MARMARA UNIVERSITY
INSTITUTE FOR GRADUATE STUDIES
IN PURE AND APPLIED SCIENCES

SYNTHESIS AND STRUCTURAL CHARACTERIZATION OF NEW DITHIOPHOSPHONIC ACID, DERIVATIVES AND COMPLEXES FROM 2,4-DIORGANYL-1,3,2,4-DITHIADIPHOSPHETANE-2,4-DISULFIDE

ELİF BULAT

Ph.D. THESIS

Department of Chemistry
Inorganic Chemistry Program

Thesis Supervisor

Prof. Dr. Ertuğrul Gazi SAĞLAM

ISTANBUL, 2023

MARMARA UNIVERSITY
INSTITUTE FOR GRADUATE STUDIES IN PURE AND APPLIED SCIENCES

SYNTHESIS AND STRUCTURAL CHARACTERIZATION OF NEW DITHIOPHOSPHONIC ACID, DERIVATIVES AND COMPLEXES FROM 2,4-DIORGANYL-1,3,2,4-DITHIADIPHOSPHETANE-2,4-DISULFIDE

ELİF BULAT

Ph.D. THESIS

Department of Chemistry
Inorganic Chemistry Program

Thesis Supervisor

Prof. Dr. Ertuğrul Gazi SAĞLAM

ISTANBUL, 2023

MARMARA UNIVERSITY
INSTITUTE FOR GRADUATE STUDIES IN PURE AND APPLIED SCIENCES

Elif BULAT, a Doctor of Philosophy student of Marmara University Institute for Graduate Studies in Pure and Applied Sciences, defended his thesis entitled "**Synthesis and Structural Characterization of New Dithiophosphonic Acid, Derivatives and Complexes from 2,4-diorganyl-1,3,2,4-dithiadiphosphetane-2,4-disulfide**", on August 2023 and has been found to be satisfactory by the jury members.

Jury Members

Prof. Dr. Ertuğrul Gazi SAĞLAM (Advisor)
Marmara University ..... (SIGN)

Prof.Dr.Bahattin YALÇIN (Jury Member)
Marmara University ..... SIGN

Prof.Dr. Ahmet Orhan GÖRGÜLÜ (Jury Member)
Marmara University SIGN

Prof.Dr. Dursun Ali KÖSE (Jury Member)
Hitit University SIGN

Prof.Dr. Yunus ZORLU (Jury Member)
Gebze Technical University SIGN

APPROVAL

Marmara University Institute for Graduate Studies in Pure and Applied Sciences Executive Committee approves that Elif BULAT be granted the degree of Doctor of Philosophy in Department of Chemistry, Inorganic Chemistry Program on …/…./20.. (Resolution no: ……).

Director of the Institute
Prof. Dr. Bülent EKİCİ

TABLE OF CONTENTS

ACKNOWLEDGEMENTS…… **i**

ÖZET…… **ii**

ABSTRACT…… **iii**

CLAIM FOR ORIGINALITY…… **iv**

ABBREVIATIONS…….. **v**

LIST OF FIGURES…….. **vi**

LIST OF TABLES…… **xxi**

1. INTRODUCTION…… **1**

2. 1,3,2,4-DITHIADIPHOSPHETANE-2,4-DISULFIDES……. **11**

2.1. 1,3,2,4- Dithiadiphosphetane-2,4-disulfides Synthesis Methods……. **11**

2.1.1. DTDP Resonance Structures……. **11**

2.1.1.1. Configuration of DTDP Isomer Structure……. **12**

2.1.1.2. Synthesis of Configuration Isomers of DTDPs……. **17**

2.1.2. Synthesis methods of 1,3,2,4-dithiadiphosphetane-2,4-disulfides… **20**

2.1.2.1. Method 1: DTDP synthesis from the reaction of thiophosphindichloride and hydrogen disulfide……. **20**

2.1.2.2. Method 2: DTDP synthesis from the reaction of phosphine and disulfide dichloride……. **21**

2.1.2.3. Method 3: Synthesis of DTDP from the reaction of diphosphene and sulphur…… **21**

2.1.2.4. Method 4: DTDP synthesis from the reaction of thiadiphosphirane and sulphur…… **22**

2.1.2.5. Method 5: Synthesis of DTDP from the reaction of thiophosphindichloride and hydrogen sulphide…….. **22**

2.1.2.6. Method 6: DTDP synthesis from phosphine and sulphur reaction……... **23**

2.1.2.7. Method 7: DTDP synthesis from the reaction of P_4S_{10} and an aromatic/aliphatic reagent…….. **25**

2.1.2.8. Synthesis of metal-containing DTDPs, DTDP S-Metal salts…. **30**

2.2. Reactions of DTDPs with RO-X (X= H, Na)…… **31**

2.2.1. Reactions with alcohols (DTDP+R-OH)…….. **31**
2.2.2. Reactions with alcoholates (DTDP+RO-Na)…… **33**
2.2.3. Reaction with diols (DTDP+HO-$(X)_n$-OH, X= -CH_2-or -Aryl-)….. **34**
2.3. DTDP Cyclisation Reactions…… **36**
2.3.1. Cyclisation Reactions with Diols…….. **36**
2.3.2. Macro-Cyclisation Reactions…… **37**
2.3.3. Cyclization with Compounds Containing -OH and Substituted Functional Groups……... **41**
2.3.4. Diels Alder Ring Reactions……... **43**
2.4. Resonance and Binding Models in Dithiophosphonic Acid Anions……. **43**
2.4.1. Synthesis of DTPOA Complexes…….. **45**
2.4.2. Synthesis of Nickel DTPOA Complexes…….. **51**
3. MATERIAL and METHOD……. **56**
3.1. Material……. **56**
3.1.1. Chemical Substances……. **56**
3.2. Instruments……... **57**
3.3. Method…….. **58**
3.3.1. Synthesis of 2,4-*bis*($R^{x,y}$)-1,3,,2,4-dithiadiphosphetane-2,4-disulfides……. **58**
3.3.2. Synthesis Method of Dithiophosphonic Acid and Dithiophosphonates; ([$R^{x,y}$(RnO)P(S)SH] and [NH_4][$S_2P(R^{x,y})$(ORn)])… **58**
3.3.3. Synthesis Method of Ni(II)-DTPOA, [Ni($S_2P(R^{x,y})$(ORn)]…….. **59**
3.4. X-ray data collection and structure refinement……. **60**
3.5. Computational Methods…… **61**
3.5.1. DFT calculations……... **61**
3.5.2. Molecular Docking Calculations……... **62**
3.6. *In vitro* cytotoxic activity studies…….. **62**
4. EXPERIMENTAL STUDIES…….. **64**
4.1. Part I. Synthesis of novel 2,4-*bis*(R^x)-1,3,2,4-dithiadiphosphetane-2,4-disulfide ([R^x-P(S)S]$_2$, R^x= 3,4-dimethoxyphenyl-, SAV-A1)……. **64**
4.1.1. General Procedure of dithiophosphonic acids and the ammonium dithiophosphonates salts for Part Ia…… **64**

4.1.2. General Procedure of dithiophosphonic acids and the ammonium salts dithiophosphonates for Part Ib……. **65**

4.1.3. General Synthesis Method of [Ni($S_2P(R^x)$(ORn)] Complexes for Part Ia…….. **65**

4.2. Synthesis of novel 2,4-*bis*(R^y)-1,3,2,4-dithiadiphosphatene-2,4-disulfide, ([R^y-P(S)S]$_2$, R^x= 2,4-dimethoxyphenyl-, SAV-A2)…… **66**

4.2.1. General Procedure of dithiophosphonic acids and the ammonium dithiophosphonates salts for Part II……. **66**

4.2.2. General Procedure of the synthesis of the complexes [Ni($S_2P(R^y)$(ORn)] for Part II…….. **67**

5. RESULT AND DISCUSSION……. **71**

5.1. Structural Characterization……... **71**

5.1.1. Comment on the IR Spectra of [R^x-P(S)S]$_2$, [NH_4][$S_2P(R^x)$(ORn)] and [Ni($S_2P(R^x)$(ORn)] for Part Ia…….. **71**

5.1.2. Comment on the IR Spectra of [NH_4][$S_2P(R^x)$(ORn)], [Ni($S_2P(R^x)$(ORn)] for Part Ib……. **95**

5.1.3. Comment on the IR Spectra of [R^y-P(S)S]$_2$, [NH_4][$S_2P(R^y)$(ORn)], [Ni($S_2P(R^y)$(ORn)] for Part II…….. **112**

5.1.4. Comment on the Mass (MS-ESI) Spectra of [NH_4][$S_2P(R^x)$(ORn)] ve [Ni($S_2P(R^x)$(ORn))$_2$] for Part Ia…….. **126**

5.1.5. Comment on the Mass (MS-ESI) Spectra of [NH_4][$S_2P(R^x)$(ORn)] ve [Ni($S_2P(R^x)$(ORn))$_2$] of Part Ib……... **141**

5.1.6. Comment on the Mass spectra of [NH_4][$S_2P(R^y)$(ORn)], [Ni($S_2P(R^y)$(ORn)] for Part II…….. **152**

5.1.7. NMR (^{1}H, ^{13}C- and ^{31}P- NMR) of compounds…….. **161**

5.1.7.1 Comment on the HSQC spectrum on the [Ni($S_2P(R^x)$(OR6))$_2$] for Part Ia…… **161**

5.1.7.2. Comment of ^{1}H-NMR Spectra of Part Ia' compounds……. **161**

5.1.7.3. Comment of ^{1}H-NMR Spectra Spectra of Part Ib' compounds……. **181**

5.1.7.4 NMR (^{1}H, ^{13}C-ve ^{31}P- NMR) Spectra of the Part II' compounds…… **193**

5.1.7.5 Comment on the HSQC spectrum on the [Ni(S2P(Ry)(OR2))2] for Part II…… **193**
5.1.7.6. Comment of ^{1}H-NMR Spectra of the Part II' compounds……. **194**
5.1.7.7. Comments on ^{13}C-NMR Spectra of Part Ia' compounds…… **204**
5.1.7.8. Comments on ^{13}C-NMR Spectra of Part Ib' compounds…… **221**
5.1.7.9. Comments on ^{13}C-NMR Spectra of the Part II' compounds….. **233**
5.1.7.10. Comments on ^{31}P-NMR Spectra of Part Ia' compounds……. **243**
5.1.7.11. Comments on ^{31}P-NMR Spectra of Part Ib' compounds……. **258**
5.1.7.12. Comments on ^{31}P-NMR Spectra of the Part II' compounds…. **269**
5.2. Crystallographic Descriptions of the Spectra of the Part Ia' Ni(II) Complexes……... **278**
5.3. Crystallographic Descriptions of the Part Ib' Ni(II) Complexes…… **307**
5.4. Crystallographic Descriptions of the Spectra of the Part II' [$Ni(S_2P(R^y)(OR2))_2$] Complex…… **324**
5.5. Optimized molecular structures of the Part Ia' Ni(II) Complexes……. **329**
5.6. Frontier orbitals and chemical parameters of the Part Ia' Ni(II) Complexes……... **332**
5.7. Optimized molecular structures of the Part Ib' Ni(II) Complexes……. **334**
5.8. Chemical parameters and HOMO and LUMO iso surfaces of Part Ib' Ni(II) Complexes……. **336**
5.9. Optimized molecular structure of the Part II' [$Ni(S_2P(R^y)(OR2))_2$] Complex…….. **338**
5.10. Part II Frontier orbitals and chemical parameters of the Part II' [$Ni(S_2P(R^y)(OR2))_2$] Complex…… **340**
5.11. The MEP surfaces of the Part Ia' Ni(II) Complexes…… **342**
5.12. Molecular electrostatic potential (MEP) surfaces of Part Ib' Ni(II) Complexes……... **344**
5.13. Part II The MEP surfaces of the Part II' [$Ni(S_2P(R^y)(OR2))_2$] Complex…….. **345**
5.14. Molecular docking studies of the Part Ia' Ni(II) complexes…… **346**
5.15. Part Ib. Molecular docking studies of [$Ni(S_2P(R^x)(OR1))_2$], [$Ni(S_2P(R^x)(OR2))_2$], [$Ni(S_2P(R^x)(OR4))_2$] and [$Ni(S_2P(R^x)(OR5))_2$] with

colon cancer antigen and liver cancer proteins……. **355**

5.16. Molecular docking studies of the Part II' $[Ni(S_2P(R^y)(OR2))_2]$ Complex…….. **362**

5.17. *In vitro* cytotoxic activity studies of the Part Ia' Compounds……. **364**

5.18. *In vitro* cytotoxic activity studies of the Part Ib' Compounds…… **368**

5.19. *In vitro* cytotoxic activity studies of the Part II' Compounds…….. **370**

6. CONCLUSIONS…….. **374**

7. REFERENCES……..……... **385**

8. CURRICULUM VITAE……... **400**

ACKNOWLEDGEMENTS

I would like to thank FDK-2021-10339, Marmara University, Project Coordination Application (2,4-*bis*(**3,4-dimethoxyphenyl**)-1,3,2,4-dithiadiphosphetane-2,4-disulfide derivatives studies) and Research Centre and Yozgat Bozok University, Application and Research Centre (2,4-*bis*(**2,4-dimethoxyphenyl**)-1,3,2,4-dithiadiphosphetane-2,4-disulfide derivatives studies) for supporting this thesis. I would also like to thank the staff of both the Project Coordination Application and Research Centres for their support in project writing.

I would also like to thank the esteemed academicians of Marmara University (Science Faculty) and Yozgat Bozok University (Science Faculty); Prof. Dr. Hamza Yılmaz, one of the doyens of Inorganic Chemistry; the Thesis Monitoring Committee (TIK) and academicians who evaluated the thesis for their scientific support.

To my seniors Mustafa HOROZOĞLU and Tugay TURKAY for their support during my doctoral education;

To my mother Leyla BULAT, my brother Halil İbrahim TEKİN, my sisters Yeşim TEKİN and Arzu BULAT, who have always provided material and spiritual support in my education and training life;

Again in this term, I would like to thank my friends Fatıma Serap ÖZKAYNAKCI, Hatice YEŞİL, Yudum ÖZER, Demet ÇEVİK, Yasemin ÖZKAN, Melek KAPLAN, Sümeyye ERBAY, Mücella Özbay KARAKUŞ, Merve YAKIŞIKLIER, İrem YILMAZ, Münevver Nur KABATEPE with my sincere love and respect.

I also remember with mercy my father Salih BULAT who passed away when I was a little girl...

I would like to express my deepest respect and gratitude to my honourable supervisor Prof. Dr. Ertuğrul Gazi SAĞLAM, who shared his knowledge, experience and academic ethics with us from my research project to my doctoral thesis studies.

ÖZET

2,4-DİORGANİL-1,3,2,4-DİTİYADİFOSFETAN-2,4-DİSÜLFÜRÜNDEN YENİ DİTİYOFOSFONİK ASİT, TÜREV ve KOMPLEKSLERİNİN SENTEZİ VE YAPISAL KARAKTERİZASYONU

Dimer olarak bilinen yeni 2,4-*bis*($R^{x,y}$)-1,3,2,2,4-ditiyadifosfetan-2,4-disülfürü ([$R^{x,y}$-P(S)S]$_2$, R^x= 3,4-dimetoksifenil, SAV-A1; R^y= 2,4-dimetoksifenil, SAV-A2) başlangıç maddesi olarak sentezlenmiştir. Bu dimerlerin alkol ile reaksiyonundan (16 adet) ditiyofosfonik asitler, [$R^{x,y}$(RnO)P(S)SH] sentezlenmiştir. Bu asitlerden 12 tanesi, [R^x(RnO)P(S)SH], SAV-A1'in alkollerle reaksiyonundan elde edilmiştir (Kısım Ia'da DTPOA sentez çalışması için kullanılan alkoller RnOH, R1=metil-, R2=Etil-, R3=n-propil-, R4=n-butil-, R5=3-pentil-, R6=3-metil-1-butil-, R7=benzil-; Kısım Ib'de DTPOA sentez çalışması için kullanılan alkoller RnOH, R1= -n-pentil; R2=2-pentil-; R3=4-tert-but-benzil-; R4= 2-propil-; R5= 2-butil-). Benzer şekilde (R^y)(RnO)PS_2H) olarak adlandırılan SAV-A2'nin alkollerle (Kısım II'de DTPOA sentez çalışması için kullanılan alkoller RnOH, R1= 2-bütil; R2= n-pentil-; R3= 4-*tert*-butil benzil-; R4= metil-) reaksiyonundan diğer asitler elde edilmiştir. Tüm asitler yapısı belirlenebilir ve kokusuz amonyum ditiyofosfonat tuzuna ([NH_4][S_2P(R^x)(ORn)] ve [NH_4][S_2P(R^y)(ORn)]) dönüştürülmüştür (16 Adet). Bu tuzlar Ni(II) iyonuyla reaksiyona girerek dört koordinasyonlu Ni(II) ditiyofosfonata kompleksleri ([Ni(S_2P(R^x)(ORn)] ve [Ni(S_2P(R^y)(ORn)]) sentezlenmiştir. Tez kapsamında toplam 50 bileşik sentezlenmiştir.

Bu çalışmada, sentezlenen yeni bileşiklerin yapısal karakterizasyonu elementel analiziyle beraber kütle, FT-IR, tek ve iki boyutlu NMR (^{1}H-, ^{13}C- ve ^{31}P-NMR) spektroskopileriyle aydınlatılmıştır. Ayrıca, komplekslerin yapısı X-ışını kırınımı yöntemi ile aydınlatıldı ([Ni(S_2P(R^x)(ORn)] X ışını analizleri kompleksleri için MÜ, BAP-FDK-2021-10339 projesiyle desteklendi; Part Ia kapsamında n= 1,2,3,4,6,7 ve Part 1b kapsamında n= 1,2,4,5). Komplekslerin teorik hesaplamalarıyla (Density Functional Theory, Molecular Docking) beraber uygulama olarak bileşiklerin antikanser çalışmalarıda gerçekleştirilmiştir.

ABSTRACT

SYNTHESIS AND STRUCTURAL CHARACTERIZATION OF NEW DITHIOPHOSPHONIC ACIDS, DERIVATIVES AND COMPLEXES FROM 2,4-DIORGANYL-1,3,2,4-DITHIADIPHOSPHETANE-2,4-DISULFIDE

Two new 2,4-*bis*($R^{x,y}$)-1,3,2,4-dithiadiphosphetane-2,4-disulfide known as dimer was synthesised as starting material ($[R^{x,y}\text{-}P(S)S]_2$, R^x= 3,4-dimethoxyphenyl, SAV-A1; R^y= 2,4-dimethoxyphenyl, SAV-A2). From the reaction of these dimers with 16 alcohols were synthesized new dithiophosphonic acids ($[R^{x,y}(RnO)P(S)SH]$). 12 of these acids ($[R^x(RnO)P(S)SH]$) were produced from the reaction of SAV1 with alcohols (RnOH= Alcohols used in DTPOA synthesis reactions for Part Ia, R1=methyl-, R2=Ethyl-, R3=n-propyl-, R4=n-butyl-, R5=3-pentyl-, R6=3-methyl-1-butyl-, R7=benzyl-; RnOH= Alcohols used in DTPOA synthesis reactions for Part Ib, RnOH, R1= n-pentyl; R2=2-pentyl-; R3=4-tert-but-benzyl-; R4= 2-propyl-; R5= 2-butyl-). Similarly, other acids which are coded as $[R^y(RnO)P(S)SH]$ were obtained from the reaction of SAV2 with alcohols (RnOH = Alcohols used for Part II for DTPOAs, R1= 2-butyl; R2= n-pentyl-; R3= 4-tert-butyl benzyl-; R4= methyl-). All acids were converted to 16 structurally determinable and odourless ammonium dithiophosphonate salts ($[NH_4][S_2P(R^x)(ORn)]$ and $[NH_4][S_2P(R^y)(ORn)]$). Ni(II) dithiophosphonato complexes were synthesized by the reaction of these salts and Ni(II) ion, as four coordination structures ($[Ni(S_2P(R^x)(ORn)]$ and $[Ni(S_2P(R^y)(ORn)]$, 16 complexes). Within the scope of the thesis, a total of 50 new compounds were synthesized.

This study elucidated the structural characterization of the synthesized new compounds by mass, FT-IR, NMR, (1D ^{1}H-, ^{13}C-, ^{31}P-NMR and 2D HSQC for $[Ni(S_2P(R^x)(OR6)]$ and $[Ni(S_2P(R^y)(OR2)]$) spectroscopies together with elemental analysis. In addition, the structure of the complexes was elucidated by the X-ray diffraction method ($[Ni(S_2P(R^x)(ORn)]$ X-ray analyses for complexes supported by MÜ, BAP-FDK-2021-10339 project; n= 1,2,3,4,6,7 under Part Ia and n= 1,2,4,5 under Part 1b). Theoretical calculations of the complexes (density functional theory, molecular docking) and anticancer studies of the compounds were carried out as applications.

CLAIM FOR ORIGINALITY

The new 2,4-diorganyl-1,3,2,4-dithiadiphosphetane-2,4-disulfide compounds (SAV-A1, SAV-A2) synthesized within the scope of this thesis are original and constitute an alternative in the synthesis of new organo-dithiophosphorus group compounds, it has a original value because it has not been studied much in terms of subject and research.

The DTDPs synthesized in this thesis provide an opportunity for many researchers studying organo-dithiophosphorus chemistry to develop new research topics. In addition, the investigation of biological and anticarcinogenic effects of the novel compounds produced in this thesis has the potential to be of interest for researchers working in different branches. The development of an alternative method in the near future for the disposal of nuclear wastes generated from nuclear power plants using the novel compounds produced in this study is among the potential outputs of the thesis.

This thesis has an original value in terms of enabling creation of new research topics related to the synthesis of new dithiophosphonic acids/dithiophosphonic acid salts/metal-DTPOA complexes.

Elif BULAT **Prof. Dr. Ertuğrul Gazi SAĞLAM**

ABBREVIATIONS

p-	*Para-*
m-	*Meta-*
o-	*Ortho-*
i-	*İso-*
Sec-	*Secondar*
Tert-	*Tertiary-*
Ar	Aromatic
Ph-	Phenyl-
Me-	Methyl-
Et-	Ethyl-
Pr-	Propyl-
But-	Butyl-
Hex-	Hexyl-
Cy-	Cyclo-
Tol-	Tolyl-
Fc-	Ferrocenyl-
P_4S_{10}	Phosphorus Penta Sulfide
Py	Pyridine
LR	Lawesson' reagent
DTDP	1,3,2,4-dithiadiphosphetane-2,4-disulfides
DTPOA	Dithiophosphonic acid
SAV-A1	2,4-*bis*(3,4-dimetoxyphenyl)-1,3,2,4-dithiadiphosphetane-2,4-disulfides
SAV-A2	2,4-*bis*(2,4-dimetoxyphenyl)- 1,3,2,4-dithiadiphosphetane-2,4-disulfides
M.P.	Melting point
HPLC	High Liquid Pressure Chromatography
Hz	Hertz
ppm	Parts Per Million

LIST OF FIGURES

Figure 1.1. Experimental setup for the supercritical extraction system…… **2**

Figure 1.2. Comparison of CYANEX 301 with the compounds synthesized within the scope of the thesis……. **4**

Figure 1.3.a. Structures of DTPOA structures ([R^x(ORn)P(S)SH]) synthesized from the newly synthesized starting material ([R^x-P(S)S]$_2$) within the scope of the thesis, (Part Ia)…… **6**

Figure 1.3.b. Structures of DTPOA structures ([R^x(ORn)P(S)SH]) synthesized from the newly synthesized starting material ([R^x-P(S)S]$_2$) within the scope of the thesis, (Part Ib)…… **7**

Figure 1.4.a. Structures of ammonium dithiophosphonate salts ([NH_4][$S_2P(R^x)$(ORn)]) synthesized from DTPOAs within the scope of the thesis, (Part Ia)…….. **7**

Figure 1.4.b. Structures of ammonium dithiophosphonate salts ([NH_4][$S_2P(R^x)$(ORn)]) synthesized from DTPOAs within the scope of the thesis, (Part Ib)……. **8**

Figure 1.5.a. Structures of Ni(II)-DTPOA complexes ([Ni($S_2P(R^x)$(ORn)]) synthesized from [NH_4][$S_2P(R^x)$(ORn)] within the scope of the thesis, (Part Ia)..... **8**

Figure 1.5.b. Structures of Ni(II)-DTPOA complexes ([Ni($S_2P(R^x)$(ORn)]) synthesized from [NH_4][$S_2P(R^x)$(ORn)] within the scope of the thesis, (Part Ib)……. **9**

Figure 1.6.a. Structures of DTPOA structures ([R^y(ORn)P(S)SH]) synthesized from the newly synthesized starting material ([R^y-P(S)S]$_2$) within the scope of the thesis,(Part II)……. **9**

Figure 1.6.b. Structures of ammonium dithiophosphonate salts ([NH_4][$S_2P(R^y)$(ORn)]) synthesized from DTPOAs within the scope of the thesis, (Part II)…….. **10**

Figure 1.6.c. Structures of Ni(II)-DTPOA complexes ([Ni($S_2P(R^y)$(ORn)]) synthesized from [NH_4][$S_2P(R^y)$(ORn)] within the scope of the thesis, (Part II).. **10**

Figure 2.1. Illustration of the discovery of phosphorus (left) and the Berzelius reagent…….. **11**

Figure 2.2. One synthesis reaction of DTDP, (R= H, aliphatic or aromatic group)……... **12**
Figure 2.3. Resonance representation of ringed covalent and dipolar structures…….. **12**
Figure 2.4. One of an examples of the DTDPs isomers, (*cis*- and *trans*-isomers)…… **14**
Figure 2.5. The equilibrium between structures I and II……. **16**
Figure 2.6. Structure of some DTDPs belonging to *trans*- and *cis*-isomers…… **17**
Figure 2.7. An example of a ringed covalent I (*cis*-isomerism) and dipolar II X-ray ORTEP diagram structure…….. **17**
Figure 2.8. Phosphane and S_2Cl_2 synthesis of dipolar II structure…… **18**
Figure 2.9. Synthesis of dipolar II structure from phosphene and elemental sulphur…….. **18**
Figure 2.10. Synthesis of dipolar II structure by heating DTDPS in the gas phase……. **18**
Figure 2.11. One of the synthesis methods for dipolar II isomer……. **19**
Figure 2.12. Synthesis of dithioxophosphorane (Dipolar structure II)……. **20**
Figure 2.13. General synthesis reaction of DTDPs according to Method 1…… **21**
Figure 2.14. General synthesis reaction of DTDPs according to Method 2…… **21**
Figure 2.15. General synthesis reaction of DTDPs according to Method 3…… **21**
Figure 2.16. General synthesis reaction of DTDPs according to method 4……. **22**
Figure 2.17. General synthesis reaction of DTDPs according to Method 5…… **22**
Figure 2.18. General synthesis reaction of DTDPs according to method 6……. **24**
Figure 2.19. Suggested DTDP reaction mechanism for Method 7…….. **25**
Figure 2.20. The best-known DTDPs are synthesized according to Method 7… **26**
Figure 2.21. DR-thiomethyl derivative one of the synthesis reaction…….. **27**
Figure 2.22. DTDP-naphthalene derivative structure…….. **28**
Figure 2.23. Structure of the first proposed DTDP of dicyclohexenyl derivative…….. **28**
Figure 2.24. Synthesis of diethylamido-DTDP analogue……. **30**
Figure 2.25. Synthesis of diethylamido-DTDP from starting material EtS-DTDP……... **30**

Figure 2.26. The general synthesis method of DTPOAs…….. **32**
Figure 2.27. General synthesis method of the reaction of DTDPs with alcoholate salts…….. **34**
Figure 2.28. Synthesis reaction of *bis*-(alkyl-/aryl-) dithiophosphonic acids….. **34**
Figure 2.29. Synthesis reactions of cyclic heterocyclic DTPOA derivatives…... **35**
Figure 2.30. Syntheses reactions of cyclic DTPOA derivatives with aromatic or aliphatic diols……...…… **37**
Figure 2.31. Synthesis of eight- to ten-membered heterocyclic DTPOA derivatives from the reaction of $[Fc\text{-}P(S)S]_2$ with alkenyl-diols and I_2……. **38**
Figure 2.32. Synthesis of ferrocene-containing heterocycles DTPOA from the reaction of $[Fc\text{-}P(S)S]_2$ with alkenyl-diols and $SOCl_2$…….. **38**
Figure 2.33. Synthesis of mono- and di-phosphorus species from $[Fc\text{-}P(S)S]_2$, aryl-diols and I_2 as an one pot synthesis…… **39**
Figure 2.34. Synthesis of non-heterocycle from $[Fc\text{-}P(S)S]_2$, but-2-in-1,4-diol and I_2……. **40**
Figure 2.35. Synthesis of sulfur-containing macrocyclic DTPOA derivatives…. **41**
Figure 2.36. Resonance structures of dithiophosphonate ligand**…….** **44**
Figure 2.37. Typical binding modes of metal-dithiophosphonates……. **44**
Figure 2.38. Synthesis reaction of metal-DTPOA coordination compound……. **46**
Figure 2.39. Synthesis reaction of organometallic-Ti-DTPOA…… **46**
Figure 2.40. Synthesis reaction of organometallic-Pb-*O*-alkyl-4-methoxyphenyl DTPOA……... **47**
Figure 2.41. Synthesis reaction of organometallic-Pb-*S*-alkyl-4-methoxyphenyl DTPOA……... **47**
Figure 2.42. $[M(PR_3)_2(S_2(S)PC_6H_4OMe)]$ synthesis reaction (M= Ni(II), Pd(II) ve Pt(II); R=Ph, Et)……... **47**
Figure 2.43. Synthesis reaction of $[Pt(PR_3)_2(S_2(S)PC_6H_4OMe)]$, (R= Ethyl-, n-butyl-)……... **48**
Figure 2.44. $[(R_3O)_2B\text{-}S\text{-}(S)PR')]$ synthesis reaction, (R'=4-CH_3O-C_6H_4- and R= *iso*-prop-, *iso*-butyl-; *tert*-butyl-, R'=4-C_2H_5O-C_6H_4 and R= *iso*-Pr-, *iso*-butyl-)……... **48**
Figure 2.45. $[Ag_{24}(PS_4)(^{i}PrSPS_3)_4S(tol)_{12}(dppe)_6)]^{+}$ $^{-}[S^{iso}Pr]$ synthesis

reaction…… **49**

Figure 2.46. Synthesis reaction of [((η^5-C_5H_5)$_2$Fe)(RO))P(S)S)M(PPh_3)$_2$], (M=Ag, R= -OCH_3, -OC_3H_7; M= Pt, R= -OCH_3)……. **49**

Figure 2.47. Nickel-dithiolene complex together with complex *trans-bis*[*O*-ethyl(4-methoxyphenyl)phosphonodithioato]-Ni(II), which was isolated in a synthesis reaction…….. **50**

Figure 2.48. Suggested reaction mechanism for the synthesis of DTPOA-Metal complexes by one-pot reaction method…… **50**

Figure 2.49. Synthesis reaction of Ni(II)-DTPOA complexes……. **51**

Figure 2.50. Nickel complex of ferrocenyl dithiophosphonic salts……. **51**

Figure 2.51. Synthesis of Nickel-DTPOA complexes of macro-structured ring complexes……. **52**

Figure 2.52. Synthesis reaction of $[NBu_4]_2[Ni_2(C_6H_5)_4(\mu\text{-}OH)_2]$ complex…….. **52**

Figure 2.53. Synthesis reaction of Zn(II)-, Cd(II)-, Hg(II)-DTPOA complexes with the two-centered ring…… **53**

Figure 2.54. Synthesis of six-coordinated DTPOA-Nickel complexes…… **53**

Figure 2.55. Six-coordinated 2,4,6-tris-2-pyridyl-1,3,5-triazine-Ni(II)-DTPOA complex…… **54**

Figure 2. 56. Synthesis reaction of the *cis*-isomer for the square-plane Ni(II)-DTPOA…… **55**

Figure 3.1. The suggested reaction mechanism for the formation of DTPOAs… **58**

Figure 3.2. Synthesis reactions of $[NH_4][S_2P(R^{x,y})(ORn)]$……... **59**

Figure 3.3. Synthesis reaction of Ni(II)-DTPOA complex…….. **60**

Figure 4.1. SAV-A1 synthesis reaction…… **64**

Figure 4.2. SAV-A2 synthesis reaction…… **66**

Figure 5.1. SAV-A1 IR spectrum (4000 cm^{-1}- 400 cm^{-1})…… **73**

Figure 5.2. $[NH_4][S_2P(R^x)(OR1)]$ IR spectrum (4000 cm^{-1}- 400 cm^{-1})……. **74**

Figure 5.3. $[NH_4][S_2P(R^x)(OR2)]$ IR spectrum (4000 cm^{-1}- 400 cm^{-1})……. **75**

Figure 5.4. $[NH_4][S_2P(R^x)(OR3)]$ IR spectrum (4000 cm^{-1}- 400 cm^{-1})…… **76**

Figure 5.5. $[NH_4][S_2P(R^x)(OR4)]$ IR spectrum (4000 cm^{-1}- 400 cm^{-1})…… **77**

Figure 5.6. $[NH_4][S_2P(R^x)(OR5)]$ IR spectrum (4000 cm^{-1}- 400 cm^{-1})……. **78**

Figure 5.7. $[NH_4][S_2P(R^x)(OR6)]$ IR spectrum (4000 cm^{-1}- 400 cm^{-1})…… **79**

Figure 5.8. $[NH_4][S_2P(R^x)(OR7)]$ IR spectrum (4000 cm^{-1}- 400 cm^{-1})…… **80**
Figure 5.9.a. $[Ni(S_2P(R^x)(OR1))_2]$ IR spectrum (4000 cm^{-1}- 400 cm^{-1})…….. **81**
Figure 5.9.b. $[Ni(S_2P(R^x)(OR1))_2]$ IR spectrum (400 cm^{-1}- 200 cm^{-1})……. **82**
Figure 5.10.a. $[Ni(S_2P(R^x)(OR2))_2]$ IR spectrum (4000 cm^{-1}- 400 cm^{-1})……. **83**
Figure 5.10.b. $[Ni(S_2P(R^x)(OR2))_2]$ IR spectrum (400 cm^{-1}- 200 cm^{-1})……. **84**
Figure 5.11.a. $[Ni(S_2P(R^x)(OR3))_2]$ IR spectrum (4000 cm^{-1}- 400 cm^{-1})…… **85**
Figure 5.11.b. $[Ni(S_2P(R^x)(OR3))_2]$ IR spectrum (400 cm^{-1}- 200 cm^{-1})…….. **86**
Figure 5.12.a. $[Ni(S_2P(R^x)(OR4))_2]$ IR spectrum (4000 cm^{-1}- 400 cm^{-1})……. **87**
Figure 5.12.b. $[Ni(S_2P(R^x)(OR4))_2]$ IR spectrum (400 cm^{-1}- 200 cm^{-1})……. **88**
Figure 5.13.a. $[Ni(S_2P(R^x)(OR5))_2]$ IR spectrum (4000 cm^{-1}- 400 cm^{-1})……. **89**
Figure 5.13.b. $[Ni(S_2P(R^x)(OR5))_2]$ IR spectrum (400 cm^{-1}- 200 cm^{-1})……. **90**
Figure 5.14.a. $[Ni(S_2P(R^x)(OR6))_2]$ IR spectrum (4000 cm^{-1}- 400 cm^{-1})…… **91**
Figure 5.14.b. $[Ni(S_2P(R^x)(OR6))_2]$ IR spectrum (400 cm^{-1}- 200 cm^{-1})…….. **92**
Figure 5.15.a. $[Ni(S_2P(R^x)(OR7))_2]$ IR spectrum (4000 cm^{-1}- 400 cm^{-1})…… **93**
Figure 5.15.b. $[Ni(S_2P(R^x)(OR7))_2]$ IR spectrum (400 cm^{-1}- 200 cm^{-1})…….. **94**
Figure 5.16. $[NH_4][S_2P(R^x)(OR1)]$ IR spectrum (4000 cm^{-1}- 400 cm^{-1})……. **97**
Figure 5.17. $[NH_4][S_2P(R^x)(OR2)]$ IR spectrum (4000 cm^{-1}- 400 cm^{-1})……. **98**
Figure 5.18. $[NH_4][S_2P(R^x)(OR3)]$ IR spectrum (4000 cm^{-1}- 400 cm^{-1})……. **99**
Figure 5.19. $[NH_4][S_2P(R^x)(OR4)]$ IR spectrum (4000 cm^{-1}- 400 cm^{-1})…….. **100**
Figure 5.20. $[NH_4][S_2P(R^x)(OR5)]$ IR spectrum (4000 cm^{-1}- 400 cm^{-1})……. **101**
Figure 5.21.a. $[Ni(S_2P(R^x)(OR1))_2]$ IR spectrum (4000 cm^{-1}- 400 cm^{-1})……. **102**
Figure 5.21.b. $[Ni(S_2P(R^x)(OR1))_2]$ IR spectrum (400 cm^{-1}- 200 cm^{-1})…….. **103**
Figure 5.22.a. $[Ni(S_2P(R^x)(OR2))_2]$ IR spectrum (4000 cm^{-1}- 400 cm^{-1})……. **104**
Figure 5.22.b. $[Ni(S_2P(R^x)(OR2))_2]$ IR spectrum (400 cm^{-1}- 200 cm^{-1})……. **105**
Figure 5.23.a. $[Ni(S_2P(R^x)(OR3))_2]$ IR spectrum (4000 cm^{-1}- 400 cm^{-1})…… **106**
Figure 5.23.b. $[Ni(S_2P(R^x)(OR3))_2]$ IR spectrum (400 cm^{-1}- 200 cm^{-1})…….. **107**
Figure 5.24.a. $[Ni(S_2P(R^x)(OR4))_2]$ IR spectrum (4000 cm^{-1}- 400 cm^{-1})……. **108**
Figure 5.24.b. $[Ni(S_2P(R^x)(OR4))_2]$ IR spectrum (400 cm^{-1}- 200 cm^{-1})……. **109**
Figure 5.25.a. $[Ni(S_2P(R^x)(OR5))_2]$ IR spectrum (4000 cm^{-1}- 400 cm^{-1})……. **110**
Figure 5.25.b. $[Ni(S_2P(R^x)(OR5))_2]$ IR spectrum (400 cm^{-1}- 200 cm^{-1})…….. **111**
Figure 5.26. SAV-A2 IR spectrum (4000 cm^{-1}- 400 cm^{-1})……. **113**
Figure 5.27. $[NH_4][S_2P(R^y)(OR1)]$ IR spectrum (4000 cm^{-1}- 400 cm^{-1})……. **114**

Figure 5.28. $[NH_4][S_2P(R^y)(OR2)]$ IR spectrum (4000 cm^{-1}- 400 cm^{-1})…… **115**
Figure 5.29. $[NH_4][S_2P(R^y)(OR3)]$ IR spectrum (4000 cm^{-1}- 400 cm^{-1})……. **116**
Figure 5.30. $[NH_4][S_2P(R^y)(OR4)]$ IR spectrum (4000 cm^{-1}- 400 cm^{-1})…….. **117**
Figure 5.31.a. $[Ni(S_2P(R^y)(OR1))_2]$ IR spectrum (4000 cm^{-1}- 400 cm^{-1})…… **118**
Figure 5.31.b. $[Ni(S_2P(R^y)(OR1))_2]$ IR spectrum (400 cm^{-1}- 200 cm^{-1})…….. **119**
Figure 5.32.a. $[Ni(S_2P(R^y)(OR2))_2]$ IR spectrum (4000 cm^{-1}- 400 cm^{-1})……. **120**
Figure 5.32.b. $[Ni(S_2P(R^y)(OR2))_2]$ IR spectrum (400 cm^{-1}- 200 cm^{-1})……. **121**
Figure 5.33.a. $[Ni(S_2P(R^y)(OR3))_2]$ IR spectrum (4000 cm^{-1}- 400 cm^{-1})…… **122**
Figure 5.33.b. $[Ni(S_2P(R^y)(OR3))_2]$ IR spectrum (400 cm^{-1}- 200 cm^{-1})…….. **123**
Figure 5.34.a. $[Ni(S_2P(R^y)(OR4))_2]$ IR spectrum (4000 cm^{-1}- 400 cm^{-1})…….… **124**
Figure 5.34.b. $[Ni(S_2P(R^y)(OR4))_2]$ IR spectrum (400 cm^{-1}- 200 cm^{-1})…….…. **125**
Figure 5.35. $[NH_4][S_2P(R^x)(OR1)]$ Mass spectrum (ESI^-)……... **127**
Figure 5.36. $[NH_4][S_2P(R^x)(OR2)]$ Mass spectrum (ESI^-)……..…… **128**
Figure 5.37. $[NH_4][S_2P(R^x)(OR3)]$ Mass spectrum (ESI^-)……..…… **129**
Figure 5.38. $[NH_4][S_2P(R^x)(OR4)]$ Mass spectrum (ESI^-)……...…. **130**
Figure 5.39. $[NH_4][S_2P(R^x)(OR5)]$ Mass spectrum (ESI^-)……...…. **131**
Figure 5.40. $[NH_4][S_2P(R^x)(OR6)]$ Mass spectrum (ESI^-)……...…. **132**
Figure 5.41. $[NH_4][S_2P(R^x)(OR7)]$ Mass spectrum (ESI^-)…….. **133**
Figure 5.42. $[Ni(S_2P(R^x)(OR1))_2]$ Mas spectrum (ESI^+)……. **134**
Figure 5.43. $[Ni(S_2P(R^x)(OR2))_2]$ Mas spectrum (ESI^+)……. **135**
Figure 5.44. $[Ni(S_2P(R^x)(OR3))_2]$ Mas spectrum (ESI^+)……. **136**
Figure 5.45. $[Ni(S_2P(R^x)(OR4))_2]$ Mas spectrum (ESI^+)……. **137**
Figure 5.46. $[Ni(S_2P(R^x)(OR5))_2]$ Mas spectrum (ESI^+)……. **138**
Figure 5.47. $[Ni(S_2P(R^x)(OR6))_2]$ Mas spectrum (ESI^+)……. **139**
Figure 5.48. $[Ni(S_2P(R^x)(OR7))_2]$ Mas spectrum (ESI^+)……. **140**
Figure 5.49. $[NH_4][S_2P(R^x)(OR1)]$ Mass spectrum (ESI^-)……... **142**
Figure 5.50. $[NH_4][S_2P(R^x)(OR2)]$ Mass spectrum (ESI^-)……..…… **143**
Figure 5.51. $[NH_4][S_2P(R^x)(OR3)]$ Mass spectrum (ESI^-)……..…… **144**
Figure 5.52. $[NH_4][S_2P(R^x)(OR4)]$ Mass spectrum (ESI^-)……...…. **145**
Figure 5.53. $[NH_4][S_2P(R^x)(OR5)]$ Mass spectrum (ESI^-)……...…. **146**
Figure 5.54. $[Ni(S_2P(R^x)(OR1))_2]$ Mas spectrum (ESI^+)……. **147**
Figure 5.55. $[Ni(S_2P(R^x)(OR2))_2]$ Mas spectrum (ESI^+)……. **148**

Figure 5.56. [Ni($S_2P(R^x)(OR3))_2$] Mas spectrum (ESI^+)……. **149**
Figure 5.57. [Ni($S_2P(R^x)(OR4))_2$] Mas spectrum (ESI^+)……. **150**
Figure 5.58. [Ni($S_2P(R^x)(OR5))_2$] Mas spectrum (ESI^+)……. **151**
Figure 5.59. [NH_4][$S_2P(R^y)(OR1)$] Mass spectrum (ESI^-)……... **153**
Figure 5.60. [NH_4][$S_2P(R^y)(OR2)$] Mass spectrum (ESI^-)……..…… **154**
Figure 5.61. [NH_4][$S_2P(R^y)(OR3)$] Mass spectrum (ESI^-)……..…… **155**
Figure 5.62. [NH_4][$S_2P(R^y)(OR4)$] Mass spectrum (ESI^-)……...… **156**
Figure 5.63. [Ni($S_2P(R^y)(OR1))_2$] Mas spectrum (ESI^+)……. **157**
Figure 5.64. [Ni($S_2P(R^y)(OR2))_2$] Mas spectrum (ESI^+)……. **158**
Figure 5. 65. [Ni($S_2P(R^y)(OR3))_2$] Mas spectrum (ESI^+)……. **159**
Figure 5.66. [Ni($S_2P(R^y)(OR4))_2$] Mas spectrum (ESI^+)……. **160**
Figure 5.67. HSQC spectrum (**I**) for the aromatic region and (**II**) for the aliphatic region of [Ni($S_2P(R^x)(OR6))_2$]…….. **162**
Figure 5.68. The numbering scheme for the compounds Part Ia……. **166**
Figure 5.69. [NH_4][$S_2P(R^x)(OR1)$] ^{1}H-NMR spectrum……... **167**
Figure 5.70. [NH_4][$S_2P(R^x)(OR2)$] ^{1}H-NMR spectrum……..…… **168**
Figure 5.71. [NH_4][$S_2P(R^x)(OR3)$] ^{1}H-NMR spectrum……..… **169**
Figure 5.72. [NH_4][$S_2P(R^x)(OR4)$] ^{1}H-NMR spectrum…….. **170**
Figure 5.73. [NH_4][$S_2P(R^x)(OR5)$] ^{1}H-NMR spectrum……..… **171**
Figure 5.74. [NH_4][$S_2P(R^x)(OR6)$] ^{1}H-NMR spectrum……..…… **172**
Figure 5.75. [NH_4][$S_2P(R^x)(OR7)$] ^{1}H-NMR spectrum……... **173**
Figure 5.76. [Ni($S_2P(R^x)(OR1))_2$] ^{1}H-NMR spectrum…… **174**
Figure 5.77. [Ni($S_2P(R^x)(OR2))_2$] ^{1}H-NMR spectrum…… **175**
Figure 5.78. [Ni($S_2P(R^x)(OR3))_2$] ^{1}H-NMR spectrum……. **176**
Figure 5.79. [Ni($S_2P(R^x)(OR4))_2$] ^{1}H-NMR spectrum…… **177**
Figure 5.80. [Ni($S_2P(R^x)(OR5))_2$] ^{1}H-NMR spectrum…… **178**
Figure 5.81. [Ni($S_2P(R^x)(OR6))_2$] ^{1}H-NMR spectrum…… **179**
Figure 5.82. [Ni($S_2P(R^x)(OR7))_2$] ^{1}H-NMR spectrum…… **180**
Figure. 5.83. The numbering scheme for compounds Part Ib…….. **181**
Figure 5.84. [NH_4][$S_2P(R^x)(OR1)$] ^{1}H-NMR spectrum…….. **183**
Figure 5.85. [NH_4][$S_2P(R^x)(OR2)$] ^{1}H-NMR spectrum…….. **184**
Figure 5.86. [NH_4][$S_2P(R^x)(OR3)$] ^{1}H-NMR spectrum…….. **185**

Figure 5.87. $[NH_4][S_2P(R^x)(OR4)]$ ^{1}H-NMR spectrum…….. **186**
Figure 5.88. $[NH_4][S_2P(R^x)(OR5)]$ ^{1}H-NMR spectrum…….. **187**
Figure 5.89. $[Ni(S_2P(R^x)(OR1))_2]$ ^{1}H-NMR spectrum…… **188**
Figure 5.90. $[Ni(S_2P(R^x)(OR2))_2]$ ^{1}H-NMR spectrum…… **189**
Figure 5.91. $[Ni(S_2P(R^x)(OR3))_2]$ ^{1}H-NMR spectrum…… **190**
Figure 5.92. $[Ni(S_2P(R^x)(OR4))_2]$ ^{1}H-NMR spectrum…… **191**
Figure 5.93. $[Ni(S_2P(R^x)(OR5))_2]$ ^{1}H-NMR spectrum…… **192**
Figure. 5.94. The numbering scheme for compounds…….. **193**
Figure. 5.95. HSQC spectrum of $[Ni(S_2P(R^y)(OR2))_2]$…… **194**
Figure 5.96. $[NH_4][S_2P(R^y)(OR1)]$ ^{1}H-NMR spectrum……... **196**
Figure 5.97. $[NH_4][S_2P(R^y)(OR2)]$ ^{1}H-NMR spectrum……... **197**
Figure 5.98. $[NH_4][S_2P(R^y)(OR3)]$ ^{1}H-NMR spectrum……... **198**
Figure 5.99. $[NH_4][S_2P(R^y)(OR4)]$ ^{1}H-NMR spectrum……... **199**
Figure 5.100. $[Ni(S_2P(R^y)(OR1))_2]$ ^{1}H-NMR spectrum…….. **200**
Figure 5.101. $[Ni(S_2P(R^y)(OR2))_2]$ ^{1}H-NMR spectrum…….. **201**
Figure 5.102. $[Ni(S_2P(R^y)(OR3))_2]$ ^{1}H-NMR spectrum…….. **202**
Figure 5.103. $[Ni(S_2P(R^y)(OR4))_2]$ ^{1}H-NMR spectrum…….. **203**
Figure 5.104. $[NH_4][S_2P(R^x)(OR1)]$ ^{13}C-NMR spectrum…… **207**
Figure 5.105. $[NH_4][S_2P(R^x)(OR2)]$ ^{13}C-NMR spectrum…… **208**
Figure 5.106. $[NH_4][S_2P(R^x)(OR3)]$ ^{13}C-NMR spectrum…… **209**
Figure 5.107. $[NH_4][S_2P(R^x)(OR4)]$ ^{13}C-NMR spectrum…… **210**
Figure 5.108. $[NH_4][S_2P(R^x)(OR5)]$ ^{13}C-NMR spectrum…… **211**
Figure 5.109. $[NH_4][S_2P(R^x)(OR6)]$ ^{13}C-NMR spectrum…… **212**
Figure 5.110. $[NH_4][S_2P(R^x)(OR7)]$ ^{13}C-NMR spectrum…… **213**
Figure 5.111. $[Ni(S_2P(R^x)(OR1))_2]$ ^{13}C-NMR spectrum……. **214**
Figure 5.112. $[Ni(S_2P(R^x)(OR2))_2]$ ^{13}C-NMR spectrum……. **215**
Figure 5.113. $[Ni(S_2P(R^x)(OR3))_2]$ ^{13}C-NMR spectrum……. **216**
Figure 5.114. $[Ni(S_2P(R^x)(OR4))_2]$ ^{13}C-NMR spectrum……. **217**
Figure 5.115. $[Ni(S_2P(R^x)(OR5))_2]$ ^{13}C-NMR spectrum……. **218**
Figure 5.116. $[Ni(S_2P(R^x)(OR6))_2]$ ^{13}C-NMR spectrum……. **219**
Figure 5.117. $[Ni(S_2P(R^x)(OR7))_2]$ ^{13}C-NMR spectrum……. **220**
Figure 5.118. $[NH_4][S_2P(R^x)(OR1)]$ ^{13}C-NMR spectrum…… **223**

Figure 5.119. $[NH_4][S_2P(R^x)(OR2)]$ ^{13}C-NMR spectrum…… **224**
Figure 5.120. $[NH_4][S_2P(R^x)(OR3)]$ ^{13}C-NMR spectrum…… **225**
Figure 5.121. $[NH_4][S_2P(R^x)(OR4)]$ ^{13}C-NMR spectrum…… **226**
Figure 5.122. $[NH_4][S_2P(R^x)(OR5)]$ ^{13}C-NMR spectrum…… **227**
Figure 5.123. $[Ni(S_2P(R^x)(OR1))_2]$ ^{13}C-NMR spectrum……. **228**
Figure 5.124. $[Ni(S_2P(R^x)(OR2))_2]$ ^{13}C-NMR spectrum……. **229**
Figure 5.125. $[Ni(S_2P(R^x)(OR3))_2]$ ^{13}C-NMR spectrum……. **230**
Figure 5.126. $[Ni(S_2P(R^x)(OR4))_2]$ ^{13}C-NMR spectrum……. **231**
Figure 5.127. $[Ni(S_2P(R^x)(OR5))_2]$ ^{13}C-NMR spectrum……. **232**
Figure 5.128. $[NH_4][S_2P(R^y)(OR1)]$ ^{13}C-NMR spectrum…… **235**
Figure 5.129. $[NH_4][S_2P(R^y)(OR2)]$ ^{13}C-NMR spectrum…… **236**
Figure 5.130. $[NH_4][S_2P(R^y)(OR3)]$ ^{13}C-NMR spectrum…… **237**
Figure 5.131. $[NH_4][S_2P(R^y)(OR4)]$ ^{13}C-NMR spectrum…… **238**
Figure 5.132. $[Ni(S_2P(R^y)(OR1))_2]$ ^{13}C-NMR spectrum……. **239**
Figure 5.133. $[Ni(S_2P(R^y)(OR2))_2]$ ^{13}C-NMR spectrum……. **240**
Figure 5.134. $[Ni(S_2P(R^y)(OR3))_2]$ ^{13}C-NMR spectrum……. **241**
Figure 5.135. $[Ni(S_2P(R^y)(OR4))_2]$ ^{13}C-NMR spectrum……. **242**
Figure 5.136. $[NH_4][S_2P(R^x)(OR1)]$ ^{31}P-NMR spectrum…… **244**
Figure 5.137. $[NH_4][S_2P(R^x)(OR2)]$ ^{31}P-NMR spectrum…… **245**
Figure 5.138. $[NH_4][S_2P(R^x)(OR3)]$ ^{31}P-NMR spectrum…… **246**
Figure 5.139. $[NH_4][S_2P(R^x)(OR4)]$ ^{31}P-NMR spectrum…… **247**
Figure 5.140. $[NH_4][S_2P(R^x)(OR5)]$ ^{31}P-NMR spectrum…… **248**
Figure 5.141. $[NH_4][S_2P(R^x)(OR6)]$ ^{31}P-NMR spectrum…… **249**
Figure 5.142. $[NH_4][S_2P(R^x)(OR7)]$ ^{31}P-NMR spectrum…… **250**
Figure 5.143. $[Ni(S_2P(R^x)(OR1))_2]$ ^{31}P-NMR spectrum…….. **251**
Figure 5.144. $[Ni(S_2P(R^x)(OR2))_2]$ ^{31}P-NMR spectrum…….. **252**
Figure 5.145. $[Ni(S_2P(R^x)(OR3))_2]$ ^{31}P-NMR spectrum…….. **523**
Figure 5.146. $[Ni(S_2P(R^x)(OR4))_2]$ ^{31}P-NMR spectrum…….. **254**
Figure 5.147. $[Ni(S_2P(R^x)(OR5))_2]$ ^{31}P-NMR spectrum…….. **255**
Figure 5.148. $[Ni(S_2P(R^x)(OR6))_2]$ ^{31}P-NMR spectrum…….. **256**
Figure 5.149. $[Ni(S_2P(R^x)(OR7))_2]$ ^{31}P-NMR spectrum…….. **257**
Figure 5.150. $[NH_4][S_2P(R^x)(OR1)]$ ^{31}P-NMR spectrum…… **259**

Figure 5.151. $[NH_4][S_2P(R^x)(OR2)]$ ^{31}P-NMR spectrum…… **260**
Figure 5.152. $[NH_4][S_2P(R^x)(OR3)]$ ^{31}P-NMR spectrum…… **261**
Figure 5.153. $[NH_4][S_2P(R^x)(OR4)]$ ^{31}P-NMR spectrum…… **262**
Figure 5.154. $[NH_4][S_2P(R^x)(OR5)]$ ^{31}P-NMR spectrum…… **263**
Figure 5.155. $[Ni(S_2P(R^x)(OR1))_2]$ ^{31}P-NMR spectrum…….. **264**
Figure 5.156. $[Ni(S_2P(R^x)(OR2))_2]$ ^{31}P-NMR spectrum…….. **265**
Figure 5.157. $[Ni(S_2P(R^x)(OR3))_2]$ ^{31}P-NMR spectrum…….. **266**
Figure 5.158. $[Ni(S_2P(R^x)(OR4))_2]$ ^{31}P-NMR spectrum…….. **267**
Figure 5.159. $[Ni(S_2P(R^x)(OR5))_2]$ ^{31}P-NMR spectrum…….. **268**
Figure 5.160. $[NH_4][S_2P(R^y)(OR1)]$ ^{31}P-NMR spectrum…… **270**
Figure 5.161. $[NH_4][S_2P(R^y)(OR2)]$ ^{31}P-NMR spectrum…… **271**
Figure 5.162. $[NH_4][S_2P(R^y)(OR3)]$ ^{31}P-NMR spectrum…… **272**
Figure 5.163. $[NH_4][S_2P(R^y)(OR4)]$ ^{31}P-NMR spectrum…… **273**
Figure 5.164. $[Ni(S_2P(R^y)(OR1))_2]$ ^{31}P-NMR spectrum…….. **274**
Figure 5.165. $[Ni(S_2P(R^y)(OR2))_2]$ ^{31}P-NMR spectrum…….. **275**
Figure 5.166. $[Ni(S_2P(R^y)(OR3))_2]$ ^{31}P-NMR spectrum…….. **276**
Figure 5.167. $[Ni(S_2P(R^y)(OR4))_2]$ ^{31}P-NMR spectrum…….. **277**
Figure 5.168. A) Crystal structure of $[Ni(S_2P(R^x)(OR1))_2]$ with displacement ellipsoids drawn at the 50% probability level. **B)** and **C)** HS of $[Ni(S_2P(R^x)(OR1))_2]$ mapped with d_{norm}, showing the CH···O hydrogen bonding interactions **D)** View of the one-dimensional CH···S hydrogen-bonded chains running along the crystallographic *c*-axis. **E)** The illustration of the 3D supramolecular network showing the honeycomb-like motif…….. **286**
Figure 5.169. A) Representations of the C8-H8A···π_{phenyl} (d(H···π) = 2.65 Å) interactions in $[Ni(S_2P(R^x)(OR1))_2]$. B) The HS shape index exhibits concave curvature, where C-H···π interaction occur……. **287**
Figure 5.170. The resolved 2D fingerprint plots showing the percentage contributions to the total HS area in $[Ni(S_2P(R^x)(OR1))_2]$…… **288**
Figure 5.171. A) Crystal structure of $[Ni(S_2P(R^x)(OR2))_2]$ with displacement ellipsoids drawn at the 50% probability level (symmetry code: i: -x+1, -y+1, -z) **B)** and **C)** HS of $[Ni(S_2P(R^x)(OR2))_2]$ mapped with d_{norm}, showing the CH···O hydrogen bonding interactions **D)** View of the CH···S hydrogen

bonding interactions in the crystal structure **E)** The illustration of the 3D supramolecular network showing 2D hydrogen-bonded layers…… **289**

Figure 5.172. A) Representations of the C8-H8A···π_{phenyl} (d(H···π) = 2.72 Å) interactions in [Ni($S_2P(R^x)(OR2))_2$]. B) The HS shape index exhibits concave curvature, where C-H···π interaction occur…….. **290**

Figure 5.173. The resolved 2D fingerprint plots showing the percentage contributions to the total HS area in [Ni($S_2P(R^x)(OR2))_2$]…… **291**

Figure 5.174. A) Crystal structure of [Ni($S_2P(R^x)(OR3))_2$] with displacement ellipsoids drawn at the 30% probability level (symmetry code: i: -x+1, -y+1, -z) **B)** and **C)** HS of [Ni($S_2P(R^x)(OR3))_2$] mapped with d_{norm}, showing the CH···O hydrogen bonding interactions. **D)** The illustration of the 3D supramolecular network showing the herringbone motif…….. **292**

Figure 5.175. A) Representations of the C10-H10B···π_{phenyl} (d(H···π) = 2.72 Å) interactions in [Ni($S_2P(R^x)(OR3))_2$]. B) The HS shape index exhibits concave curvature, where C-H···π interactions occur……. **293**

Figure 5.176. The resolved 2D fingerprint plots showing the percentage contributions to the total HS area in [Ni($S_2P(R^x)(OR3))_2$]…… **294**

Figure 5.177. A) Crystal structure of [Ni($S_2P(R^x)(OR4))_2$] with displacement ellipsoids drawn at the 50% probability level (symmetry code: i: -x+1, -y+2, -z+1) **B)** and **C)** HS of [Ni($S_2P(R^x)(OR4))_2$] mapped with d_{norm}, showing the CH···O hydrogen bonding interactions. **D)** The 2D layers connected by the short CH···O and CH···C interactions **E)** Representation of 3D supramolecular network……. **295**

Figure 5.178. A) Representations of the π_{phenyl} ···π_{phenyl} ($d_{(H\cdots\pi)}$ = 4.255 Å) interactions in [Ni($S_2P(R^x)(OR4))_2$]. B) The HS shape index exhibits the evidence of the adjacent red and blue triangles on the shape index surface…….. **296**

Figure 5.179. The resolved 2D fingerprint plots showing the percentage contributions to the total HS area in [Ni($S_2P(R^x)(OR4))_2$]…… **297**

Figure 5.180. A) Crystal structure of [Ni($S_2P(R^x)(OR5))_2$] with displacement ellipsoids drawn at the 30% probability level (symmetry code: i: -x+1, -y+1, -z) **B)** and **C)** HS of [Ni($S_2P(R^x)(OR5))_2$] mapped with d_{norm}, showing the CH···O hydrogen bonding interactions. **D)** Illustration of 3D supramolecular

network…… **298**

Figure 5.181. A) Representations of the C11-H11C···π_{phenyl} ($d_{(H\cdots\pi)}$ = 2.73 Å) interactions in [Ni($S_2P(R^x)(OR5))_2$]. B) The HS shape index exhibits concave curvature, where C-H···π interactions occur……. **299**

Figure 5.182. The resolved 2D fingerprint plots showing the percentage contributions to the total HS area in [Ni($S_2P(R^x)(OR5))_2$]…….... **300**

Figure 5.183. A) Crystal structure of [Ni($S_2P(R^x)(OR6))_2$] with displacement ellipsoids drawn at the 30% probability level (symmetry code: i: -x+1, -y+1, -z) **B)** Perspective view of the CH···O hydrogen bonding and the short π ···π interaction **C)** HS of [Ni($S_2P(R^x)(OR6))_2$] mapped with d_{norm}, showing the CH···O hydrogen bonding interactions. **D)** The view of the 3D supramolecular network showing the herringbone motif…….. **301**

Figure 5.184. A) Representations of the π_{phenyl} ···π_{phenyl} ($d_{(\pi\cdots\pi)}$ = 3.838 Å) interactions in [Ni($S_2P(R^x)(OR6))_2$]. B) The HS shape index exhibits the evidence of the adjacent red and blue triangles on the shape index surface…….... **302**

Figure 5.185. The resolved 2D fingerprint plots showing the percentage contributions to the total HS area in [Ni($S_2P(R^x)(OR6))_2$]…… **303**

Figure 5.186. A) Crystal structure of [Ni($S_2P(R^x)(OR7))_2$] with displacement ellipsoids drawn at the 50% probability level (symmetry code: i: -x+1, -y+2, -z+1) **B)** and **C)** Perspective view of the CH···O and CH···S hydrogen bonding interactions **D)** HS of [Ni($S_2P(R^x)(OR7))_2$] mapped with d_{norm}, showing the CH···S hydrogen bonding interactions. **E)** View of the 3D supramolecular network……. **304**

Figure 5.187. A) Representations of the C15-H15···π_{phenyl} ($d_{(H\cdots\pi)}$ = 2.95 Å) interactions in [Ni($S_2P(R^x)(OR7))_2$]. B) The HS shape index exhibits concave curvature, where C-H···π interactions occur…… **305**

Figure 5.188. The resolved 2D fingerprint plots showing the percentage contributions to the total HS area in [Ni($S_2P(R^x)(OR7))_2$]…… **306**

Figure 5.189. A[Ni($S_2P(R^x)(OR1))_2$] crystal structure with displacement ellipsoids drawn at the 25% probability level **B.** The C—H···S hydrogen bonding interactions in the crystal structure view **C.** Hirshfeld surfaces of [Ni($S_2P(R^x)(OR1))_2$] mapped with d_{norm}, showing the C—H···O hydrogen

bonding interactions **D.** The illustration of the 3D supramolecular network showing the herringbone motif. **E.** The π···π interactions between the phenyl rings in [Ni($S_2P(R^x)(OR1))_2$] **F.** [Ni($S_2P(R^x)(OR1))_2$]'s Hirshfeld surfaces mapped with shape index depicting the areas of the π···π interactions……. **316**

Figure 5.190. The resolved 2D fingerprint plots showing the contributions to the overall Hirshfeld surface area in [Ni($S_2P(R^x)(OR1))_2$]…….. **317**

Figure 5.191. A. [Ni($S_2P(R^x)(OR2))_2$] crystal structure with displacement ellipsoids drawn at the 30% probability level **B.** View of the C—H···O hydrogen bonding interactions in the crystal structure **C.** [Ni($S_2P(R^x)(OR2))_2$] Hirshfeld surfaces mapped with d_{norm}, showing the C—H···O hydrogen bonding interactions **D.** The view of the 2D supramolecular network with the herringbone motif. **E.** The CH···π interaction in [Ni($S_2P(R^x)(OR2))_2$] **F.** [Ni($S_2P(R^x)(OR2))_2$] Hirshfeld surfaces mapped with shape index representing the areas of the CH···π interaction…… **318**

Figure 5.192. The resolved 2D fingerprint plots showing the contributions to the overall Hirshfeld surface area in [Ni($S_2P(R^x)(OR2))_2$]…… **319**

Figure 5.193. A. Crystal structure of [Ni($S_2P(R^x)(OR4))_2$] with displacement ellipsoids drawn at the 30% probability level **B.** View of the C—H···O hydrogen bonding interactions **C.** Hirshfeld surfaces of [Ni($S_2P(R^x)(OR4))_2$] mapped with d_{norm}, showing the C—H···O hydrogen bonding interactions **D.** The view of the 3D supramolecular network of crystal structure of [Ni($S_2P(R^x)(OR4))_2$]. **E.** The CH···π interaction in [Ni($S_2P(R^x)(OR4))_2$] **F.** Hirshfeld surfaces of [Ni($S_2P(R^x)(OR4))_2$] mapped with shape index showing the areas of the CH···π interaction……. **320**

Figure 5.194. The resolved 2D fingerprint plots showing the contributions to the overall Hirshfeld surface area in [Ni($S_2P(R^x)(OR4))_2$]…… **321**

Figure 5.195. A. Crystal structure of [Ni($S_2P(R^x)(OR5))_2$] with displacement ellipsoids drawn at the 30% probability level **B.** View of the C—H···O hydrogen bonding interactions **C.** Hirshfeld surfaces of [Ni($S_2P(R^x)(OR5))_2$] mapped with d_{norm}, showing the C—H···O hydrogen bonding interactions **D.** The view of the 3D supramolecular network of crystal structure of [Ni($S_2P(R^x)(OR5))_2$]. **E.** The CH···π interaction in [Ni($S_2P(R^x)(OR5))_2$] **F.**

Hirshfeld surfaces of [Ni($S_2P(R^x)(OR5))_2$] mapped with shape index showing the areas of the CH···π interaction…….. **322**

Figure 5.196. The resolved 2D fingerprint plots showing the contributions to the overall Hirshfeld surface area in [Ni($S_2P(R^x)(OR5))_2$]…… **323**

Figure 5.197. A. A view of the structure of [Ni($S_2P(R^y)(OR2))_2$], showing the atom-labeling scheme. Displacement ellipsoids are drawn at the 50% probability level. Symmetry code: (a) 2 −x , 1 −y , 2 –z. **B.** HS of [Ni($S_2P(R^y)(OR2))_2$] mapped with d norm , showing the C —H ···O (red dotted lines) and C —H ···S (green dotted lines) hydrogen bonding interactions. **C.** Perspective view of the 2D constructed from the C —H ···O hydrogen bonds. **D.** The 1D chains constructed from the hydrogen bonding rings with R2,2(18)-graph-set notation…….…… **327**

Figure 5.198. A. The resolved 2D fingerprint plots showing the percentage contributions to the total HS area. **B.** HS mapped with shape index (left) and curvedness (right) of [Ni($S_2P(R^y)(OR2))_2$]. The HS shape index exhibits concave curvature, where C —H ···πinteraction occurs…….. **328**

Figure 5.199. The optimized structures (**A**), HOMO and LUMO surfaces electron density and band gap values (eV) (**B**) of the Ni(II) complexes…….. **333**

Figure 5.200 A. The optimized structures of the complexes by DFT with B3LYP/LANL2DZ level. **B.** Superimposition of the DFT-optimized (dark blue) and X-ray (yellow) structures of the complexes…… **335**

Figure 5.201. The band gap levels and isosurfaces of HOMOs and LUMOs for the complexes [Ni($S_2P(R^x)(OR1))_2$], [Ni($S_2P(R^x)(OR2))_2$], [Ni($S_2P(R^x)(OR4))_2$] and [Ni($S_2P(R^x)(OR5))_2$]…… **338**

Figure 5.202. The optimized structures of the complex [Ni($S_2P(R^y)(OR2))_2$] by DFT…….. **340**

Figure 5.203. HOMO and LUMO electron density isosurfaces and band gap values (eV) of the complex [Ni($S_2P(R^y)(OR2))_2$]……. **342**

Figure 5.204. Molecular electrostatic potential (MEP) surfaces of the Ni(II) complexes……. **343**

Figure 5.205. [Ni($S_2P(R^x)(OR1))_2$], [Ni($S_2P(R^x)(OR2))_2$], [Ni($S_2P(R^x)(OR4))_2$]

and [Ni($S_2P(R^x)(OR5))_2$]'s MEP surfaces…… **345**
Figure 5.206. Molecular electrostatic potential (MEP) surfaces for the complex [Ni($S_2P(R^y)(OR2))_2$]……. **346**
Figure 5.207. Energetically most favorable docked poses obtained from the rigid molecular docking of each complex with 3WZE and 2HQ6 (**A**) and the non-covalent interactions of the Ni(II) complexes (**B**)……. **354**
Figure 208 A. The docked poses obtained from the rigid molecular docking [Ni($S_2P(R^x)(OR1))_2$], [Ni($S_2P(R^x)(OR2))_2$], [Ni($S_2P(R^x)(OR4))_2$] and [Ni($S_2P(R^x)(OR5))_2$] with 2HQ6 and 3WZE. **B.** non-covalent interactions with 2HQ6 and 3WZE…….. **361**
Figure 5.209. Energetically most favorable docked poses were obtained from the rigid molecular docking of [Ni($S_2P(R^y)(OR2))_2$] with 3WZE and 2HQ6…… **363**
Figure 5.210. The non-covalent interactions of [Ni($S_2P(R^y)(OR2))_2$] with 3WZE and 2HQ6…….. **364**
Figure 5.211. Dose-dependent antiproliferative effect of compounds and *cis*-platin on HepG2 cells for 48 h…….. **367**
Figure 5.212. Dose-dependent antiproliferative effect of compounds and *cis*-platin on DLD-1 cells for 48 h…….. **367**
Figure 5.213. Anticancer effect of compounds on cancer cells…… **370**
Figure 5.214. Antiproliferative effect of compounds on DLD-1 cells……. **373**
Figure 5.215. Antiproliferative effect of compounds on HepG2 cells……. **373**
Figure 6.1. The article published within the scope of the thesis 1…… **378**
Figure 6.2. The article published within the scope of the thesis 2…… **378**
Figure 6.3. The international congress 1 within the scope of the thesis…… **380**
Figure 6.4. The international congress 2 within the scope of the thesis…… **381**
Figure 6.5. National congress 1 within the scope of the thesis……..…… **382**
Figure 6.6. National congress 2 within the scope of the thesis……..… **383**

LIST OF TABLES

Table 2.1. Chemical shift values of DTDP isomers (in $CDCl_3$) synthesised by reaction of phosphines with sulphur……..... **13**

Table 2.2. ^{31}P chemical shift values of some DTDPs (σ_{iso}= ^{31}P isotropic chemical shift of the solid; recrystallized from a. benzene b.tetrachloromethane)…….. **15**

Table 2.3. DTDPs are synthesised according to Method 5……. **23**

Table 2.4. General synthesis reaction of DTDPs according to method 6……. **24**

Table 2.5. DTDPs synthesized in accordance with method 7…….. **29**

Table 2.6. Synthesis and reaction parameters of $[M\text{-}S\text{-}P(S)S]_2$……... **31**

Table 2.7. Starting reagent and alcohols used in the synthesis of DTPOAs…… **33**

Table 2.8. Synthesis of DTPOA from DTDP and alcoholates…… **34**

Table 2.9. List of ringed heterocyclic DTPOA derivatives……. **35**

Table 2.10. List of compounds containing a ringed disubstituted functional group……... **42**

Table 2.11. Ringed disubstituted functional groups…… **43**

Table 3.1. List of chemicals and solvents…… **56**

Table 5.1. Selected IR data (cm^{-1}) assignment of vibrational bands of the compounds for Part Ia……. **72**

Table 5.2. Part Ib Selected IR data (cm^{-1}) assignment of vibrational bands for the compounds…… **96**

Table 5.3. IR data (cm^{-1}) assignment of vibrational bands of the compounds for Part II…….. **112**

Table 5.4. Part Ia ^1H-NMR data of $[NH_4][S_2P(R^x)(ORn)]$, (D_2O; δ in ppm, *J* in Hz, s: *singlet*, d: *doublet*, dd: *doublet of doublets*, t: *triplet*, and m: *multiplet*)….. **164**

Table 5.5. Part Ia ^1H-NMR data of $[Ni(S_2P(R^x)(ORn))_2]$, ($CDCl_3$; δ in ppm, *J* in Hz, s: *singlet*, d: *doublet*, dd: *doublet of doublets*, t: *triplet*, and m: *multiplet*)….. **165**

Table 5.6. ^1H-NMR data of $[NH_4][S_2P(R^x)(ORn)]$ (D_2O) and $[Ni(S_2P(R^x)(ORn))_2]$ for Part Ib ($CDCl_3$) (δ in ppm, *J* in Hz, s: *singlet*, d: *doublet*, dd: *doublet of doublets*, t: *triplet*, and m: *multiplet*)…… **182**

Table 5.7. ^1H-NMR data of the compounds . (D_2O for $[NH_4][S_2P(R^y)(ORn)]$, $CDCl_3$ for $[Ni(S_2P(R^y)(ORn))_2]$; δ in ppm, *J* in Hz, s: *singlet*, d: *doublet*, dd:

doublet of doublets, t: *triplet*, and m: *multiplet*)……. **195**

Table 5.8 ^{13}C-NMR data of Part [NH_4][$S_2P(R^x)(ORn)$] ligands (D_2O; δ in ppm, *J* in Hz)…… **205**

Table 5.9. ^{13}C-NMR data of Part Ia [$Ni(S_2P(R^x)(ORn))_2$] complexes ($CDCl_3$; δ in ppm, *J* in Hz)……... **206**

Table 5.10. Part Ib ^{13}C-NMR data of [NH_4][$S_2P(R^x)(ORn)$] (D_2O) and [$Ni(S_2P(R^x)(ORn))_2$] ($CDCl_3$) (δ in ppm, *J* in Hz)…….. **222**

Table 5.11 ^{13}C-NMR data of the compounds. (D_2O for [NH_4][$S_2P(R^y)(ORn)$], $CDCl_3$ for [$Ni(S_2P(R^y)(ORn))_2$]; δ in ppm, *J* in Hz)…….. **234**

Table 5.12. ^{31}P-NMR data of the compounds……. **243**

Table 5.13. ^{31}P-NMR data of the compounds…… **258**

Table 5.14. ^{31}P-NMR data of the compounds…… **269**

Table 5.15. Crystal data and refinement parameters for Part Ia' [$Ni(S_2P(R^x)(ORn))_2$] (n=1-7) complexes…… **279**

Table 5.16. The intermolecular C-H···X (X= O, S, π) interactions (Å and °) for the complexes……. **282**

Table 5.17. Crystal data and refinement details for [$Ni(S_2P(R^x)(ORn))_2$] (n=1,2,4,5)…….. **283**

Table 5.18. Selected experimental and calculated at B3LYP/LANL2DZ level bond lengths (Å), bond angles (°) and torsion angles for [$Ni(S_2P(R^x)(OR1))_2$], [$Ni(S_2P(R^x)(OR2))_2$], [$Ni(S_2P(R^x)(OR4))_2$] and [$Ni(S_2P(R^x)(OR5))_2$]……... **312**

Table 5.19. The intermolecular C—H···X (X= O, S) interactions (Å and °) for the complexes……. **315**

Table 5.20. Crystal data and structure refinement details for [$Ni(S_2P(R^y)(OR2))_2$]…….. **324**

Table 5.21. The intermolecular C—H···X (X= O, S, π) interactions (Å and °) for [$Ni(S_2P(R^y)(OR2))_2$]……... **326**

Table 5.22. Selected experimental and calculated bond lengths (Å) and bond angles (°) for Ni(II) complexes…… **330**

Table 5.23. Calculated total energies, dipole moments and chemical parameters of the complexes……. **332**

Table 5.24 Calculated total energies, dipole moments and chemical parameters **337**

of the complexes.

Table 5.25. Selected experimental and calculated [B3LYP/LANL2DZ/6-31+G(d,p) level in the ground state] bond lengths (Å), bond angles (°) and torsion angles for [Ni($S_2P(R^y)(OR2))_2$]…….. **338**

Table 5.26. Calculated total energies, dipole moments and chemical parameters of the compounds [Ni($S_2P(R^y)(OR2))_2$]…….. **341**

Table 5.27. The RMSD values and bonding energies as outcome of MD for [Ni($S_2P(R^x)(OR1))_2$], [Ni($S_2P(R^x)(OR2))_2$], [Ni($S_2P(R^x)(OR4))_2$] and [Ni($S_2P(R^x)(OR5))_2$] by using AutoDock-Vina software…… **356**

Table. 5.28. The predicted bonding energies and RMSD values as a consequence of molecular docking for [Ni($S_2P(R^y)(OR2))_2$] by using AutoDock-Vina software…….. **362**

Table 5.29. IC_{50} results for compounds against cancer cell lines…….. **365**

Table 5.30. IC_{50} results for [NH_4][$S_2P(R^x)(ORn)$] and [Ni($S_2P(R^x)(ORn))_2$] against cancer cell lines…….. **368**

Table 5.31.IC_{50} results for the compounds against cancer cell lines…….. **372**

1. INTRODUCTION

Long after the discovery of the phosphorus element in 1669, Köhler synthesized phenylmonothiophosphonic acid in 1877 and introduced the first organothiophosphorus compound to the literature [1]. However, at the beginning of the 20th century, no progress could be made in this field for many years due to the difficulties in the supply of the starting materials required for the synthesis of organo-dithiophosphorus compounds, the insufficient purity of the chemicals, the infrastructure problems in the creation of reaction conditions, the by-products formed during the synthesis of the target substance and the toxic and bad odours released with it. In 1947, just after World War II, Malatesta showed that different types of organo-dithiophosphorus acids could be synthesized, albeit in low yields, by reacting the compound P_4S_{10} with Grignard reagents [2]. In the following years, studies on these substances gained impetus with the realization of their importance especially in the industrial field as emphasised in the latter sentences. Namely, Organodithiophosphorus compounds find practical uses in, for example, agriculture as insecticides, pesticides [3, 4], industry as antioxidant-additives for lubricants [5] and medicine as potential antibiotics, antimicrobial or possible anticancer agents [6-11].

These type compounds are also used in industry as a solvent-extraction reagents for metals [12], flotation agents for mineral ores [13, 14] as well as antioxidant-additives for lubricants [5].

It is a fact that the ever-increasing energy need in the world and our country could not be provided from fossil fuels and hydroelectric sources. Nuclear power plants are one of the alternative energy needs in supplying the energy needs required in the industrialization process of our country. In recent years, the rate of meeting Turkey's energy demand through imports has reached 75%. Turkey's rapid industrialization, especially in recent years, and its population reaching 85 million have increased the country's energy demand and led to the need to meet this demand from an alternative energy source. Although Turkey has attempted to establish a nuclear power plant several times (in 1969, 1977, 1985 and 1995) to realize its policies towards nuclear energy, these attempts have failed for different reasons. In order to reduce Turkey's dependence on foreign energy and to diversify its energy sources, the construction of two nuclear power plants in Akkuyu and Sinop in Gülnar, Mersin. It is a certain fact that Turkey will obtain a large amount of

energy from these plants when they are commissioned in the very near future. Considering the energy production process of nuclear power plants, they are more environmentally friendly in terms of greenhouse gas emissions compared to fossil fuels. As a result of the small amount of waste from nuclear power plants compared to others, they can be stored safely [15]. However, it is obvious that in the coming years these wastes will pose a problem in terms of accumulation and inability to completely eliminate them. In the face of this situation, scientists have already turned to some alternative solutions. Consequently, scientists have already turned to some alternative approaches [16, 17].

Due to the sulfur atoms in their structure, Organo-dithiophosphorus compounds can complex with most metals in the periodic system including radioactive lanthanide and actinide elements. Because of these properties, these compounds find applications in medicine or nuclear chemistry. For example, some of these complexes are used in medical imaging devices [18]. They compounds are promising in eliminating the harmful effects of heavy metals in wastewater solutions used in industry [19]. It is also a good alternative for qualitative or quantitative separation and purification of radioactive metals formed in nuclear reactors by extraction method at a certain pH [20-24]. A research conducted in this context are briefly described and pictured in Figure 1.1. In that picture simply represents the steps of a supercritical extraction system. Each part of is represents as follow: (1) CO_2 cylinder, (2) column consisting of molecular sieve and silica gel, (3) chiller, (4) pump head cooler, (5) HPLC pump, (6) needle valve, (7) spring coil preheater, (8) modifier vessel, (9) spring coil preheater, (10) waste vessel, (11) oven, (12) needle valve, (13) Back Pressure Regulator (BPR) valve, (14) extracted sample collection vessel.

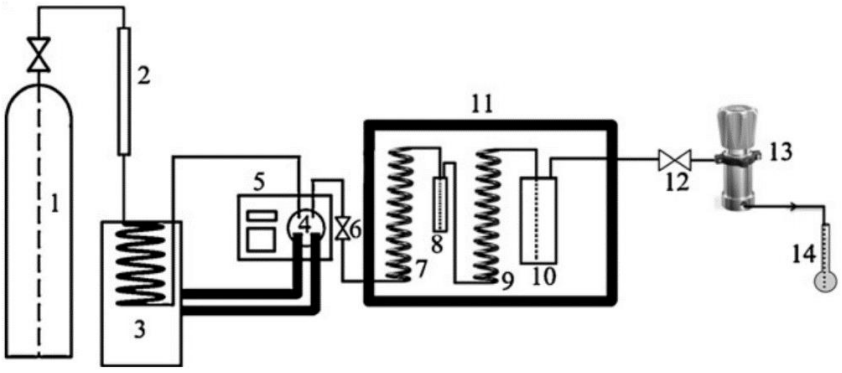
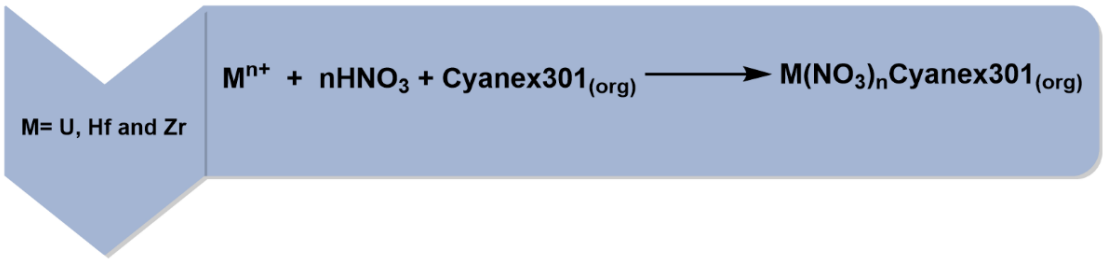


Figure 1.1. Experimental setup for the supercritical extraction system.

To increase the purity of the CO_2, which is stored in a CO_2 cylinder (1), it is passed through a column of molecular sieve beads and a silica gel filter (2). Then, CO_2 is cooled down in a chiller and pump head cooler (3, 4) in the range of −5 to 0°C. Then liquified CO_2 is charged by a feed pump (5) through the needle valve (6) and is fed to the oven (11). Two vessels (modifier storage column and extraction column) are placed in the oven. The first one (8) is filled with methanol as the modifier; the aqueous radioactive waste which is mixed with the chelating agent by a magnetic stirrer is charged to the second column (10). CO_2 is preheated using a spring coil preheater (7) before entering the modifier vessel (8) which is inside the oven. Then CO_2 first is charged into the first vessel (8) and saturated with methanol. Then itis preheated using a spring coil preheater (9) before entering the extraction column (10). Subsequently, modified SC-CO_2 is passed through the second vessel and carried out the extraction of toxic heavy metal ions which are chelated by Cyanex 301 according to the following overall reaction as below:



The chelating ligand used in this study [25], which involved the extraction of toxic heavy metals such as uranium (U), hafnium (Hf) and zirconium (Zr) from a synthetic radioactive wastewater sample using supercritical carbon dioxide (SC-CO2) and a chelating agent, is an organo-dithiophosphorus class compound, *bis*(2,4,4-trimethylpentyl) dithiophosphinic acid, known as Cyanex 301, which is commercially available.

To summarise within the scope of this information; the compounds synthesised in this thesis are similar to the structure of the compound CYANEX 301 mentioned above (Figure 1.2).

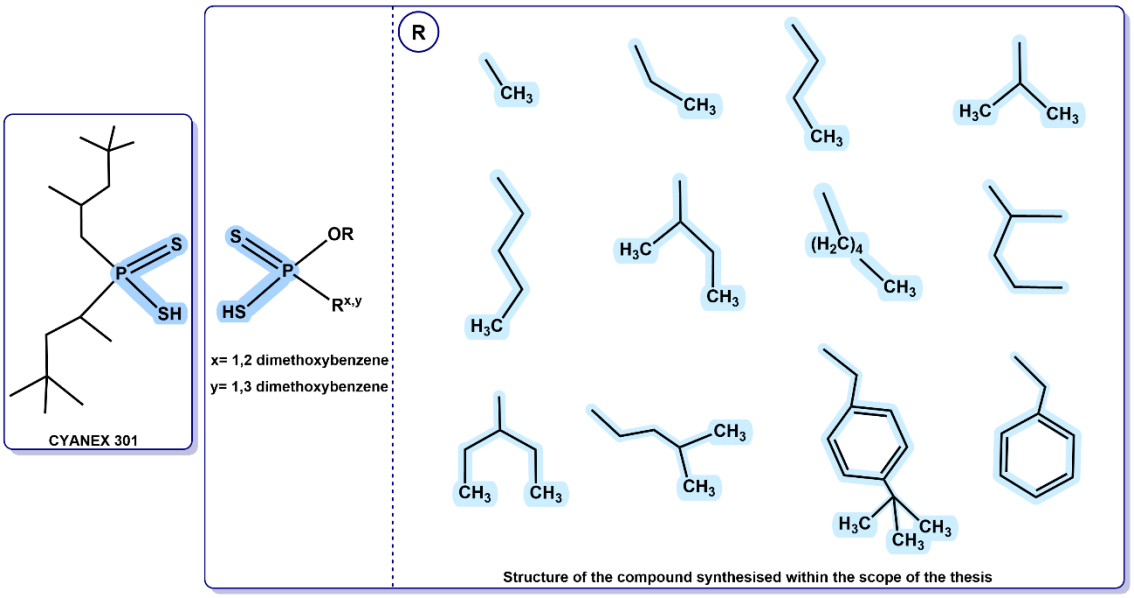


Figure 1.2. Comparison of CYANEX 301 with the compounds synthesized within the scope of the thesis.

It could be said that the compounds synthesised in this thesis have an effect such as CYANEX 301 or better than this compound in the disposal of wastes released over time in nuclear power plants established in our country to meet the energy needs. Despite the difficulties encountered in the synthesis process of this study, such as the difficulties in obtaining the starting material, the COVID-19 process and despite the challenge of organising a laboratory researching infrastructure, in the production of electricity from nuclear reactors, we expect that it will contribute, however indirectly, to the disposal of the wastes released to provide the energy of our country.

There are also studies on the antimicrobial effect of organo-dithiophosphorus compounds. S-tributylstannyl dithiophosphates and dithiophosphonates were prepared and the bactericidal activity of *S*-tributylstannyl dithiophosphates was tested on *Staphylococcus aureus* (ATCC 29213), *Escherichia coli* (ATCC 25922), and *Bacillus cereus* [26]. These compounds tested had more activity towards B. cereus than control Nika-Politsid (10 mm) and Slayt (12 mm) with growth inhibition zone of 23-24 mm. In a different study. In a different study, some Ni(II) complexes of dithiophosphonic acids were synthesized and their biological activities were tested against *Pseudomonas aeruginosa* (ATCC 27853), *Escherichia coli* (ATCC 25922), and *Acinetobacter baumannii* (ATCC 19606) using disk diffusion method [27]. The results demonstrated that the most sensitive

bacterial strains on the compounds tested were gram-negative bacteria, *A. Baumannii*, *E. coli*, and *P. aeruginosa*. Dithiophosphonates and amidodithiophosphonates compounds were synthesized [28], and screened against seven gram-positive bacteria, seven gram-negative bacteria, and three different *Methicillin-Resistant Staphylococcus aureus* (*MRSA*) strains. The results showed that a compound had potent *anti-MRSA* activity.

The anticancer effects of these compounds have started to be investigated in recent years. Especially, there are few published studies on the cytotoxic activities of dithiophoshorus compounds, let alone on the dithiophosphinic acid [29] and dithiophosphonic acid [30-32] compounds. In contrast, antiproliferative activity studies on dithiophosphoric acid compounds appear to be more frequent [33]. For example, a study by Lowe et al. showed that Pt(II)-dithiophosphoric acid complexes have cytotoxic activity [34]. In another study by Kumar et al., it is reported that some vanadium-based dithiophosphate complexes were active against lung, prostate and leukemia cancers [35]. These studies obviously need some supporting research to arrive at a more conclusive idea about the anticancer activity of dithiophoshorus derivatives as a whole. So, this thesis is also expected to be one of the pioneering studies in anticancer pharmaceutical research in the future by investigating the effects of new DTPOA ligands and complexes on cancer activity.

Such research conducted not only with this thesis, but also with previously conducted researches, ongoing researches, and also with further researches, has a vision in terms of contributing to the education of scientists in this field in our country.

Within the scope of the thesis, new 2,4-*bis*(3,4-dimethoxyphenyl)-1,3,2,4-dithiadiphosphetane-2,4-disulfide, (SAV-A1, $[R^x\text{-}P(S)S]_2$) and 2,4-*bis*(2,4-dimethoxyphenyl)-1,3,2,4-dithiadiphosphetane-2,4-disulfide, (SAV-A2, $[R^y\text{-}P(S)S]_2$), were obtained from the reaction of P_4S_{10} with 1,2-dimethoxybenzene and 1,3-dimethoxybenzene, respectively. We also synthesized 16 new dithiophosphonic acids (DTPOA) from the interaction of these two compounds with various structures alcohols $[R^{x,y}(RnO)P(S)SH]$. Twelve crude acids ($[R^x(RnO)P(S)SH]$) were produced from the reaction of SAV1 with alcohols (RnOH= alcohols used in DTPOA synthesis reactions for Part Ia, R1=methyl-, R2=ethyl-, R3=n-propyl-, R4=n-butyl-, R5=3-pentyl-, R6=3-methyl-1-butyl-, R7=benzyl-; RnOH= alcohols as used in DTPOA synthesis reactions for Part Ib, RnOH, R1= n-pentyl-; R2=2-pentyl-; R3=4-tert-but-benzyl-; R4=2-propyl-;

R5=2-butyl-). Analogously, other acids coded as [R^y(RnO)P(S)SH] were also obtained from the reaction of SAV2 with alcohols (RnOH = alcohols used in Part II for DTPOAs, R1= 2-butyl; R2= n-pentyl-; R3= 4-tert-butyl benzyl-; R4= methyl-). These foul-smelling and oily acids, whose structures could not be directly determined, were converted to their ammonium dithiophosphonates, with dry ammonia gas, ([NH_4][$S_2P(R^{x,y})$(ORn)]). Original square planar Ni(II) dithiophosphonato complexes of these salts with nickel(II) ion were synthesized, ([Ni($S_2P(R^{x,y})$(ORn)]).

The structures and codes of the dithiophosphonic acids, ammonium dithiophosphonate salts and Ni(II) dithiophosphonato complexes are pictured in Figure 1.3-Figure 1.6 for the thesis:

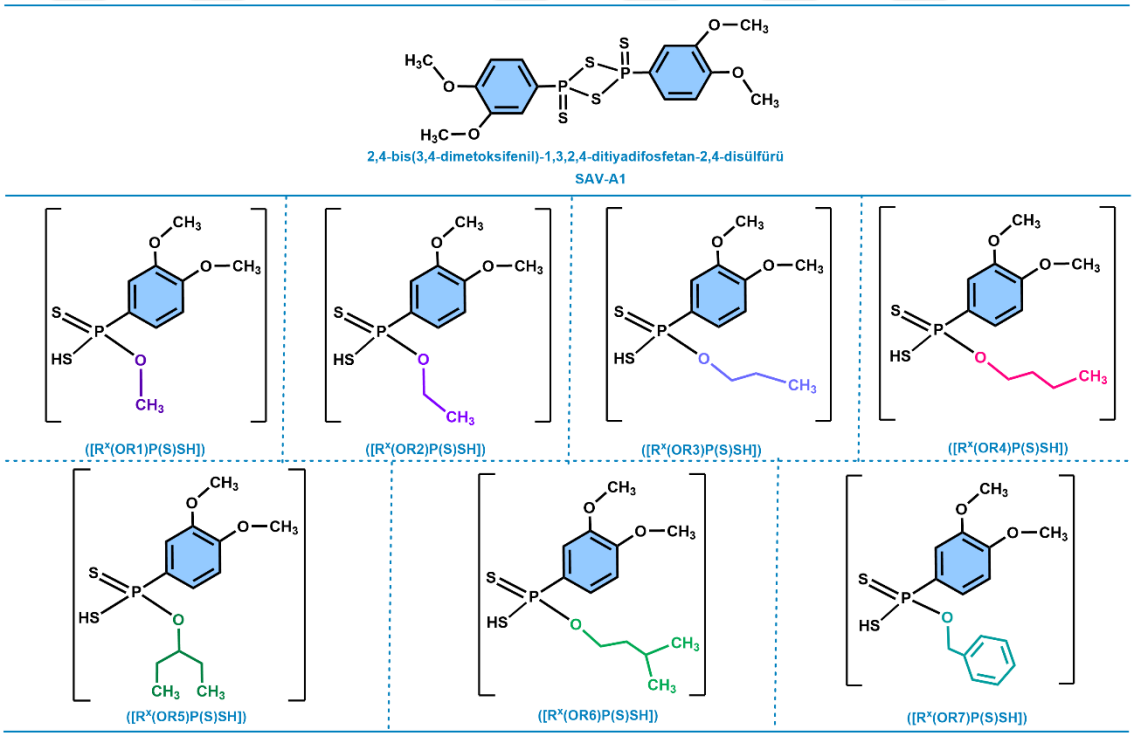


Figure 1.3.a. Structures of DTPOA structures ([R^x(ORn)P(S)SH]) synthesized from the newly synthesized starting material ([R^x-P(S)S]$_2$) within the scope of the thesis,(**Part Ia**).

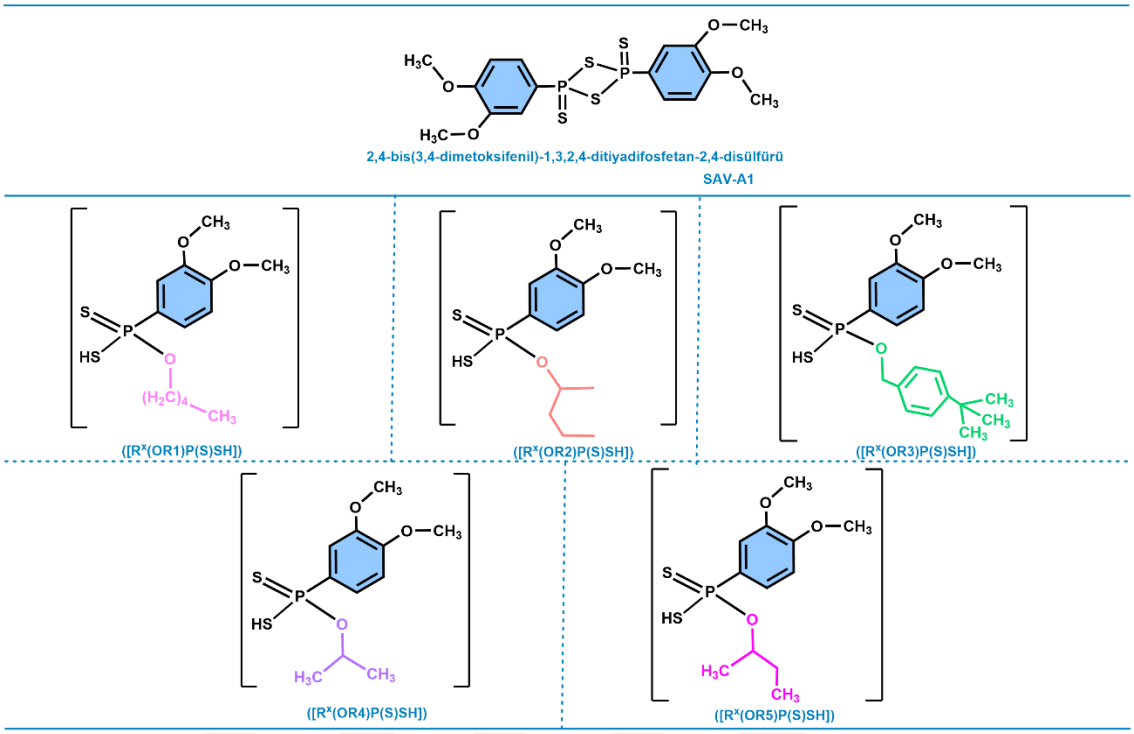


Figure 1.3.b. Structures of DTPOA structures ([R^X(ORn)P(S)SH]) synthesized from the newly synthesized starting material ([R^X-P(S)S]$_2$) within the scope of the thesis,(**Part Ib**).

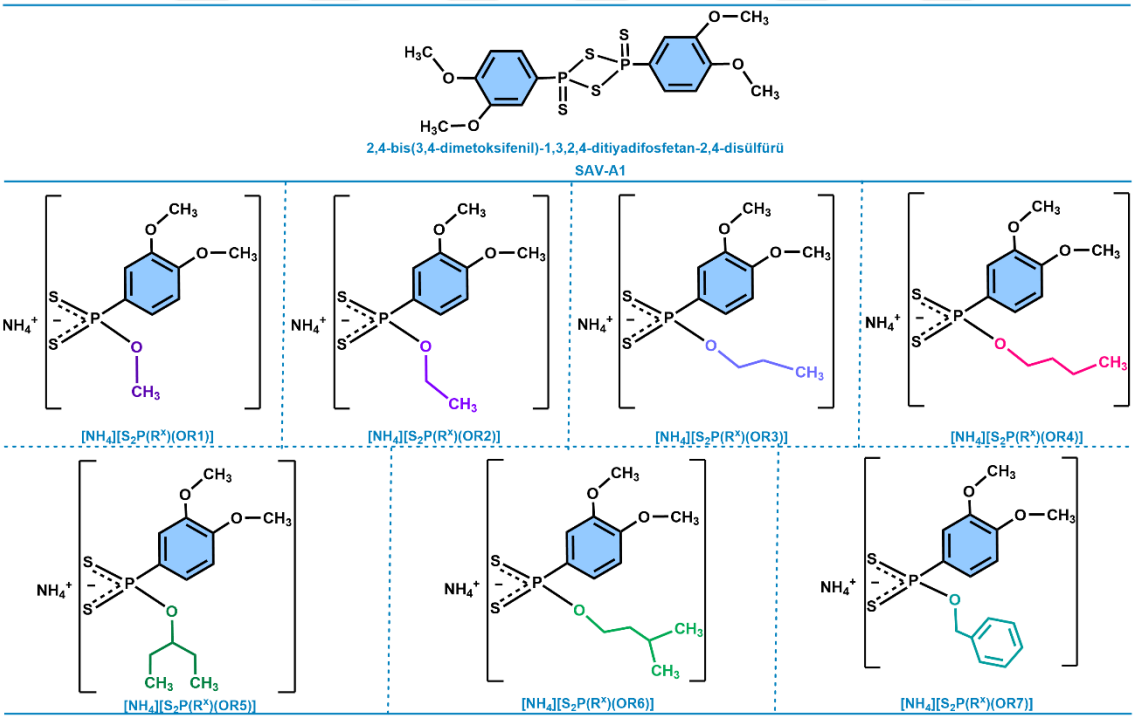


Figure 1.4.a. Structures of ammonium dithiophosphonate salts ([NH_4][$S_2P(R^X)$(ORn)]) synthesized from DTPOAs within the scope of the thesis, (**Part Ia**).

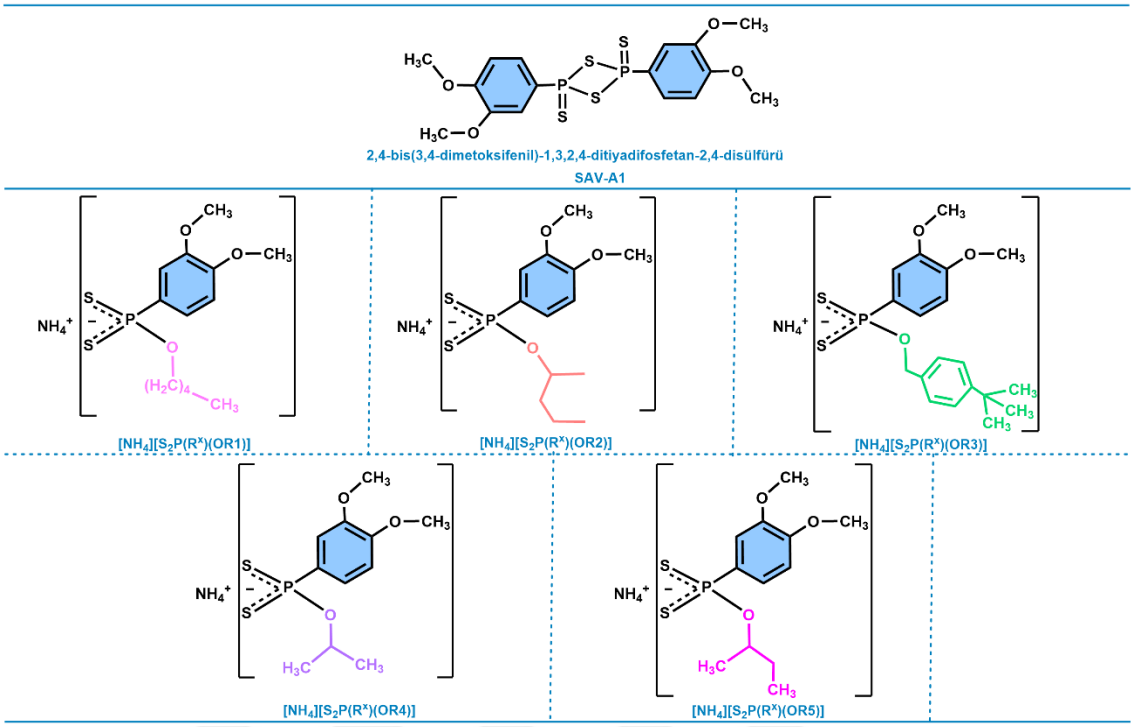


Figure 1.4.b. Structures of ammonium dithiophosphonate salts ($[NH_4][S_2P(R^X)(ORn)]$) synthesized from DTPOAs within the scope of the thesis, (**Part Ib**).

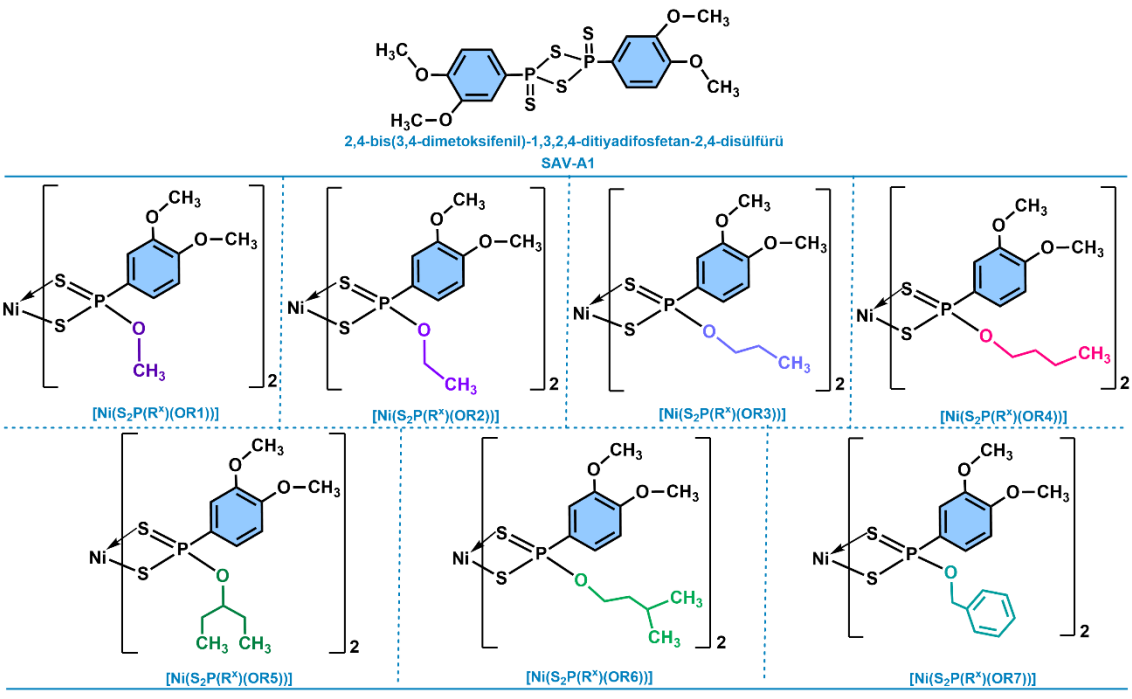


Figure 1.5.a. Structures of Ni(II)-DTPOA complexes ($[Ni(S_2P(R^X)(ORn)])$ synthesized from $[NH_4][S_2P(R^X)(ORn)]$ within the scope of the thesis, (**Part Ia**).

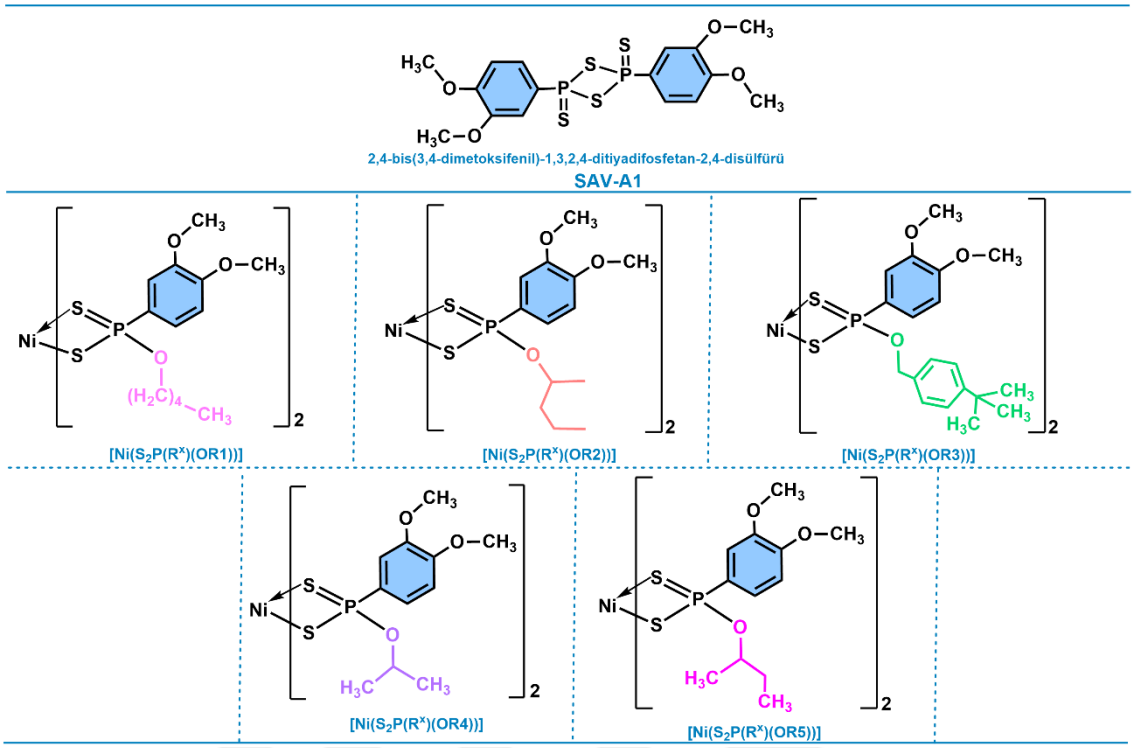


Figure 1.5.b. Structures of Ni(II)-DTPOA complexes ([Ni($S_2P(R^x)(ORn)$]) synthesized from [NH_4][$S_2P(R^x)(ORn)$] within the scope of the thesis, (**Part Ib**).

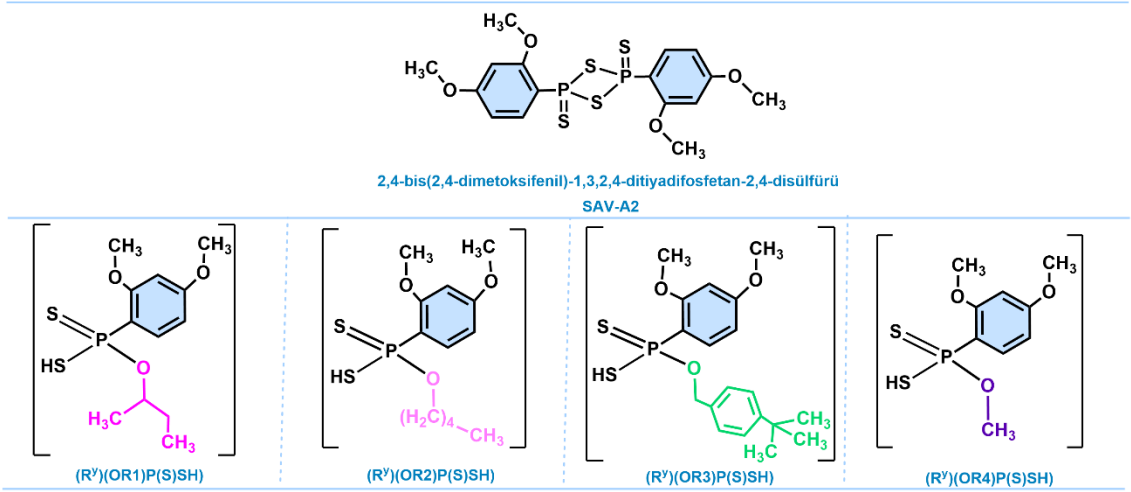


Figure 1.6.a. Structures of DTPOA structures ([R^y(ORn)P(S)SH]) synthesized from the newly synthesized starting material ([R^y-P(S)S]$_2$) within the scope of the thesis,(**Part II**).

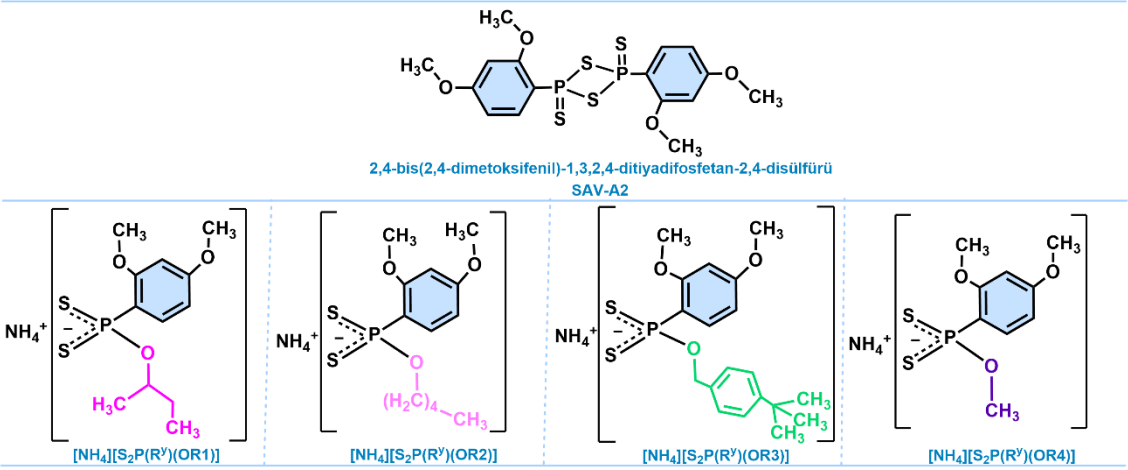


Figure 1.6.b. Structures of ammonium dithiophosphonate salts ([NH_4][$S_2P(R^y)(ORn)$]) synthesized from DTPOAs within the scope of the thesis, (**Part II**).

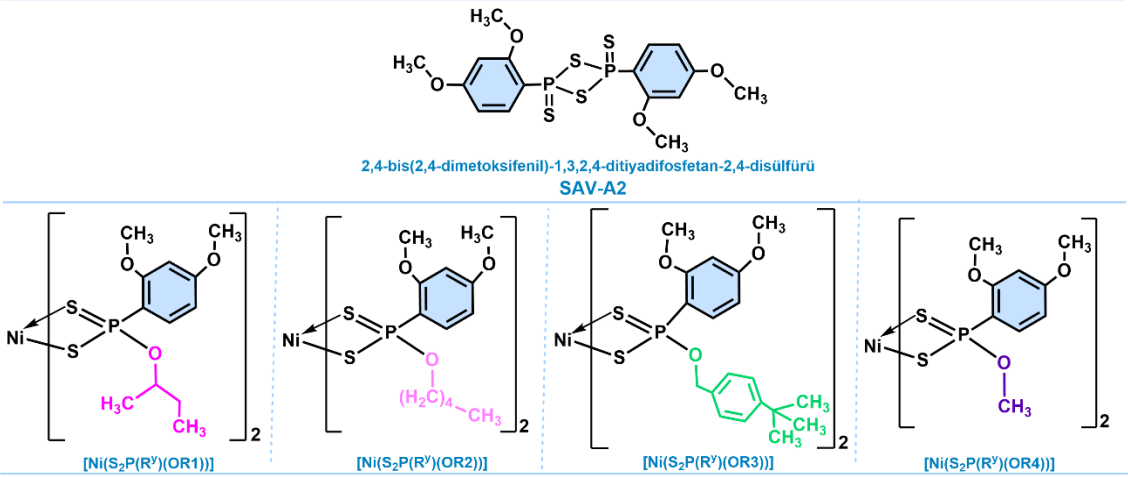


Figure 1.6.c. Structures of Ni(II)-DTPOA complexes ([$Ni(S_2P(R^y)(ORn)]$]) synthesized from [NH_4][$S_2P(R^y)(ORn)$] within the scope of the thesis, (**Part II**).

2. 1,3,2,4-DITHIADIPHOSPHETANE-2,4-DISULFIDES

2.1. 1,3,2,4-dithiadiphosphetane-2,4-disulfides Synthesis Methods

One of the nine simple objects known in antiquity was the element sulfur. It was theorized as an element by Lavoisier in 1777, but in 1810 the theory was confirmed experimentally by Gay Lussac and Thenard. On the other hand, while searching for the "Philosopher's Stone", a substance believed to transform base metals into gold, Hennig Brand accidentally discovered the Greek element phosphorus, "Light-Bearing" (1669).

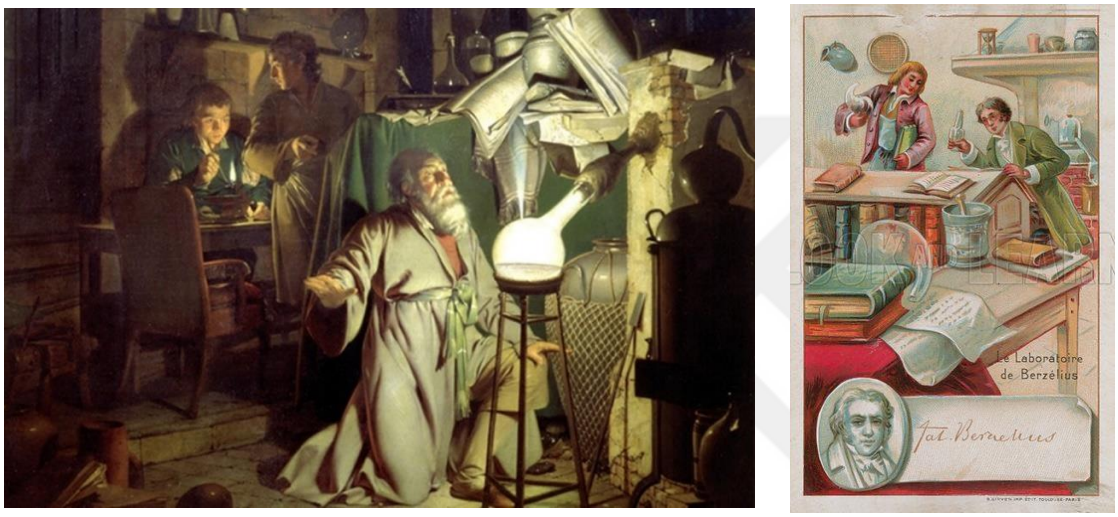


Figure 2.1. Illustration of the discovery of phosphorus (left) and the Berzelius reagent.

The reaction of phosphorus with sulphur atoms was known about 300 years ago. In fact, although it is assumed that this reaction was known before that, there was no evidence of such research. The first recorded research begins with the synthesis of phosphorpentasulphide as formulated P_4S_{10} in 1843 by the famous Swedish chemist Jöns Jacob Berzelius (1779-1848), which he named as Berzelius reagent after the reaction of white phosphorus and sulphur. This reagent was also obtained by the reaction of elemental sulphur or pyrite (FeS_2) with ferrophosphorus (Fe_2P), a by-product of the production of white phosphorus from phosphate rock [36, 37]. Berzelius reagent has been used in organic [37] and inorganic chemistry in synthesis reactions for many years since its discovery [38]. This compound is also important as a starting material in the synthesis of Organo-dithiophosphorus compounds. For instance, dithiophosphoric acids are obtained by direct interaction of Berzelius reagent with a nucleophile [39, 40], while 1,3,2,4-dithiadiphosphatene-2,4-disulfides (DTDP) are obtained when interacted with

aromatic or aliphatic reagents (Figure 2.2, [41]). DTDPs are also known as Perthiophosphonic Acid Anhydrides, Thionophosphindisulfide or Dimers and formulated as $[R\text{-}P(S)S]_2$.

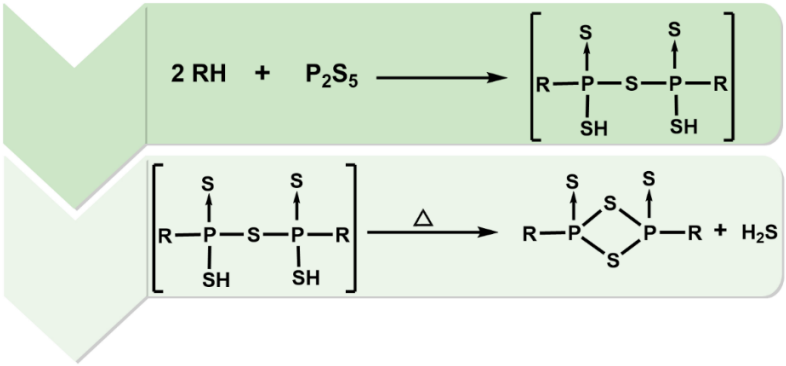


Figure 2.2. One synthesis reaction of DTDP, (R= H, aliphatic or aromatic group).

2.1.1. DTDP Resonance Structures

In the first suggested scientific studies on the structure of dimeric DTDP together with its synthesis, it is in the form of a ringed covalent structure (ring covalent I) in the solid state [42, 43] or a bimolecular dipolar structure (dipolar structure II) in the solution [42, 44], (Figure 2.3). In the following times, the existence of both theoretically hypothesized structures was confirm by spectroscopic studies.

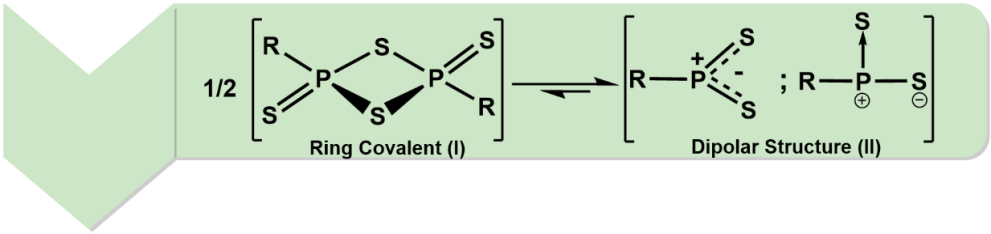


Figure 2.3. Resonance representation of ringed covalent and dipolar structures.

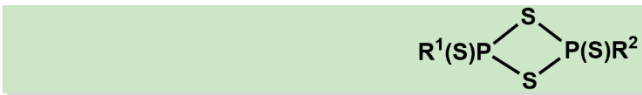
The ringed covalent I structure of DTDP is known as “dithiadiphosphetane”, while the dipolar II structure, a resonance of the ionic dipolar structure, is known as “dithioxophosphorane” [45, 46]. The existence of these two structures was supported by mass spectroscopy [47] and the existence of equilibrium between structures I and II was supported experimentally and theoretically [48-50].

2.1.1.1. Configuration of DTDP Isomer Structure

^{1}H-, ^{31}P- and ^{13}C-NMR spectra of DTDPs with different alkyl- and aryl- groups show that

these compounds usually prefer a dimeric structure in solution. Although dipolar II structure is known in the solution phase; ring covalent I structure is also known to exist in the solution. Thioxo moieties in DTDPs form configuration isomers that differ according to their position in the ring plane. These isomers show *cis*- or *trans*- isomers depending on the polarity of the solvent used (Table 2.1), [51].

Table 2.1. Chemical shift values of DTDP isomers (in $CDCl_3$) synthesised by reaction of phosphines with sulphur.



	$R^1=R^2$				R^2= *i*-Pr					
	trans-		*cis*-			*trans*-			*cis*-	
R^1	δ(P)	$^2J_{PP}$	δ(P)	*trans : cis*	δ(P^1)	δ(P^2)	$^2J_{PP}$	δ(P^1)	δ(P^2)	$^2J_{PP}$
Me-	23.7	-	14.2	3 : 1	26.1	49.0	1.8	16.6	42.0	< 3
Et-	39.9	-	31.2	5 : 1	40.4	51.2	3.9	31.8	44.0	2.0
Pr-	36.6	-	27.8	5 : 1	36.6	51.8	3.8	28.2	44.1	2.3
i-Pr-	52.0	4.8	44.5	8 : 1	-	-	-	-	-	-
Bu-	37.4	2.5	28.4	5 : 1	37.5	52.0	3.8	29.0	44.4	2.4
t-Bu-	61.4	2.5	-	-	61.1	51.8	6.2	56.8	45.3	5.7
cy-Hex-	48.7	6.7	41.3	9 : 1	47.1	53.6	4.9	40.0	45.6	3.5
Ph-	18.5	4.9	16.3	16 : 1	20.6	50.4	1.2	18.2	43.5	< 1
Xy-	19.7	1.0	17.1	12 : 1	21.8	50.7	1.2	19.2	44.1	< 1
An-	**17.1**	-	-	-	20.0	49.4	0.6	18.2	43.1	< 1

Another investigation of *cis*- and *trans*- isomerism in dimer DTDPs is the NMR (^{1}H-, ^{13}C- and ^{31}P-) study of *iso*-propyl-DTDP (Figure 2.4), [52]. In proton-decoupled ^{31}P-

NMR, this value has a chemical shift value at different locations in both isomers (4.8 Hz for the *trans*- isomer and 4.1 Hz for the *cis*- isomer). The formation of these isomers varies depending on the concentrations of the solutions. In the *cis*- and *trans*-conversion, which occurs slowly at low temperatures (-30 - 0°C), the proportion of the *cis*- form decreases with increasing temperature.

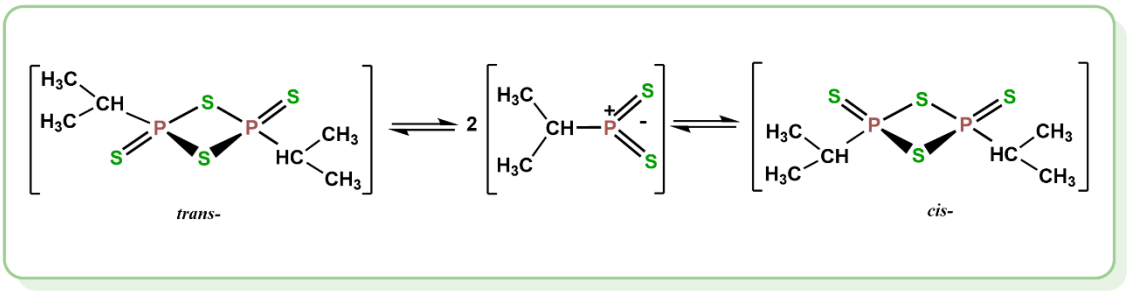


Figure 2.4. One of an examples of the DTDPs isomers, (*cis*- and *trans*- isomers).

According to NMR studies and ^{31}P chemical shift values together with crystal structure investigations of DTDPs; $[R\text{-}P(S)S]_2$ (R=methyl- [43], R=phenyl- [53], R=2,4,6-tri methylphenyl- [54]) *cis*- ve *trans*- isomers in solution:

- in apolar solvents, the balance is completely shifted toward the *trans*-isomer,
- in polar solvents, it is known that *cis*- ve *trans*- isomers exist in equilibrium [52].

The first DTDP structure known to have a *cis*- crystal structure is the bridged 1,8-naphthyl-DTDP compound [55]. However, the NMR study with the 2,4-*diiso*-propyl-DTDP derivative [56] suggests that this derivative of the compound crystallizes in the *cis*- configuration. Comparising of the chemical shift values of the *cis*- and *trans*- isomers show that the *cis*- isomer always has a smaller chemical shift than the latter (Table 2.2) [50, 52, 57].

NMR (^{31}P-NMR) studies show that, when the chemical shift values (σ_p) of the *trans*- and *cis*- isomers of S atoms with respect to the 4-membered P_2S_2 ring of dithiadiphosphetanes in solution are compared, it is observed that the *cis*-isomer always has a smaller chemical shift. This is thought to be due to the fact that the *cis*-configuration of the P_2S_2 ring further reduces the P-P distance between atoms due to the de-idealization (wrinkling) of the ring plane.

Solid-state NMR (^{31}P-NMR) investigations of dithiadiphosphetanes are characterized by a large anisopy ($\Delta\sigma$) of the chemical shift. Depending on the symmetry of the P_2S_2 ring,

one or two sideband systems are observed in the spectrum (^{31}P CP-MAS), indicating that the structure consists of an asymmetric unit molecular half and the whole molecule with two P atoms. The ^{31}P isotropic chemical shift (σ_{iso}) of the solid of DTDP is larger than that of the dimers of DTDP dissolved in solution. While this difference is high in compounds with small organic substituents, dithiadiphosphetanes with bulky organic substituents show very similar isotropic chemical shifts. These differences are known to be due to the effect of solvent on the P_2S_2 ring. An NMR study (^{31}P CP-MAS) performed with a derivative of DTDP ([R-P(S)S]$_2$, R=4-methoxy-phenyl-) similar isotropic chemical shifts of the solid and dissolved compound are observed in cases where the dithiadiphosphetane contains a stoichiometric amount of the organic solvent (e.g. benzene, toluene, o-dichlorobenzene) used for recrystallisation of the sample. If the 4-methoxy-phenyl compound crystallises without the addition of solvent molecules, the σ_{iso} is about 27 ppm higher than the ^{31}P chemical shift of the same compound in solution [57].

Table 2.2. ^{31}P chemical shift values of some DTDPs (σ_{iso}= ^{31}P isotropic chemical shift of the solid; recrystallized from a. benzene b. tetrachloromethane).

R[1]	δsol (ppm) trans	δsol (ppm) cis	δiso (ppm)	Δδ (ppm)	δiso-δsol (ppm)
Me-	23.7	14.2	52.6	317	28.9
i-Pr-	52.0 -	44.5 -	52.2 50.6	415 422	7.7 6.1
t-Bu-	61.4	-	63.0	443	1.6
cy-Hex-	48.7	41.3	53.2	417	4.5
Ph-	18.5	16.3	30.7	405	12.2
4-MeO-Ph[a]	17.1	-	22.2	446	5.1
4-MeO-Ph[b]	17.1	-	43.8	370	26.7
1,8-Naphthyl-	- -	18.0 -	30.2 22.8	307 323	12.2 4.8

In general, single crystal X-ray studies of the ring covalent I structure (dithiadiphosphetanes) of the configuration isomers of dimer $[R\text{-}P(S)S]_2$ compounds (R= methyl- [43, 58], R= phenyl- [53] and R= 2,4,6-trimethylphenyl- [50, 54]), show that the two R groups (or position of the sulfur atoms) are in the *trans*- configuration [43, 50, 54-56, 58-74]. The dipolar II structure, on the other hand, is confirmed to exist from heating DTDP derivatives (methyl or ethyl) in the gas phase in a vacuum [75] or by photoelectron spectroscopy of a monomer (ethyl thithioxophosphorane) [48].

The reactions of DTDPs with nucleophiles are characterized by an equilibrium between the *cis*- or *trans*-cyclic covalent I structure (dithiadiphosphetanes) and the dipolar II structure (dithioxophosphoranes), and the reaction of the dipolar II structure with nucleophiles [50, 51, 76, 77] is important for the initiation of the reaction [78, 79]. On the other hand, many references assume that the reaction starts with the direct attack of the reacting nucleophile on the four-membered ring of the ringed covalent I structure [43, 44].

A reaction mechanism for the *cis*- and *trans*-formations is not yet known. Previously, although dipolar II could not be detected with the ^{31}P-NMR spectrum; an equilibrium between the ring covalent I and dipolar II structures were found to exist, and MS studies with the 4-methoxyphenyl derivative showed that [80], this equilibrium was on the dipolar II side, (Figure 2.5).

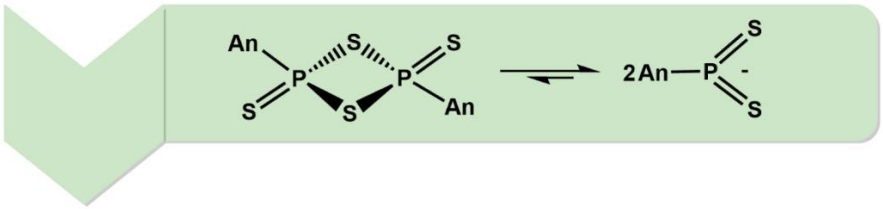


Figure 2.5. The equilibrium between structures I and II.

Many DTDPs such as methyl- [43, 58], phenyl- [53] and 2,4,6-trimethylphenyl- [43, 46, 50-54, 56, 58, 65, 81] (Figure 2. 6) can also be determined by ^{31}P-NMR spectroscopy as *trans*- and *cis*- isomers [78] in solution.

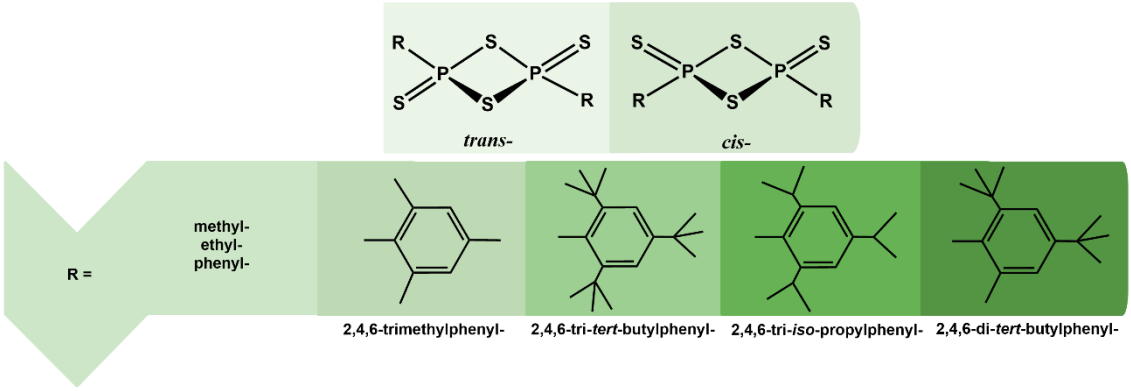


Figure 2.6. Structure of some DTDPs belonging to *trans*- and *cis*-isomers.

There is some research on the dipolar II structure supported by theoretical study together with NMR spectroscopy of the monomer dithioxophosphorane [49].

There are studies supporting the ring covalent I and dipolar II structures by NMR studies and explaining both structures by single crystal X-ray diffraction spectroscopy by crystallizing both structures simultaneously and mechanically separating the two isomers. In that study, the structure of the ring covalent *cis*-DTDP in solid form was also elucidated by crystallographic method (Figure 2.7), [50].

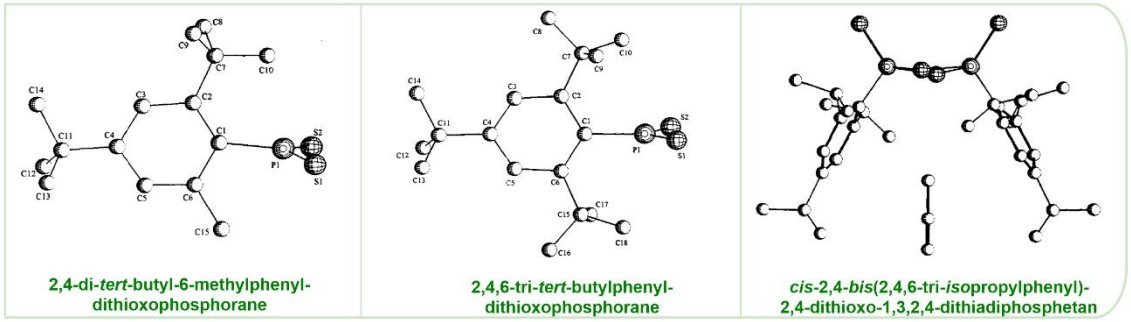


Figure 2.7. An example of a ringed covalent I (*cis*-isomerism) and dipolar II X-ray ORTEP diagram structure.

2.1.1.2. Synthesis of Configuration Isomers of DTDPs

Dipolar II structure dithioxophosphoranes are isolated from the reaction of phosphines with sulphur according to the general synthesis method of DTDPs [50, 66, 82-84]. Sterically hindered dithioxophosphoranes are obtained from the reaction of (trimethylsilyl)(tri-*tert*-butylphenyl)phosphane, (Figure 2.8.A) with disulfide dichloride (Figure 2.8.B) (R=2,4,6-tri *tert*-butylphenyl) (Figure 2.8.C) [46].

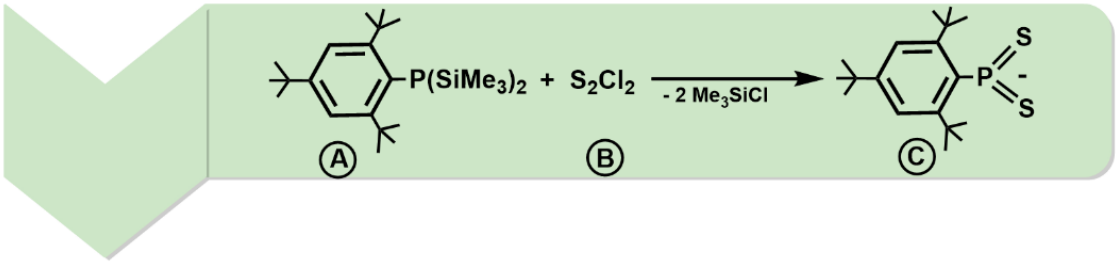


Figure 2.8. Phosphane and S_2Cl_2 synthesis of dipolar II structure.

In addition, the dipolar II structure (Figure 2.9.A) is obtained from the reaction of phosphaallenes with excessive sulfur (R= 2,4,6-di-*tert*-butyl-6-methoxyphenyl-) [85]. Another method for obtaining the II structure is the reaction of phosphenes with sulfur (Figure 2.9.B and Figure 2.9.C) [86-88].

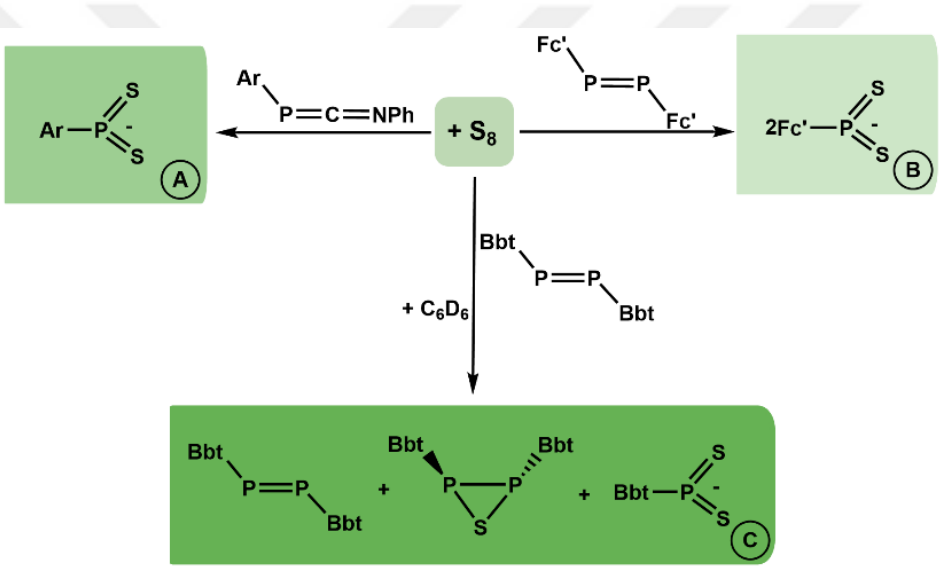


Figure 2.9. Synthesis of dipolar II structure from phosphene and elemental sulphur.

Another synthesis of the dipolar II structure; they are obtained from the synthesis of DTDP derivatives ([R-P(S)S], R= methyl- or ethyl-) in the gas phase (Figure 2.10) by heating in a vacuum [75].

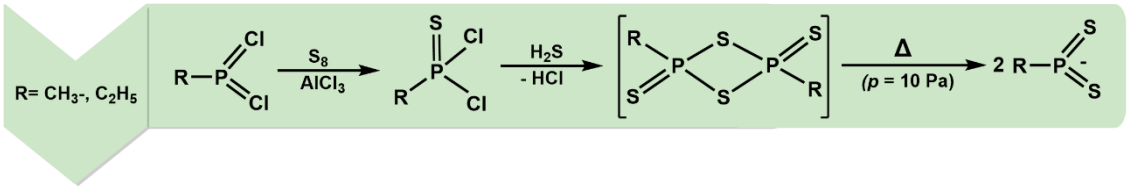


Figure 2.10. Synthesis of dipolar II structure by heating DTDPS in the gas phase.

In a recent study, a dipolar II structure ([$(CH_3O\text{-}C_6H_5)$P(S)S]) was synthesized under

special reaction conditions and its structure was supported by theoretical study together with spectroscopic methods (Figure 2.11), [89]. The isolation of the structure as well as IR and UV/Vis spectroscopic characterization of phosphine disulfide ([(Ar-P(S)S], Ar= 4-methoxyphenyl-) in argon matrices at 10 K. Dipolar II structure proved to be highly photolabile; irradiation with UV light (λ= 334 nm) led to rearrangement to the dithiaphosphirane, namely, (4-methoxyphenyl)-1,2,3-dithiaphosphirane. Photoreversion could be achieved upon irradiation at λ= 465 nm.

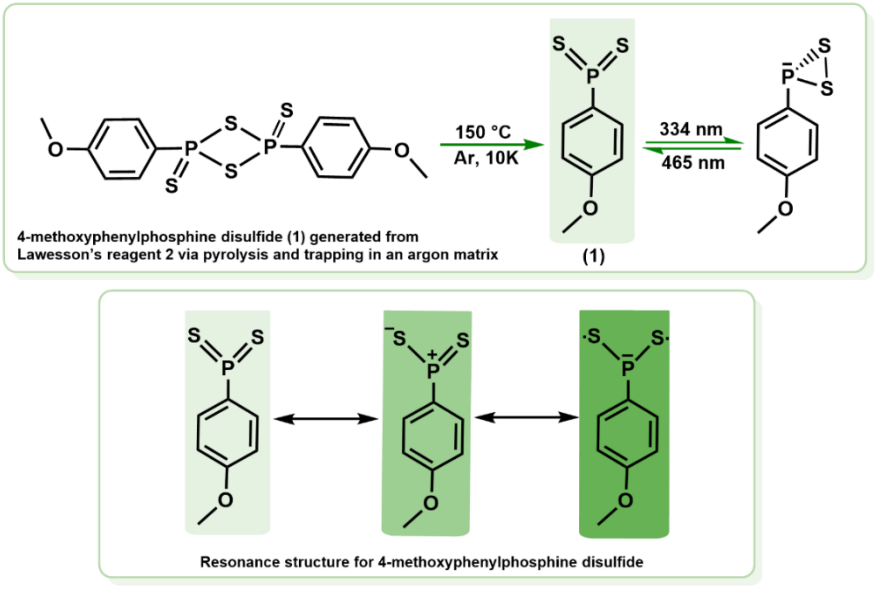


Figure 2.11. One of the synthesis methods for dipolar II isomer.

Under an inert atmosphere, dithioxophosphorane (R=2,4,6-di-*tert*-butyl-6-methoxyphenyl-, [90]) in solution remains stable for several days in non-polar solvents, while in the solid state or concentration gives dimeric products, the *trans*- (Figure 2.12.B) and *cis*- isomer (Figure 2.12.C) (1:0.8 mole ratio). Both dimers (Figure 2.12.B and Figure 2.12.C) are converted to monomer A by heating [91].

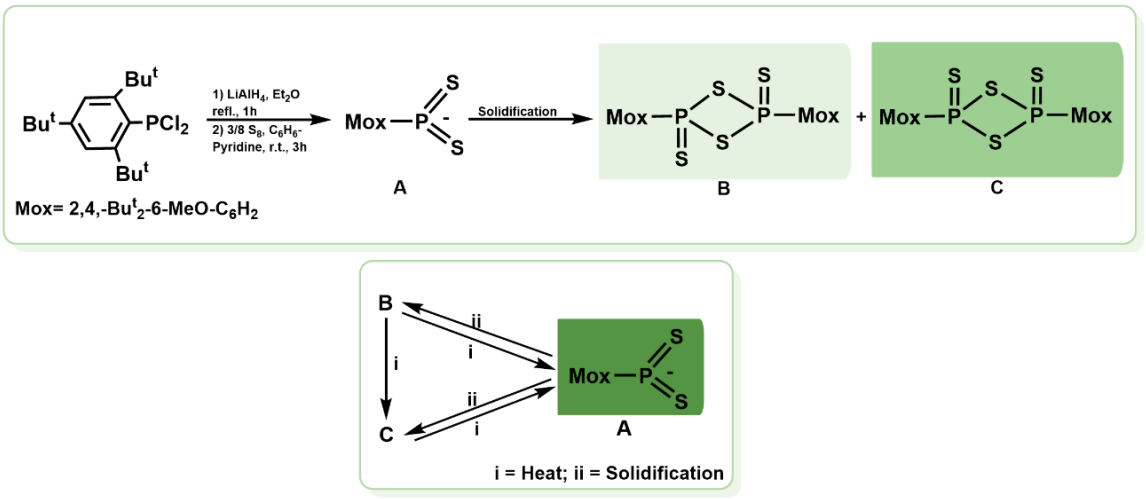


Figure 2.12. Synthesis of dithioxophosphorane (Dipolar structure II).

2.1.2. Synthesis Methods of 1,3,2,4-dithiadiphosphetane-2,4-disulfides

There are some various methods for the synthesis of 1,3,2,4-dithiadiphosphetane-2,4-disulfides. Among these methods, Methods 1-6 are used less frequently. But, method 7 is the most preferred method by researchers in DTDP synthesis because of some of its advantages, which will be mentioned later.

2.1.2.1. Method 1: DTDP Synthesis from the Reaction of Thiophosphindichloride and Hydrogen Disulfide

This method includes that the reaction of dichlorophosphines with H_2S_2 at low temperatures in an inert atmosphere. In the reactions, HCl gas is removed from dithiophosphonic acid chloride, (RP(S)SCl), formed HCl by the reaction of dichlorophosphine $RPCl_2$ (R = phenyl-, ethyl-, methyl-), with hydrogen disulfide (H_2S_2) in CS_2 as a starting material. The dimerization of dithiophosphonic acid chloride leads to DTDP (Figure 2.13) [60]. Decreasing the mole fraction of H_2S_2 from the reactants increases the yield of the product. Dimer, ($[R\text{-}P(S)S]_2$, R= *tert*-butyl-) can also be obtained by preferring Li_2S_2 instead of H_2S_2 as starting material [56]. Although the compounds have exactly the same properties as DTDPs synthesized by other routes, they have similar difficulties with other methods.

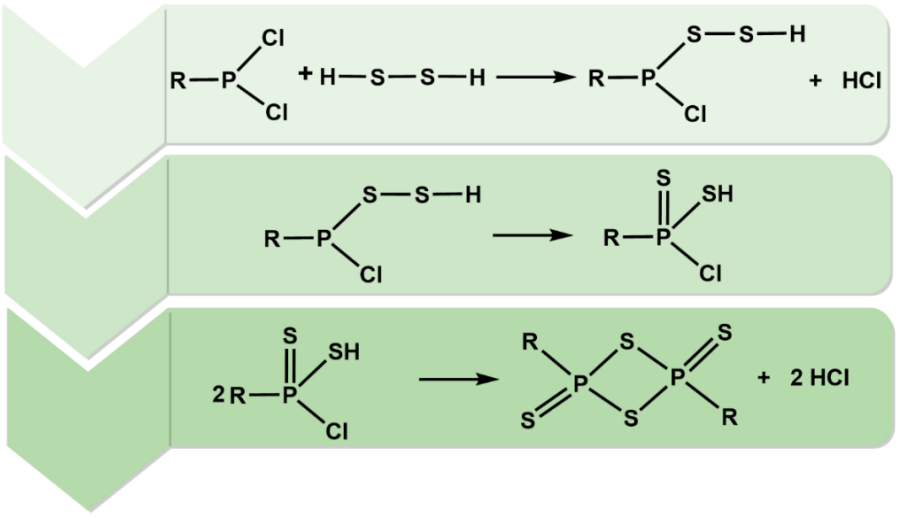


Figure 2.13. General synthesis reaction of DTDPs according to Method 1.

2.1.2.2. Method 2: DTDP Synthesis from the Reaction of Phosphine and Disulfide Dichloride

The synthesis method of DTDP, which is not well known, is the reaction of trimethylsilylphosphines with S_2Cl_2, (Figure 2.14) [46].

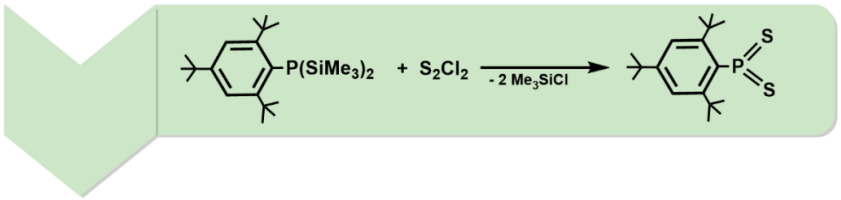


Figure 2.14. General synthesis reaction of DTDPs according to Method 2.

2.1.2.3. Method 3: Synthesis of DTDP from the Reaction of Diphosphene and Sulphur

DTDP is formed from the reaction of phosphines with sulphur as well as from the reaction of diphosphenes with sulphur [92]. The structure of *bis*(2,4,6-tri-*tert*-butylphenyl)diphosphene, which was first isolated, is synthesized from the dimerization of the intermediate (phosphinidene) formed from the reaction of 1,3,5-tri-*tert*-butylbenzyl dichloro phosphine with Mg metal (Figure 2.15) [93].

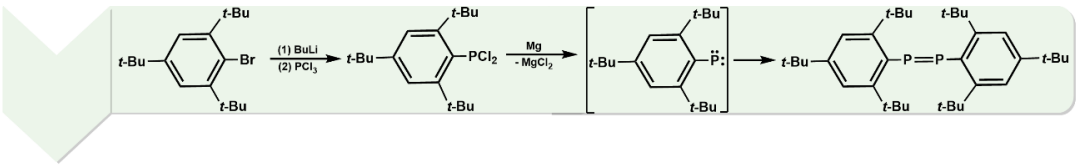


Figure 2.15. General synthesis reaction of DTDPs according to Method 3.

2.1.2.4. Method 4: DTDP Synthesis from the Reaction of Thiadiphosphirane and Sulphur

From the reactions of diphosphenes [93] with sulphur, the intermediate transition product thiadiphosphirane derivatives are formed [86, 94-96]. DTDP is synthesized from the reaction of these derivatives with elemental sulfur (Figure 2.16), [87, 88, 97].

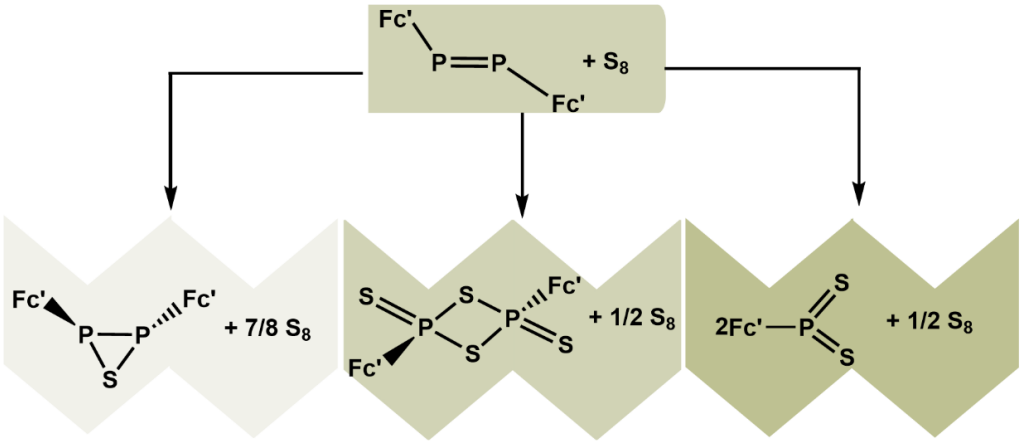


Figure 2.16. General synthesis reaction of DTDPs according to method 4.

2.1.2.5. Method 5: Synthesis of DTDP from the Reaction of Thiophosphindichloride and Hydrogen Sulphide

DTDPs are obtained from the reaction of an alkyl or aryl thiophosphindichlorides with hydrogen sulphide gas at high temperatures (Figure 2.17).

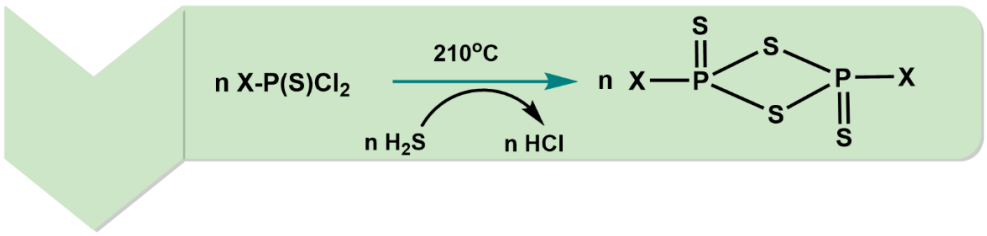


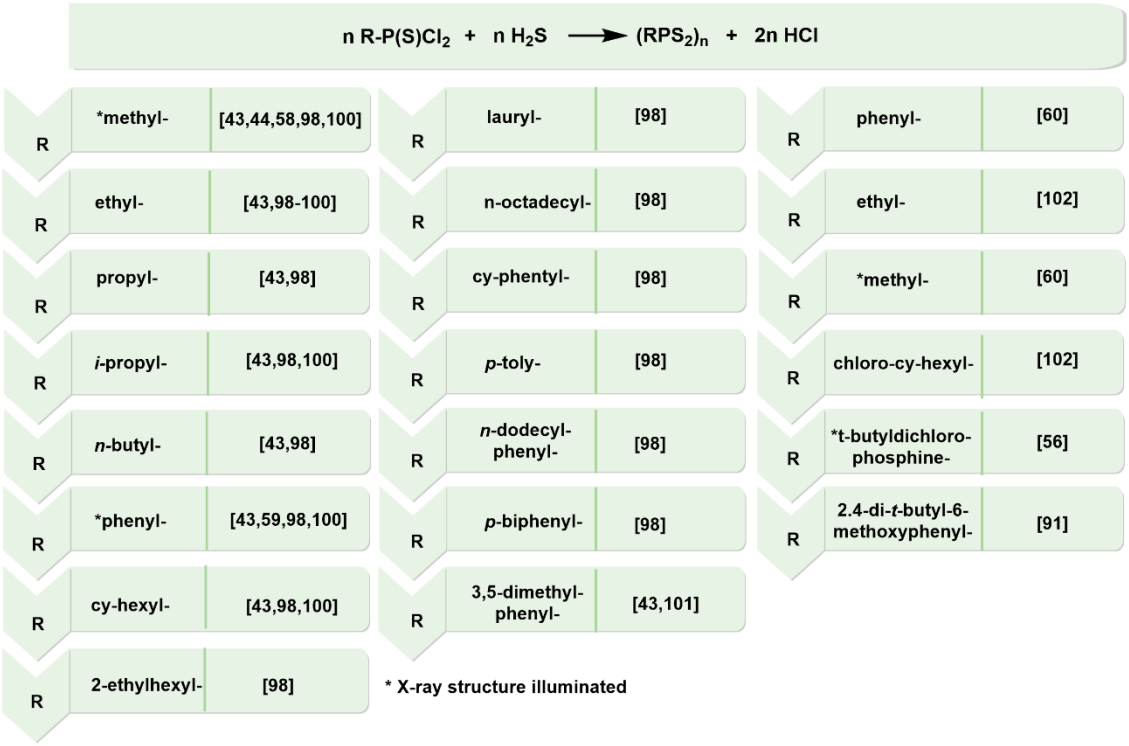
Figure 2.17. General synthesis reaction of DTDPs according to Method 5.

The temperature of the reaction depends on the thiophosphindichlorides used. Excess hydrogen sulphide and long periods of heating have no significant effect on the yield or purity of the product. These compounds are generally high melting point solids that are insoluble in most aprotic solvents and react with protic solvents [44, 98, 99]. Although DTDP can be obtained with an acceptable yield in this method, it is not a frequently preferred method due to the difficulties in obtaining the starting materials, the long

reaction time (16-24 hours), the dangerous and corrosive effects of HCl gas, the difficulties in controlling of the flow rate of hydrogen sulphide gas in the reaction medium, the exothermic reaction and the need for control of the reaction temperature.

DTDPs synthesized using this method are given in Table 2.3 [43, 44, 56, 58-60, 91, 98-102].

Table 2.3. DTDPs are synthesised according to Method 5.



R		
R	*methyl-	[43,44,58,98,100]
R	ethyl-	[43,98-100]
R	propyl-	[43,98]
R	*i*-propyl-	[43,98,100]
R	*n*-butyl-	[43,98]
R	*phenyl-	[43,59,98,100]
R	cy-hexyl-	[43,98,100]
R	2-ethylhexyl-	[98]
R	lauryl-	[98]
R	n-octadecyl-	[98]
R	cy-phentyl-	[98]
R	*p*-toly-	[98]
R	*n*-dodecyl-phenyl-	[98]
R	*p*-biphenyl-	[98]
R	3,5-dimethyl-phenyl-	[43,101]
R	phenyl-	[60]
R	ethyl-	[102]
R	*methyl-	[60]
R	chloro-cy-hexyl-	[102]
R	*t-butyldichloro-phosphine-	[56]
R	2.4-di-*t*-butyl-6-methoxyphenyl-	[91]

* X-ray structure illuminated

2.1.2.6. Method 6: DTDP Synthesis from Phosphine and Sulphur Reaction

Method 6 is not a frequently used method due to the variety of undesired by-products depending on the amount of sulphur and the difficulties in purifying the target compound. DTDPs are performed from the reaction of alkyl-/aryl- phosphines with sulphur by elimination of H_2S, preferably in benzene. The synthesis of P_2S_2 ring systems by the reaction of phosphines with sulphur has been known for a very long time [50, 92]. The formation of DTDP starts with the formation of the intermediate ring tetraphosphine tetrasulfide (Figure 2.18.A) [81, 103]. In the next step, DTDP is produced by the reaction of the intermediate with additional sulphur (Figure 2.18), [104, 105].

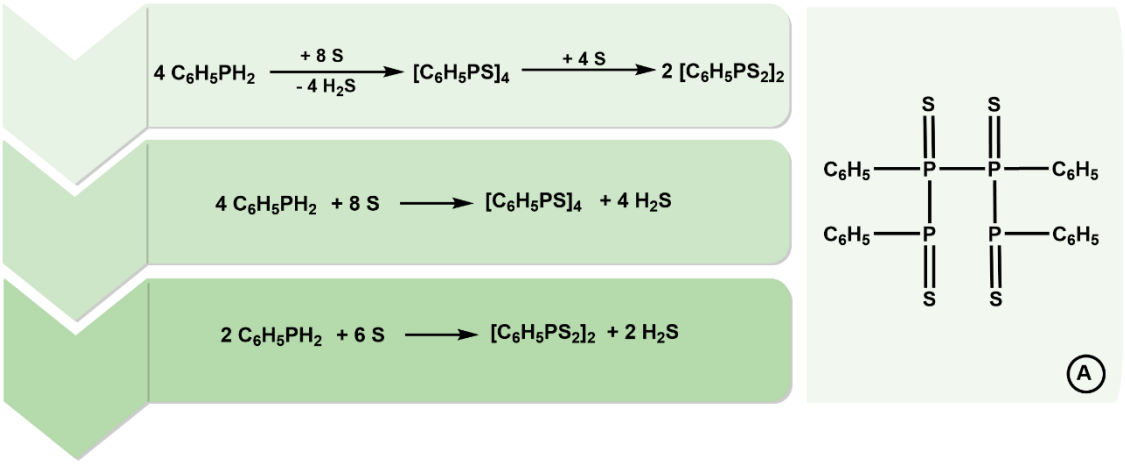


Figure 2.18. General synthesis reaction of DTDPs according to method 6.

There are also DTDPs obtained as by-products from the reaction of elemental sulphur with cyclic monocarbatetraphosphines [61]. According to this method, DTDP is synthesized by reacting various aryl and/or alkyl groups with sulphur (Table 2.4), [46, 50, 53, 54, 56, 61, 81, 105-107].

Table 2.4. General synthesis reaction of DTDPs according to method 6.

$2\ R\text{-}PH_2 + 6\ S \longrightarrow [R\text{-}PS_2]_2 + 2\ H_2S$

R*	phenyl-	[53,61,81,105]	R*	n-heptyl-	[105]	R*	4-phenylethyl phenyl-	[105]	R*	cyanoethyl-	[105]
R	methyl-	[105]	R	n-octyl-	[105]	R	trifuoromethyl-	[105]	R	dichloroacetyl-	[105]
R	ethyl-	[105]	R	n-stearyl-	[105]	R	2-chloroethyl-	[105]	R	trichloroacetyl-	[105]
R	propyl-	[105]	R	allyl-	[105]	R	perfuoroethyl-	[105]	R	3,5-di-*t*.-butyl-4-hydroxyphenyl-	[107]
R	*i*-propyl-	[105]	R	benzyl-	[105]	R	4-chlorophenyl-	[105]	R*	2,4,6-tri-*i*-propylphenyl-	[50]
R	*n*-butyl-	[105]	R	cy-pentyl-	[105]	R	4-bromophenyl-	[105]	R*	2,4-di-*t*-butyl-6-methylphenyl-	[50]
R	*i*-butyl-	[105]	R	cy-hexyl-	[105]	R	hydroxyethyl-	[105]	R*	2,4,6-trimethyl phenyl-	[50]
R*	*t*-butyl-	[56,105,106]	R*	4-methylphenyl-	[105]	R*	methoxyethyl-	[105]	R*	2,4,6-tri-*tert*-butyl phenyl-	[46,50]
R	n-amyl-	[105]	R	2,4,5-trimethyl phenyl-	[105]	R	acetoxy ethyl-	[105]	R*	1,3,5-trimethyl phenyl-	[54]
R	*i*-amyl-	[105]	R	2,4,6-trimethyl phenyl-	[105]	R	benzoyloxyethyl-	[105]			

* X-ray structure illuminated

To summarise, for the synthesis of DTDP, it is important to optimize the mole ratios of starting materials and sulphur in the reactions in the above-mentioned methods [53, 54, 87, 97]. These methods are not favoured due to the difficulties in the reaction environment, the variety of by-products formed depending on the amount of sulphur and the difficulties in purifying the target compound.

The most favoured synthesis method used by researchers for the synthesis of DTDPs is the chemical reaction of the Berzelius compound with several reagents. The details of the method are given below.

2.1.2.7. Method 7: DTDP Synthesis from the Reaction of P_4S_{10} and an Aromatic/Aliphatic Reagent

The best-preferred method for the synthesis of DTDPs is the reaction of P_4S_{10} with an aromatic or aliphatic reagent. Although this method is the most practical, the mole ratios of the starting materials, time and temperature parameters are important for the DTDPs to be synthesized. Therefore, for each DTDP synthesis, these three parameters should be well optimized for maximum yield of product and minimum amount of by-product. In the suggested reaction mechanism for the formation of DTDP (Figure 2.19), it starts with the attack of nucleophiles on the electrophilic central phosphorus atoms of the ionic P_4S_{10} [42] and DTDP is obtained by elimination of H_2S gas.

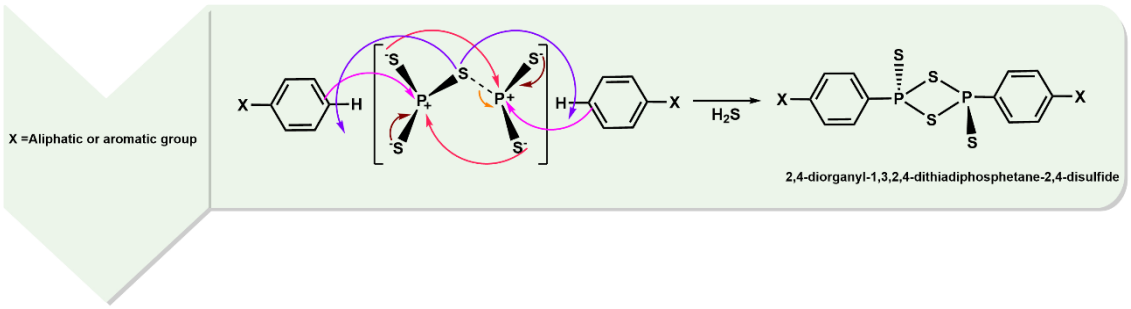


Figure 2.19. Suggested DTDP reaction mechanism for Method 7.

Depending on the amounts of starting materials in the synthesis of DTDP, hydrogen sulphide elimination may be more or less [42]. In general, for DTDPs, the optimum temperature range is kept as low as possible. High temperatures also result in lower yields of the product. Low temperatures are therefore preferable, which allow a reasonably rapid diffusion of the gas in the reactions. The reaction yield can also be increased (up to 10 times or even 20 times) by an excess of the aromatic reagent over P_4S_{10} [108, 109]. For the reaction performed in an inert atmosphere under reflux, the starting materials must be of analytical purity and their stoichiometry must be well established (sometimes, calculated mole ratios of the starting material could be greater than the mole ratios of P_4S_{10}, for example, one tenth of P_4S_{10} [41, 44, 110, 111]), and the optimum conditions of time and temperature parameters are determined until the starting materials are

completely dissolved or dissolved in each other; in order to reduce the number of by-products to be formed in the reaction and to form DTDP at maximum yield. Moreover, DTDP should be kept in a desiccator in an inert atmosphere since the formed product is influenced by the humidity and oxygen of the air in a short time. The decomposition of DTDPs, which usually have a light yellow colour, yields a white, viscous, unknown polymeric substance.

The reason why the last method is preferred by researchers compared to other methods is that the by-products are low, the effluents are not quickly affected by moisture and oxygen in the air and are easily available.

There are many DTDPs achieved by this method. The best known of these dimers [R-$P(S)S]_2$, are the Lawesson reagent (R= anisyl-), [112, 113], Ferrocenyl Lawesson reagent (R= Fc-) [62], Belleau reagent (R= 4-phenoxyphenyl-) [114], Yokoyama reagent (R= thioanisyl-) [115] and Davy (R= thiomethyl-) reagents, (Figure 2.20), [115-118]. These compounds are usually named after the inventor. It is interesting that the Belleau reagent [114] and Lawesson's reagent [112, 113] of DTDP analogues were first synthesized by Lecher et al [42]. Probably, the modification of the synthesis method or the discovery of the thionation property led to the personalized names of these compounds. Another interesting example, the thiomethyl derivative of DTDP (together with the *p*-tolylthio derivative, also called Heimgartner reagent), was synthesized by Scott and co-workers, but due to the incomplete description of its structure [116], it was named Davy's reagent (DR) after Davy modified the method and described the structure [118].

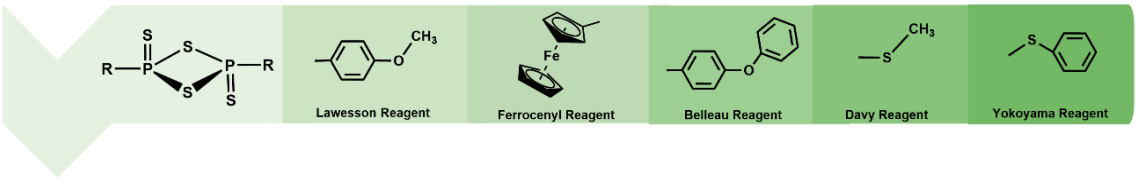


Figure 2.20. The best-known DTDPs are synthesized according to Method 7.

This reagent is obtained by reactions of P_4S_{10} with alkyl- or aryl- groups containing thio groups. On the other hand, only the DR-thiomethyl derivative is also obtained from the direct reaction of dimethyl dithiophosphoric acid with P_4S_{10} in a methanol medium (Figure 2.21), [119]. These DTDPs can be synthesized in the laboratory [62] but not the commercially available such as Lawesson, Davy or Japanese reagents.

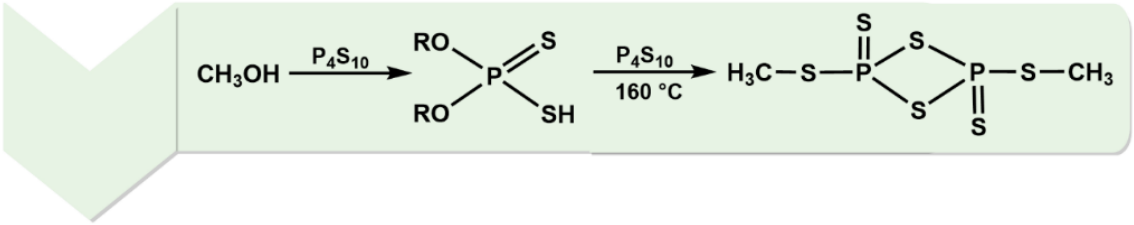


Figure 2.21. DR-thiomethyl derivative one of the synthesis reaction.

Actually, the first studies on the synthesis of DTDP with PS-ring compound and different type alkyl/aryl reagents started in the early 19th century. In that process, which started with DTDP-naphthalene analogue for the first time, J.Mai began his researchers with Berzelius reagent and naphthalene reaction. In Mai's research, he tried reacting P_4S_3 and P_4S_7 with sulfur in the presence of naphthalene, but each time he obtained P_4S_{10}. [120]. In fact, it was expected that P_4S_{10} would be obtained as a product under those reaction conditions [120]. A long time later, the naphthalene derivative of DTDP, which was synthesized in 1930 and named as "organic-thio-phosphoric naphthalene compound" in during those years, was synthesized for the first time. The synthesis of this substance was important because the mine stood as a good alternative as an additive in the flotation of ores [121]. In the following years, with the studies conducted with naphthalene, it began to be investigated which carbon atom phosphorus binds to naphthalene through.

Whether the phosphorus atom in DTDP binds to naphthalene at the "position 2" (β position) [42] or the "position 1" (α position) [63] has been a matter of debate. Although the α, α; β, β and α, β isomer structures of the crude products formed by refluxing P_4S_3 compound with sulphur to α-bromonaphthalenele at high temperature [120] or by heating P_4S_{10} to α-bromonaphthalenele at high temperature (in the naphthyl-DTDP derivative) were tried to be explained by ^{31}P-NMR spectroscopy [62]; spectroscopic and crystallographic studies have shown that phosphorus atoms are bound to carbon atoms' position 1 and 8 in naphthyl (Figure 2.22), [55, 63, 122].

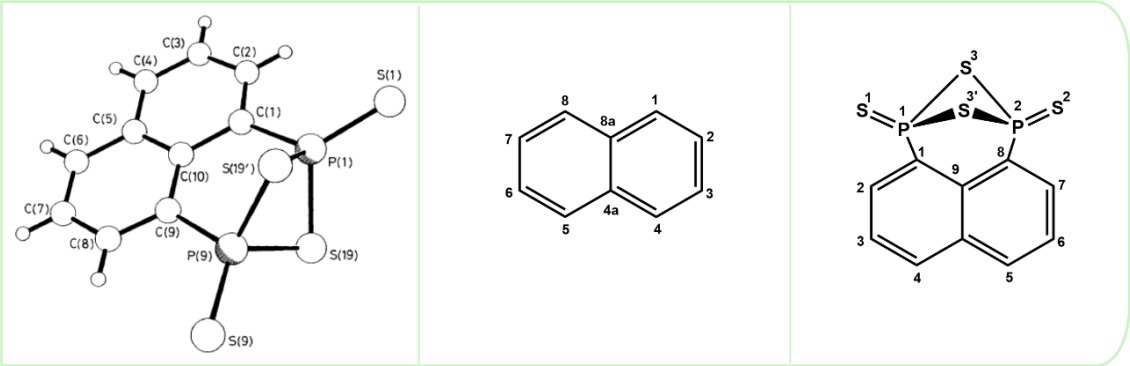


Figure 2.22. DTDP-naphthalene derivative structure.

DTDP analogues were synthesized in the years after 1930 with various reagents (*iso*-butylene [123], turpentine or pinene produced from a pine oil, etc. [124, 125]) using P_4S_{10} as starting material. The first suggestions on the structure of DTDP are found in a patent study for a dicyclohexenyl- derivative (Figure 2.23), [110, 111].

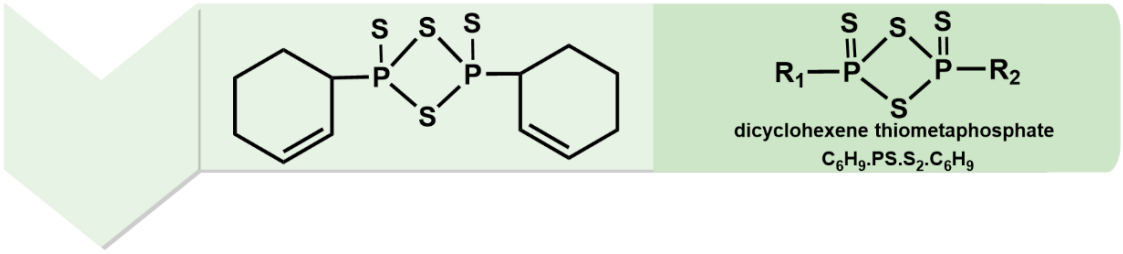
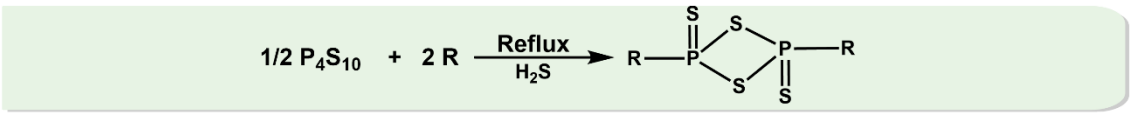


Figure 2.23. Structure of the first proposed DTDP of dicyclohexenyl derivative.

The first scientific finding supporting the structure was brought to the literature by Fay et al. in 1952. Although the synthesis reaction of DTDP is not suggested in that study, it is the first descriptive compound in terms of the structure and method [111].

Shortly after this study, DTDPs were synthesized by applying the reaction method of an aromatic or aliphatic reagent with compound P_4S_{10} in the synthesis of benzene, o-xylene, anisole, phenetole, 2-*iso*-propylnaphthalene and naphthalene derivatives [42]. This method is still preferred by researchers today. DTDPs synthesized using this method between 1930-2023 are given in Table 2.5, [41, 42, 55, 62-66, 68-74, 98, 101, 108-111, 113, 115-119, 121, 123-134].

Table 2.5. DTDPs synthesized in accordance with method 7.



R	naphthyl-	[42,108,121]
R*	1-bromonaphthyl-; naphthyl-1,8-diyl	[55,62-64]
R*	4-methoxynaphthyl--1,8 1-Methoxynaphthalei	[63]
R	1-naphthyl-	[63]
R	2-naphthyl-	[63,98]
R*	1-methoxynaphtyl-	[63]
R	2-*i*-propyl-naphthyl-	[42,108]
R	*i*-butylene-	[123]
R	turpentyl- (pinen)	[124,125]
R	dipentene- terpinolene-	[125]
R	cy-hexyl	[110,111]
R	*p*-thiotolyl-	[117,118]
R*	*p*-methoxyphenylthio-	[42,115]
R*	thiophenol-	[115]
R	di-*i*-butyl-	[109]
R	ferrocenyl-	[62]
R*	1,1'-dimethylferrocenyl-	[62]
R	anisyl-; 1,1'-dimethylferrocenyl-	[62]
R	3-*t*-butyl-4-methoxyphenyl-	[42]
R	3,5-di-*tert*-butyl-4-hydroxyphenyl-	[101]
R	3-brominephenyl-1-*i*-amyl ether	[71]
R	butylphenyl ether	[71]

R	n-hexadecyl	[41]
R*	benzyl-	[42,108]
R*	*o*-xylene-	[42,108]
R	anisyl-	[42,65,66,108,113]
R	thiophenyl-	[42,108]
R*	phenetole-	[108]
R	anthracene-	[108]
R	phenanthrene-	[108]
R	thiofen-	[126,127]
R	thiomethyl-	[67,116,118,119]
R	thioethyl-	[69,118]
R	heptadecafluorododecyl phenyl ether	[128]
R*	tridecafluorodecyl phenyl ether	[128]
R*	fluorous anisole derivative	[129]
R	dimethylamido	[72-74,130]
R	diethylamido	[73,74,130]
R*	trifluoroethyl-	[74]
R	3-methoxytoluene	[131]
R	2-methoxytoluene	[131]
R	1,2-dimetoxybenzene	[132]
R	1,3-dimetoxybenzene	[133]
R	fluorene	[134]

* X-ray structure illuminated

Nitrogen-containing DTDPs ($[R_2N\text{-}P(S)S]_2$, R= H, alkyl- or aryl) can also be obtained

according to Method 7. The dimethyl amido derivative of DTDP was first obtained from the reaction of dimethylaminosulfan ([$S(N(CH_3)_2)_2$]) P_4S_3 [72]. The diethylamido-DTDP derivatives are formed by [2+2] cycloaddition of the monomethaphosphate derivative formed by heating pyridine-stabilized dithiomonomethaphosphoryl diethylamide (Figure 2.24), [135].

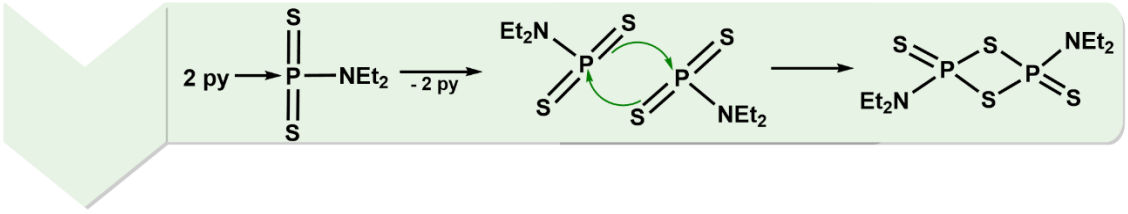


Figure 2.24. Synthesis of diethylamido-DTDP analogue.

Another method for the synthesis of diethylamido-DTDP is the reaction of Davy's reagent with trimethyl-(diethylamino)silane ($(Et_2N)_2SiMe_2$) to the reaction product (*S*-trimethylsilyl *S*-ethyl(diethylamido)trithiophosphate). It is obtained from thermal decomposition at 99°C (Figure 2.25), [73].



Figure 2.25. Synthesis of diethylamido-DTDP from starting material EtS-DTDP.

In another study on the synthesis of methyl- and ethyl- amido-DTDP derivatives, spectroscopic results of the products obtained from the reaction of P_4S_{10} with alkylsulfendialkyl amides (R_2NSR') revealed that this method is not a suitable approach for the synthesis of alkyl amido-DTDPs and the products are undefined compounds [74]. Instead of this method, synthesis of dialkyl amido-DTDPs by reaction of $(Py)PS_2NR_2$ compound with Lewis acid $AlCl_3$ was preferred [74].

2.1.2.8. Synthesis of Metal-Containing DTDPs, DTDP S-Metal Salts

DTDP S-Metal salts ([M-S-P(S)S]$_2$) are synthesized in specially made glassware and under-sensitive reaction conditions. They are usually prepared by heating stoichiometric mixtures of metal, red phosphorus and chalcogen at high temperatures in Vycor or quartz glass ampoules. The use of transparent quartz glass furnaces provides an advantage in

better controlling the course of the reaction. X-ray analyses showed that the compounds belong to hexachalcogenohypodiphosphates [136].

Table 2.6. Synthesis and reaction parameters of $[M\text{-}S\text{-}P(S)S]_2$.

	Starting compounds	Reaction temperature °C
$Mg_3P_2S_6$	Mg, P, S	500-800
$Ca_2P_2S_6$	Ca, P, S	700-800
$V_2P_2S_6$	V, P, S	400-470
$Mn_2P_2S_6$	Mn, P, S	600-780
$Fe_2P_2S_6$	Fe, P, S	400-650
$Co_2P_2S_6$	Co, P, S	400-650
$Ni_2P_2S_6$	Ni, P, S	570-710
$Pd_2P_2S_6$	Pd, P, S	450-500
$Zn_2P_2S_6$	Zn, P, S	450-490
$Cd_2P_2S_6$	Cd, P, S	600-670
$Hg_2P_2S_6$	Hg, P, S	320-500
$Sn_2P_2S_6$	Sn, P, S	350-450 400-500
$Pb_2P_2S_6$	PbS, P, S	500-650
$Mg_2P_2Se_6$	Mg, P, Se	480-690
$Mg_2CaP_2Se_6$	Mg, Ca, P, Se	450-500
$Mn_2P_2Se_6$	Mn, P, Se	600-720
$Fe_2P_2Se_6$	Fe, P, Se FeSe, P, Se	550-700
$Ni_2P_2Se_6$	Ni, P, Se	500-560
$Cd_2P_2Se_6$	Cd, P, Se	550-650
$Hg_2P_2Se_6$	Hg, P, Se HgSe, P, Se	340-500
$Sn_2P_2Se_6$	SnSe, P, Se	450-550
$Pb_2P_2Se_6$	PbSe, P, Se	500-600

After the synthesis studies of the above-mentioned DTDP-metal salts, (M= Ag [137], Tl [138], Cs and K [139], U [140, 141], Rb [112, 142, 143], U and Pu [144], Na, K and Rb [143], Cu [145], Li [140]), other metal salts were synthesized and their structures were elucidated by single-crystal X-ray spectroscopy.

2.2. Reactions of DTDPs with RO-X (X= H, Na)

2.2.1. Reactions with Alcohols (DTDP+R-OH)

Dithiophosphonic acids (DTPOA) are obtained from organo-dithiophosphorus derivatives as products of the reaction of DTDPs with alcohols. Originally, the reaction of DTDPs with alcohols was known since the 1930s [121, 124, 125] but the reaction could not be described. Fay et al. first described the synthesis of cyclohexyl-dithiophosphonic acid and *O*-methyl(cyclohexyl) dithiophosphonic acid from the reaction of cyclohexyl-DTDP derivative with water and methyl alcohol, respectively [111]. Afterward, Lecher

et al. synthesized the corresponding DTPOAs by hydrolysis of anisyl-, phenethyl-, naphthyl-, benzyl-, *iso*-propyl naphthyl-DTDP derivatives with water [42]. This method of synthesis of DTPOAs was quite practical and easy compared to other synthesis methods [38, 99, 146]. For this reasons, the method was highly preferred by researchers in the synthesis of DTPOAs, and many DTPOAs have been synthesized using this method in the following years (Figure 2.26), [42, 59, 63, 107, 108, 131-133, 146-168]. Optically active DTPOAs are also synthesized by this method [59, 159, 164, 169-173]. These optically active compounds were found to be effective against some fungal species [157, 164, 165, 171-174].

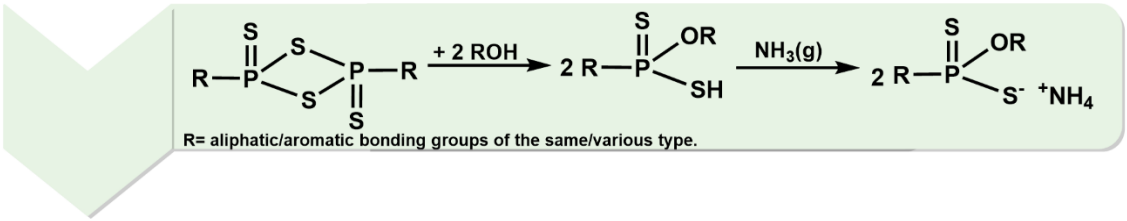
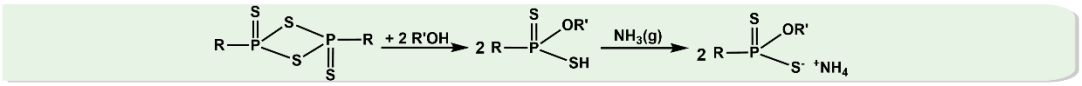


Figure 2.26. The general synthesis method of DTPOAs.

DTPOAs synthesized in this way are used in the separation and purification of ores by separation and beneficiation processes by floating some of the minerals with different surface properties in an aqueous slurry and precipitating the others [121], as an oxidation inhibitor in viscous engine oils against the harmful effects of oxidation [125], in the production of insecticides and fungicides [105, 127], as an intermediate for the production of wear inhibitors in lubricating oils [105], as an additive for its antimicrobial [164] and insecticidal properties [98].

DTPOAs formed by the reaction of DTDPs and alcohols are given in Table 2.7 [42, 107, 108, 111, 121, 124, 125, 127, 147, 175-179].

Table 2.7. Starting reagent and alcohols used in the synthesis of DTPOAs.



R, ([R-P(S)S]$_2$)	R', (R'-OH)	Literature
Naphthyl-	Ethyl-, methyl-, propyl-, phenol-	[108,121]
Turpenthyl- (pinen)	Eapryl- (octanol-2),hexyl, Lauryl-, octadecyl,methyl-	[124]
Dipenthyl-, terpinolene	Oleyl-, stearyl-, butyl-, Amyl-, 2-ethyl-, hexyl-	[125]
cy-hexyl-	H_2O, methyl-	[111]
Anisil-, phenethyl-, naphthyl-, benzyl-, *i*-propyl,	H_2O	[42,108]
Benzyl-, *o*-xylyl-, 2-*i* propylnaphthyl-	H_2O	[108]
Methyl-	Methyl, ethyl, *i*-propyl, cy-hexyl-, phenyl-	[175]
Thiophene	Ethyl-	[127]
Ethyl-	Ethyl-	[176]
Ethyl-, phenyl-	Methyl-, ethyl-, *i*-propyl-, n- butyl-	[177]
3,5-di-*tert*-butyl-4-hydroxyphenyl-	Methyl-,ethyl-, *i*-propyl-, n- butyl-	[107,178]
1-Bromonaphthalene; Naphthalene-1,8-diyl	Methyl-	[63,147]
Anisil-, phenyl-	Pyrogallol	[148]
Anisil- (Lawesson reagent)	Resorcinol,hydroquinone	[148]
Ferrocenyl-	1-octyl-, phenyl-, *tri*phenylsilanide	[59]
Anisil- (Lawesson reagent)	Ethyl-, butyl-, 2-butyl-, 3-pentyl-, 1-octyl-, pentyl-	[59]
Benzyl-	Allyl-, ethyl-, adamantyl-, pentyl-, benzyl-	[59]
Anisil- (Lawesson reagent)	(1S,5R,2S)-(-)-menthyl	[168]
Ferrocenyl-	Hydroxymethyl,benzotriazole	[149]
Ferrocenyl-	Ethyl-, *iso*-propyl-, *sec*-butyl-, *i*-butyl-	[151]
Anisil- (Lawesson reagent)	2-(*N*-benzylidenamino)ethyl; 1-(*N*-benzylidenamino)-2-propyl	[152]

R, ([R-P(S)S]$_2$)	R', (R'-OH)	Literature
Ferrocenyl-	Bornyl, myrtenyl, adamantyl	[156]
3,5-di-*tert*-butyl-4-hydroxyphenyl-; Ferrocenyl-	Paracetamol, 4-(1*H*-pyrrol-1yl)phenol	[174]
3,5-di-*tert*-butyl-4-hydroxyphenyl	Thymol	[159]
Ferrocenyl-	2-(3-Thienyl)ethanol	[160]
3,5-di-*tert*-butyl-4-hydroxyphenyl	Paracetamol	[161]
Ferrocenyl-	*i*-Pr-, *tert*-Bu-,Ph-	[162]
Ferrocenyl-	*N*-aryl-pyrrole	[163]
4-phenoxyphenyl; 4-*i*-pentyloxyphenyl	4-(1*H*-pyrrol-1-yl)phenol	[164]
Ferrocenyl-	9H-carbazol-2-ol	[179]
Anisil- (Lawesson reagent)	3-ph-1-propyl	[146]
Ferrocenyl-	3-methyl-1-butyl,1-ph-1-propyl, 3-pentyl, 3-ph-1-propyl	[146]
Anisil- (Lawesson reagent)	1-ph-1-propyl, 3-pentyl, 4-*t*-butylcyhexyl	[167]
Anisil- (Lawesson reagent)	Dimethylaminomethyl-2-naphthol-7-dimethylaminomethyl-	[153]
Phenethyl-	Methyl-, ethyl-, *i*-propyl-,	[154]
Ferrocenyl-	3-benzyloxybenzyl-; 4-n-butylbenzyl-; benzyl-	[155]
Anisil- (Lawesson reagent)	4-*t*-butylbenzyl, diphenyl methanol,	[167]
2-methoxytolyl-	Ethyl- *i*-propyl,	[131]
Ferrocenyl-	4-*t*-cyhexyl , 2-phenyl- 1-propyl	[166]
3-methoxytolyl- Ferrocenyl-	Ethyl-, *i*-propyl,3-pentyl, *i*-butyl, 2-pentyl	[131,166]
1,2-dimethoxybenzene	Methyl-, Ethyl-, *n*-propyl,3-pentyl, 3-methyl-1-butyl-, benzyl-	[132]
1,3-dimethoxybenzene	*i*-butyl, ,n-pentyl, 4-*t*-butylbenzyl,	[133]

2.2.2. Reactions with Alcoholates (DTDP+RO-Na)

Alternative to alcohols in the synthesis of DTPOAs, it is sometimes obtained from the reaction of alcoholate salts (usually sodium salt) with DTDPs (Figure 2.27), [114, 150, 180-182].

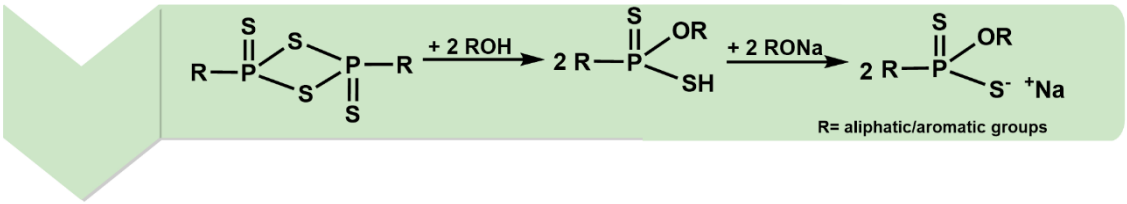


Figure 2.27. General synthesis method of the reaction of DTDPs with alcoholate salts.

The DTPOAs can be formed by the reaction of DTDPs and alcoholate salts from past to present are given in Table 2.8.

Table 2.8. Synthesis of DTPOA from DTDP and alcoholates.

R, ([R-P(S)S]$_2$)	R', (R'-OH)	Literature
Methyl-	*i*-propanol	[180]
Ethyl-	*i*-propanol	[180]
Methyl-	Methyl-*t*-butyl-carbinol	[180]
Methyl-	cy-hexanol	[180]
Anisil- (Lawesson reagent)	Sodium methoxide Sodium n-propoxide	[114]
Ferrocenyl-	Sodium methoxide Sodium n-propoxide	[150]
Ferrocenyl-	Sodium ethoxide	[181]
Anisil- (Lawesson reagent)	Sodium *t*-butoxide	[182]

2.2.3. Reaction with Diols (DTDP+HO-(X)$_n$-OH, X= -CH$_2$-or -Aryl-)

DTDPs react with mono alcohols as well as 1,2-substituted aliphatic diols [98, 158, 183-189], long-chain aliphatic diols (Figure 2.28 A), [98, 158, 174, 185, 188, 190-195], aromatic diols containing aromatic [158, 191, 196] or functional groups (Figure 2.28 B), [158, 194, 196-198] or aryloxy or alkylenoxy dialcohols (Figure 2.28 C), [193, 196-199] to form *bis*-(alkyl/aryl)dithiophosphonic acids.

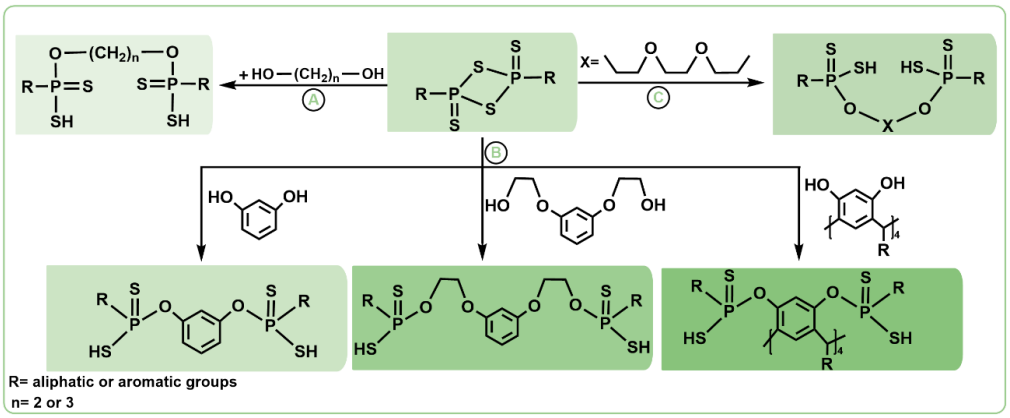


Figure 2.28. Synthesis reaction of *bis*-(alkyl-/aryl-) dithiophosphonic acids.

But when DTDPs are refluxed with alkyl or aryl dithiols in toluene, cyclic heterocyclic compounds are synthesised (Figure 2.29), [200].

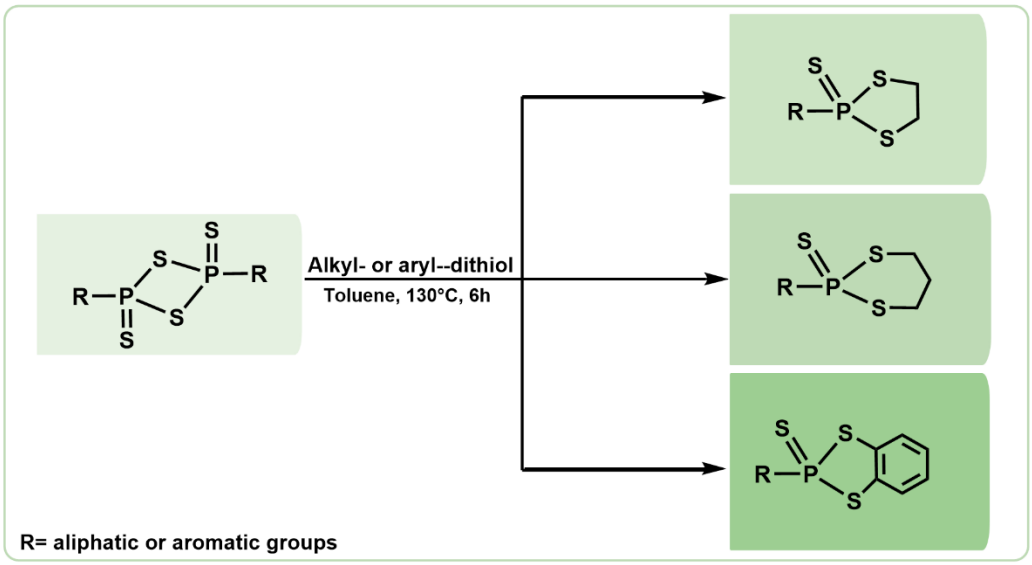


Figure 2.29. Synthesis reactions of cyclic heterocyclic DTPOA derivatives.

Table 2.9. List of ringed heterocyclic DTPOA derivatives.

DTDP	Diol HO-(CH_2)n-OH	Literature
Methyl -	1,2-ethylene glycol 1,2-propylene glycol	[98,190]
Ethyl -	1,2-propylene glycol	[98]
Phenyl -	1,2-ethylene glycol	[98]
n-propyl -	1,2-ethylene glycol 1,2-propylene glycol	[98]
n-butyl -	1,2-ethylene glycol	[98]
cy-hexyl -	1,2-ethylene glycol 1,2-butylene glycol	[98]
i-amyl -	1,2-ethylene glycol	[98]
2-ethylhexyl-	1,2-ethylene glycol	[98]
Lauryl -	1,2-ethylene glycol 1,2-penthylene glycol	[98]
n-octadecyl-	1,2-ethylene glycol	[98]
Benzyl -	1,2-ethylene glycol	[98]

DTDP	Diol HO-(CH_2)n-OH	Literature
2-naphthyl -	1,2-n-hexylene glycol	[98]
Tetrahyronaphthyl -	1,2-ethylene glycol	[98]
4-biphenyl-	1,2-ethylene glycol 1,2-n-hexylene glycol	[98]
Terphenyl-	1,2-ethylene glycol	[98]
Indanyl-	1,2-ethylene glycol	[98]
Phenanthryl-	1,2-ethylene glycol	[98]
1,3-propylene-	1,2-ethylene glycol	[98]
n-dodecylphenyl-	1,2-ethylene glycol	[98]
3,5-xylyl-	1,2-ethylene glycol	[98]
Naphthalene-1,8-diyl-	1,2-ethylene glycol	[63,184]
Anisil- (Lawesson reagent)	1,2-ethanediol	[185]

DTDP	Diol HO-(CH_2)n-OH	Literature
Anisil-Lawesson reagent	Biphenyl-2,2′-diol 1,2-ethylene glycol	[191]
Anisil-Lawesson reagent	1,3-propandiol, 1,5-pentyldiol	[191]
3,5-di-*t*-butyl-4-hydroxyphenyl	(+)-dimethyl L-tartrate	[186]
4-phenoxyphenyl	(+)-dimethyl L-tartrate	[186]
2,4-Di-*t*-butyl-phenol;Ferrocenyl-	(+)-dimethyl L-tartrate	[158]
Ferrocenyl-	1,2-ethanediol *t*-1,2-*cy*-hexanediol	[188]
Phenethyl-	*t*-1,2-*cy*-hexanediol	[158]
2,4-Di-*t*-butylphenol	Thymol	[174]
2,4-Di-*t*-butylphenol	1,2:5,6-di-*O*-*cy*-hexylidene-*D*-mannitol	[189]
Methyl-	1,4-butylene glycol 1,6-hexamethylene glycol	[98,190]
Methyl-	2,2-dimethyl-1,3-propylene glycol	[98]

DTDP	Diol HO-(CH_2)n-OH	Literature
Phenyl-	1,4-butylene glycol 1,6-hexylene glycol	[98]
Lauryl-	1,4-butylene glycol	[98]
n-octadecyl-	1,3-n-pentylene glycol	[98]
n-amyl-	1,6-hexylene glycol	[98]
2-naphthyl-	1,5-pentylene glycol	[98]
4-ethylphenyl-	1,3-propylene glycol	[98]
1,8 naphthyl-	Ethane- 1,2-diols	[183]
Anisil-Lawesson reagent	1,4-butanediol	[192]
Phenethyl, 2,4-Di-*t*-butylphenol	1,4-butylene glycol	[193]
2,4-Di-*t*-butyl-phenol	Resorcinol	[196-198]
Anisil-Lawesson reagent	2-amino ethanol ; 2-(2-aminoethoxy)ethanol	[194]

2.3. DTDP Cyclisation Reactions

2.3.1. Cyclisation Reactions with Diols

The reaction of DTDPs ([R-P(S)S]$_2$ R= 4-methoxyphenyl-, *p*-phenoxyphenyl-) with aliphatic diols at different reaction temperatures and in different molar ratios give alkyl 1,3,2-dioxaphosphorinane-2-sulfide, thioacetamide and ringed aliphatic structures as products (Figure 2.30 A, [191, 201]). From the refluxing of DTDPs with mono or disubstituted aromatic diols (Figure 2.30 B, [62, 191, 202]; Figure 2.30 C, [63, 148, 183]) in a solvent (usually toluene) at a constant temperature, ringed aryldioxaphospholanes are synthesized.

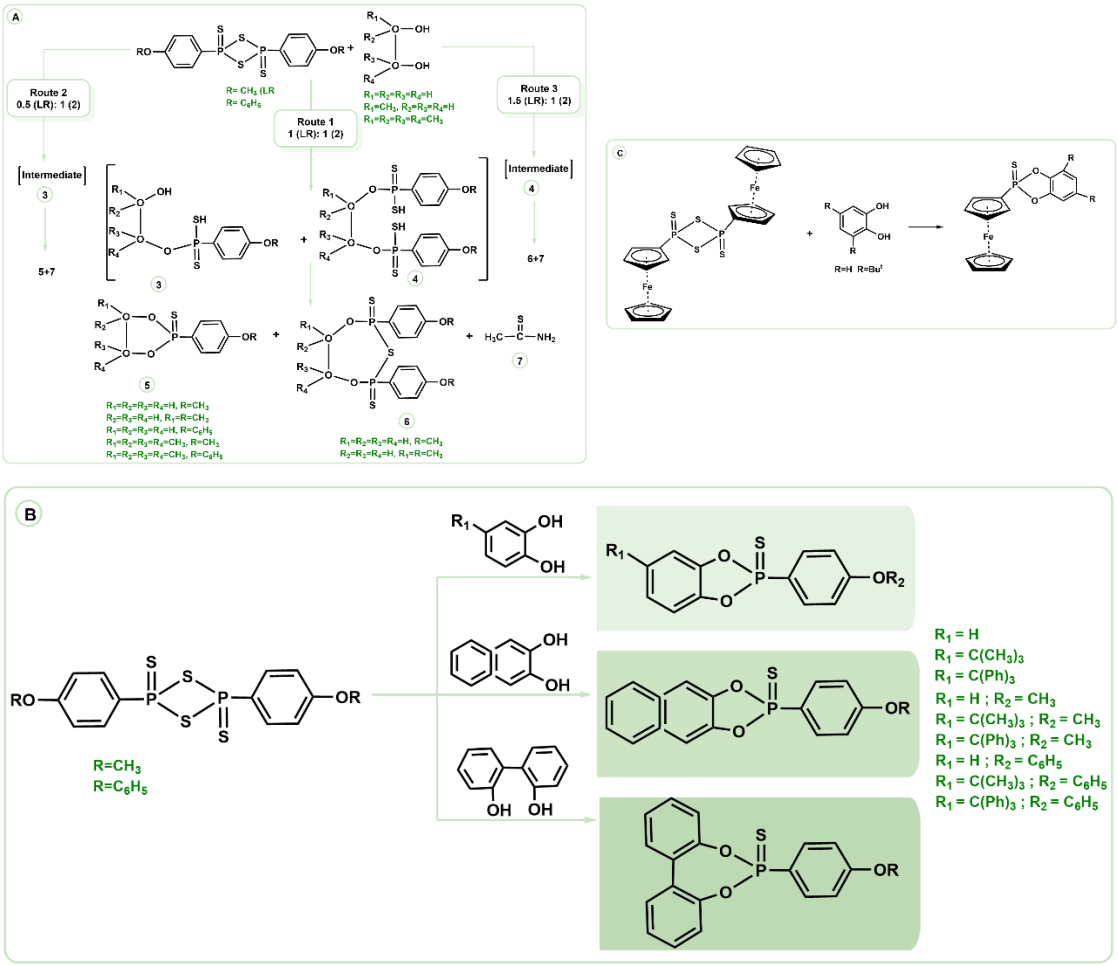


Figure 2.30. Syntheses reactions of cyclic DTPOA derivatives with aromatic or aliphatic diols.

2.3.2. Macro-Cyclisation Reactions

Macrocyclic compounds continue to be investigated in various fields including drug development, materials science, coordination chemistry and supramolecular chemistry [203-215]. Although these compounds are difficult to synthesize, research of these compounds related to antibiotics, immunosuppressants and anticancer continues to increase [206, 216]. Macrocyclic phosphorus 1,1-dithiolates of phosphorus containing two phosphorus atoms and two chalcogen atoms and two oxygen atoms (DTPOA) have been synthesized from the reaction of DTDP with alkyl diols [216] or alkyl dithiols [217] in the presence of dihalogenated alkanes with NaH.

Macrocyclic DTPOAs have also been obtained from the synthesis reaction of alkyl diols with I_2 or $SOCl_2$ in the presence/in the presence of a *tert*-amine of DTDP [218].

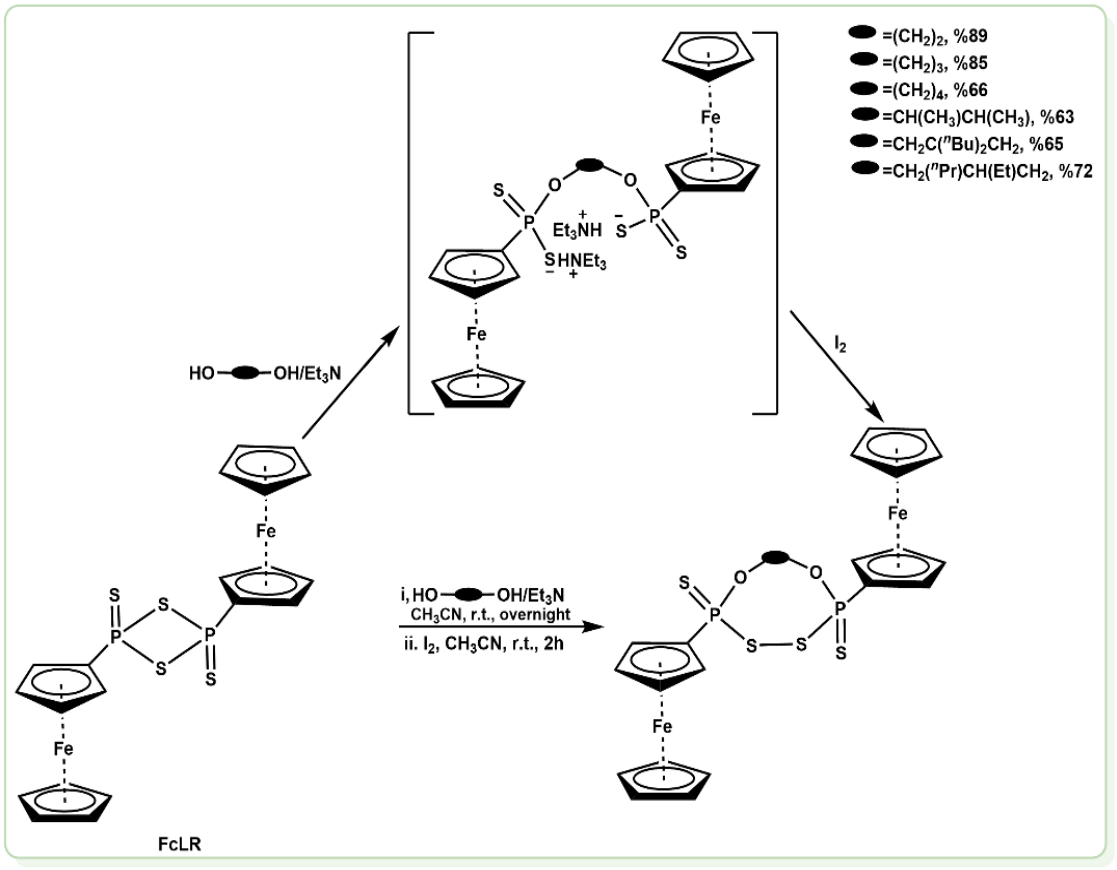


Figure 2.31. Synthesis of eight- to ten-membered heterocyclic DTPOA derivatives from the reaction of [Fc-P(S)S]$_2$ with alkenyl-diols and I_2.

In the case of $SOCl_2$ was added under the same reaction conditions, it was observed that the yield decreased as the size of the ring increased.

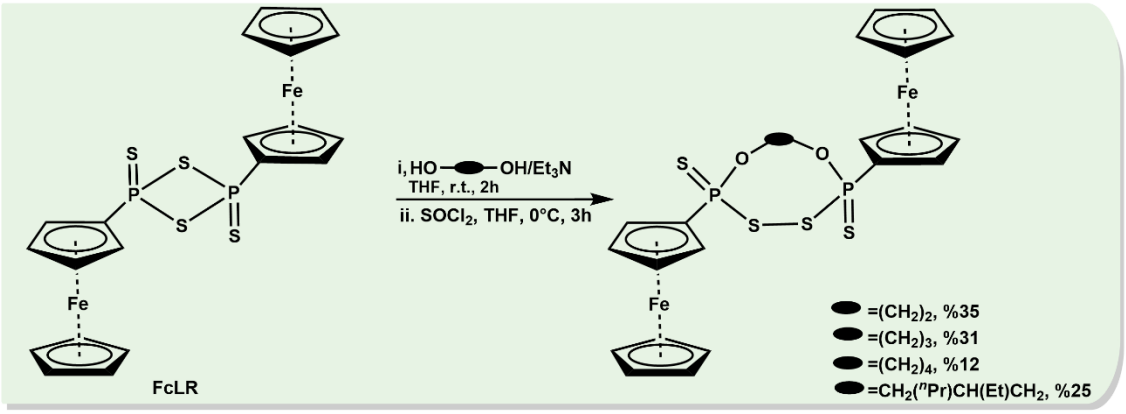


Figure 2.32. Synthesis of ferrocene-containing heterocycles DTPOA from the reaction of [Fc-P(S)S]$_2$ with alkenyl-diols and $SOCl_2$.

Similarly, the reaction of [Fc-P(S)S]$_2$, with an equimolar amount of aryl-diol in the

presence of two equimolar amounts of triethylamine at room temperature, followed by the oxidation using iodine, gave rise to the additional mono-phosphorus species (Figure 2.33).

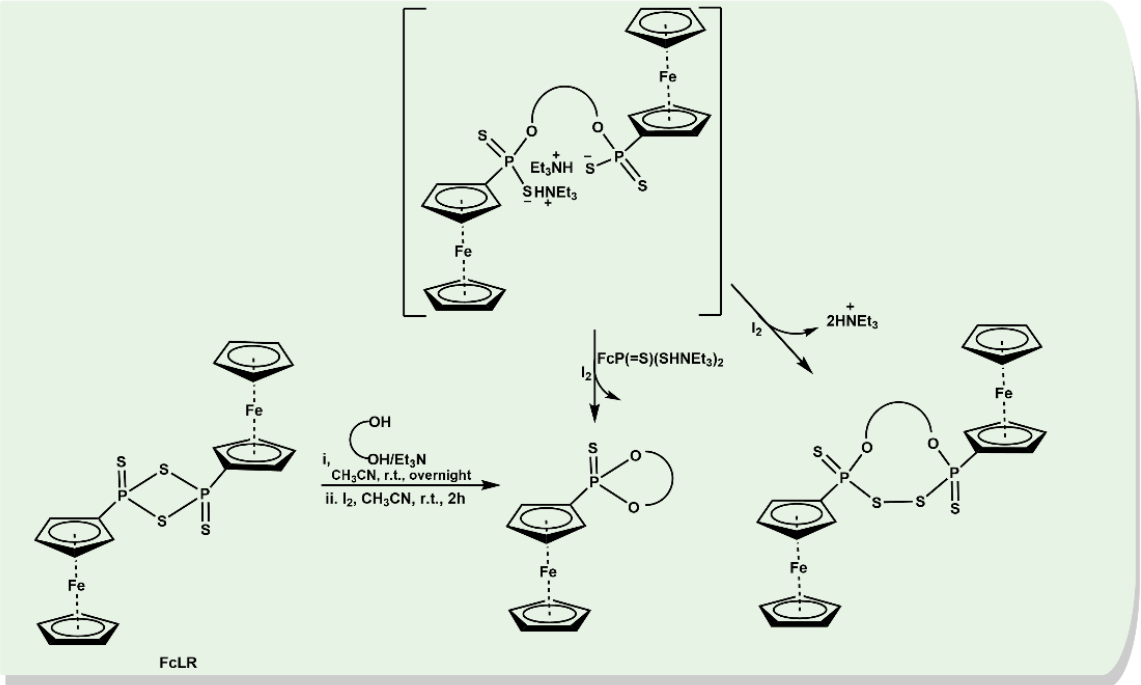


Figure 2.33. Synthesis of mono- and di-phosphorus species from [Fc-P(S)S]$_2$, aryl-diols and I_2 as an one pot synthesis.

Under similar reaction conditions, if but-2-in-1,4-diol was used as the starting material, the diol product was obtained in high yield instead of the ten-membered heterocyclic derivative. The previously synthesised diol product in high yield by iodine oxidation of this compound obtained from the reaction of Ferrocenyl Lawesson reagent with methylate salt [219] is a diastereomer due to its chiral centre.

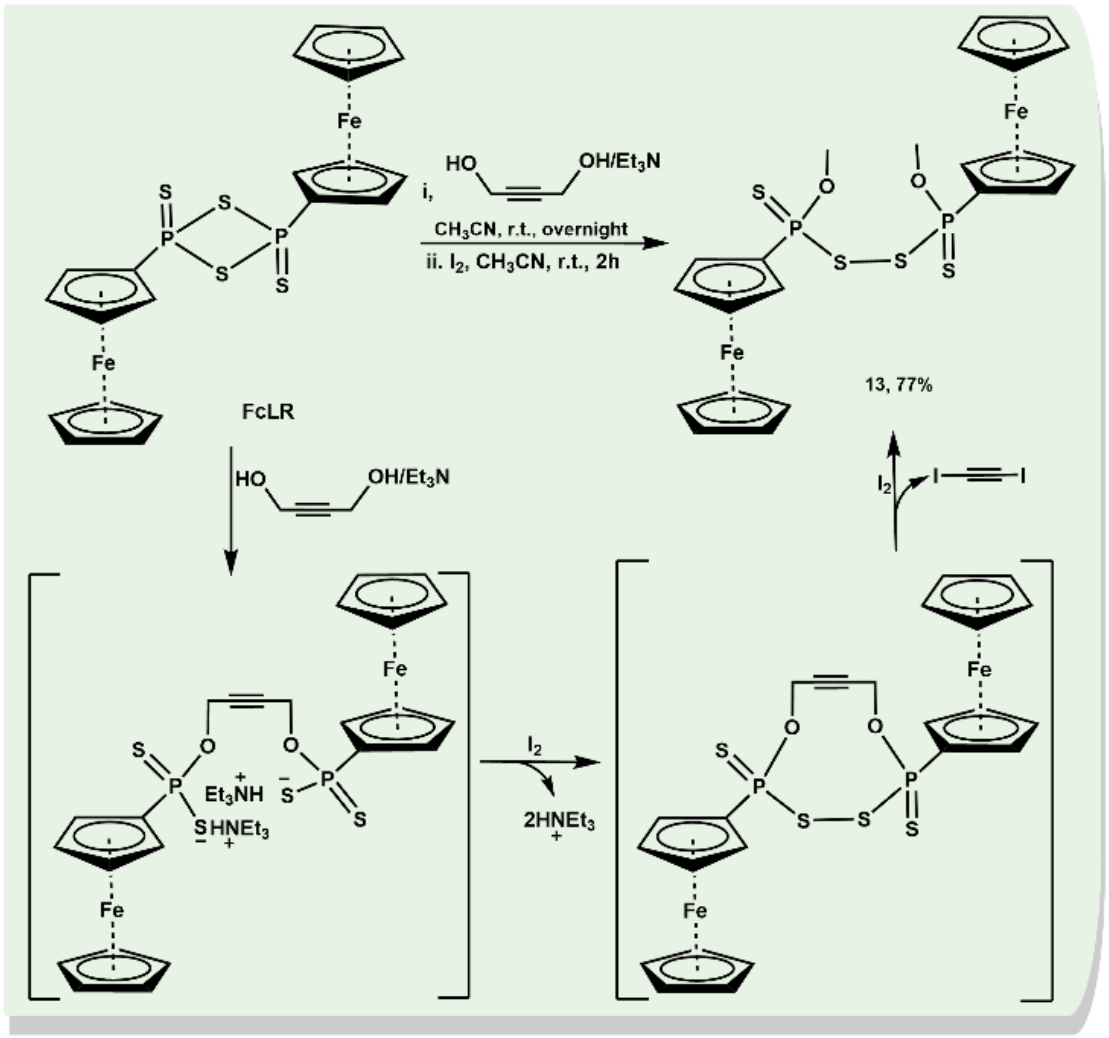


Figure 2.34. Synthesis of non-heterocycle from [Fc-P(S)S]$_2$, but-2-in-1,4-diol and I_2.

Macrocyclic DTPOA derivatives have also been synthesized from the reaction of DTDP with dihalogenated alkanes, alkyl or aryl dithiols [203] in the presence of a *tert*-amine.

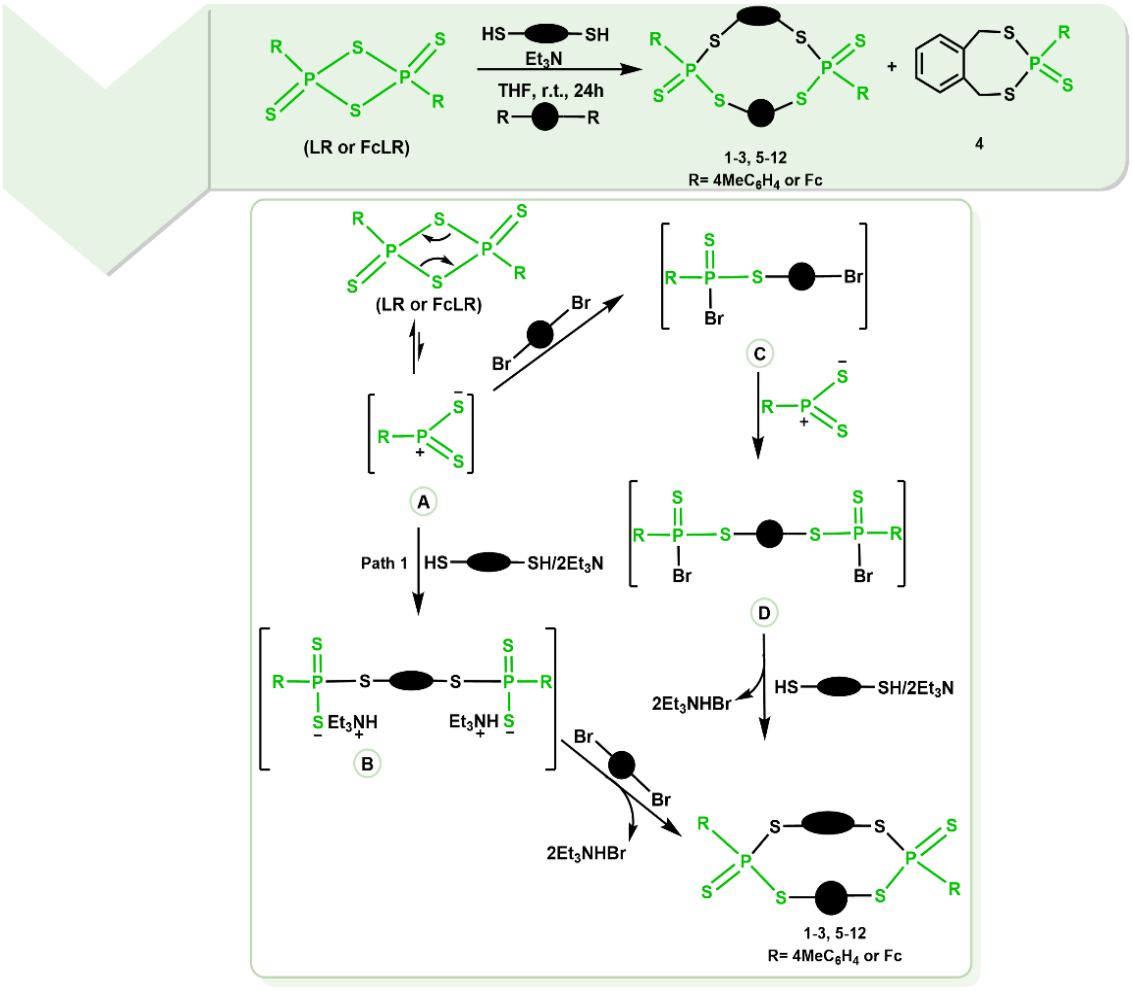


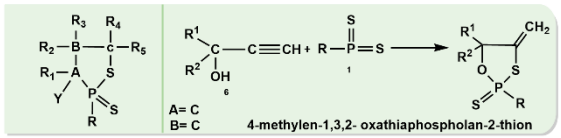
Figure 2.35. Synthesis of sulfur-containing macrocyclic DTPOA derivatives.

2.3.3. Cyclization with Compounds Containing -OH and Substituted Functional Groups

Heterocyclic P-S systems have been of interest in industry for many years due to their use as commercially important additives [220]. These compounds include alkyn alcohols of DTDPs, hydroxy nitriles, amino nitriles, salicylic acid derivative [45], unsaturated ketones (chalcone), hydroxy ketones, benzylanilines [221], pyridinium derivatives (pyridinium phenacylides) [222], phosphines [77], alkyl phosphites, coumarins [223], hydroxy amino benzoic acid derivatives [224], oxa- or thiadiazole derivatives [225], amidoximes [226], aryldianilines [227], thio-phosphorus-containing four-ring [228], from reaction with bifunctional compounds such as cyanamides, carboimides [229, 230], aldehydes [202, 203], naphthol, hydroquinolines [153], oxime derivatives (indanone) [231], ethane 1,2 dione derivative [232], etc. [77, 231, 232], five-ring [45, 77, 221-223,

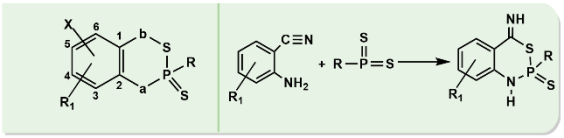
225, 226] or six-ring [45, 77, 153, 221, 224, 227-229, 231, 233] hetero ring structures are found [76].

Table 2.10. List of compounds containing a ringed disubstituted functional group [45].



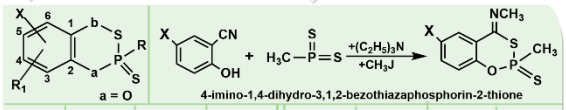
[23]	R	R_2	R_3	R_5
	CH_3	CH_3	CH_3	$=CH_2$
	CH_3	C_2H_5	CH_3	$=CH_2$
	C_2H_5	CH_3	CH_3	$=CH_2$
	C_3H_7	CH_3	CH_3	$=CH_2$
	iso-C_4H_9	CH_3	CH_3	$=CH_2$

[23]	R	R_2	R_3	R_5
	CH_3	$-(CH_2)_5-$		$=CH_2$
	Ph	CH4	CH_3	$=CH_2$
	Ph	$-(CH_2)_5-$		$=CH_2$
	C_3H_7	$-(CH_2)_5-$		$=CH_2$



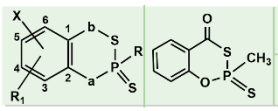
[23]	a	b	R	R_1
	N-H	C=NH	CH_3	H
	N-H	C=NH	*iso*-C_4H_9	H
	N-H	C=NH	Ph	H
	N-H	C=NH	CH_3	6-Cl
	N-H	C=NH	CH_3	6-Cl

[23]	a	b	R	R_1
	N-H	C=NH	C_3H_7	6-Cl
	N-H	C=NH	C_6H_{11}	6-Cl
	N-H	C=NH	Ph-CH_2-	6-Cl
	N-H	C=NH	CH_3	5-CH_3



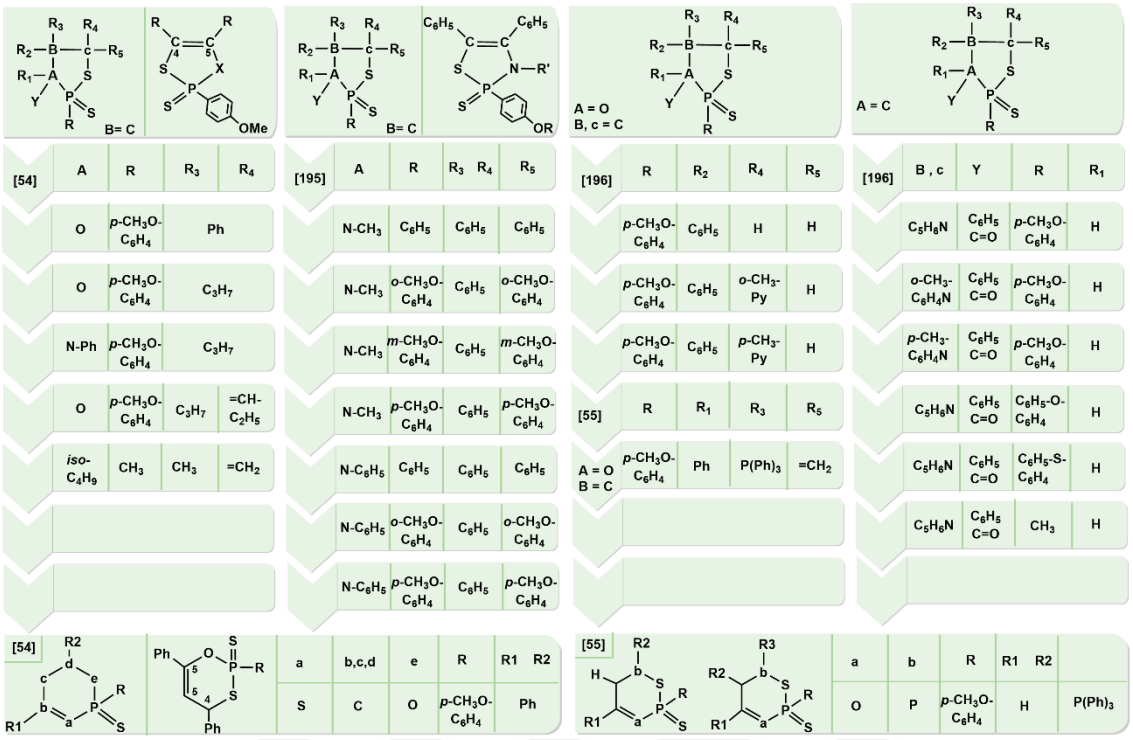
b	X	R	R_1
CH_3 C=NH-	4-CH_3	CH_3	5-CH_3
CH_2-	4-NO_2	CH_3	-

b	X	R	R_1
CH_2-	4-NO_2	C_2H_5	-
CH_2-	4-NO_2	C_4H_9	-



a	b	R	R_1
O	C=O	-	CH_3

Table 2.11. Ringed disubstituted functional groups.



[54]	A	R	R_3	R_4
	O	*p*-CH_3O-C_6H_4	Ph	
	O	*p*-CH_3O-C_6H_4	C_3H_7	
	N-Ph	*p*-CH_3O-C_6H_4	C_3H_7	
	O	*p*-CH_3O-C_6H_4	C_3H_7	=CH-C_2H_5
	iso-C_4H_9	CH_3	CH_3	$=CH_2$

[195]	A	R	R_3 R_4	R_5
	N-CH_3	C_6H_5	C_6H_5	C_6H_5
	N-CH_3	*o*-CH_3O-C_6H_4	C_6H_5	*o*-CH_3O-C_6H_4
	N-CH_3	*m*-CH_3O-C_6H_4	C_6H_5	*m*-CH_3O-C_6H_4
	N-CH_3	*p*-CH_3O-C_6H_4	C_6H_5	*p*-CH_3O-C_6H_4
	N-C_6H_5	C_6H_5	C_6H_5	C_6H_5
	N-C_6H_5	*o*-CH_3O-C_6H_4	C_6H_5	*o*-CH_3O-C_6H_4
	N-C_6H_5	*p*-CH_3O-C_6H_4	C_6H_5	*p*-CH_3O-C_6H_4

[196]	R	R_2	R_4	R_5
	p-CH_3O-C_6H_4	C_6H_5	H	H
	p-CH_3O-C_6H_4	C_6H_5	*o*-CH_3-Py	H
	p-CH_3O-C_6H_4	C_6H_5	*p*-CH_3-Py	H

[55]	R	R_1	R_3	R_5
A = O B = C	*p*-CH_3O-C_6H_4	Ph	$P(Ph)_3$	$=CH_2$

[196]	B , c	Y	R	R_1
	C_5H_6N	C_6H_5 C=O	*p*-CH_3O-C_6H_4	H
	o-CH_3-C_6H_4N	C_6H_5 C=O	*p*-CH_3O-C_6H_4	H
	p-CH_3-C_6H_4N	C_6H_5 C=O	*p*-CH_3O-C_6H_4	H
	C_5H_6N	C_6H_5 C=O	C_6H_5-O-C_6H_4	H
	C_5H_6N	C_6H_5 C=O	C_6H_5-S-C_6H_4	H
	C_5H_6N	C_6H_5 C=O	CH_3	H

[54]	a	b,c,d	e	R	R1 R2
	S	C	O	*p*-CH_3O-C_6H_4	Ph

[55]	a	b	R	R1 R2	
	O	P	*p*-CH_3O-C_6H_4	H	$P(Ph)_3$

2.3.4. Diels Alder Ring Reactions

DTDPs give ring addition reactions (cycloaddition reactions) with unsaturated systems such as dienes [229, 230, 234-236]. The reaction products are four-ring [229, 230, 234-236] or six-ring [229, 230, 234-236] structures containing thio-phosphorus as in compounds containing double functional groups. Cycloaddition reactions take place via Diels-Alder reactions.

2.4. Resonance and Binding Models in Dithiophosphonic Acid Anions

Dithiophosphonic acid anions ($DTPOA^-$) are also known as dithiophosphonate salts, dithiophosphonate or phosphonodithioate ligands, DTPOA phosphorus 1,1-dithiolates. Dithiophosphonic acids (DTPOA) obtained from the nucleophilic reaction of DTDPs with alcohols form complexes with almost all metals in the periodic system in different types and various coordination numbers [237, 238]. The resonance structures are due to the [S-P-S] moiety in the structure of the anion (Figure 2.37.). Namely, the electron charges belonging to the S-P-S moiety in the dithiophosphonate ligand form complexes by single or double bonding to the metal due to the distribution of the negative charge formed by the delocalization of these bonds to the sulfur atoms.

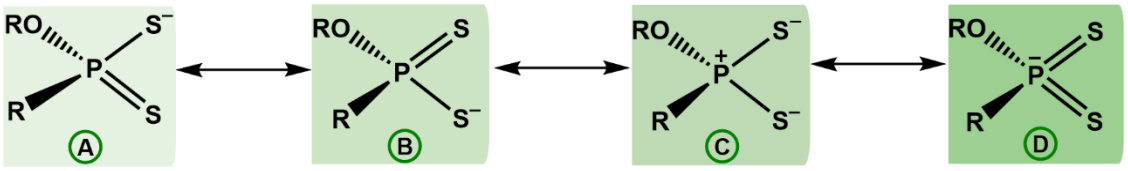


Figure 2.36. Resonance structures of dithiophosphonate ligand**.**

Such a resonance in the ligand allows the formation of monocentric or poly-centric complexes with various types of bonding, based on the structure characteristic of the metal to which it binds. The types of bonding associated with this class of ligands are shown in Figure 2.37. These types of binding are largely related to the property of the Lewis acid (metal ion) to which they are attached [237-239].

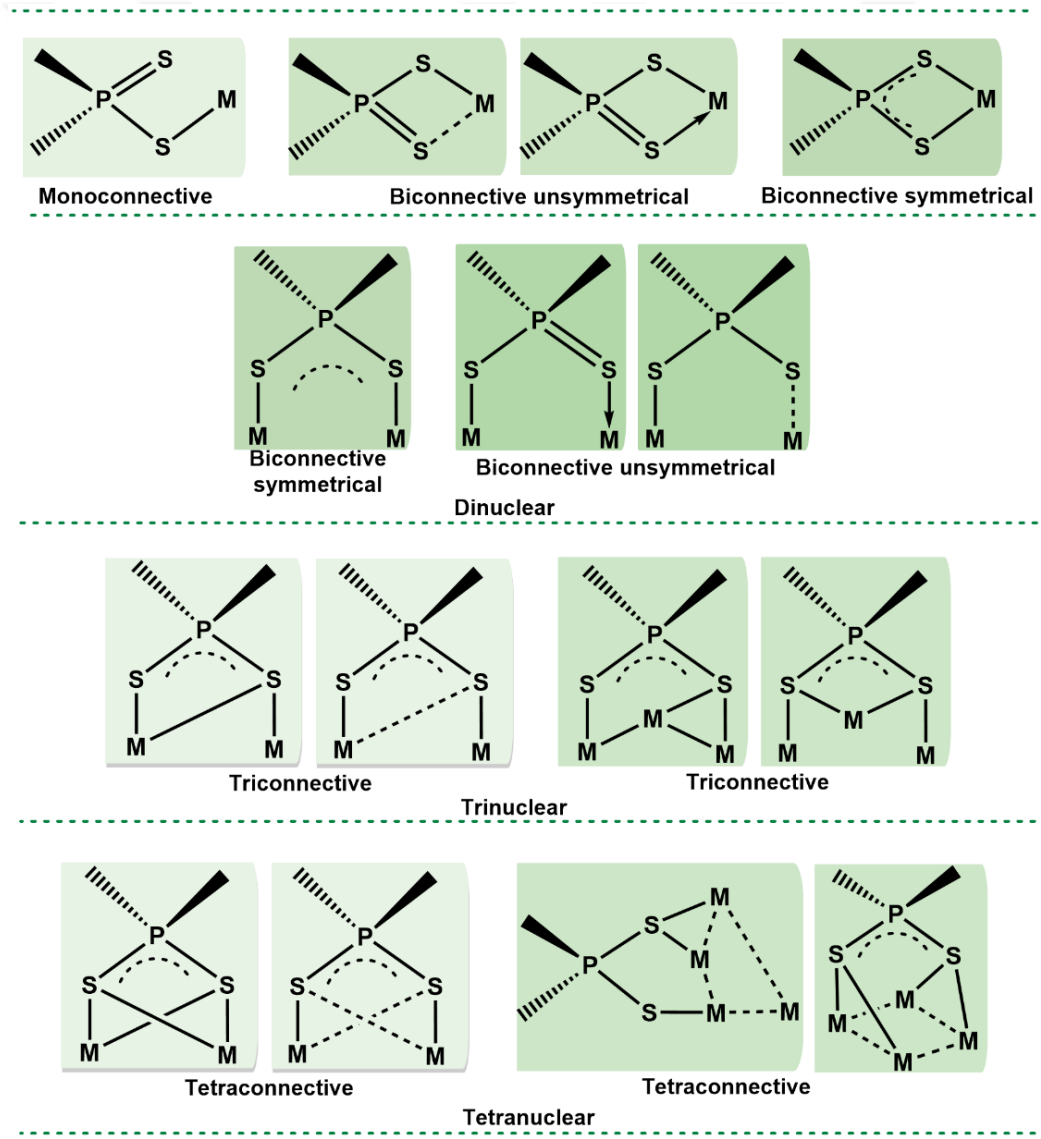


Figure 2.37. Typical binding modes of metal-dithiophosphonates.

When the ligand and metal forming DTPOA complexes are evaluated according to the hard and soft acid-base theory; it helps to explain which binding geometry the resonance of the ligand prefers in the formation of metal complexes. The theory is related to the principle of Lewis acids and bases. In general, the so-called "hard" species are small (when considered in terms of atomic radius), have a large positive charge (mainly applied to positive species called acids) and are not easily polarised [240]. For the so-called "soft" species we can think of the opposite. That is, the species are usually structures with low charge and large atomic radii that are easily polarised. In general, 'hard' acids form stable compounds only with 'hard' bases; soft acids form stable compounds with soft bases [240].

The class of dithiophosphonate ligands are Lewis bases and are generally included in the soft species class. However, they can behave softer or harder according to the property of the Lewis acid (metal ion) to which the ligands are connected by coordination bond. The types of coordinative bonding shown in Figure 2.37 are examples of one-centered single or one-centered double bonding. In two-centered double bonding, electron-donating sulfur atoms can bond with the metal symmetrically or asymmetrically. In P/S type ligands, three-centered triple bonding and four-centered quadruple bonding are also available [238]. Soft double metal-centered complexes such as Hg(II) or Au(I) form coordination according to A and B resonance structures as seen in the Figure 2.36. Only the single bonding system involves the sulfur atom, which retains the character of more double bond to the phosphorus atom and does not undergo coordination. However, the coordination of the other sulfur atom with the metal center is not very common. The harder metals favour the (C) resonance structure, which is the hard base form of dithiophosphonates in the same figure.

In Ni(II)-DTPOA complexes, the sulfur atoms in the ligand are bonded to the nickel atom in the center in the form of two teeth.

2.4.1. Synthesis of DTPOA Complexes

In the synthesis of DTPOA complexes, dithiophosphonic acid is generally converted into ammonium salts. The coordination compound is formed from the reaction of the dithiophosphonate anion and the metal ion in an alcohol solution (Figure 2.38.A). Another method can be synthesized by direct reaction of DTDP, metal salt and alcohol

(alcohol to be used as a ligand) (one-pot synthesis) (Figure 2.38.B) [241].

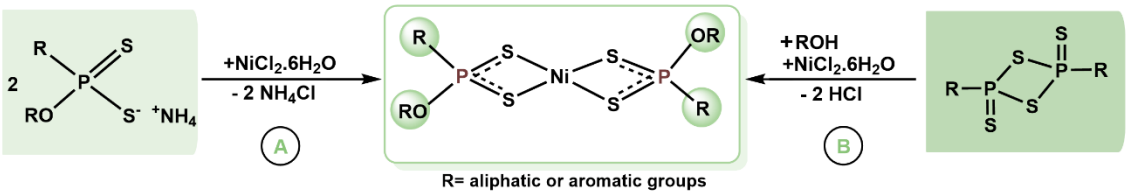


Figure 2.38. Synthesis reaction of metal-DTPOA coordination compound.

In fact, the synthesis of the coordination compound in the latter method is nothing else but the sequential chemical reaction of the crude acid formed by the reaction of DTDP with alcohol in the same solution immediately with the metal ion solution the so-called one-pot synthesis. Experience has shown that if the alcohol is solid, the reaction is carried out in an apolar solvent. This method is also important as a contribution to Green Chemistry [241].

Unusual DTPOA class organometallic derivatives can be prepared by direct reaction of DTDPs with organometallic compounds. In a study carried out in this context, the organometallic compound $[(\eta^5\text{-}C_5H_4R')_2Ti(P(S)SR)_2]$ was synthesized from the direct reaction of the dimer $[R\text{-}P(S)S]_2$ (R= 4-CH_3O-C_6H_4-; C_6H_5-O-C_6H_4) and $[(\eta^5\text{-}C_5H_4R')_2Ti(CO)_2]$ (R'= H, -CH_3) in THF. The same compounds can be prepared with the dimer $[(\eta^5\text{-}C_5H_4R')_2TiCl_2]$ and $LiHBEt_3$. If the reaction rate is slower than the reaction rate of the organometallic compound $[(\eta^5\text{-}C_5H_4R')_2Ti(P(S)SR)_2]$ with the dimer $[R\text{-}P(S)S]_2$ (R= *tert*-Bu-; C_6H_4-CH_2-) and $[(\eta^5\text{-}C_5H_4CH_3)_2Ti(CO)_2]$, the organometallic compound, namely, $[(\eta^5\text{-}C_5H_4CH_3)_2Ti(P(S)_2SR)_2]$ is synthesized [242].

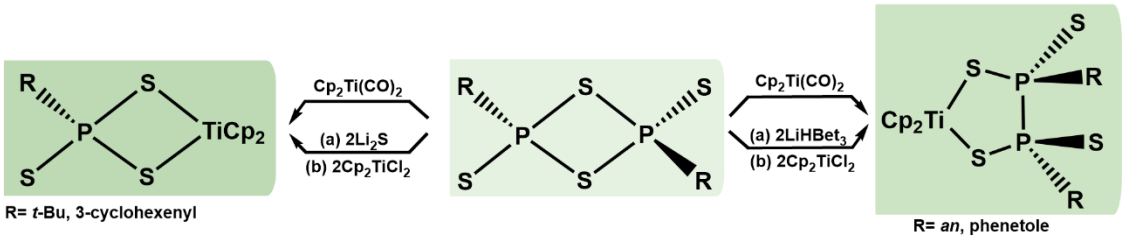


Figure 2.39. Synthesis reaction of organometallic-Ti-DTPOA.

If triethyl- and tri-phenyl(alkylthio)plumbanes that are thio- derivatives react with the dimer under the same reaction conditions, then triethyl- and tri-phenyllead (IV) *S*-(*S*'-alkyl-4-methoxyphenyltrithiophosphonates) organometallic compounds are obtained [243].



Figure 2.40. Synthesis reaction of organometallic-Pb-*O*-alkyl-4-methoxyphenyl DTPOA.

If triethyl- and triphenyl(alkylthio)plumbanes react with the dimer under the same reaction conditions, then triethyl- and triphenyl lead (IV) *S*-(*S*'-alkyl-4-methoxyphenyltrithiophosphonates) organometallic compounds (Figure 2.41) are obtained [243].

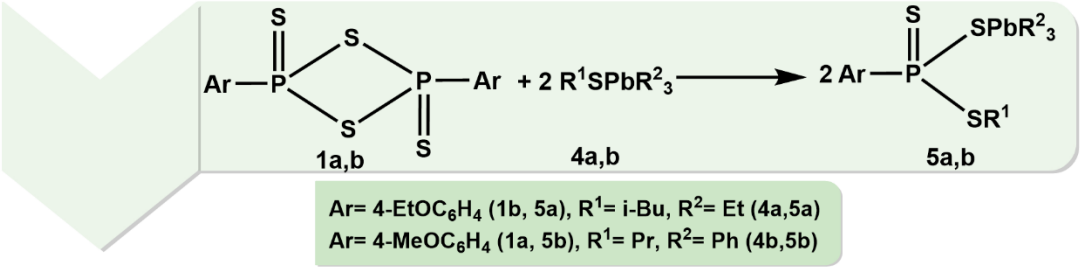


Figure 2.41. Synthesis reaction of organometallic-Pb-*S*-alkyl-4-methoxyphenyl DTPOA.

Organometallic complexes of the type $[M(PR_3)_2(S_2(S)PC_6H_4OMe)]$ were obtained by one-pot synthesis of Lawesson's reagent with phosphine dihalides of Group 10 metals (MCl_2-$(PR_3)_2$, (M= Ni(II), Pd(II) ve Pt(II); R=Ph, Et) in dry and oxygen-free THF [244, 245]. These compounds are quite stable in the solid form in an oxygen-free medium but lose this property in the solution phase, that is unstable (Figure 2.42).

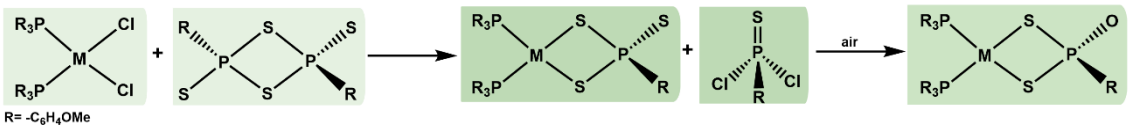


Figure 2.42. $[M(PR_3)_2(S_2(S)PC_6H_4OMe)]$ synthesis reaction (M= Ni(II), Pd(II) ve Pt(II); R=Ph, Et).

The organometallic ferrocenyl dimer $[(\eta^5\text{-}C_5H_5)_2Fe\text{-}P(S)S]_2$ forms DTPOA class organometallic compounds ($[PtCl_2\text{-}(PR_3)_2]$), R= Ethyl-, n-butyl-) with organometallic-Pt derivatives in a similar reaction condition (Figure 2.43), [62].

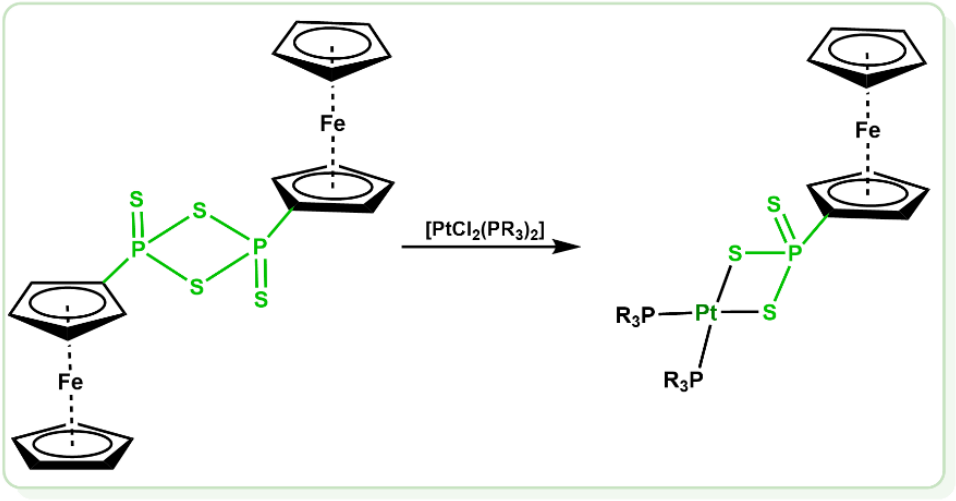


Figure 2.43. Synthesis reaction of $[Pt(PR_3)_2(S_2(S)PC_6H_4OMe)]$, (R= Ethyl-, n-butyl-).

The direct reaction of the dimer $[R\text{-}P(S)S]_2$ (R= 4-CH_3O-C_6H_4-; R'=4-C_2H_5O-C_6H_4-) of trialkylborates, in anhydrous toluene in an ultrasonic bath gives the compound *S*-alkoxyborate-*O*-4-aryl-dithiophosphonate, ($[(R_3O)_2BS\text{-}(S)PR']$), (Figure 2.44). The product is purified by a special distillation method (falling-film distillation) [246].

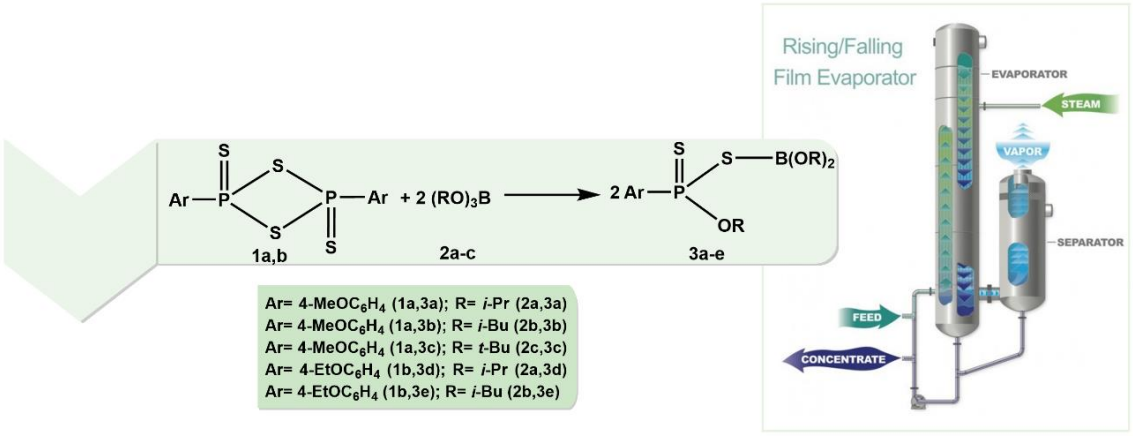


Figure 2.44. $[(R_3O)_2B\text{-}S\text{-}(S)PR']$ synthesis reaction, (R'=4-CH_3O-C_6H_4- and R= *iso*-prop-, *iso*-butyl-; *tert*-butyl-, R'=4-C_2H_5O-C_6H_4 and R= *iso*-Pr-, *iso*-butyl-).

The reaction of 1,2-bis(diphenylphosphino)ethane (dppe) with alkyl silver thiolate in THF with Davy's reagent yielded colourless and highly structurally complex crystals, (Figure 2.45), [247].

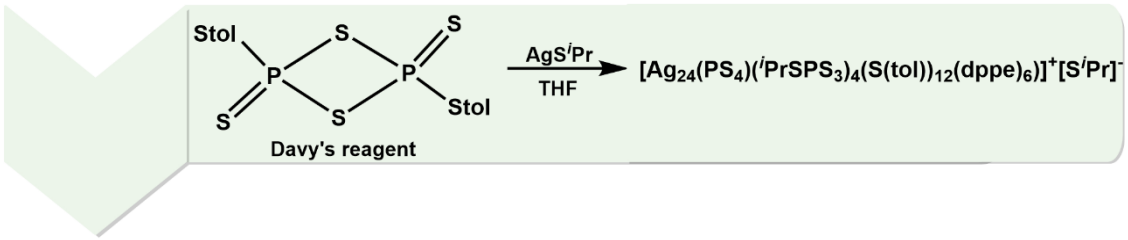


Figure 2.45. $[Ag_{24}(PS_4)(^{i}PrSPS_3)_4S(tol)_{12}(dppe)_6)]^{+}$ $^{-}[S^{iso}Pr]$ synthesis reaction.

Another organometallic complex, $[(\eta^5\text{-}C_5H_5)_2Fe\text{-}P(S)S]_2$ in an alcohol solution of *n*-propyl alchol, is obtained from the reaction of n-propanoxysodium salt and silver salt ($[Ag(PPh_3)_2NO_3]$) (Figure 2.46A and 2.46B). A similar reaction occurs with the salt $[Pd(MeCN)_2Cl_2]$ (Figure 2.46C). The organometallic derivatives obtained in both products also contain a ferrocenyl group; the compound formed gains a heterobimetallic complex feature [248].

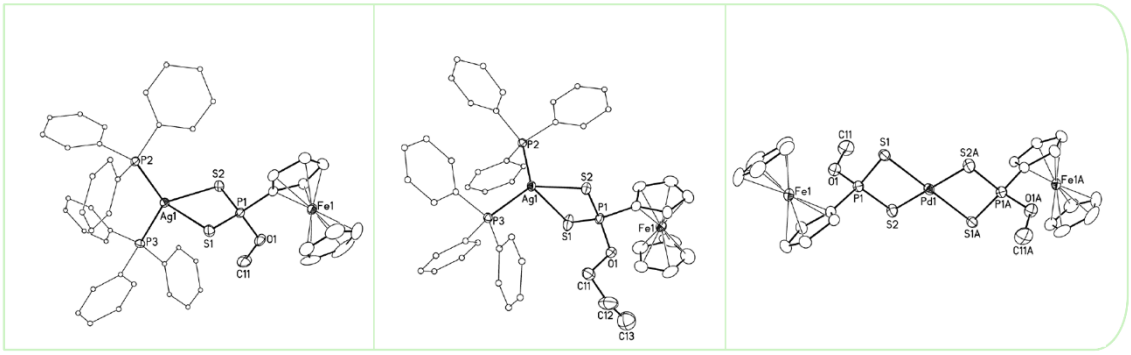


Figure 2.46. Synthesis reaction of $[((\eta^5\text{-}C_5H_5)_2Fe)(RO))P(S)S)M(PPh_3)_2]$, (M=Ag, R= -$OCH_3$, -$OC_3H_7$; M= Pt, R= -$OCH_3$)

These organometallic complexes are all synthesized by a one-pot method. However, coordination compounds of metal salt, DTDP and alcohol in the same medium can also be synthesized.

In addition to the use of DTDPs as starting materials in the synthesis of organo-dithiophosphorus compounds, they also exhibit thiolation properties. In a study carried out for this purpose [249], the Nickel-dithiolene complex was synthesized from the reaction of disubstituted imidazolidine-2-thione-4,5-diones compound with powdered nickel metal or metal salt after thiolation with Lawesson reagent. But, besides this complex, the *trans-bis*[*O*-ethyl(4-methoxyphenyl)phosphonodithioato]-Ni(II) complex was also isolated as a by-product [249]. In that study, complexes with Pd and Pt salts

were also synthesized by the same method.

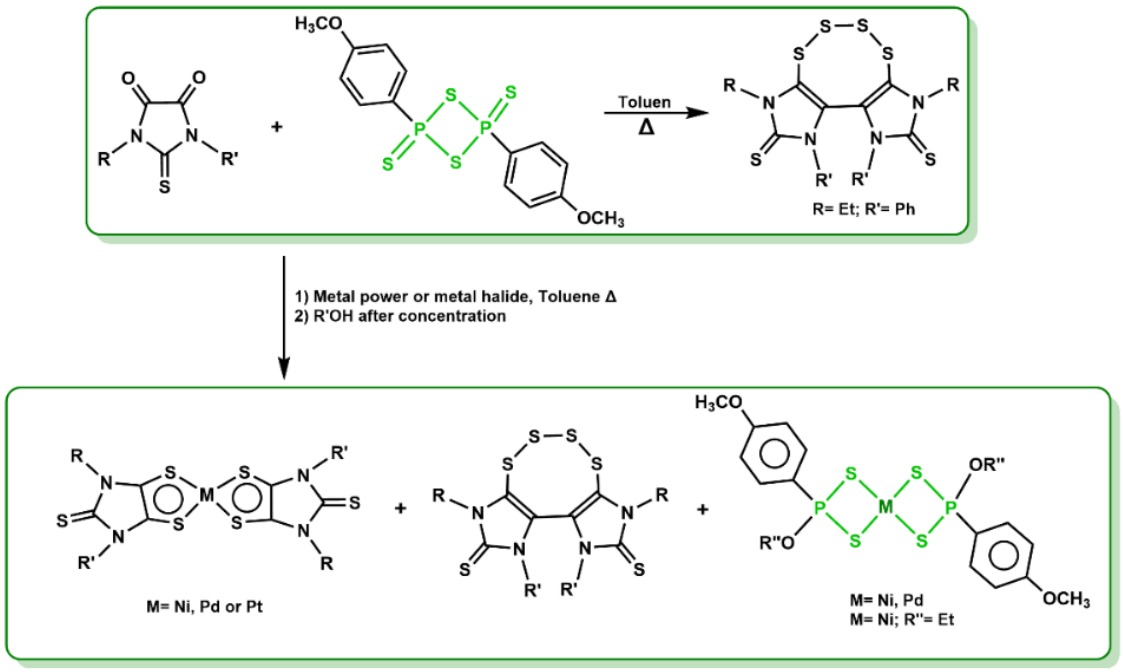


Figure 2.47. Nickel-dithiolene complex together with complex *trans-bis*[*O*-ethyl(4-methoxyphenyl)phosphonodithioato]-Ni(II), which was isolated in a synthesis reaction.

After such study, the DTPOA metal complex was synthesized by first direct reaction of the metal salt ($NiCl_2$, $Co(CH_3COO)_2$) with DTPA and alcohol (methanol) [241].

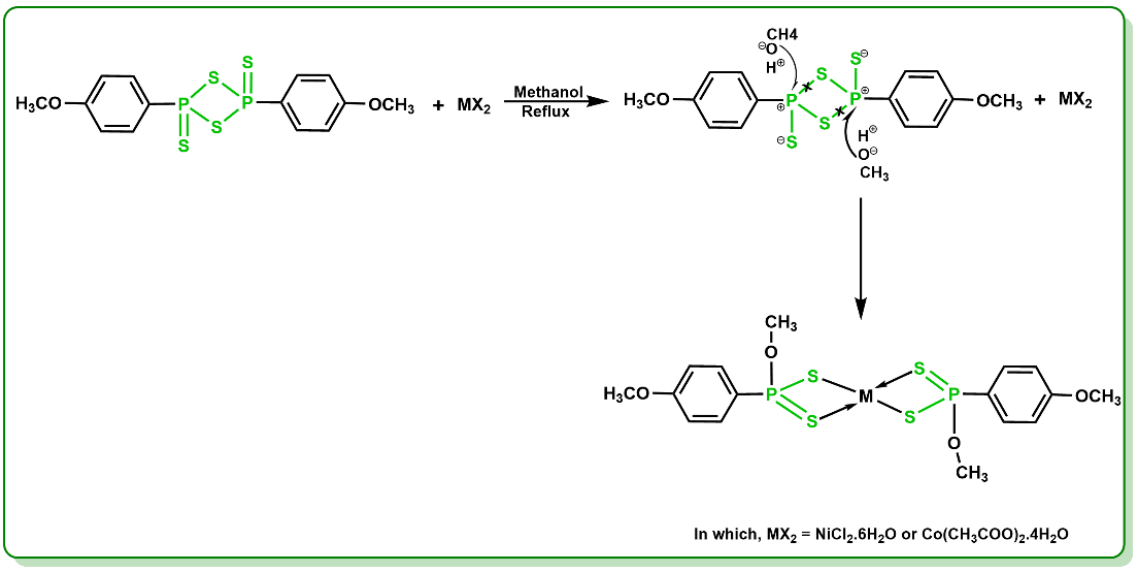


Figure 2.48. Suggested reaction mechanism for the synthesis of DTPOA-Metal complexes by one-pot reaction method.

2.4.2. Synthesis of Nickel DTPOA Complexes

As known, DTPOAs give easy complexes with metals due to the two sulphur atoms in their structure [59]. Ni(II)-DTPOA complexes are the most widely known dithiophosphonate complexes of all the metals in this ligand class [237, 250-252]. The synthesis of the first Ni(II)-DTPOA complex [$Ni(S_2PPh(OEt))_2$] and its crystal structure were published in 1967 [253]. Other Pd(II)- and Pt(II)-DTPOA complexes in the same group as nickel have been synthesized less frequently than Ni-DTPOA complexes [167, 254-257], (Figure 2.49).

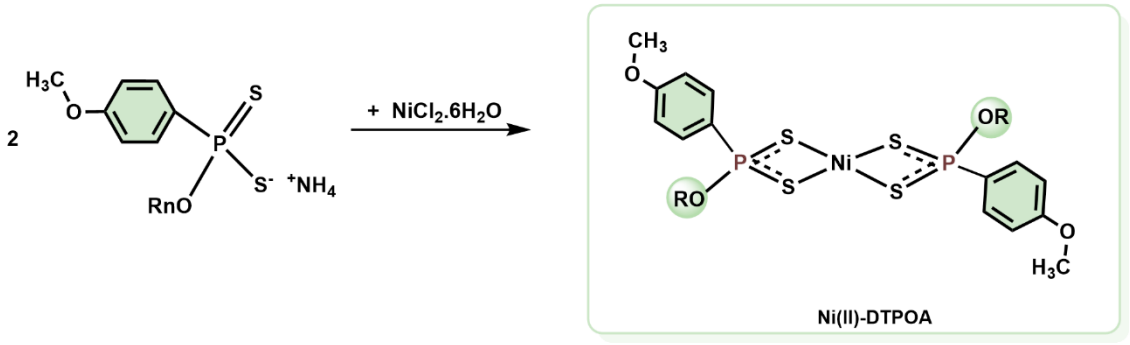


Figure 2.49. Synthesis reaction of Ni(II)-DTPOA complexes.

In general, Ni(II)-DTPOA complexes have a mononuclear and square plane geometry. Ferrocenyl-containing Ni(II)-DTPOA complexes have also been synthesised (Figure 2.50), [237, 241, 258, 259].

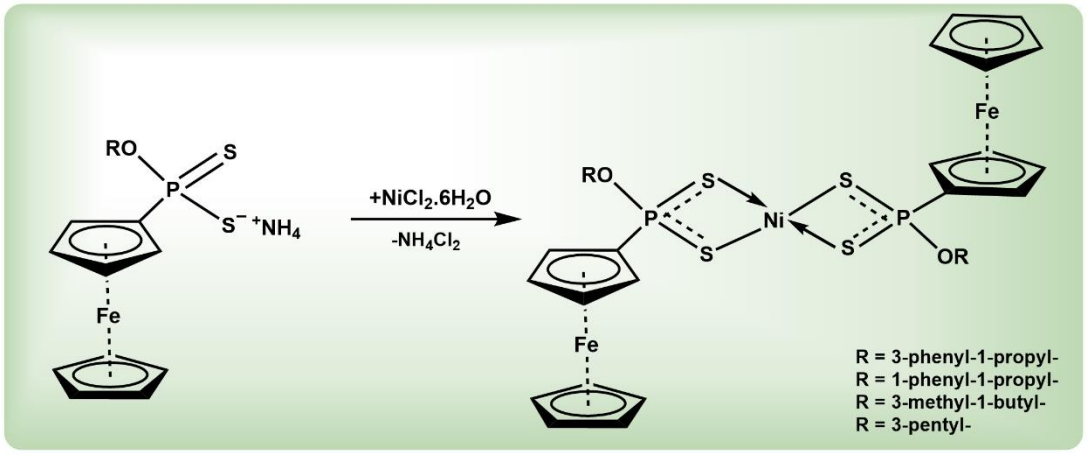


Figure 2.50. Nickel complex of ferrocenyl dithiophosphonic salts.

Macrostructured complexes of nickel-DTPOA complexes have also been designed. Gataulina et al. also synthesized macro-structured four-coordinated, double metal-

centered ring Ni-DTPOA complexes with some great chelating ligands (podand ligands) (Figure 2.51), [150].

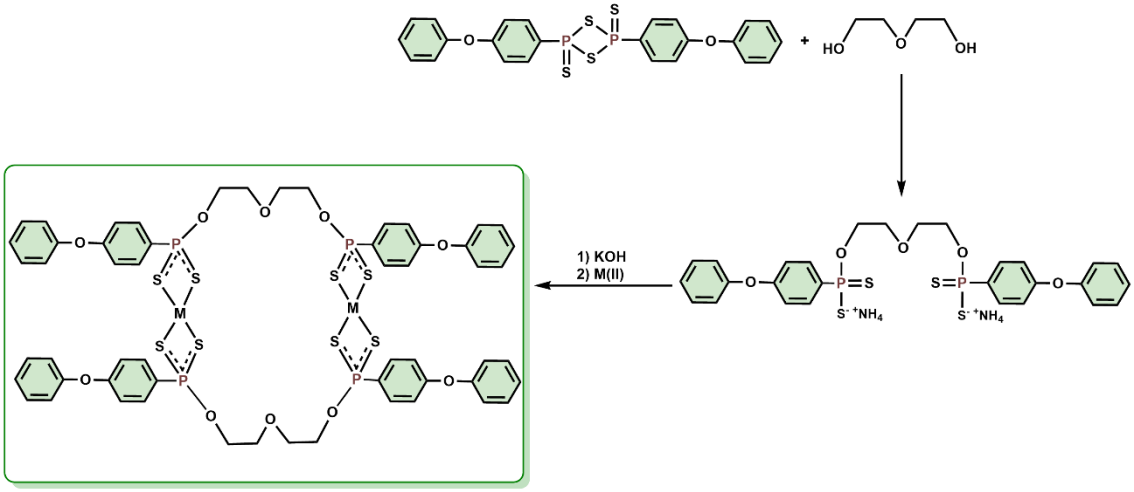


Figure 2.51. Synthesis of Nickel-DTPOA complexes of macro-structured ring complexes.

It is possible to obtain new DTPOA complexes from the reaction of complexes such as the organometallic $[NBu_4]_2[Ni_2(C_6H_5)_4(\mu\text{-}OH)_2]$ complex with DTPOA acids and salts (Figure 2.52), [260].

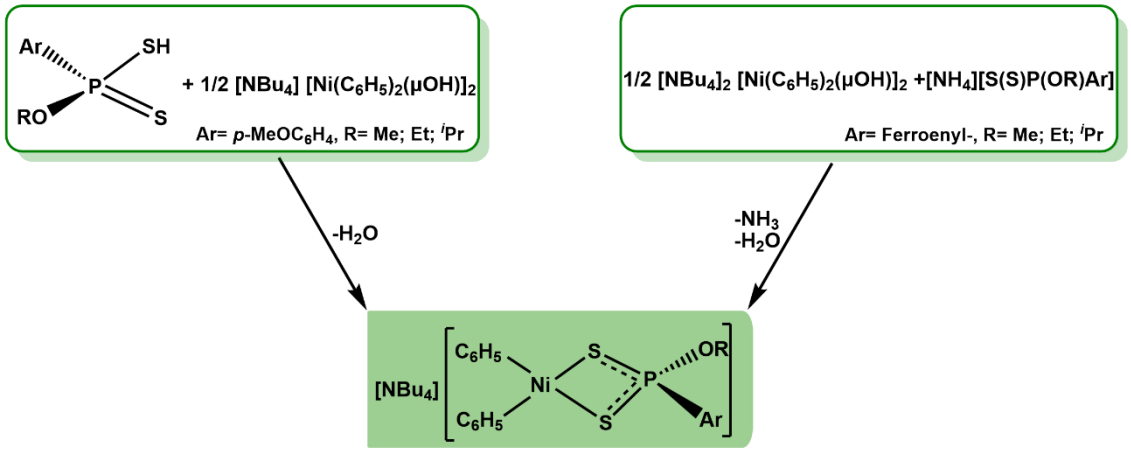


Figure 2.52. Synthesis reaction of $[NBu_4]_2[Ni_2(C_6H_5)_4(\mu\text{-}OH)_2]$ complex.

DTPOAs form complexes with Group 12 elements in two metal-centered ring structures (Figure 2.53.). In this case, in the structure of Zn(II), Cd(II)- or Hg(II)-DTPOA complex; two of the four sulphur atoms are directly bonded to the metal and the other two are bridged to the metal (Figure 2.53), [185, 259, 261-263]

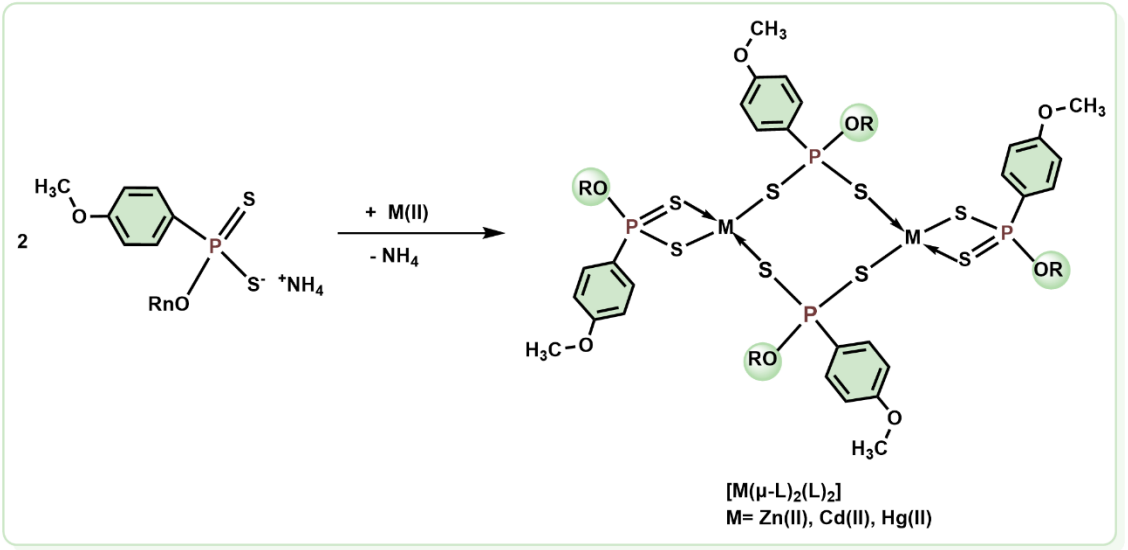


Figure 2.53. Synthesis reaction of Zn(II)-, Cd(II)-, Hg(II)-DTPOA complexes with the two-centered ring.

Square plane nickel(II)-DTPOA complexes in quaternary coordination have unsaturated coordination and have a tendency to transform into a six-coordination structure by increasing their coordination with Lewis bases such as pyridine (Figure 2.54). In this case, the complex transforms from a square plane structure to a smooth octahedral structure (Figure 2.54) [133, 167].

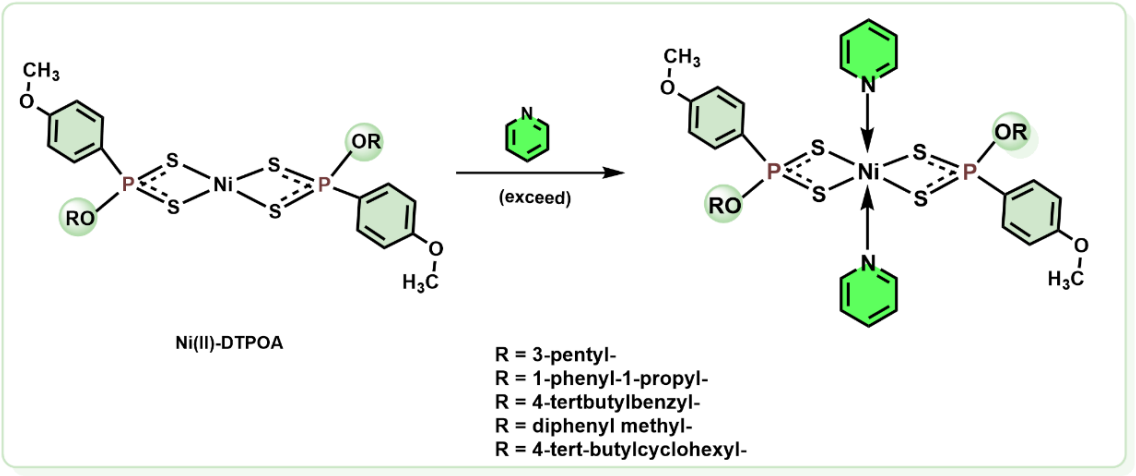


Figure 2.54. Synthesis of six-coordinated DTPOA-Nickel complexes

Another 6-coordinated complex of Ni(II)-DTPOA complex has been synthesized as various types of coordination polymers with various ligands such as pyridinyl-alkyne,

pyridyl tetrazine, bipyridine or pyridinyl-1,4-diamine containing N-donor [264, 265].

Macrostructured complexes of Ni(II)-DTPOA complexes with large Lewis bases such as 2,4,6-tris-2-pyridyl-1,3,5-triazine [266] have also been synthesized (Figure 2.55).

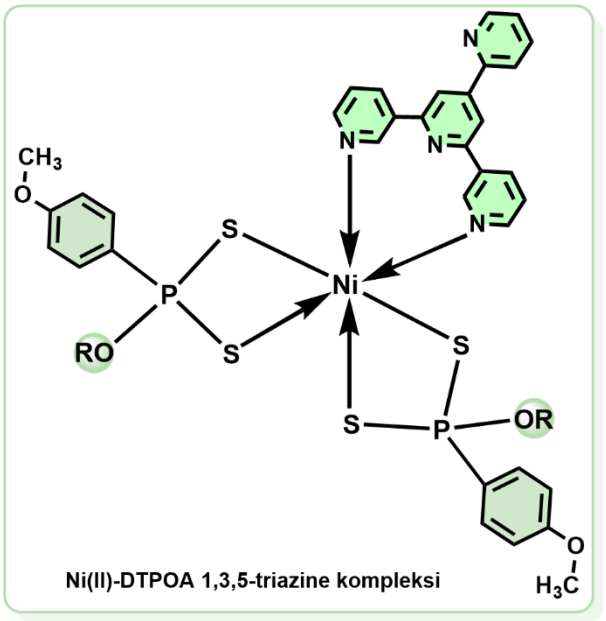


Figure 2.55. Six-coordinated 2,4,6-tris-2-pyridyl-1,3,5-triazine-Ni(II)-DTPOA complex.

Square plane DTPOA complexes of nickel can be in *cis*- or *trans*-isomeric configuration (Figure 2. 56). In complex structures, mostly *trans*-configuration is preferred in terms of stability; however, there are also *cis*- structures [151, 267, 268].

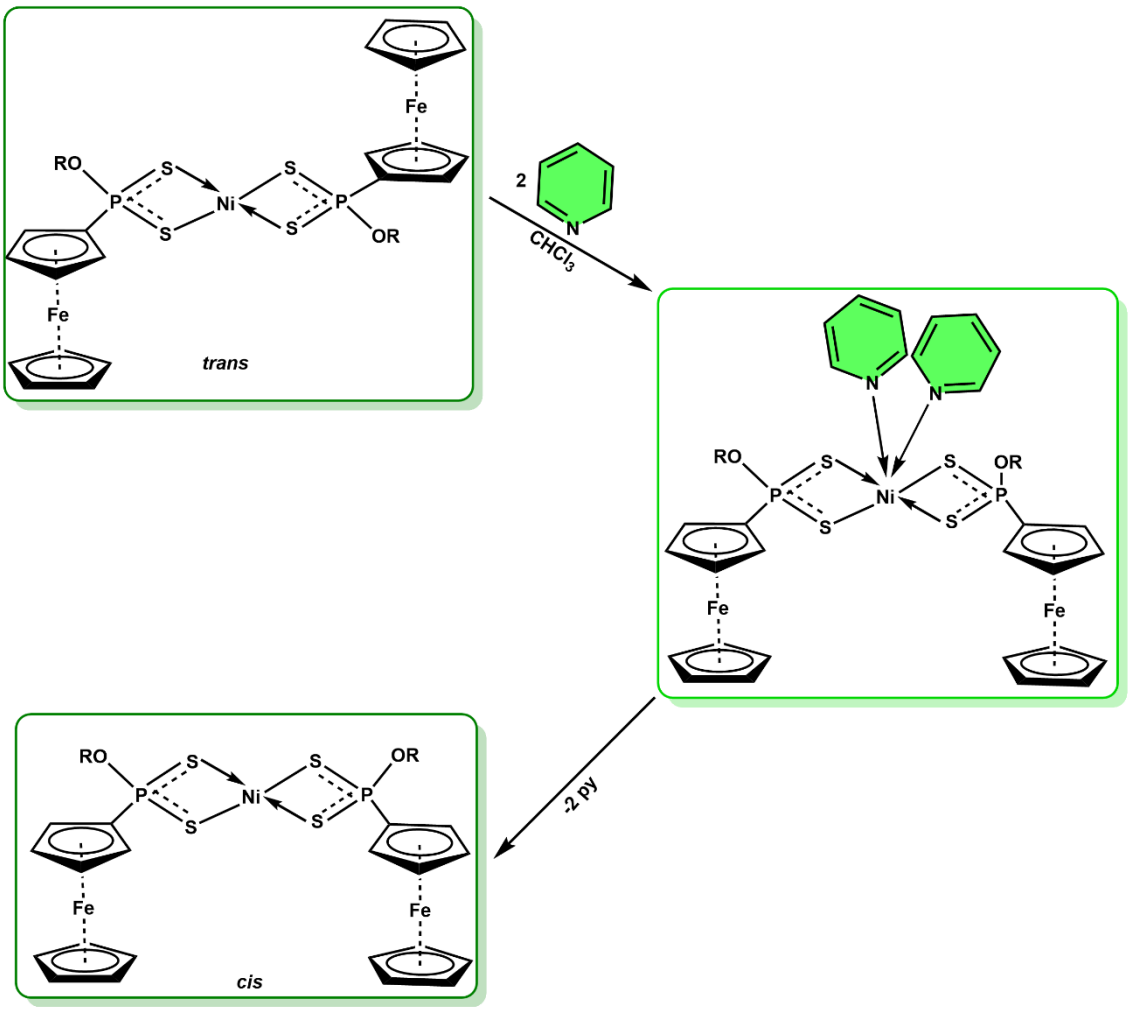


Figure 2. 56. Synthesis reaction of the *cis*-isomer for the square-plane Ni(II)-DTPOA.

3. MATERIAL and METHOD

50 new compounds were synthesized and characterizated by Mass, FT-IR, NMR (^{1}H-, ^{13}C- and ^{31}P-NMR for 1D- and HSQC for 2D) spectroscopies together with elemental analysis in this thesis. Furthermore, the structures of the complexes were elucidated by X-ray diffraction. Along with density functional theory and molecular docking studies as theoretical calculations of the complexes and anticancer studies of the compounds (except for SAV-A1 and SAV-A2) were also carried out as an application.

3.1. Material

3.1.1. Chemical Substances

The chemical compounds and solvents used in the thesis experimental studies are presented in Table 3.1.

Table 3.1. List of chemicals and solvents.

	Compound Name	Supplier	Purity	Density (g/mL)
1	Phosphoruspenta sülfür	Sigma-Aldrich	99%	-
2	1,2-dimethoxy benzene	Across	99%	1.084
3	1,3-dimethoxy benzene	Across	98%	1.055
4	Methanol	Merck	99.8%	0.792
5	Ethanol	Merck	99.8%	0.792
6	n-propanol	Sigma-Aldrich	98%	0.802
7	2-propanol	Sigma-Aldrich	98%	0.785
8	n-butanol	Sigma-Aldrich	98%	0.810
9	2-butanol	Sigma-Aldrich	98%	0.808
10	n-pentanol	Sigma-Aldrich	98%	0.811
11	2-pentanol	Sigma-Aldrich	98%	0.812

	Compound Name	Supplier	Purity	Density (g/mL)
12	3-pentanol	Sigma-Aldrich	98%	0.815
13	3-methyl-1-butanol	Sigma-Aldrich	98%	0.809
14	Benzyl alcohol	Sigma-Aldrich	97%	0.809
15	4-*tert*-butylbenzyl alcohol	Sigma-Aldrich	95%	0.928
16	$NiCl_2.6H_2O$	Merck	99.9%	-
17	Benzene	Sigma-Aldrich	99.5%	0.876
18	Diethyl ether	Sigma-Aldrich	99%	0.713
19	Chloroform	Sigma-Aldrich	99%	1.49
20	Acetic acid	Sigma-Aldrich	99.9%	1.05
21	Ammonia gas	Linde Industrial Gases Türkiye	99.9%	-
22	Argon gas	Linde Industrial Gases Türkiye	99.9%	-

3.2. Instruments

Melting Point

Melting points were measured using an BUCHI-M-560 melting point apparatus with a capillary tube in Marmara University, Science Faculty, Department Chemistry, Inorganic Chemistry Laboratory.

Elemental Analysis Instrument

Microanalyses were performed using a LECO CHNS-932C elemental analyzer in Yozgat Bozok University, Science Faculty, Department Chemistry, Instrumental Analysis Laboratory.

Infrared Spectrophotometer

IR spectral studies were recorded on a Perkin Elmer Spectrum 400 FTIR spectrophotometer (200-4000 cm^{-1}) in Yozgat Bozok University, Science Faculty, Department Chemistry, Instrumental Analysis Laboratory.

NMR Spectrometer

^{1}H (500 MHz), ^{13}C (^{1}H decoupled; 125 MHz) and ^{31}P-NMR (^{1}H decoupled; 202.4 MHz) analyses were done on a Bruker FT spectrometer at 298°K. ^{1}H- and ^{13}C-NMR chemical shifts (δ) are given in ppm and referenced to the internal signal of TMS. 85% H_3PO_4 was used as the external standard for ^{31}P-NMR. D_2O was the solvent of choice for $[NH_4][S_2P(R^{x,y})(ORn)]$ and $CDCl_3$ for $[Ni(S_2P(R^{x,y})(ORn)]$ complexes in Çankırı Karatekin University Research Center. Diagnostic correlations which are based on Hetero Nuclear Single Quantum Coherence (HSQC) experiments were also performed on a Bruker FT spectrometer at 298°K for $[Ni(S_2P(R^{x})(OR6)]$ and $[Ni(S_2P(R^{y})(OR2)]$ in Ankara University Faculty of Pharmacy Central Laboratory.

Mass Spectrometer

The LC/MS system was composed of a Waters Alliance HPLC with a C-18 column and a Waters Micromass ZQ connected to an ESI ionizer in Ankara University Faculty of Pharmacy Central Laboratory.

X-ray Difractometer

X-ray data were obtained with Bruker APEX II QUAZAR three-circle diffractometer.

Indexing was performed using APEX2 [269] in Gebze Technical University. Data integration and reduction were carried out with SAINT [270]. Absorption correction was performed by the multi-scan method implemented in SADABS [271].

3.3. Method

3.3.1. Synthesis of 2,4-*bis*($R^{x,y}$)-1,3,,2,4-dithiadiphosphetane-2,4-disulfides

The new 2,4- *bis*($R^{x,y}$)-1,3,,2,4-dithiadiphosphetane-2,4-disulfide known as dimer was synthesized according to Method 7 [42] as starting material ([$R^{x,y}$-P(S)S]$_2$, R^x =3,4-dimethoxyphenyl-, SAV-A1; R^y= 2,4-dimethoxyphenyl-, SAV-A2). Experiments were carried out by adjusting the parameters such as the temperature at which the experiment should be started, the temperature should remain constant, the mole ratios of the reagents should be well calculated, and the materials used should be dry and away from moisture. The details of the method are mentioned in the section "4. EXPERIMENTAL STUDIES".

3.3.2. Synthesis Method of Dithiophosphonic Acid and Dithiophosphonates; ([$R^{x,y}$(RnO)P(S)SH] and [NH_4][$S_2P(R^{x,y})$(ORn)])

The reaction method of DTDPs with alcohols is preferred by researchers for the synthesis of DTPOAs. Since the crude acid formed at the end of the reaction is malodorous, it is converted into odorless derivatives (salt or complex) [262]. The DTPOAs are an oily and viscous mixture. These acids are converted to ammonium salts and stabilized.

In a nucleophile reaction such as alcohol, DTDPs can be explained as a reaction in which the free electron pair on the oxygen of the alcohol attack electrophilic phosphorus atom. The proton on the alcohol oxygen attacks to one of the sulfides attached to the phosphorus to form DTPOA (Figure 3.1).

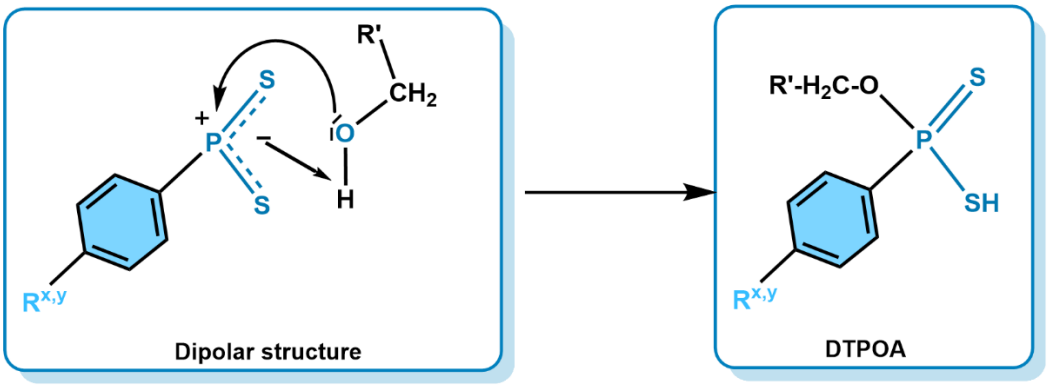


Figure 3.1. The suggested reaction mechanism for the formation of DTPOAs.

From the reaction of SAV-A1 reagent, $[R^x\text{-}P(S)S]_2$, with various alcohols, twelve dithiophosphonic acids of aliphatic and aromatic subsititued were synthesized, ($[R^x(RnO)P(S)SH]$, DTPOA). The synthesis of DTPOA from these alcohols consisted of two parts: Part Ia, synthesis of seven DTPOA from RnOH (R1=methyl-; R2=ethyl-; R3=n-propyl-; R4=n-butyl-; R5=3-pentyl-; R6=3-methyl-1-butyl-; R7=benzyl-). Part Ib includes the synthesis of 5 DTPOA from RnOH alcohols (R1= -n-pentyl; R2=2-pentyl-; R3=4-tert-but-benzyl-; R4=2-propyl-; R5=2-butyl-). By similar reactions, dithiophosphonic acids were synthesized from the reaction of SAV-A2 reagent, $[R^y\text{-}P(S)S]_2$, with four various alcohols, (Part II, $[R^y(RnO)P(S)SH]$, RnOH; R1= 2-butyl-; R2=n-pentyl-; R3=4-tert-but-benzyl-; R4= Methyl-). All of them were prepared according to the method in the literature [250, 254].

These acids were converted to structurally determinable and odorless sixteen ammonium dithiophosphonate salts ($[NH_4][S_2P(R^{x,y})(ORn)]$; Part Ia, Part Ib and Part II). The crude dithiophosphonic acid, ($[R^{x,y}(RnO)P(S)SH]$), was poured into 50-60 mL of benzene. The benzene solution was filtered (filter paper) and cooled to 0°C. Through this solution, dry ammonia gas was bubbled at a rate of 20 mL/min until the precipitation was complete. The white, amorphous precipitate ($[NH_4][S_2P(R^{x,y})(ORn)]$) was filtered (filter paper), washed with benzene and dried in a vacuum desiccator. (Figure 3.2). The details of the method are summarized in the section "4. EXPERIMENTAL STUDIES".

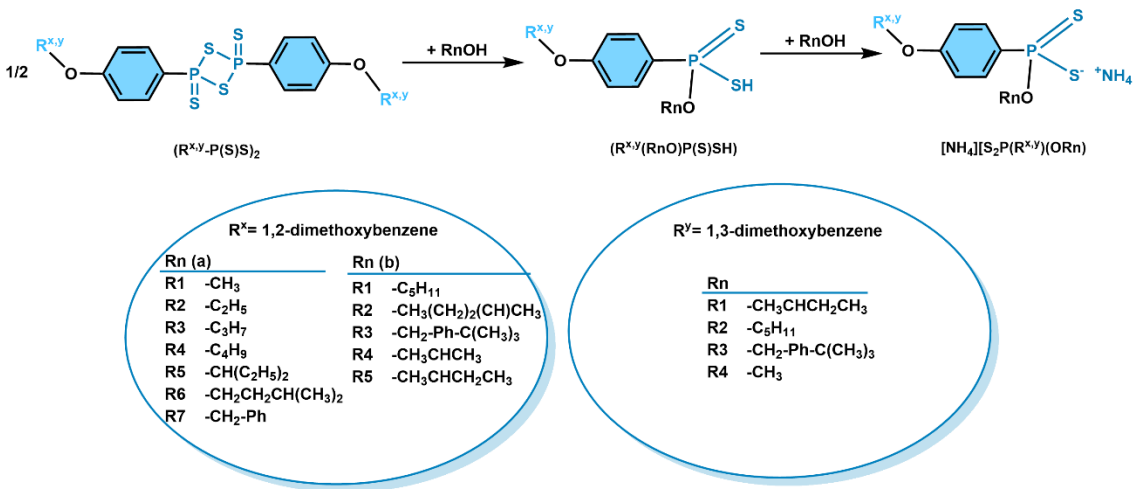


Figure 3.2. Synthesis reactions of $[NH_4][S_2P(R^{x,y})(ORn)]$.

3.3.3. Synthesis Method of Ni(II)-DTPOA, $[Ni(S_2P(R^{x,y})(ORn)]$

In a 100 ml beaker, ammonium-DTPOA salt is taken and dissolved in ethyl alcohol. Stoichiometric amount in another beaker and dissolve $NiCl_2.6H_2O$ in the same solvent. $NiCl_2.6H_2O$ solution is added to dropwise to the dissolved $[NH_4][S_2P(R^{x,y})(ORn)]$. The clear solution turns violet as Ni(II) metal is added dropwise. After turning violet, the mixture is heated for another 5 min, the precipitated complex ($[Ni(S_2P(R^{x,y})(ORn)]$) is filtered and recrystallized (Figure 3.3).

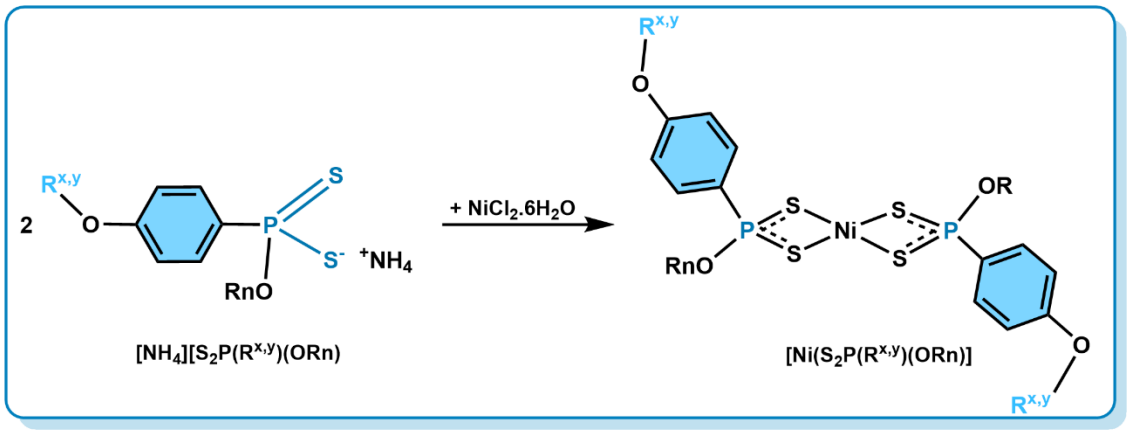


Figure 3.3. Synthesis reaction of Ni(II)-DTPOA complex.

Sixteen new Ni(II) dithiophosphonato complexes which are four-coordinated were synthesized from the reaction of these salts with $NiCl_2.6H_2O$ (seven $[Ni(S_2P(R^x)(ORn)]$ complexes from Part Ia, five $[Ni(S_2P(R^x)(ORn)]$ complexes from Part Ib; four $[Ni(S_2P(R^y)(ORn)]$ complexes from Part II).

Consequently, 50 compounds were synthesized in this study. The details of the method are explained in the section "4. EXPERIMENTAL STUDIES".

3.4. X-ray data collection and structure refinement

As mentioned in the ABSTRACT and 3.3. METHOD sections; since the experimental studies of the thesis consists of three parts, the X-ray structure studies and the theoretical studies also comprise three parts, namely, $[Ni(S_2P(R^x)(ORn))_2]$ (n=1-7) for Part Ia; $[Ni(S_2P(R^x)(ORn))_2]$ (n=1, 2, 4 and 5) for Part Ib and $[Ni(S_2P(R^x)(OR2))_2]$ for Part II. All complexes structures were solved using SHELXT [272] and then refined by full-matrix least-squares refinements on F^2 using the SHELXL [273] in Olex2 Software Package [274]. The positions of all hydrogen atoms which were bonded to carbon were geometrically optimized with the following HFIX instructions in SHELXL: HFIX 137

for the -CH_3 and HFIX 43 for the CH of the aromatic rings. Finally, their displacement parameters were set to isotropic thermal displacements parameters ($U_{iso}(H) = 1.2\times U_{eq}$ for $CH_{aromatic}$ and ($U_{iso}(H) = 1.5\times U_{eq}$ (CH_3 groups). Crystal structure validations and geometrical calculations were performed using Platon software [275]. Mercury software [276] was applied for the cif files visualization. Additional crystallographic data with CCDC reference numbers (2054965 for $[Ni(S_2P(R^x)(OR1))_2]$, 2054966 for $[Ni(S_2P(R^x)(OR2))_2]$, 2104693 for $[Ni(S_2P(R^x)(OR3))_2]$, 2054967 for $[Ni(S_2P(R^x)(OR4))_2]$, 2018565 for $[Ni(S_2P(R^x)(OR5))_2]$, 2097183 for $[Ni(S_2P(R^x)(OR6))_2]$ and 2061755 for $[Ni(S_2P(R^x)(OR7))_2]$ for Part Ia, 2176951 for $[Ni(S_2P(R^x)(OR1))_2]$, 2218375 for $[Ni(S_2P(R^x)(OR2))_2]$, 2254587 for $[Ni(S_2P(R^x)(OR4))_2]$ and 2254588 for $[Ni(S_2P(R^x)(OR5))_2]$ for Part Ib and 2054970 for $[Ni(S_2P(R^y)(OR2))_2]$ Part II have been deposited within the Cambridge Crystallographic Data Center via www.ccdc.cam.ac.uk/deposit. The crystallographic data and structure refinement parameters are listed in Tables (Table 5.11 for Part Ia; Table 5.14 for Part Ib and Table 5.27 for Part II).

When its come to Hirshfeld Surface (HS) Analysis; in order to get a better insight into the intermolecular interactions in $[Ni(S_2P(R^x)(ORn))_2]$ (n=1-7) for Part Ia, $[Ni(S_2P(R^x)(ORn))_2]$ (n=1, 2, 4 and 5) for Part Ib and $[Ni(S_2P(R^y)(OR2))_2]$ for Part II Hirshfeld surfaces (HS) [277] incorporating two-dimensional (2D) fingerprint plots [278] using Crystal Explorer [279] program was used. The normalized contact distance (d_{norm}) surface, which is expressed in terms of distances to the surface from the nuclei inside and outside the HS (d_i, and d_e, respectively) and the vdW radii of the atoms, defined as Eq. 1 gives identification of the regions of particular importance to intermolecular interactions [280, 281]. The 2D fingerprint plots, which were derived from the combination of d_i, and d_e, were used for quantifying the intermolecular contacts in the crystal.

$$d_{norm} = \frac{d_i - r_i^{vdw}}{r_i^{vdw}} + \frac{d_e - r_e^{vdw}}{r_e^{vdw}} \qquad \text{Equation (1)}$$

3.5. Computational Methods

3.5.1. DFT calculations

The quantum mechanical DFT calculations of the Ni(II) dithiophosphonato complexes (($[Ni(S_2P(R^x)(ORn))_2]$ (n=1-7) for Part Ia, $[Ni(S_2P(R^x)(OR1))_2]$, $[Ni(S_2P(R^x)(OR2))_2]$,

[$Ni(S_2P(R^x)(OR4))_2$] and [$Ni(S_2P(R^x)(OR5))_2$] for Part Ib and [$Ni(S_2P(R^y)(OR2))_2$] for Part II) were performed by the Gaussian 09 software package and the Gauss-view visualization program [282, 283]. The X-ray diffraction experimental data of the complexes were used to prepare the input file for the geometry in Gaussian. The complexes were optimized at B3LYP/LANL2DZ/6-31+G(d,p) level in ground state [284-286] is used in DFT calculation to predict the geometry optimizations, total energies, HOMO and LUMO orbitals and MEP surfaces of the compounds.

3.5.2. Molecular Docking Calculations

The molecular docking calculations of the Ni(II) complexes ([$Ni(S_2P(R^x)(ORn))_2$] (n=1-7) for Part Ia, [$Ni(S_2P(R^x)(ORn))_2$] (n=1-2, 4-5) for Part Ib and [$Ni(S_2P(R^y)(OR2))_2$]for Part II) with liver cancer protein, PDB ID: 3WZE and colon cancer antigen proteins, ID 2HQ6 to predict the interaction mechanism were performed by using AutoDock-Vina software [287]. 3D molecular structures of the liver cancer protein, PDB ID: 3WZE and colon cancer antigen proteins, ID 2HQ6 were obtained from Protein Data Bank (PDB). All residues were removed and then polar hydrogens were added to produce favorable protonation states for molecular docking using Discover Studio Visualizer 4.0 software [288]. AutoDockTools (ADT) were used for creating docking data entry files [289]. ADT was performed to add partial charges using the Geistener method and to define torsions and rotatable bonds. The active sites of the proteins were defined to include residues of the active site within the grid size of 30×30×30 Å. To evaluate the quality of docking results, it is common to calculate the Root Mean Square Deviation (RMSD) between the docked pose and the known crystal structure confirmation. Docking results are acceptable when the RMSD value is lower than 2 Å [290]. At the same time, between molecular docking executions were performed, the most favorable ones being represented by the lowest free-bond energy (ΔG) [291]. The interactions figures were drafted using Discover Studio Visualizer 4.0 software [292].

3.6. *In vitro* cytotoxic activity studies

Human liver hepatocellular carcinoma cell line (HepG2) (ATCC® HB-8065™) and human colon cancer cell line (DLD-1) (ATCC® CCL-221™) were purchased from American Type Culture Collection (ATCC, USA). Dulbecco's modified eagle's medium-high glucose (DMEM), fetal bovine serum (FBS), 3-(4,5-dimethylthiazol-2-yl)-2,5-

diphenyl tetrazolium bromide (MTT), phosphate-buffered saline (PBS) and pentahydrate (*bis*-benzimide) for the cell culture studies were purchased.

The cytotoxic activity studies were done according to the literature procedures [293, 294]. The HepG2 and DLD-1 cells were seeded into sterile 96-well plates at a density of 5 x 10^3 cells/well. After 24 h, cells were exposed to compounds at six different concentrations for 48 h. After this period was completed, 5 mg/mL of MTT stock solution was added to each well, and plates were incubated for 2 h. The measure of absorbance values was done using the Promega plate reader device at 560 nm. IC_{50} values were calculated using GraphPad Prism software 5.

4. EXPERIMENTAL STUDIES

This section is of three parts (Part Ia, Part Ib and Part II) as presented in the section "1. INTRODUCTION", ABSTRACT and pictured Figure 1.3. - Figure 1.6.

4.1. Part I. Synthesis of novel 2,4-*bis*(R^x)-1,3,2,4-dithiadiphosphetane-2,4-disulfide ([R^x-P(S)S]$_2$, R^x= 3,4-dimethoxyphenyl-, SAV-A1)

A 4.00 g (8.99 mmol) sample of P_4S_{10} was put into a three-neck flask and the flask was heated to 120°C in an oil bath with constant stirring by a magnet. Onto this material, 1,2-dimethoxy benzene (4.97 g, 35.96 mmol) was added drop-wise from a funnel (1-2 drops/second). One-batch addition of 1,2-dimethoxybenzene proved to be much less effective. An inert atmosphere was provided by bubbling Ar gas through one of the necks. A tap-water reflux was connected to avoid evaporation. A liquid product with pale-yellow colour was obtained in about one hour. After keeping at the same temperature for another two hours, the mixture was left cooling with the inert atmosphere in the place. A solid product formed. The solid was filtered; washed with diethyl ether and kept in a desiccator under an inert atmosphere. The product was stable at room temperature as such but turns into a pale-yellow gel if gets in touch with open air (Figure 4.1), [132].

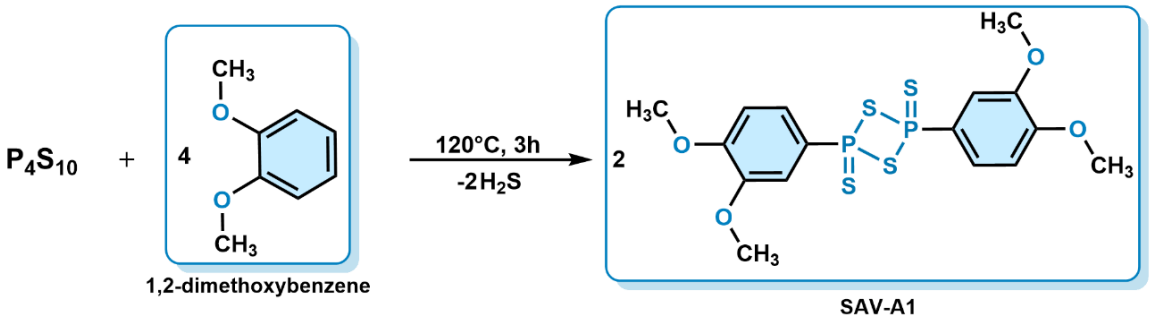


Figure 4.1. SAV-A1 synthesis reaction.

4.1.1. General Procedure of dithiophosphonic acids and the ammonium dithiophosphonates salts for Part Ia

4.30 mmol (2.00 g) of the SAV-A1 reagent was taken into a three-necked flask, and onto it, an 8.60 mmol of one of the alcohols (0.28 g of methanol; 0.40 g of ethanol; 0.52 g of n-propanol; 0.64 g of n-butanol; 0.76 g of 3-pentanol; 0.76 g of 3-methyl-1-butanol; 0.93 g of benzyl alcohol) was added dropwise. The mixture was heated to 50-60°C, kept at this temperature range until complete dissolution and then left aside to cool. The crude

dithiophosphonic acid ([R^x(RnO)P(S)SH]) an oily, viscous mixture), was poured into 50-60 mL of benzene. The benzene solution was filtered (filter paper) and was cooled to 0°C. Through this solution, dry ammonia gas was bubbled at a rate of 20 mL/min until the precipitation was complete. The white, amorphous ammonium dithiophosphonates ([NH_4][$S_2P(R^x)$(ORn)]), was filtered (filter paper), washed with benzene and dried in a vacuum desiccator.

4.1.2. General Procedure of dithiophosphonic acids and the ammonium salts dithiophosphonates for Part Ib

To 4.30 mmol (2.00 g) of the SAVA 1 reagent was carefully added to 8.60 mmol an alcohol (0.76 g for n-pentyl alcohol; 0.76 g for 2-pentyl alcohol; 1,41 g for 4-tert-but-benzyl alcohol; 0.52 g for 2-propyl alcohol; 0.64 g for 2-butyl alcohol) under an inert atmosphere. The mixture was heated (~50-60°C) until dissolved, then allowed to cool. The oily-viscous crude acid ([R^x(RnO)P(S)SH]) was taken into benzene solvent, filtered and cooled to 0°C. Ammonia gas was passed in this solution to obtained ammonium salt, [NH_4][$S_2P(R^x)$(ORn)]. The precipitated white amorphous salt was washed with anhydrous benzene and dried in a vacuum desiccator.

4.1.3. General Synthesis Method of [Ni($S_2P(R^x)$(ORn)] Complexes for Part Ia

4.21 mmol sample of the ammonium salt interested (1.18 g of [NH_4][$S_2P(R^x)$(OR1)]; 1.24 g of [NH_4][$S_2P(R^x)$(OR2)]; 1.30 g of [NH_4][$S_2P(R^x)$(OR3)]; 1.36 g of [NH_4][$S_2P(R^x)$(OR4)]; 1.42 g of [Ni($S_2P(R^x)$(OR5)]; 1.42 g of [Ni($S_2P(R^x)$(OR6)]; 1.50 g of [NH_4][$S_2P(R^x)$(OR7)]) was dissolved in 30-40 mL ethanol. Onto this, a solution of 2.1 mmol (0.5 g) $NiCl_2.6H_2O$ in the same solvent was added dropwise. The mixture was heated to 50-60^{0}C; kept as such for 5-10 min and filtered through filter paper without letting excess cooling. Tiny, violet crystals form upon cooling. This compound was recrystallized from ethanol.

4.1.3. General Synthesis Method of [Ni($S_2P(R^x)$(ORn)] Complexes for Part Ib

An ethanolic solution of $NiCl_2.6H_2O$ (2.1 mmol; 0.5 g) was added to ammonium salt (4.21 mmol; 1.42 g for [NH_4][$S_2P(R^x)$(OR1)] and [NH_4][$S_2P(R^x)$(OR2)]; 1.74 g for [NH_4][$S_2P(R^x)$(OR3)]; 1.30 g for [NH_4][$S_2P(R^x)$(OR4)]; 1.36 g for [NH_4][$S_2P(R^x)$(OR5)]) in ethyl alcohol by stirring and heated to the boiling temperature of the solution. After cooling, the precipitated solid was crystallized from ethanol.

4.2. Synthesis of novel 2,4-*bis*(R^y)-1,3,2,4-dithiadiphosphatene-2,4-disulfide, ([R^y-P(S)S]$_2$, R^x= 2,4-dimethoxyphenyl-, SAV-A2)

In a 145°C oil-bath under a fume hood, 1,3-dimetoxybenzene (4.97 g, 35.96 mmol) was added dropwise, with constant stirring, onto a P_4S_{10} sample (4g, 8,99 mmol) in a round-bottom flask while passing Ar gases to provide an inert atmosphere. The mixture turned into a clear, pale-yellow solution in about 1 hour after the dropwise addition step. The stirring procedure was continued and a yellow precipitate started to form in 2 hours. After 3 hours, the mixture was taken out of the oil bath and left aside for cooling to room temperature. A deep yellow solid was formed at the bottom of the flask. The solid was filtered; washed with dry diethyl ether and then crushed in ether medium with a spatula. The ether-washed solid was filtered again and dried in an inert (Ar) atmosphere. Our experience is that the yellow product decomposes in 1 hour under humid atmosphere (Figure 4.2), [133].

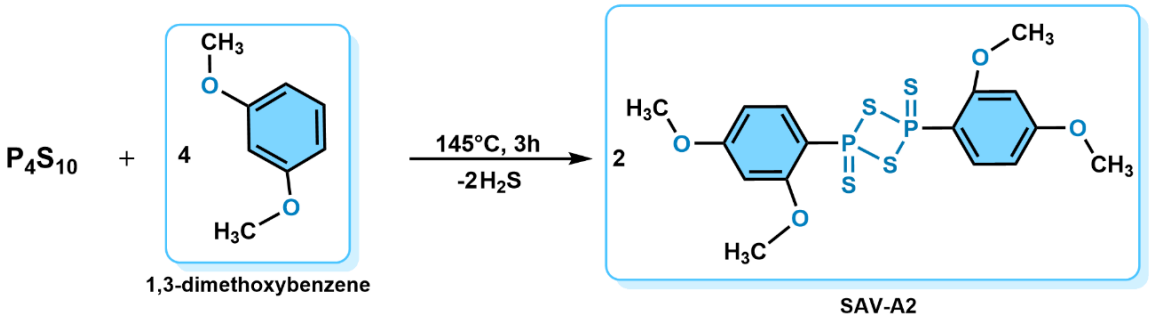


Figure 4.2. SAV-A2 synthesis reaction.

4.2.1. General Procedure of dithiophosphonic acids and the ammonium dithiophosphonates salts for Part II

2.00 g (4.30 mmol) of the SAV-A2 reagent was taken into a three-necked flask, and onto it, an 8.60 mmol of one of the alcohols (0.64 g of 2-butanol; 0.76 g of *n*-pentanol; 1.41 g of 4-*tert*-butylbenzyl alcohol; 0.28 g of methanol) was added dropwise. The mixture was heated to 50-60°C, kept at this temperature range until complete dissolution and then left aside to cool. The crude dithiophosphonic acid (an oily, viscous mixture), was poured into 50-60 mL of benzene. The benzene solution was filtered (filter paper) and was cooled to 0°C. Through this solution dry ammonia gas was bubbled at a rate of 20 mL/min until the precipitation was complete. The white, amorphous precipitate ([NH_4][$S_2P(R^y)$(ORn)) was filtered (filter paper), washed with benzene and dried in a vacuum desiccator.

4.2.2. General Procedure of the synthesis of the complexes [Ni($S_2P(R^y)$(ORn)] for Part II

4.21 mmol sample of the ammonium salt interested (1.36 g of $[NH_4][S_2P(R^y)(OR1)$; 1.42 g of $[NH_4][S_2P(R^y)(OR2)$; 1.74 g of $[NH_4][S_2P(R^y)(OR4)$; 1.18 g of $[NH_4][S_2P(R^y)(ORn))$ was dissolved in 30-40 mL ethanol. Onto this, a solution of 2,10 mmol (0.5 g) $NiCl_2.6H_2O$ in the same solvent was added dropwise. The mixture was heated to 50-60°C; kept as such for 5-10 min and filtered through filter paper without letting excess cooling. Tiny, violet crystals form upon cooling. This compound was recrystallized from ethanol or chloroform.

Experimental details and analytical data for compounds are follows:

Part Ia;

SAV-A1: Yield: 3.29 g (78%). Yellow. m.p. 160-163°C. Anal. Calcd.for: $C_{16}H_{18}O_4P_2S_4$ (464.52 $g.mol^{-1}$): C, 41.37; H, 3.91; S, 27.61; found: C, 41.42; H, 3.97; S, 27.66 %.

$[NH_4][S_2P(R^x)(OR1)]$: Yield: 1.78 g (73%). White. m.p. 162-163°C, decomposition. LC/MS: m/z 263.69($[M-NH_4]^-$, 100%). Anal. Calcd.for: $C_9H_{16}NO_3PS_2$ (281.33 $g.mol^{-1}$): C, 38.42; H, 5.73; N, 4.98; S, 22.80; found: C, 38.50 ; H, 5.80; N, 5.05; S, 22.93 %.

$[NH_4][S_2P(R^x)(OR2)]$: Yield: 1.91 g (75%). White. m.p. 156-157°C, decomposition. LC/MS: m/z 277.78 ($[M-NH_4]^-$, 100%). Anal. Calcd.for: $C_{10}H_{18}NO_3PS_2$ (295.36 $g.mol^{-1}$): C, 40.66; H, 6.14; N, 4.74; S, 21.71; found: C, 40.88; H, 6.36; N, 4.96; S, 21.89 %.

$[NH_4][S_2P(R^x)(OR3)]$: Yield: 2.01 g (75%). White. m.p. 210-212°C. LC/MS: m/z 291.75 ($[M-NH_4]^-$, 100%). Anal. Calcd.for: $C_{11}H_{20}NO_3PS_2$ (309.39 $g.mol^{-1}$): C, 42.70; H, 6.52; N, 4.53; S, 20.73; found: C, 42.80; H, 6.62; N, 4.61; S, 20.82 %.

$[NH_4][S_2P(R^x)(OR4)]$: Yield: 2.05 g (73 %). White. m.p. 194-196°C, decomposition. LC/MS: m/z 305.78 ($[M-NH_4]^-$, 100%). Anal. Calcd.for: $C_{12}H_{22}NO_3PS_2$ (323.41 $g.mol^{-1}$): C, 44.56; H, 6.86; N, 4.33; S, 19.83; found: C, 44.62; H, 6.91; N, 4.40; S, 19.94 %.

$[NH_4][S_2P(R^x)(OR5)]$: Yield: 2.20 g (75%). White. m.p. 190-192°C, decomposition. LC/MS: m/z 319.80 ($[M-NH_4]^-$, 100%). Anal. Calcd.for: $C_{13}H_{24}NO_3PS_2$ (337.44 $g.mol^{-1}$): C, 46.27; H, 7.17; N, 4.15; S, 19.00; found: C, 46.37; H, 7.28; N, 4.26; S, 19.11 %.

$[NH_4][S_2P(R^x)(OR6)]$: Yield: 1.93 g (66%). White. m.p. 192-194°C, decomposition. LC/MS: m/z 319.82 ($[M-NH_4]^-$, 100%). Anal. Calcd.for:$C_{13}H_{24}NO_3PS_2$ (337.44 $g.mol^{-1}$): C, 46.27; H, 7.17; N, 4.15; S, 19.00; found: C, 46.31; H, 7.24; N, 4.21; S, 19.05 %.

[NH_4][$S_2P(R^x)(OR7)$]: Yield: 2.24 g (72%). White. m.p. 185-186°C, decomposition. LC/MS: m/z 339.80 ([M-NH_4]$^+$, 100%). Anal. Calcd.for: $C_{15}H_{20}NO_3PS_2$ (357.43 g.mol^{-1}): C, 50.40; H, 5.64; N, 3.92; S, 17.94; found: C, 50.42; H, 5.67; N, 3.99; S, 18.01 %.

[Ni($S_2P(R^x)(OR1)$]: Yield: 0.96 g (78%). Violet. m.p.125-127°C. LC/MS: m/z 362.71 ([(NiL1+AcCN]$^+$, 100%), 585.9 ([M+H]$^+$, 78%). Anal. Calcd.for: $C_{18}H_{24}NiO_6P_2S_4$ (585.28 g.mol^{-1}): C, 36.94; H, 4.13; S, 21.91; found: C, 37.01; H, 4.20; S, 22.02 %.

[Ni($S_2P(R^x)(OR2)$]: Yield: 0.89 g (69%). Violet. m.p.146-148°C. LC/MS: m/z 614.03 ([M+H]$^+$, 100%). Anal. Calcd.for: $C_{20}H_{28}NiO_6P_2S_4$ (613.33 g.mol^{-1}): C, 39.17; H, 4.60; S, 20.91; found: C, 39.23; H, 4.65; S, 20.98 %.

[Ni($S_2P(R^x)(OR3)$]: Yield: 1.05 g (78%). Violet. m.p.158-160°C. LC/MS: m/z 140.35 ([(C_6H_3-$(OCH_3)_2$+2H]$^+$, 100%), 642.01 ([M-H]$^+$, 54%). Anal. Calcd.for: $C_{22}H_{32}NiO_6P_2S_4$ (641.39 g.mol^{-1}): C, 41.20; H, 5.03; S, 20.00; found: C, 41.27; H, 5.10; S, 20.07 %.

[Ni($S_2P(R^x)(OR4)$]: Yield: 1.24 g (88%). Violet. m.p.90-91°C. LC/MS: m/z 692.09 ([M+Na]$^+$, 100%). Anal. Calcd.for: $C_{23}H_{36}NiO_6P_2S_4$ (669.44 g.mol^{-1}): C, 43.06; H, 5.42; S, 19.16; found: C, 43.14; H, 5.50; S, 19.23 %.

[Ni($S_2P(R^x)(OR5)$]: Yield: 1.02 g (69%). Violet. m.p.140-141°C. LC/MS: m/z 698.14 ([M+H]$^+$, 100%). Anal. Calcd.for: $C_{26}H_{40}NiO_6P_2S_4$ (697.49 g.mol^{-1}): C, 44.77; H, 5.78; S, 18.39; found: C, 44.84; H, 5.86; S, 18.44 %.

[Ni($S_2P(R^x)(OR6)$]: Yield: 1.34 g (92%). Violet. m.p.96-98°C. LC/MS: m/z 139.89 ([(C_6H_3-$(OCH_3)_2$+2H]+, 100%), 698.09 ([M-H]$^+$, 39%). Anal. Calcd.for: $C_{26}H_{40}NiO_6P_2S_4$ (697.49 g.mol^{-1}): C, 44.77; H, 5.78; S, 18.39;found: C, 44.83; H, 5.82; S, 18.45 %.

[Ni($S_2P(R^x)(OR7)$]: Yield: 1.29 g (83%). Violet. m.p.170-172°C. LC/MS: m/z 140.27 ([(C_6H_3-$(OCH_3)_2$+2H]$^+$, 100%), 738.38 ([M+H]$^+$, 12%). Anal. Calcd.for: $C_{30}H_{32}NiO_6P_2S_4$ (737.47 g.mol^{-1}): C, 48.86; H, 4.37; S, 17.39; found: C, 48.92; H, 4.44; S, 17.43 %.

Part Ib;

[NH_4][$S_2P(R^x)(OR1)$]: Yield: 2.20 g (75%). White. m.p. 149-150ºC. LC/MS: m/z 319.80 ([M-NH_4]$^-$, 100%). Anal. Calcd. for: $C_{13}H_{24}NO_3PS_2$ (337.44 g.mol^{-1}): C, 46.27; H, 7.17; N, 4.15; S, 19.00; found: C, 46.33; H, 7.22; N, 4.20; S, 19.05 %.

[NH_4][$S_2P(R^x)(OR2)$]: Yield: 1.93 g (62%). White. m.p. 151-153ºC. LC/MS: m/z 319.82 ([M-NH_4]$^-$, 100%). Anal. Calcd. for: $C_{13}H_{24}NO_3PS_2$ (337.44 g.mol^{-1}): C, 46.27; H, 7.17;

N, 4.15; S, 19.00; found: C, 46.24; H, 7.15; N, 4.11; S, 18.97 %.

[NH_4][$S_2P(R^x)(OR3)$]: Yield: 2.78 g (78%). White. m.p. 174-175 ºC. LC/MS: m/z 395.95 ([M-NH_4]$^+$, 100%). Anal. Calcd. for: $C_{19}H_{28}NO_3PS_2$ (413.53 g.mol^{-1}): C, 55.18; H, 6.82; N, 3.39; S, 15.51; found: C, 55.21; H, 6.84; N, 3.43; S, 15.57 %.

[NH_4][$S_2P(R^x)(OR4)$]: Yield: 1.87 g (65%). White. m.p. 203-204°C. LC/MS: m/z 291.74 ([M-NH_4]$^-$, 100%). Anal. Calcd.for: $C_{11}H_{20}NO_3PS_2$ (309.39 g.mol^{-1}): C, 42.70; H, 6.52; N, 4.53; S, 20.73; found: C, 42.74; H, 6.67; N, 4.58; S, 20.80 %.

[NH_4][$S_2P(R^x)(OR5)$]: Yield: 2.17 g (72 %). White. m.p. 197-198°C, decomposition. LC/MS: m/z 305.78 ([M-NH_4]$^-$, 100%). Anal. Calcd.for: $C_{12}H_{22}NO_3PS_2$ (323.41 g.mol^{-1}): C, 44.56; H, 6.86; N, 4.33; S, 19.83; found: C, 44.50; H, 6.79; N, 4.27; S, 19.77 %.

[Ni($S_2P(R^x)(OR1)$]: Yield: 1.36 g (93%). Violet. m.p. 96-97 ºC. m/z 140.24 ([(C_6H_3-(OCH_3)$_2$+2H]$^+$, 100%), 698.09 ([M-H]$^+$, 28%). Anal. Calcd. for: $C_{26}H_{40}NiO_6P_2S_4$ (697.49 g.mol^{-1}): C, 44.77; H, 5.78; S, 18.39; found: C, 44.74; H, 5.73; S, 18.36 %.

[Ni($S_2P(R^x)(OR2)$]: Yield: 1.15 g (78%). Violet. m.p. 120-121 ºC. LC/MS: m/z 720.16 ([M+Na]$^+$, 100%), 720.16 ([M]$^+$, 72%). Anal. Calcd. for: $C_{26}H_{40}NiO_6P_2S_4$ (697.49 g.mol^{-1}): C, 44.77; H, 5.78; S, 18.39; found: C, 44.80; H, 5.80; S, 18.45 %.

[Ni($S_2P(R^x)(OR3)$]: Yield: 1.27 g (71%). Violet. m.p. 128-130 ºC. LC/MS: m/z 140.16 ([(C_6H_3-(OCH_3)$_2$+2H]$^+$, 100%), 850.33 ([M-H]$^+$, 12%). Anal. Calcd. for: $C_{38}H_{48}NiO_6P_2S_4$ (849.69 g.mol^{-1}): C, 53.71; H, 5.69; S, 15.10; found: C, 53.71; H, 5.74; S, 15.15 %.

[Ni($S_2P(R^x)(OR4)$]: Yield: 1.16 g (86%). Violet. m.p.159-161°C. LC/MS: m/z 642.01 ([M+H]$^+$, 100%). Anal. Calcd.for: $C_{22}H_{32}NiO_6P_2S_4$ (641.3%9 g.mol^{-1}): C, 41.20; H, 5.03; S, 20.00; found: C, 41.27; H, 5.10; S, 20.07 %.

[Ni($S_2P(R^x)(OR5)$]: Yield: 0.98 g (70%). Violet. m.p.150-151°C. LC/MS: m/z 692.09 ([M+Na]$^+$, 100%), 692.09 ([M]$^+$, 100%). Anal. Calcd.for: $C_{23}H_{36}NiO_6P_2S_4$ (669.44 g.mol^{-1}): C, 43.06; H, 5.42; S, 19.16; found: C, 43.14; H, 5.50; S, 19.23 %.

Part II;

SAV-A2: Yield: 3.01 g (72%). Yellow. M.P.: 92°C. Anal. Calcd. for: $C_{16}H_{18}O_4P_2S_4$ (464.52 g.mol^{-1}): C, 41.37; H, 3.91; S, 27.61; found: C, 41.40; H, 3.95; S, 27.64 %.

[NH_4][$S_2P(R^y)(OR1)$]: Yield: 1.98 g (71%). White. M.P.:167-168°C. ^{31}P NMR: δ=99.8. LC/MS: m/z 351.9 ([(M-NH_4)(EtOH]$^+$, 100%). Anal. Calcd. for: $C_{12}H_{22}NO_3PS_2$ (323.41

g.mol^{-1}): C, 44.56; H, 6.86; N, 4.33; S, 19.83; found: C, 44.66; H, 6.96; N, 4.42; S, 19.90 %.

[NH_4][$S_2P(R^y)(OR2)$]: Yield: 2.15 g (73%). White. M.P.: 178°C. ^{31}P NMR: δ=102.3. LC/MS: m/z 365.8 ([(M-NH_4)(EtOH]$^+$, 100%). Anal. Calcd. for: $C_{13}H_{24}NO_3PS_2$ (337.44 g.mol^{-1}): C, 46.27; H, 7.17; N, 4.15; S, 19.00; found: C, 46.40; H, 7.30; N, 4.27; S, 19.12 %.

[NH_4][$S_2P(R^y)(OR3)$]: Yield: 2.63 g (73%). White. M.P.:187-188°C. ^{31}P NMR: δ=103.4. LC/MS: m/z 442.0 ([(M-NH_4)(EtOH]$^+$, 100%). Anal. Calcd. for: $C_{19}H_{28}NO_3PS_2$ (413.53 g.mol^{-1}): C, 55.18; H, 6.82; N, 3.39; S, 15.51; found: C, 55.21; H, 6.84; N, 3.43; S, 15.57 %.

[NH_4][$S_2P(R^y)(OR4)$]: Yield: 1.87 g (77%). White. m.p. 157-158°C. LC/MS: m/z 263.70 ([M-NH_4]$^-$, 19%). Anal. Calcd.for: $C_9H_{16}NO_3PS_2$ (281.33 g.mol^{-1}): C, 38.42; H, 5.73; N, 4.98; S, 22.80; found: C, 38.46 ; H, 5.77; N, 5.02; S, 22.83 %.

[Ni($S_2P(R^y)(OR1)$]: Yield: 0.98 g (70%). Violet. M.P.:167°C. ^{31}P NMR: δ=98.5. LC/MS: m/z 670.1 ([M+H]$^+$, 100%). Anal. Calcd. for: $C_{23}H_{36}NiO_6P_2S_4$ (669.44 g.mol^{-1}): C, 43.06; H, 5.42; S, 19.16; found: C, 43.14; H, 5.50; S, 19.24 %.

[Ni($S_2P(R^y)(OR2)$]: Yield: 1.28 g (87%). Violet. M.P.:107°C. ^{31}P NMR: δ=101.4. LC/MS: m/z 698.2 ([M+H]$^+$, 100%). Anal. Calcd. for: $C_{26}H_{40}NiO_6P_2S_4$ (697.49 g.mol-1): C, 44.77; H, 5.78; S, 18.39; found: C, 44.89; H, 5.90; S, 18.51 %.

[Ni($S_2P(R^y)(OR3)$]: Yield: 1.32 g (74%). Violet. M.P.:179°C. ^{31}P NMR: δ=102.6. LC/MS: m/z 185.6 ([NiS_4]$^+$, 100%), 850.27 ([M+H]$^+$, 82%). Anal. Calcd. for: $C_{38}H_{48}NiO_6P_2S_4$ (849.69 g.mol^{-1}): C, 53.71; H, 5.69; S, 15.10; found: C, 53.71; H, 5.74; S, 15.15 %.

[Ni($S_2P(R^y)(OR4)$]: Yield: 0.92 g (75%). Violet. m.p. 229°C. LC/MS: m/z 585.80 ([M+H]$^+$, 100%), 100%), 585.9 ([M+H]$^+$, 78%). Anal. Calcd.for: $C_{18}H_{24}NiO_6P_2S_4$ (585.28 g.mol^{-1}): C, 36.94; H, 4.13; S, 21.91; found: C, 37.06; H, 4.25; S, 22.03 %.

5. RESULT AND DISCUSSION

The structures of the compounds were characterized by spectroscopic methods (mass spectrometry (ESI), FT-IR spectroscopy, 1D ^{1}H-NMR, ^{13}C-NMR, ^{31}P-NMR and 2D HSQC techniques (for [Ni($S_2P(R^x)$(OR6)] and [Ni($S_2P(R^y)$(OR2)]) and elemental analysis. The structures of complexes were elucidated by single crystal X-ray diffraction analysis and DFT and Molecular Docking calculations ([Ni($S_2P(R^x)$(ORn)], n=1-7 for Part Ia, [Ni($S_2P(R^x)$(ORn)], n=1,2,4 and 5 Part Ib and [Ni($S_2P(R^y)$(OR2)] for Part II). In vitro cytotoxic activity studies were also performed for all compounds except for SAV-A1 and SAV-A2.

5.1. Structural Characterization

Since dithiophosphonic acids are viscous liquid, as mentioned earlier, their structures analyses are performed indirectly. That is, the structures of salts or complexes derived from their DTDP are indirectly determined by comparison with the structure of the dimers.

5.1.1. Comment on the IR Spectra of [R^x-P(S)S]$_2$, [NH_4][$S_2P(R^x)$(ORn)] and [Ni($S_2P(R^x)$(ORn)] for Part Ia

Selected IR data (cm^{-1}) assignment of vibrational bands for the compounds are given in Table 5.1. for Part Ia. IR spectra of the compounds are also presented in Figures 5.1-5.15. The characteristic ν_{N-H} stretching bands of the ligands appear at 3190-2931 cm^{-1} on IR. These bands disappear on the IR spectra of the complexes proving the substitution of the ammonium group by metal cations. For the ligands, symmetric and asymmetric PS stretching bands ($\nu(PS)_{sym}$ and $\nu(PS)_{asym}$) are observed at 610-544 cm^{-1} cm^{-1} and 689-641 cm^{-1}, respectively. The IR spectra of the complexes all show two bands in the ranges 562-553 cm^{-1} and 663-630 cm^{-1} attributable to the ν_{sym} and ν_{asym} PS stretching vibrations, respectively. The complexes also display Ni-S bands. IR spectral symmetric and asymmetric Ni-S stretching bands ($\nu(Ni-S)_{sym}$ and $\nu(Ni-S)_{asym}$) are located at 263-296 cm^{-1} and 323-351 cm^{-1}, respectively. IR data reported for similar compounds agree well with our findings [29, 30, 131, 295].

Table 5.1. Selected IR data (cm^{-1}) assignment of vibrational bands of the compounds for Part Ia.

Compounds	$\nu(Ni\text{-}S)_{sym}$	$\nu(Ni\text{-}S)_{asym}$	$\nu(PS)_{sym}$	$\nu(PS)_{asym}$	$\nu(N\text{-}H)$
SAV-A1	-	-	544	679	-
$[NH_4][S_2P(R^x)(OR1)]$	-	-	556	689	3189
$[NH_4][S_2P(R^x)(OR2)]$	-	-	558	667	3181
$[NH_4][S_2P(R^x)(OR3)]$	-	-	556	667	3197
$[NH_4][S_2P(R^x)(OR4)]$	-	-	556	646	3188
$[NH_4][S_2P(R^x)(OR5)]$	-	-	566	641	3193
$[NH_4][S_2P(R^x)(OR6)]$	-	-	557	649	3191
$[NH_4][S_2P(R^x)(OR7)]$	-	-	558	665	3179
$[Ni(S_2P(R^x)(OR1))_2]$	263	331	558	663	-
$[Ni(S_2P(R^x)(OR2))_2]$	296	341	558	630	-
$[Ni(S_2P(R^x)(OR3))_2]$	263	336	562	663	-
$[Ni(S_2P(R^x)(OR4))_2]$	289	327	558	663	-
$[Ni(S_2P(R^x)(OR5))_2]$	266	323	553	661	-
$[Ni(S_2P(R^x)(OR6))_2]$	278	324	560	630	-
$[Ni(S_2P(R^x)(OR7))_2]$	284	351	562	636	-

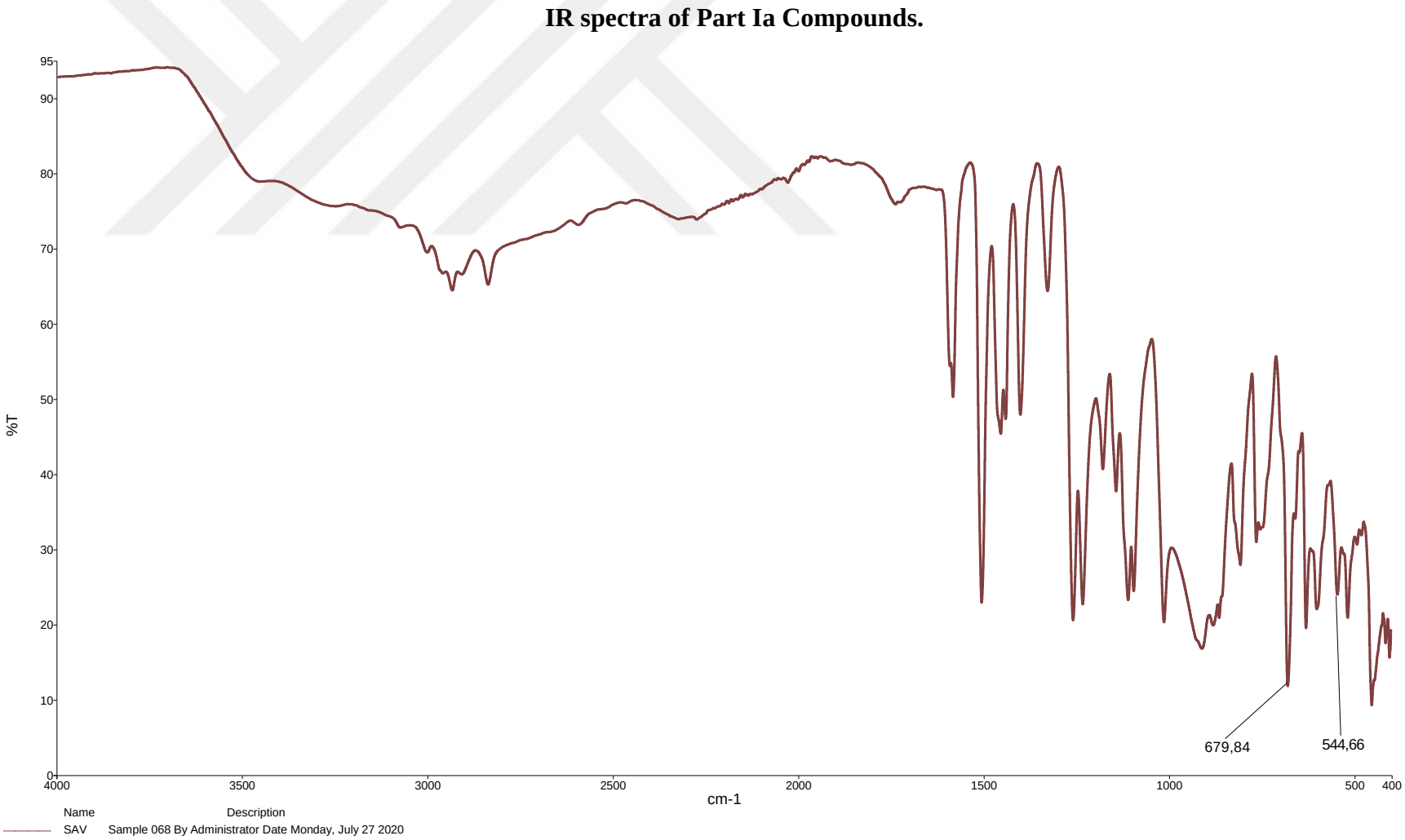


Figure 5.1. SAV-A1 IR spectrum (4000 cm^{-1}- 400 cm^{-1}).

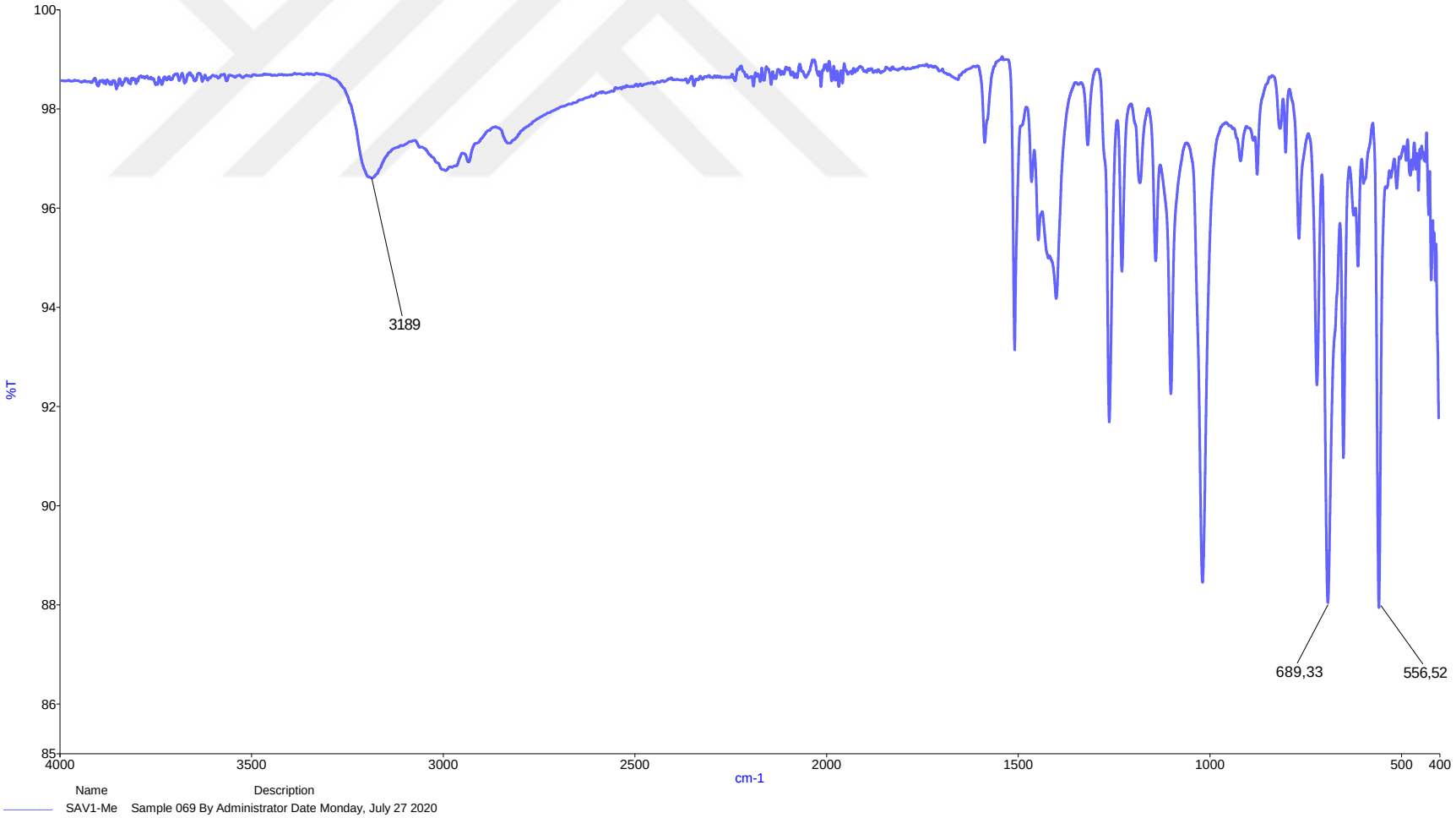


Figure 5.2. $[NH_4][S_2P(R^x)(OR1)]$ IR spectrum (4000 cm^{-1}- 400 cm^{-1}).

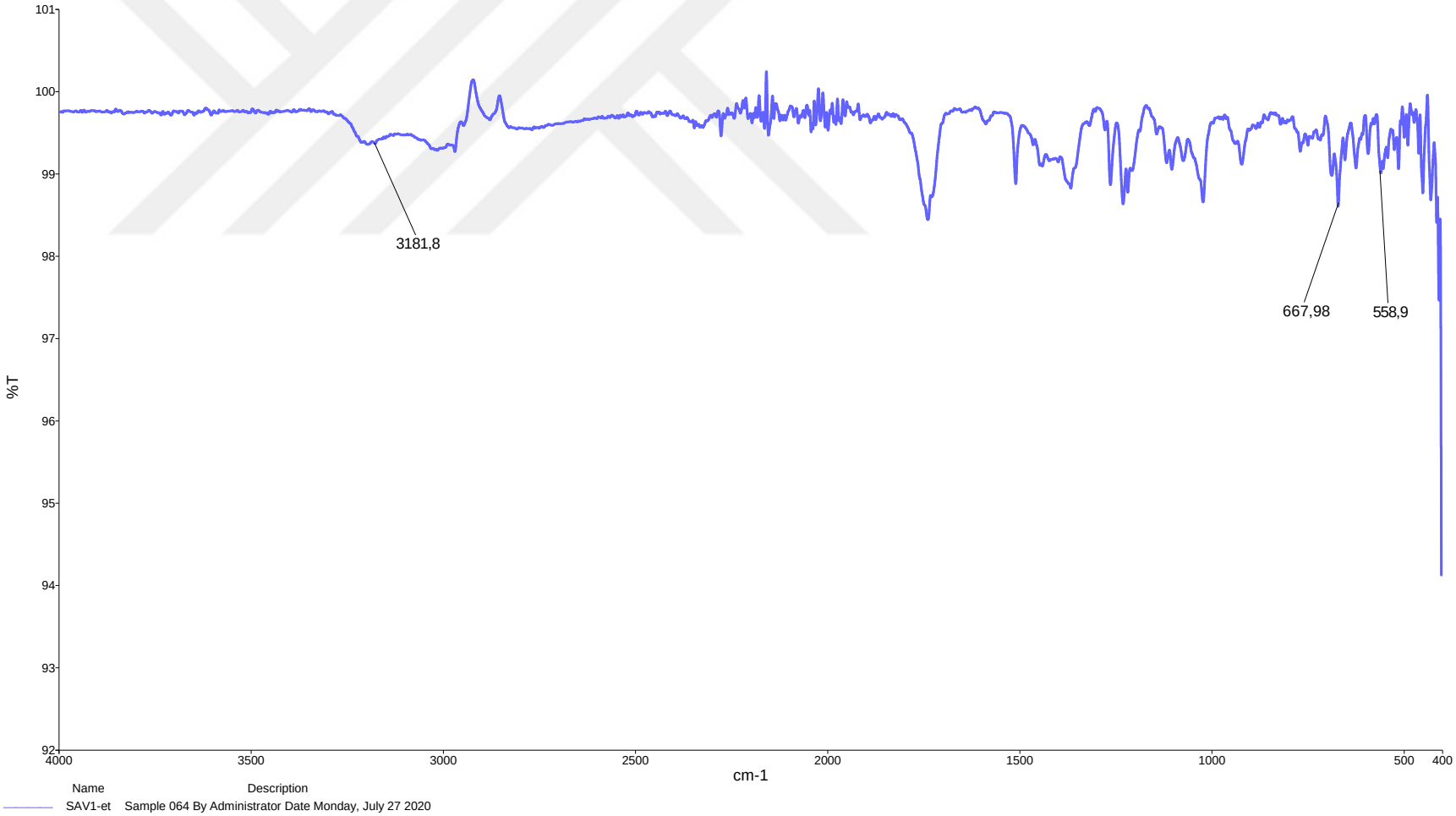


Figure 5.3. $[NH_4][S_2P(R^x)(OR2)]$ IR spectrum (4000 cm^{-1}- 400 cm^{-1}).

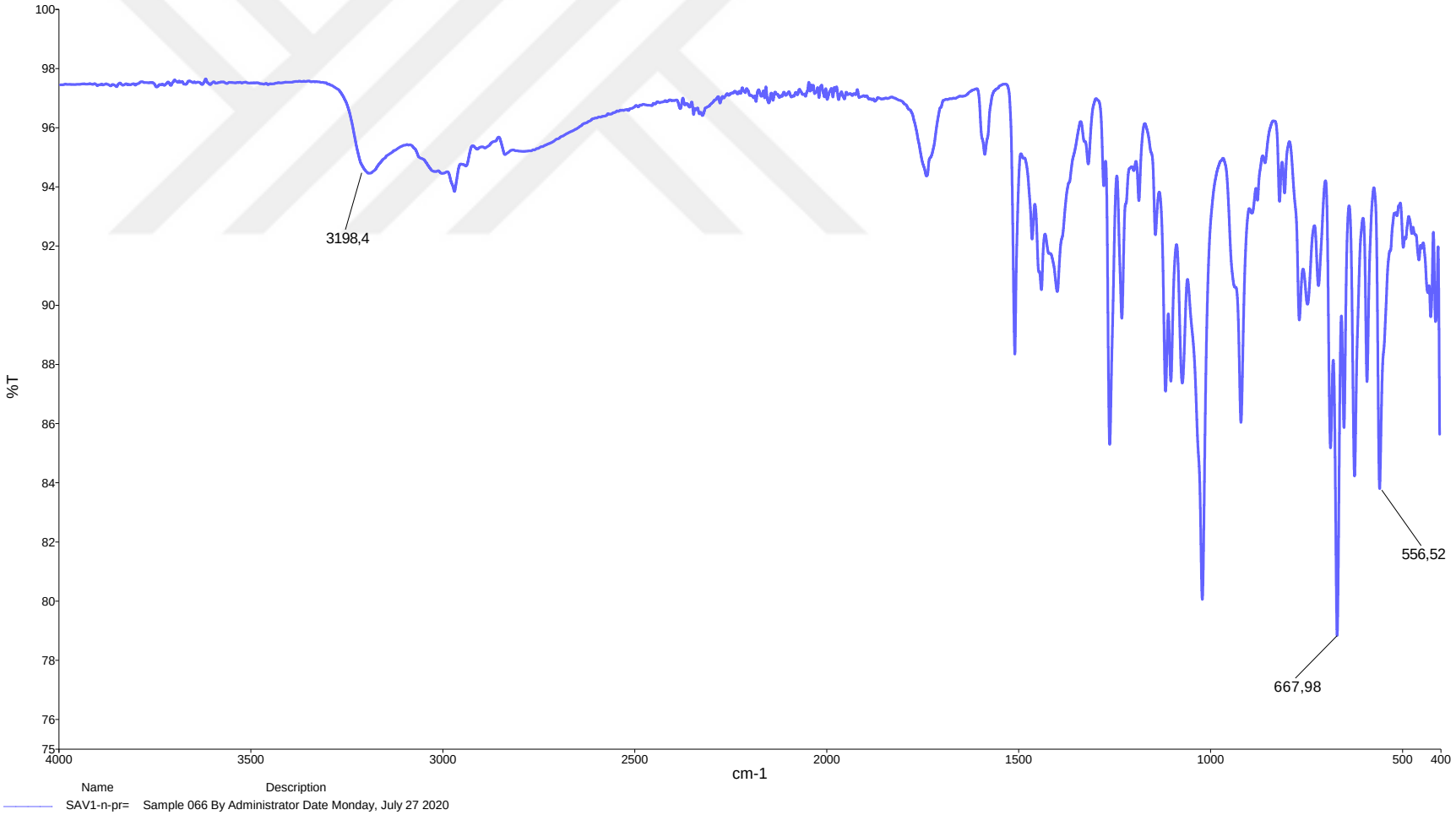


Figure 5.4. $[NH_4][S_2P(R^x)(OR3)]$ IR spectrum (4000 cm^{-1}- 400 cm^{-1}).

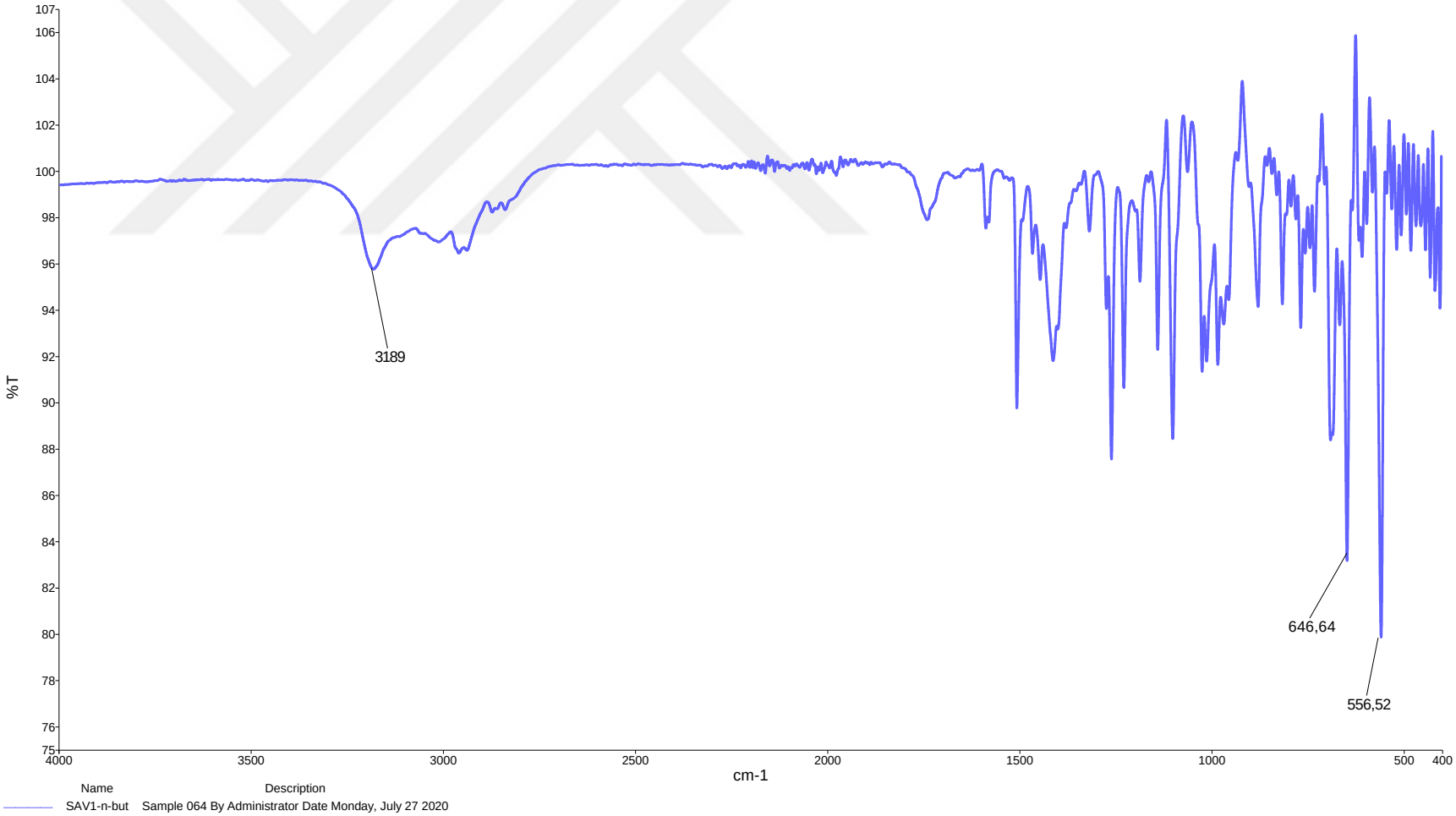


Figure 5.5. $[NH_4][S_2P(R^x)(OR4)]$ IR spectrum (4000 cm^{-1}- 400 cm^{-1}).

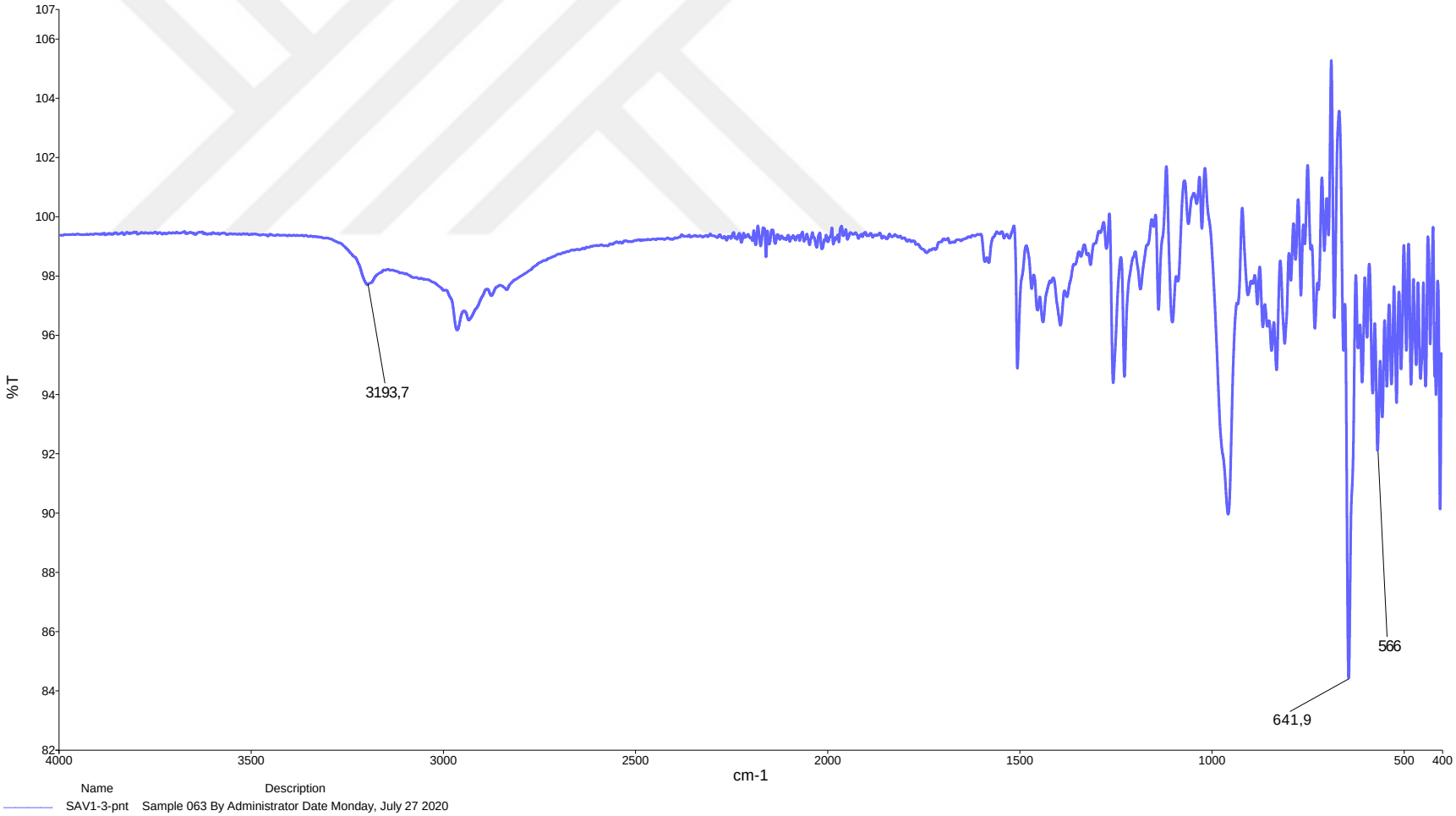


Figure 5.6. $[NH_4][S_2P(R^x)(OR5)]$ IR spectrum (4000 cm^{-1}- 400 cm^{-1}).

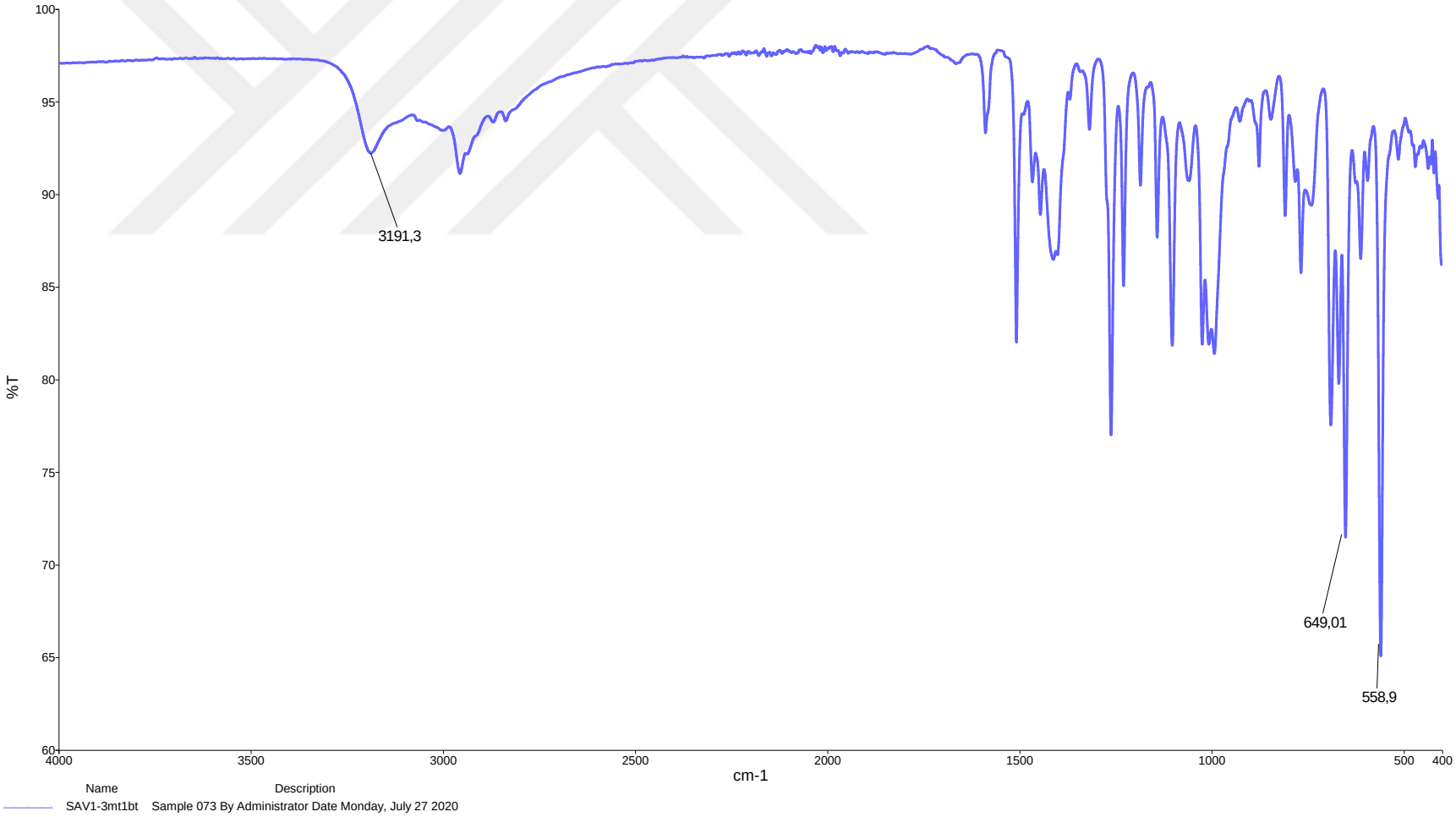


Figure 5.7. $[NH_4][S_2P(R^x)(OR6)]$ IR spectrum (4000 cm^{-1}- 400 cm^{-1}).

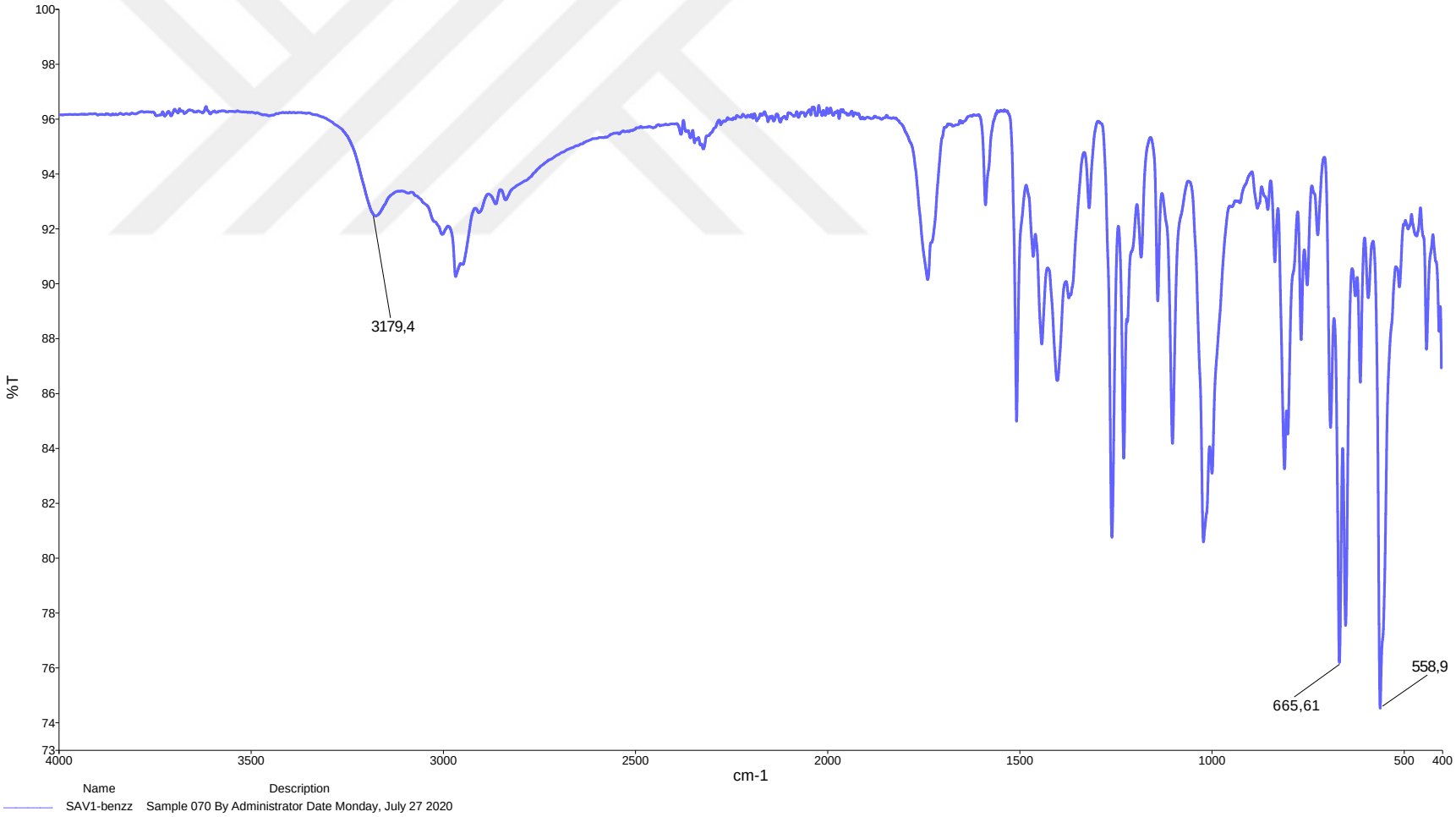


Figure 5.8. $[NH_4][S_2P(R^x)(OR7)]$ IR spectrum (4000 cm^{-1}- 400 cm^{-1}).

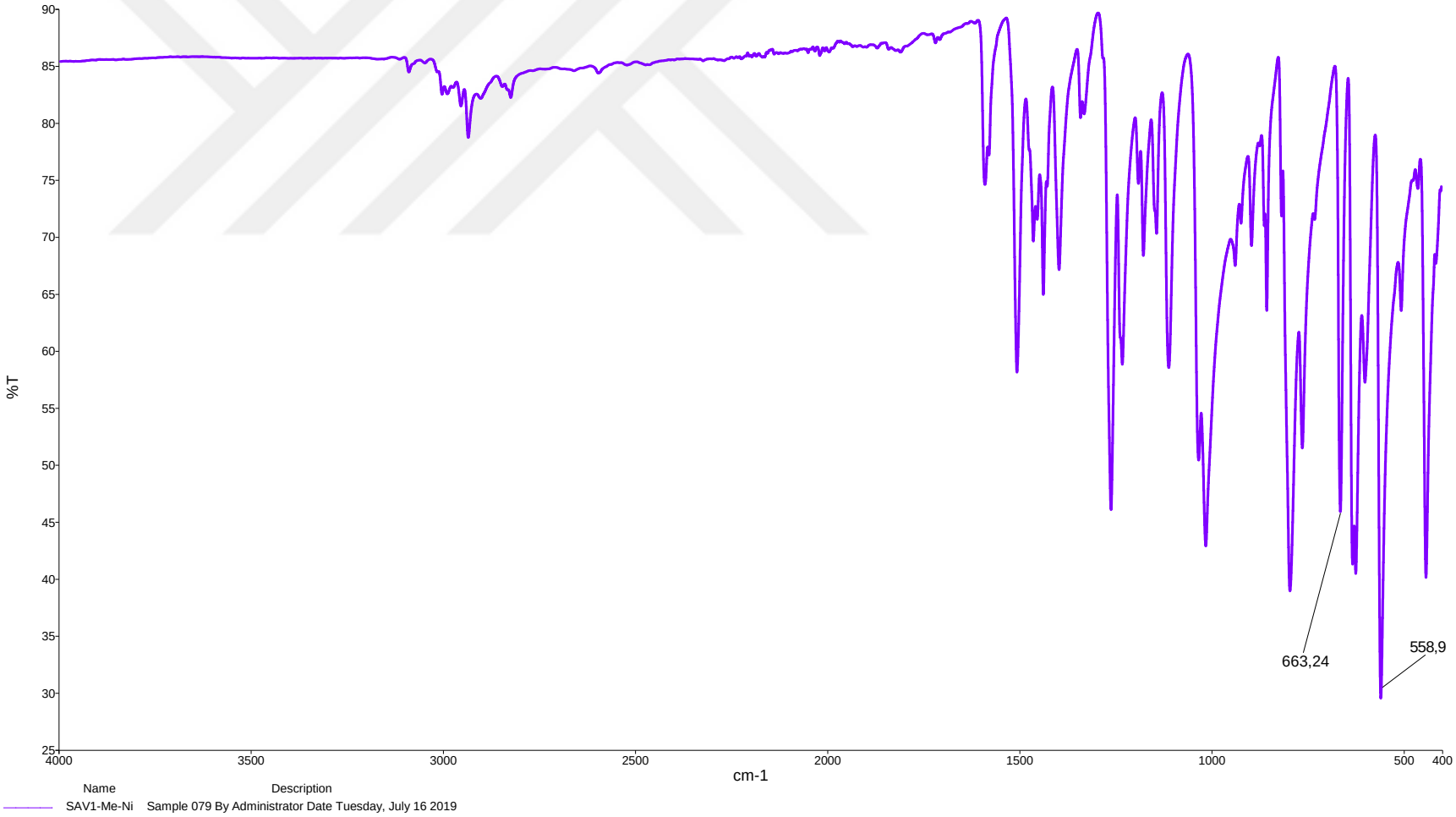


Figure 5.9.a. $[Ni(S_2P(R^x)(OR1))_2]$ IR spectrum (4000 cm^{-1}- 400 cm^{-1}).

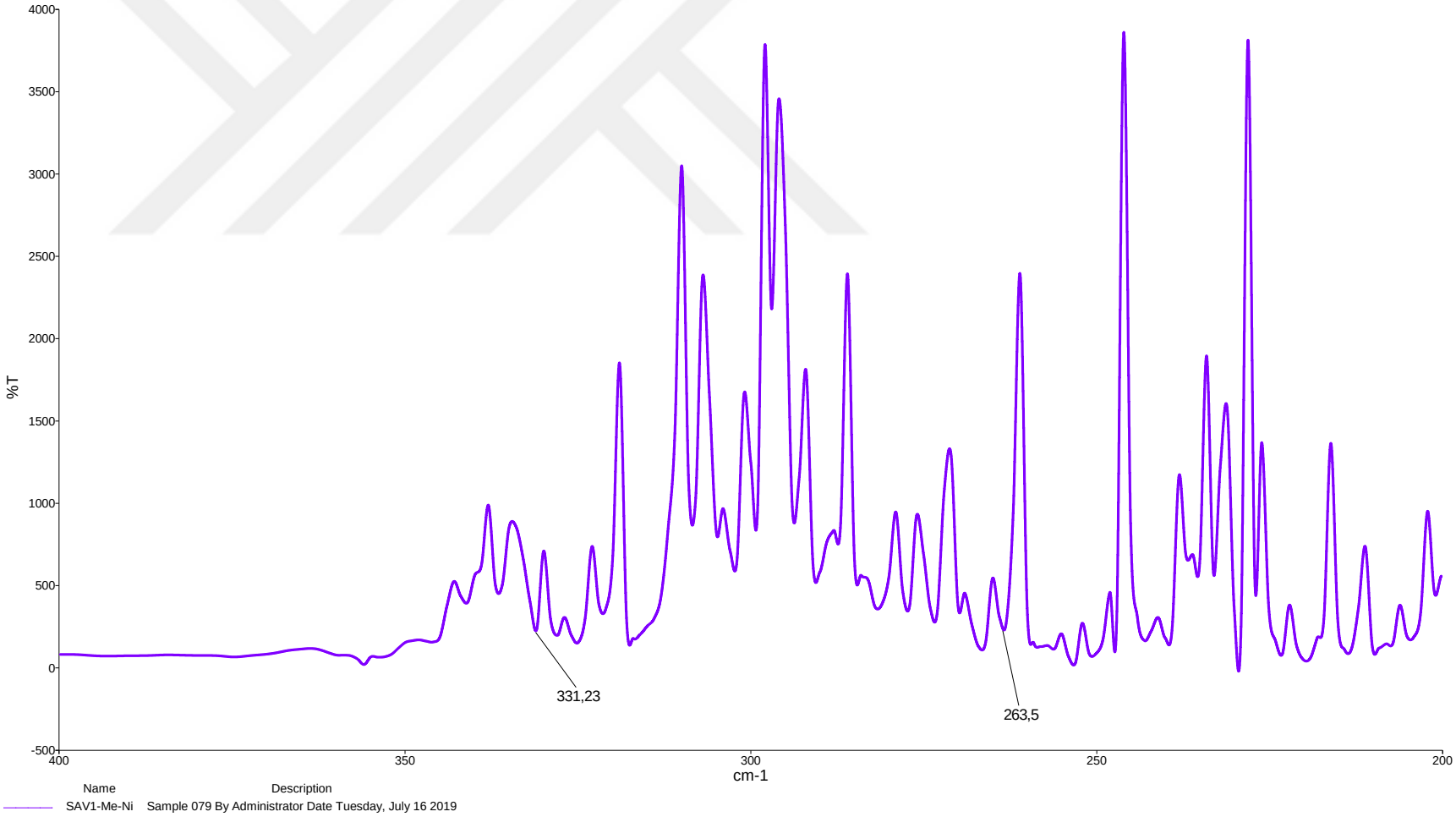


Figure 5.9.b. [Ni($S_2P(R^x)(OR1))_2$] IR spectrum (400 cm^{-1}- 200 cm^{-1}).

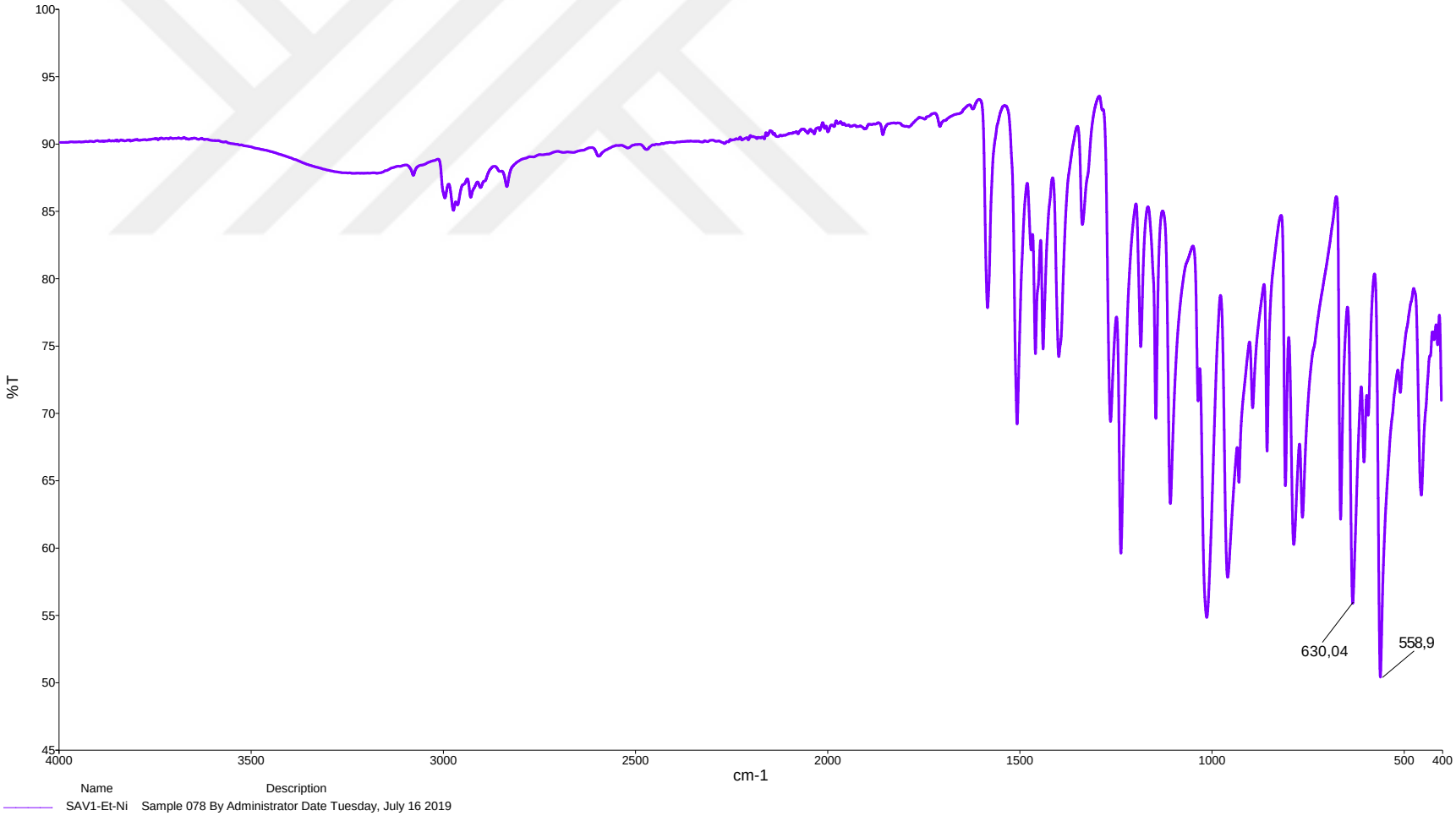


Figure 5.10.a. $[Ni(S_2P(R^x)(OR2))_2]$ IR spectrum (4000 cm^{-1}- 400 cm^{-1}).

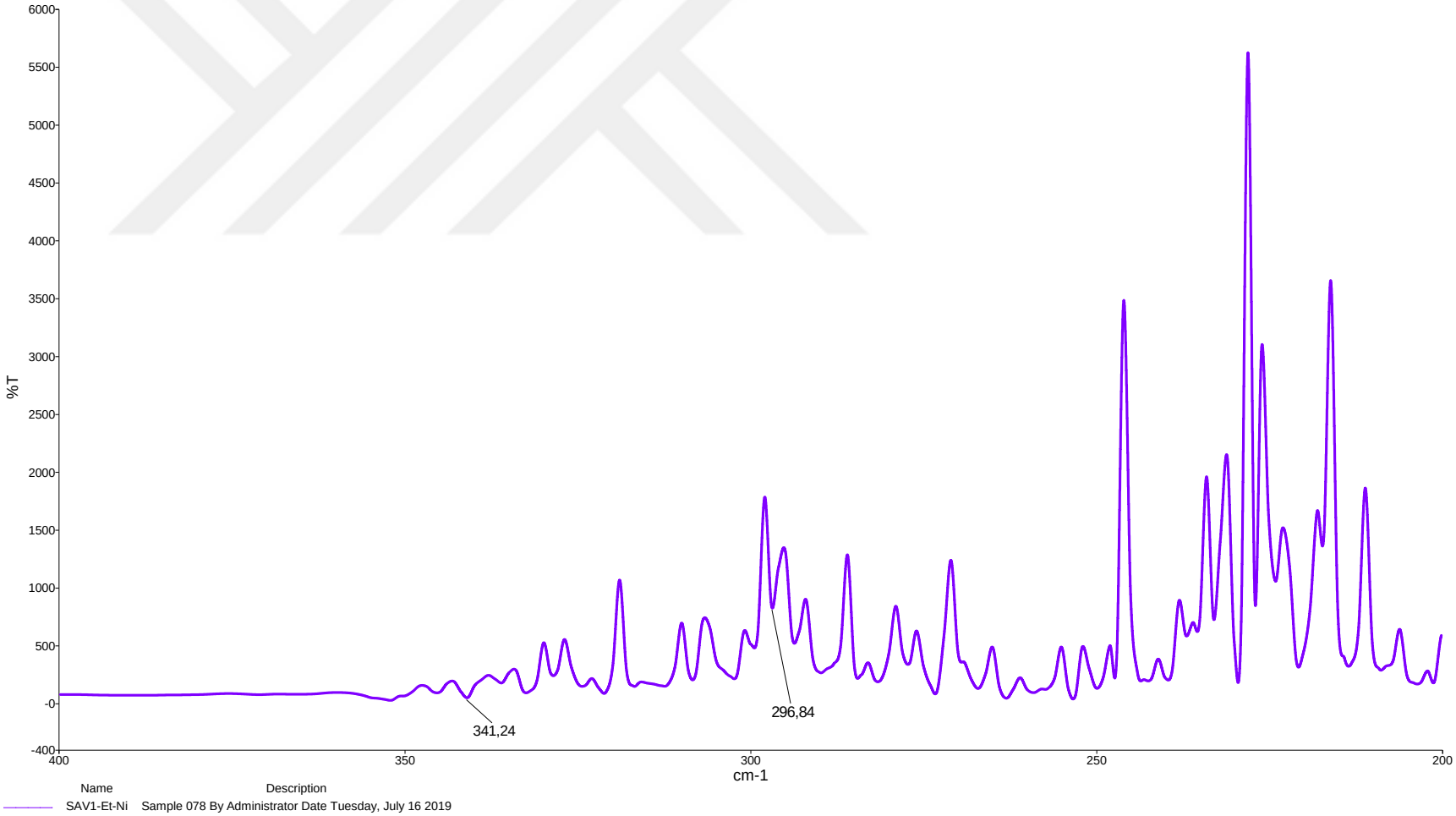


Figure 5.10.b. $[Ni(S_2P(R^x)(OR2))_2]$ IR spectrum (400 cm^{-1}- 200 cm^{-1}).

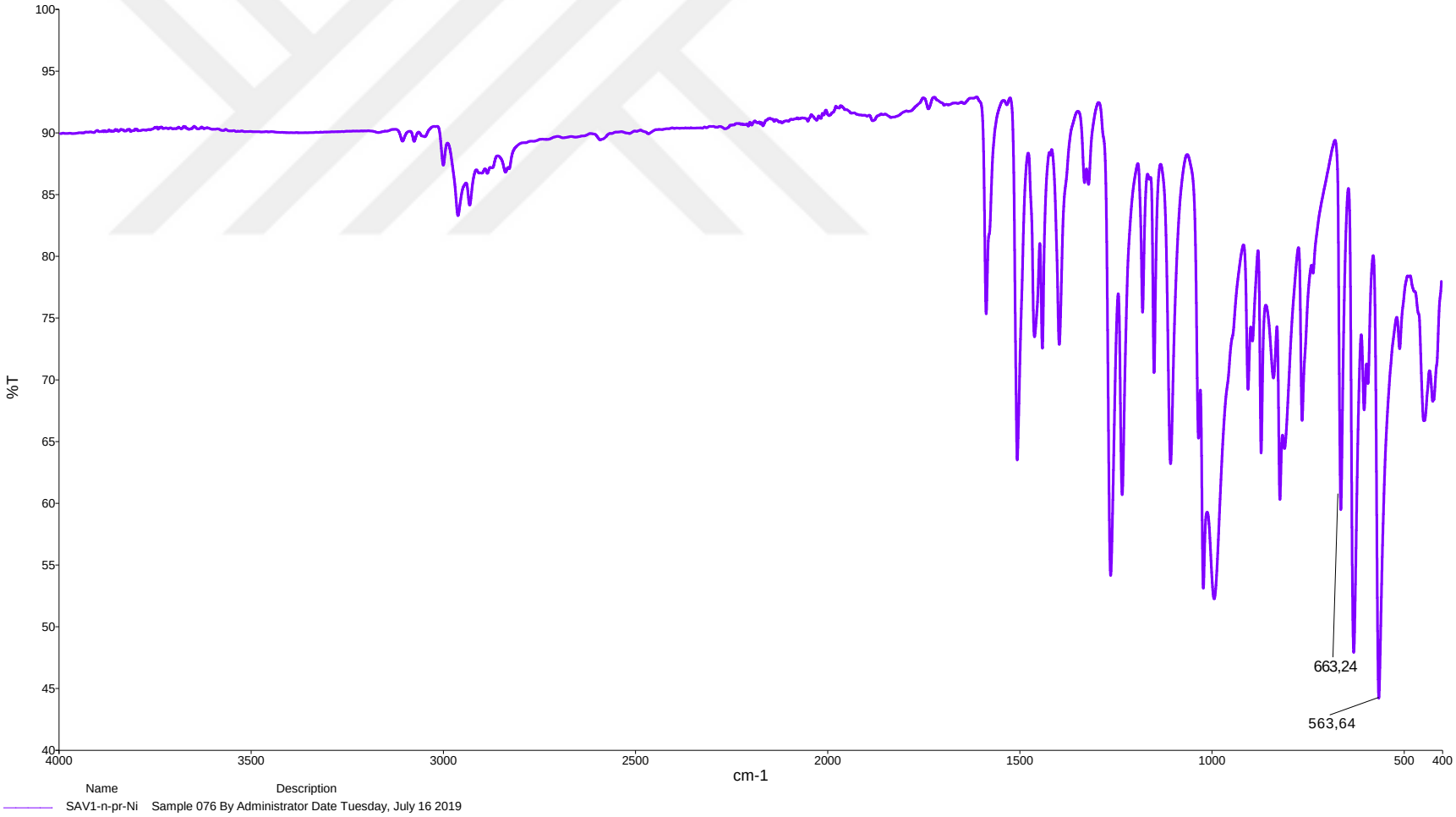


Figure 5.11.a. $[Ni(S_2P(R^x)(OR3))_2]$ IR spectrum (4000 cm^{-1}- 400 cm^{-1}).

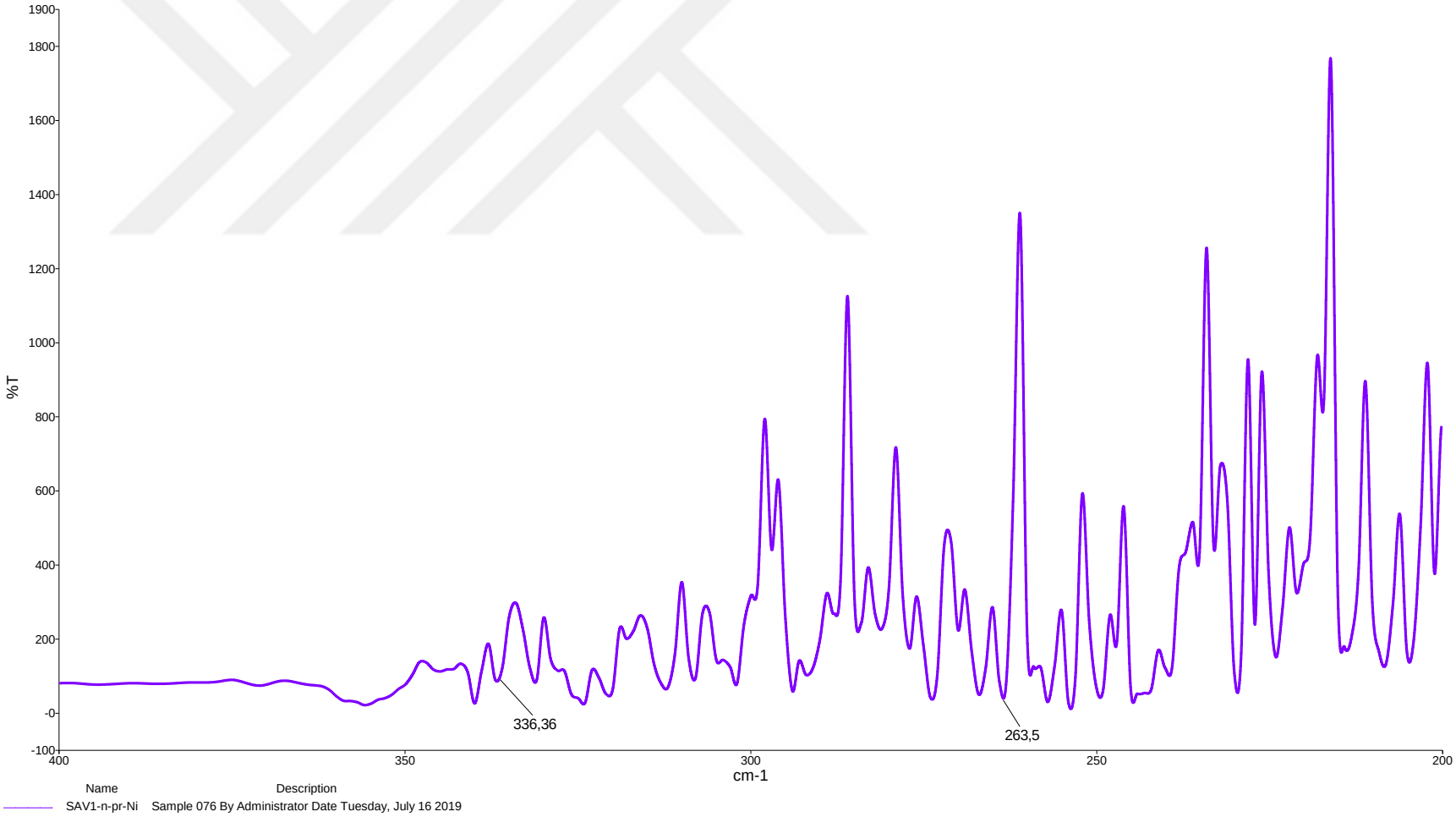


Figure 5.11.b. [Ni($S_2P(R^x)(OR3))_2$] IR spectrum (400 cm^{-1}- 200 cm^{-1}).

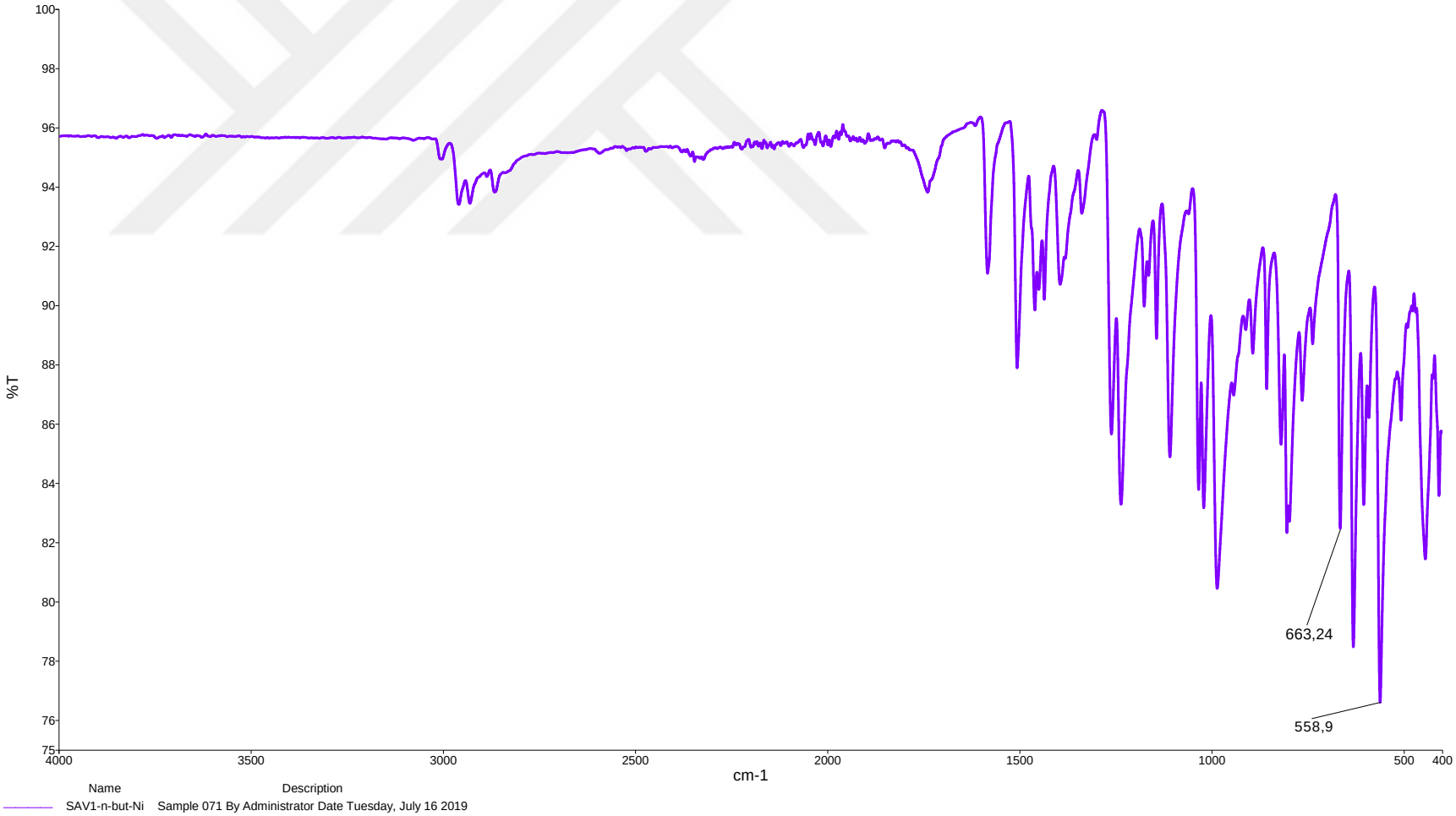


Figure 5.12.a. $[Ni(S_2P(R^x)(OR4))_2]$ IR spectrum (4000 cm^{-1}- 400 cm^{-1}).

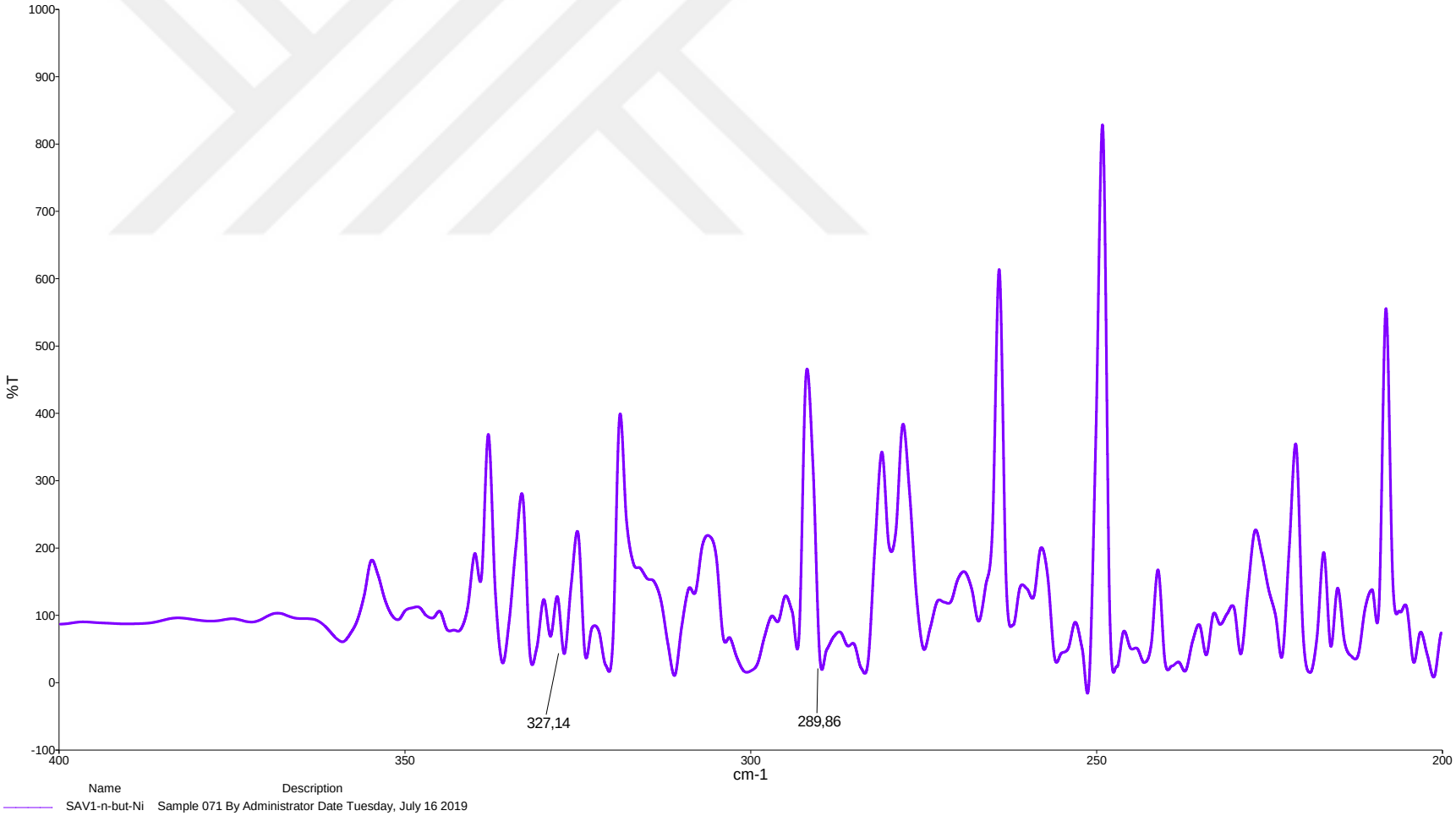


Figure 5.12.b. [Ni($S_2P(R^x)(OR4))_2$] IR spectrum (400 cm^{-1}- 200 cm^{-1}).

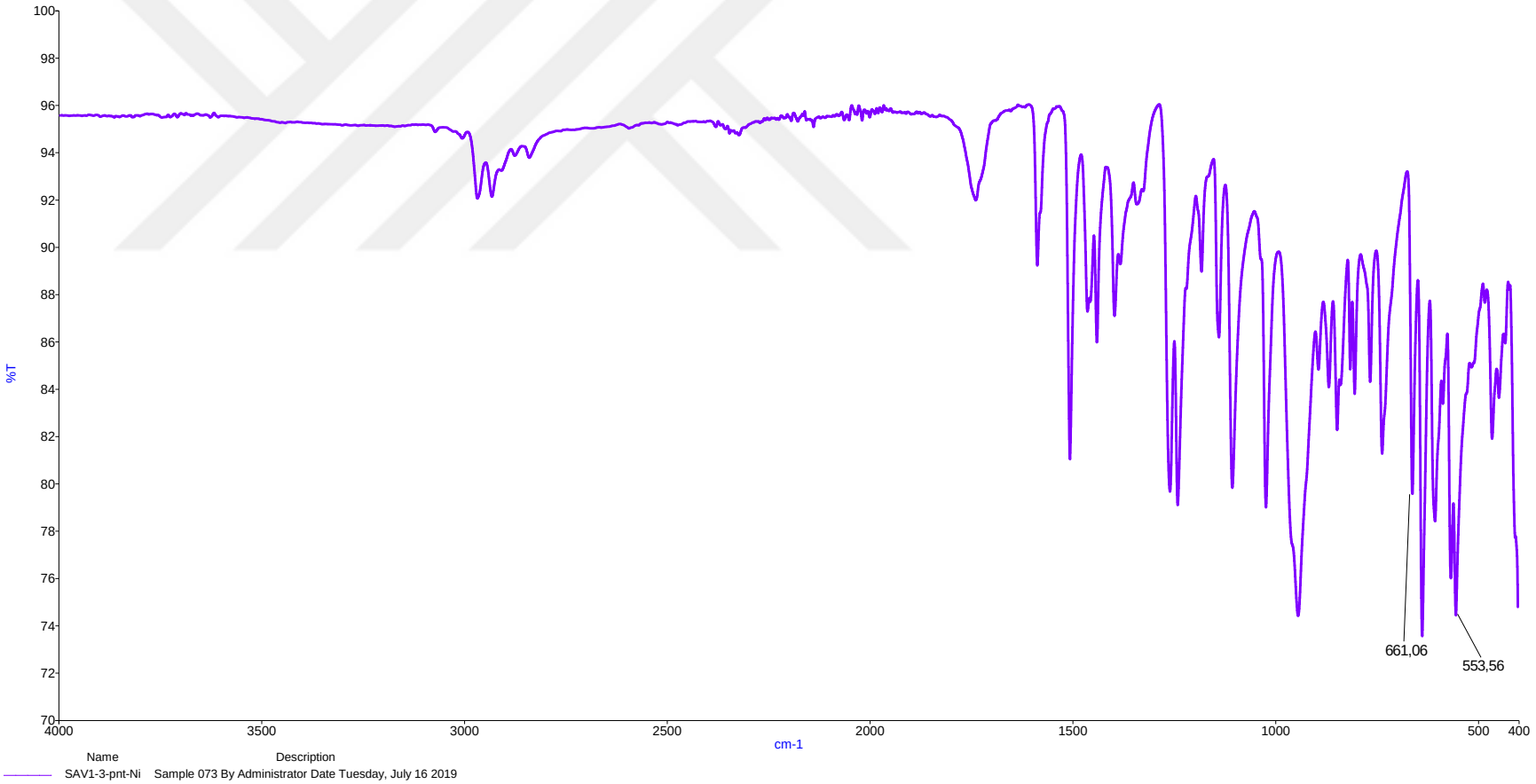


Figure 5.13.a. $[Ni(S_2P(R^x)(OR5))_2]$ IR spectrum (4000 cm^{-1}- 400 cm^{-1}).

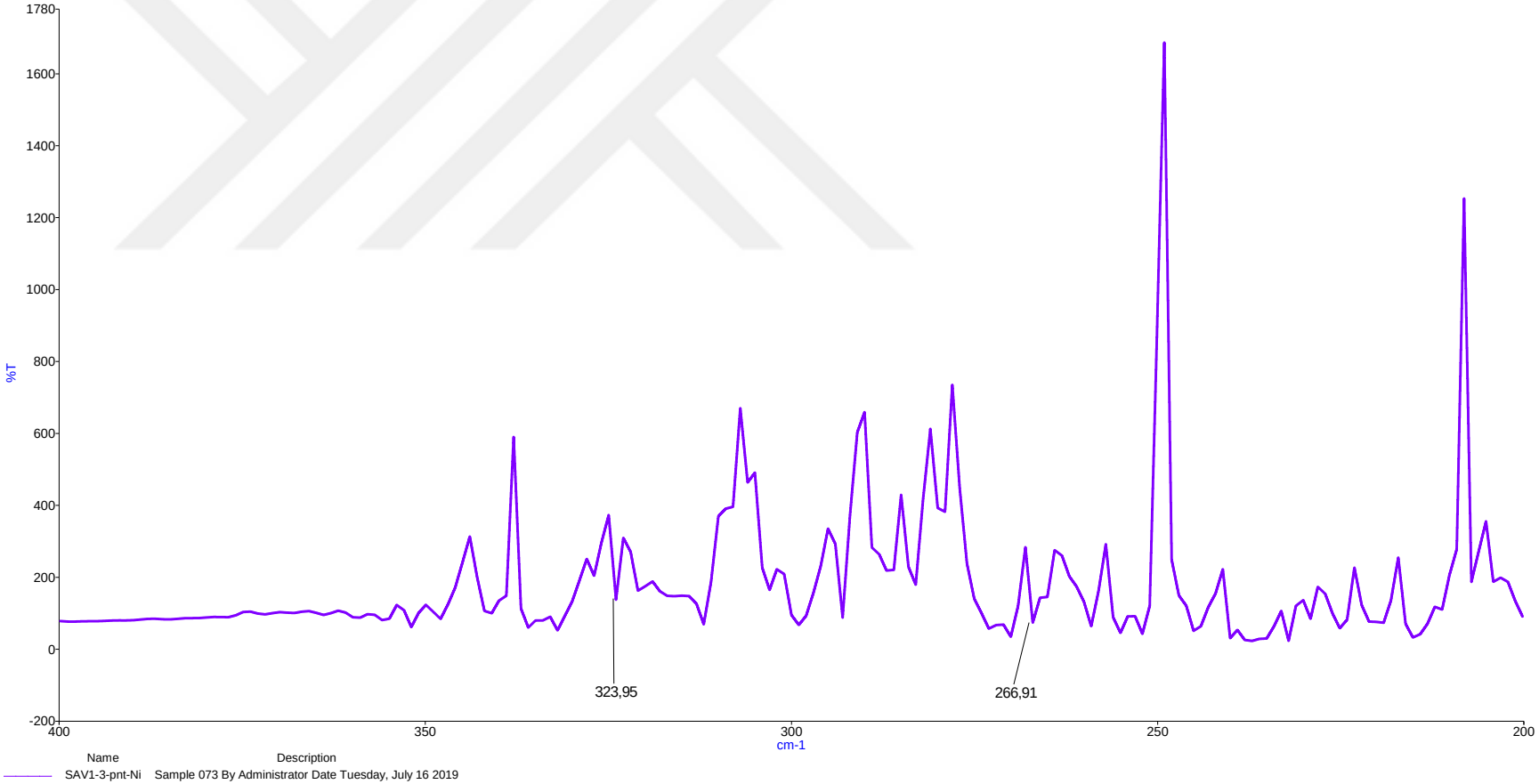


Figure 5.13.b. [Ni($S_2P(R^x)(OR5)$)$_2$] IR spectrum (400 cm^{-1}- 200 cm^{-1}).

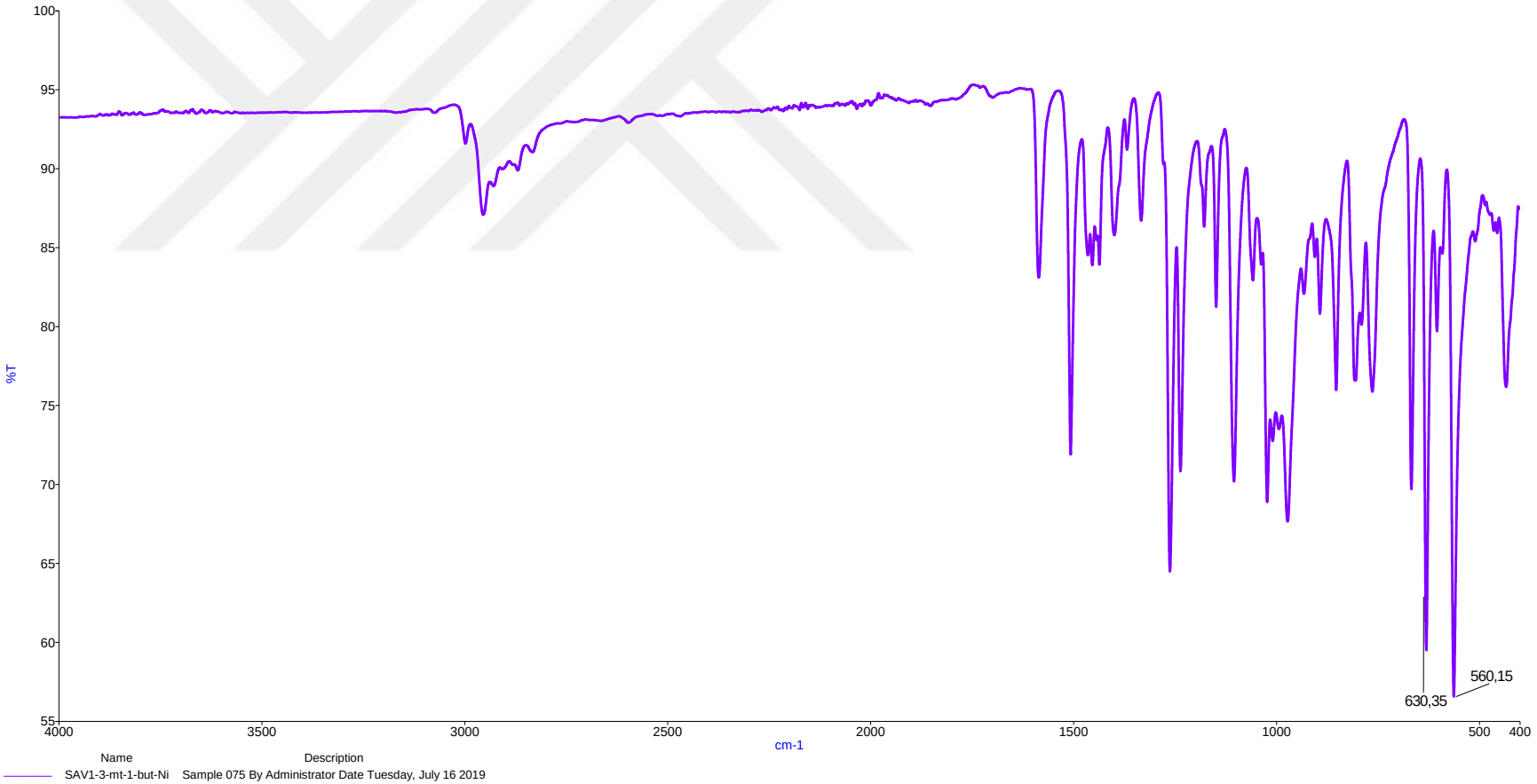


Figure 5.14.a. $[Ni(S_2P(R^x)(OR6))_2]$ IR spectrum (4000 cm^{-1}- 400 cm^{-1}).

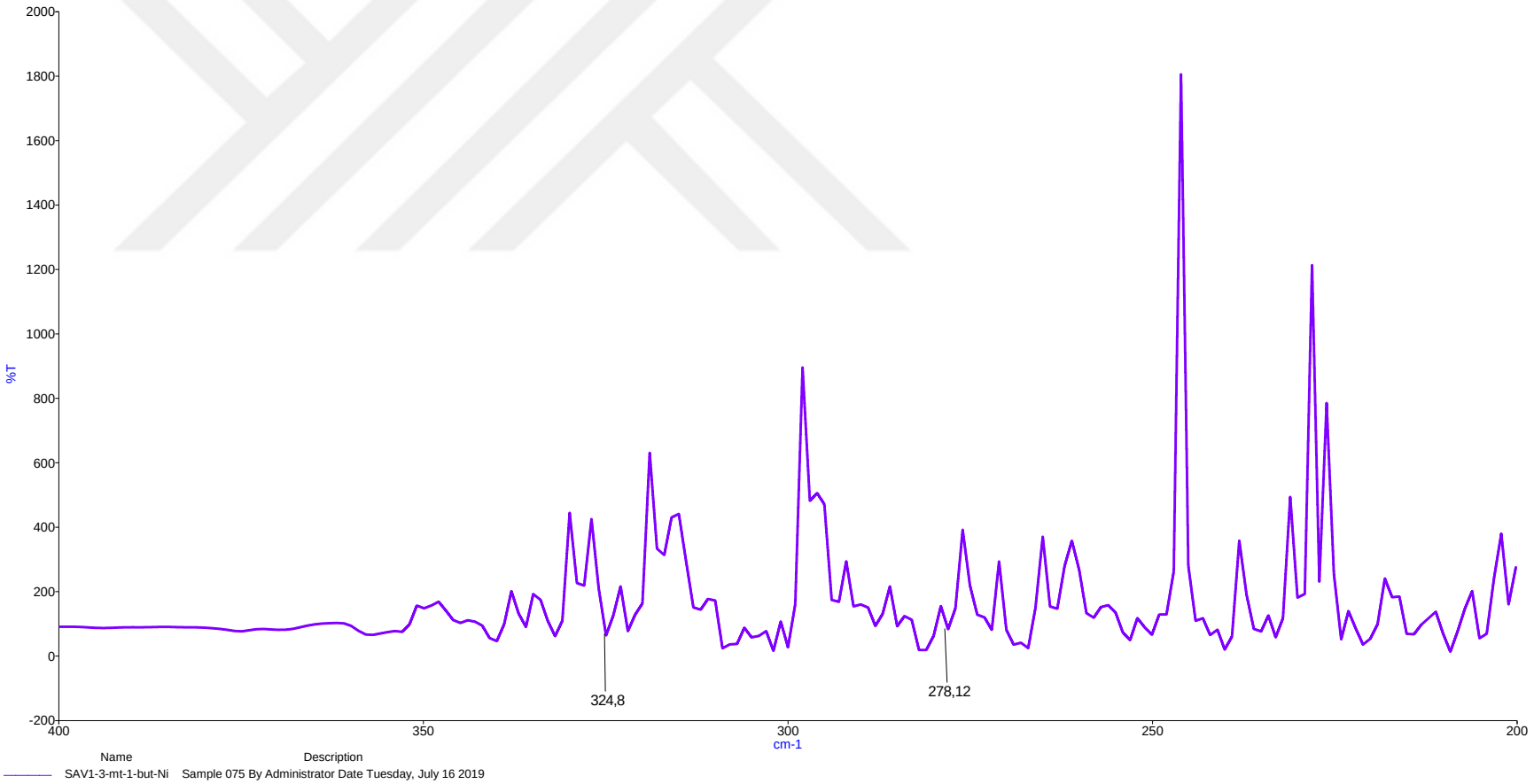


Figure 5.14.b. [Ni($S_2P(R^x)(OR6)$)$_2$] IR spectrum (400 cm^{-1}- 200 cm^{-1}).

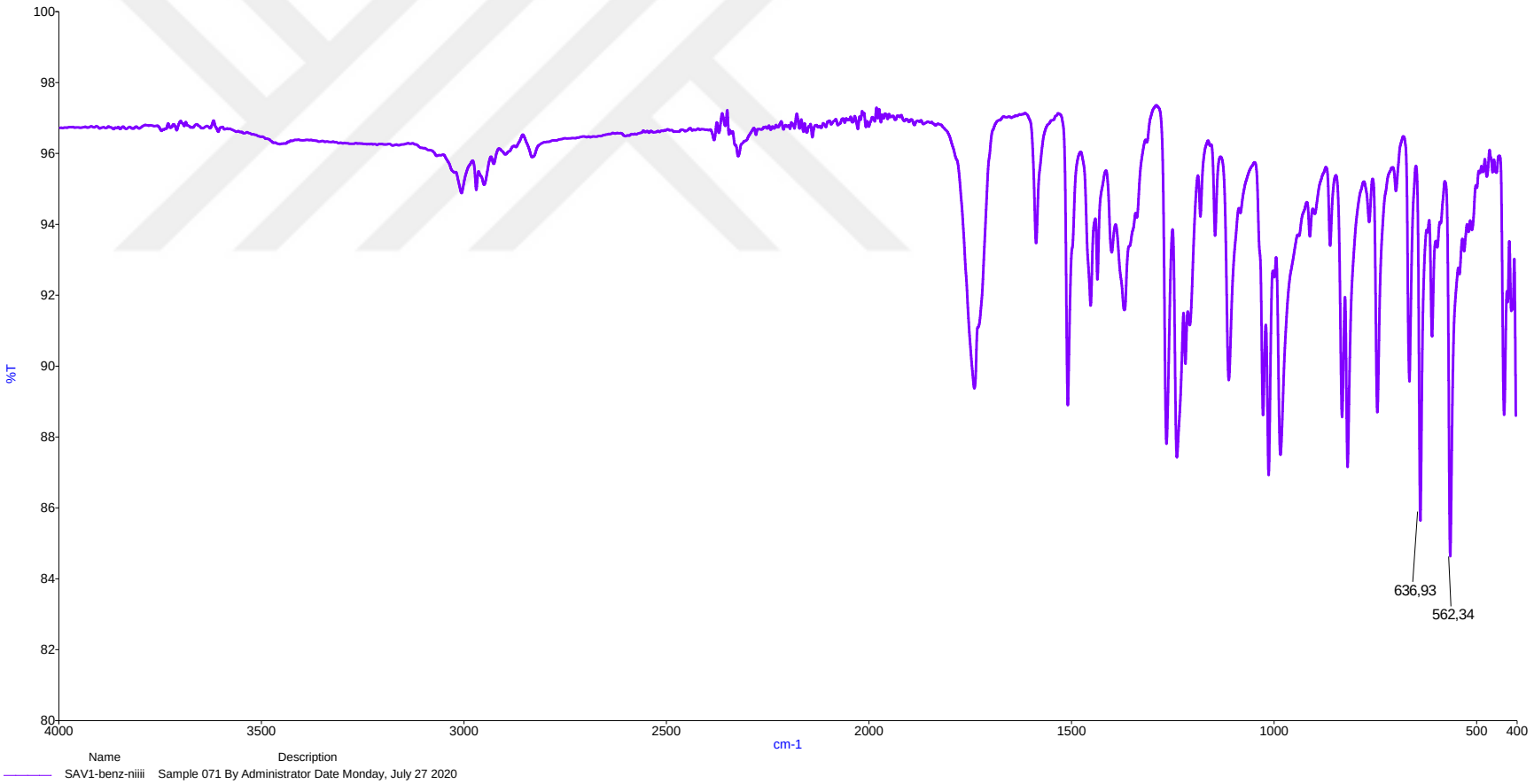


Figure 5.15.a. [Ni($S_2P(R^x)(OR7))_2$] IR spectrum (4000 cm^{-1}- 400 cm^{-1}).

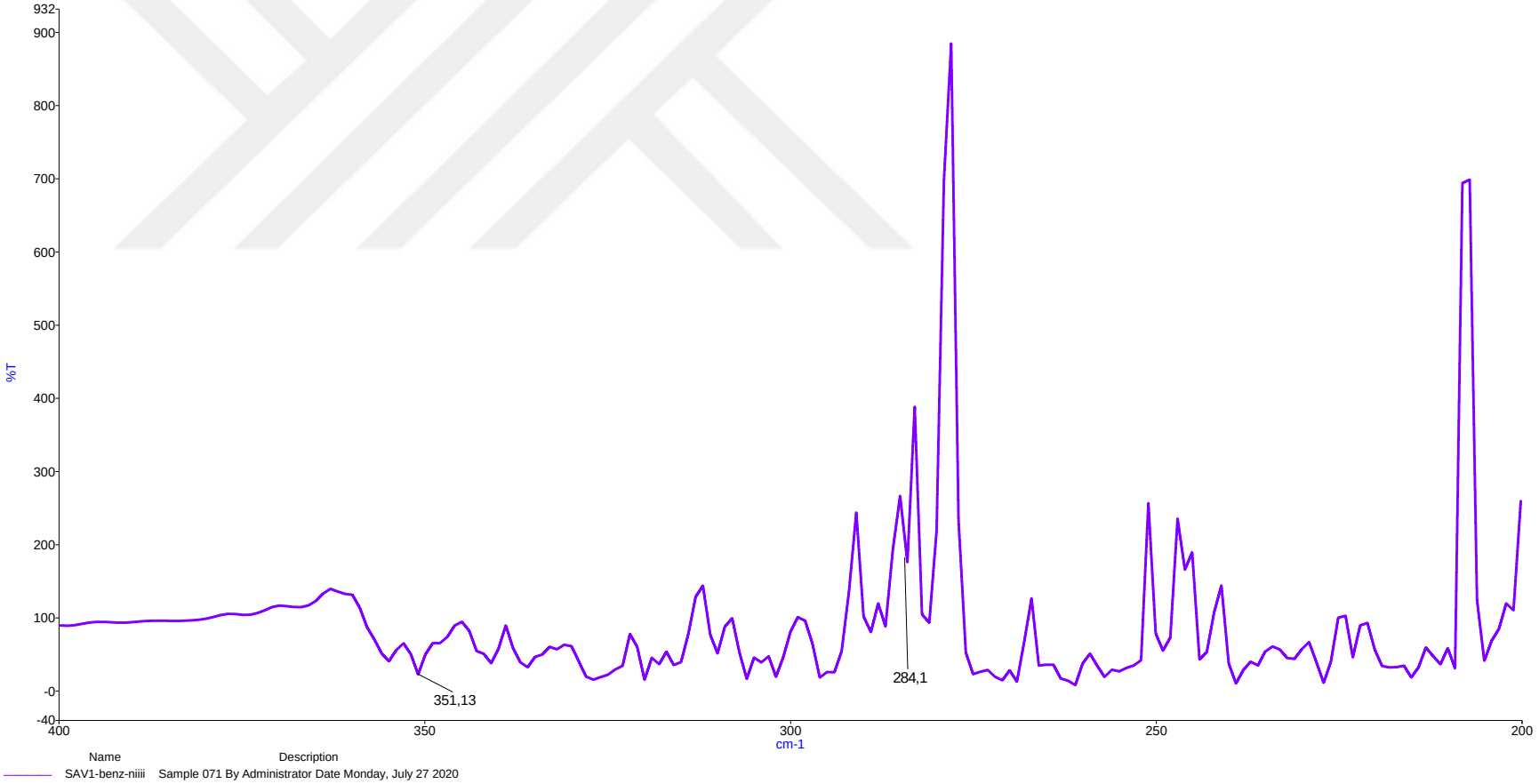


Figure 5.15.b. $[Ni(S_2P(R^x)(OR7))_2]$ IR spectrum (400 cm^{-1}- 200 cm^{-1}).

5.1.2. Comment on the IR Spectra of $[NH_4][S_2P(R^x)(ORn)]$, $[Ni(S_2P(R^x)(ORn)]$ for Part Ib

Some of the prominent IR vibration bands (cm^{-1}) for the ligands and the complexes are presented in Table 5.2. Part Ib. IR spectra of the compounds are presented in Figures 5.16-5.25. The characteristic vibrational ν(N-H) stretching peaks appear at 3189-2960 cm^{-1} (the ligands). This bands is absent in the IR spectra of the complexes, indicating the formation of nickel-sulfur bonds. In the IR spectra of the ligands, the vibration bands at 567-557 cm^{-1} and 684-641 cm^{-1} belong to the symmetric and asymmetric PS stretching modes ($\nu(PS)_{sym}$ and $\nu(PS)_{asym}$), respectively. For the Ni(II) complexes, these bands are shifted to 562-555 cm^{-1} for $\nu(PS)_{sym}$ and 660-629 cm^{-1} for $\nu(PS)_{asym}$. Symmetric and asymmetric Nickel-sulfur vibration frequencies ($\nu(Ni\text{-}S)_{sym}$ and $\nu(Ni\text{-}S)_{asym}$) are also discernable at 293-263 cm^{-1} and 335-317 cm^{-1}, respectively. Literature values for the same vibrations on similar structures confirm the assignments given [63, 71, 183, 236].

Table 5.2. Part Ib Selected IR data (cm^{-1}) assignment of vibrational bands for the compounds.

Compounds	$\nu(Ni\text{-}S)_{sym}$	$\nu(Ni\text{-}S)_{asym}$	$\nu(PS)_{sym}$	$\nu(PS)_{asym}$	$\nu(N\text{-}H)$
$[NH_4][S_2P(R^x)(OR1)]$	-	-	557	685	3179
$[NH_4][S_2P(R^x)(OR2)]$	-	-	557	641	3192
$[NH_4][S_2P(R^x)(OR3)]$	-	-	560	665	3190
$[NH_4][S_2P(R^x)(OR4)]$	-	-	557	667	3194
$[NH_4][S_2P(R^x)(OR5)]$	-	-	557	678	3197
$[Ni(S_2P(R^x)(OR1))_2]$	265	331	560	630	-
$[Ni(S_2P(R^x)(OR2))_2]$	263	321	562	636	-
$[Ni(S_2P(R^x)(OR3))_2]$	267	335	557	643	-
$[Ni(S_2P(R^x)(OR4))_2]$	293	317	562	636	-
$[Ni(S_2P(R^x)(OR5))_2]$	279	324	560	636	-

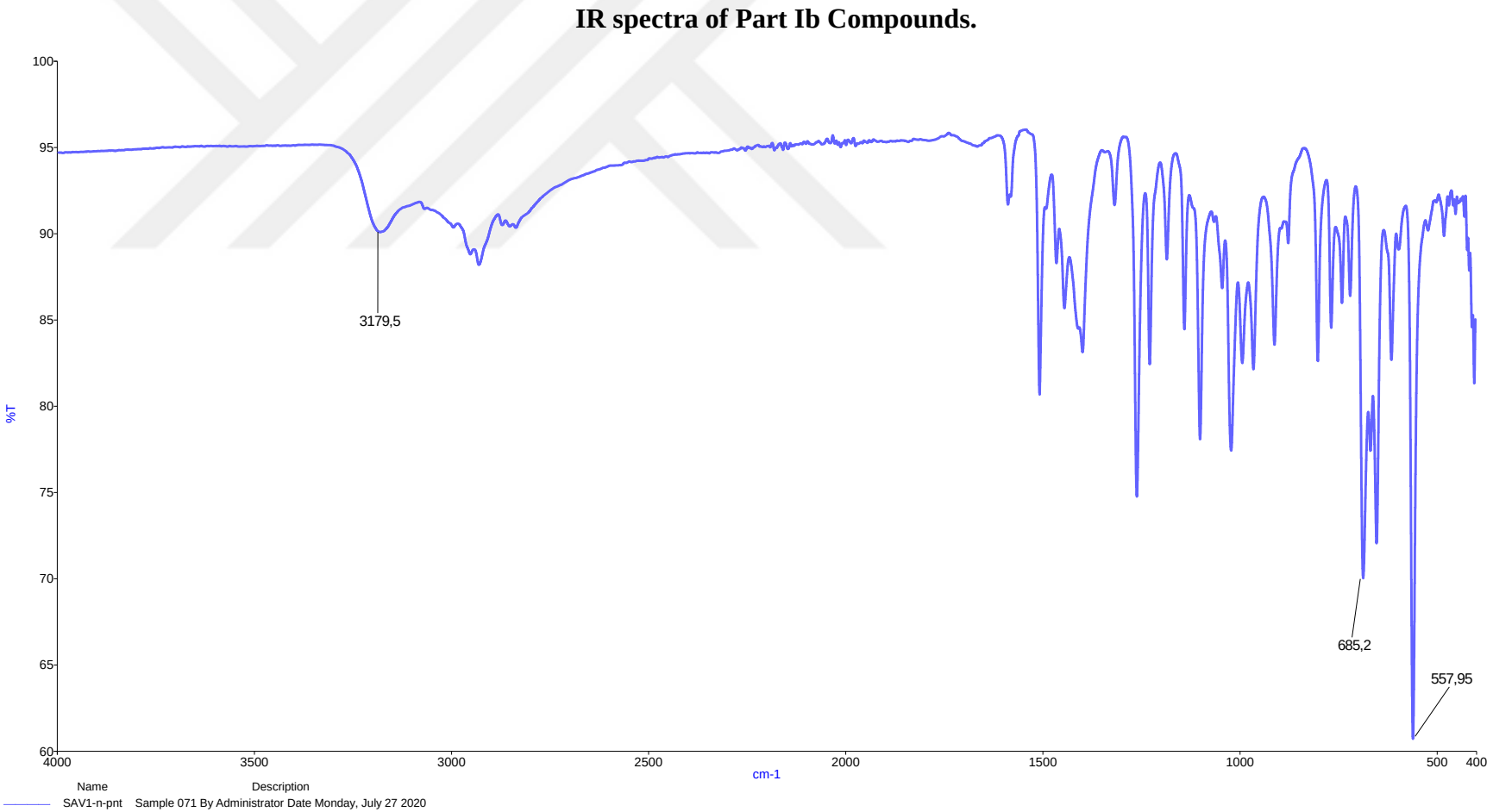


Figure 5.16. $[NH_4][S_2P(R^x)(OR1)]$ IR spectrum (4000 cm^{-1}- 400 cm^{-1}).

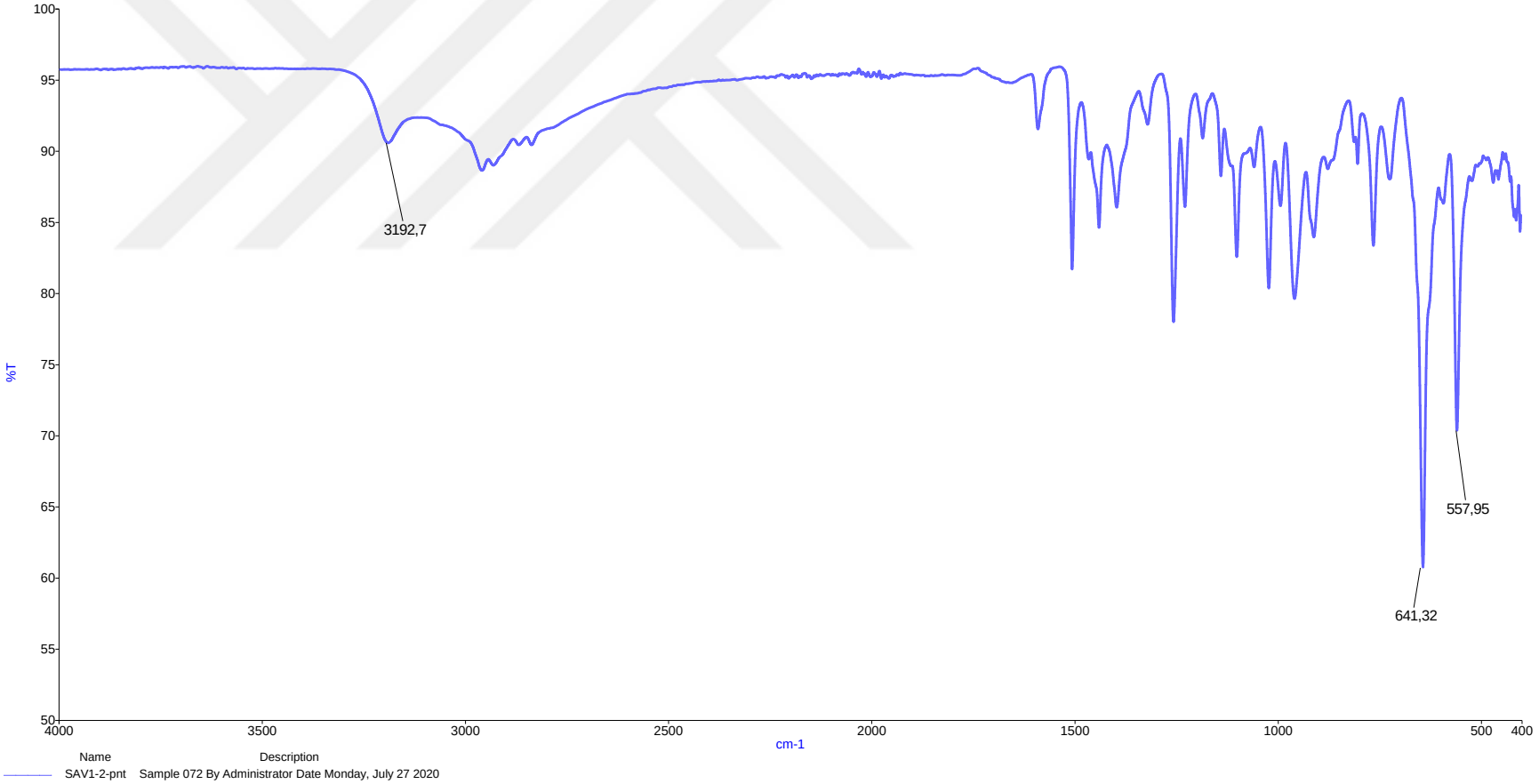


Figure 5.17. $[NH_4][S_2P(R^x)(OR2)]$ IR spectrum (4000 cm^{-1}- 400 cm^{-1}).

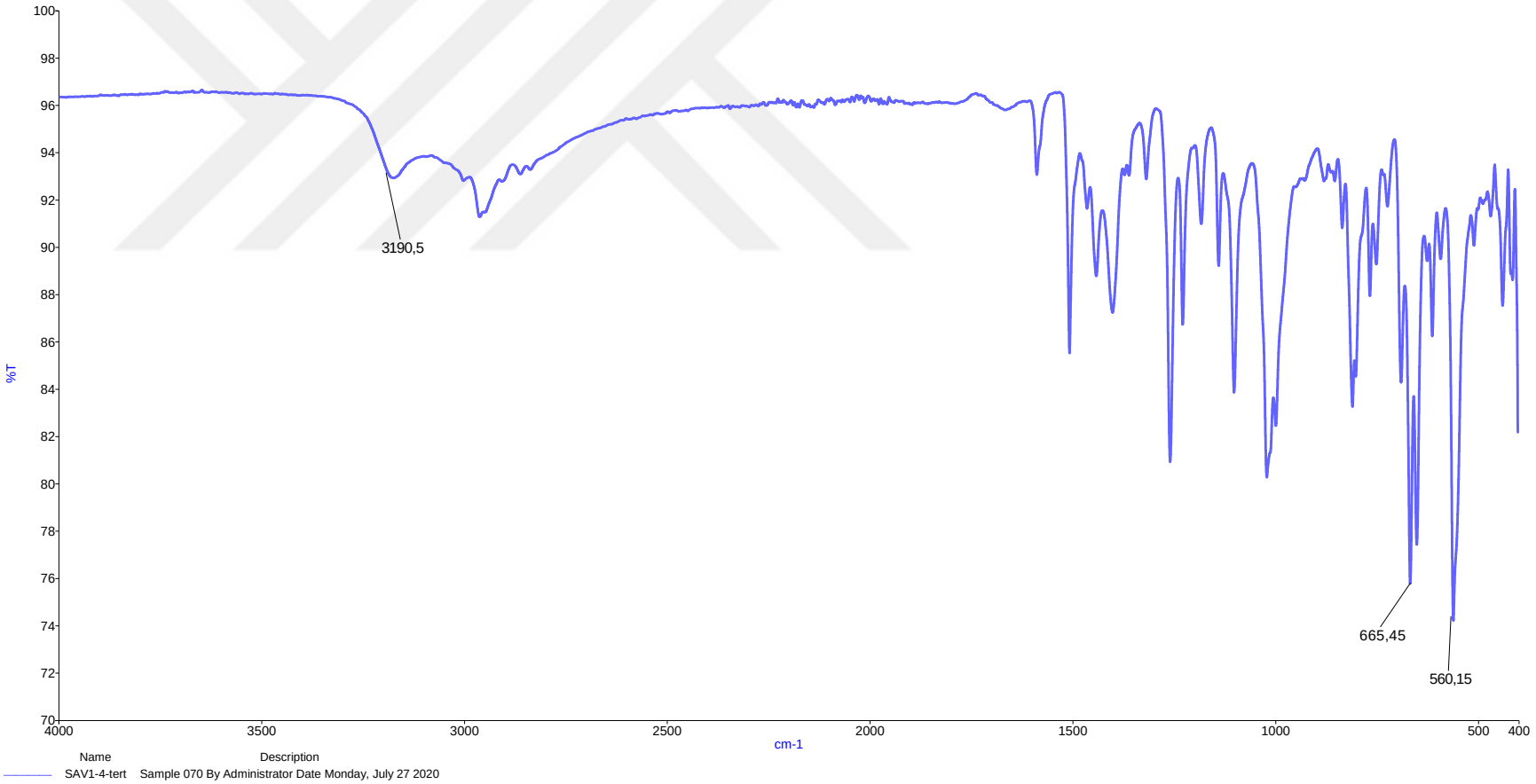


Figure 5.18. $[NH_4][S_2P(R^x)(OR3)]$ IR spectrum (4000 cm^{-1}- 400 cm^{-1}).

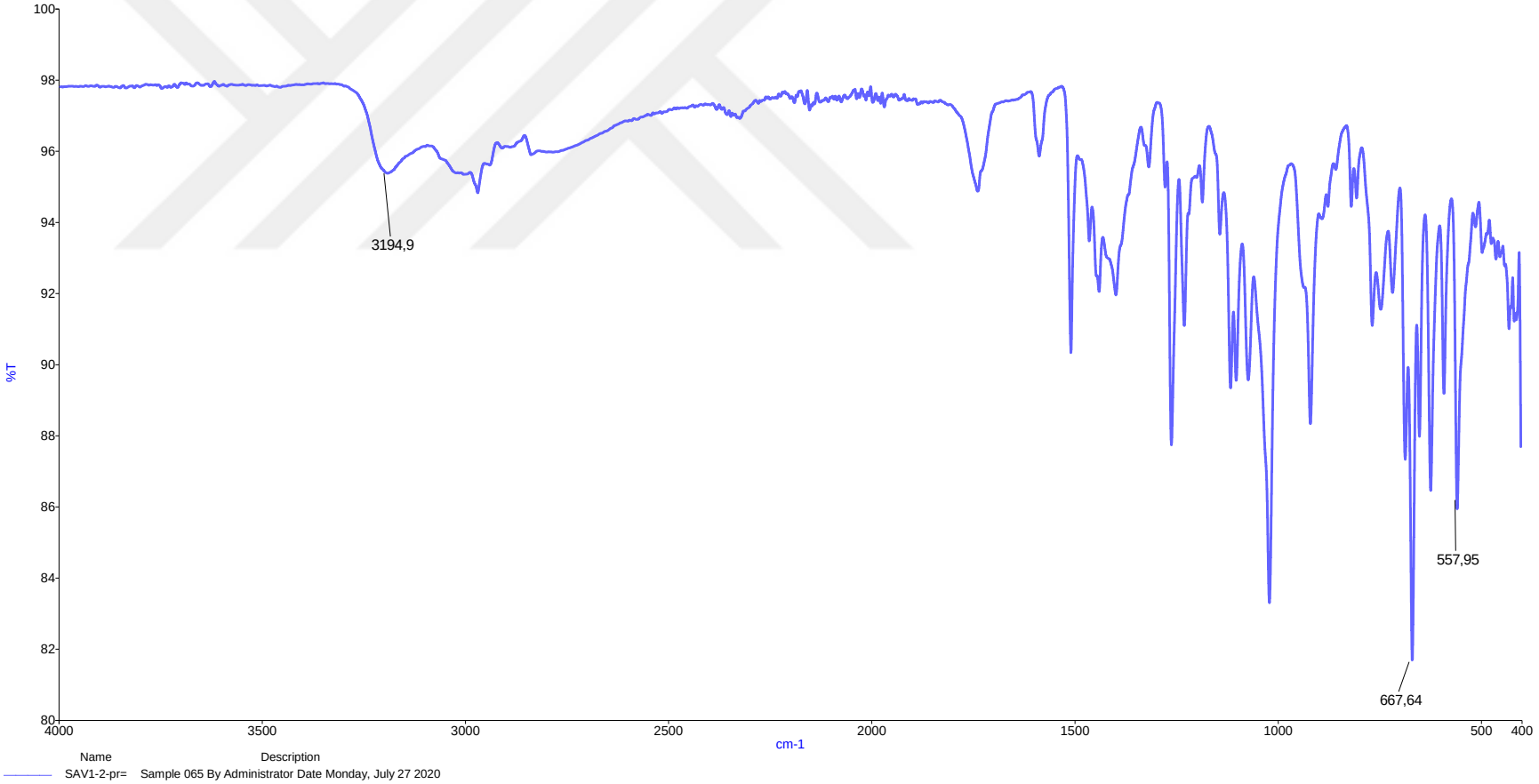


Figure 5.19. $[NH_4][S_2P(R^x)(OR4)]$ IR spectrum (4000 cm^{-1}- 400 cm^{-1}).

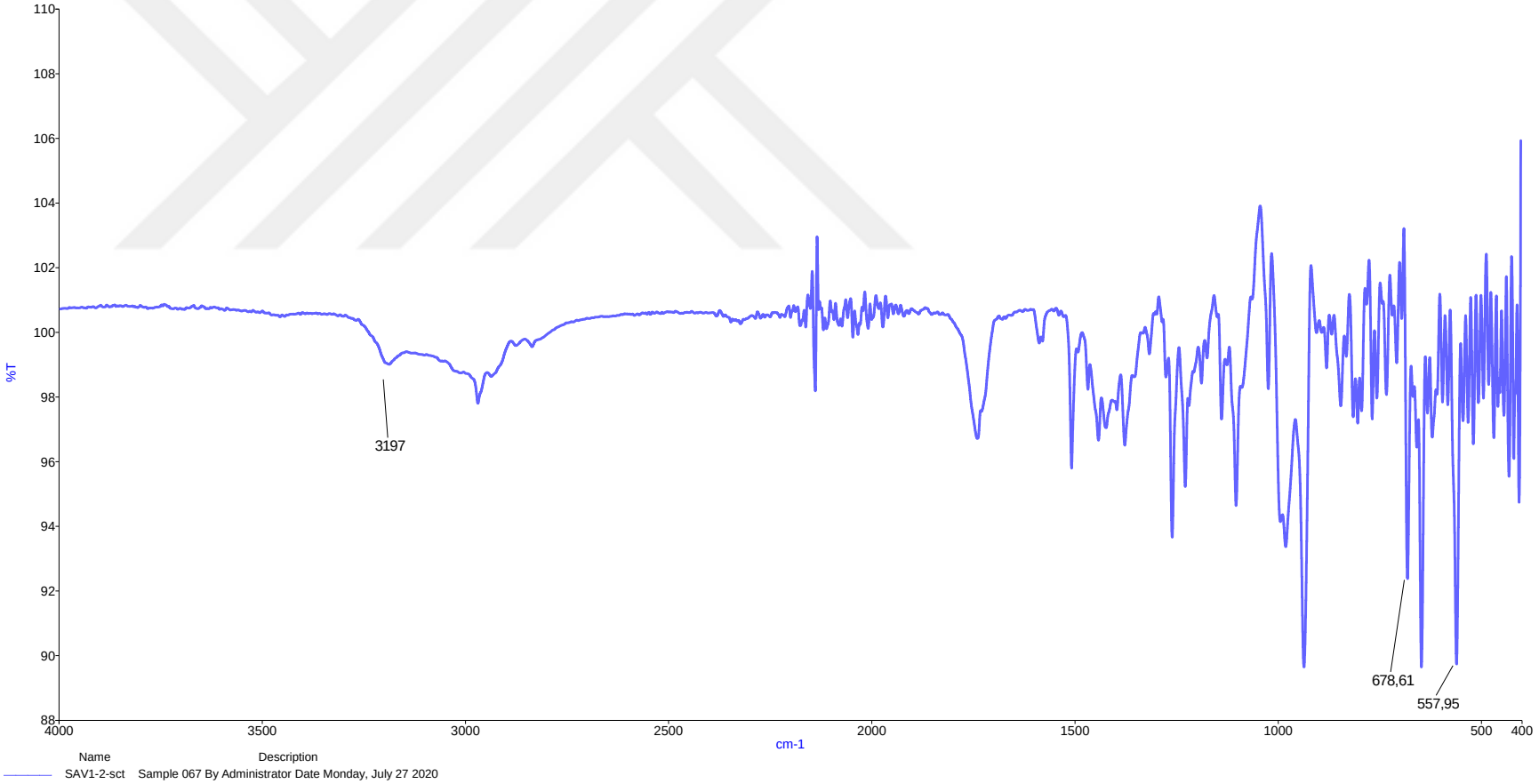


Figure 5.20. $[NH_4][S_2P(R^x)(OR5)]$ IR spectrum (4000 cm^{-1}- 400 cm^{-1}).

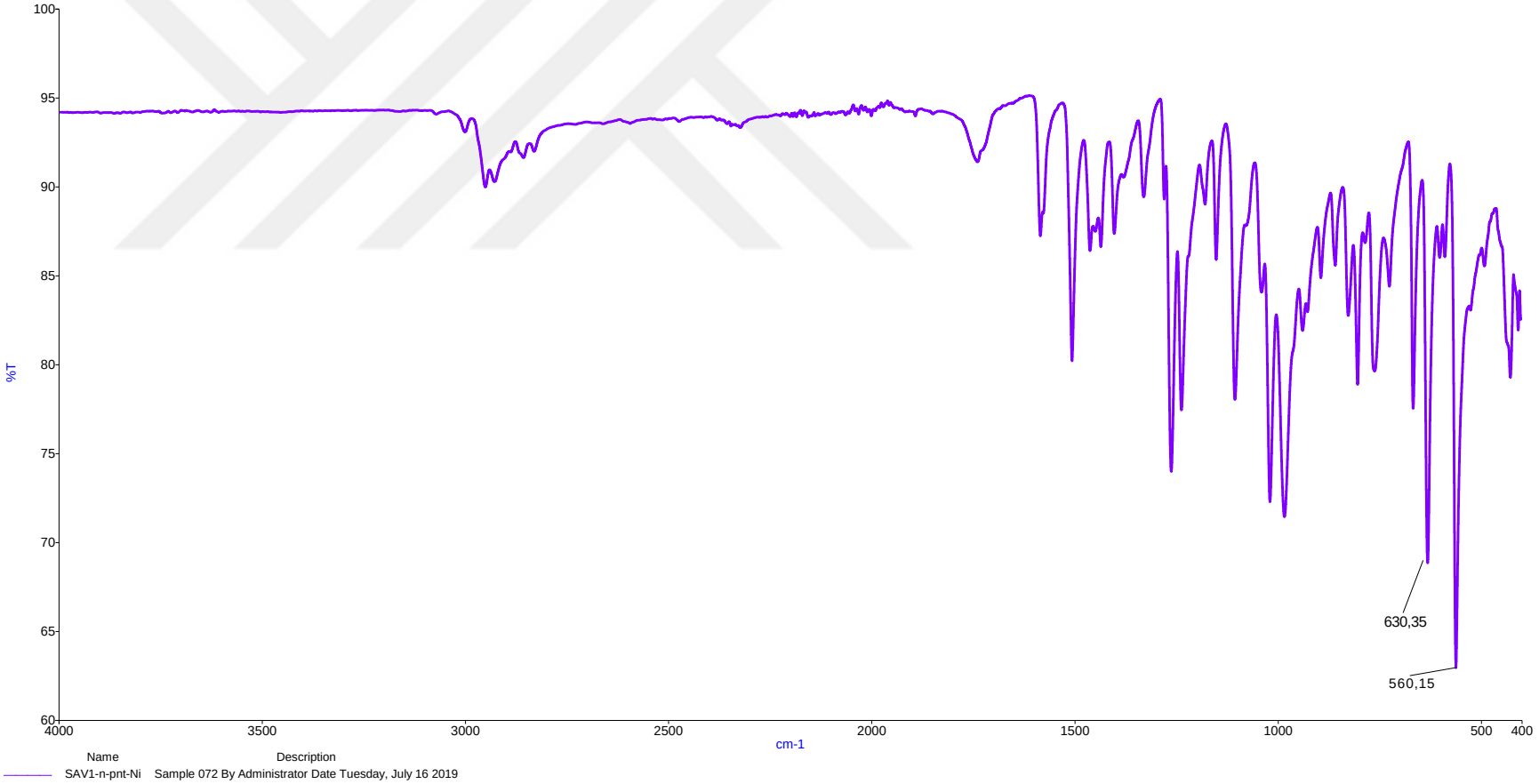


Figure 5.21.a. [Ni($S_2P(R^x)(OR1))_2$] IR spectrum (4000 cm^{-1}-400 cm^{-1})

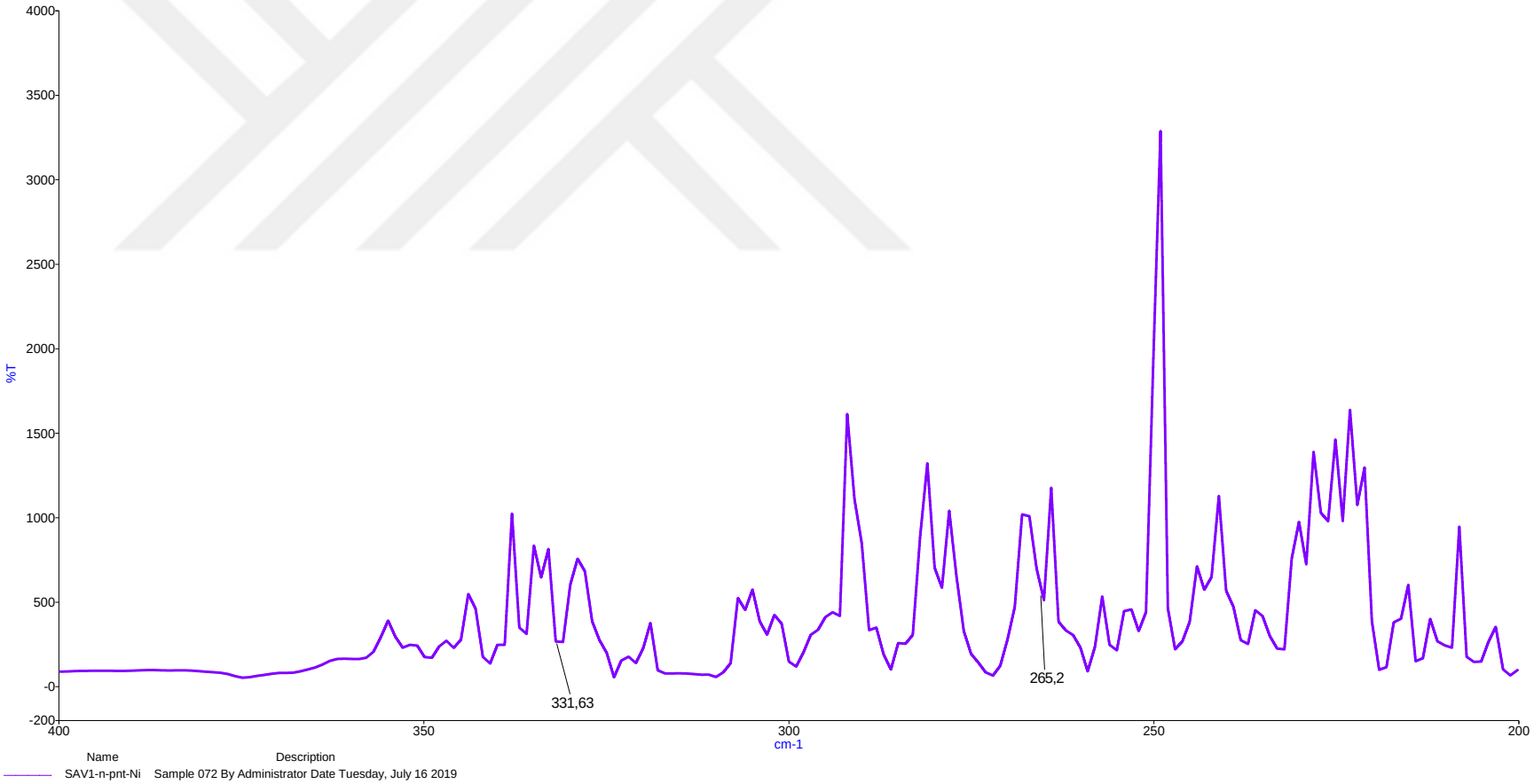


Figure 5.21.b. [Ni($S_2P(R^x)(OR1))_2$] IR spectrum (400 cm^{-1}- 200 cm^{-1})

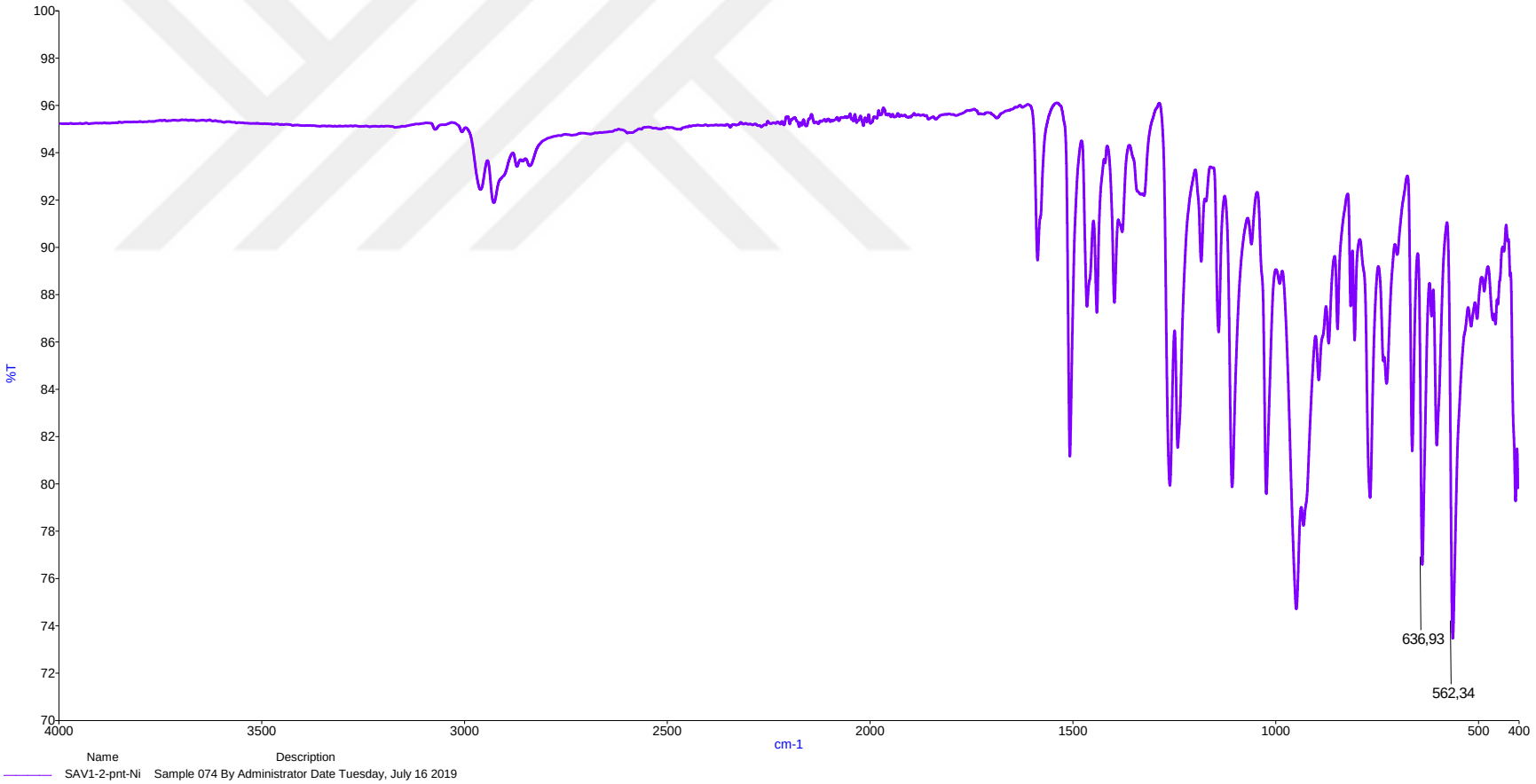


Figure 5.22.a. [Ni($S_2P(R^x)(OR2)_2$] IR spectrum (4000 cm^{-1}- 400 cm^{-1}).

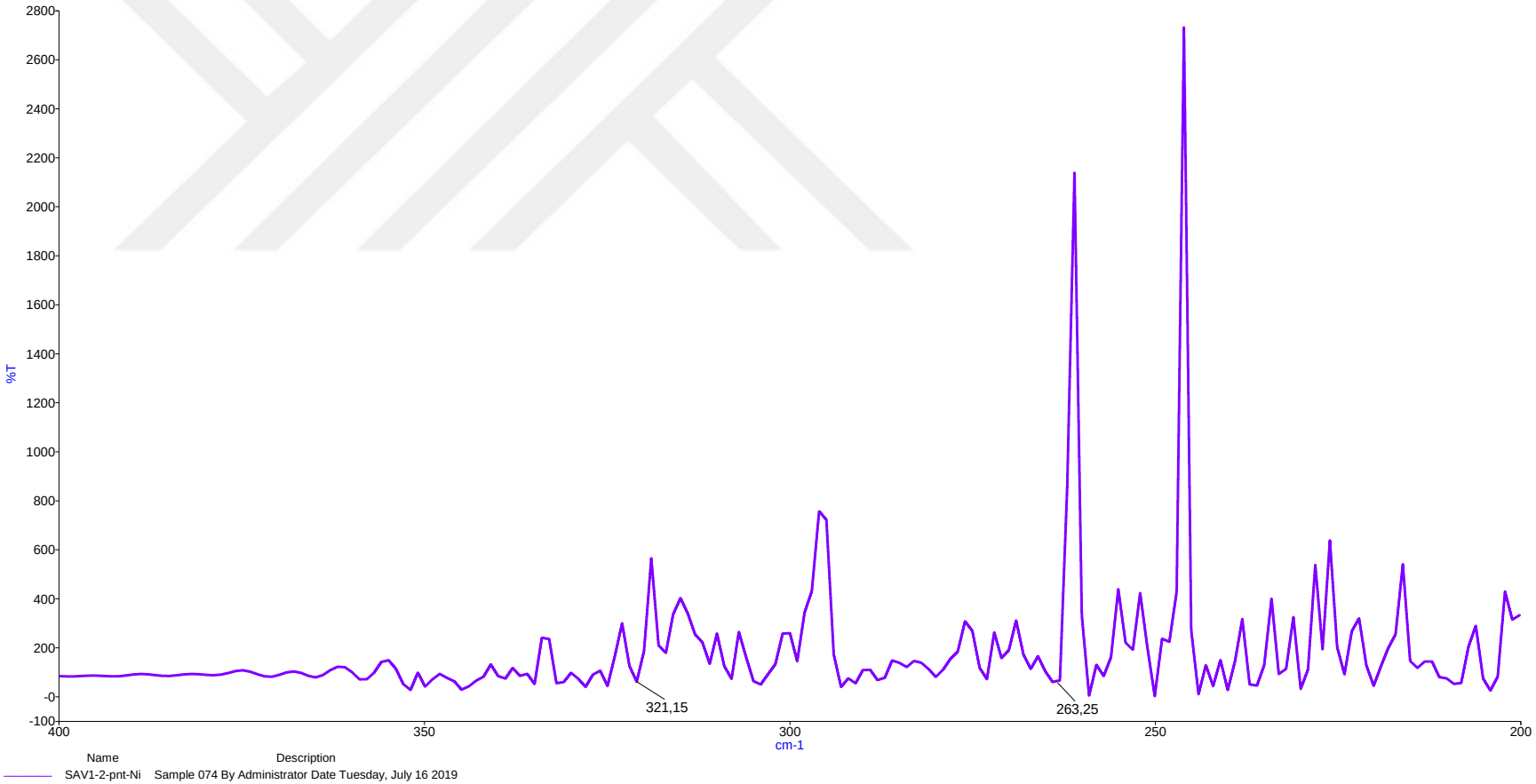


Figure 5.22.b. [Ni($S_2P(R^x)(OR2)$)$_2$] IR spectrum (400 cm^{-1}- 200 cm^{-1})

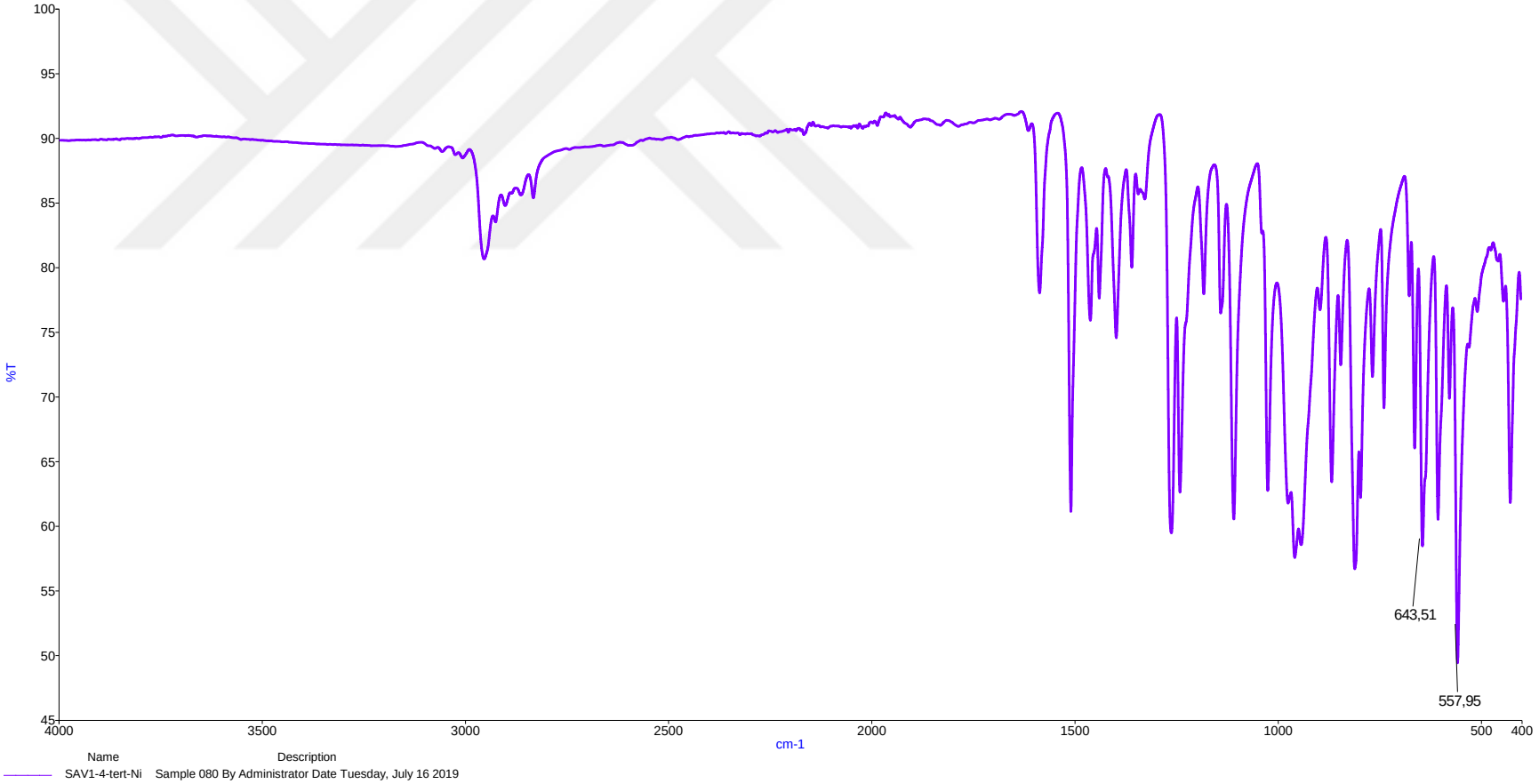


Figure 5.23.a. [Ni($S_2P(R^x)(OR3))_2$] IR spectrum (4000 cm^{-1}- 400 cm^{-1})

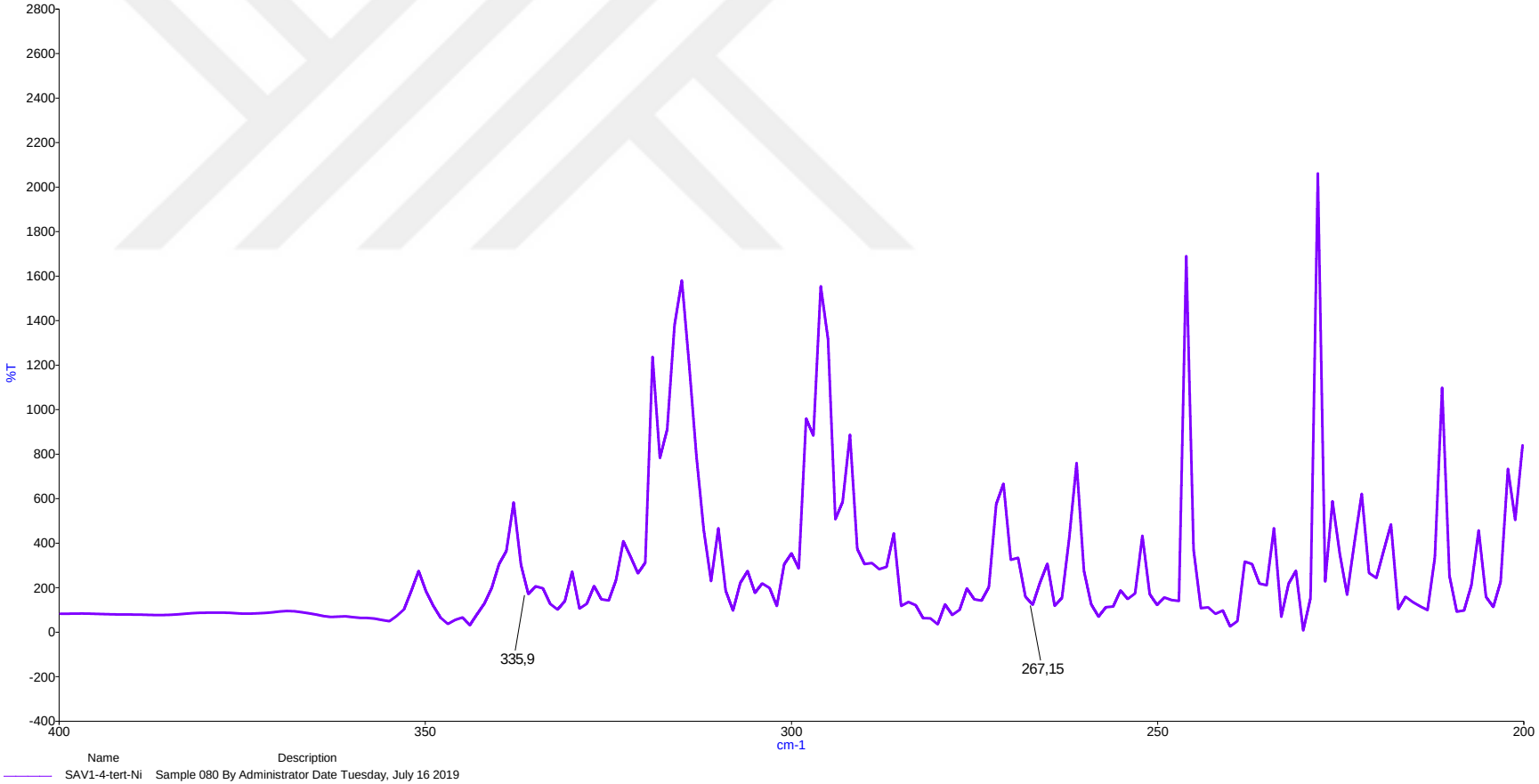


Figure 5.23.b. [Ni($S_2P(R^x)(OR3))_2$] IR spectrum (400 cm^{-1}- 200 cm^{-1})

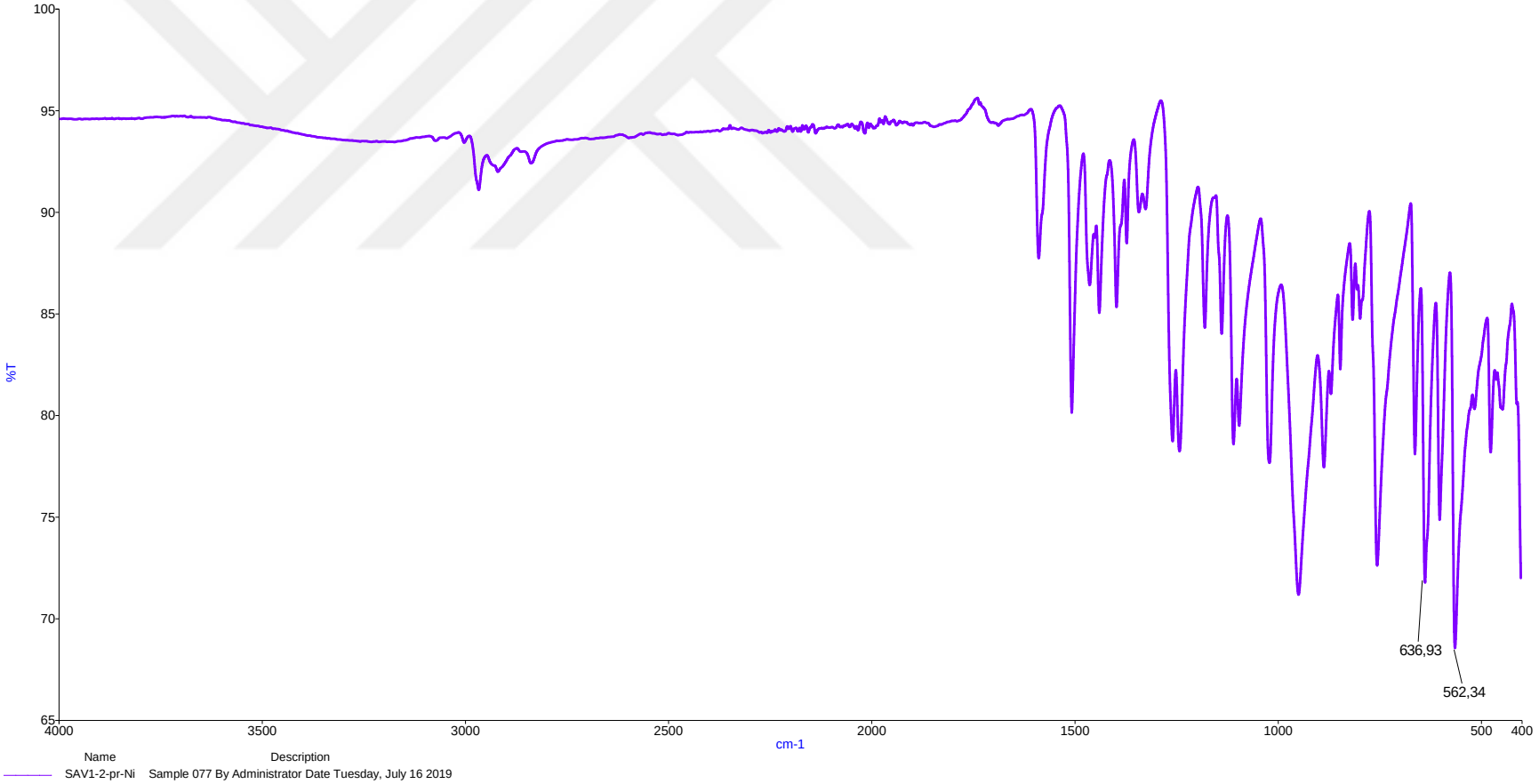


Figure 5.24.a. [Ni($S_2P(R^x)(OR4))_2$] IR spectrum (4000 cm^{-1}- 400 cm^{-1})

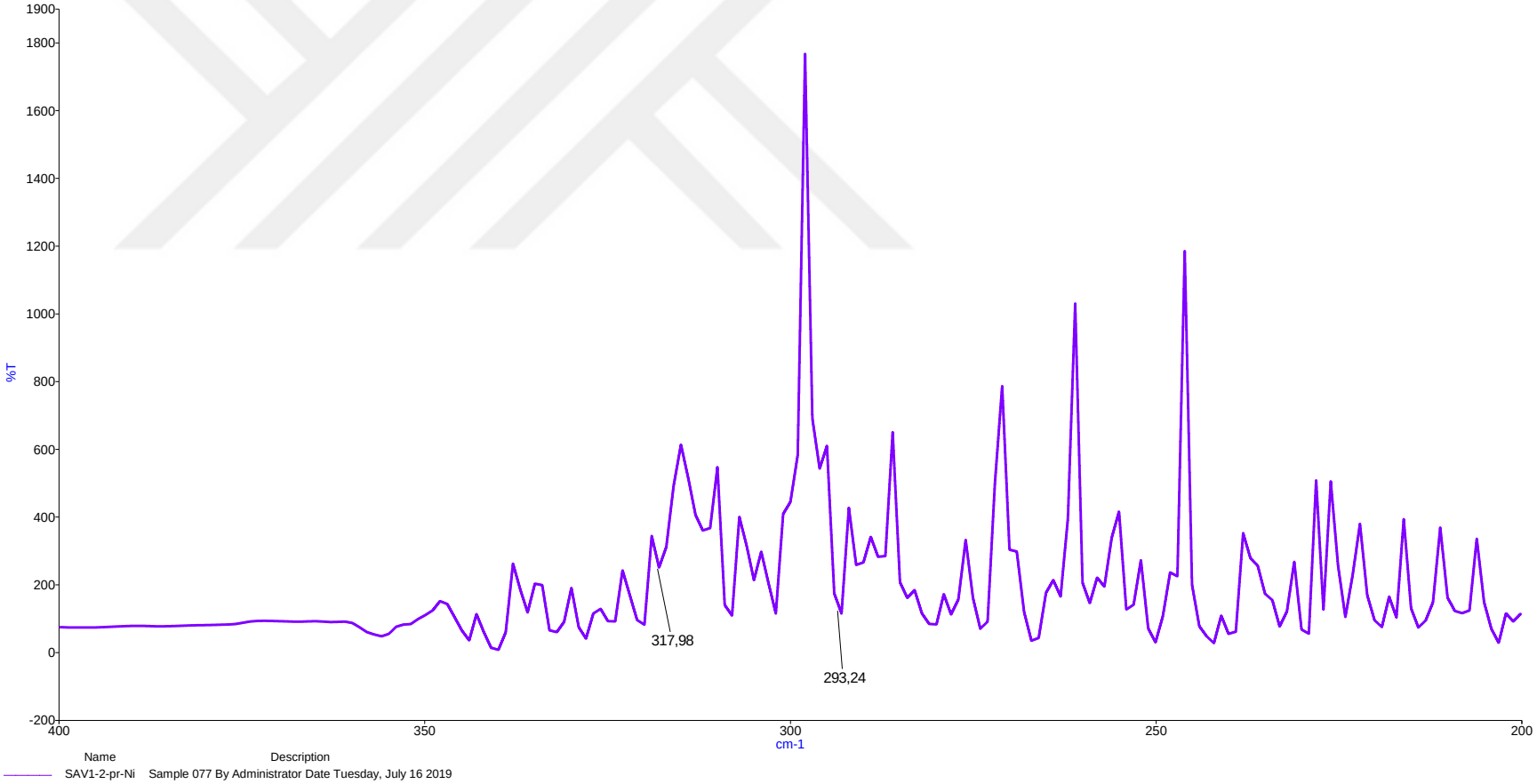


Figure 5.24.b. [Ni($S_2P(R^x)(OR4))_2$] IR spectrum (400 cm^{-1}- 200 cm^{-1})

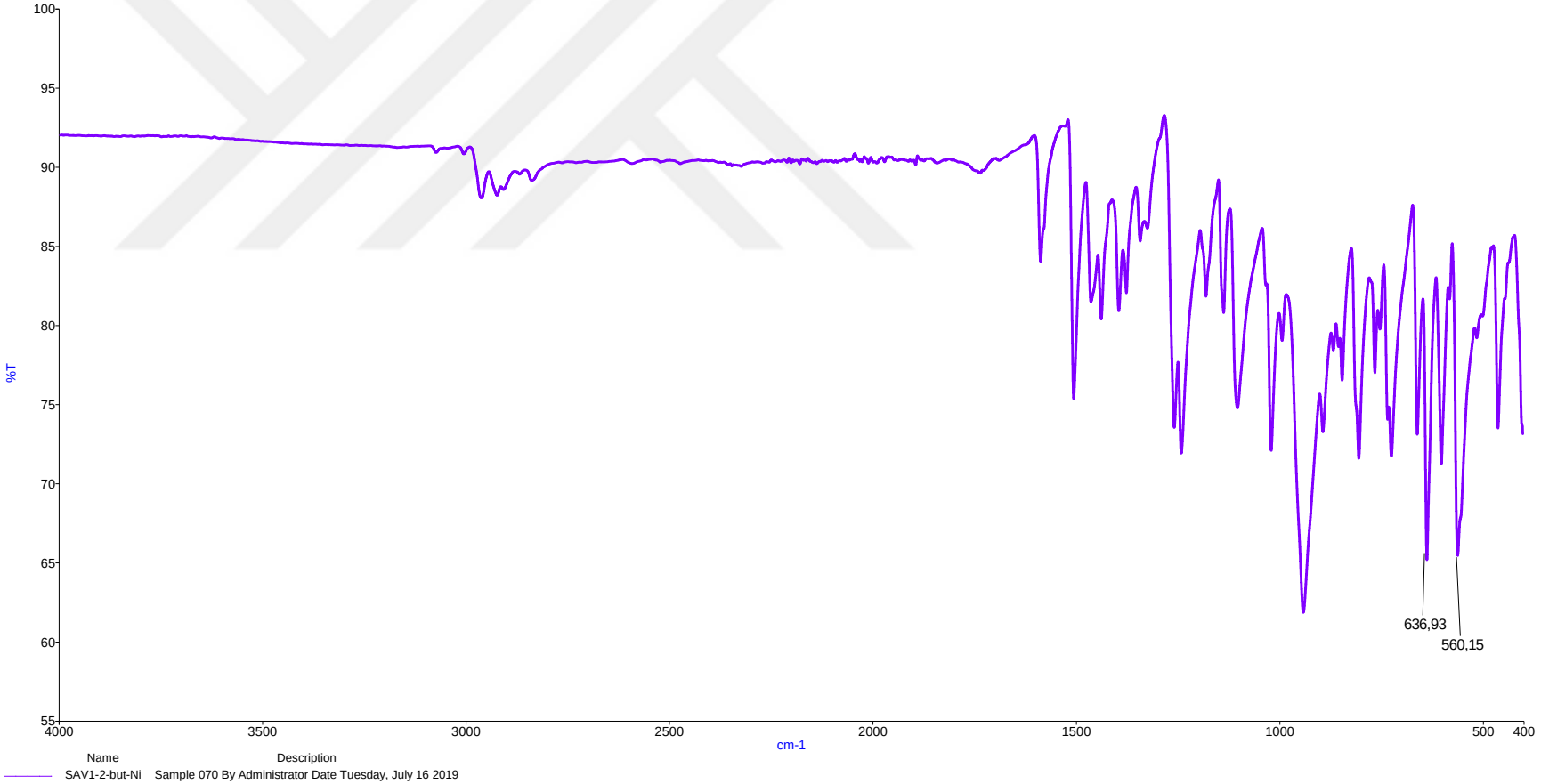


Figure 5.25.a. [Ni($S_2P(R^x)(OR5)$)$_2$] IR spectrum (4000 cm^{-1}- 400 cm^{-1})

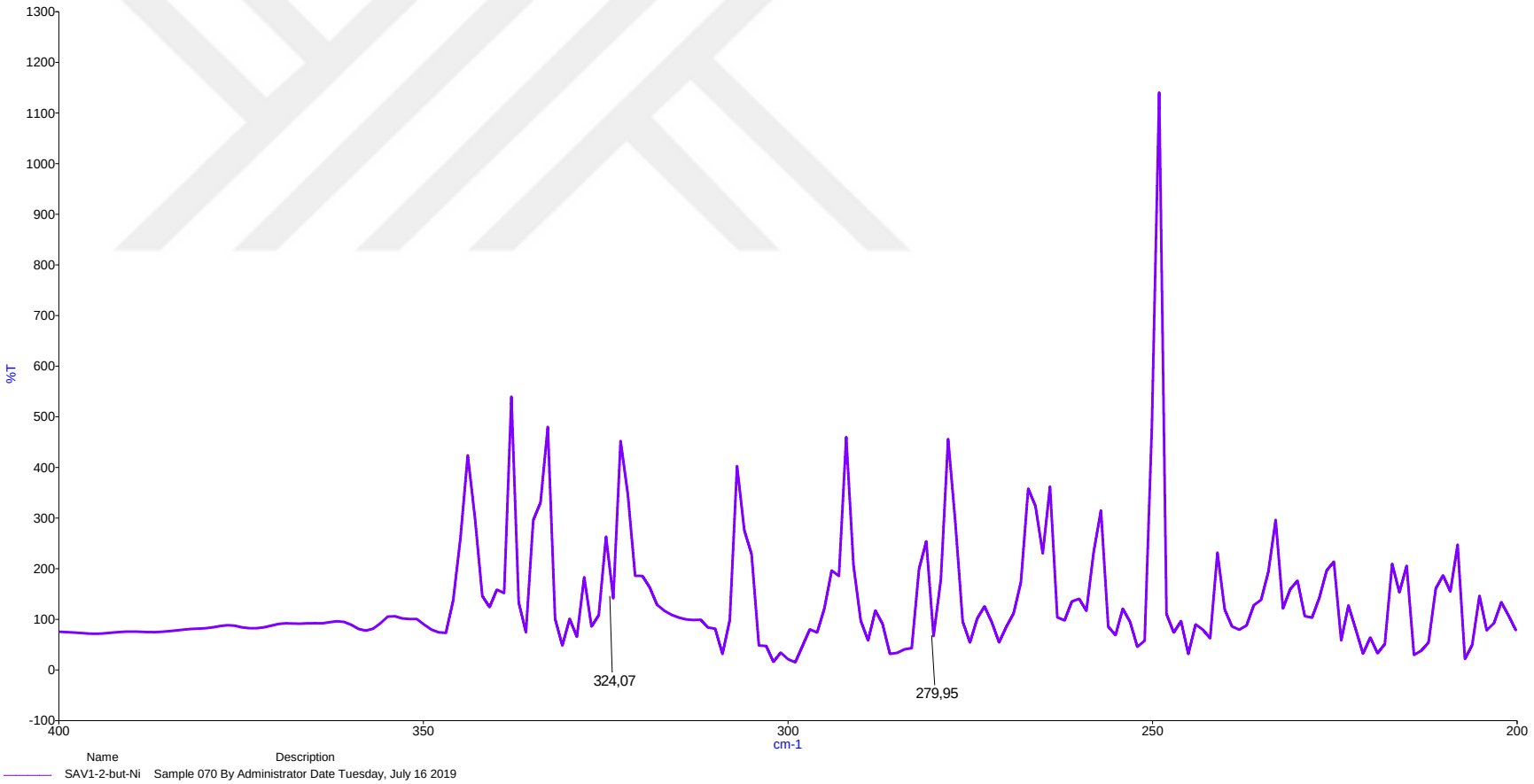


Figure 5.25.b. [$Ni(S_2P(R^x)(OR5))_2$] IR spectrum (400 cm^{-1}- 200 cm^{-1})

5.1.3. Comment on the IR Spectra of $[R^y\text{-}P(S)S]_2$, $[NH_4][S_2P(R^y)(ORn)]$, $[Ni(S_2P(R^y)(ORn)]$ for Part II

The IR data of the compounds are presented in Table 5.3 and their spectra are in Figures 5.26-5.34. The characteristic ν(N-H) stretching bands of the ligands appear at 2967-2953 cm^{-1} on IR. These bands disappear on the IR spectra of the complexes proving the substitution of the ammonium group by metal cations. Symmetric and asymmetric PS stretching vibrations ($\nu(PS)_{sym}$ and $\nu(PS)_{asym}$) of the ligands are shown up at 559-554 cm^{-1} cm^{-1} and 665-651 cm^{-1}, respectively. On the other hand, the spectra of the complexes all show two bands in the ranges 560-549 cm^{-1} and 682-669 cm^{-1} attributable to the ν_{sym} and ν_{asym} PS stretching bands, respectively. The complexes also display Ni-S bands ($\nu(Ni\text{-}S)_{sym}$ and $\nu(Ni\text{-}S)_{asym}$) that are located at 271-287 cm^{-1} and 330-342 cm^{-1}, respectively. IR data reported for similar compounds agree well with our findings [131, 296-298].

Table 5.3. IR data (cm^{-1}) assignment of vibrational bands of the compounds for Part II.

Compounds	$\nu(Ni\text{-}S)_{sym}$	$\nu(Ni\text{-}S)_{asym}$	$\nu(PS)_{sym}$	$\nu(PS)_{asym}$	ν(N-H)
SAV-A2	-	-	566	685	-
$[NH_4][S_2P(R^y)(OR1)]$	-	-	555	654	3017
$[NH_4][S_2P(R^y)(OR2)]$	-	-	557	652	3019
$[NH_4][S_2P(R^y)(OR3)]$	-	-	559	665	3018
$[NH_4][S_2P(R^y)(OR4)]$	-	-	553	655	3019
$[Ni(S_2P(R^y)(OR1))_2]$	271	342	560	674	-
$[Ni(S_2P(R^y)(OR2))_2]$	287	330	549	669	-
$[Ni(S_2P(R^y)(OR3))_2]$	285	332	557	680	-
$[Ni(S_2P(R^y)(OR4))_2]$	281	328	557	680	-

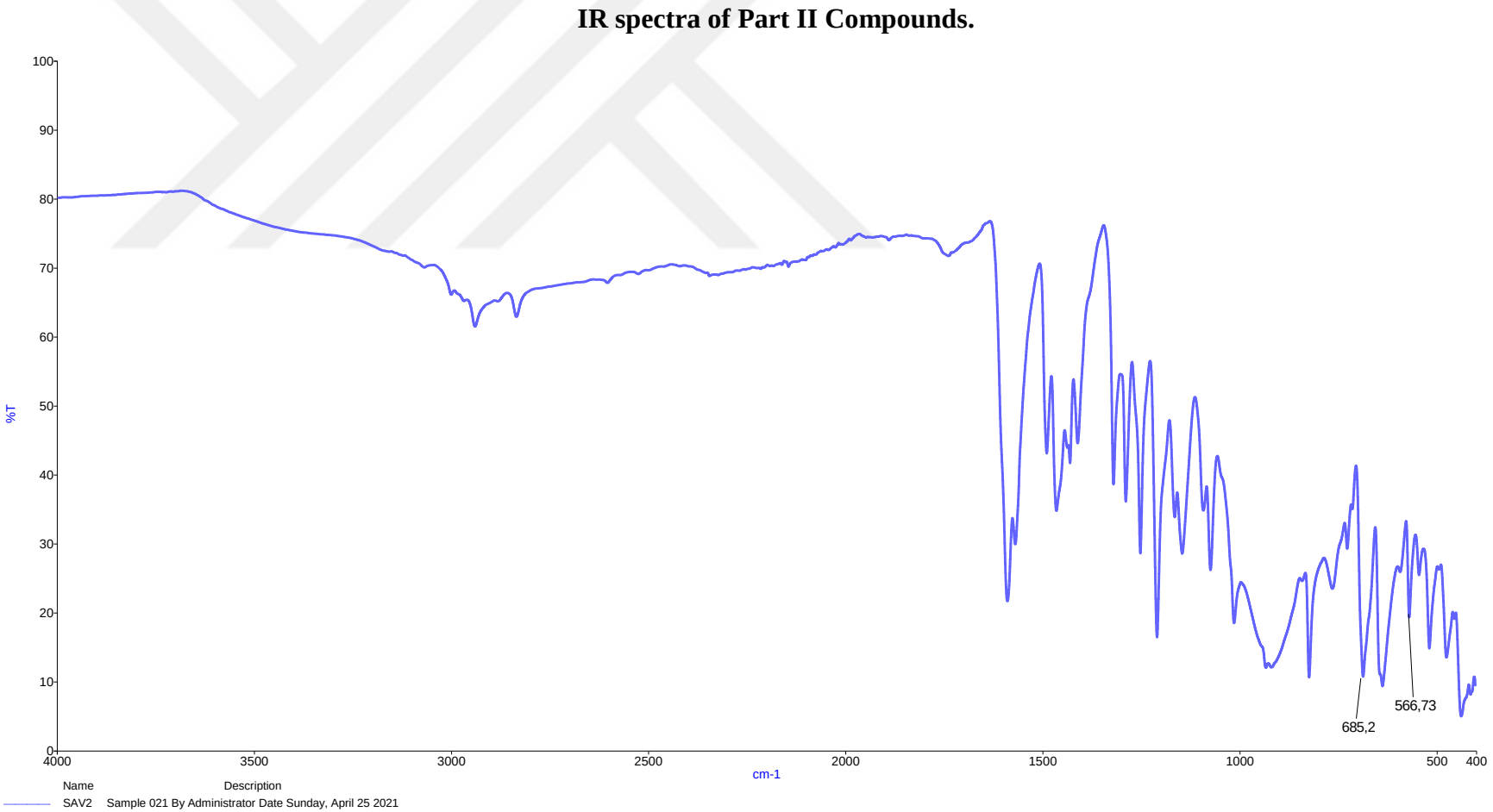


Figure 5.26. SAV-A2 IR spectrum (4000 cm^{-1}- 400 cm^{-1}).

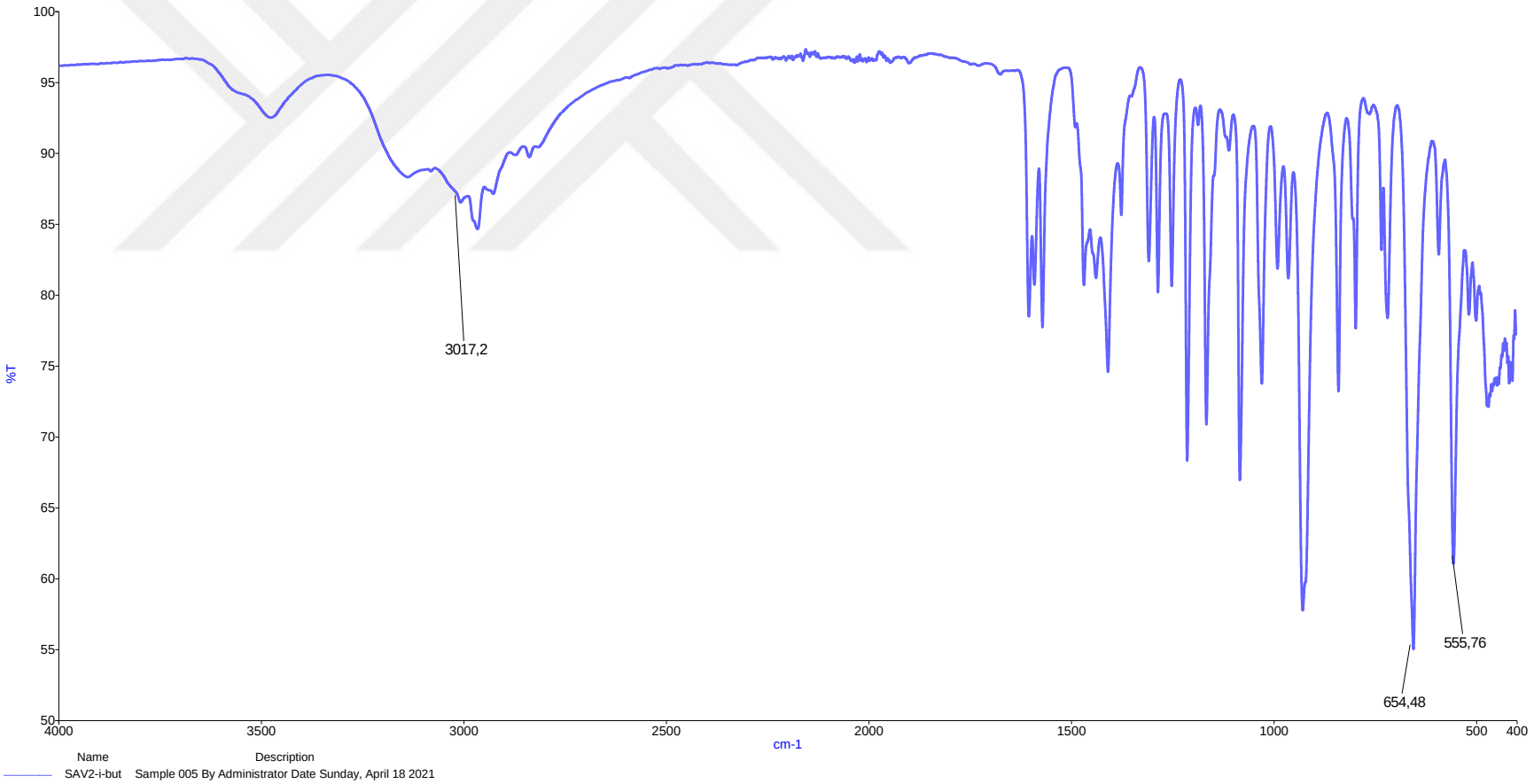


Figure 5.27. $[NH_4][S_2P(R^y)(OR1)]$ IR spectrum (4000 cm^{-1}- 400 cm^{-1})

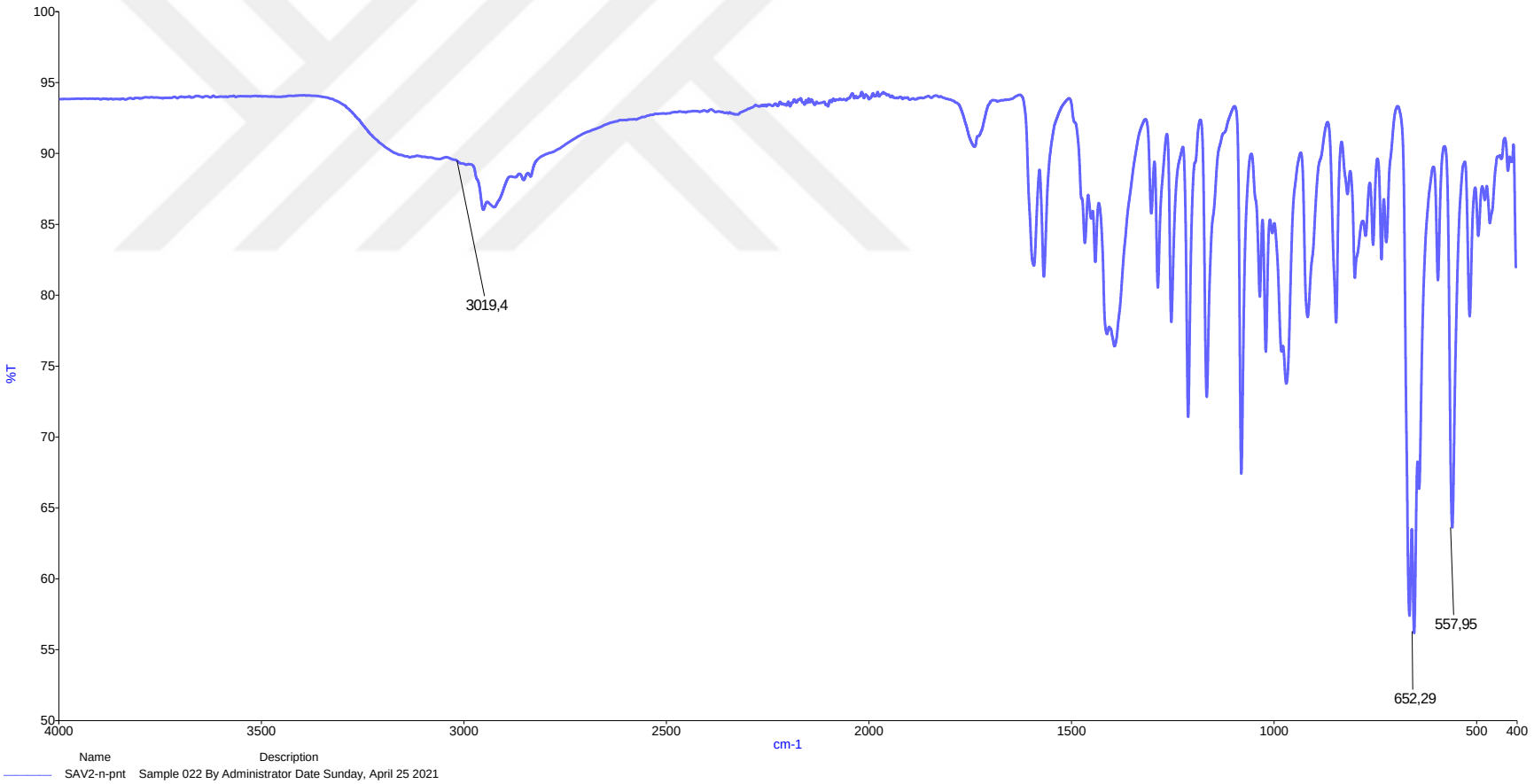


Figure 5.28. $[NH_4][S_2P(R^y)(OR2)]$ IR spectrum (4000 cm^{-1}- 400 cm^{-1}).

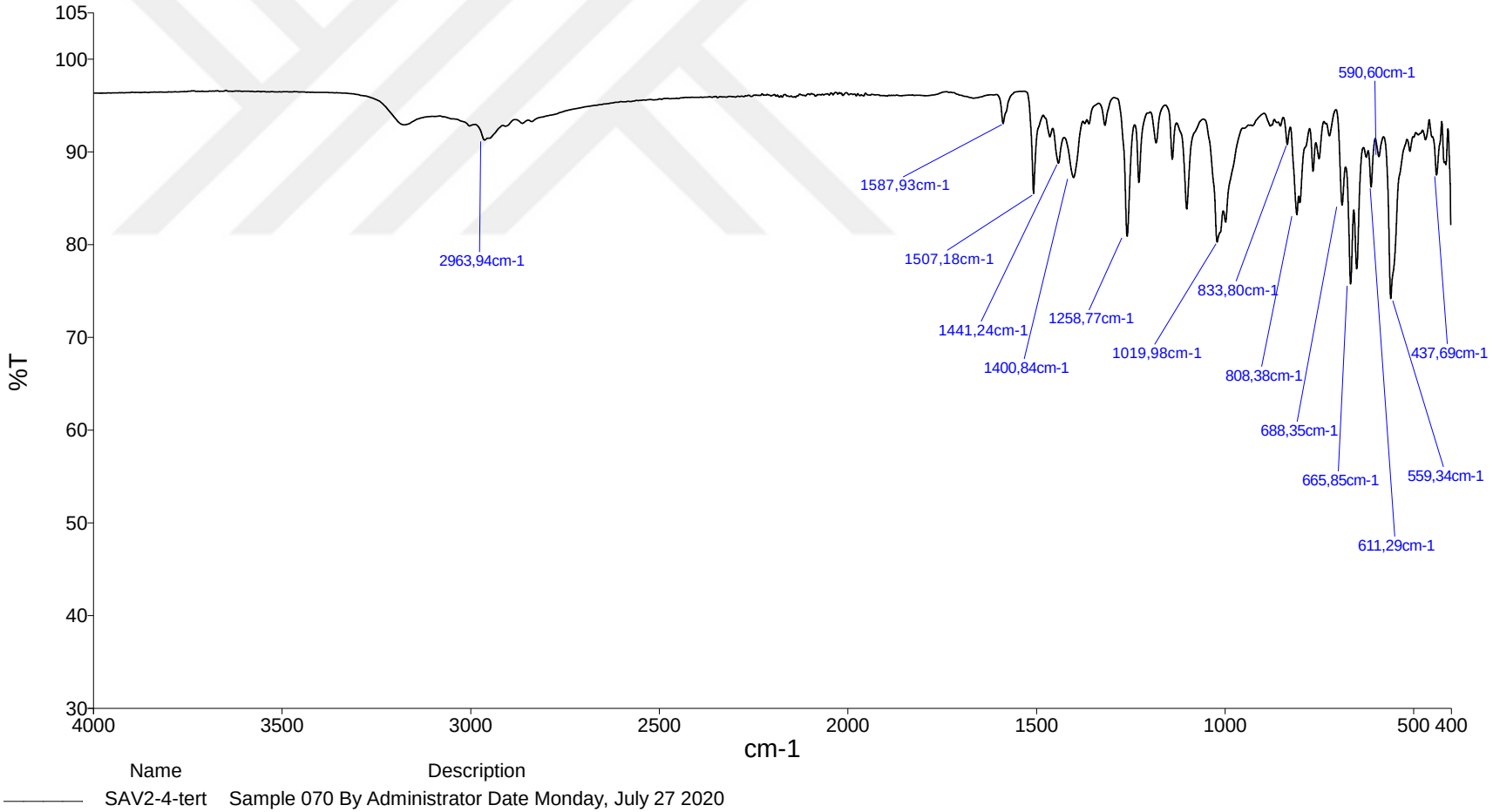


Figure 5.29. $[NH_4][S_2P(R^y)(OR3)]$ IR spectrum (4000 cm^{-1}- 400 cm^{-1}).

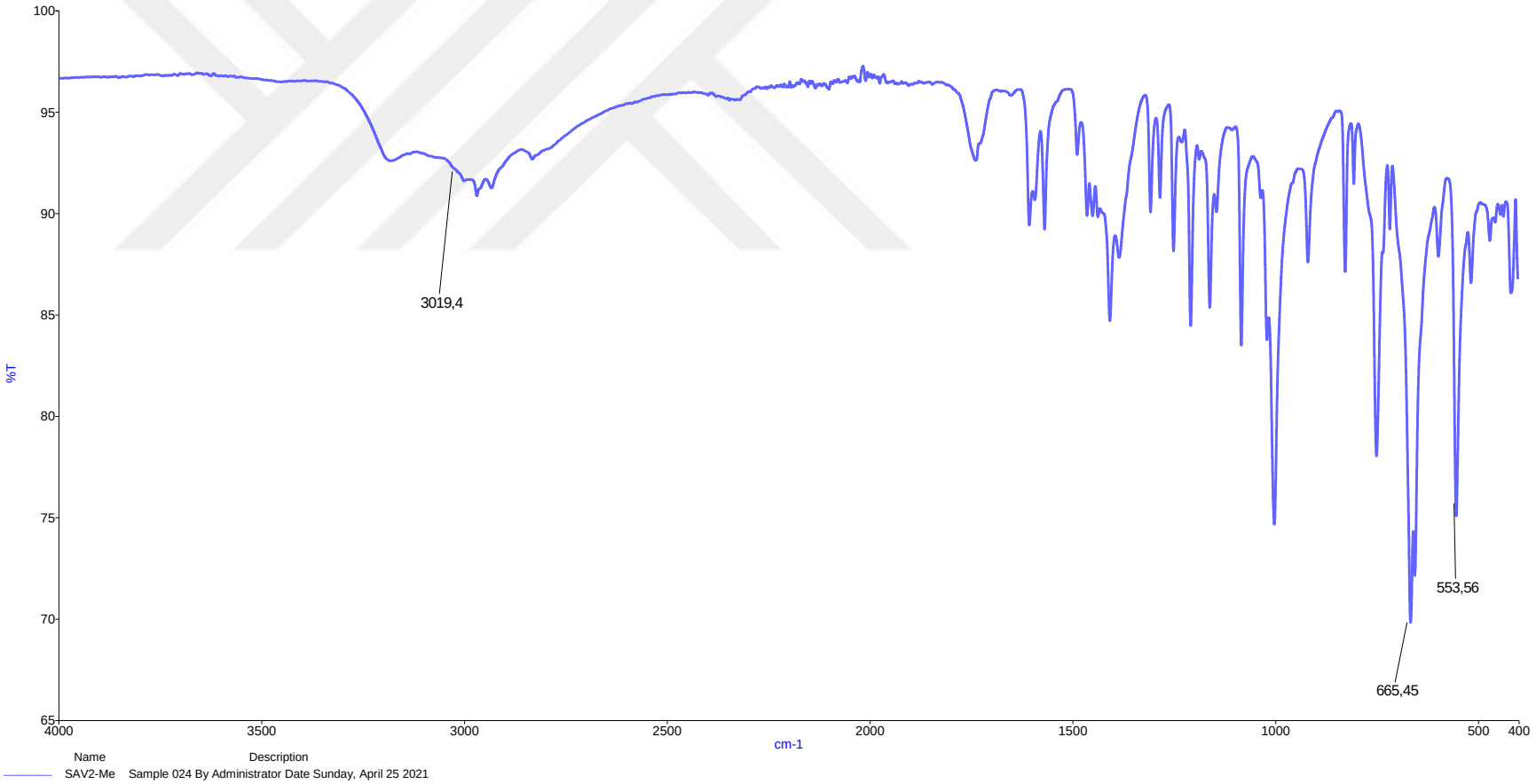


Figure 5.30. $[NH_4][S_2P(R^y)(OR4)]$ IR spectrum (4000 cm^{-1}- 400 cm^{-1}).

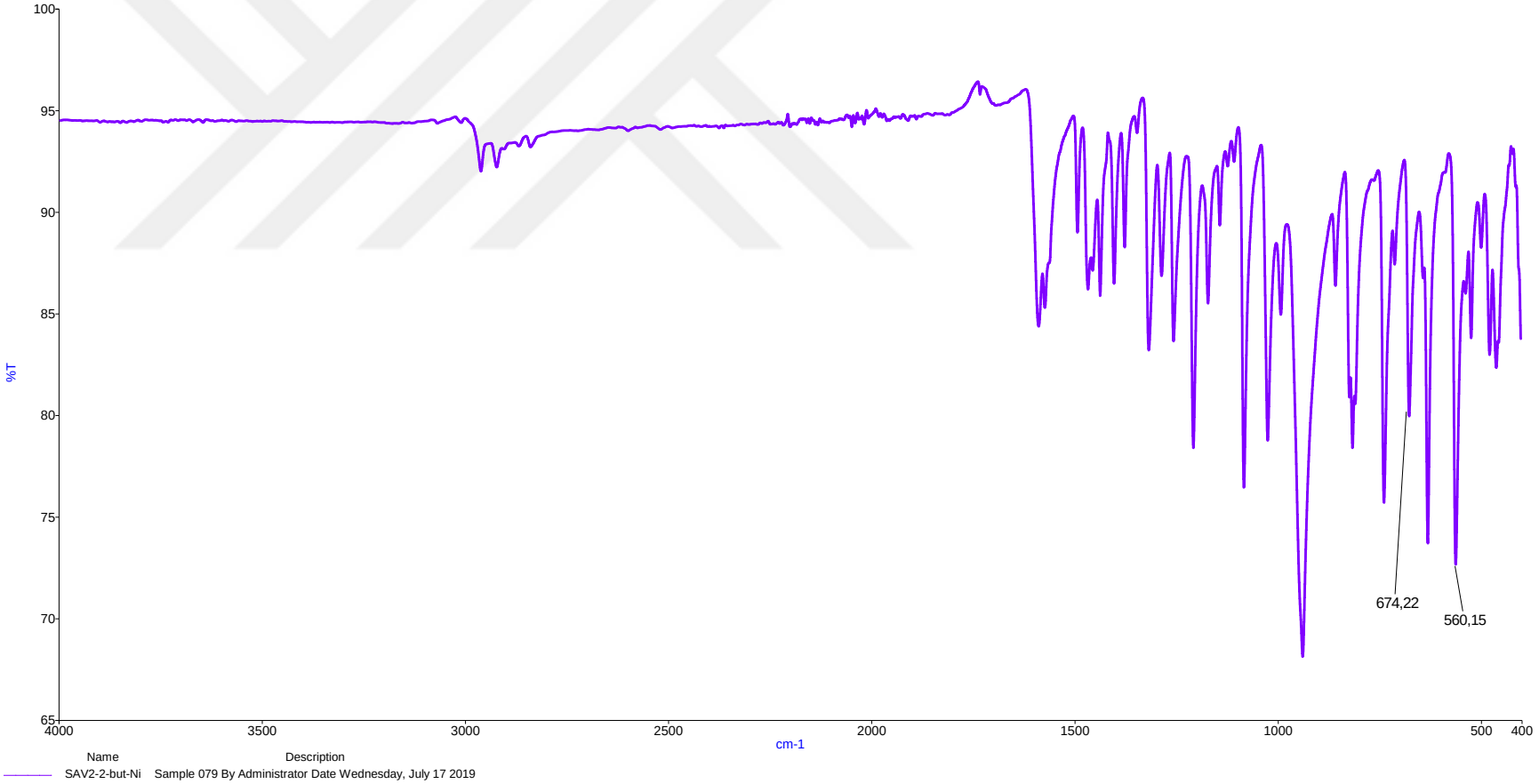


Figure 5.31.a. [Ni($S_2P(R^y)(OR1))_2$] IR spectrum (4000 cm^{-1}- 400 cm^{-1}).

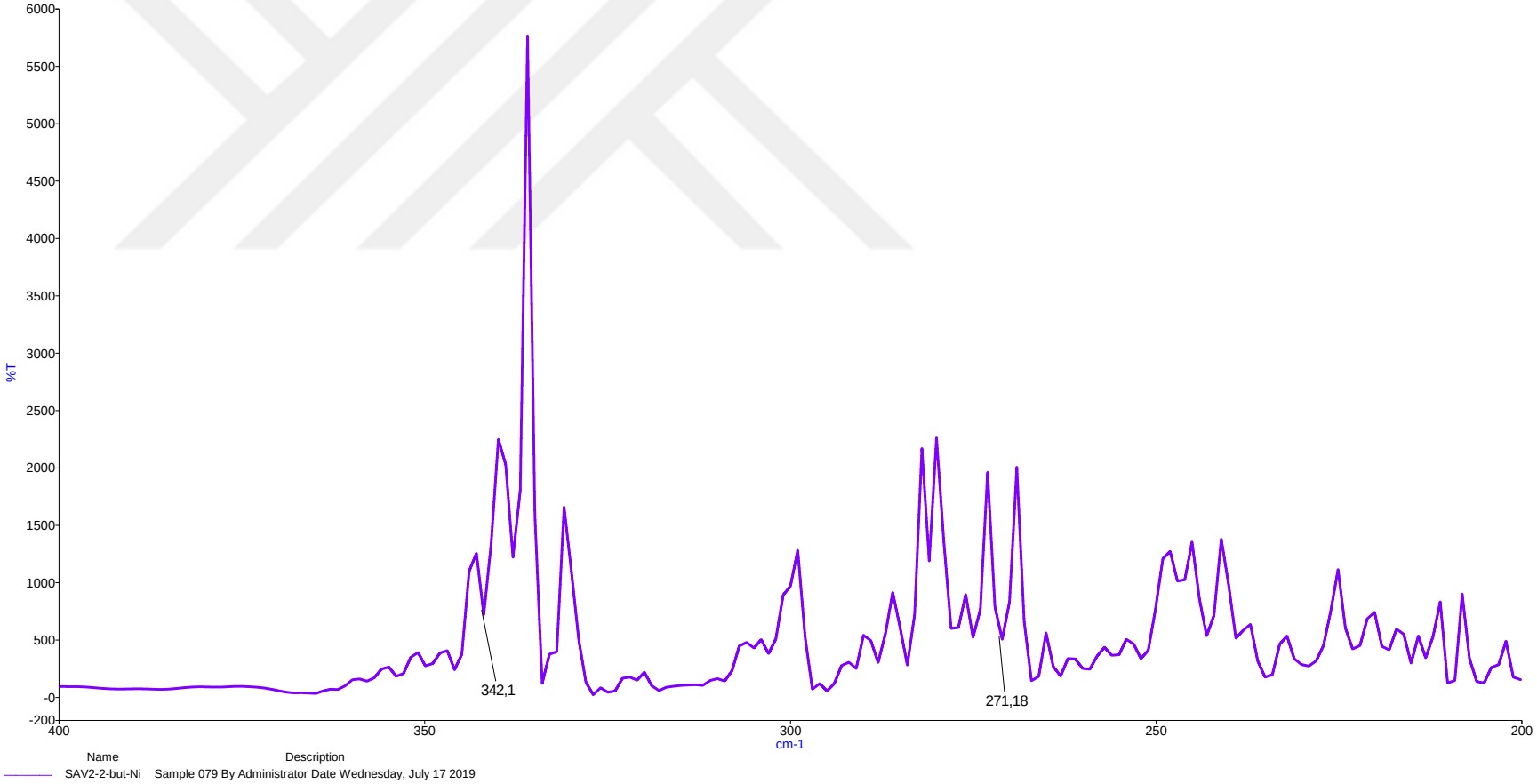


Figure 5.31.b. $[Ni(S_2P(R^y)(OR1))_2]$ IR spectrum (400 cm^{-1}- 200 cm^{-1}).

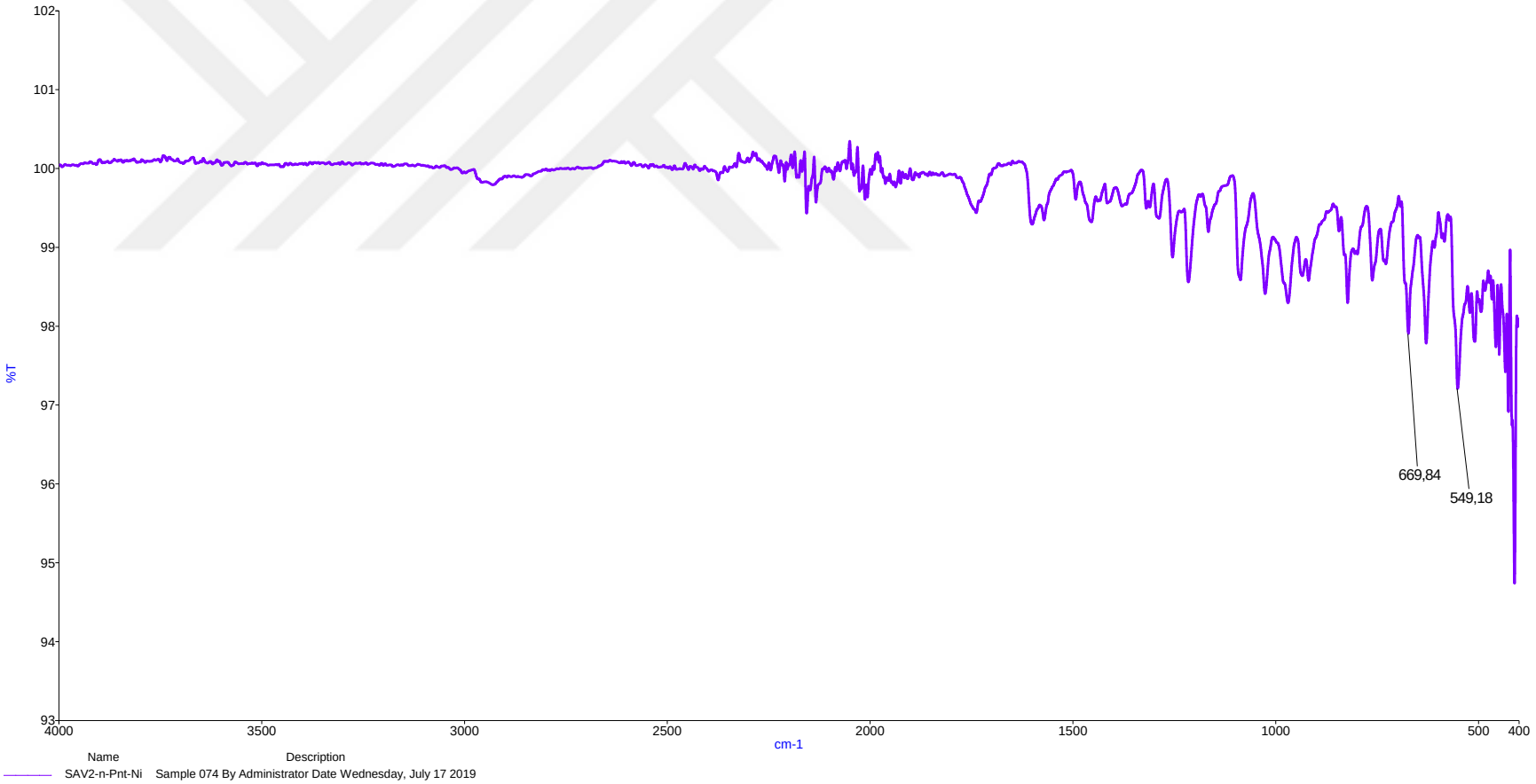


Figure 5.32.a. [Ni($S_2P(R^y)(OR2)$)$_2$] IR spectrum (4000 cm^{-1}- 400 cm^{-1}).

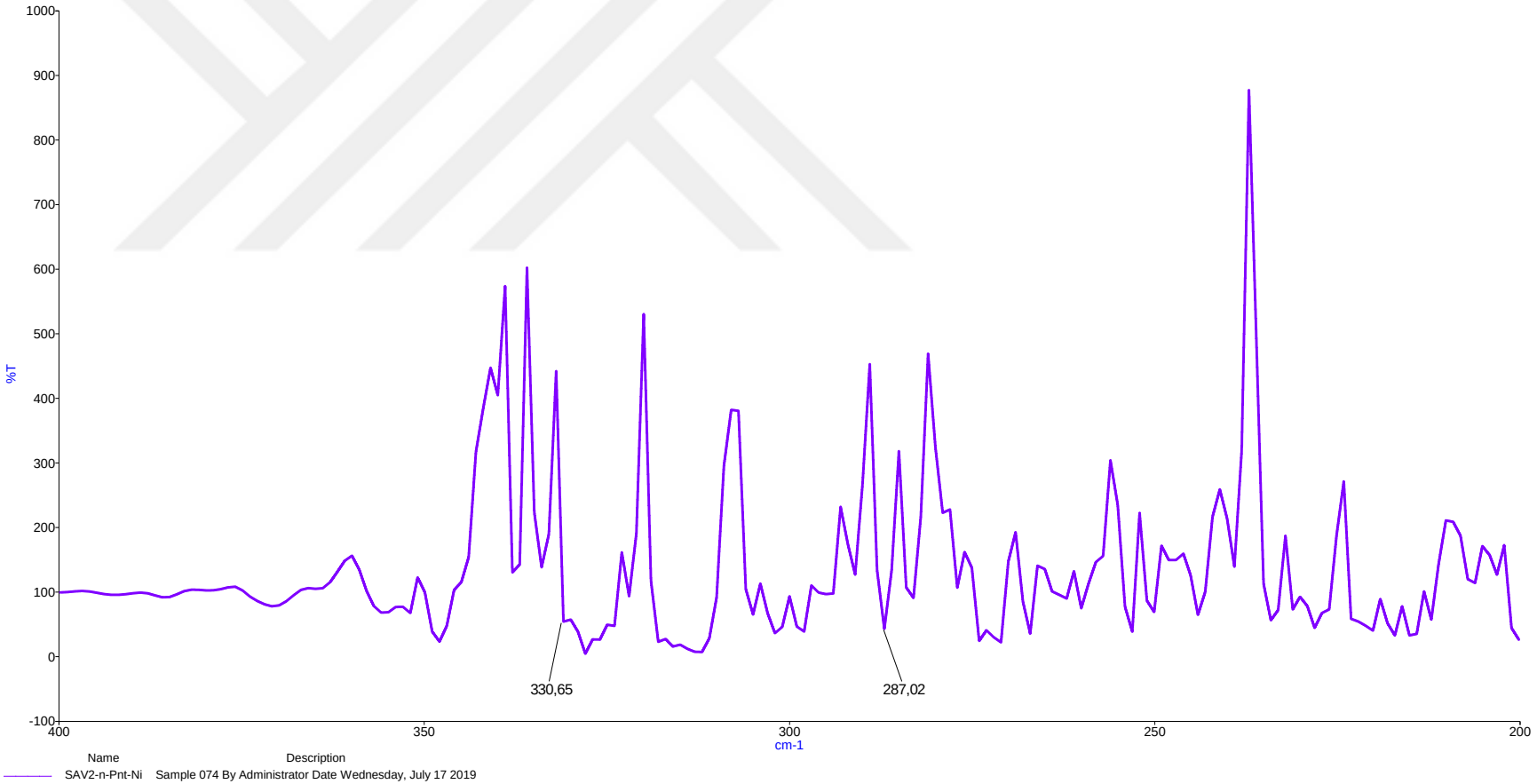


Figure 5.32.b. $[Ni(S_2P(R^y)(OR2))_2]$ IR spectrum (400 cm^{-1}- 200 cm^{-1})

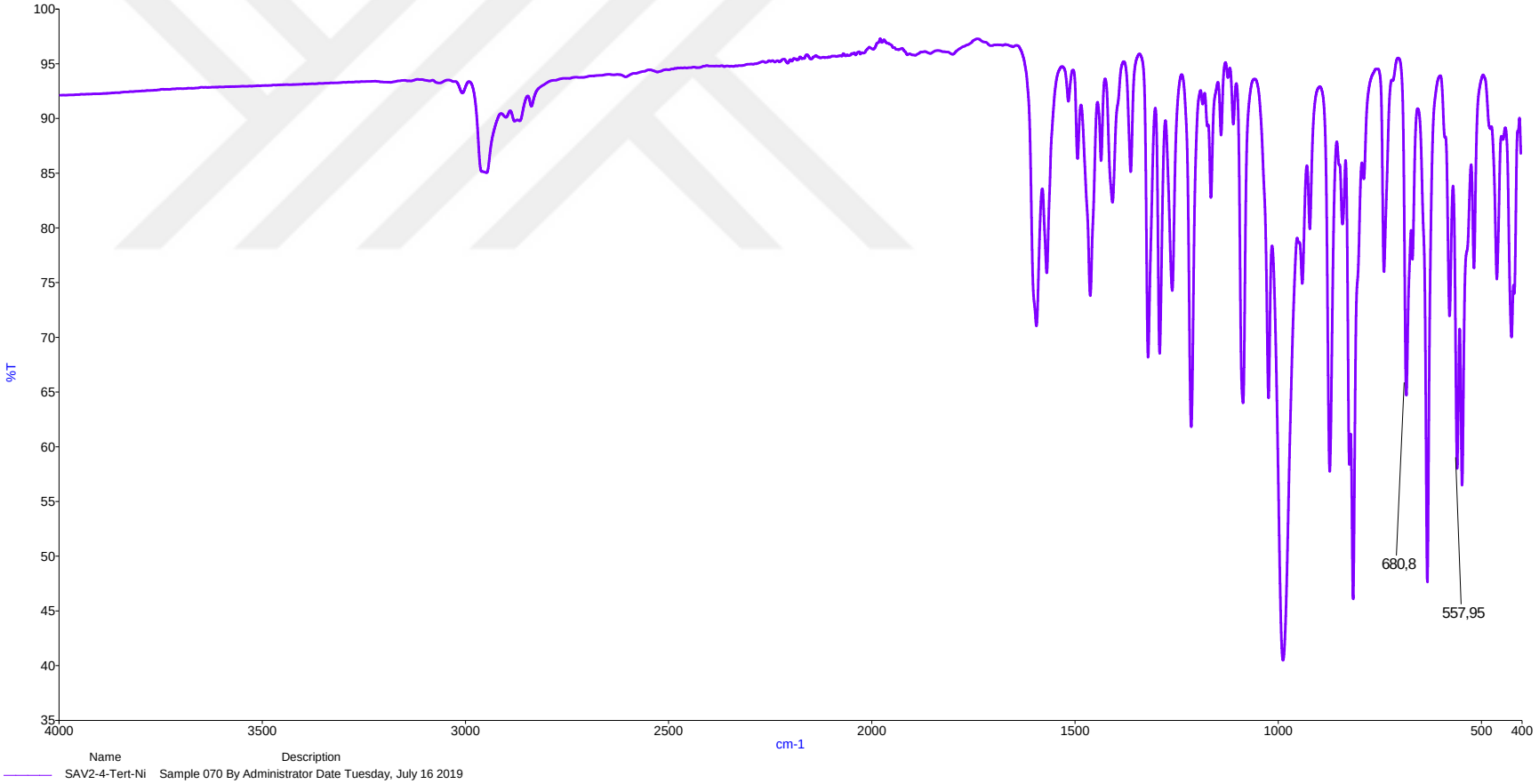


Figure 5.33.a. [Ni($S_2P(R^y)(OR3))_2$] IR spectrum (4000 cm^{-1}- 400 cm^{-1})

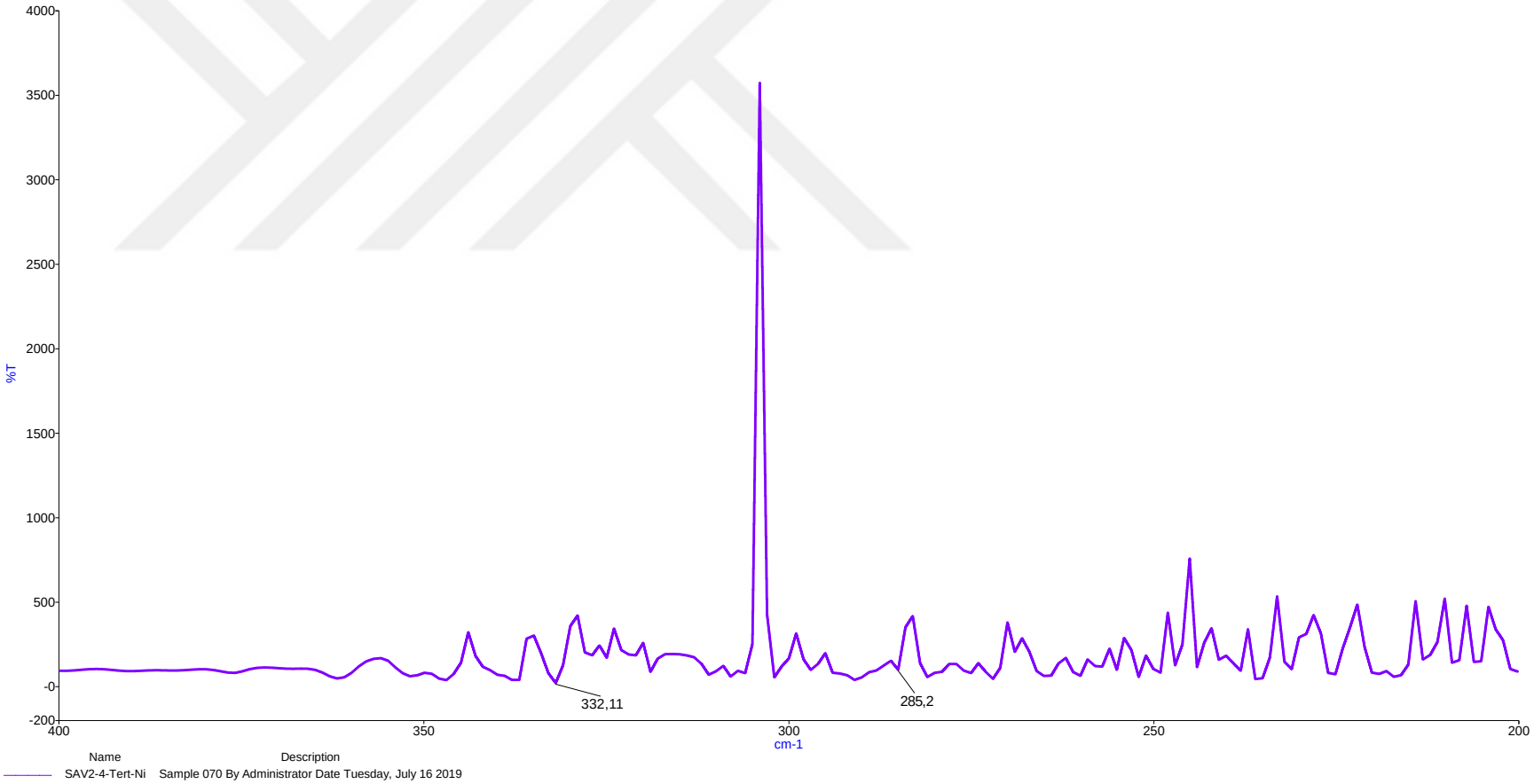


Figure 5.33.b. [Ni($S_2P(R^y)(OR3))_2$] IR spectrum (400 cm^{-1}- 200 cm^{-1})

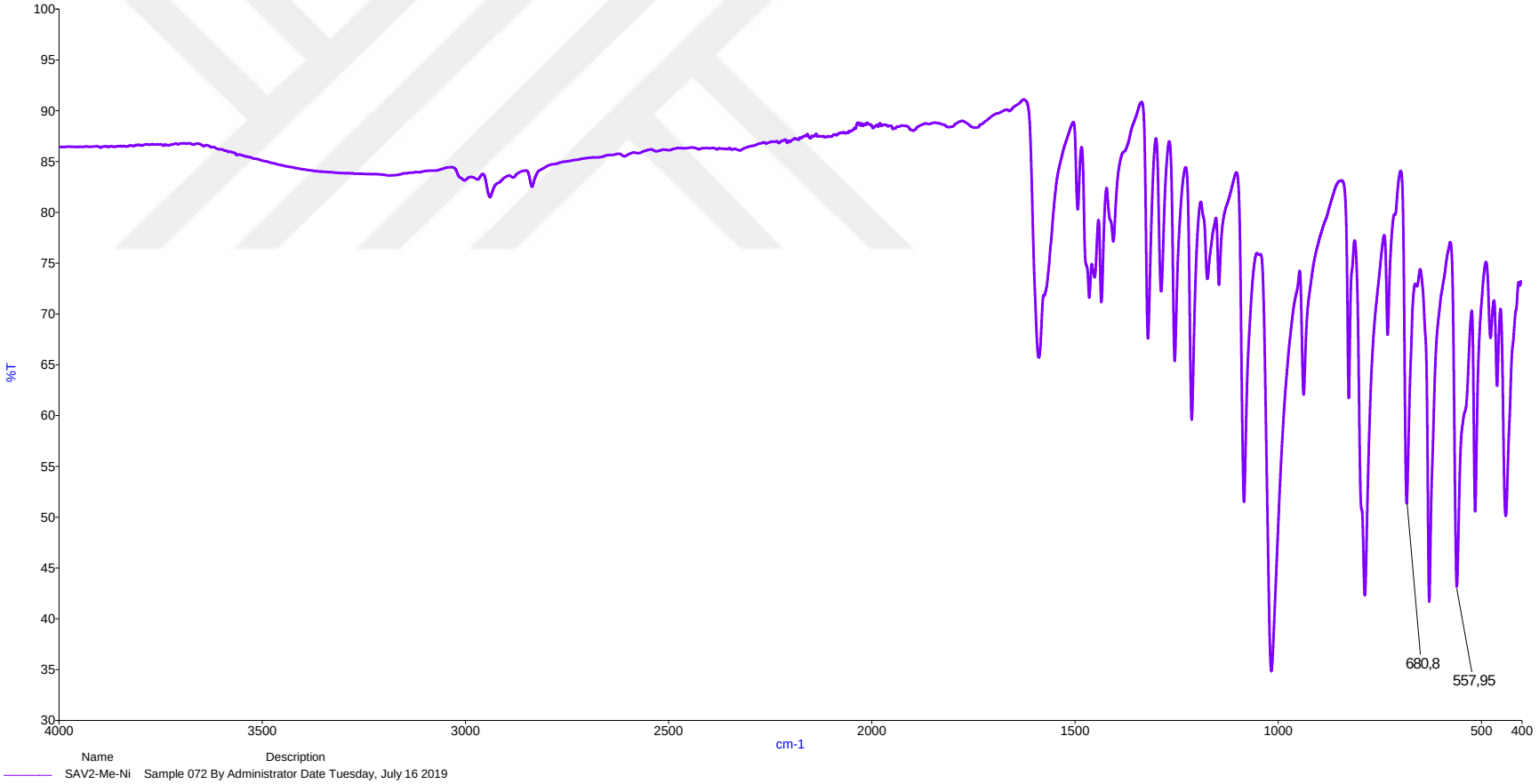


Figure 5.34.a. $[Ni(S_2P(R^y)(OR4))_2]$ IR spectrum (4000 cm^{-1}- 400 cm^{-1})

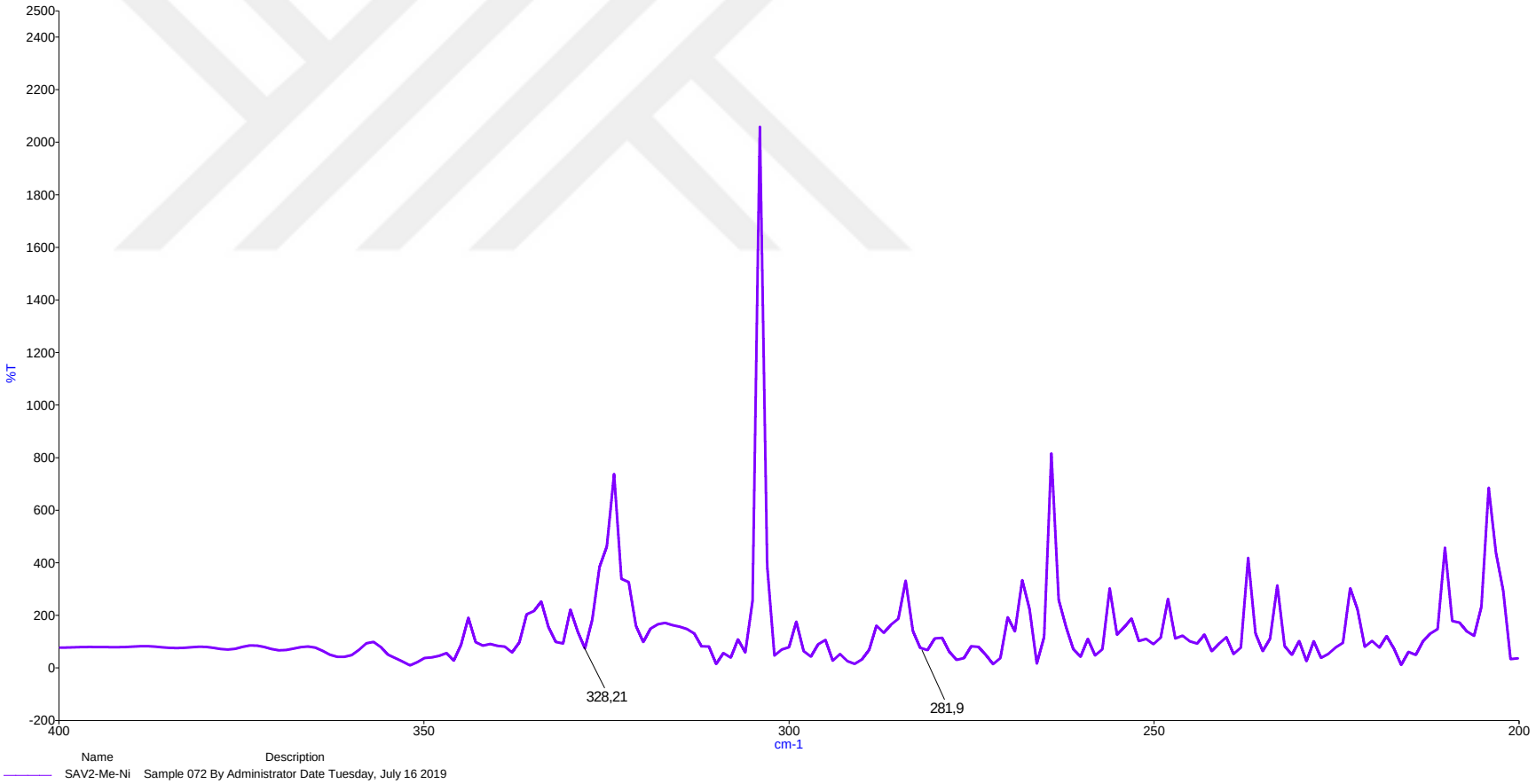


Figure 5.34.b. $[Ni(S_2P(R^y)(OR4))_2]$ IR spectrum (400 cm^{-1}- 200 cm^{-1})

5.1.4. Comment on the Mass (MS-ESI) Spectra of $[NH_4][S_2P(R^x)(ORn)]$ ve $[Ni(S_2P(R^x)(ORn))_2]$ for Part Ia

The ESI-MS spectra of the compounds are given in Figures 5.35-5.48. Some MS peaks display m/z values that are 23 or 41 units higher than the value corresponding to the m/z of the probably-candidate species. This is attributed to the attachment of sodium or acetonitrile contaminations from the buffer or the solvent. In the MS spectra of the ligands, the peak pertaining to the molecular ion $[M\text{-}NH_4]^+$ is the principal peak. The molecular ion peak is also the principle one in the spectra of the complexes except for those $[Ni(S_2P(R^x)(ORn))_2]$ complexes with n= 1, 3, 6 and 7.

Mass spectra of Part Ia $[NH_4][S_2P(R^x)(ORn)]$ and $[Ni(S_2P(R^x)(ORn))_2]$ compounds.

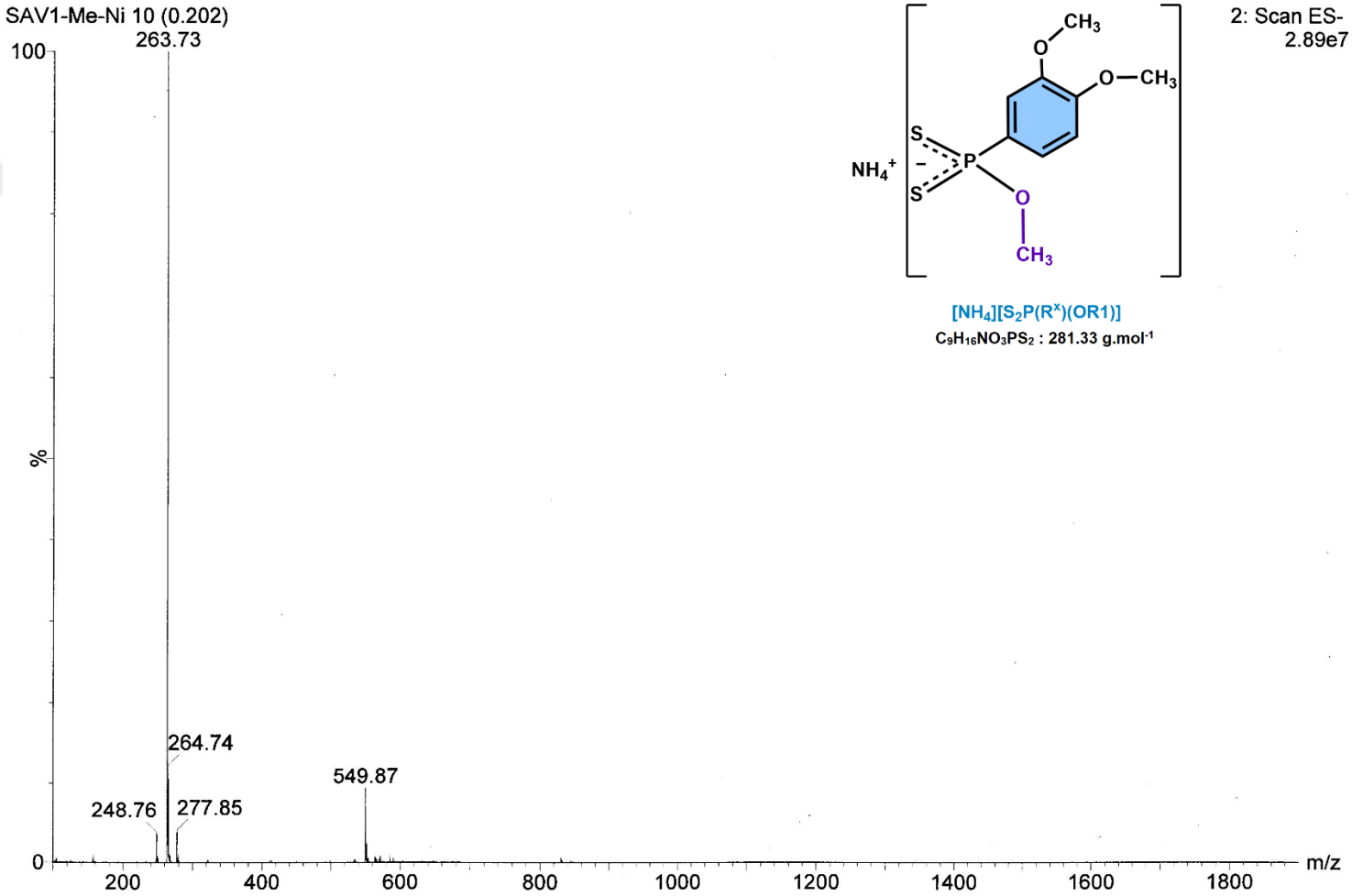


Figure 5.35. $[NH_4][S_2P(R^x)(OR1)]$ Mass spectrum (ESI^-).

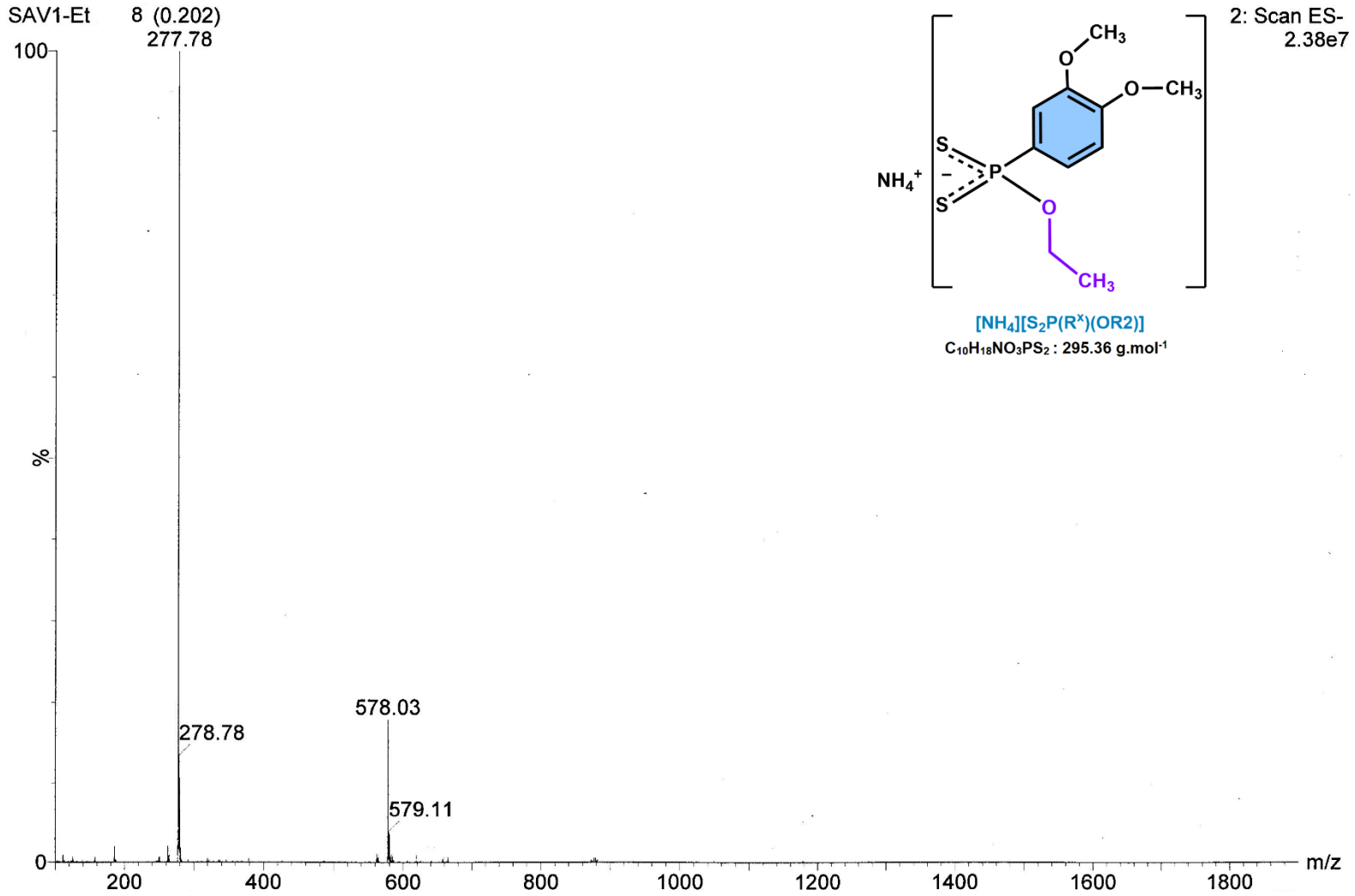


Figure 5.36. $[NH_4][S_2P(R^x)(OR2)]$ Mass spectrum (ESI^-).

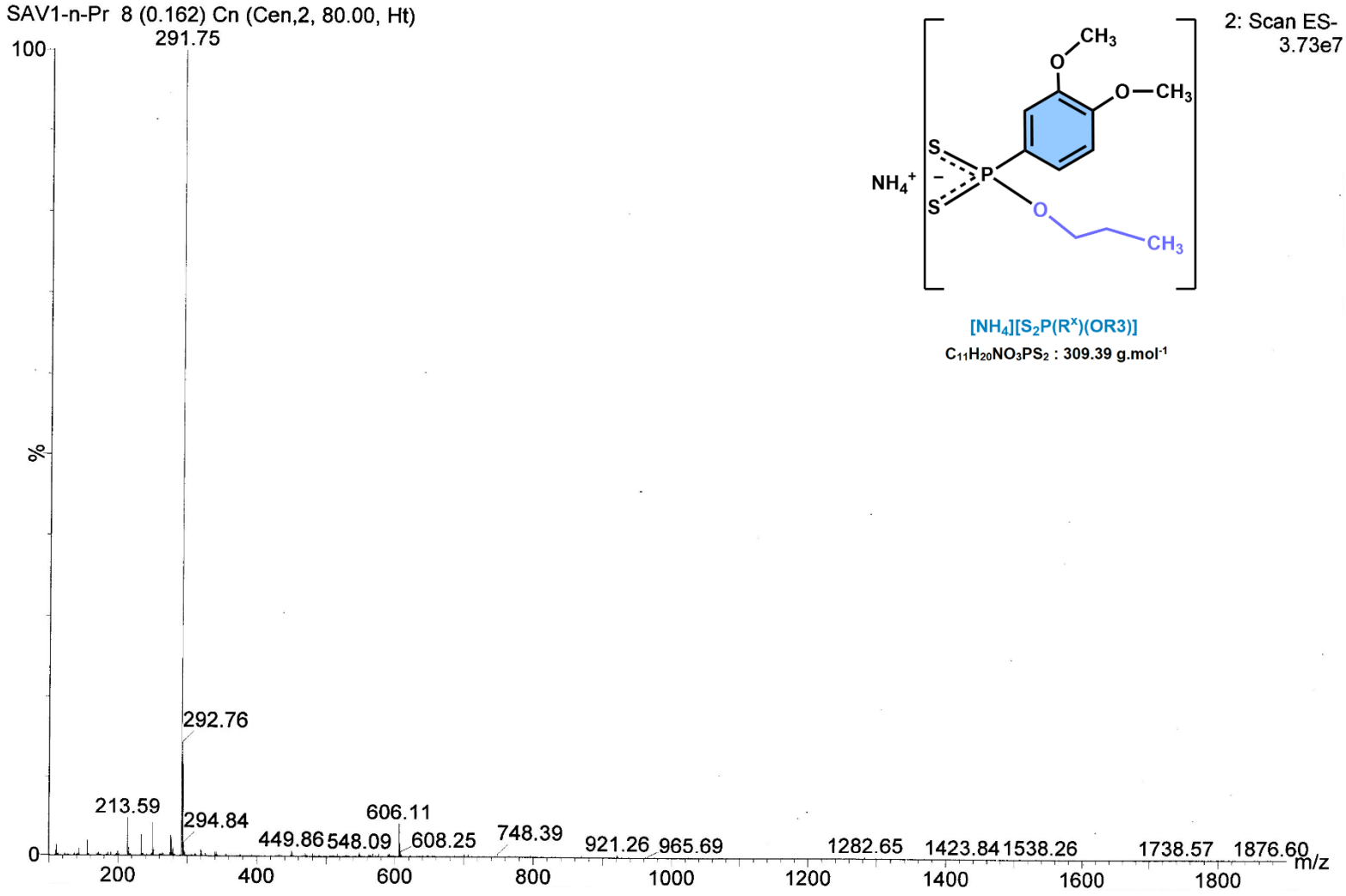


Figure 5.37. $[NH_4][S_2P(R^x)(OR3)]$ Mass spectrum (ESI^-).

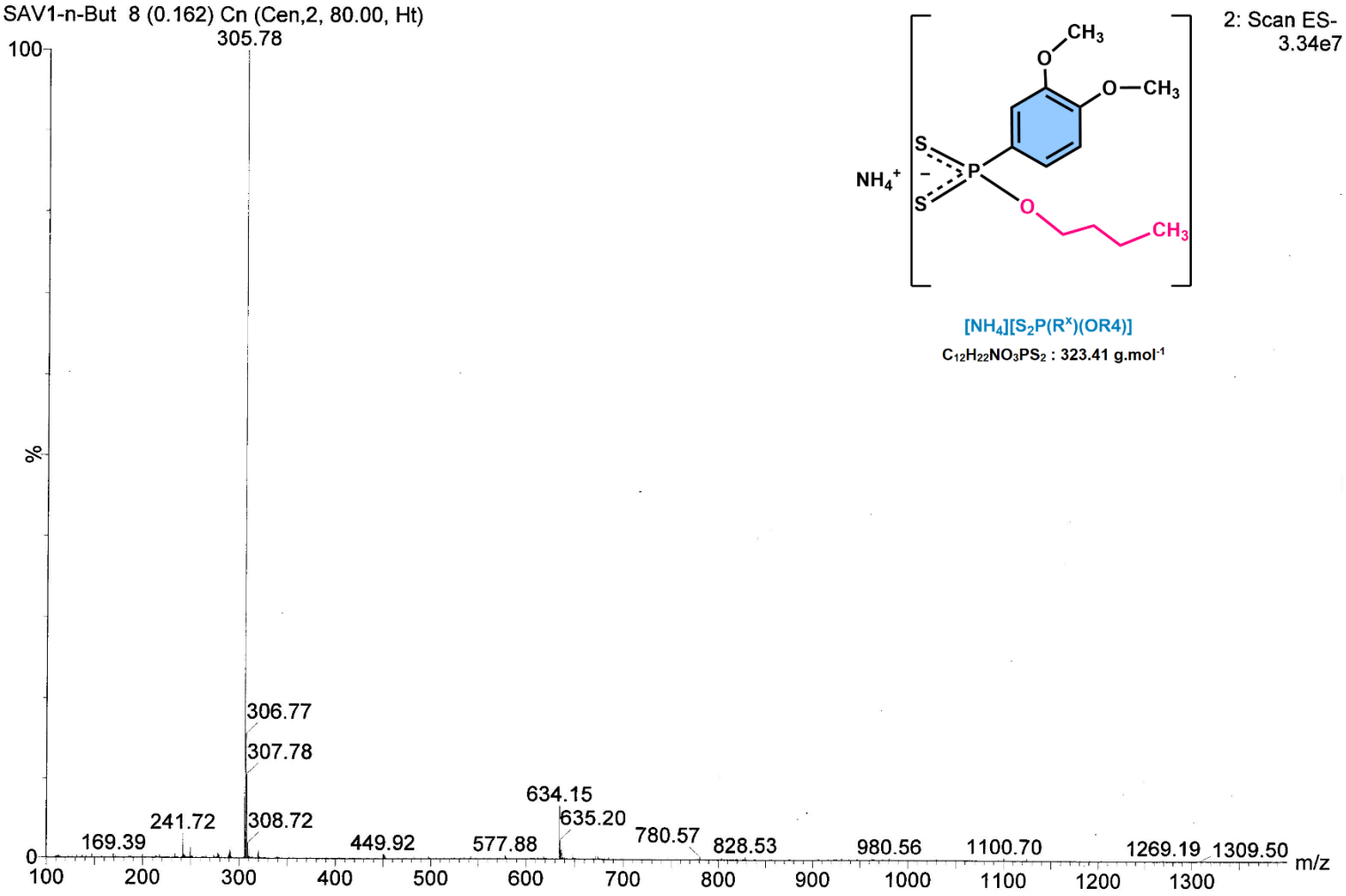


Figure 5.38. $[NH_4][S_2P(R^x)(OR4)]$ Mass spectrum (ESI^-).

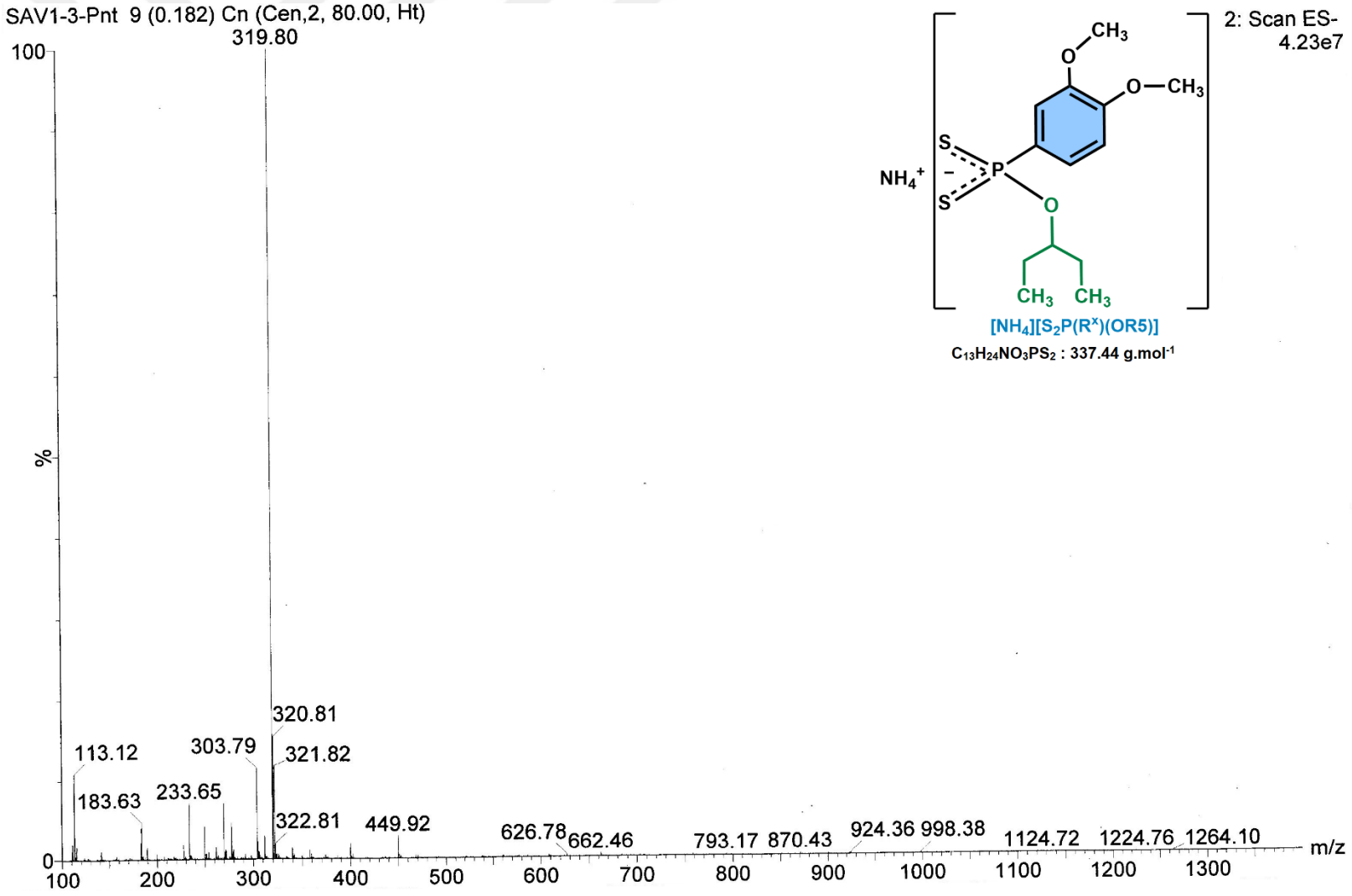


Figure 5.39. $[NH_4][S_2P(R^x)(OR5)]$ Mas spectrum (ESI^-).

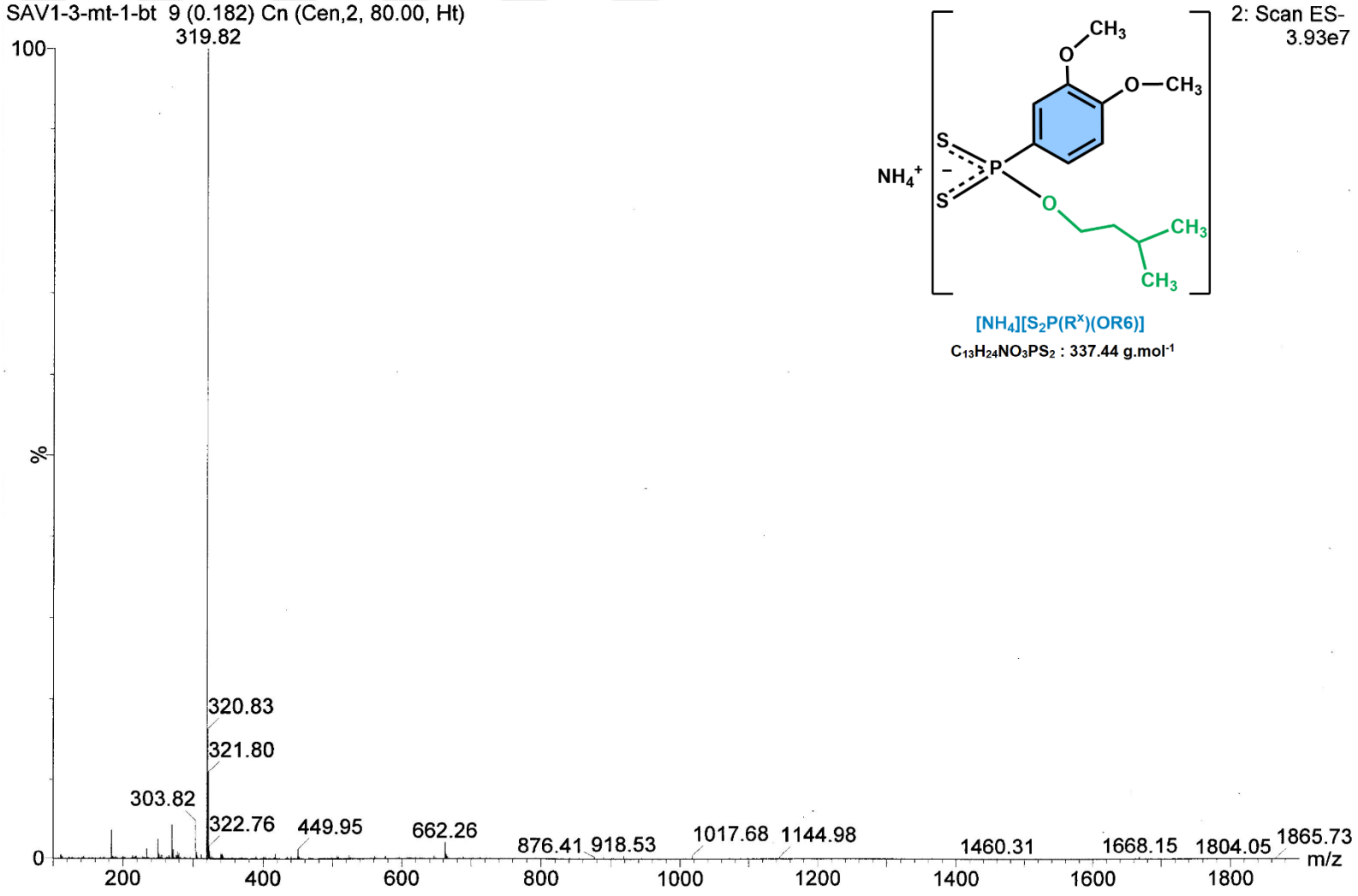


Figure 5.40. [NH_4][$S_2P(R^x)$(OR6)] Mas spectrum (ESI^-).

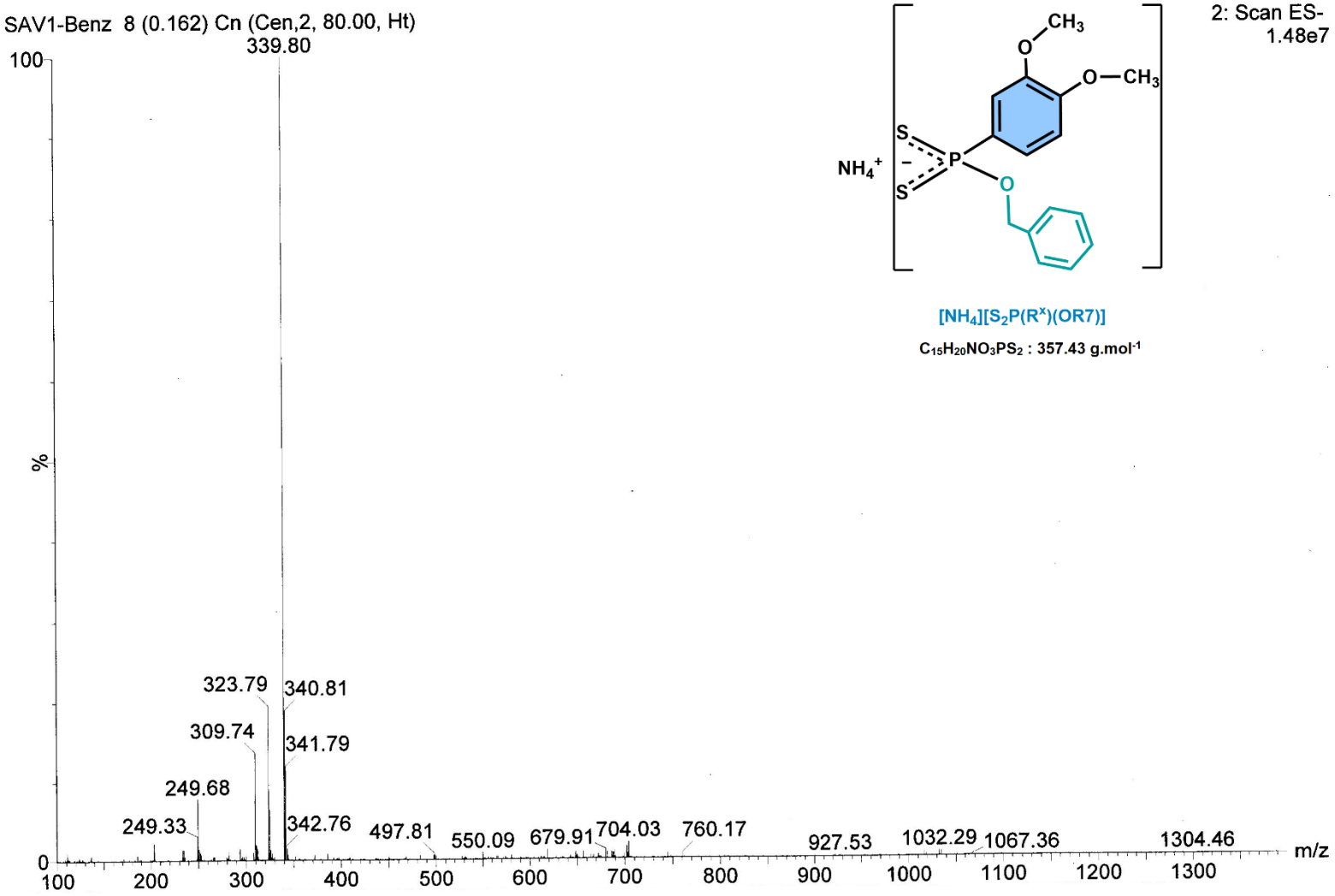


Figure 5.41. $[NH_4][S_2P(R^x)(OR7)]$ Mas spectrum (ESI^-).

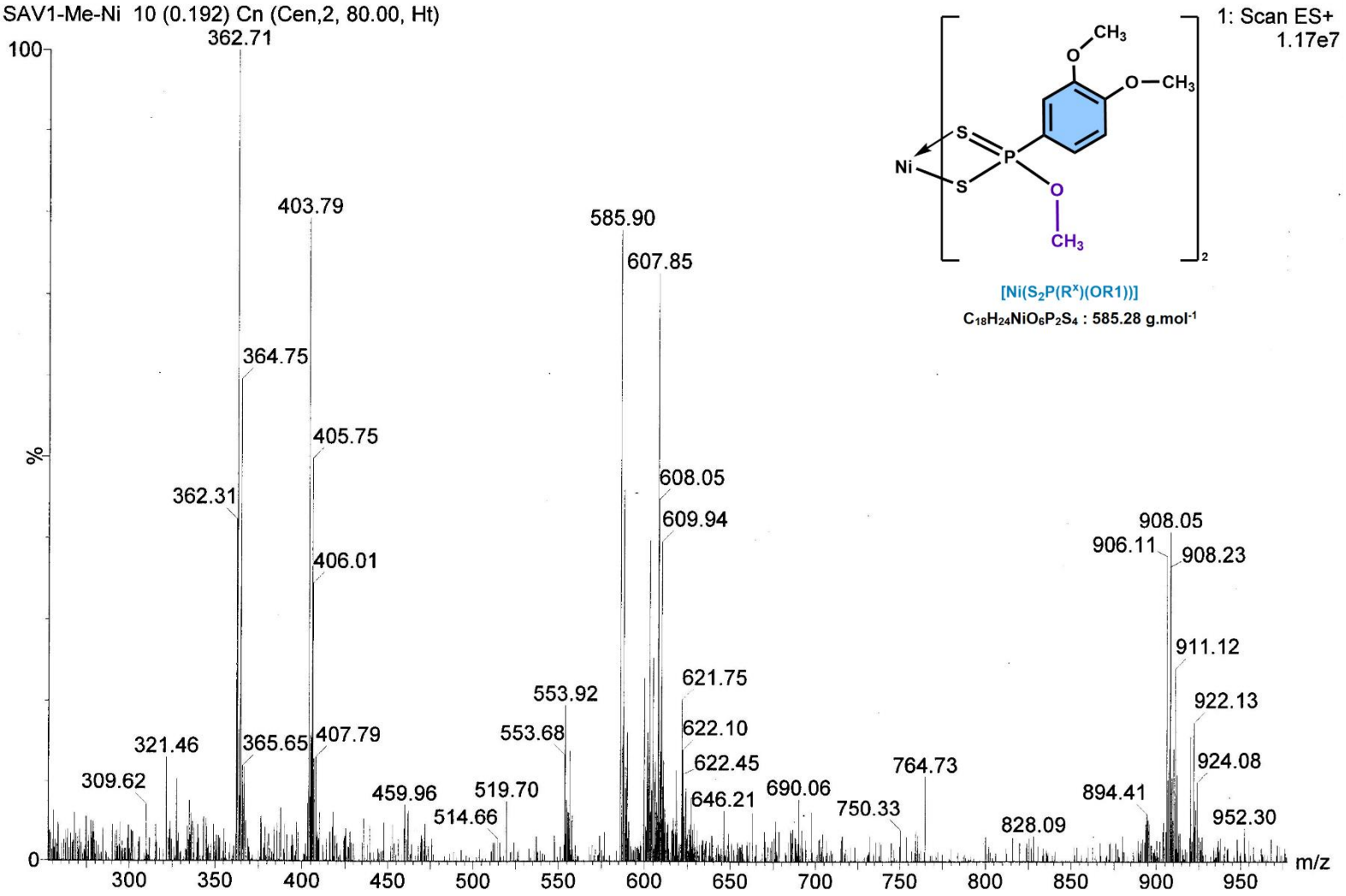


Figure 5.42. $[Ni(S_2P(R^x)(OR1))_2]$ Mas spectrum (ESI^+).

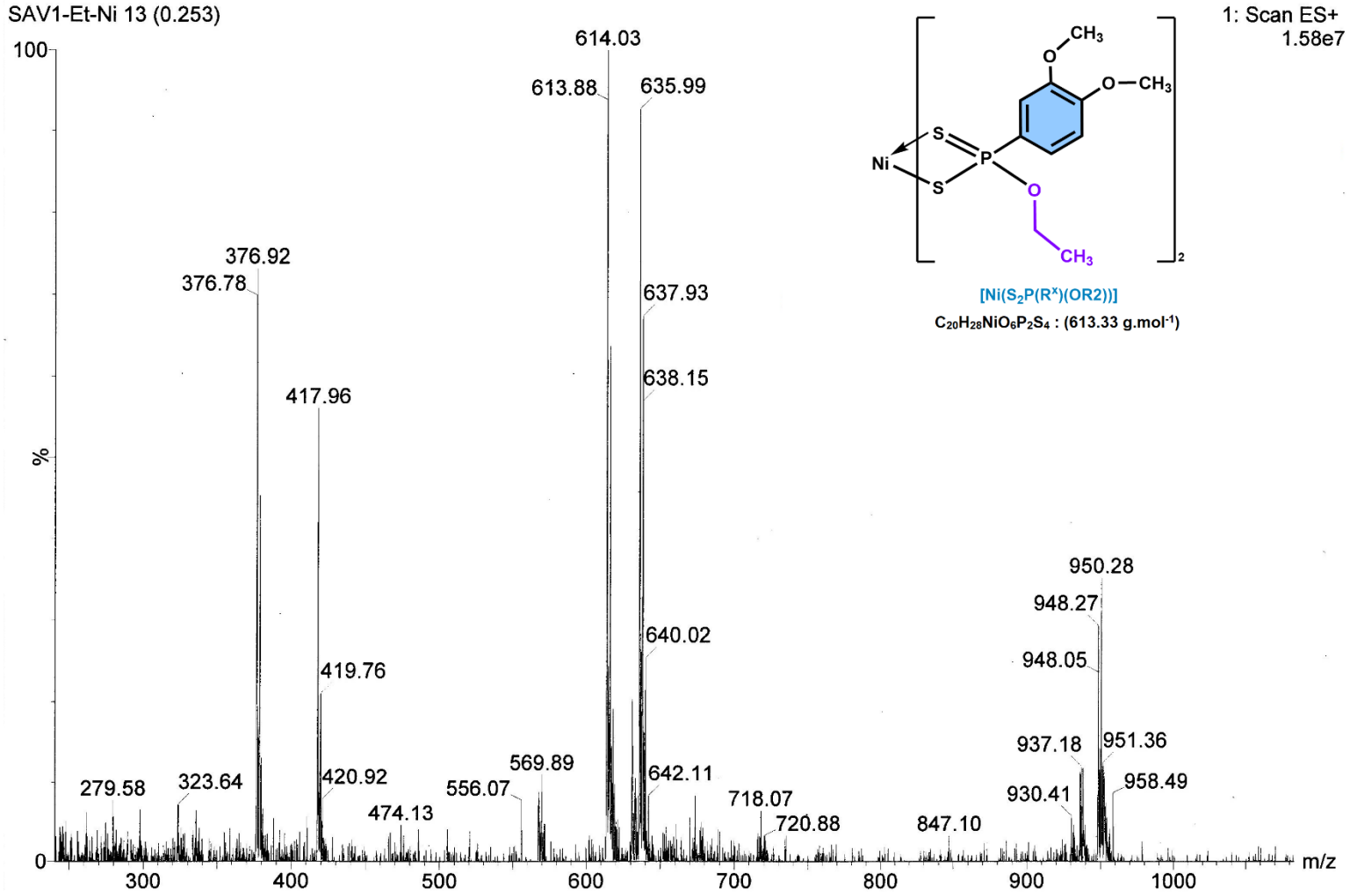


Figure 5.43. $[Ni(S_2P(R^x)(OR2))_2]$ Mas spectrum (ESI^+).

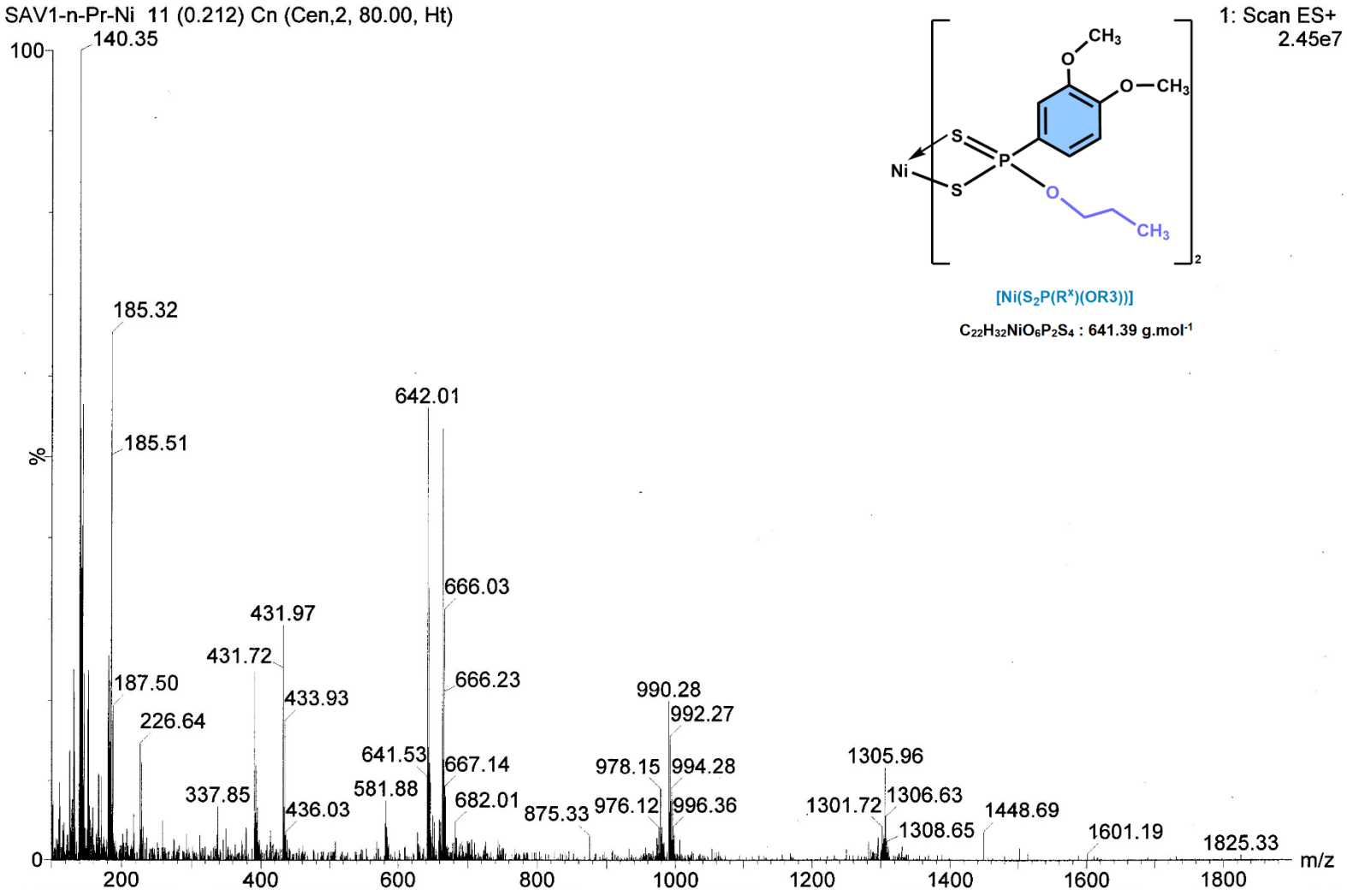


Figure 5.44. $[Ni(S_2P(R^x)(OR3))_2]$ Mas spectrum (ESI^+).

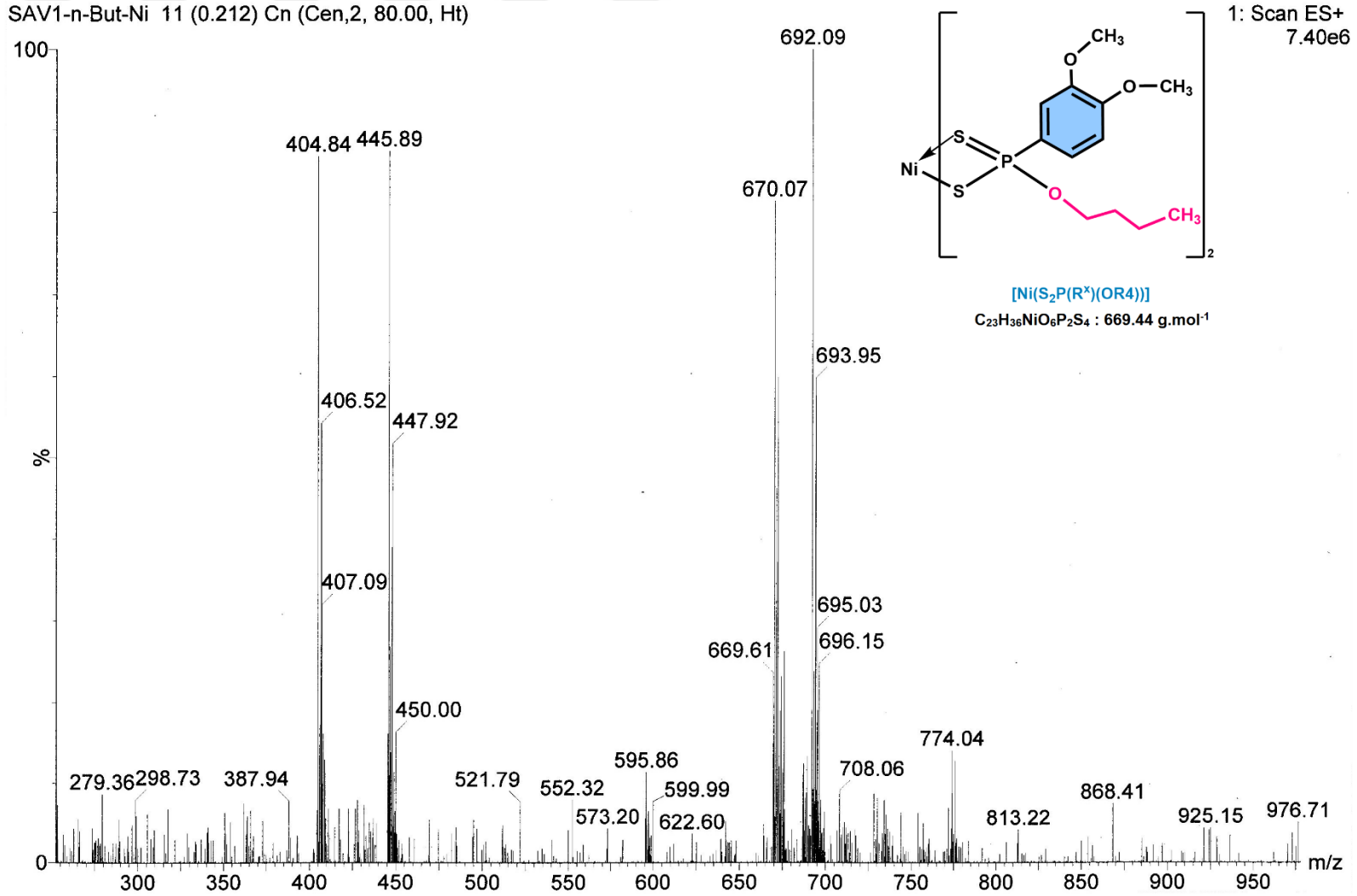


Figure 5.45. $[Ni(S_2P(R^x)(OR4))_2]$ Mas spectrum (ESI^+).

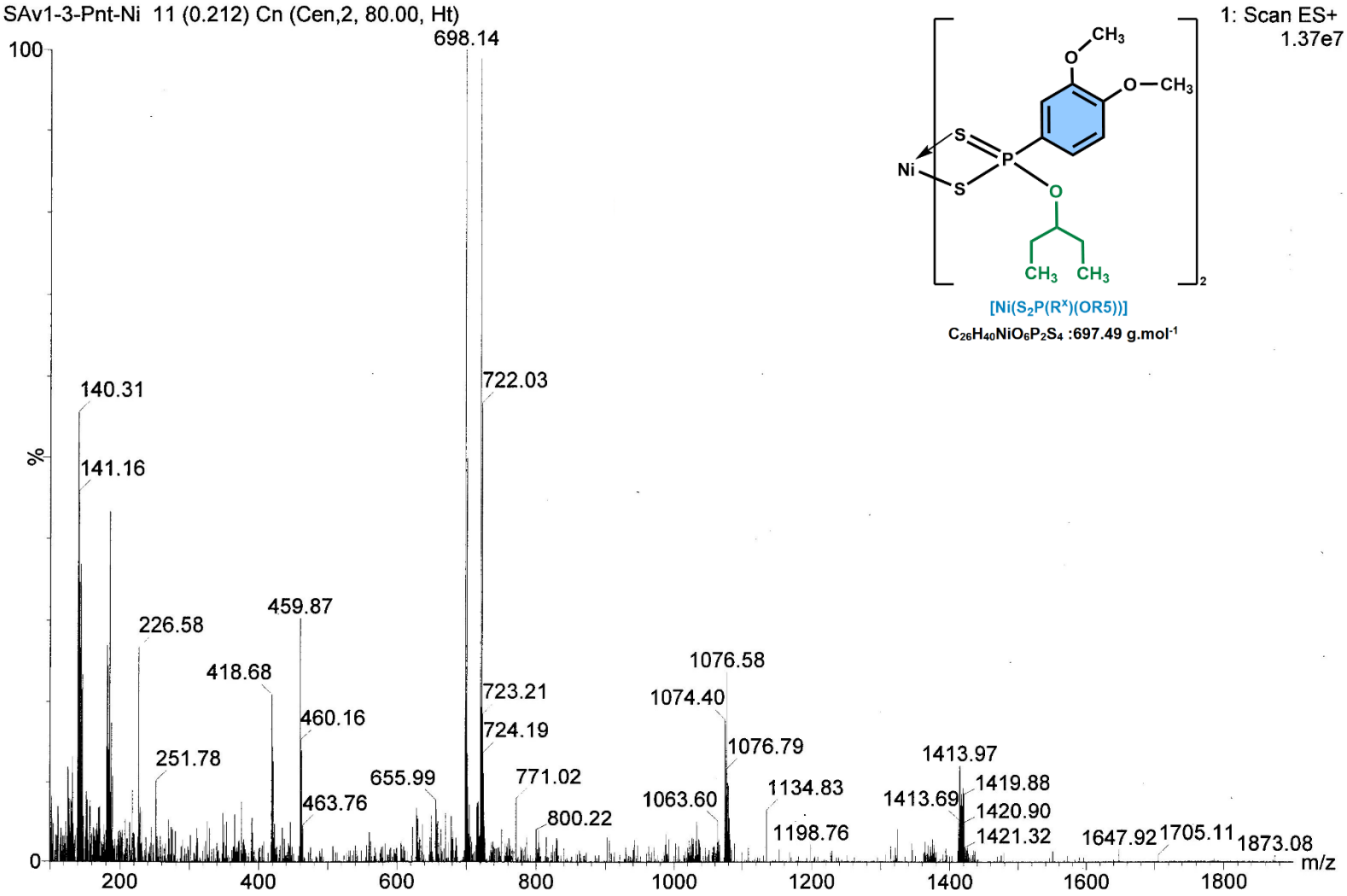


Figure 5.46. $[Ni(S_2P(R^x)(OR5))_2]$ Mas spectrum (ESI^+).

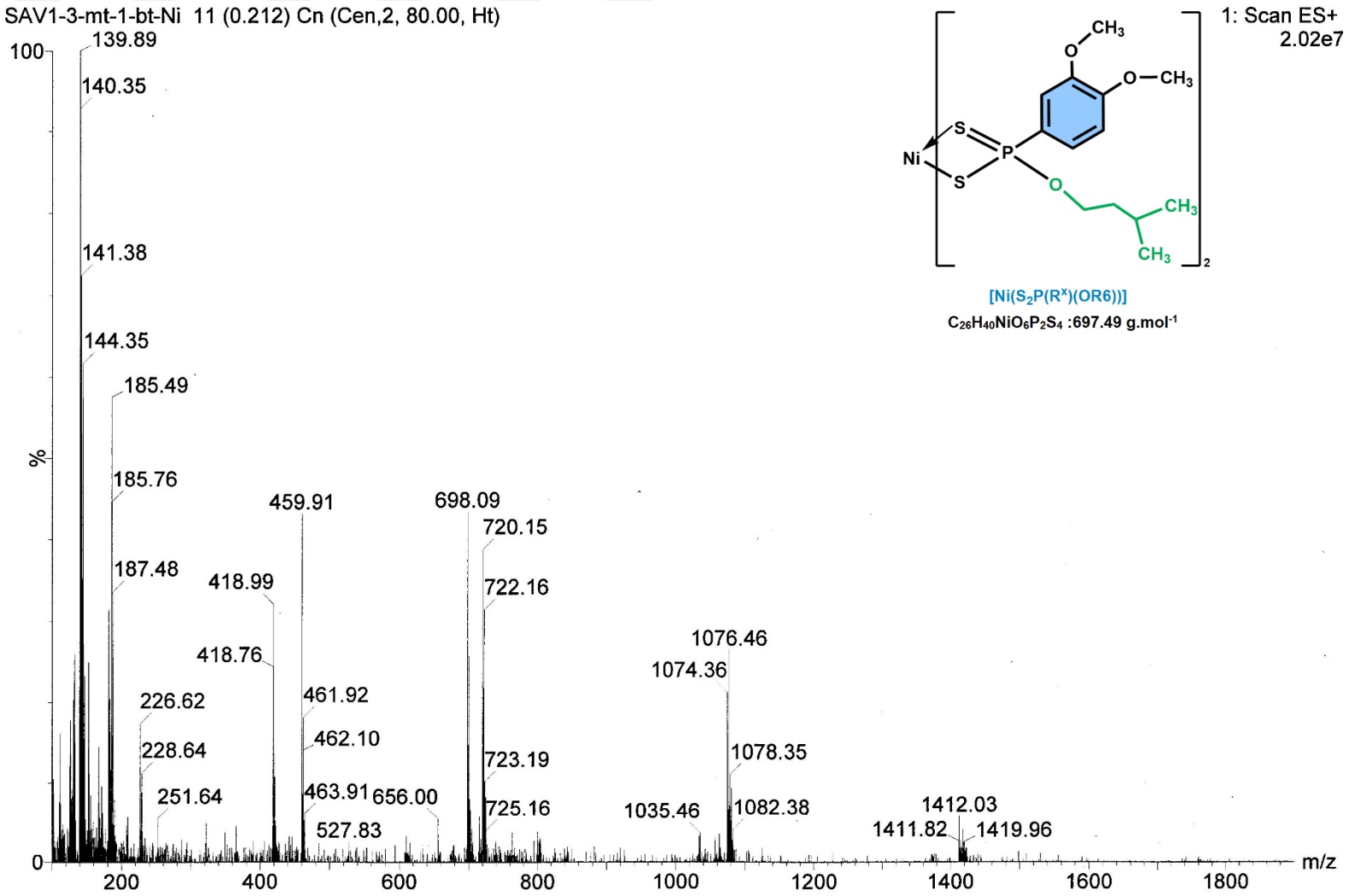


Figure 5.47. [Ni($S_2P(R^x)(OR6)$)$_2$] Mas spectrum (ESI^+).

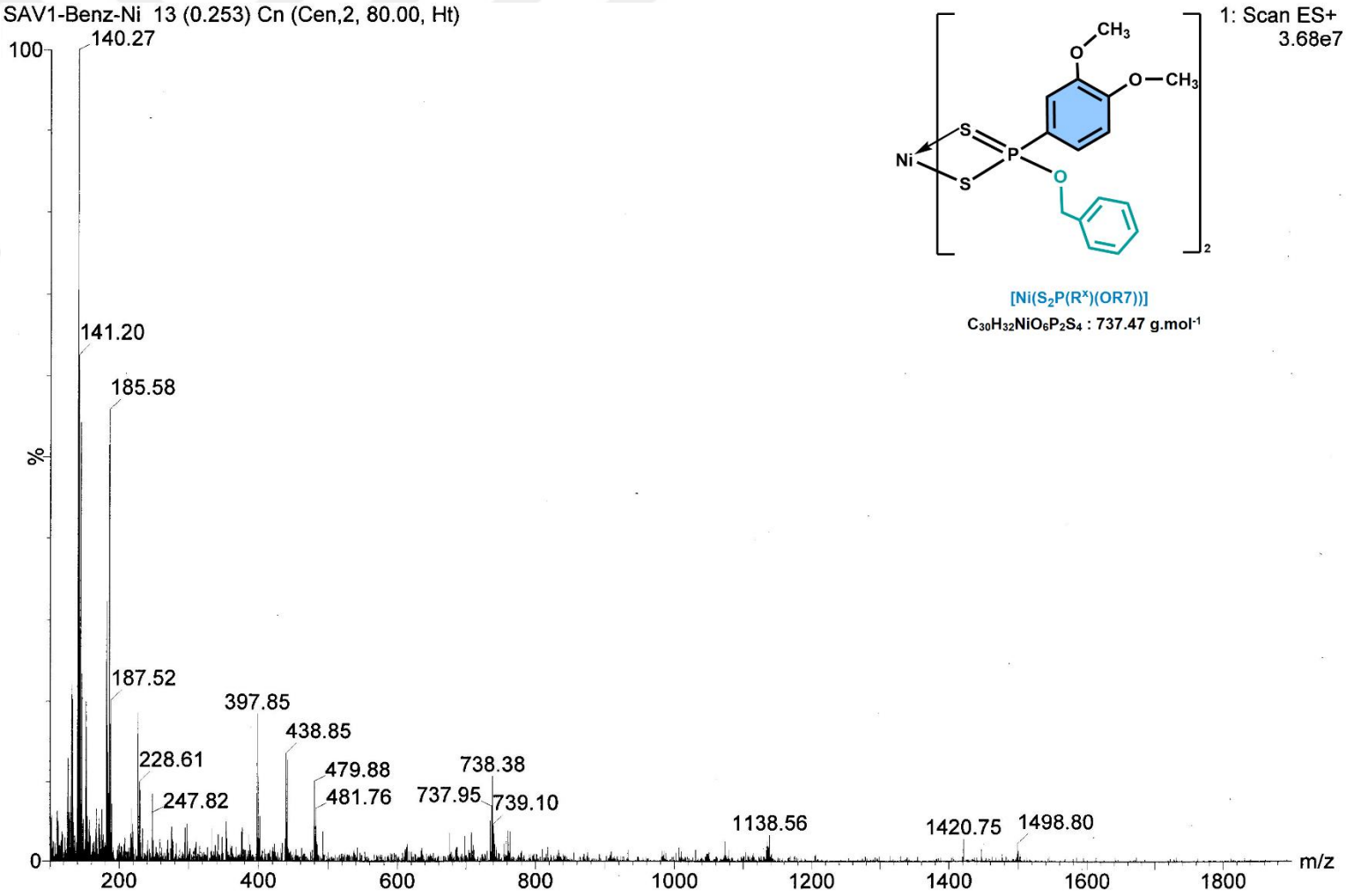


Figure 5.48. $[Ni(S_2P(R^x)(OR7))_2]$ Mas spectrum (ESI^+).

5.1.5. Comment on the Mass (MS-ESI) Spectra of $[NH_4][S_2P(R^x)(ORn)]$ ve $[Ni(S_2P(R^x)(ORn))_2]$ of Part Ib

The spectra of the compounds are given in Figures 5.49-5.58. The molecular ion peaks shown up in the MS spectra of the synthesized ligands are also the main peaks which is represented as $[M\text{-}NH_4]^+$. The molecular ion peaks for $[Ni(S_2P(R^x)(OR2))_2]$, $[Ni(S_2P(R^x)(OR4))_2]$ and $[Ni(S_2P(R^x)(OR5))_2]$ complexes are also the principal peaks, which are not the case for $[Ni(S_2P(R^x)(OR1))_2]$ and $[Ni(S_2P(R^x)(OR3))_2]$.

Mass spectra of Part Ib [NH_4][$S_2P(R^x)(ORn)$] and [$Ni(S_2P(R^x)(ORn))_2$] compounds.

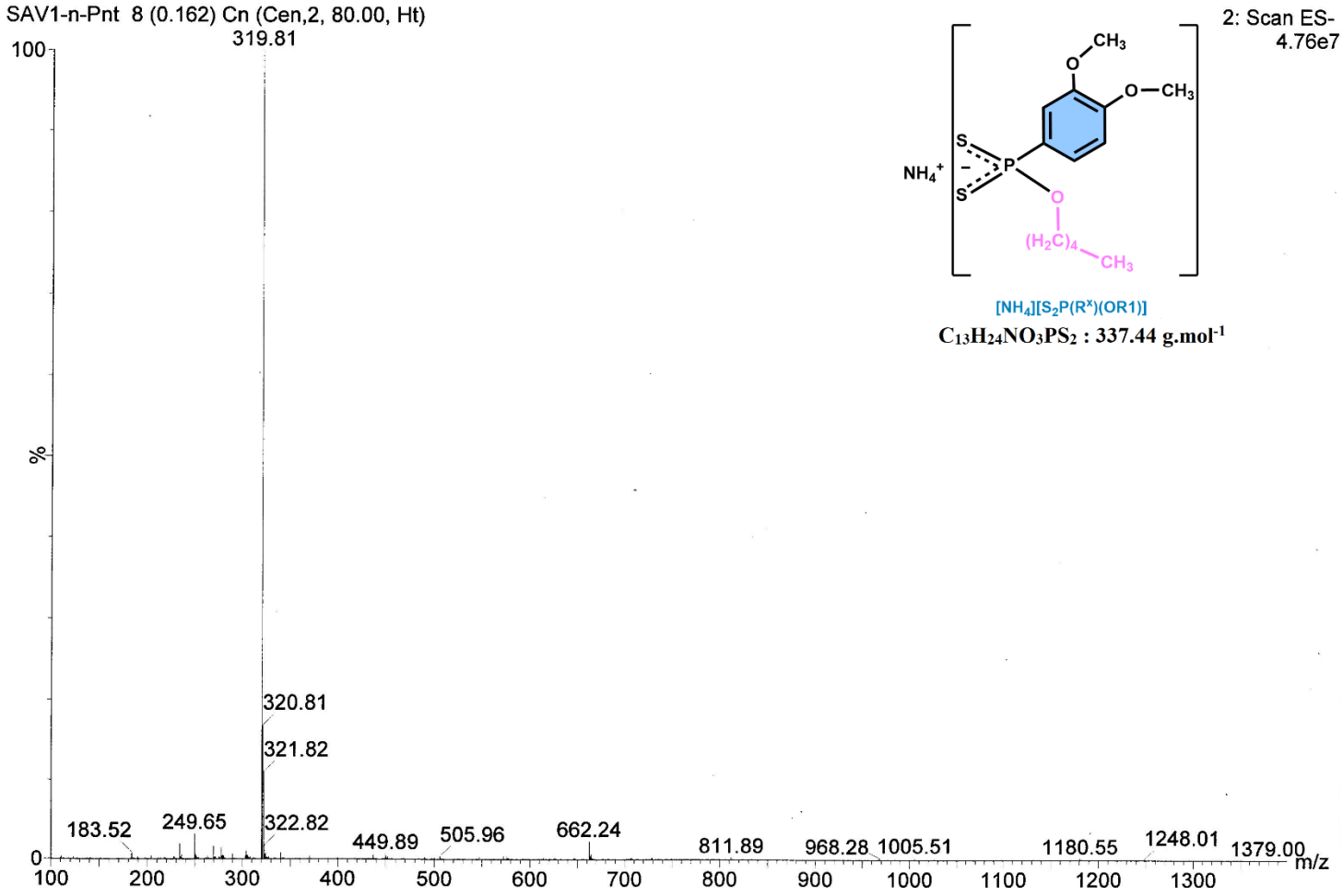


Figure 5.49. [NH_4][$S_2P(R^x)(OR1)$] Mass spectrum.

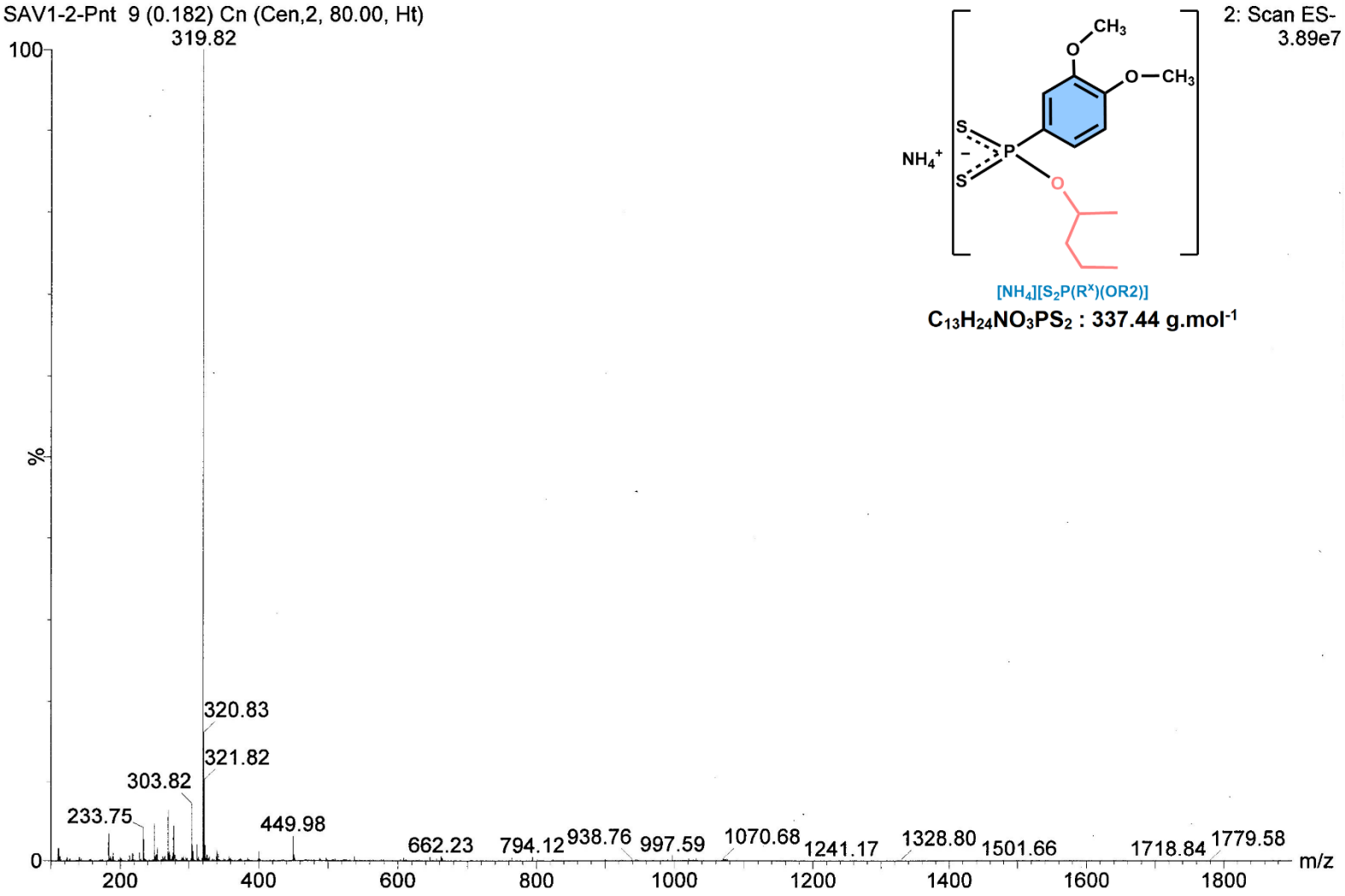


Figure 5.50. $[NH_4][S_2P(R^x)(OR2)]$ Mass spectrum.

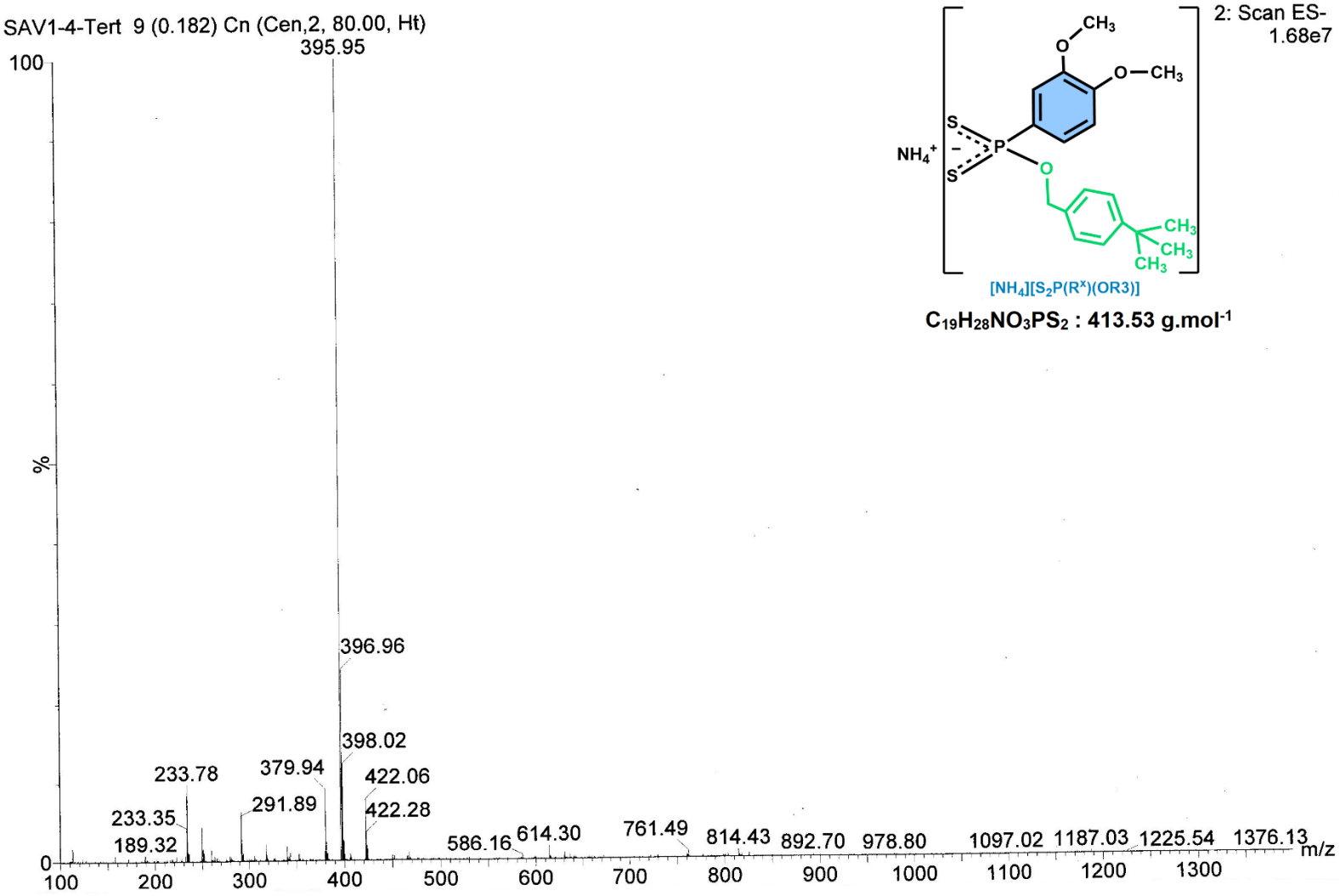


Figure 5.51. [NH_4][$S_2P(R^x)(OR3)$] Mass spectrum.

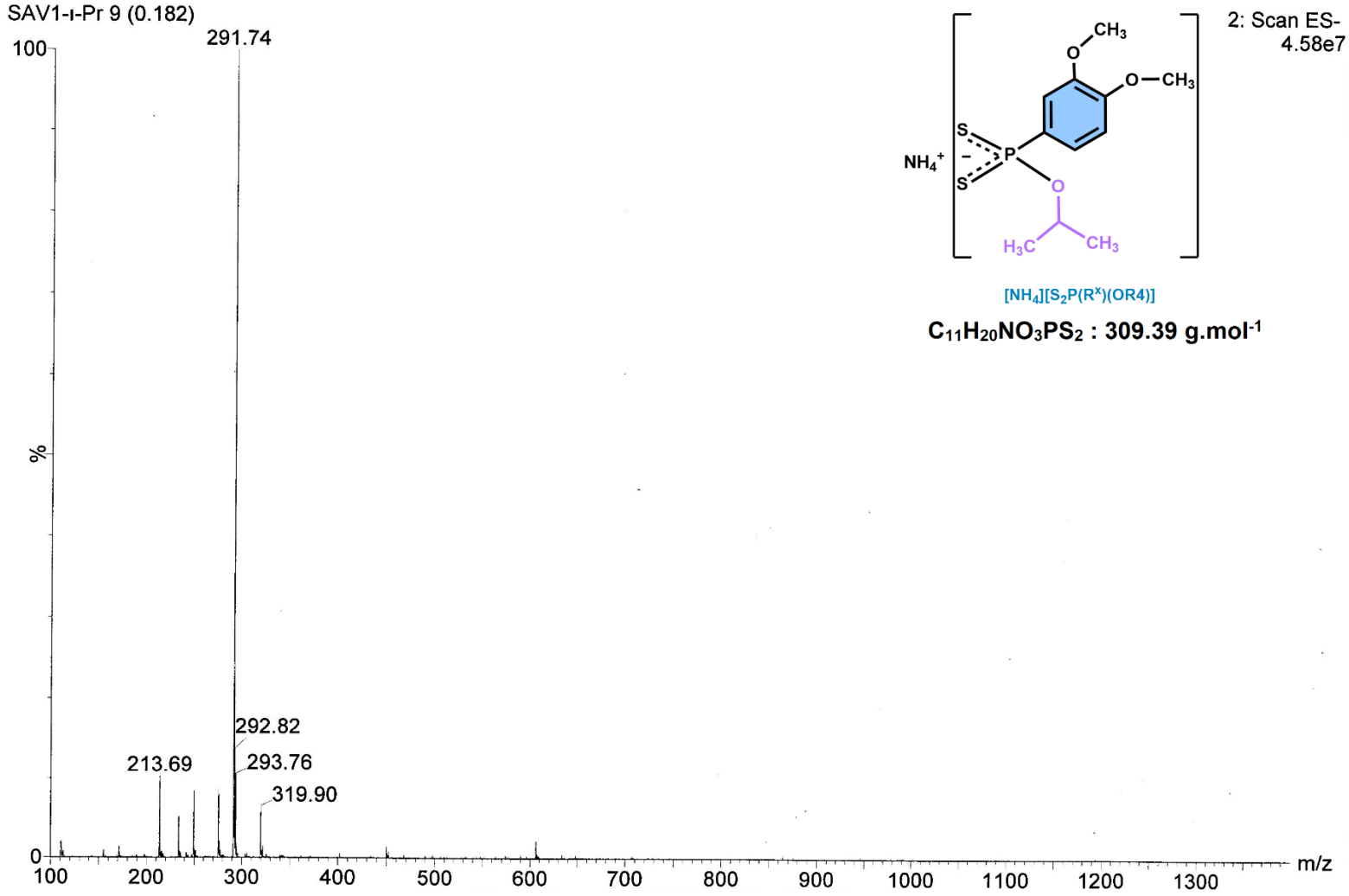


Figure 5.52. [NH_4][$S_2P(R^x)$(OR4)] Mass spectrum.

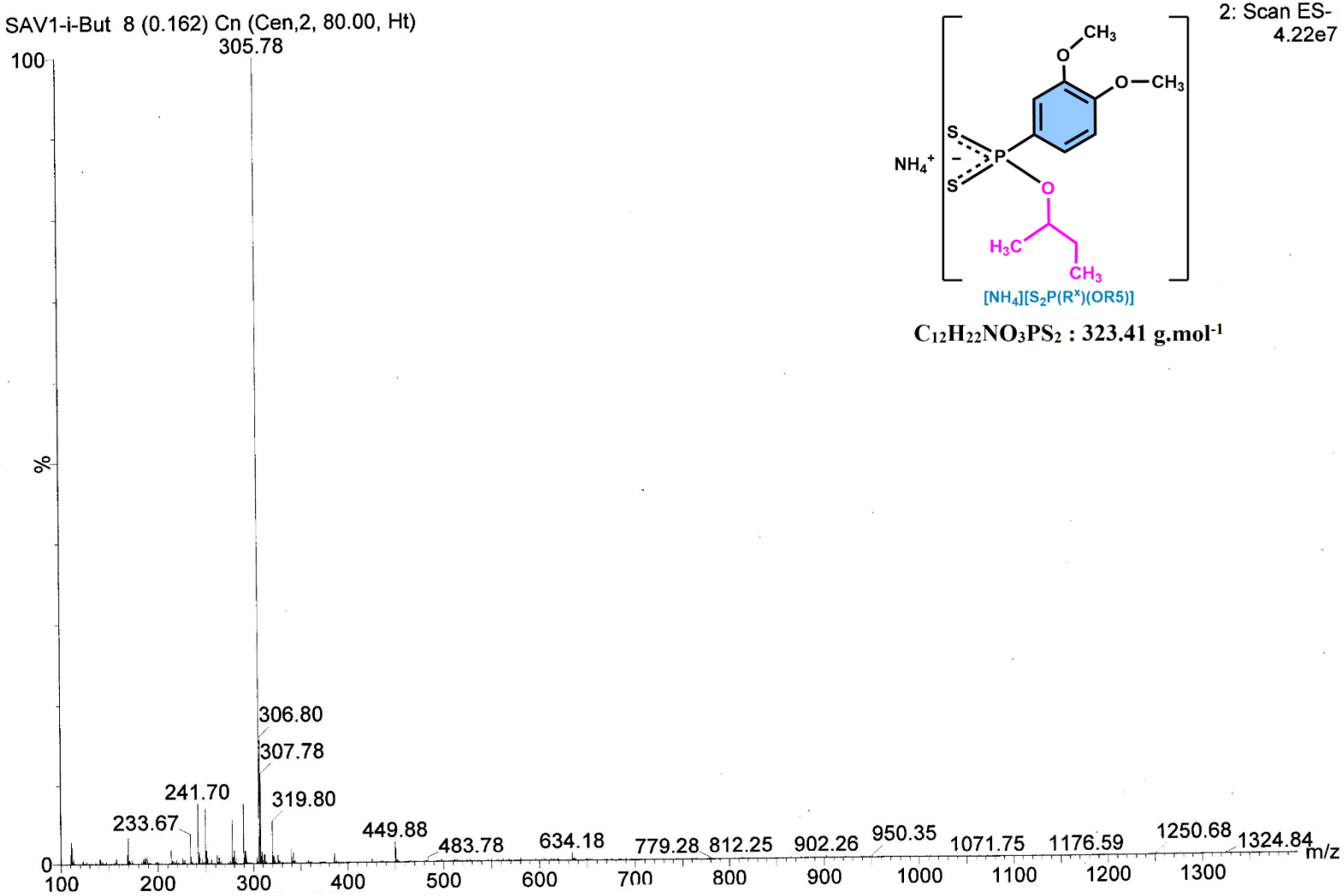


Figure 5.53. $[NH_4][S_2P(R^x)(OR5)]$ Mass spectrum.

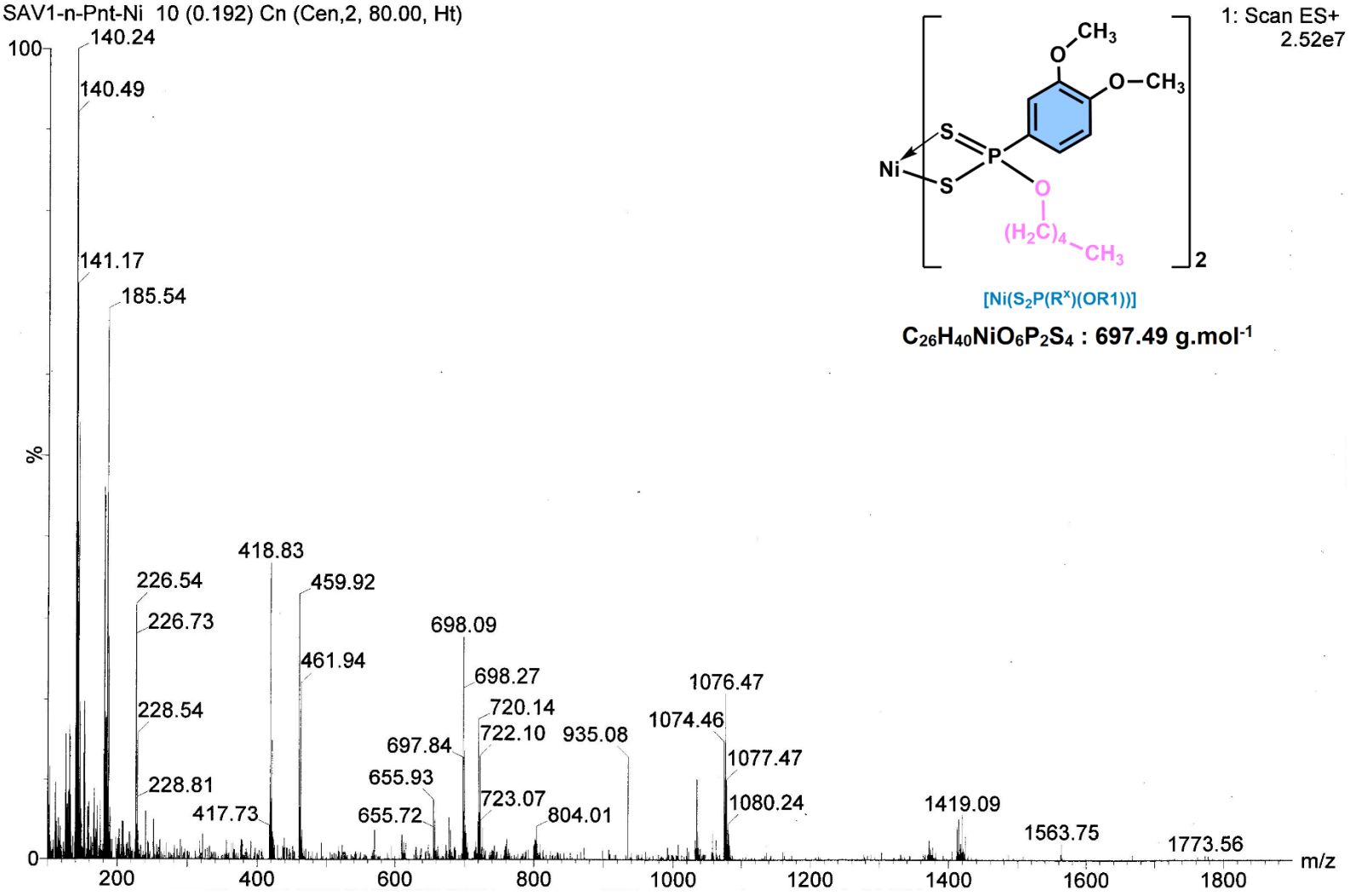


Figure 5.54. [Ni($S_2P(R^x)(OR1)$)$_2$] Mass spectrum.

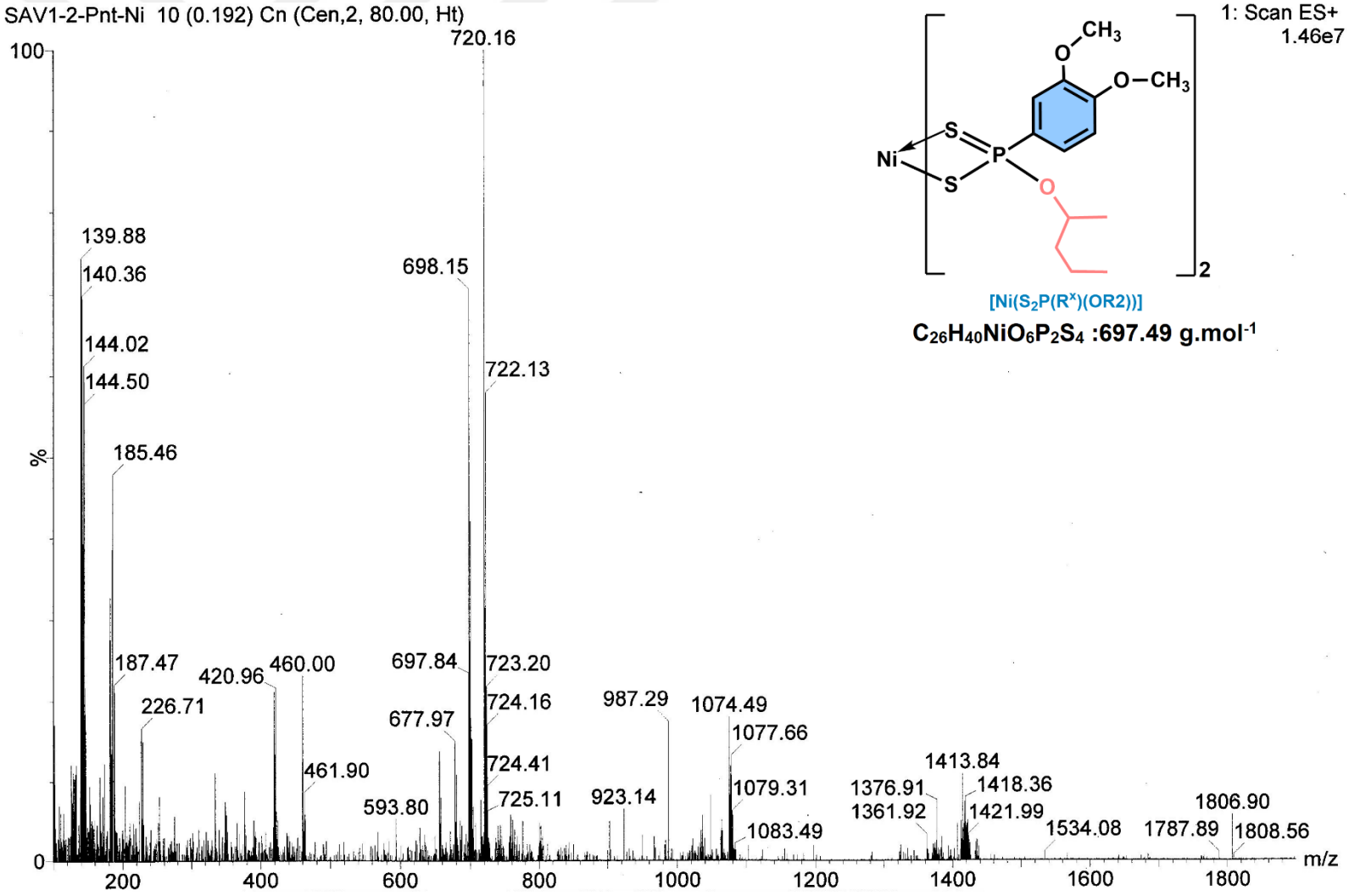


Figure 5.55. [Ni($S_2P(R^x)(OR2))_2$] Mass spectrum.

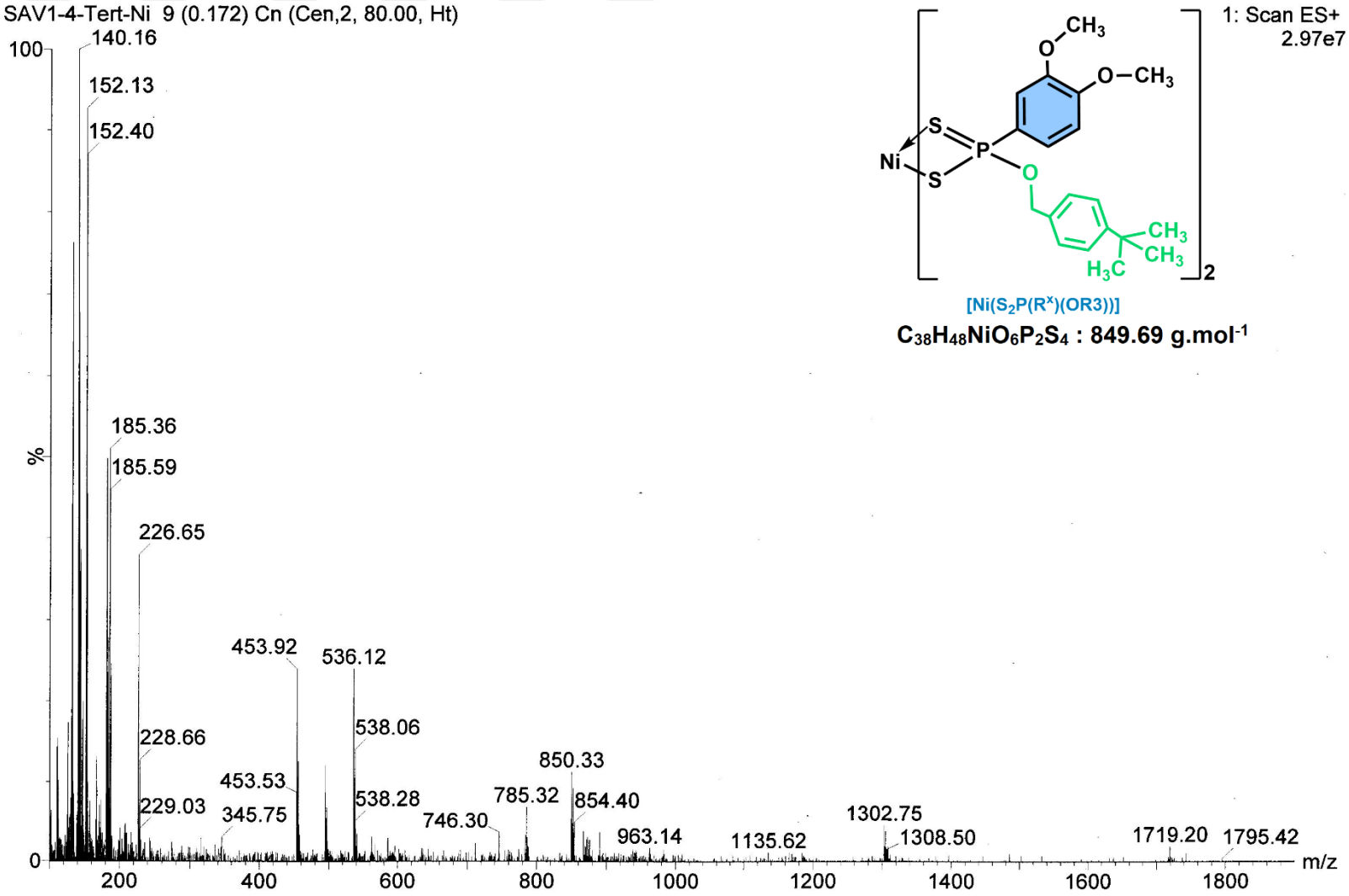


Figure 5.56. [$Ni(S_2P(R^x)(OR3))_2$] Mass spectrum.

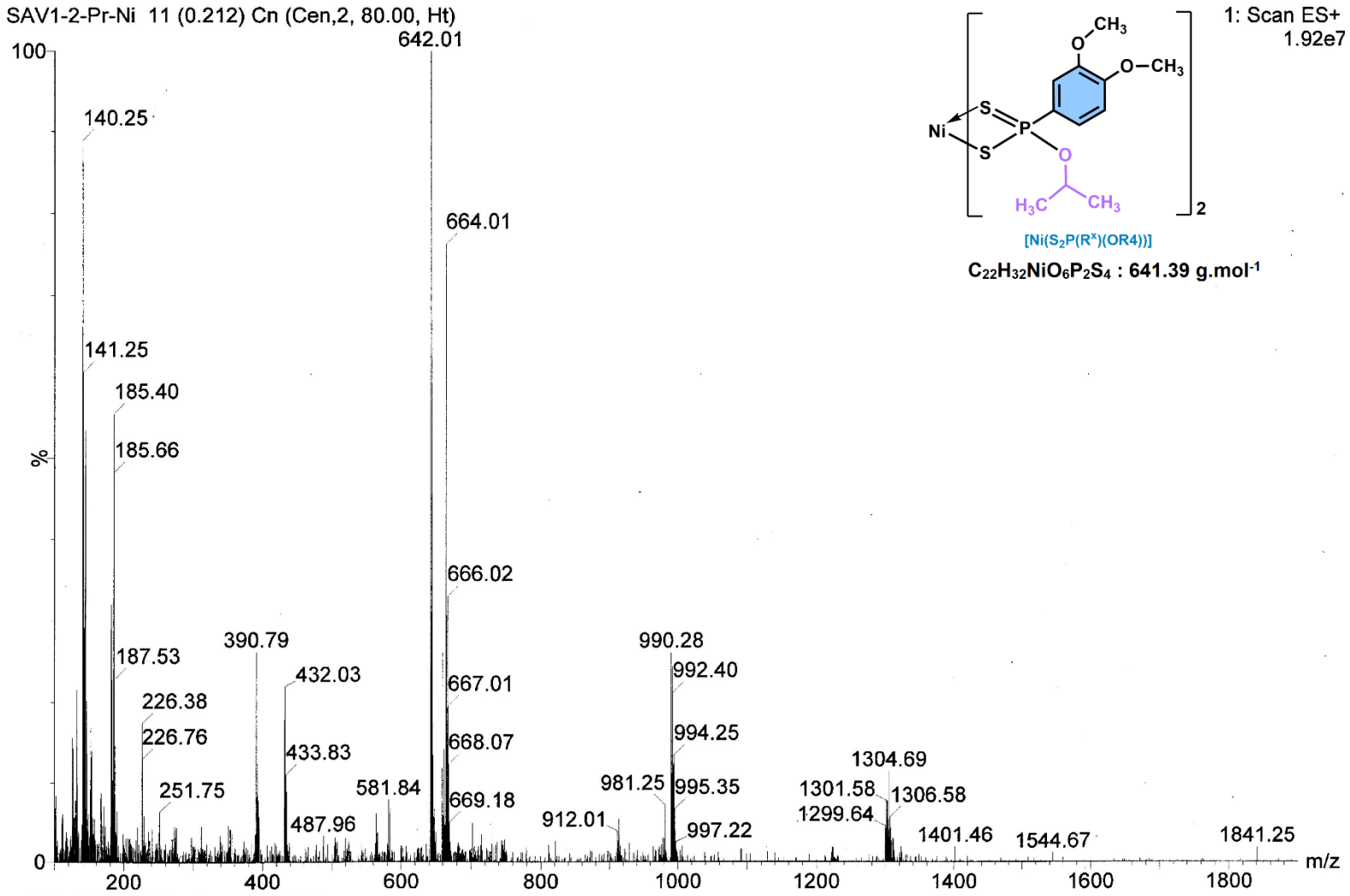


Figure 5.57. [Ni($S_2P(R^x)(OR4))_2$] Mass spectrum.

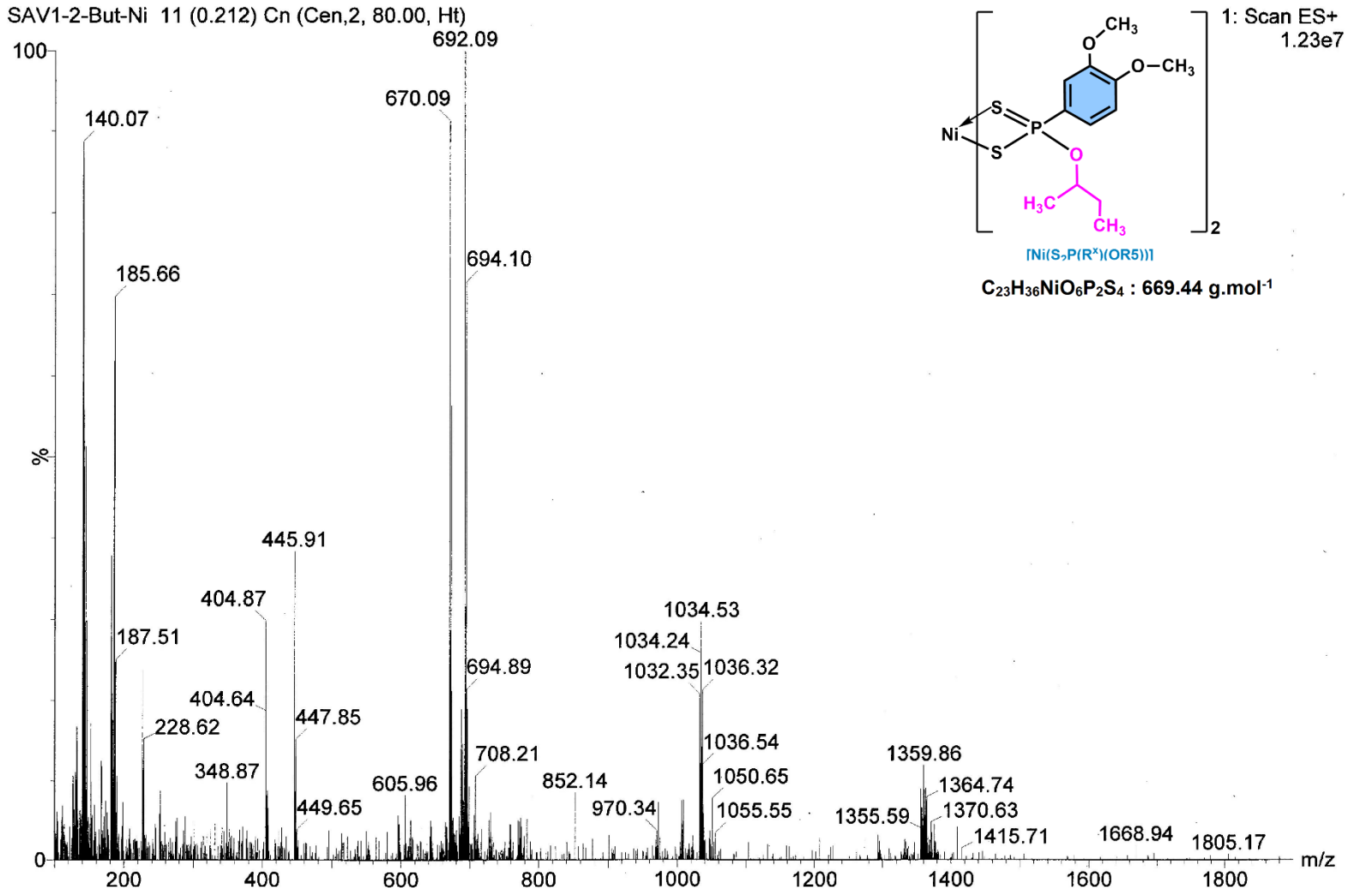


Figure 5.58. [Ni($S_2P(R^x)(OR5)$)$_2$] Mass spectrum.

5.1.6. Comment on the Mass spectra of $[NH_4][S_2P(R^y)(ORn)]$, $[Ni(S_2P(R^y)(ORn)]$ for Part II

The spectra of the compounds are pictured in Figures 5.59-5.162. All the ligands and complexes display intense molecular ion peaks. The ammonium salts display the corresponding dithiophosphonic acids as the molecular ion. In the section, experimental, we represent the molecular ions by $[M\text{-}NH_4]^+$. In general, all the $[M\text{-}NH_4]^+$ species are accompanied by one molecule of EtOH. These peaks are the most intense (principal) ones on all the MS spectra. The molecular ion peaks of the complexes, $[M+H]^+$, are also the principal peak, except for $[Ni(S_2P(R^y)(OR3))_2]$.

Mass spectra of Part II $[NH_4][S_2P(R^y)(ORn)]$ and $[Ni(S_2P(R^y)(ORn))_2]$ compounds.

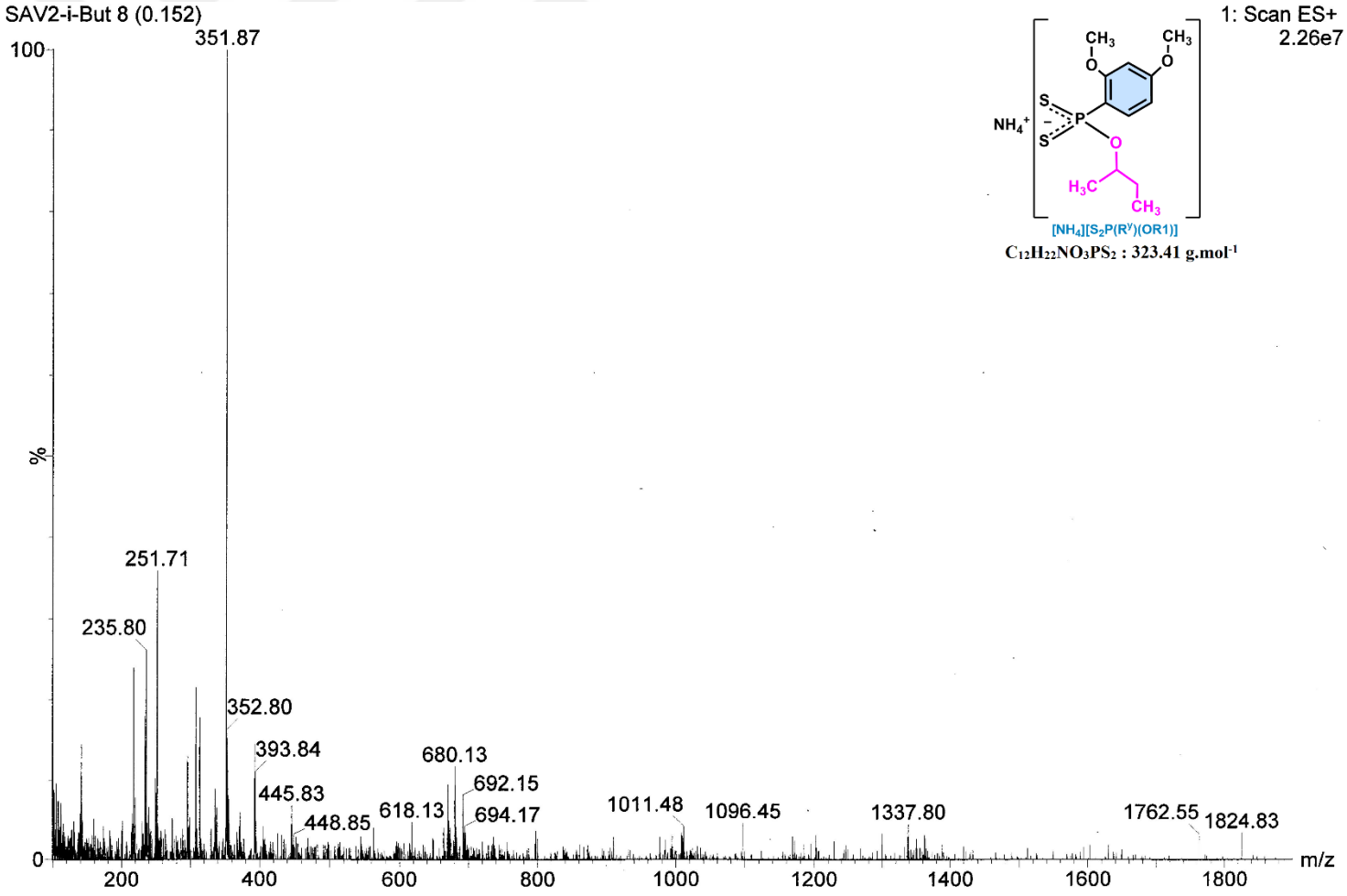


Figure 5.59. $[NH_4][S_2P(R^y)(OR1)]$ Mass spectrum.

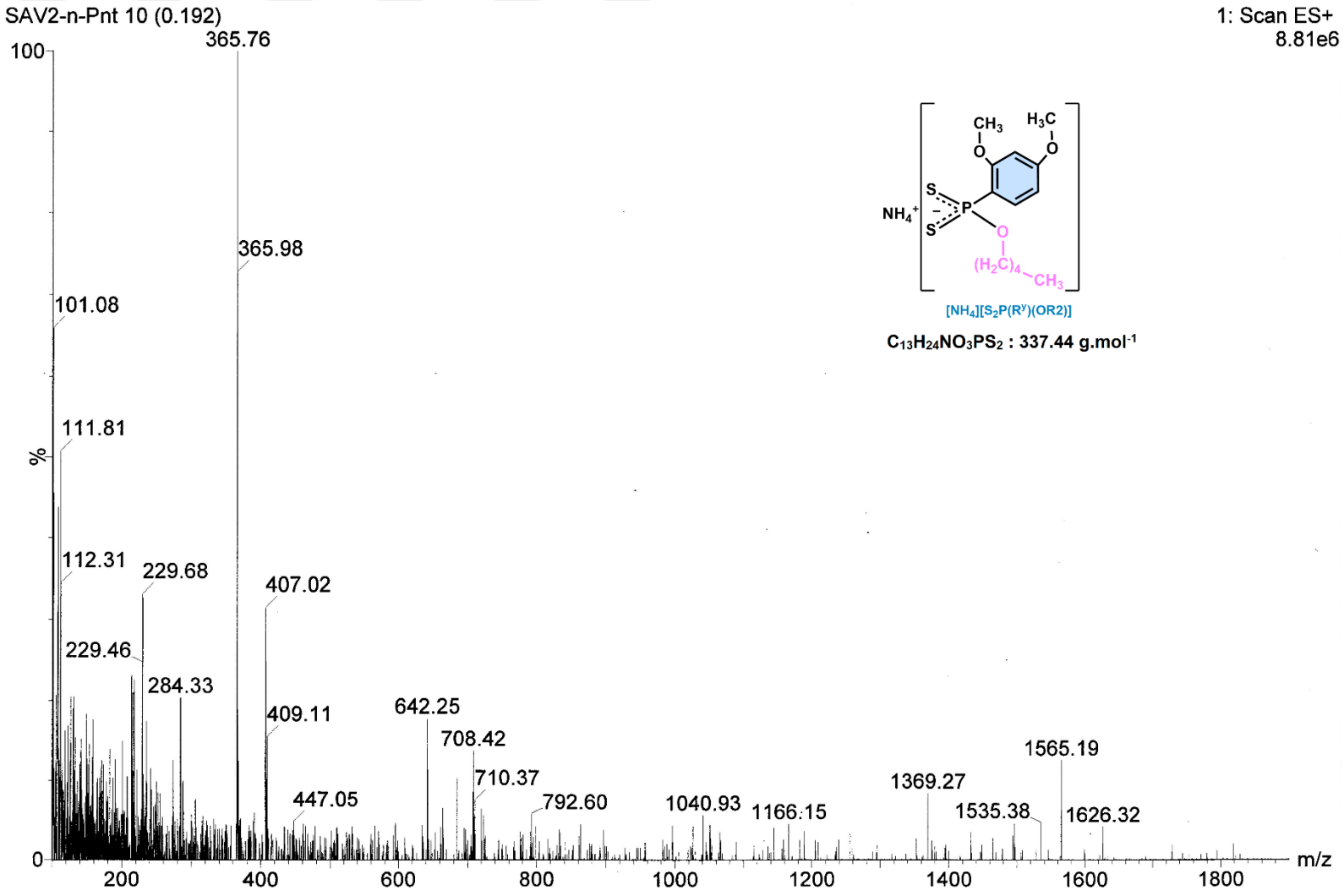


Figure 5.60. $[NH_4][S_2P(R^y)(OR2)]$ Mass spectrum.

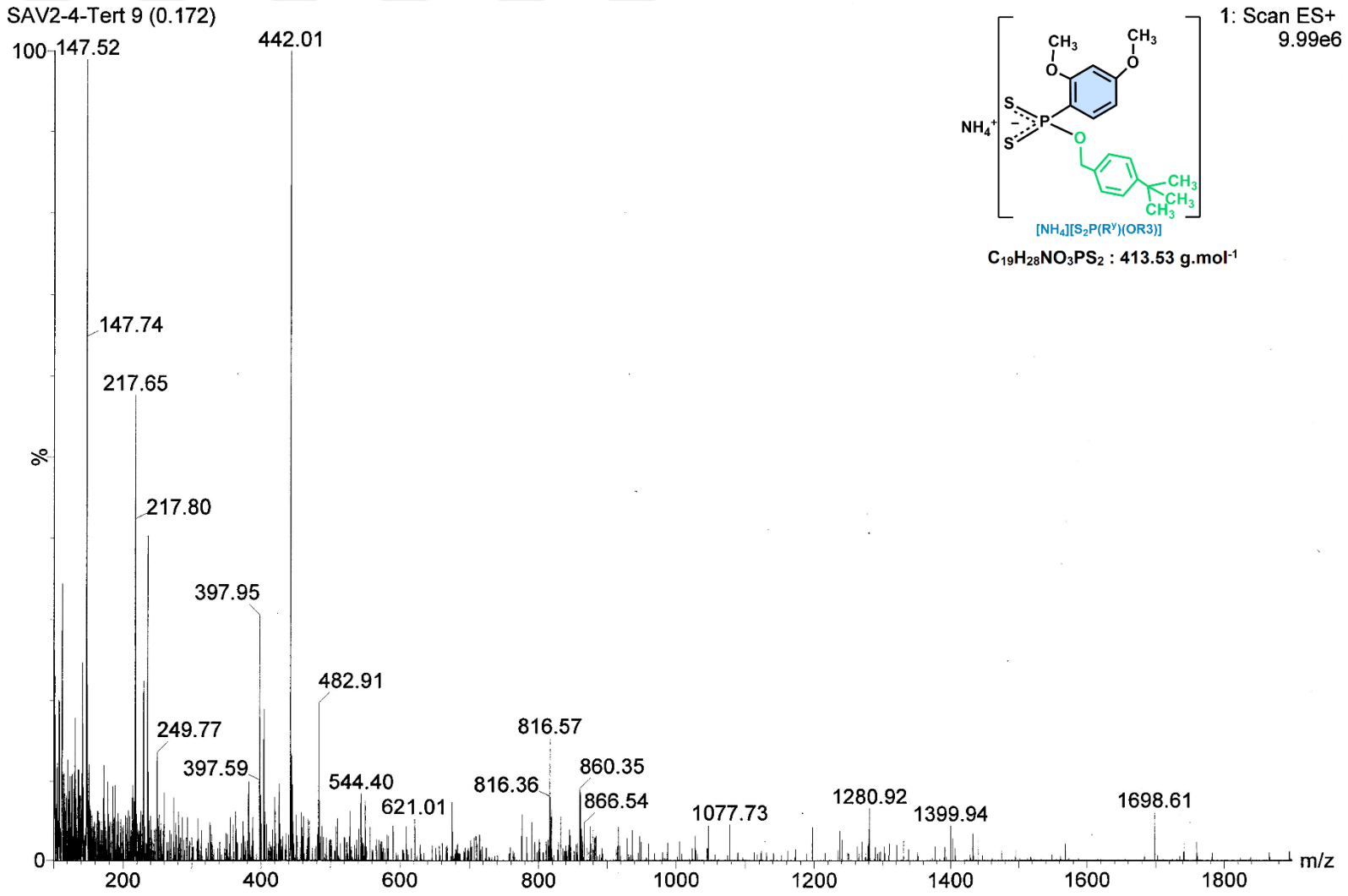


Figure 5.61. $[NH_4][S_2P(R^y)(OR3)]$ Mass spectrum.

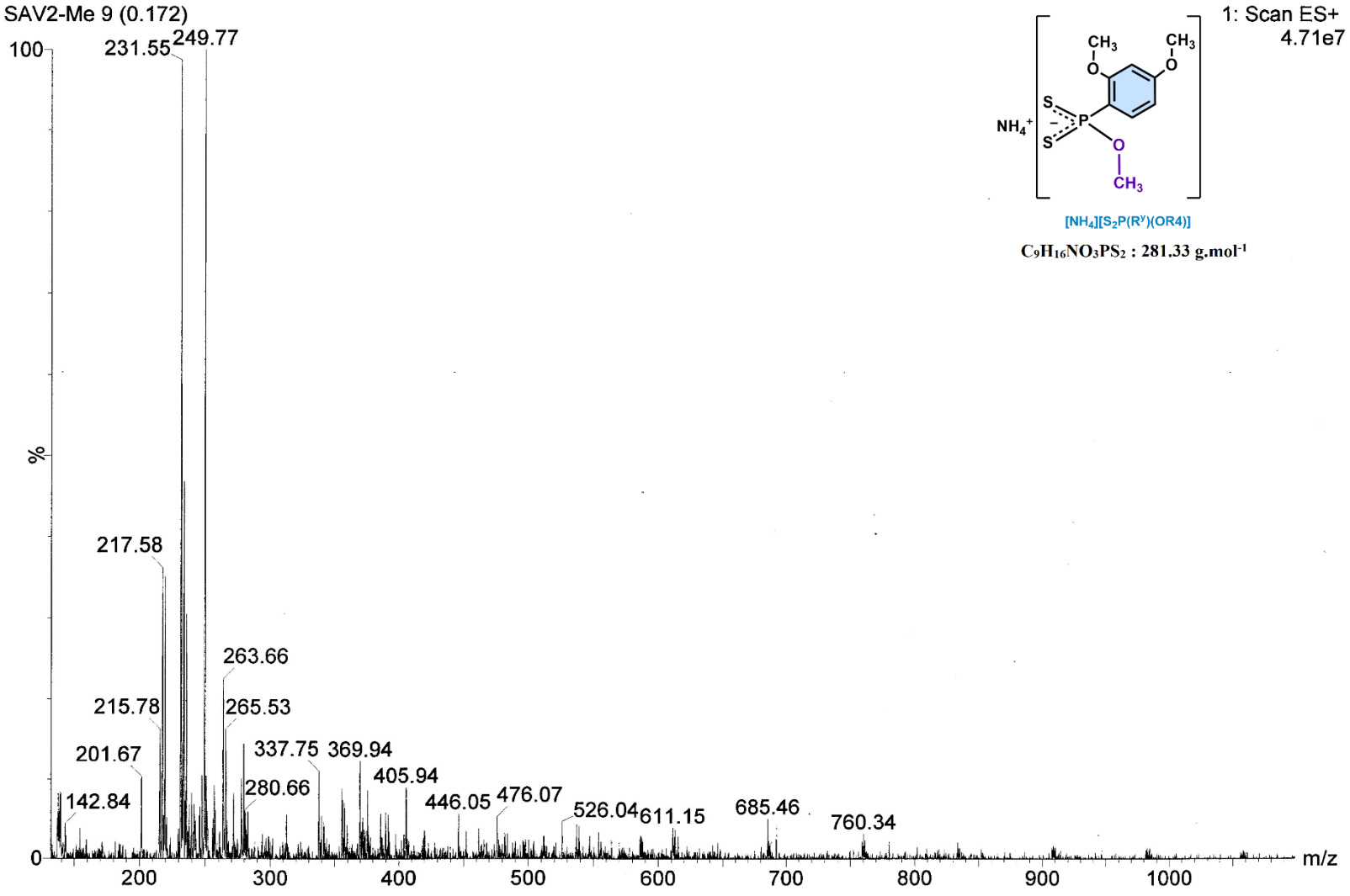


Figure 5.62. $[NH_4][S_2P(R^y)(OR4)]$ Mass spectrum.

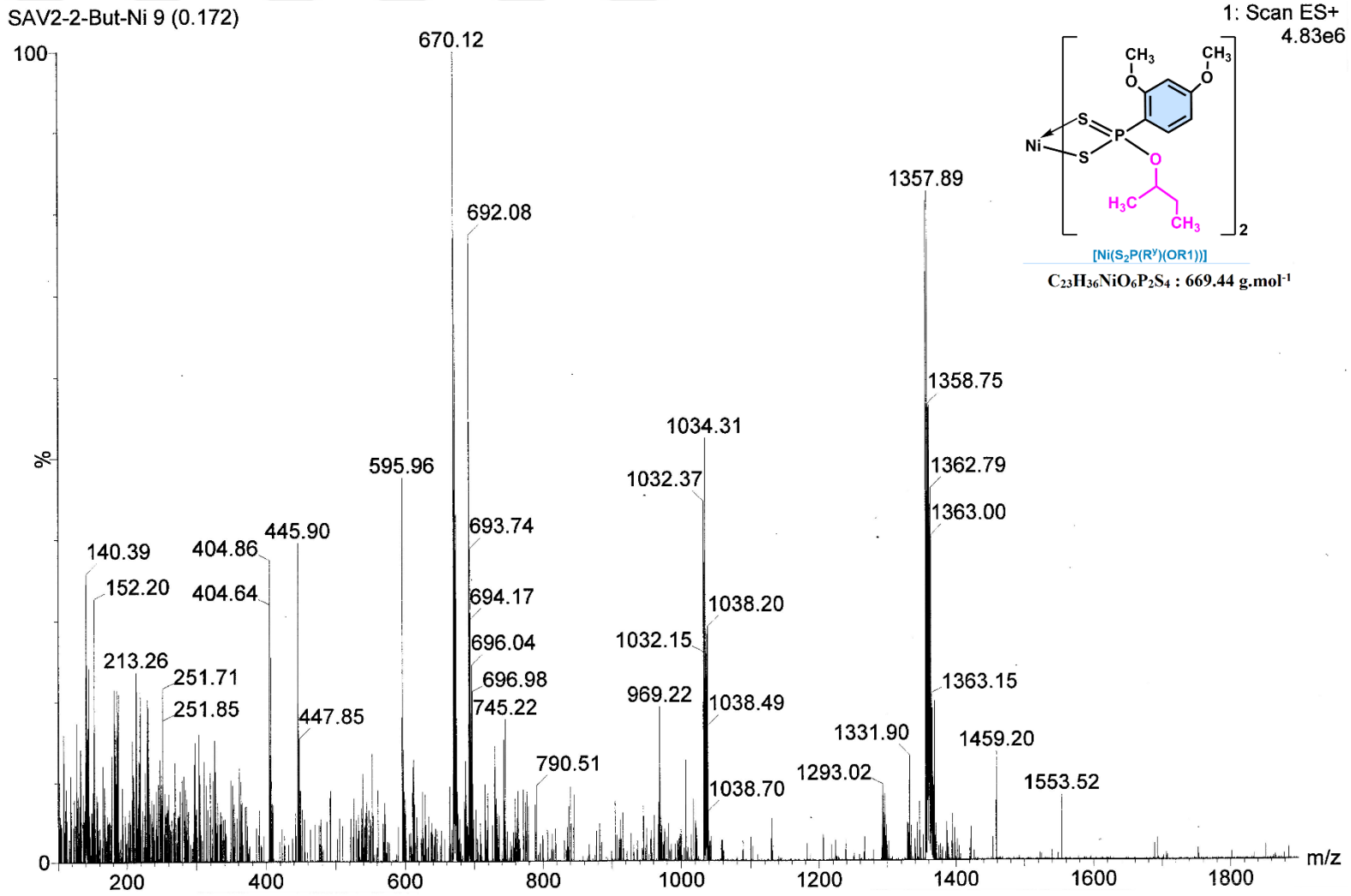


Figure 5.63. [Ni($S_2P(R^y)(OR1)$)$_2$] Mass spectrum.

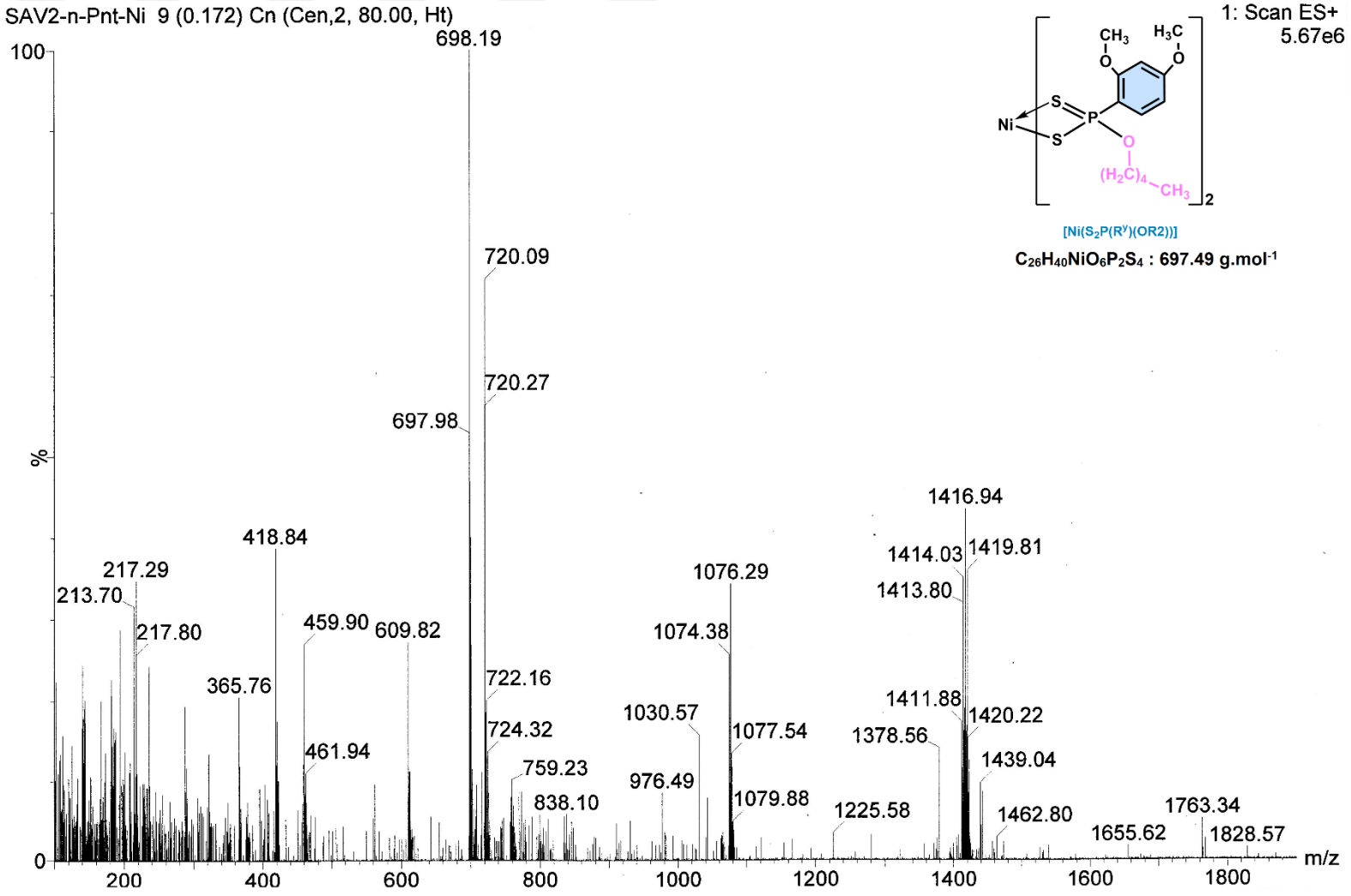


Figure 5.64. [Ni($S_2P(R^y)(OR2))_2$] Mass spectrum.

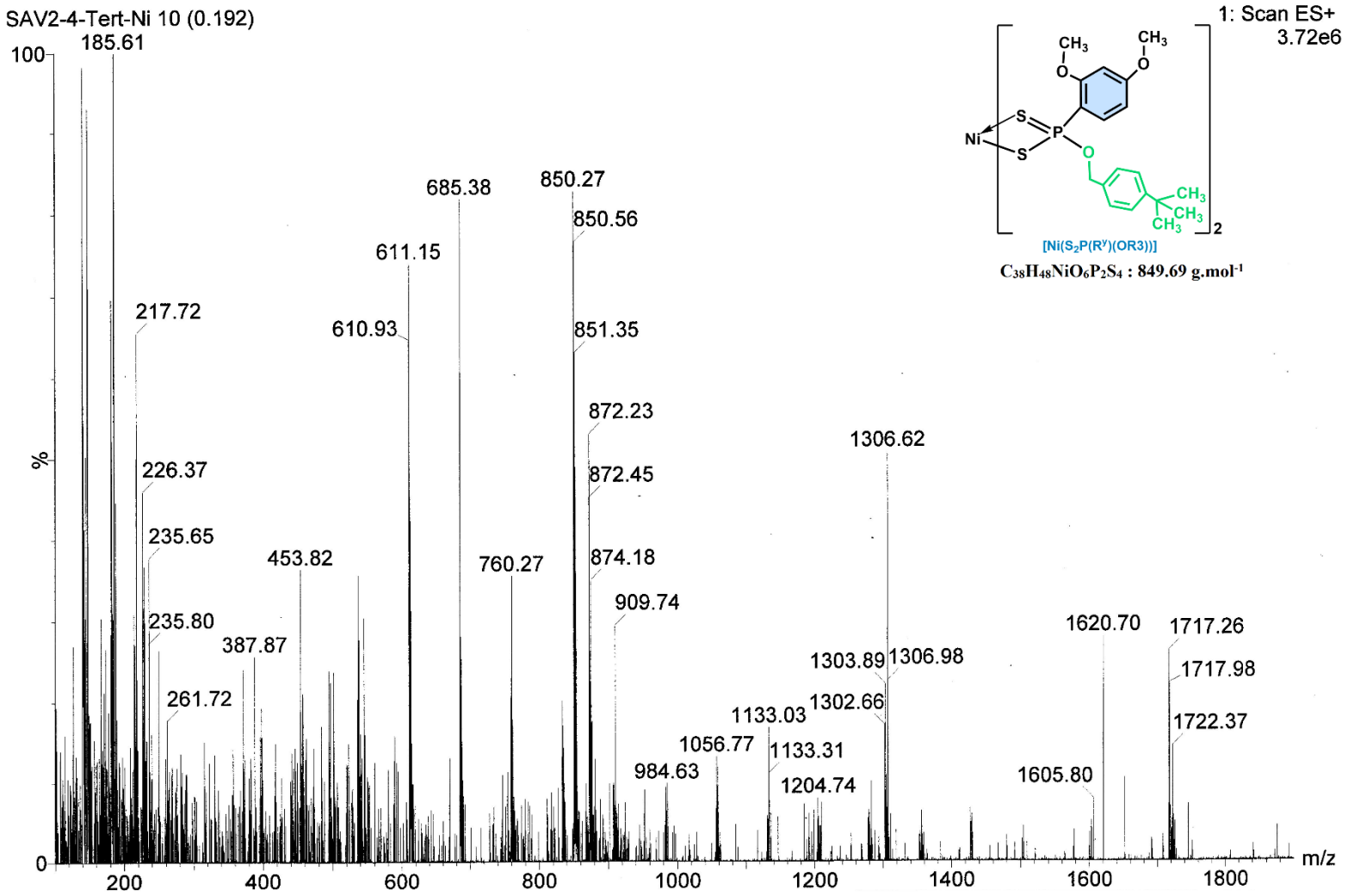


Figure 5.65. $[Ni(S_2P(R^y)(OR3))_2]$ Mass spectrum.

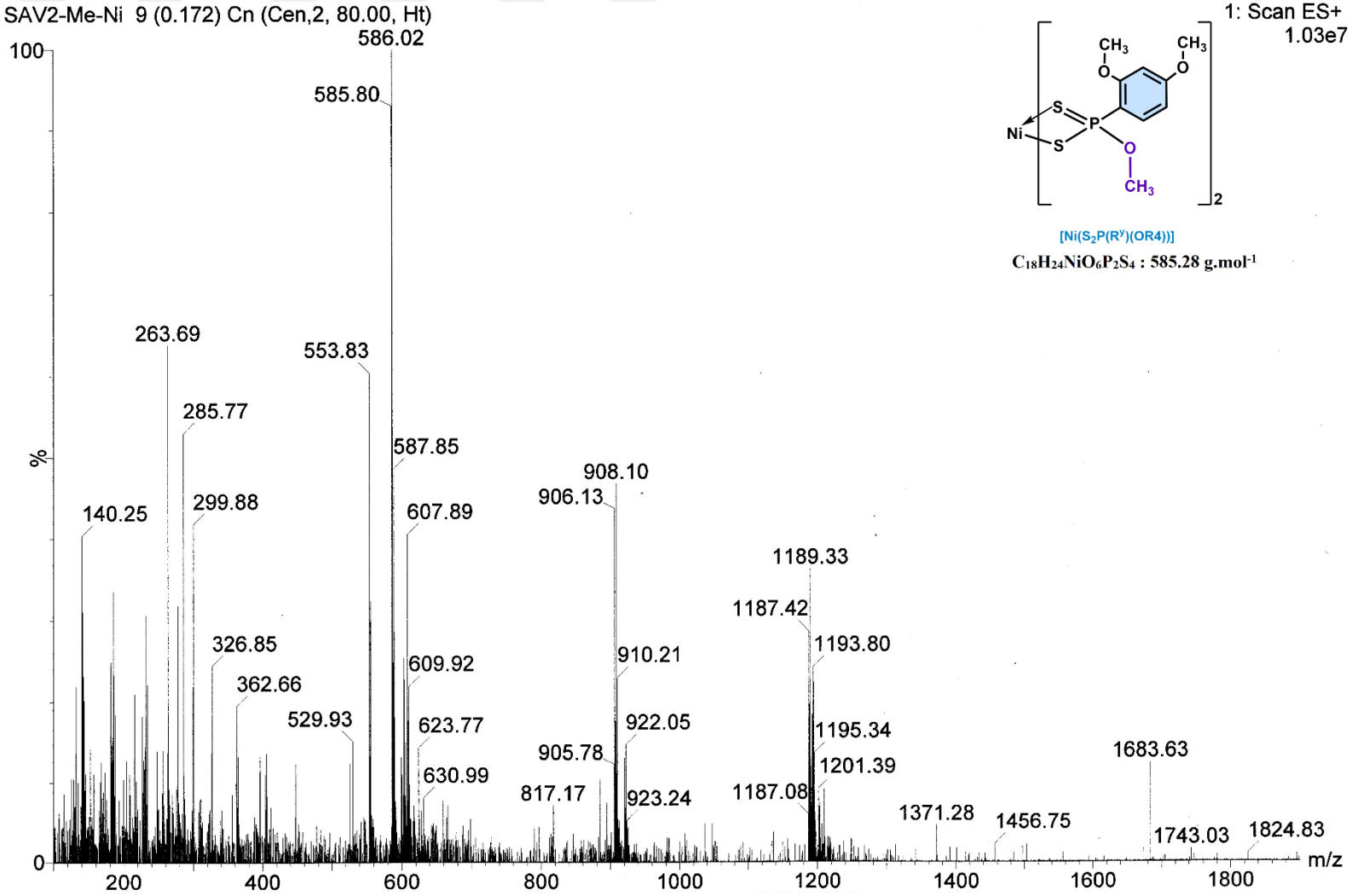


Figure 5.66. [Ni($S_2P(R^y)(OR4))_2$] Mass spectrum.

5.1.7. NMR (^{1}H, ^{13}C- and ^{31}P- NMR) of compounds

For NMR spectra measurements, the NMR solvent D_2O was used for ligands. $CDCl_3$ was used for the complexes. ^{13}C-NMR and ^{31}P-NMR analyses were performed as proton-decoupled. In the spectra, the chemical shift "δ" is given in ppm and the splitting constant *J* values are given in Hz (s: single; d: double; t: triple; dd: pair of two; m: multiple). The starting materials, $[R^{x,y}\text{-}P(S)S]_2$, are insoluble in the common NMR solvents, so no NMR data were provided for it.

All the NMR values compare well with the literature reports for similar structures [101, 122, 185, 261, 298-301].

5.1.7.1 Comment on the HSQC spectrum on the $[Ni(S_2P(R^x)(OR6))_2]$ for Part Ia

The ambiguity regarding the assignments of ^{1}H- and ^{13}C-NMR peaks of $[Ni(S_2P(R^x)(OR6))_2]$ complex was dealt with by using HSQC spectra (Figure 5.67).

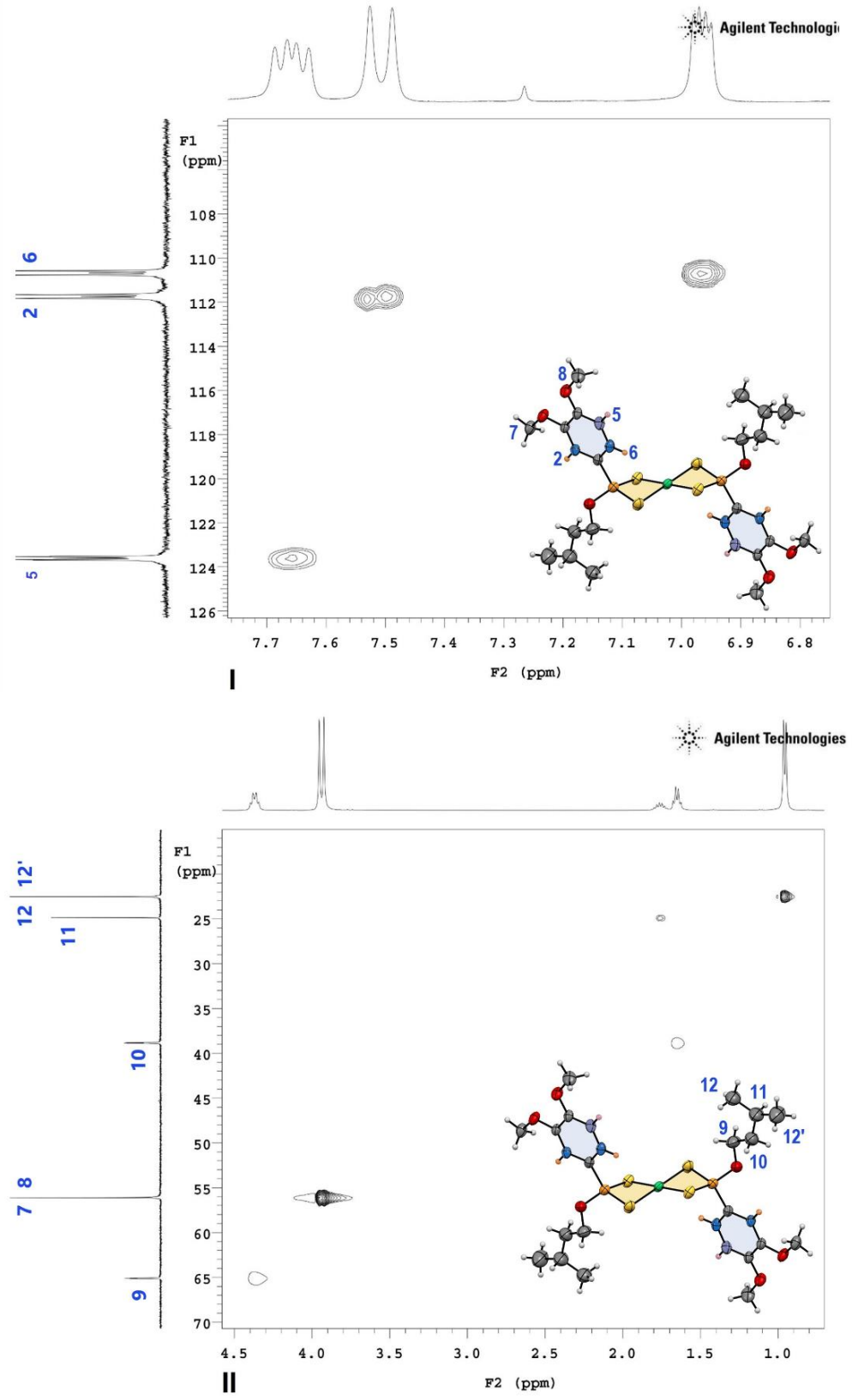


Figure 5.67. HSQC spectrum (**I**) for the aromatic region and (**II**) for the aliphatic region of $[Ni(S_2P(R^x)(OR6))_2]$.

5.1.7.2. Comment of ^{1}H-NMR Spectra of Part Ia' compounds

The NMR spectra and important NMR data for the ligands and their nickel(II) complexes are presented in Table 5.4 and Table 5.5. The numbering system used for assignments of the carbon atoms is also given in Figure 5.68. The spectra of the compounds are also given in Figures 5.69-5.82.

Table 5.4. Part Ia ^{1}H-NMR data of $[NH_4][S_2P(R^x)(ORn)]$, (D_2O; δ in ppm, J in Hz, s: *singlet*, d: *doublet*, dd: *doublet of doublets*, t: *triplet*, and m: *multiplet*).

	$[NH_4][S_2P(R^x)(OR1)]$	$[NH_4][S_2P(R^x)(OR2)]$	$[NH_4][S_2P(R^x)(OR3)]$	$[NH_4][S_2P(R^x)(OR4)]$	$[NH_4][S_2P(R^x)(OR5)]$	$[NH_4][S_2P(R^x)(OR6)]$	$[NH_4][S_2P(R^x)(OR7)]$
C_2-H	7.6 (d, H), $^{3}J_{PH}$= 14.7	7.7 (d, H), $^{3}J_{PH}$= 13.8	7.6 (d, H), $^{3}J_{PH}$= 14.6	7.6 (d, H), $^{3}J_{PH}$= 14.6	7.7 (d, H), $^{3}J_{PH}$= 14.7	7.6 (d, H), $^{3}J_{PH}$= 14.6	7.4 (d, H),$^{3}J_{PH}$= 14.7
C_5-H	7.0 (dd, H) $^{4}J_{PH}$= 3.8 , $^{3}J_{HH}$= 8.3	6.9 (dd, H) $^{4}J_{PH}$= 3.6, $^{3}J_{HH}$= 8.2	7.1 (dd, H) $^{4}J_{PH}$= 3.7, $^{3}J_{HH}$= 8.3	7.1 (dd, H) $^{4}J_{PH}$= 3.8, $^{3}J_{HH}$= 8.3	7.1 (dd, H) $^{4}J_{PH}$= 3.7, $^{3}J_{HH}$= 8.2	7.1 (dd, H) $^{4}J_{PH}$= 3.7, $^{3}J_{HH}$= 8.3	6.8 (dd, H) $^{4}J_{PH}$= 3.7, $^{3}J_{HH}$= 8.2
C_6-H	7.7 (dd, H) $^{3}J_{PH}$= 14.3, $^{3}J_{HH}$= 8.3	7.7 (dd, H) $^{3}J_{PH}$= 12.6 , $^{3}J_{HH}$= 7.9	7.7 (dd, H) $^{3}J_{PH}$= 14.3, $^{3}J_{HH}$=8.3	7.7 (dd, H) $^{3}J_{PH}$= 14.3, $^{3}J_{HH}$=8.4	7.7 (dd, H) $^{3}J_{PH}$= 13.4, $^{3}J_{HH}$= 8.3	7.7 (dd, H) $^{3}J_{PH}$= 14.2, $^{3}J_{HH}$= 8.3	7.5 (dd, H) $^{3}J_{PH}$= 14.4,$^{3}J_{HH}$= 8.3
C_7-H	3.9 (s, 3H)	3.9 (s, 3H)	3.9 (s, 3H)	3.9 (s, 3H)	3.9 (s, 3H)	3.9 (s, 3H)	3.7 (s, 3H)
C_8-H	3.9 (s, 3H)	3.8 (s, 3H)	3.9 (s, 3H)	3.9 (s, 3H)	3.9 (s, 3H)	3.9 (s, 3H)	3.6 (s, 3H)
C_9-H	3.6 (d, 3H) , $^{3}J_{PH}$= 14.7	3.9 (m, 2H)	3.8 (dd, 2H) $^{3}J_{HH}$= 6.3, $^{3}J_{PH}$= 14.8	3.9 (dd, 2H) $^{3}J_{HH}$= 6.6, $^{3}J_{PH}$= 15.0	4.4 (m, H)	3.8 (m, 2H)	4.7 (d, 2H), $^{3}J_{PH}$= 10.2
C_{10}-H	-	1.2 (t, 3H), $^{3}J_{HH}$= 7.3	1.6 (m, 2H)	1.6 (m, 2H)	1.6 (m, 4H)	1.5 (m, 2H)	-
C_{11}-H	-	-	0.9 (t, 3H), $^{3}J_{HH}$= 7.5	1.4 (m, 2H)	0.8 (t, 6H),$^{3}J_{HH}$= 7.5	1.6 (m, H)	-
C_{12}-H	-	-	-	0.9 (t, 3H), $^{3}J_{HH}$= 7.5	-	0.8 (d, 6H), $^{3}J_{HH}$= 6.7	-
$C_{11,12,13}$-H	-	-	-	-	-	-	7.2 (m, 5H)

Table 5.5. Part Ia ^{1}H-NMR data of [Ni($S_2P(R^x)(ORn))_2$], ($CDCl_3$; δ in ppm, *J* in Hz, s: *singlet*, d: *doublet*, dd: *doublet of doublets*, t: *triplet*, and m: *multiplet*).

	[Ni($S_2P(R^x)(OR1))_2$]	[Ni($S_2P(R^x)(OR2))_2$]	[Ni($S_2P(R^x)(OR3))_2$]	[Ni($S_2P(R^x)(OR4))_2$]	[Ni($S_2P(R^x)(OR5))_2$]	[Ni($S_2P(R^x)(OR6))_2$]	[Ni($S_2P(R^x)(OR7))_2$]
C_2-H	7.5 (d, 2H), $^{3}J_{PH}$= 15.2	7.5 (d, 2H), $^{3}J_{PH}$= 15.1	7.5 (d, 2H), $^{3}J_{PH}$= 15.2	7.5 (d, 2H), $^{3}J_{PH}$= 15.2	7.6 (d, 2H), $^{3}J_{PH}$= 15.2	7.5 (d, 2H), $^{3}J_{PH}$= 15.2	7.5 (d, 2H),$^{3}J_{PH}$= 15.3
C_5-H	7.0 (dd, 2H) $^{4}J_{PH}$= 4.2 , $^{3}J_{HH}$= 8.3	7.0 (dd, 2H) $^{4}J_{PH}$= 3.9, $^{3}J_{H}$H= 8.2	7.0 (dd, 2H) $^{4}J_{PH}$= 3.3, $^{3}J_{HH}$= 7.8	7.0 (dd, 2H) $^{4}J_{PH}$= 4.2, $^{3}J_{HH}$= 8.4	7.0 (dd, 2H) $^{4}J_{PH}$= 4.2, $^{3}J_{HH}$= 8.3	7.0 (dd, 2H) $^{4}J_{PH}$= 4.2, $^{3}J_{HH}$= 8.4	7.0 (dd, 2H) $^{4}J_{PH}$= 4.0, $^{3}J_{HH}$= 8.3
C_6-H	7.7 (dd, 2H) $^{3}J_{PH}$= 15.1, $^{3}J_{HH}$= 8.3	7.7 (dd, 2H) $^{3}J_{PH}$= 14.2 , $^{3}J_{HH}$= 8.5	7.7 (dd, 2H) $^{3}J_{PH}$= 14.5, $^{3}J_{HH}$=8.4	7.7 (dd, 2H) $^{3}J_{PH}$= 14.9, $^{3}J_{HH}$=8.5	7.7 (dd, 2H) $^{3}J_{PH}$= 14.7, $^{3}J_{HH}$= 8.3	7.7 (dd, 2H) $^{3}J_{PH}$= 14.9, $^{3}J_{HH}$= 8.3	7.7 (dd, 2H) $^{3}J_{PH}$= 14.8,$^{3}J_{HH}$= 8.6
C_7-H	4.0 (s, 6H)	4.0 (s, 6H)	4.0 (s, 6H)	4.0 (s, 6H)	4.0 (s, 6H)	4.0 (s, 6H)	3.9 (s, 6H)
C_8-H	4.0 (s, 6H)	3.9 (s, 6H)	4.0 (s, 6H)	3.9 (s, 6H)	3.9 (s, 6H)	3.9 (s, 6H)	3.9 (s, 6H)
C_9-H	4.0 (d, 6H) , $^{3}J_{PH}$= 14.9	4.4 (m, 4H)	4.3 (dd, 4H) $^{3}J_{HH}$= 6.7, $^{3}J_{PH}$= 14.7	4.4 (dd, 4H) $^{3}J_{HH}$= 6.7, $^{3}J_{PH}$= 15.7	4.8 (m , 2H)	4.4 (dd, 4H) $^{3}J_{HH}$= 6.6, $^{3}J_{PH}$= 15.5	5.4 (d, 4H), $^{3}J_{PH}$= 8.9
C_{10}-H	-	1.4 (t, 6H), $^{3}J_{HH}$= 7.0	1.8 (dd, 4H) $^{3}J_{HH}$= 13.8, $^{4}J_{PH}$= 6.8	1.8 (m, 4H)	1.8 (m, 8H)	1.7 (dd, 4H), $^{3}J_{HH}$= 6.7	-
C_{11}-H	-	-	1.0 (t, 6H), $^{3}J_{HH}$= 7.2	1.5 (m, 4H)	1.0 (t, 12H),$^{3}J_{HH}$= 7.4	1.8 (m, 2H)	-
C_{12}-H	-	-	-	1.0 (t, 6H), $^{3}J_{HH}$= 7.4	-	1.0 (d, 12H), $^{3}J_{HH}$= 6.6	-
$C_{11,12,13}$-H	-	-	-	-	-	-	7.4 (m, 10H)

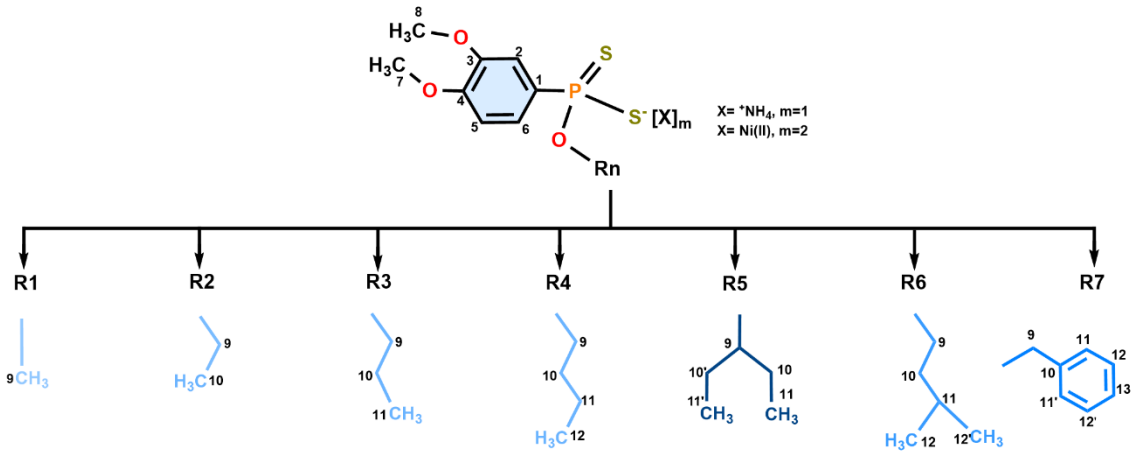


Figure 5.68. The numbering scheme for the compounds Part Ia.

The C_6-***H*** proton in the 3,4-dimethoxyphenyl ring appears as a doublet of doublets due to splittings by the phosphorous ($^3J_{PH}$= 12.6-14.4 Hz for the ligands and $^3J_{PH}$= 14.2-15.1 Hz for the complexes) and also by C_5-***H*** proton ($^3J_{HH}$= 8.2-8.4 Hz for the ligands and $^3J_{HH}$= 7.8-8.4 Hz for the complexes). Splittings by the other aromatic proton are not observable. The C_2-***H*** proton gives rise to a doublet as it is split by phosphorous ($^3J_{PH}$= 13.8-14.7 Hz for the ligands and $^3J_{PH}$= 15.1-15.3 Hz for the complexes). Here again, splittings by distant aromatic protons are below the observable limit. C_5-***H*** proton displays a four-bond coupling to phosphorus ($^4J_{PH}$= 3.6-3.8 Hz for ligands and $^4J_{PH}$= 3.3-4.2 Hz for complexes); therefore this proton also appears as a doublet of doublets. The chemical shifts of the methoxy protons are virtually the same (δ=~3.6-4.0 ppm in all compounds).

The chemical shifts of the P-O-C_9-***H*** protons in the ligands tend to move to lower fields in the spectra of the corresponding nickel complexes. These protons appear very close to the aromatic ring O-C***H***$_3$ protons on the spectra of the ligands; but more distant on those of the complexes because the aromatic ring O-C***H***$_3$ protons are less effected by the complexation. The ***H***-C10-***H*** protons on the ligand $[NH_4][S_2P(R^x)(OR6)]$ are typically diastereotopic and remain the same on the spectrum of the corresponding nickel complex.

^{1}H-NMR spectra of Part Ia [NH_4][$S_2P(R^x)(ORn)$] and [$Ni(S_2P(R^x)(ORn))_2$] compounds.

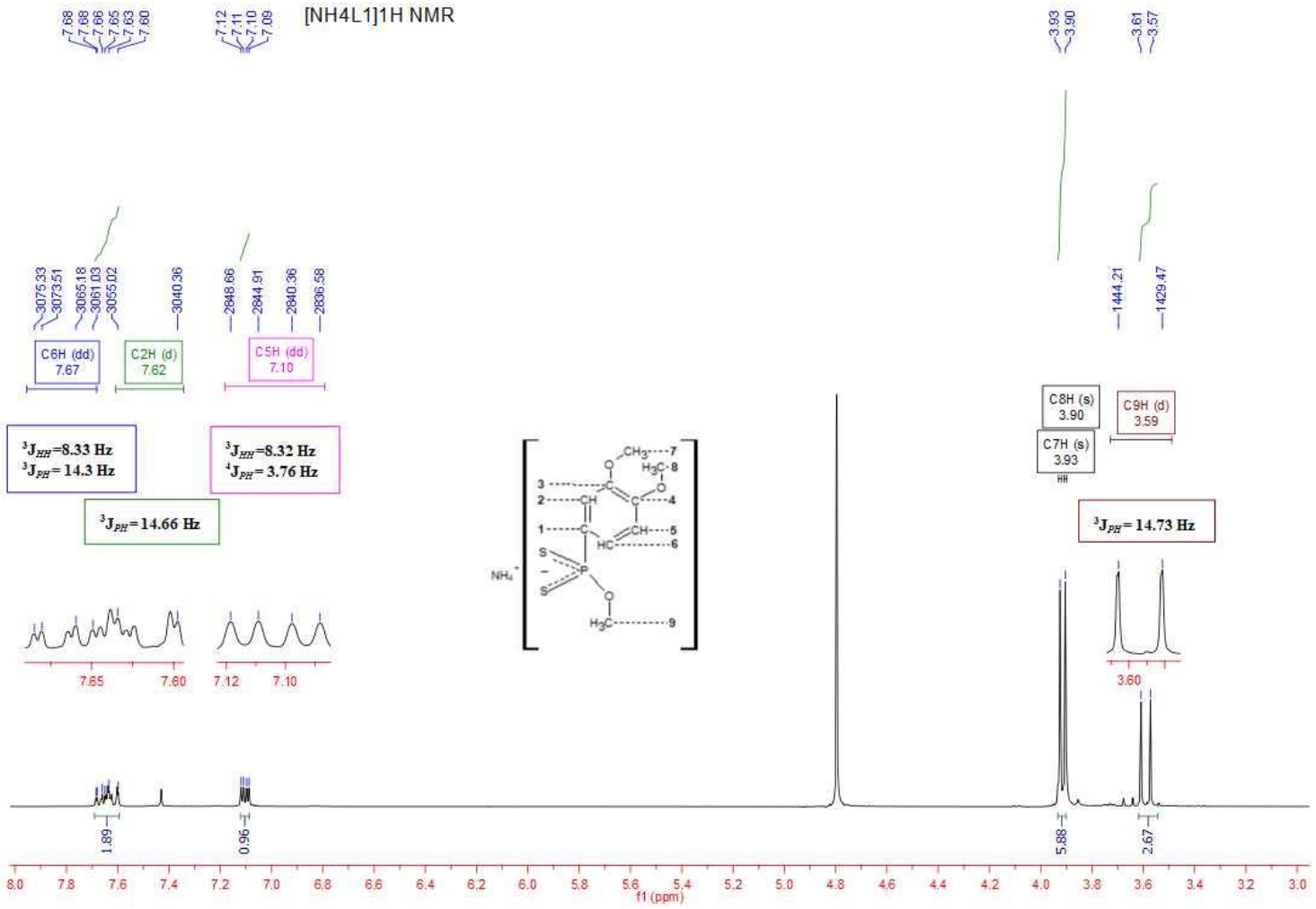


Figure 5.69. [NH_4][$S_2P(R^x)(OR1)$] ^{1}H-NMR spectrum.

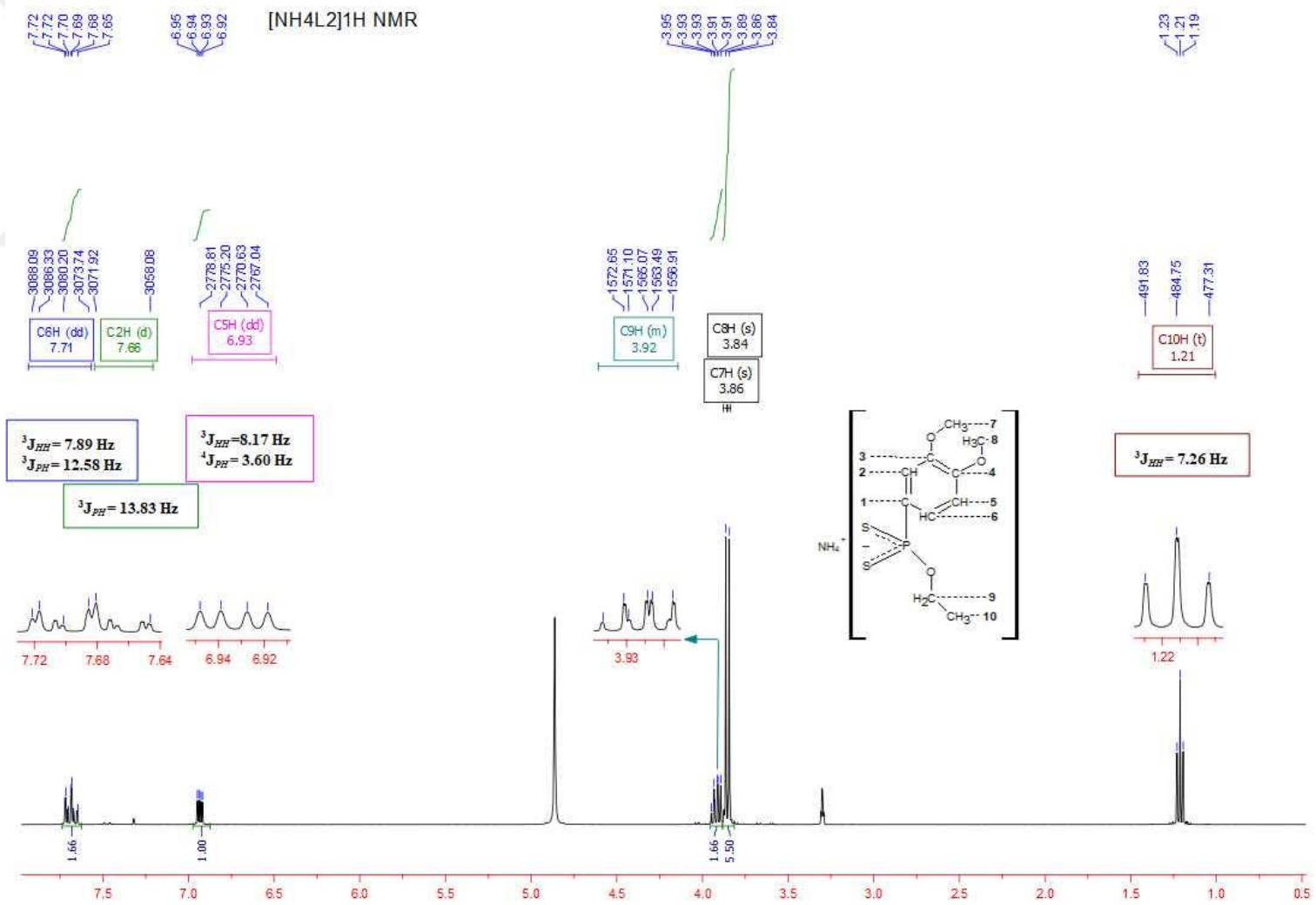


Figure 5.70. $[NH_4][S_2P(R^x)(OR2)]$ ^{1}H-NMR spectrum.

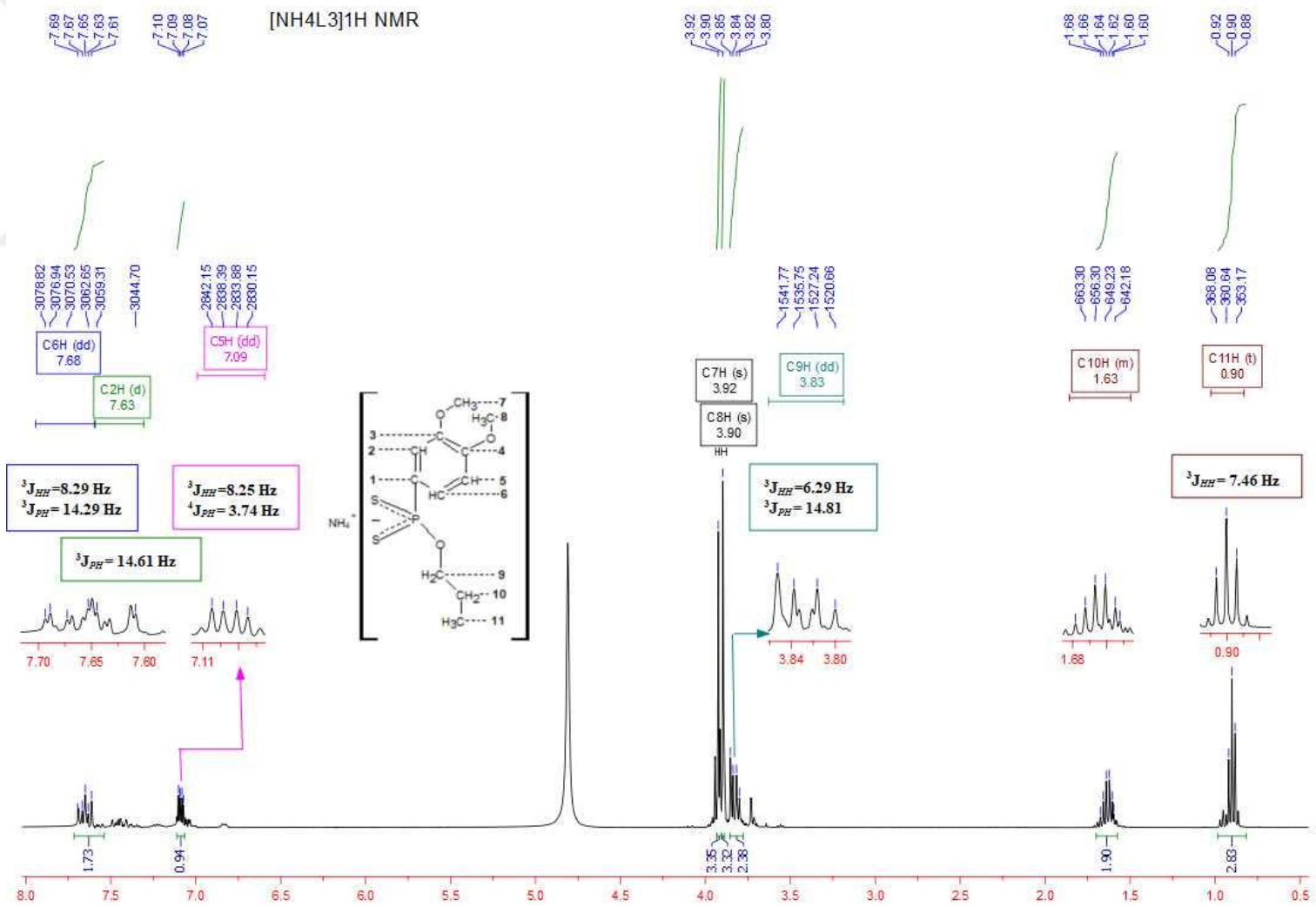


Figure 5.71. $[NH_4][S_2P(R^x)(OR3)]$ ^{1}H-NMR spectrum.

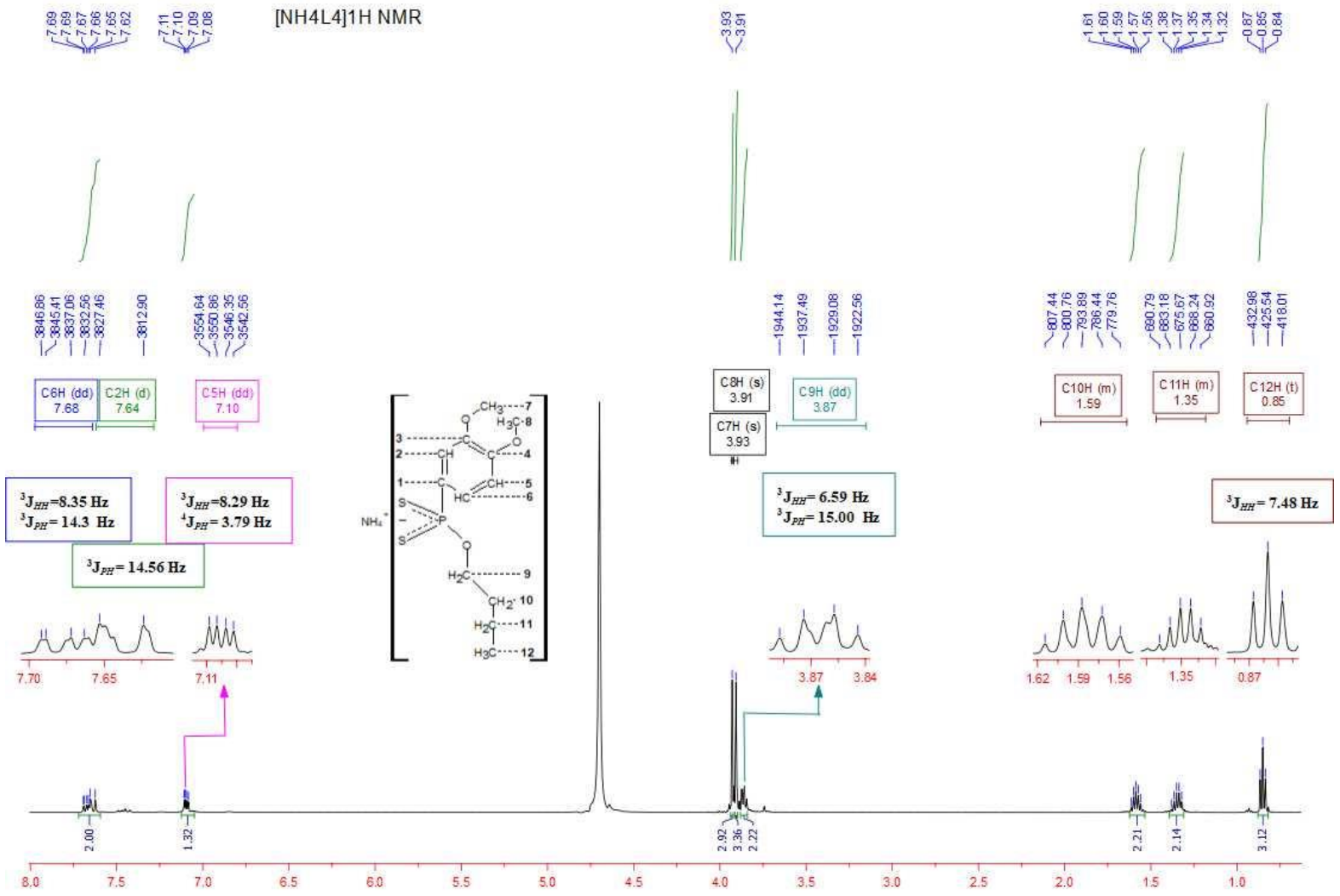


Figure 5.72. $[NH_4][S_2P(R^x)(OR4)]$ ^{1}H-NMR spectrum.

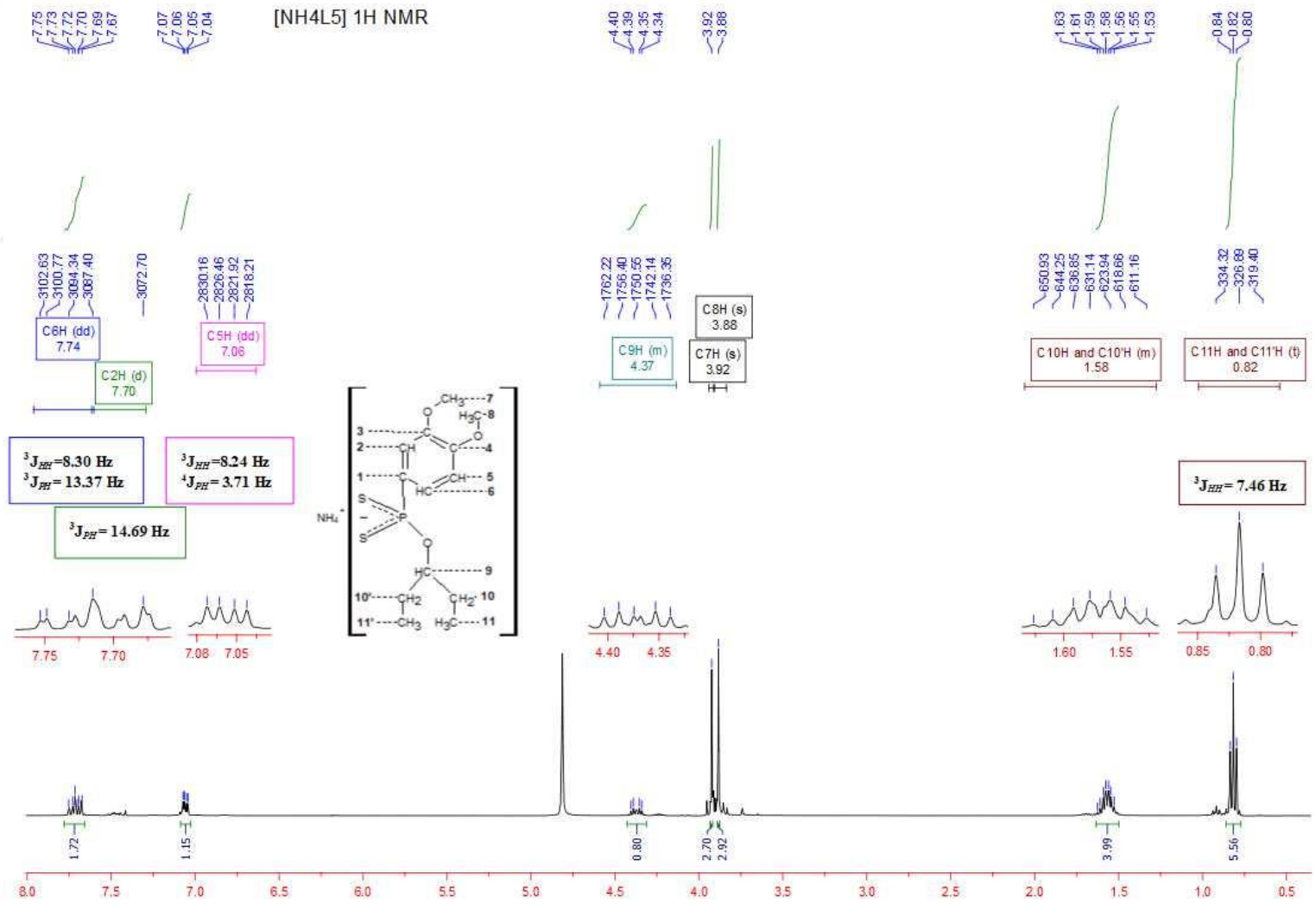


Figure 5.73. $[NH_4][S_2P(R^x)(OR5)]$ ^{1}H-NMR spectrum.

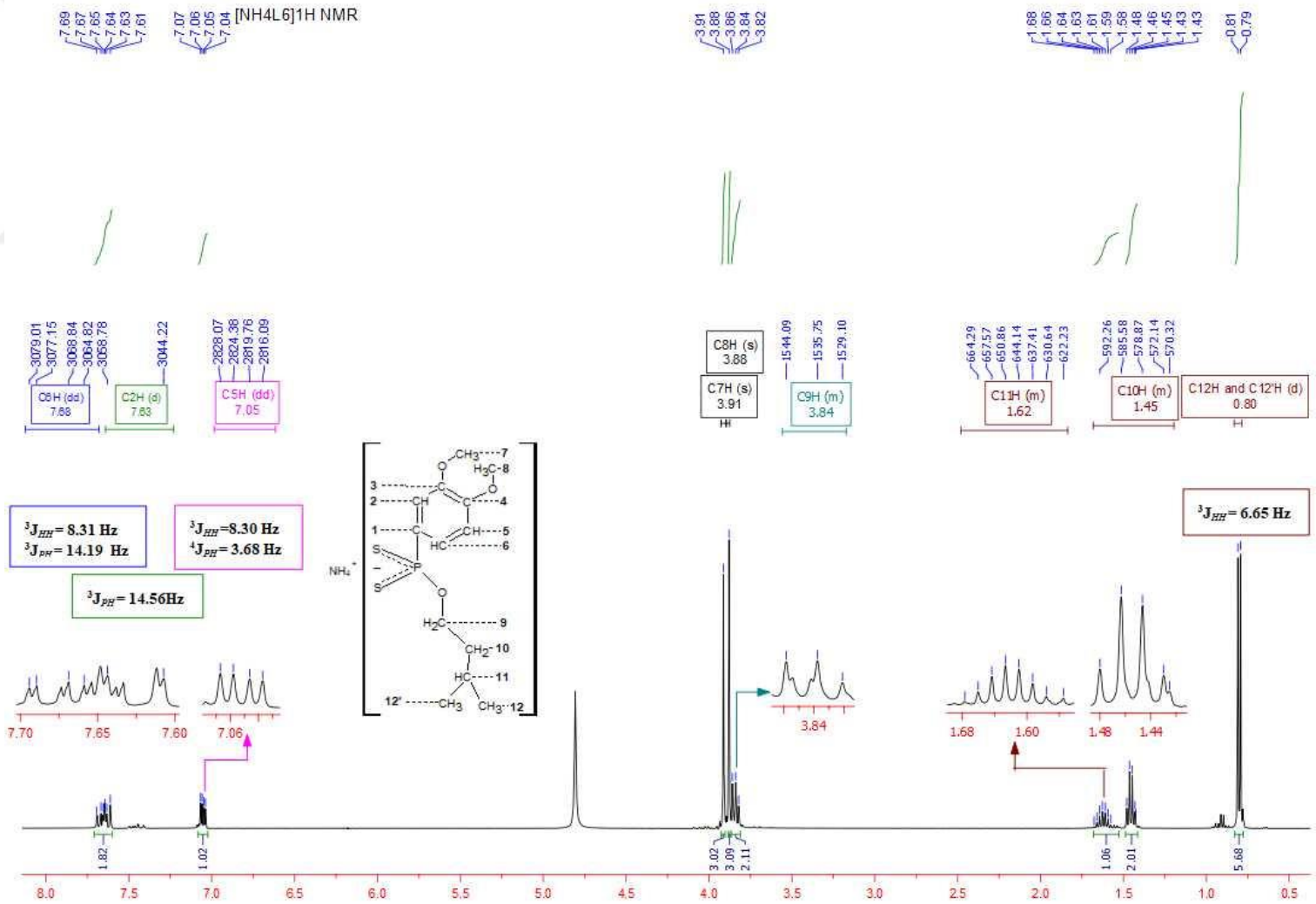


Figure 5.74. $[NH_4][S_2P(R^x)(OR6)]$ ^{1}H-NMR spectrum.

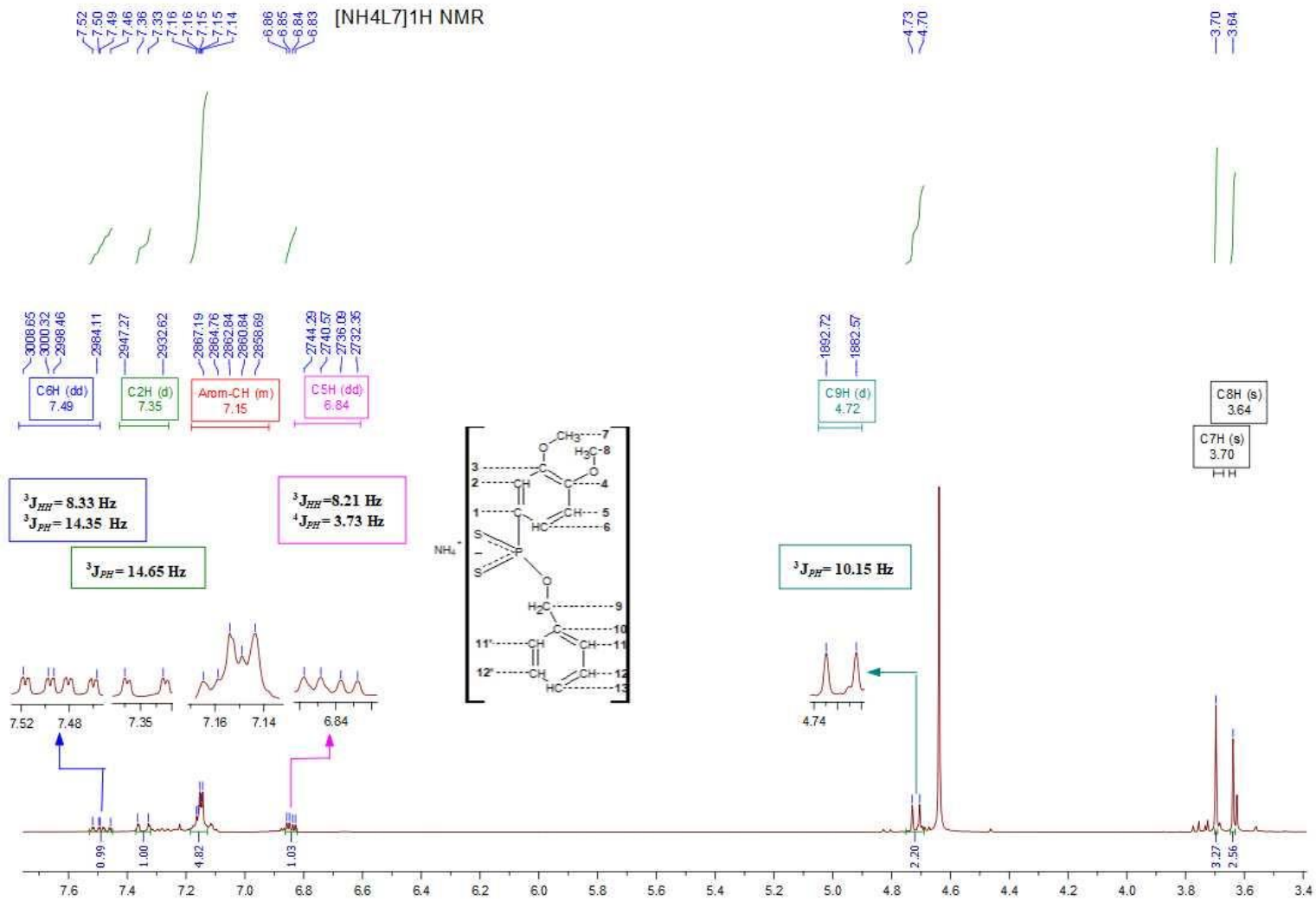


Figure 5.75. $[NH_4][S_2P(R^x)(OR7)]$ ^{1}H-NMR spectrum.

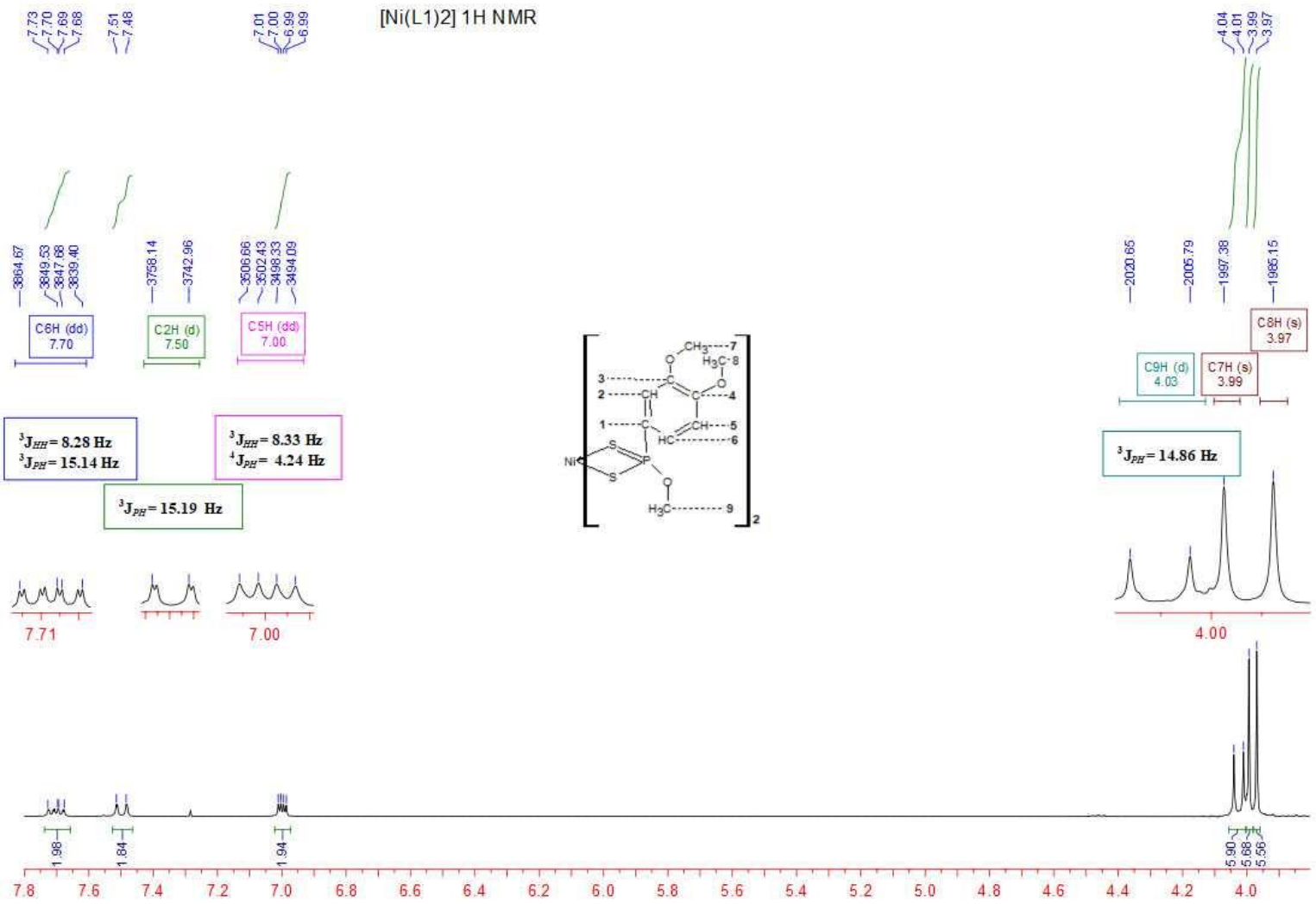


Figure 5.76. $[Ni(S_2P(R^x)(OR1))_2]$ ^{1}H-NMR spectrum.

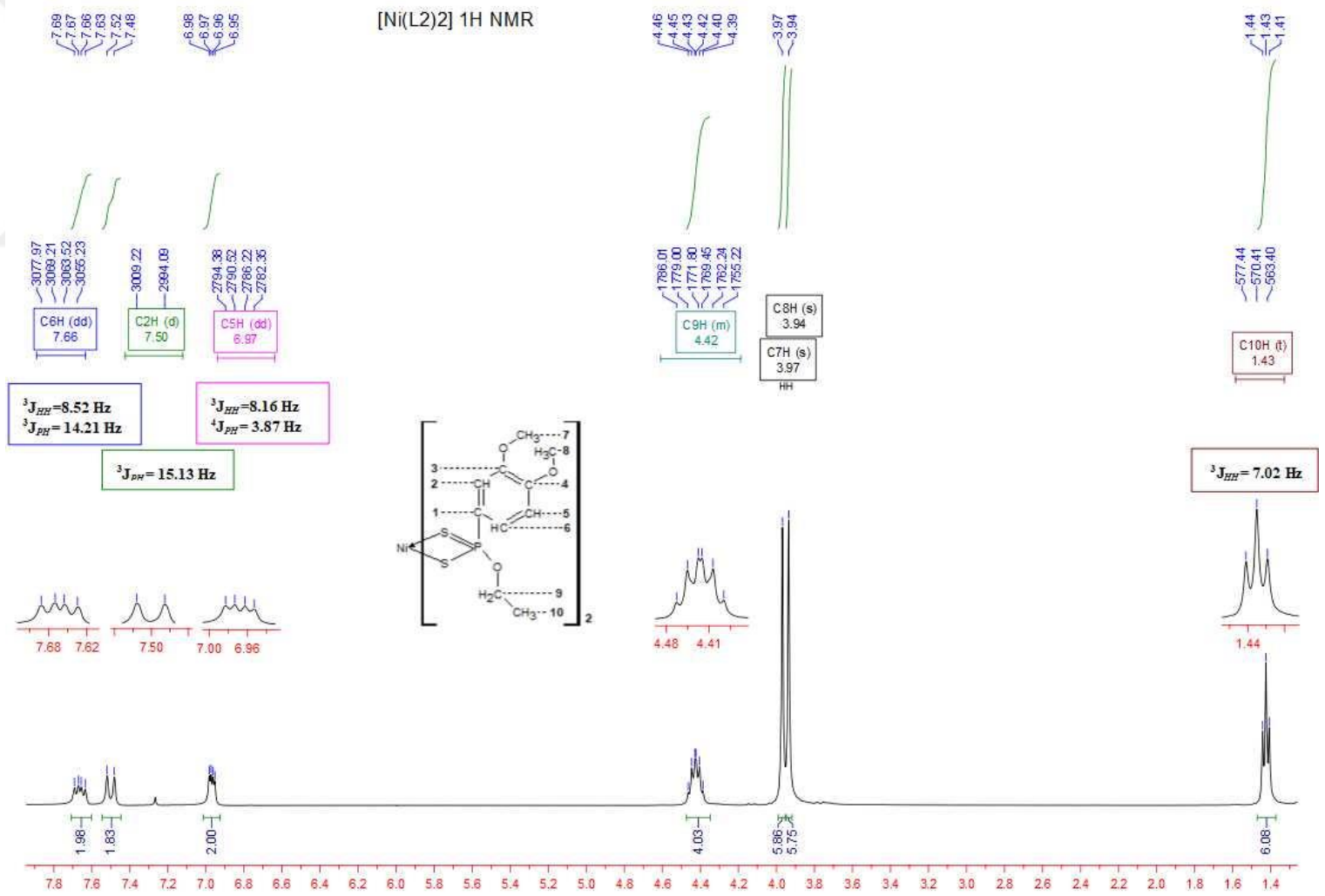


Figure 5.77. $[Ni(S_2P(R^x)(OR2))_2]$ ^{1}H-NMR spectrum.

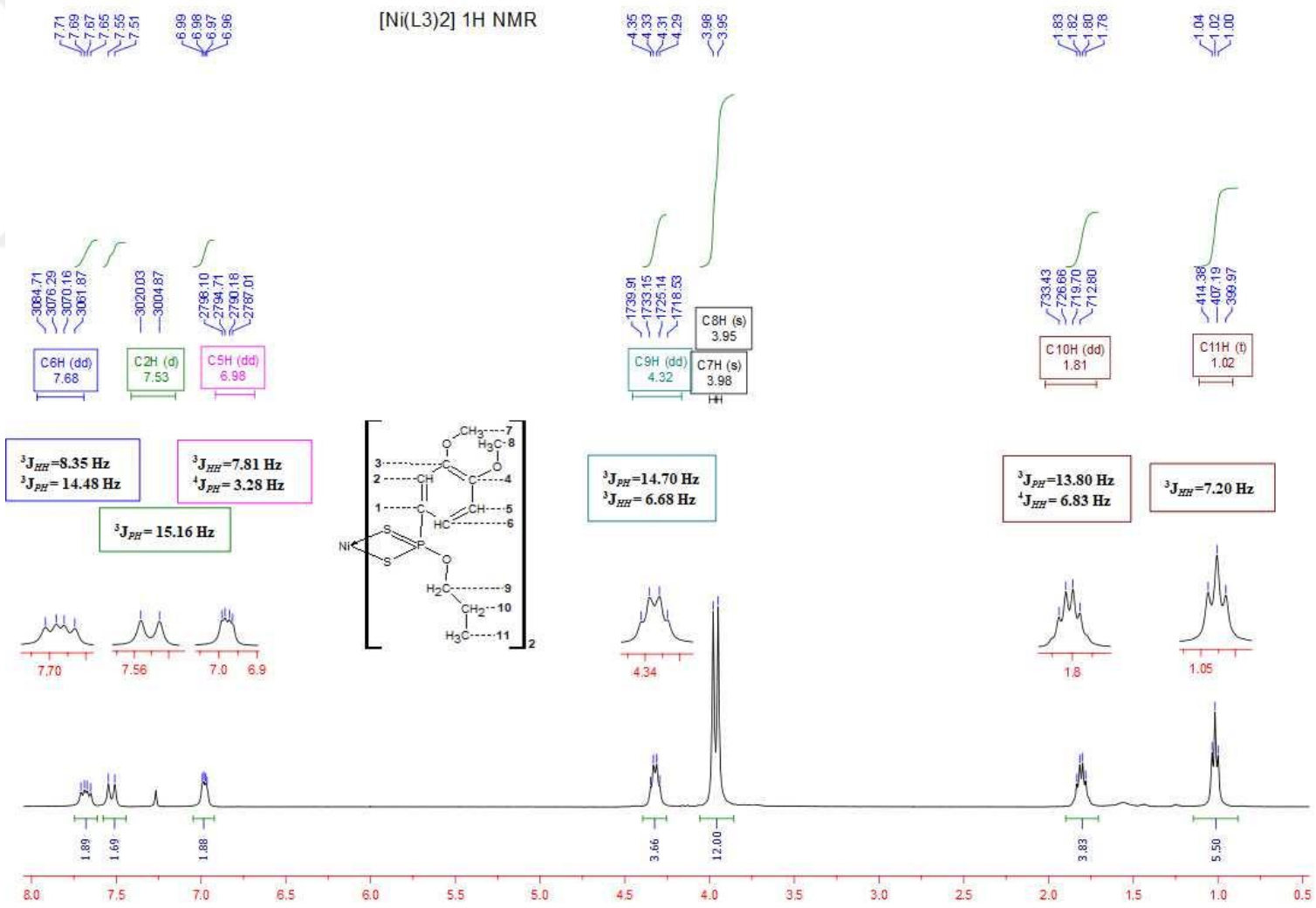


Figure 5.78. $[Ni(S_2P(R^x)(OR3))_2]$ ^{1}H-NMR spectrum.

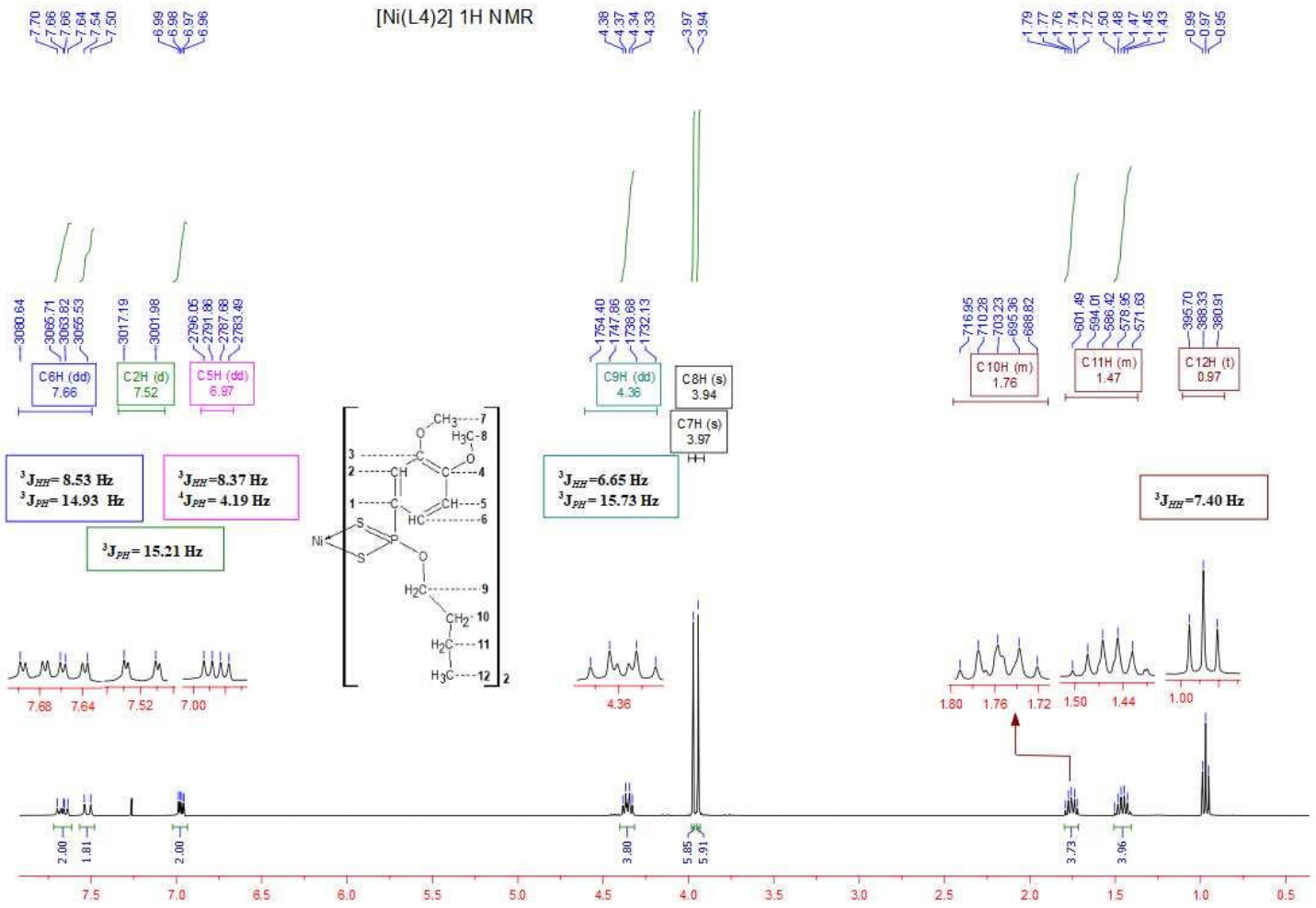


Figure 5.79. [Ni($S_2P(R^x)(OR4)$)$_2$] ^{1}H-NMR spectrum.

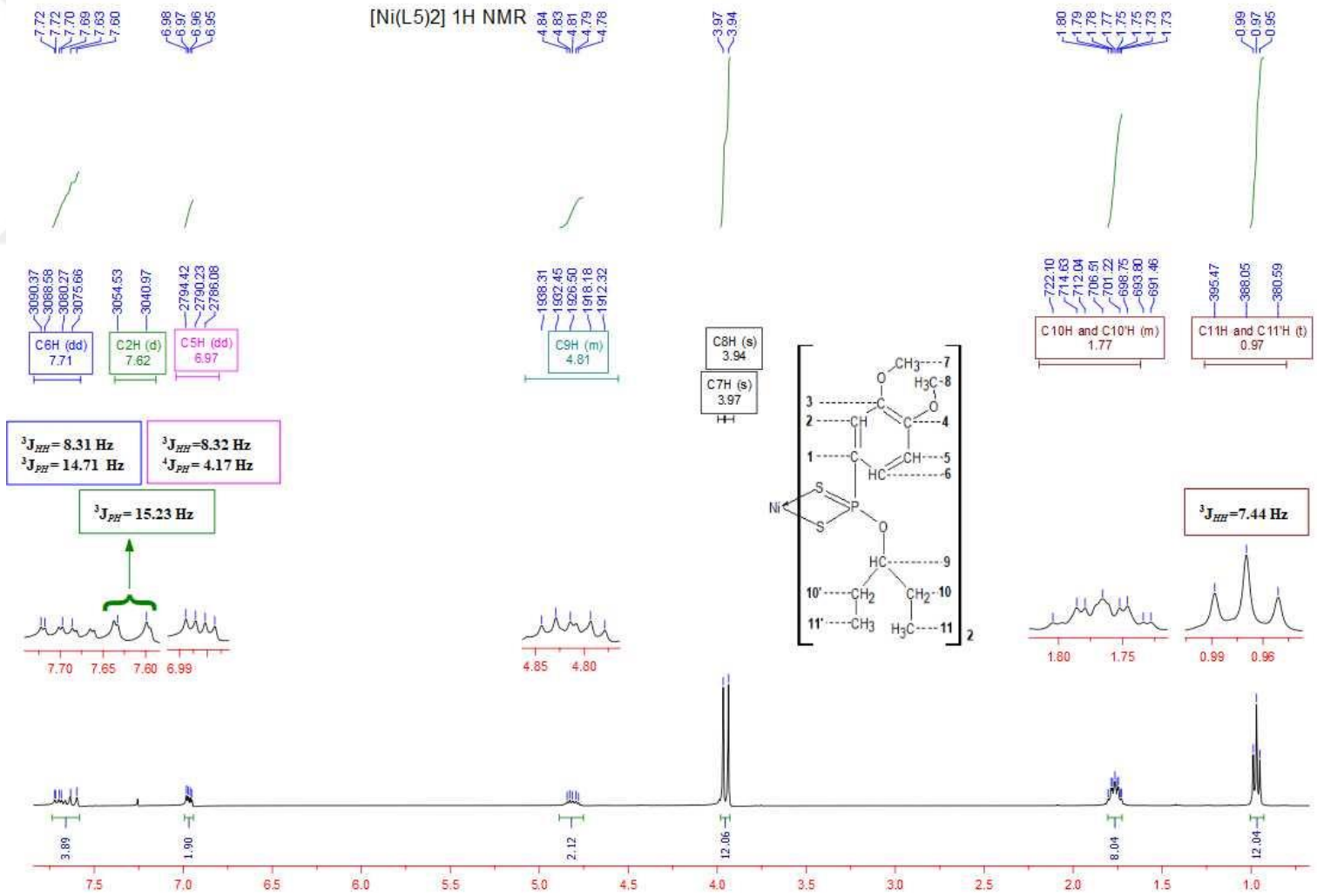


Figure 5.80. $[Ni(S_2P(R^x)(OR5))_2]$ ^{1}H-NMR spectrum.

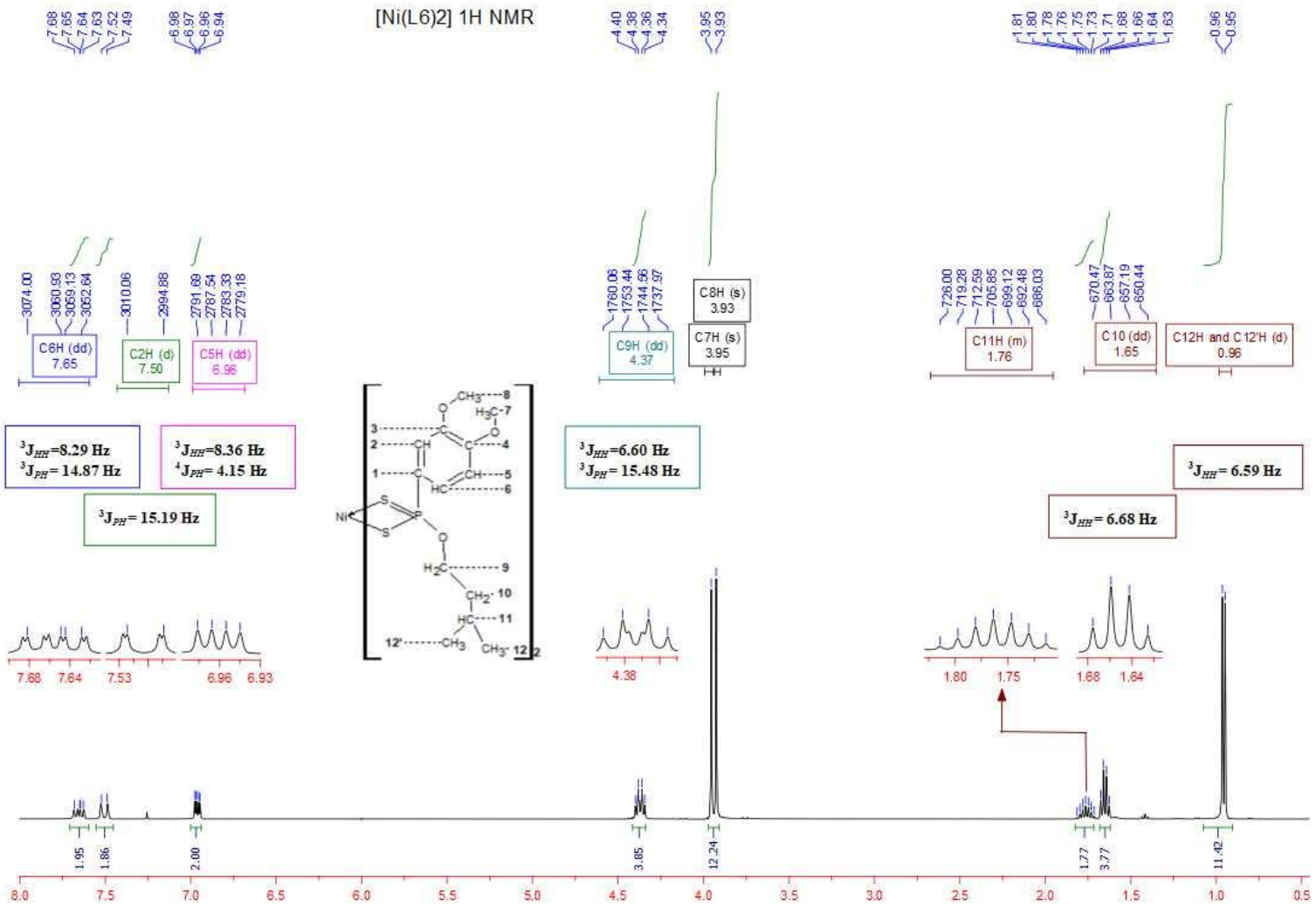


Figure 5.81. $[Ni(S_2P(R^x)(OR6))_2]$ ^{1}H-NMR spectrum.

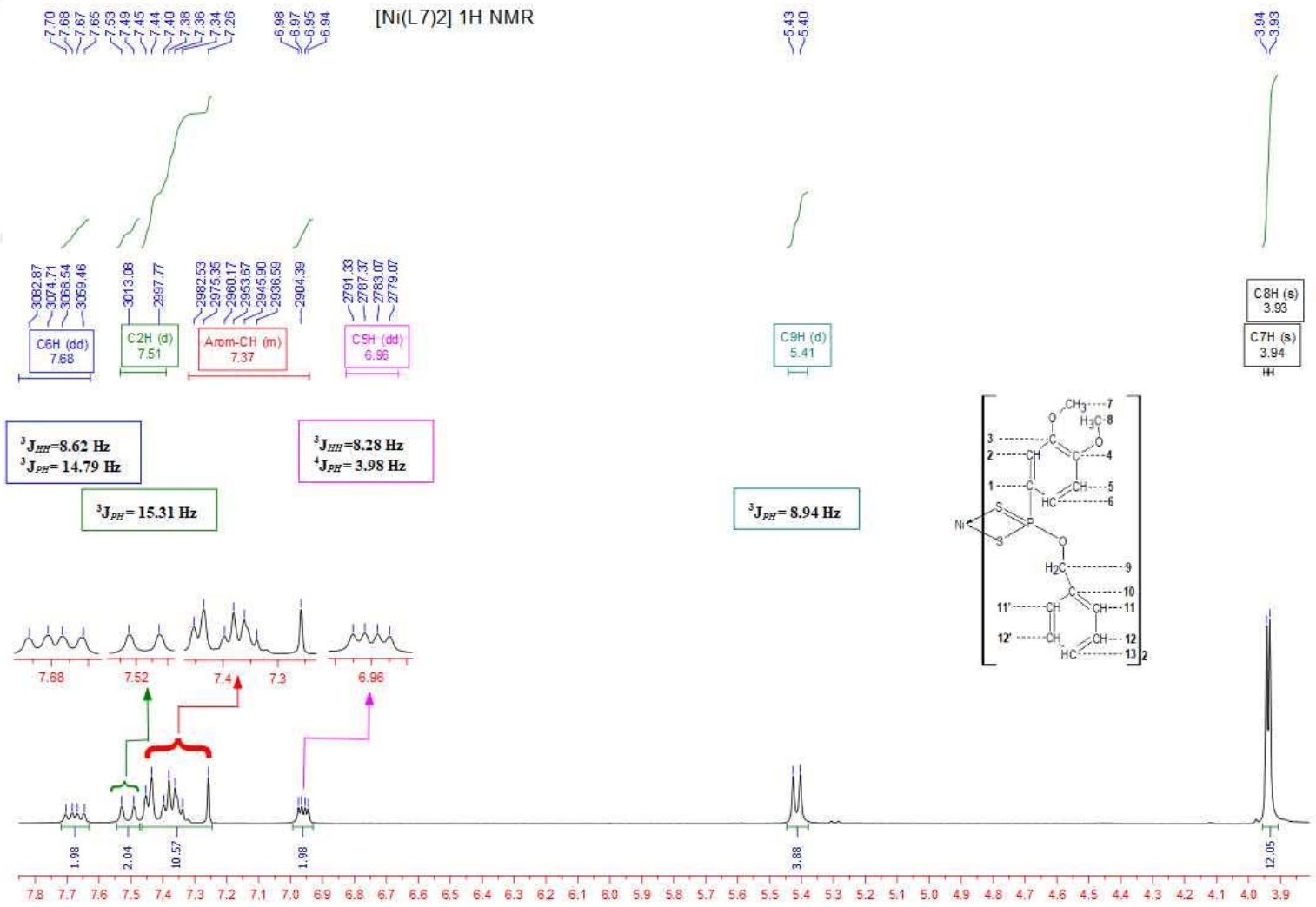


Figure 5.82. $[Ni(S_2P(R^x)(OR7))_2]$ ^{1}H-NMR spectrum.

5.1.7.3. Comment of ^{1}H-NMR Spectra Spectra of Part Ib' compounds

The numbering scheme of the carbon atoms is depicted in Figure 5.83 and ^{1}H-NMR spectra are given in Figure 5.84-5.93. The NMR data of the compounds are presented in Tables 5.6.

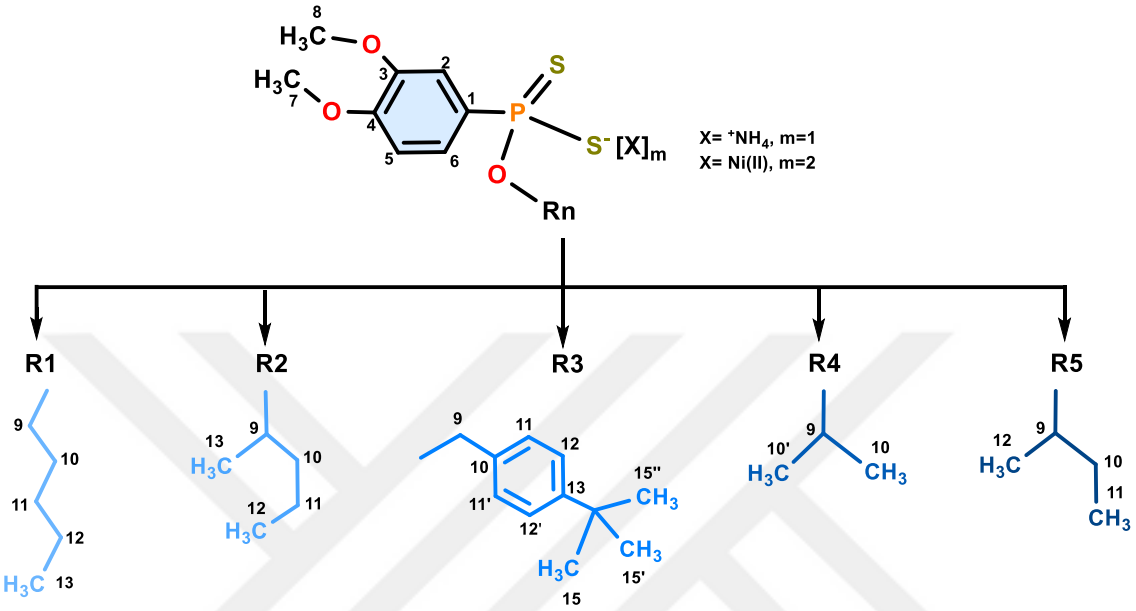


Figure. 5.83. The numbering scheme for compounds Part Ib.

The splitting pattern of the aromatic C_6-***H*** proton (doublet of doublets) indicates a three-bond coupling to the phosphorous atom (~ $^{3}J_{PH}$= 14 Hz for $[NH_4][S_2P(R^x)(ORn)]$ and $[Ni(S_2P(R^x)(ORn))_2]$) and *meta*- coupling to C_5-***H*** proton ($^{3}J_{HH}$= 8.3 Hz for $[NH_4][S_2P(R^x)(ORn)]$; $^{3}J_{HH}$= 8.0-8.6 Hz for the $[Ni(S_2P(R^x)(ORn))_2]$). Similarly, C_5-***H*** proton appears as a doublet of doublets with a four-bond coupling to phosphorus atom (~$^{4}J_{PH}$= 3.7 Hz for ligands; $^{4}J_{PH}$= 3.6-4.2 Hz for complexes). The coupling constants of the C_2-***H*** proton to phosphorous are $^{3}J_{PH}$= 14.0-15.3 Hz for $[NH_4][S_2P(R^x)(ORn)]$ and $[Ni(S_2P(R^x)(ORn))_2]$. The coupling between C_2-***H*** and C_5-***H*** protons is unobservable. Methoxy protons appear in the range 3.7-4.0 ppm.

As to the general trends [132], the P-O-C_9-***H*** protons' chemical shifts in the complexes are higher than those relating to their counterparts in the ligands. Methoxy protons in the *o*-dimethoxyphenyl moiety are very close to each other in the ligand spectra, but they are quite far away compared to those of the complexes.

Table 5.6. ^{1}H-NMR data of $[NH_4][S_2P(R^x)(ORn)]$ (D_2O) and $[Ni(S_2P(R^x)(ORn))_2]$ for Part Ib ($CDCl_3$) (δ in ppm, *J* in Hz, s: *singlet*, d: *doublet*, dd: *doublet of doublets*, t: *triplet*, and m: *multiplet*).

$[NH_4][S_2P(R^x)(OR1)]$	$[NH_4][S_2P(R^x)(OR2)]$	$[NH_4][S_2P(R^x)(OR3)]$	$[NH_4][S_2P(R^x)(OR4)]$	$[NH_4][S_2P(R^x)(OR5)]$		$[Ni(S_2P(R^x)(OR1))_2]$	$[Ni(S_2P(R^x)(OR2))_2]$	$[Ni(S_2P(R^x)(OR3))_2]$	$[Ni(S_2P(R^x)(OR4))_2]$	$[Ni(S_2P(R^x)(OR4))_2]$
7.6 (d, 1H), $^3J_{PH}$= 14.6	7.7(d, 1H), $^3J_{PH}$ =14.7	7.6 (d, 1H), $^3J_{PH}$= 14.8	7.4 (d, 1H), $^3J_{PH}$=14.0	7.5 (d, 1H), $^3J_{PH}$= 14.7	C_2-H	7.5 (d, 2H), $^3J_{PH}$= 15.1	7.6 (d, 2H), $^3J_{PH}$= 14.7	7.6 (d, 2H), $^3J_{PH}$= 15.1	7.4 (d, 2H), $^3J_{PH}$= 13.8	7.6 (d, 2H), $^3J_{PH}$= 15.3
7.1 (dd, 1H) $^4J_{PH}$= 3.7, $^3J_{HH}$= 8.3	7.1 (dd, 1H) $^4J_{PH}$= 3.7, $^3J_{HH}$= 8.3	6.8 (dd, 1H) $^4J_{PH}$= 3.7, $^3J_{HH}$= 8.5	7.1 (dd, 1H) $^4J_{PH}$= 3.7, $^3J_{HH}$= 8.2	6.9 (dd, 1H) $^4J_{PH}$= 3.8, $^3J_{HH}$= 8.1	C_5-H	7.0 (dd, 2H) $^4J_{PH}$= 3.9, $^3J_{HH}$= 8.1	7.0 (dd, 2H) $^4J_{PH}$= 3.8, $^3J_{HH}$= 8.0	7.0 (dd, 2H) $^4J_{PH}$= 3.6, $^3J_{HH}$= 7.9	7.1 (dd, 2H) $^4J_{PH}$= 3.7, $^3J_{HH}$= 8.2	7.0 (dd, 2H) $^4J_{PH}$= 4.2, $^3J_{HH}$= 8.4
7.7 (dd,1H); $^3J_{PH}$= 14.2, $^3J_{HH}$= 8.3	7.7 (dd, 1H) $^3J_{PH}$= 14.3, $^3J_{HH}$= 8.3	7.7 (dd, 1H) $^3J_{PH}$= 14.1, $^3J_{HH}$=8.3	7.5 (dd, 1H) $^3J_{PH}$= 13.3, $^3J_{HH}$= 8.3	7.5 (dd, 1H) $^3J_{PH}$= 14.2, $^3J_{HH}$= 8.3	C_6-H	7.7 (dd, 2H) $^3J_{PH}$= 14.3, $^3J_{HH}$= 8.2	7.7 (dd, 2H) $^3J_{PH}$= 13.7, $^3J_{HH}$= 8.6	7.7 (dd, 2H) $^3J_{PH}$= 14.3, $^3J_{HH}$=8.3	7.5 (dd, 2H); $^3J_{PH}$= 14.9, $^3J_{HH}$= 8.0	7.7 (dd, 2H) $^3J_{PH}$= 14.8 $^3J_{HH}$= 8.3
3.9 (s, 3H)	3.9 (s, 3H)	3.7 (s, 3H)	3.9 (s, 3H)	3.8 (s, 3H)	C_7-H	4.0 (s, 6H)	4.0 (s, 6H)	4.0 (s, 6H)	3.9 (s, 6H)	4.0 (s, 6H)
3.9 (s, 3H)	3.9 (s, 3H)	3.7 (s, 3H)	3.9 (s, 3H)	3.7 (s, 3H)	C_8-H	3.9 (s, 6H)	4.0 (s, 6H)	4.0 (s, 6H)	3.9 (s, 6H)	3.9 (s, 6H)
3.8 (dd, 2H) $^3J_{PH}$= 15.2, $^3J_{HH}$= 6.6	4.5 (dd, 1H) $^3J_{PH}$= 14.1, $^3J_{HH}$= 6.3	4.8 (s, 2H)	4.5 (m, H)	4.3 (m, H)	C_9-H	4.3 (dd, 4H) $^3J_{PH}$= 15.4, $^3J_{HH}$= 6.7	5.1 (m, 2H)	5.4 (d, 2H), $^3J_{PH}$= 8.7	4.5 (m, 2H)	5.0 (m, 2H)
1.6 (m, 2H)	1.5 (m, 2H)	-	1.2 (dd, 6H) $^4J_{PH}$= 6.2, $^3J_{HH}$= 11.6	1.4 (m, 2H)	C_{10}-H	1.8 (m, 4H)	1.7 (m, 4H)	-	1.2 (dd, 12H) $^4J_{PH}$= 6.2 $^3J_{HH}$= 11.6	1.7 (m, 4H)
1.2 (m, 4H)	1.3 (m, 2H)	7.1 (d, 2H), $^3J_{HH}$= 8.5 (Arom-C11-H)	-	0.7 (t, 3H), $^3J_{HH}$= 7.5	C_{11}-H	1.4 (s, 8H)	1.5 (s, 4H)	7.4 (m, 8H) (Arom-C11,12-H)	-	1.0 (t, 6H), $^3J_{HH}$= 7.4
-	1.2 (d, 3H), $^3J_{HH}$= 6.3	7.0 (d, 2H), $^3J_{HH}$= 8.4 (Arom-C12-H)	-	1.0 (dd, 3H) $^3J_{PH}$= 2.4 ; $^3J_{HH}$= 6.3	C_{12}-H	-	1.5 (s, 6H)	-	-	1.4 (d, 6H), $^3J_{HH}$= 6.2
0.8 (t, 3H), $^3J_{HH}$= 7.1	0.8 (t, 3H), $^3J_{HH}$= 7.4	-	-	-	C_{13}-H	0.9 (t, 6H), $^3J_{HH}$= 6.6	1.0 (t, 6H), $^3J_{HH}$= 7.2	-	-	-
-	-	0.9 (s, 9H)	-	-	$C_{15,15',15''}$-H	-	-	1.4 (s, 18H)	-	-

^{1}H-NMR of Part Ib [NH_4][$S_2P(R^x)(ORn)$] and [$Ni(S_2P(R^x)(ORn))_2$] compounds.

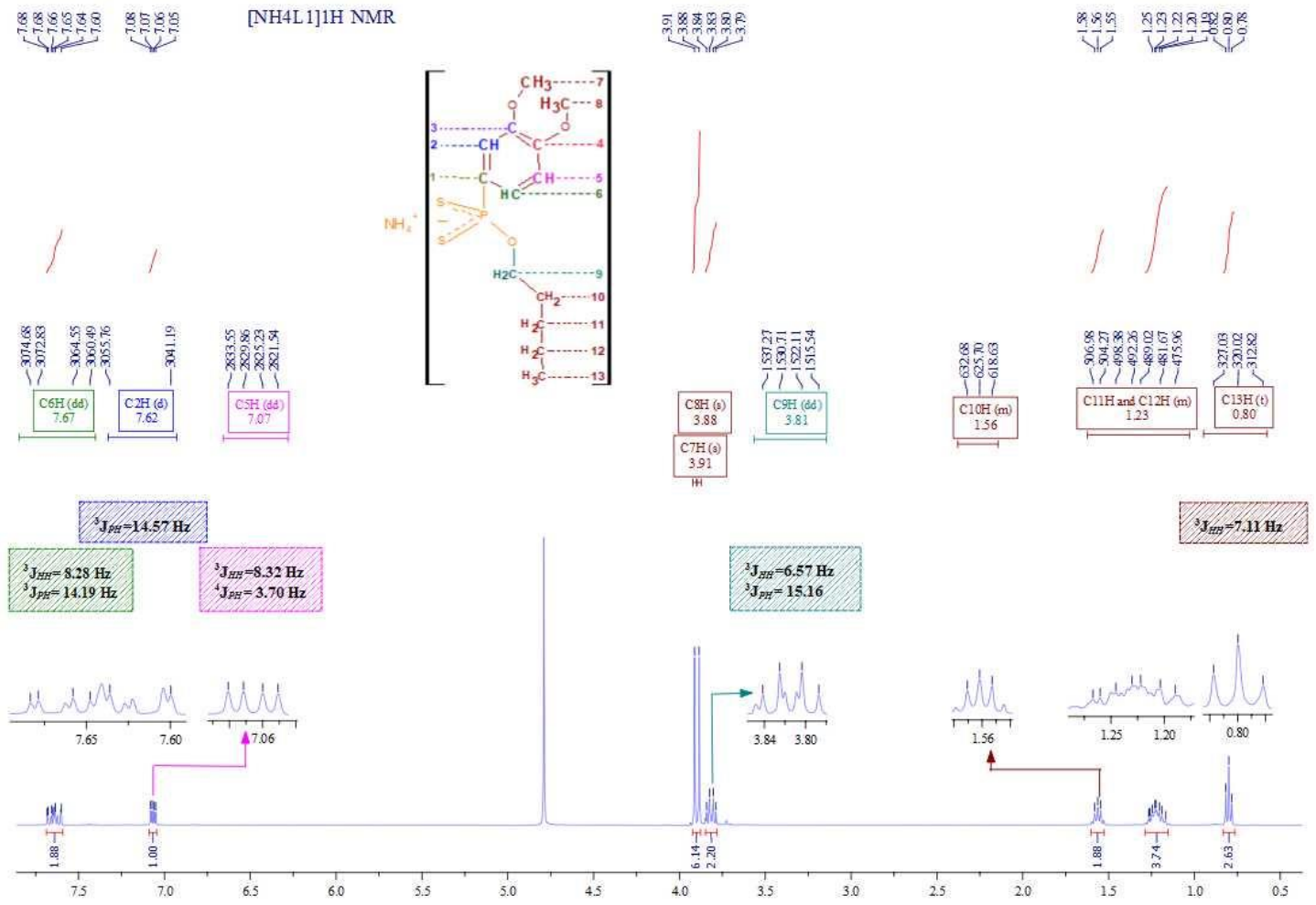


Figure 5.84. [NH_4][$S_2P(R^x)(OR1)$] ^{1}H-NMR spectrum.

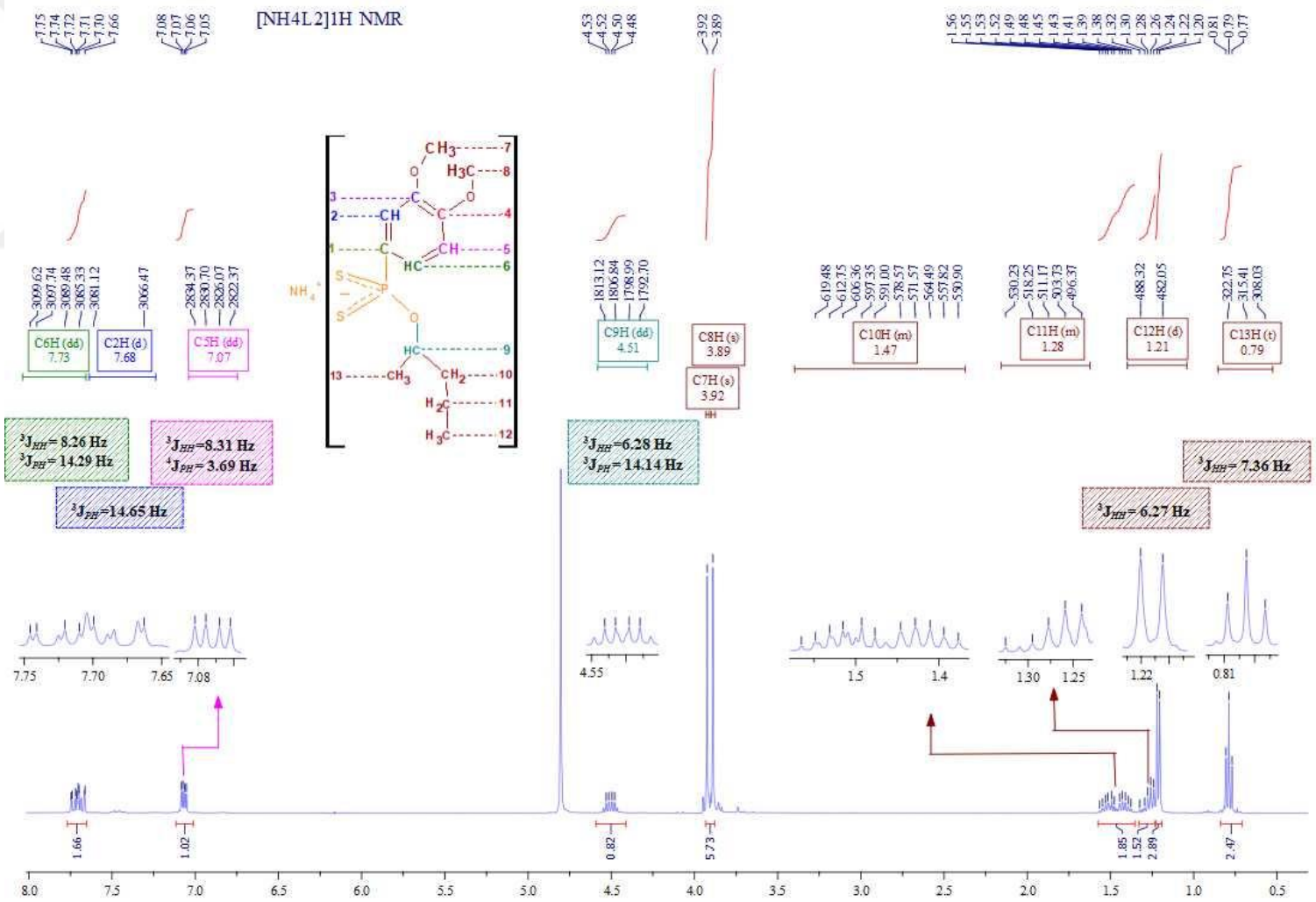


Figure 5.85. $[NH_4][S_2P(R^x)(OR2)]$ ^{1}H-NMR spectrum.

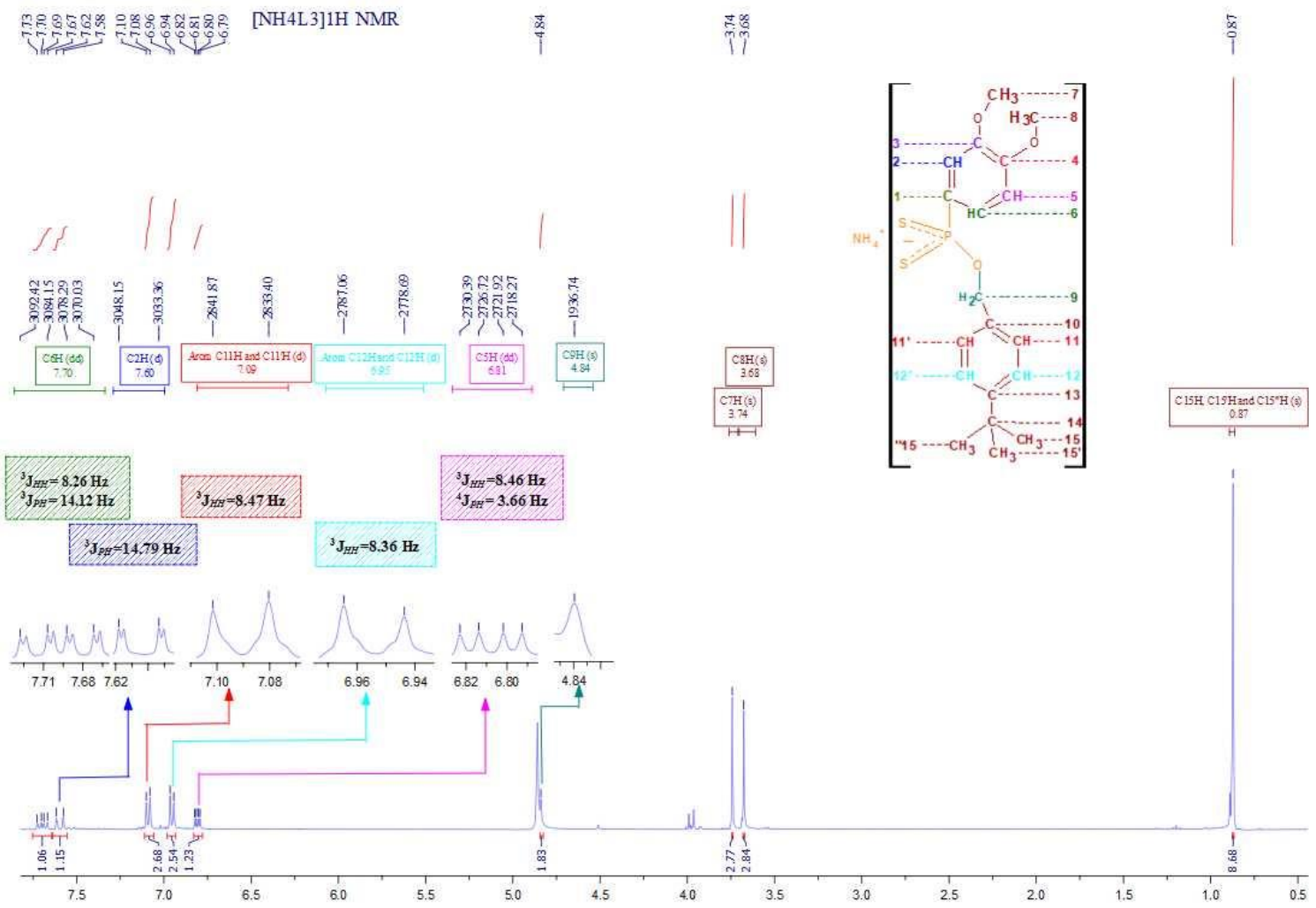


Figure 5.86. $[NH_4][S_2P(R^x)(OR3)]$ ^{1}H-NMR spectrum.

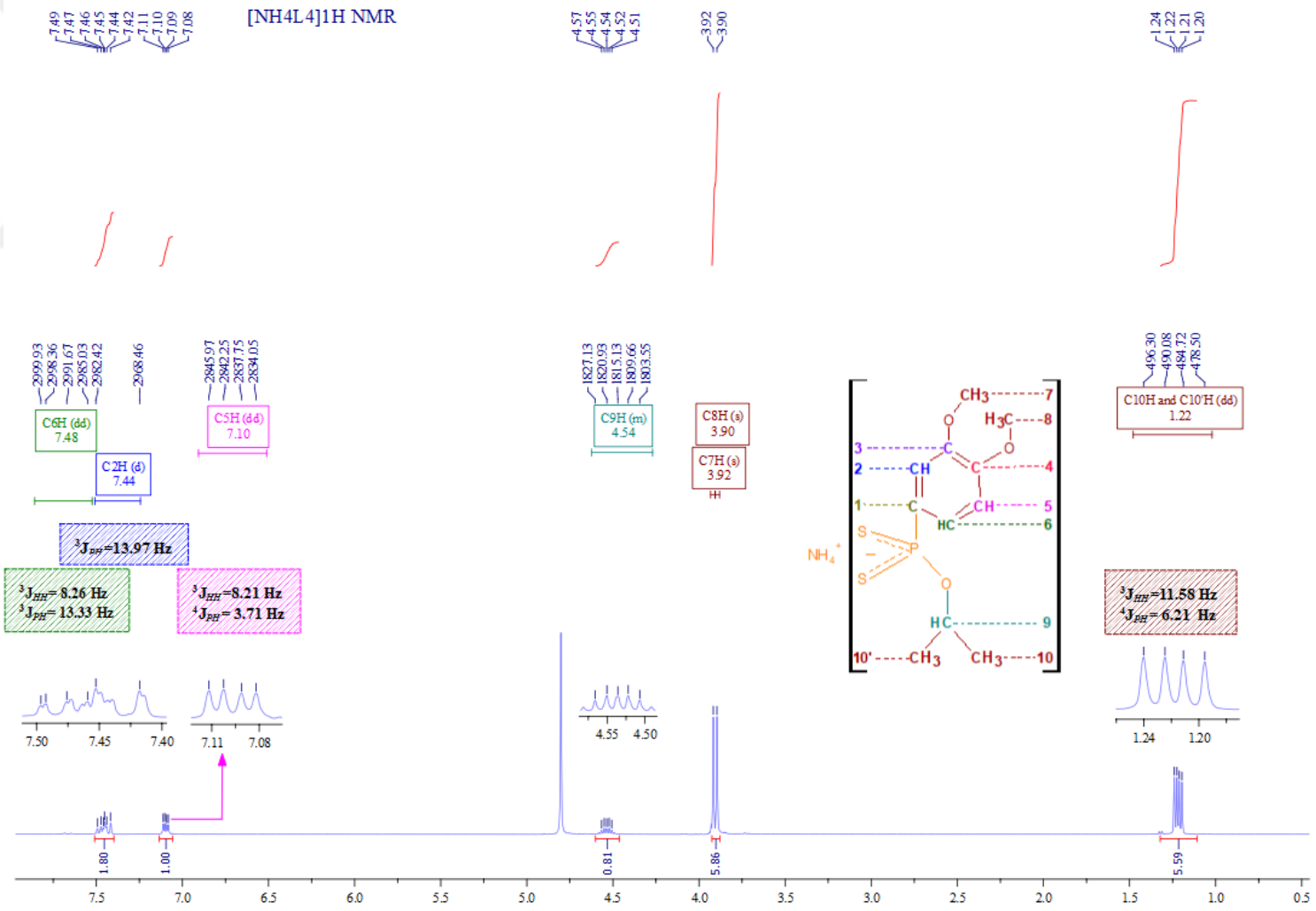


Figure 5.87. $[NH_4][S_2P(R^x)(OR4)]$ ^{1}H-NMR spectrum.

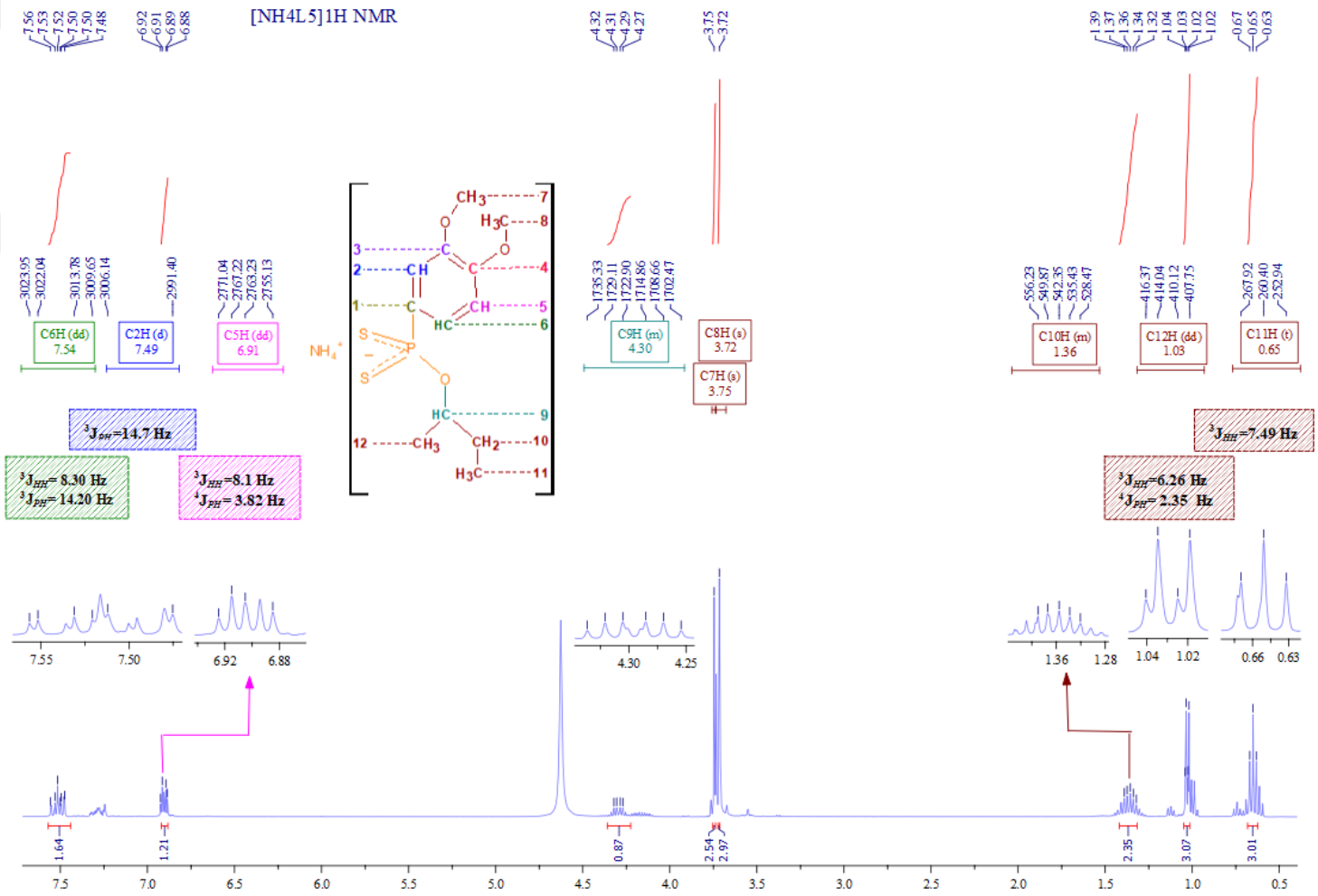


Figure 5.88. $[NH_4][S_2P(R^x)(OR5)]$ ^{1}H-NMR spectrum.

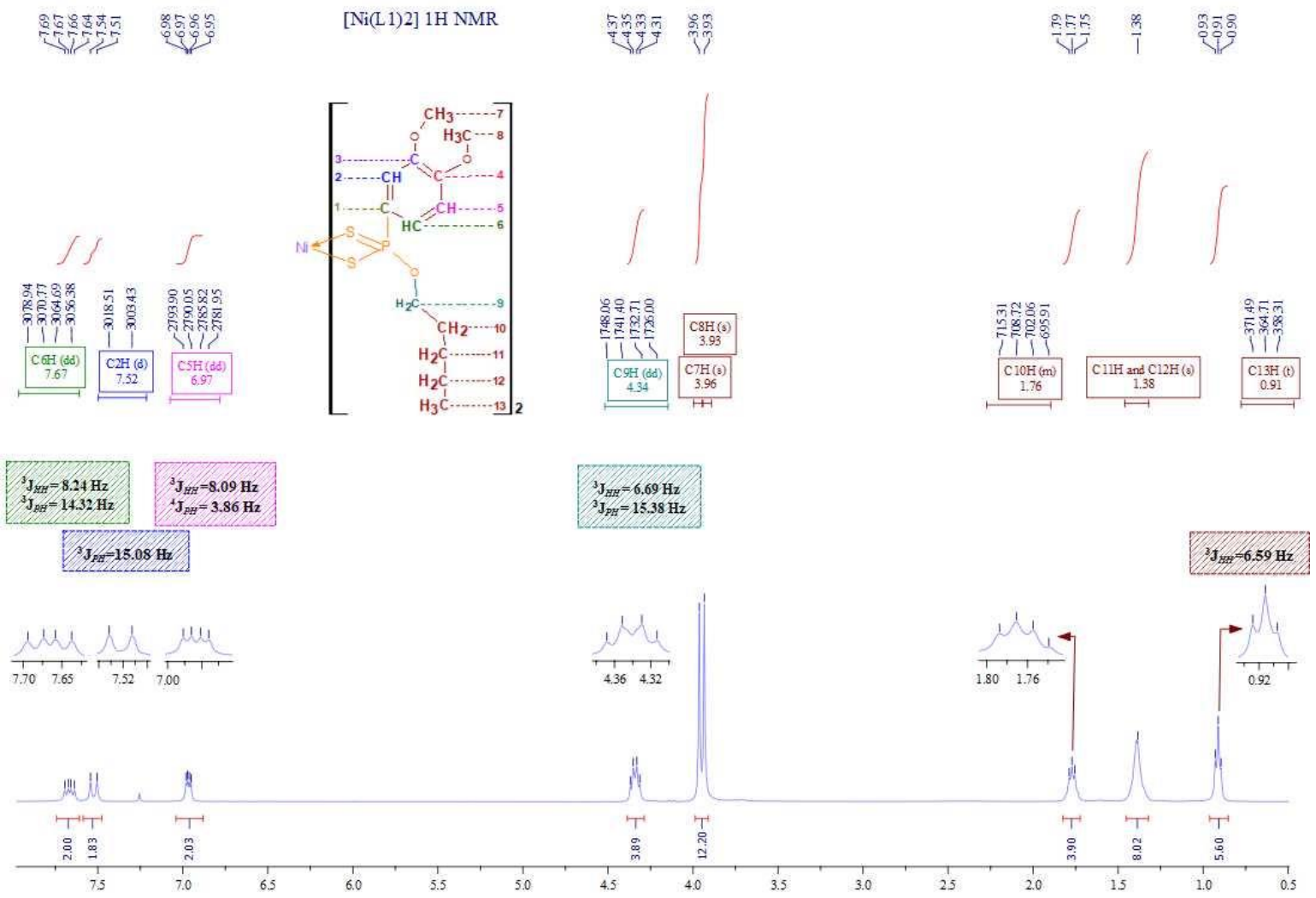


Figure 5.89. $[Ni(S_2P(R^x)(OR1))_2]$ ^{1}H-NMR spectrum.

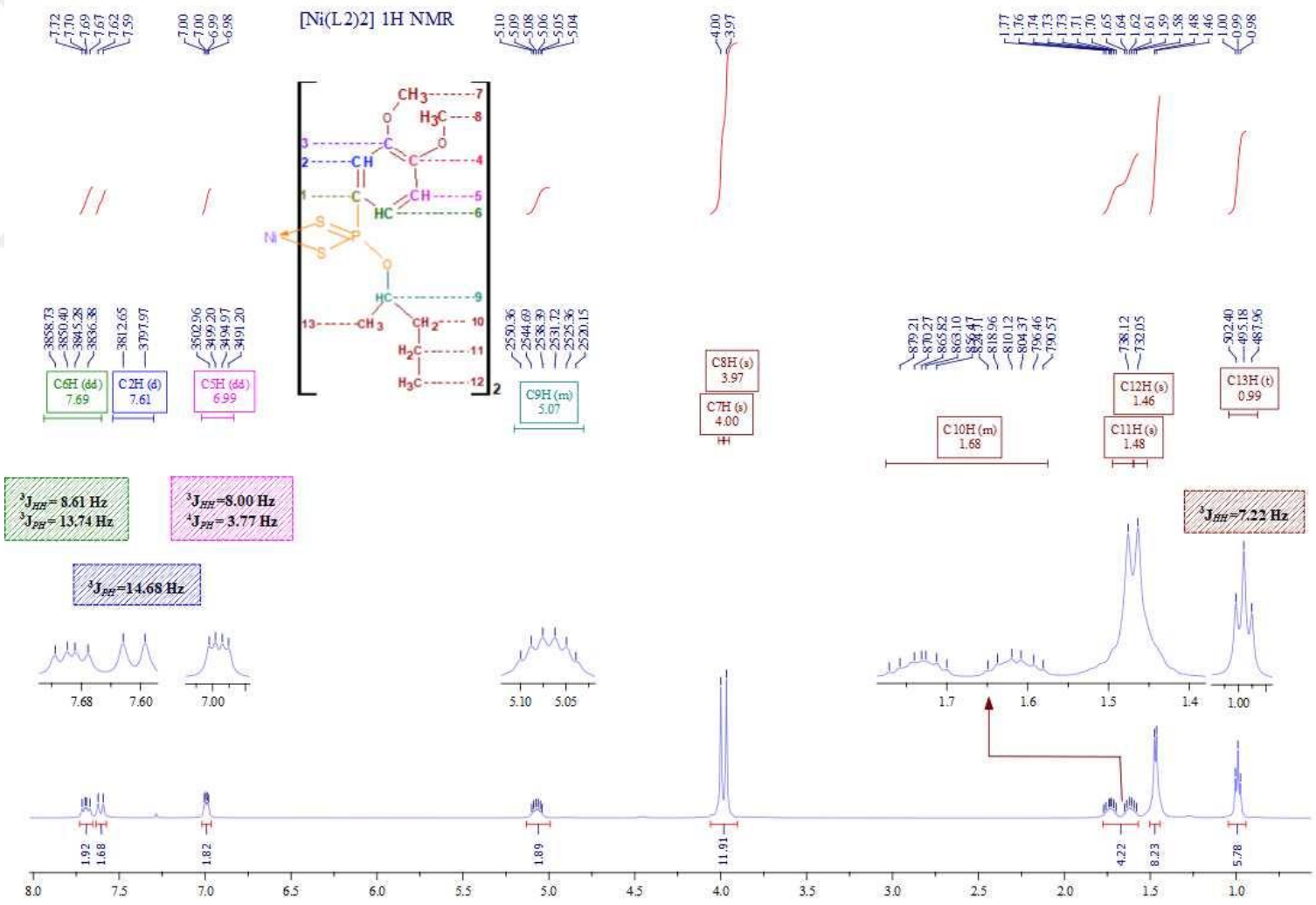


Figure 5.90. $[Ni(S_2P(R^x)(OR2))_2]$ ^{1}H-NMR spectrum.

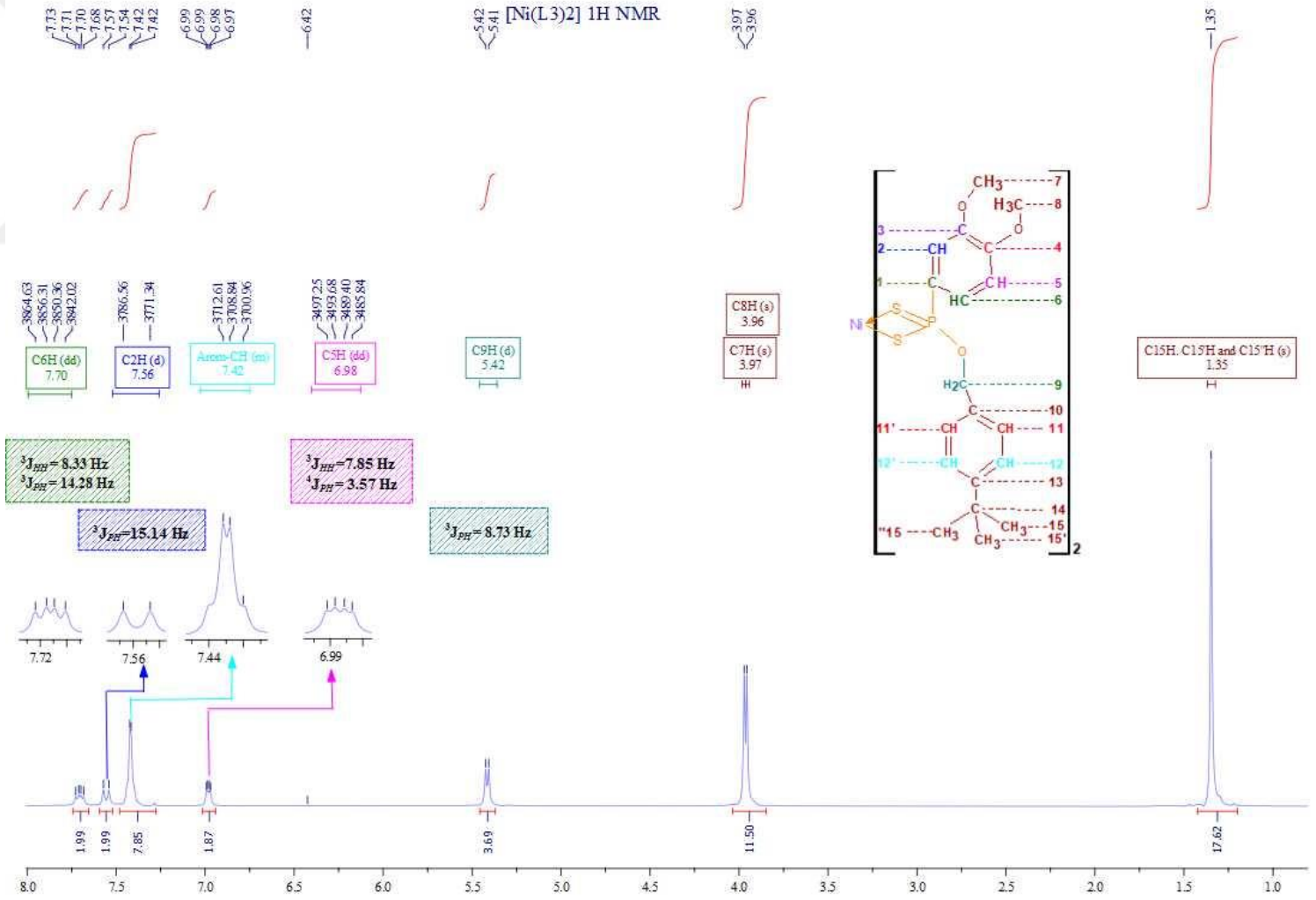


Figure 5.91. $[Ni(S_2P(R^x)(OR3))_2]$ ^{1}H-NMR spectrum.

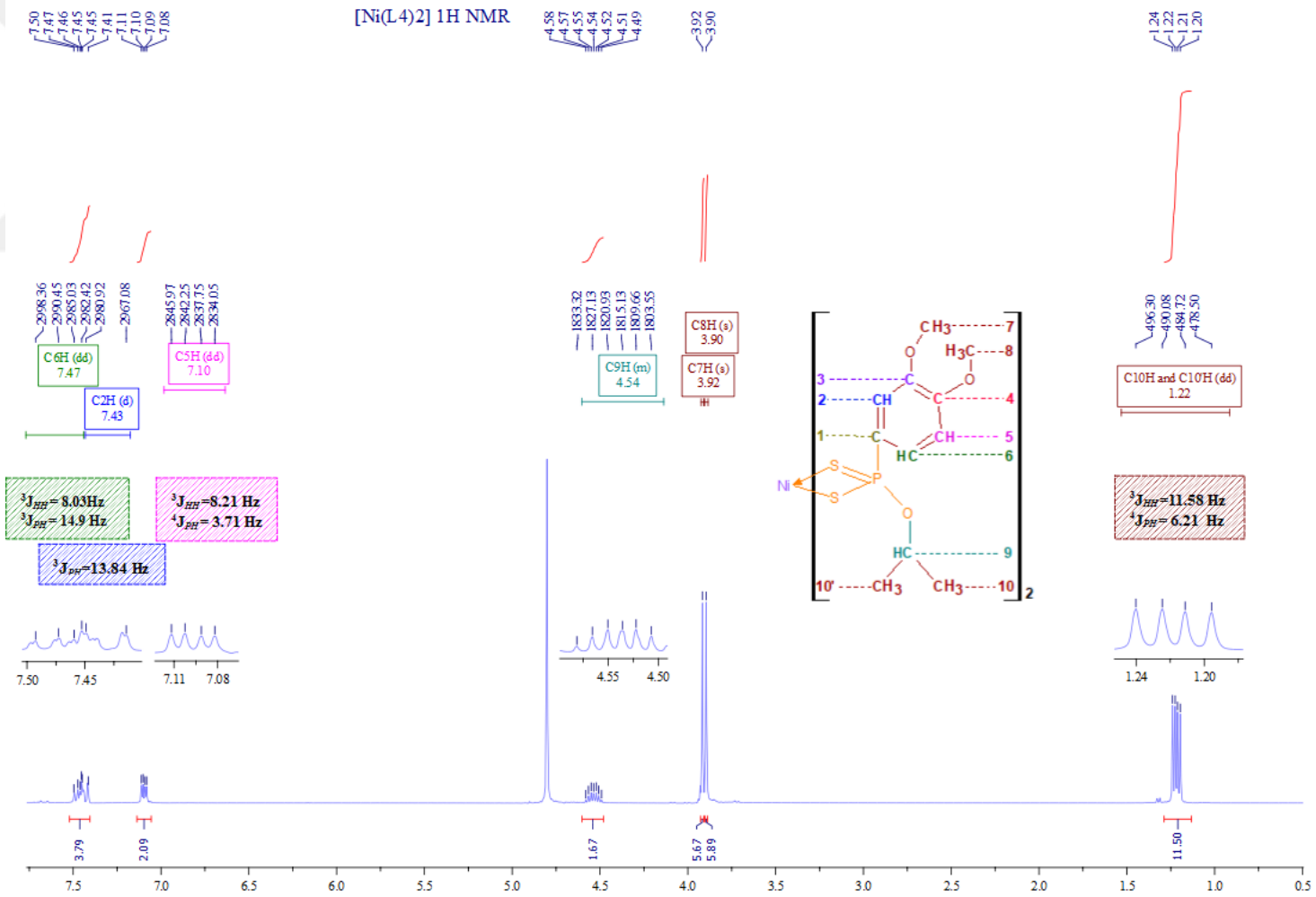


Figure 5.91. [Ni($S_2P(R^x)(OR4))_2$] ^{1}H-NMR spectrum.

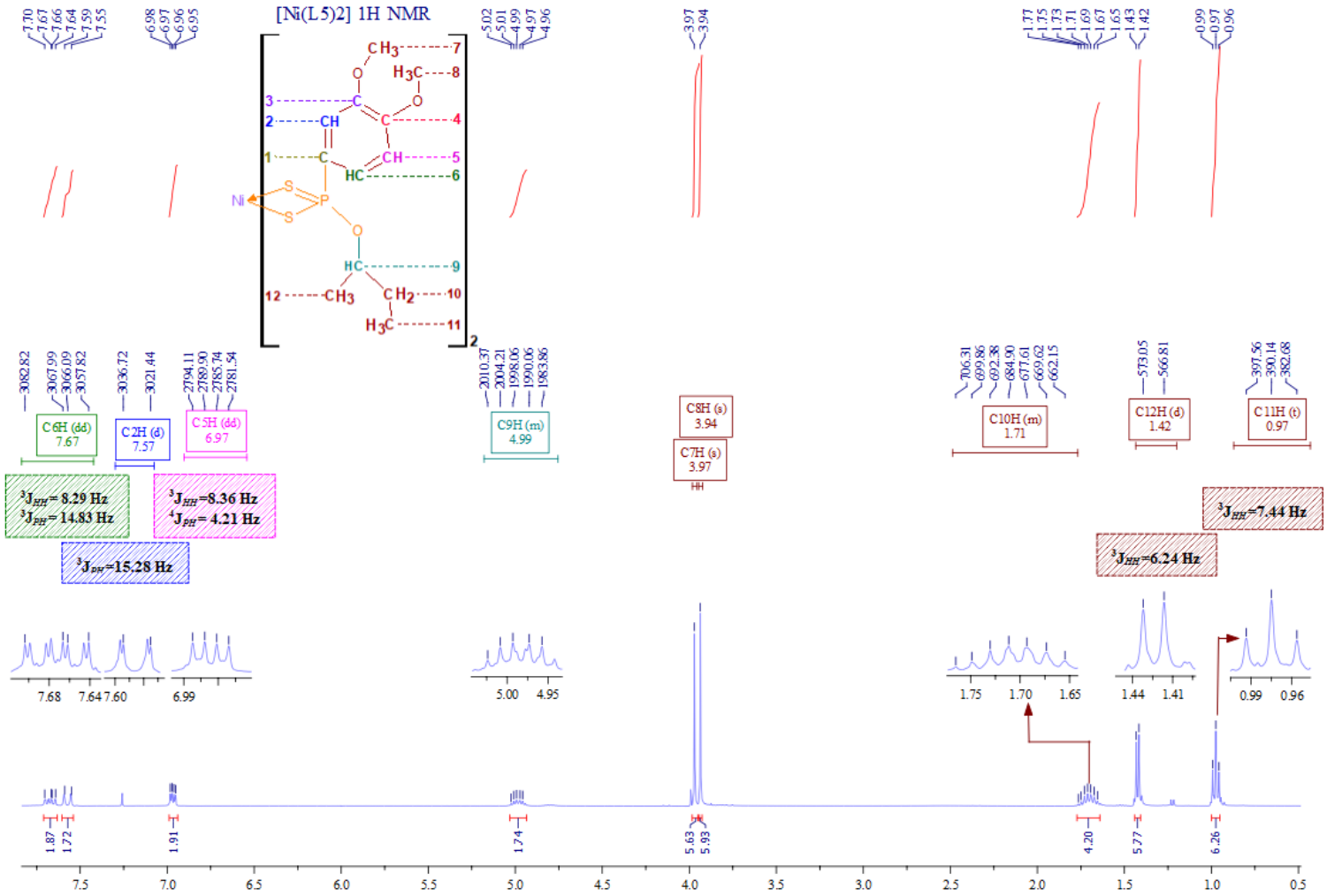


Figure 5.92. [Ni($S_2P(R^x)(OR5)$)$_2$] ^{1}H-NMR spectrum.

5.1.7.4 NMR (^{1}H, ^{13}C-ve ^{31}P- NMR) Spectra of the Part II' compounds

As mentioned before, the starting material, SAV-A2, is insoluble in the common NMR solvents, so no NMR data were provided for it. The numbering system used for assignments of the protons is also given in Figure 5.94.

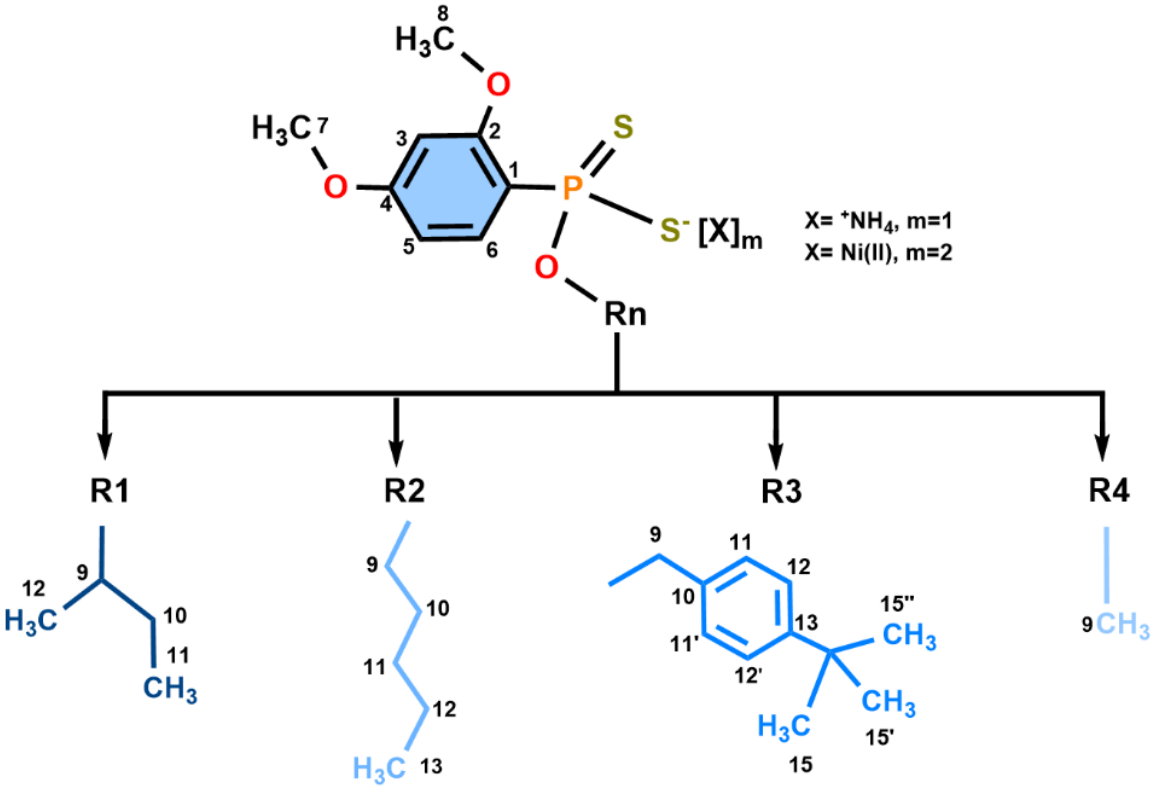


Figure. 5.94. The numbering scheme for compounds.

As a general pattern, NMR (^{1}H-, ^{13}C- and ^{31}P-) signals of the complexes are also displayed at higher fields relative to those observed for the corresponding ligands. Here in, all the NMR data are reasonably consistent with the literature reports for similar structures [101, 122, 297, 298, 301-303].

5.1.7.5 Comment on the HSQC spectrum on the [Ni($S_2P(R^y)(OR2)$)$_2$] for Part II

The ambiguity regarding the assignments of ^{1}H- and ^{13}C-NMR peaks of [Ni($S_2P(R^y)(OR2)$)$_2$] complex was dealt with by using HSQC spectra (Figure 5.95).

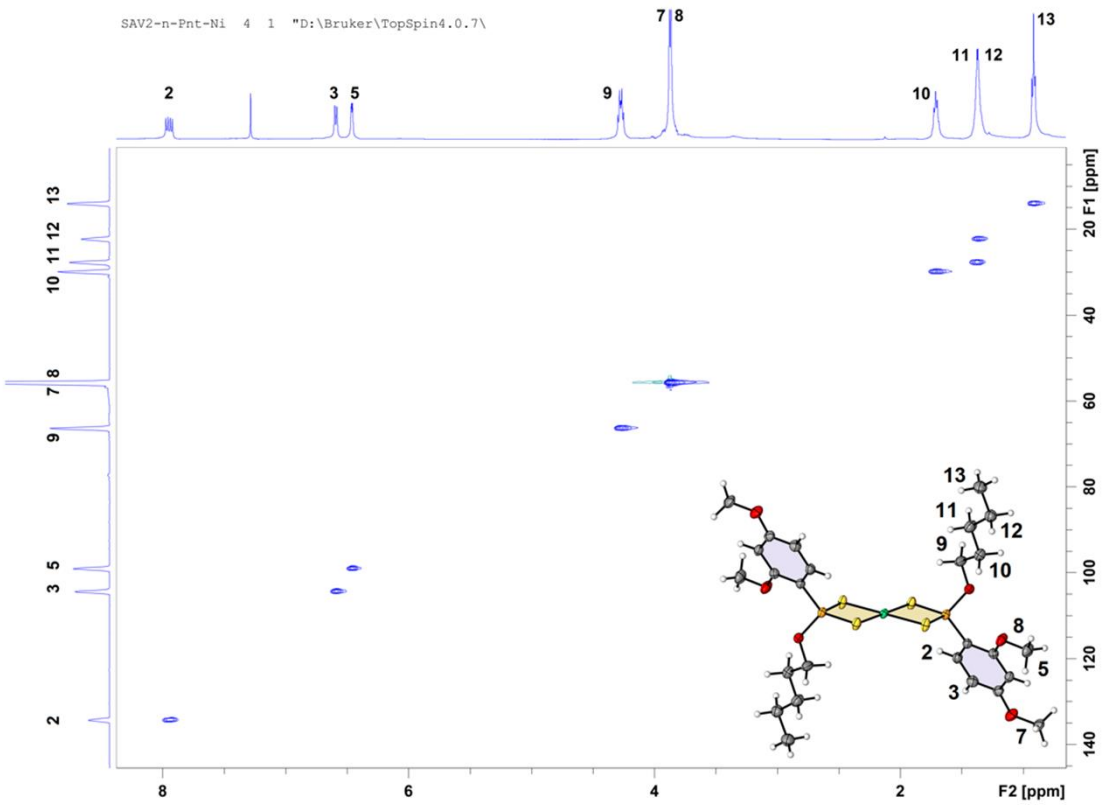


Figure. 5.95. HSQC spectrum of $[Ni(S_2P(R^y)(OR2))_2]$.

5.1.7.6. Comment of ^{1}H-NMR Spectra of the Part II' compounds

The ^{1}H-NMR data is given in Table 5.7 In the ^{1}H-NMR spectra of all the compounds tested, the C_6-***H*** proton on the 2,4-dimethoxyphenyl ring appears as a doublet of doublets indicating splittings by the phosphorus ($^3J_{PH}$= 16.6-17.0 Hz for the ligands and $^3J_{PH}$= 17.7-18.1 Hz for the complexes) and also by C_5-***H*** proton ($^3J_{HH}$= 8.4-8.7 Hz for the ligands and $^3J_{HH}$= 8.2-8.6 Hz for the complexes). The methoxy protons C_7-***H*** and C_8-***H*** on the aromatic moiety were overlapped. The chemical shifts of the methoxy protons are δ=~3.8-3.9 ppm in ligands and complexes.

The signals of the C_3-***H*** and C_5-***H*** protons are adjacent to each other for the ligands. These protons are somewhat (C_3-***H***; $^4J_{PH}$= 3.4-3.5 Hz, C_5-***H***; $^3J_{HH}$=8.0-8.6 Hz) separated from each other in the spectra of the complexes. On the spectra of the ligand $[NH_4][S_2P(R^y)(OR3)]$, the P-O-C_9-***H*** proton is very close to O-C***H***$_3$ (attached to the aromatic ring) protons. But more distant on that of the complex; obviously because the aromatic ring O-C***H***$_3$ protons are effected by complexation.

Table 5.7. ^{1}H-NMR data of the compounds . (D_2O for $[NH_4][S_2P(R^y)(ORn)]$, $CDCl_3$ for $[Ni(S_2P(R^y)(ORn))_2]$; δ in ppm, J in Hz, s: *singlet*, d: *doublet*, dd: *doublet of doublets*, t: *triplet*, and m: *multiplet*).

$[NH_4][S_2P(R^y)(OR1)]$	$[NH_4][S_2P(R^y)(OR2)]$	$[NH_4][S_2P(R^y)(OR3)]$	$[NH_4][S_2P(R^y)(OR4)]$		$[Ni(S_2P(R^y)(OR1))_2]$	$[Ni(S_2P(R^y)(OR2))_2]$	$[Ni(S_2P(R^y)(OR3))_2]$	$[Ni(S_2P(R^y)(OR4))_2]$
6.6 (m, 2H)	6.6 (m, 2H)	6.5 (m, 2H)	6.7 (m, 2H)	C_3-*H*	6.4 (s, 2H)	6.4 (d, 2H); $^{4}J_{PH}$= 3.4	6.4 (d, 2H); $^{3}J_{PH}$= 3.5	6.4 (d, 2H); $^{3}J_{PH}$= 3.6
C_3*H* is adjacent to C_5*H*				C_5-*H*	6.6 (d, 2H); $^{3}J_{HH}$=8.0	6.6 (d, 2H); $^{3}J_{HH}$=8.5	6.6 (d, 2H); $^{3}J_{HH}$=8.6	6.6 (d, 2H); $^{3}J_{HH}$=8.7
8.1 (dd, H) $^{3}J_{PH}$= 17.0 ; $^{3}J_{HH}$= 8.4	8.1 (dd, H) $^{3}J_{PH}$= 16.7 ;$^{3}J_{HH}$= 8.7	8.2 (dd, H) $^{3}J_{PH}$= 16.6 ; $^{3}J_{HH}$= 8.5	8.1 (dd, H) $^{3}J_{PH}$= 16.7 ; $^{3}J_{HH}$= 8.3	C_6-*H*	8.0 (dd, 2H) $^{3}J_{PH}$= 17.7 ; $^{3}J_{HH}$= 8.2	7.9 (dd, 2H) $^{3}J_{PH}$= 17.9 ; $^{3}J_{HH}$= 8.6	7.9 (dd, 2H) $^{3}J_{PH}$= 18.1 ; $^{3}J_{HH}$= 8.6	7.9 (dd, H) $^{3}J_{PH}$= 18.3 ; $^{3}J_{HH}$= 8.7
3.9 (s, 6H)	3.8 (s, 3H)	3.8 (s, 6H)	3.9 (s, 3H)	C_7-*H*	3.9 (s, 6H)	3.9 (s, 6H)	3.8 (s, 12H)	3.9 (s, 12H)
	3.9 (s, 3H)		3.9 (s, 3H)	C_8-*H*	3.8 (s, 6H)	3.8 (s, 6H)		
4.5 (m, H)	3.8 (dd, 2H) $^{3}J_{PH}$= 15.5; $^{3}J_{HH}$= 6.8	4.9 (d, 2H); $^{3}J_{PH}$= 8.8	3.7 (d, 3H); $^{3}J_{PH}$= 14.4	C_9-*H*	4.9 (m, 2H)	4.3 (dd, 4H) $^{3}J_{PH}$= 15.8 ; $^{3}J_{HH}$= 6.4	5.3 (d, 4H); $^{3}J_{PH}$= 9.5	3.9 (d, 6H); $^{3}J_{PH}$= 15.3
1.6 (m, 2H)	1.6 (m, 2H)	-	-	C_{10}-*H*	1.6 (m, 4H)	1.7 (m, 4H)	-	-
0.9 (t, 3H); $^{3}J_{HH}$= 7.5	-	-	-	C_{11}-*H*	1.0 (t, 6H); $^{3}J_{HH}$= 6.8	-	-	-
1.2 (d, 3H); $^{3}J_{HH}$= 6.3	-	-	-	C_{12}-*H*	1.4 (d, 6H); $^{3}J_{HH}$= 5.6	-	-	-
-	0.8 (t, 3H); $^{3}J_{HH}$= 7.0	-	-	C_{13}-*H*	-	0.9 (t, 6H); $^{3}J_{HH}$= 6.3	-	-
-	-	1.3 (s, 9H)	-	C_{15}-*H*	-	-	1.3 (s, 18H)	-
-	1.3 (m, 4H)	7.3 (s, 4H)	-	$C_{11,12}$-*H*	-	1.4 (s, 8H)	7.4 (s, 8H)	-

^{1}H-NMR of Part II [NH_4][$S_2P(R^y)(ORn)$] and [$Ni(S_2P(R^y)(ORn))_2$] compounds.

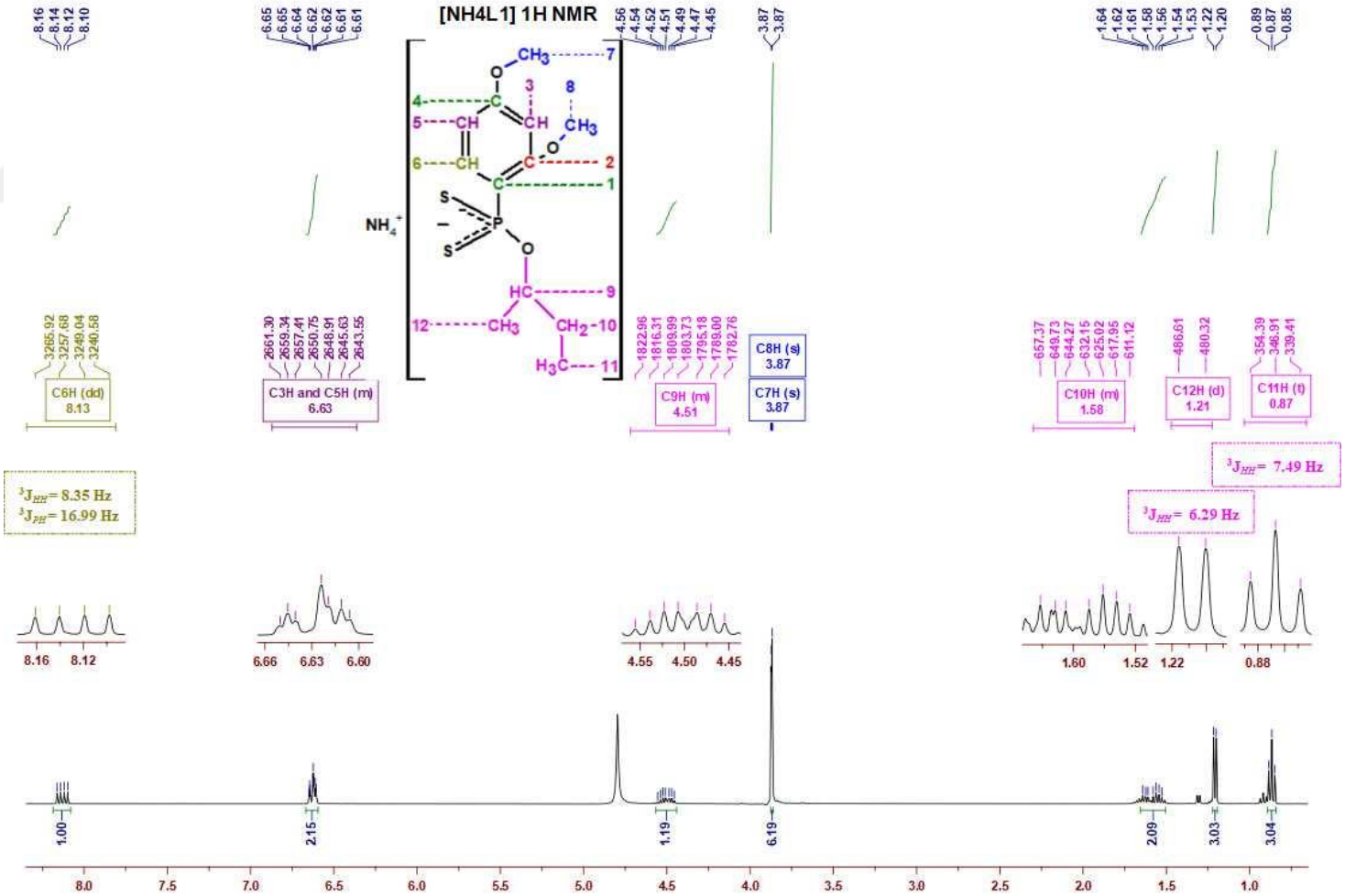


Figure 5.96. [NH_4][$S_2P(R^y)(OR1)$] ^{1}H-NMR spectrum.

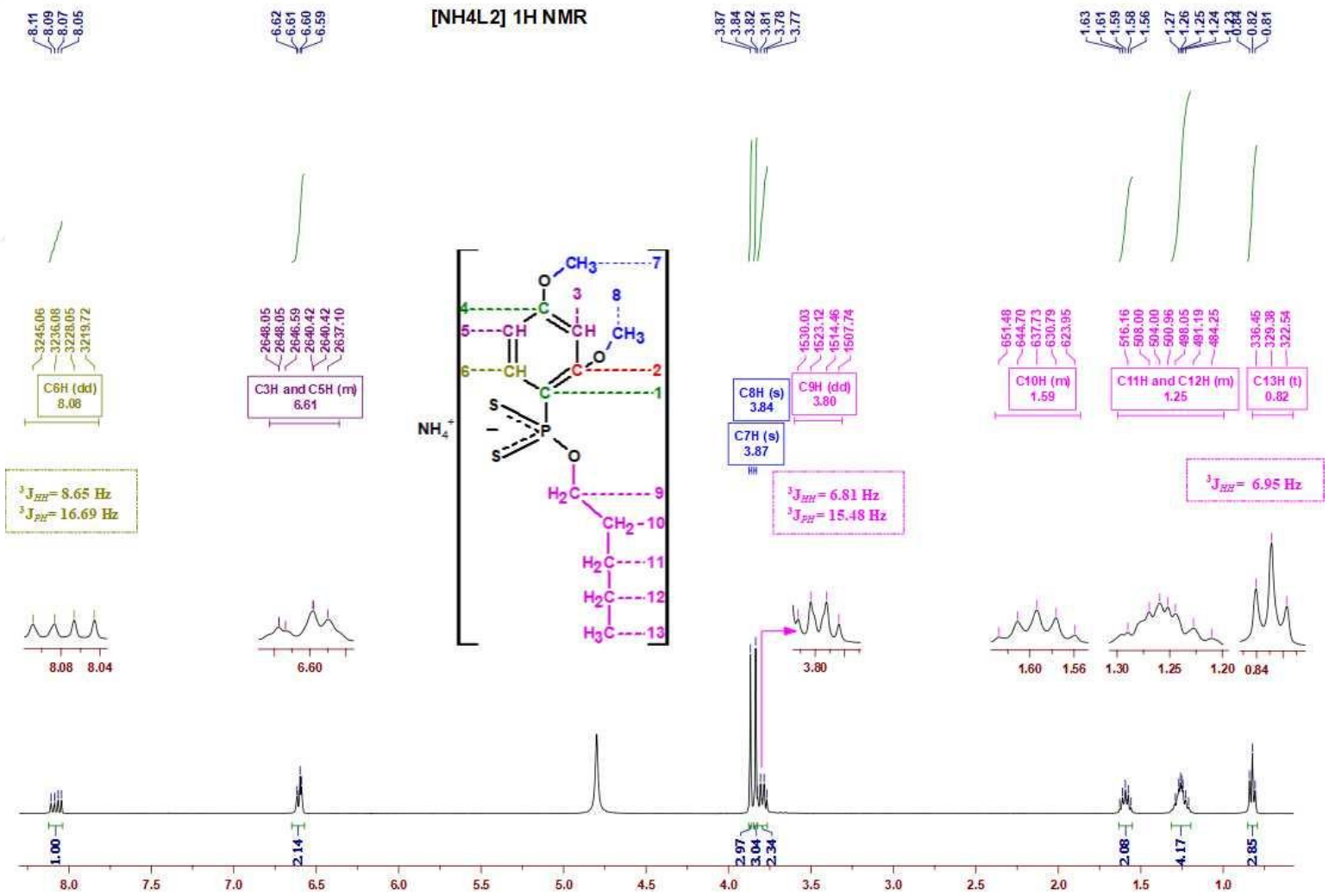


Figure 5.97. $[NH_4][S_2P(R^y)(OR2)]$ ^{1}H-NMR spectrum.

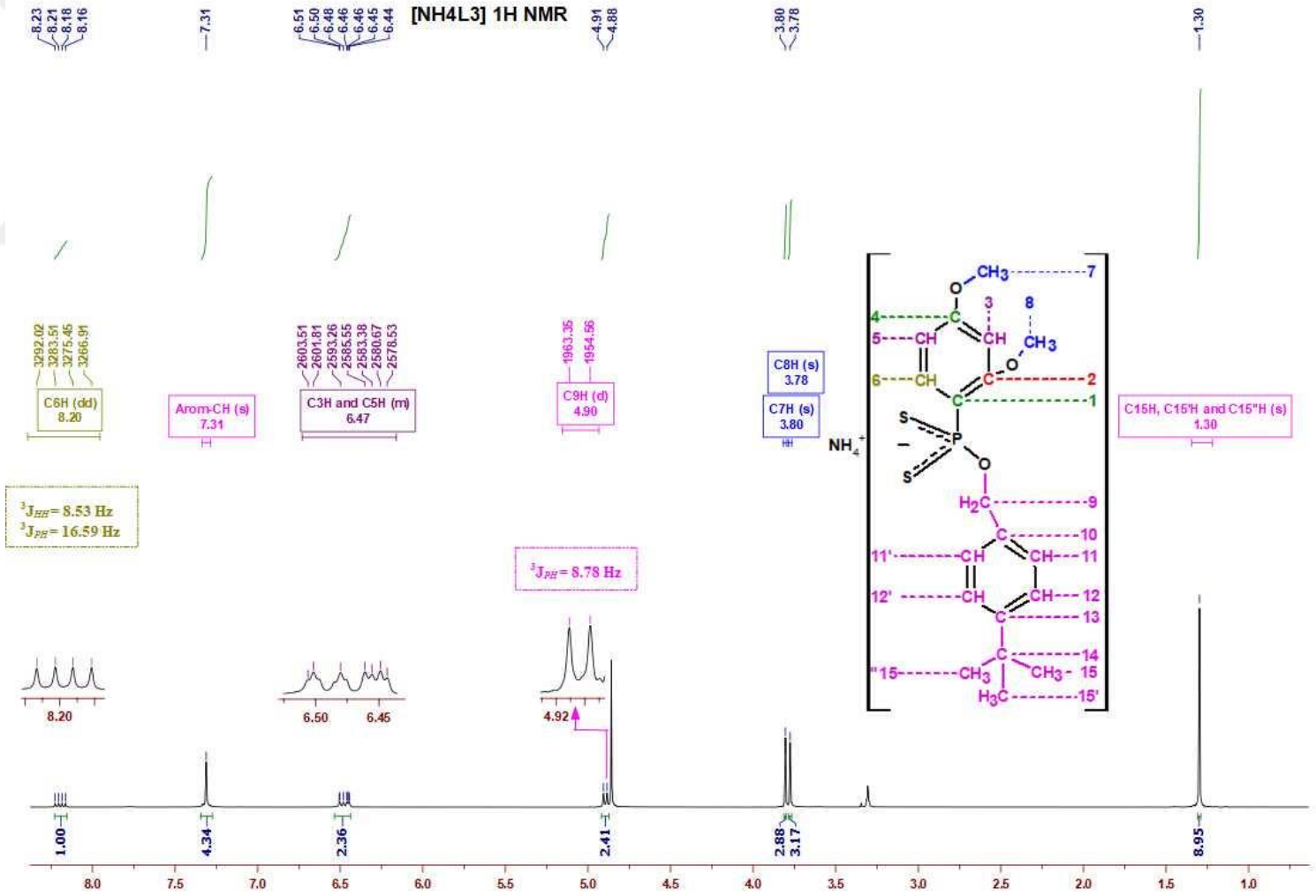


Figure 5.98. $[NH_4][S_2P(R^y)(OR3)]$ ^{1}H-NMR spectrum.

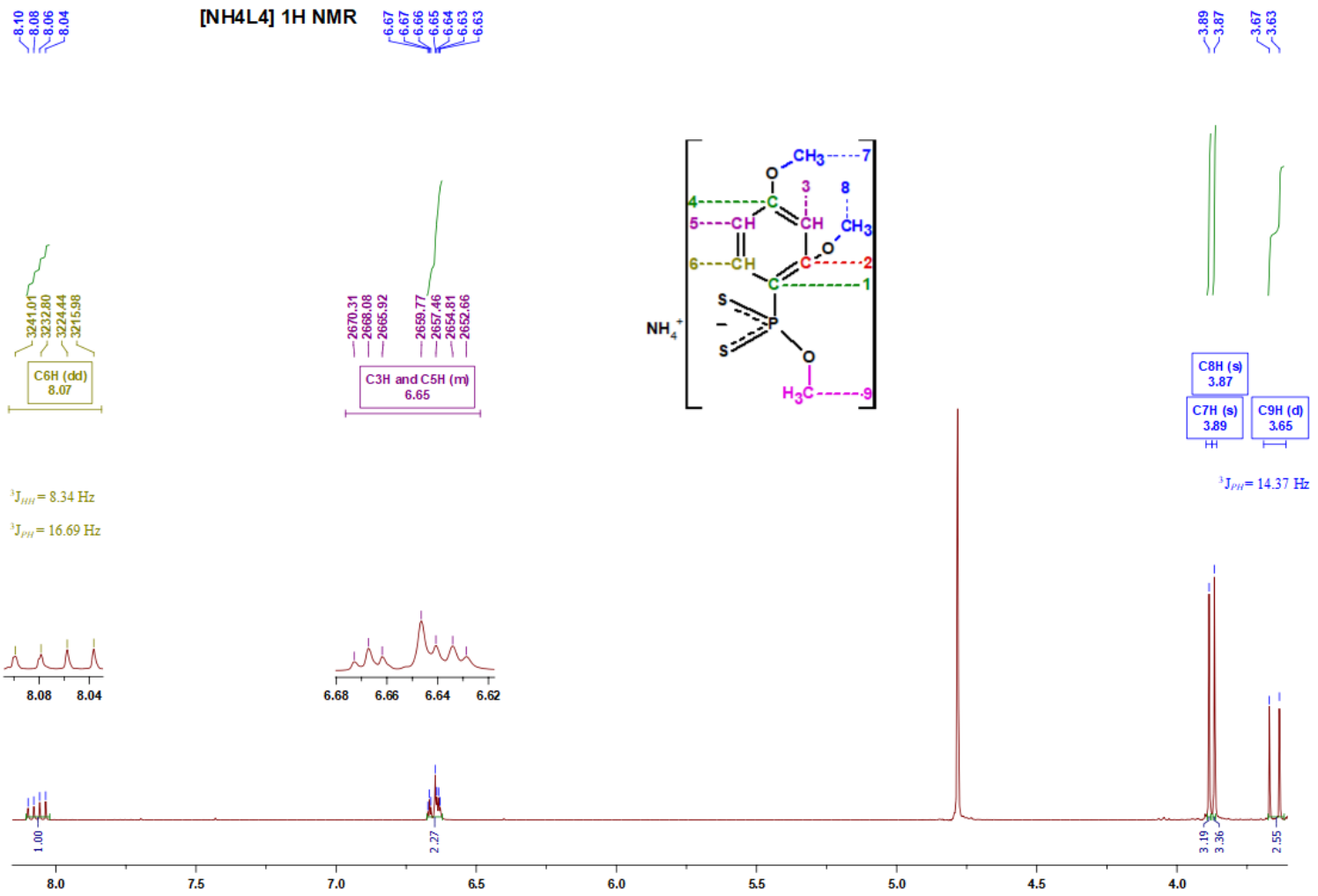


Figure 5.99. $[NH_4][S_2P(R^y)(OR4)]$ ^{1}H-NMR spectrum.

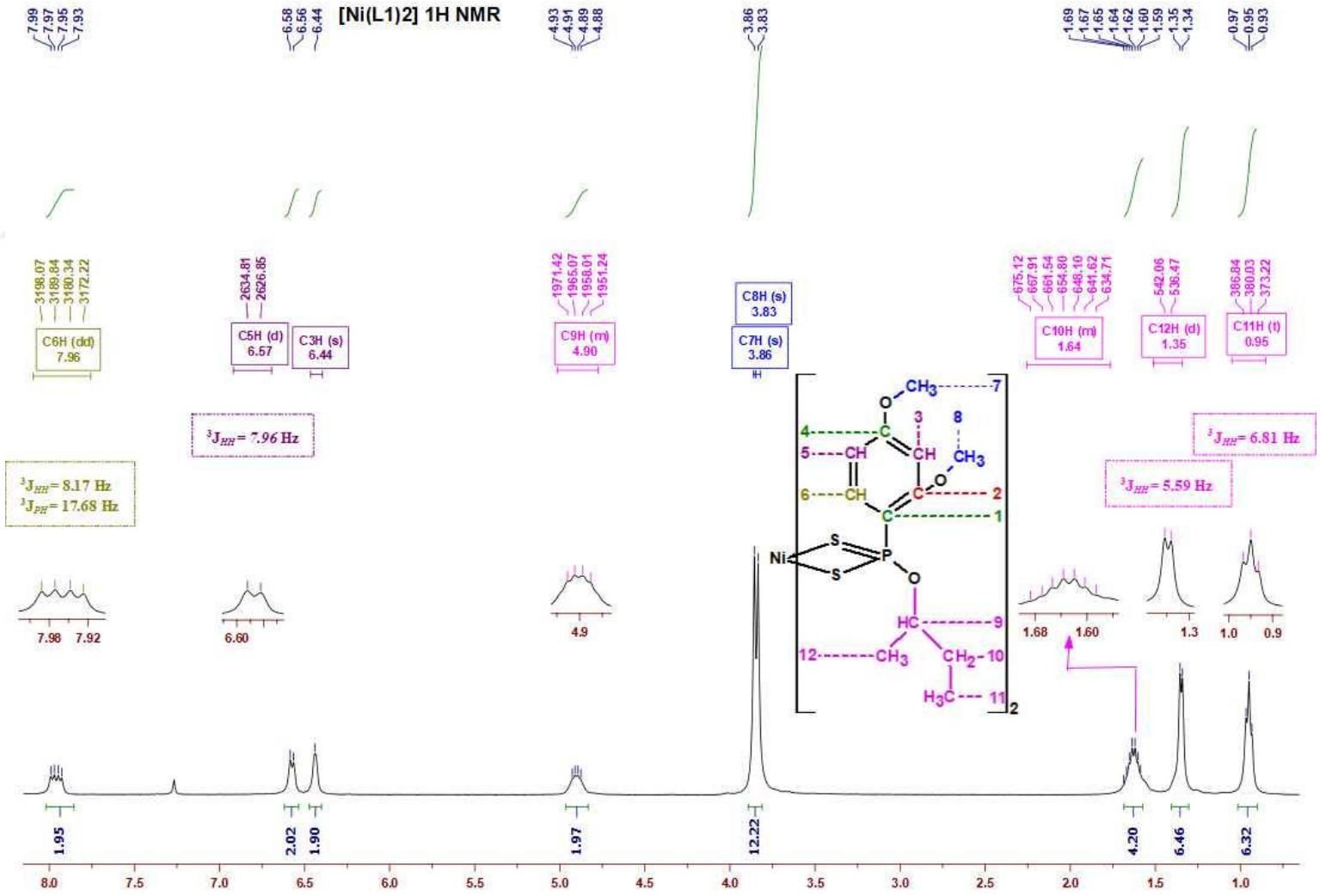


Figure 5.100. $[Ni(S_2P(R^y)(OR1))_2]$ ^{1}H-NMR spectrum.

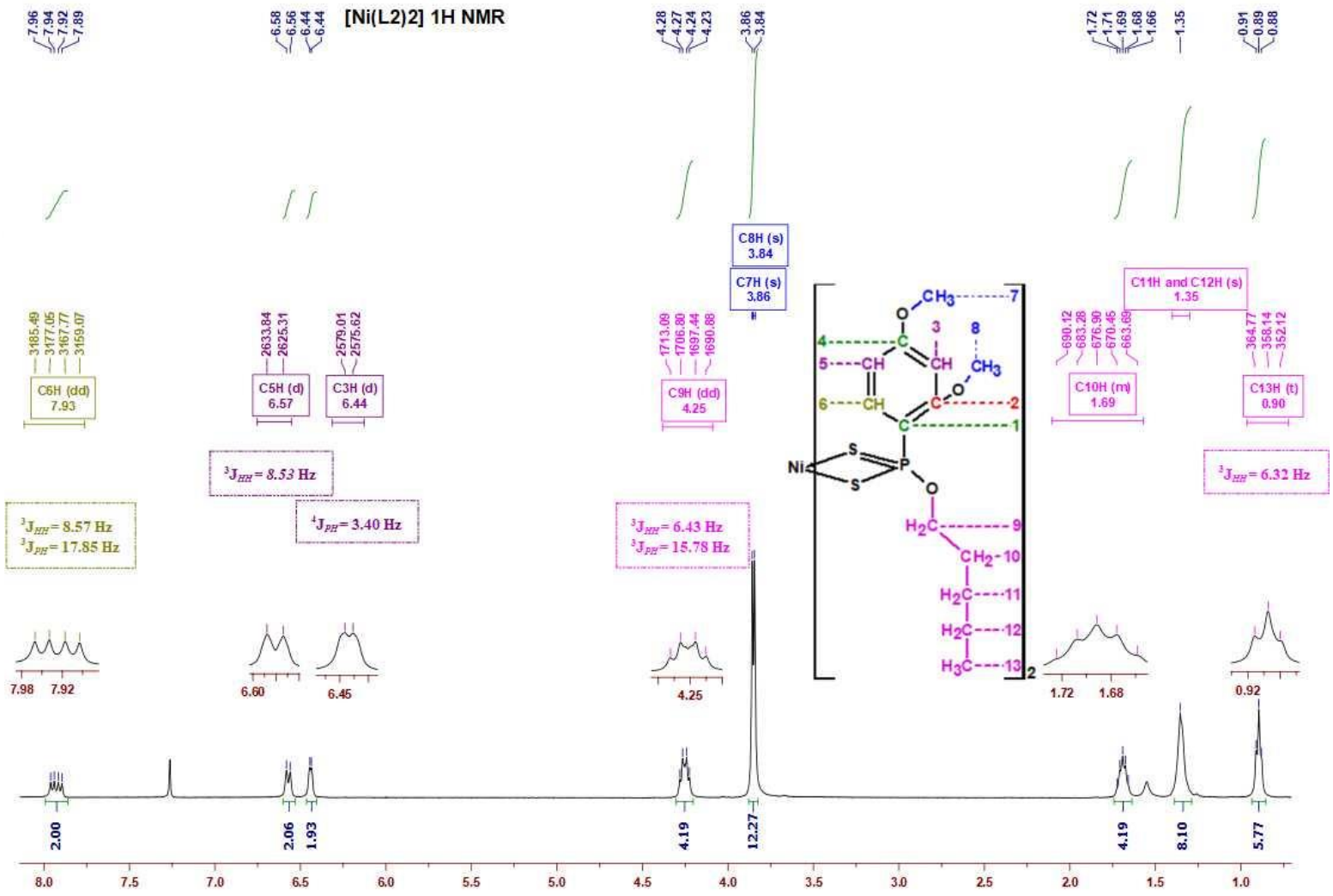


Figure 5.101. $[Ni(S_2P(R^y)(OR2))_2]$ ^{1}H-NMR spectrum.

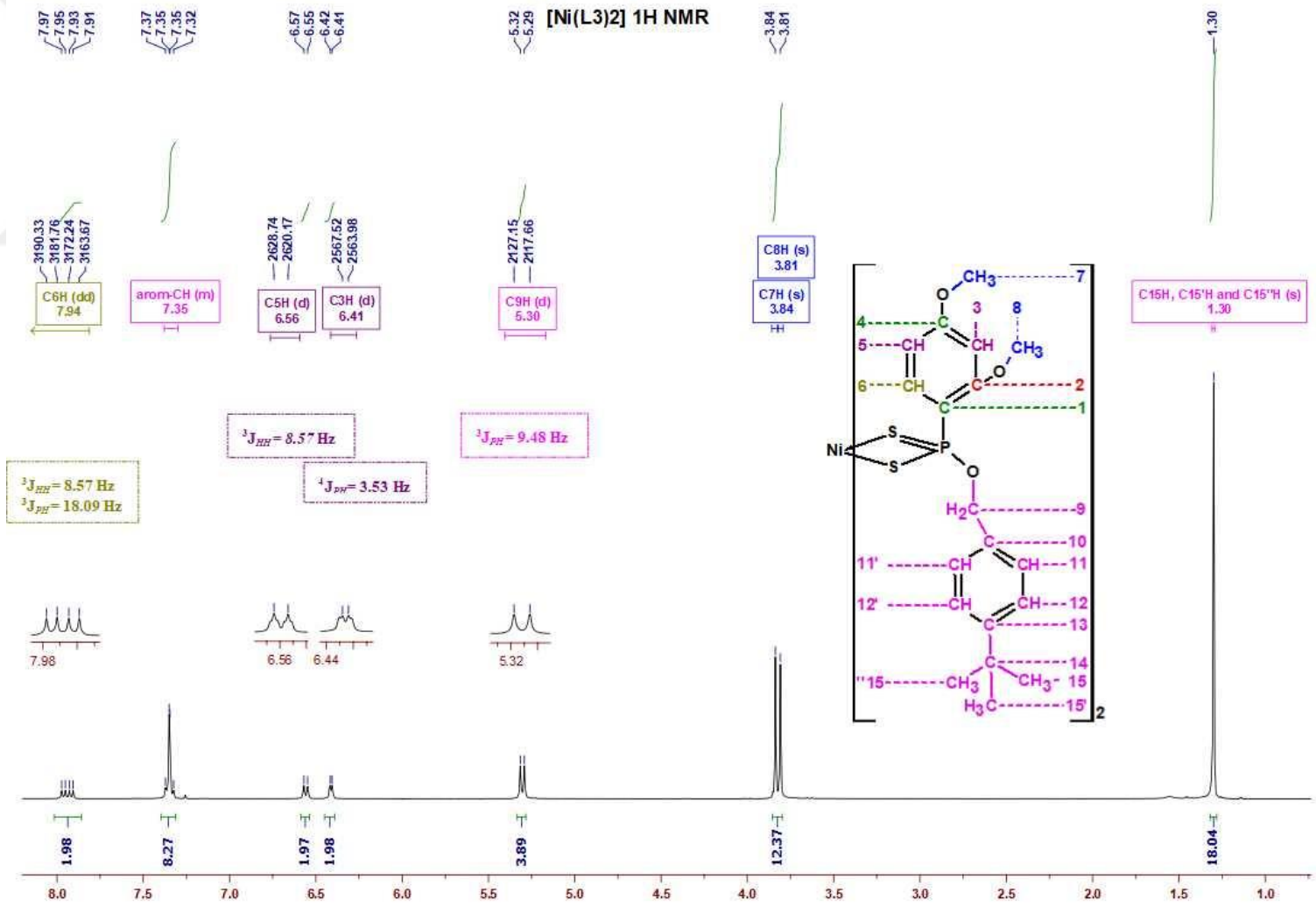


Figure 5.102. $[Ni(S_2P(R^y)(OR3))_2]$ ^{1}H-NMR spectrum.

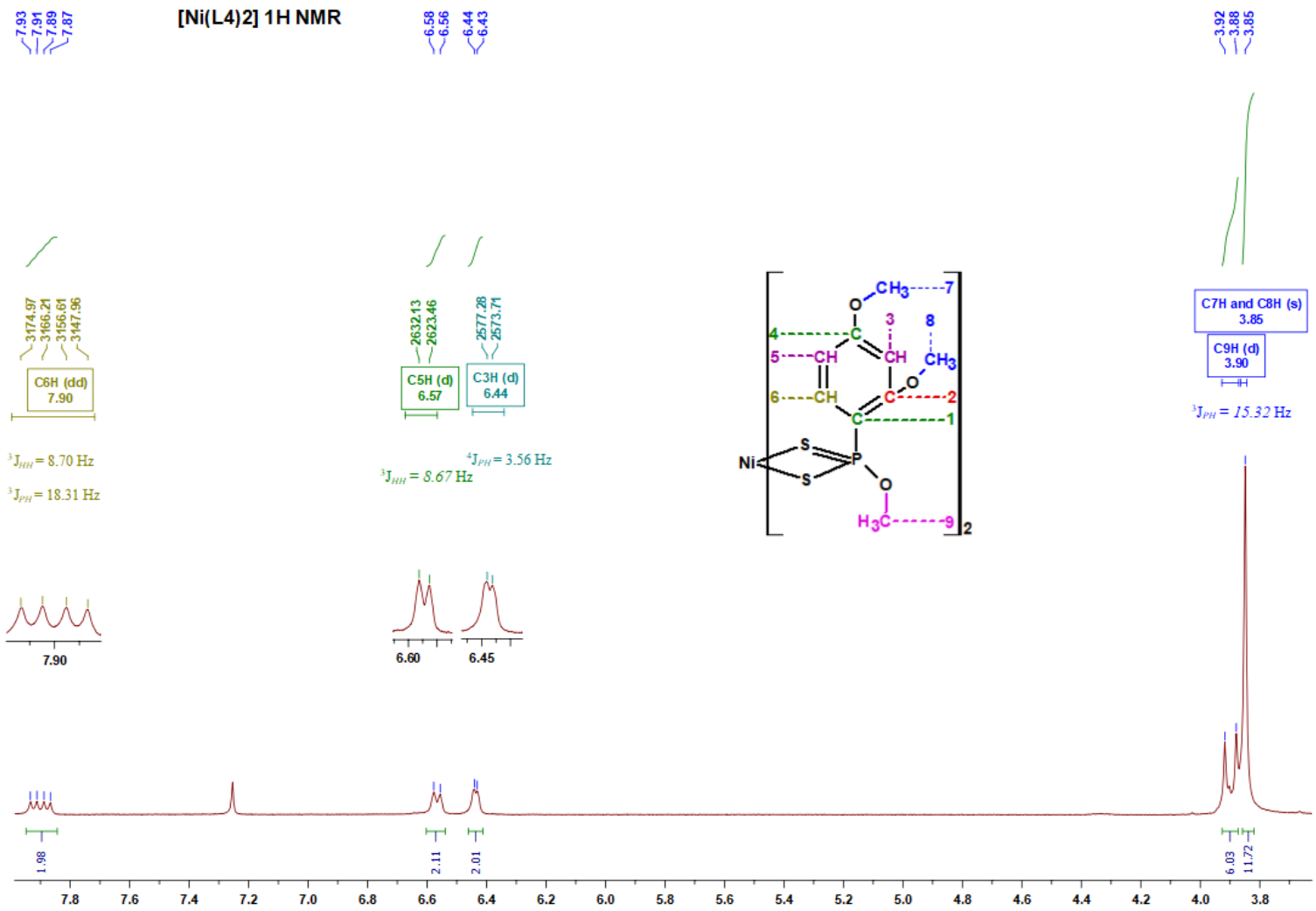


Figure 5.103. [Ni($S_2P(R^y)(OR4))_2$] ^{1}H-NMR spectrum.

5.1.7.7. Comments on ^{13}C-NMR Spectra of Part Ia' Compounds

On the ^{13}C-NMR spectra of the ligands, the nuclei $\boldsymbol{C}_2$ and $\boldsymbol{C}_6$ are split by the phosphorus in the ranges, $^2J_{PC}$= 14.6-15.0 Hz and 12.2-12.8 Hz, respectively. These values lie in the expected domain [131]. As is the case in many similar structures the three-bond P-$\boldsymbol{C}$ coupling displayed by the nuclei $\boldsymbol{C}_3$ and $\boldsymbol{C}_5$ ($^3J_{PC}$= 16.8-17.4 Hz and 16.8-18.3 Hz, respectively) are higher than the two-bond couplings of $\boldsymbol{C}_2$ and $\boldsymbol{C}_6$.

The difference between the ^{13}C-NMR spectra of the complexes and those of the corresponding ligands is not worth commenting on.

The NMR spectra and important NMR data for the ligands and their nickel(II) complexes are presented in Tables 5.8-5.9. Spectrum peaks of ^{13}C-NMR are given in Figure 5.104-5.117.

Table 5.8 ^{13}C-NMR data of Part $[NH_4][S_2P(R^x)(ORn)]$ ligands (D_2O; δ in ppm, J in Hz).

	$[NH_4][S_2P(R^x)(OR1)]$	$[NH_4][S_2P(R^x)(OR2)]$	$[NH_4][S_2P(R^x)(OR3)]$	$[NH_4][S_2P(R^x)(OR4)]$	$[NH_4][S_2P(R^x)(OR5)]$	$[NH_4][S_2P(R^x)(OR6)]$	$[NH_4][S_2P(R^x)(OR7)]$
C_1	135.3, J_{PC}= 113.8	128.6, J_{PC}= 115.8	128.7, J_{PC}= 115.6	128.8, J_{PC}= 115.7	129.4, J_{PC}= 117.6	128.7, J_{PC}= 115.6	128.3, J_{PC}= 115.1
C_2	113.4, $^2J_{PC}$= 14.6	111.6, $^2J_{PC}$= 16.6	111.7, $^2J_{PC}$= 16.3	111.8, $^2J_{PC}$= 16.3	112.0, $^2J_{PC}$= 16.3	111.7, $^2J_{PC}$= 16.3	111.8, $^2J_{PC}$= 16.7
C_3	147.7, $^3J_{PC}$= 16.9	148.6	148.8, $^3J_{PC}$= 19.8	148.8, $^3J_{PC}$= 18.5	148.8, $^3J_{PC}$= 18.6	148.8, $^3J_{PC}$= 18.6	148.8, $^3J_{PC}$= 20.0
C_4	150.5, $^4J_{PC}$= 3.0	150.4, $^4J_{PC}$= 3.0	150.3, $^4J_{PC}$= 2.9	150.4, $^4J_{PC}$= 3.0	152.9, $^4J_{PC}$= 3.0	153.1, $^4J_{PC}$= 3.0	153.1, $^4J_{PC}$= 3.0
C_5	109.8, $^3J_{PC}$= 16.9	109.8, $^3J_{PC}$= 18.3	109.7, $^3J_{PC}$= 16.8	109.8, $^3J_{PC}$= 16.8	113.5, $^3J_{PC}$= 17.2	113.6, $^3J_{PC}$= 17.0	113.6, $^3J_{PC}$= 17.1
C_6	123.4, $^2J_{PC}$= 12.3	123.3, $^2J_{PC}$= 12.2	123.3, $^2J_{PC}$= 12.2	123.3, $^2J_{PC}$= 12.2	126.4, $^2J_{PC}$= 12.7	126.5, $^2J_{PC}$= 12.6	126.6, $^2J_{PC}$= 12.8
C_7	55.0	59.6	54.9	54.9	58.6	58.6	58.6
C_8	54.9	59.6			58.5	58.5	58.4
C_9	49.7, $^2J_{PC}$= 6.8	55.0	68.0, $^2J_{PC}$= 6.0	63.4, $^2J_{PC}$= 7.2	83.1, $^2J_{PC}$= 8.6	66.8, $^2J_{PC}$= 7.6	69.8, $^2J_{PC}$= 6.9
C_{10}	-	15.2, $^3J_{PC}$= 9.1	23.1, $^3J_{PC}$= 4.0	32.3, $^3J_{PC}$= 8.9	29.3, $^3J_{PC}$= 3.8	41.3, $^3J_{PC}$= 8.2	130.9, $^3J_{PC}$= 13.4
C_{11}	-	-	22.9, $^4J_{PC}$= 4.6	18.7	11.5	27.0	139.9, $^4J_{PC}$= 8.1
C_{12}	-	-	-	12.7	-	24.6	131.4
C_{13}	-	-	-	-	-	-	131.0

Table 5.9. ^{13}C-NMR data of Part Ia [Ni($S_2P(R^x)(ORn))_2$] complexes ($CDCl_3$; δ in ppm, J in Hz).

	[Ni($S_2P(R^x)(OR1))_2$]	[Ni($S_2P(R^x)(OR2))_2$]	[Ni($S_2P(R^x)(OR3))_2$]	[Ni($S_2P(R^x)(OR4))_2$]	[Ni($S_2P(R^x)(OR5))_2$]	[Ni($S_2P(R^x)(OR6))_2$]	[Ni($S_2P(R^x)(OR7))_2$]
C_1	128.2, J_{PC}= 115.9	128.6, J_{PC}= 115.8	128.7, J_{PC}= 115.6	128.8, J_{PC}= 115.7	129.4, J_{PC}= 117.6	128.7, J_{PC}= 115.6	128.3, J_{PC}= 115.1
C_2	111.4, $^2J_{PC}$= 16.5	111.6, $^2J_{PC}$= 16.6	111.7, $^2J_{PC}$= 16.3	111.8, $^2J_{PC}$= 16.3	112.0, $^2J_{PC}$= 16.3	111.7, $^2J_{PC}$= 16.3	111.8, $^2J_{PC}$= 16.7
C_3	148.8, $^3J_{PC}$= 20.0	148.6	148.8, $^3J_{PC}$= 19.8	148.8, $^3J_{PC}$= 18.5	148.8, $^3J_{PC}$= 18.6	148.8, $^3J_{PC}$= 18.6	148.8, $^3J_{PC}$= 20.0
C_4	152.7	152.6	152.6	152.6	152.4	152.6	152.8
C_5	110.6, $^3J_{PC}$= 19.7	110.6, $^3J_{PC}$= 20.1	110.7, $^3J_{PC}$= 19.1	110.6, $^3J_{PC}$= 18.6	110.6, $^3J_{PC}$= 18.5	110.7, $^3J_{PC}$= 18.8	110.7, $^3J_{PC}$= 19.1
C_6	123.7, $^2J_{PC}$= 14.4	123.6, $^2J_{PC}$= 13.7	123.6, $^2J_{PC}$= 13.7	123.6, $^2J_{PC}$= 13.6	123.5, $^2J_{PC}$= 13.2	123.6, $^2J_{PC}$= 13.6	123.7, $^2J_{PC}$= 13.9
C_7	56.1	56.1	56.1	56.1	56.1	56.1	56.1
C_8							
C_9	52.6, $^2J_{PC}$= 5.8	62.8	68.0, $^2J_{PC}$= 6.0	66.3, $^2J_{PC}$= 6.2	81.1, $^2J_{PC}$= 6.9	65.1, $^2J_{PC}$= 6.0	67.7, $^2J_{PC}$= 5.2
C_{10}	-	16.2, $^3J_{PC}$= 3.4	23.6, $^3J_{PC}$= 7.5	32.2, $^3J_{PC}$= 7.5	27.4	38.8, $^3J_{PC}$= 7.5	128.2
C_{11}	-	-	10.3	18.9	9.3	24.9	135.7, $^4J_{PC}$= 9.0
C_{12}	-	-	-	13.7	-	22.5	128.6
C_{13}	-	-	-	-	-	-	128.5

^{13}C-NMR spectra of Part Ia [NH_4][$S_2P(R^x)(ORn)$] and [$Ni(S_2P(R^x)(ORn))_2$] compounds.

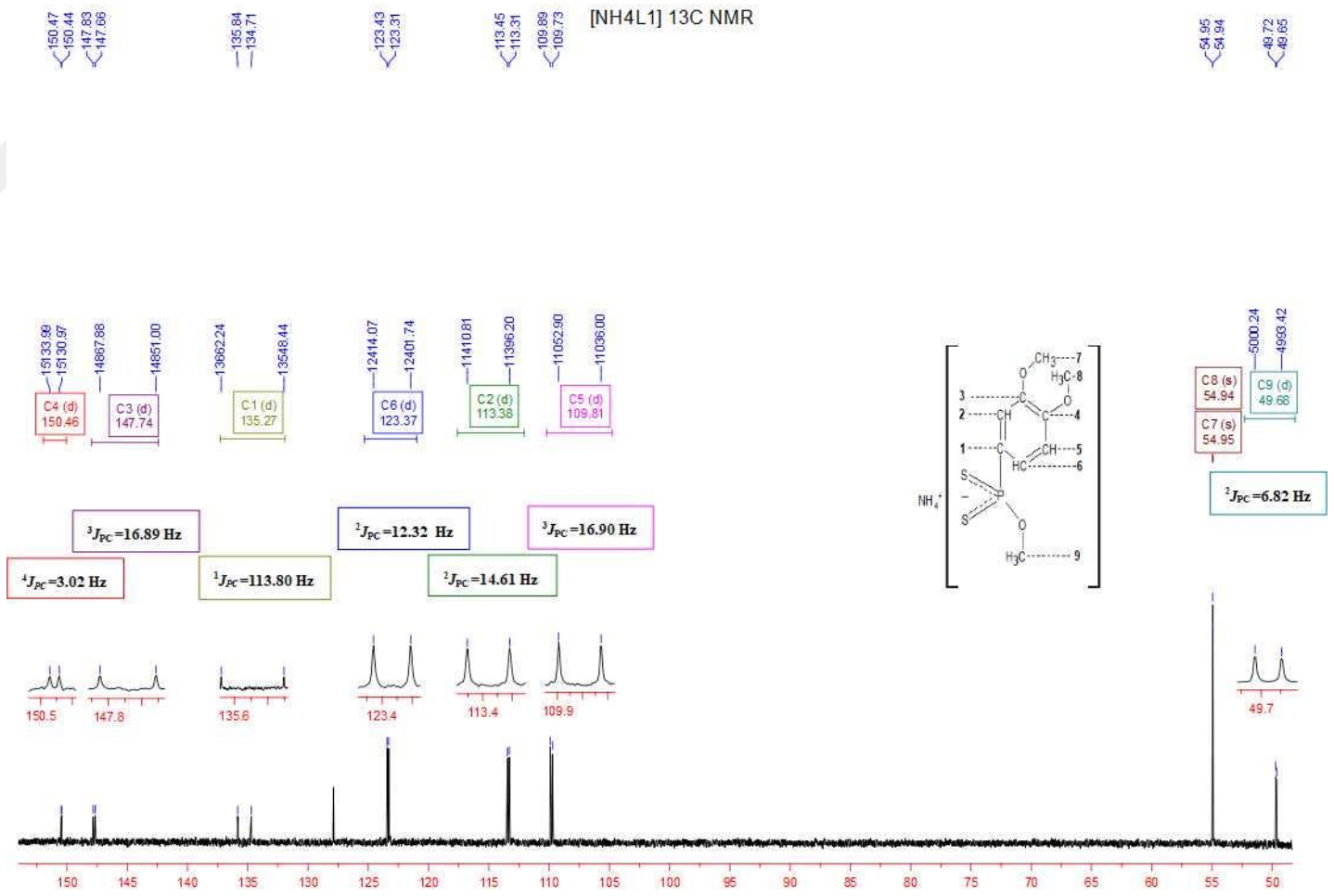


Figure 5.104. [NH_4][$S_2P(R^x)(OR1)$] ^{13}C-NMR spectrum.

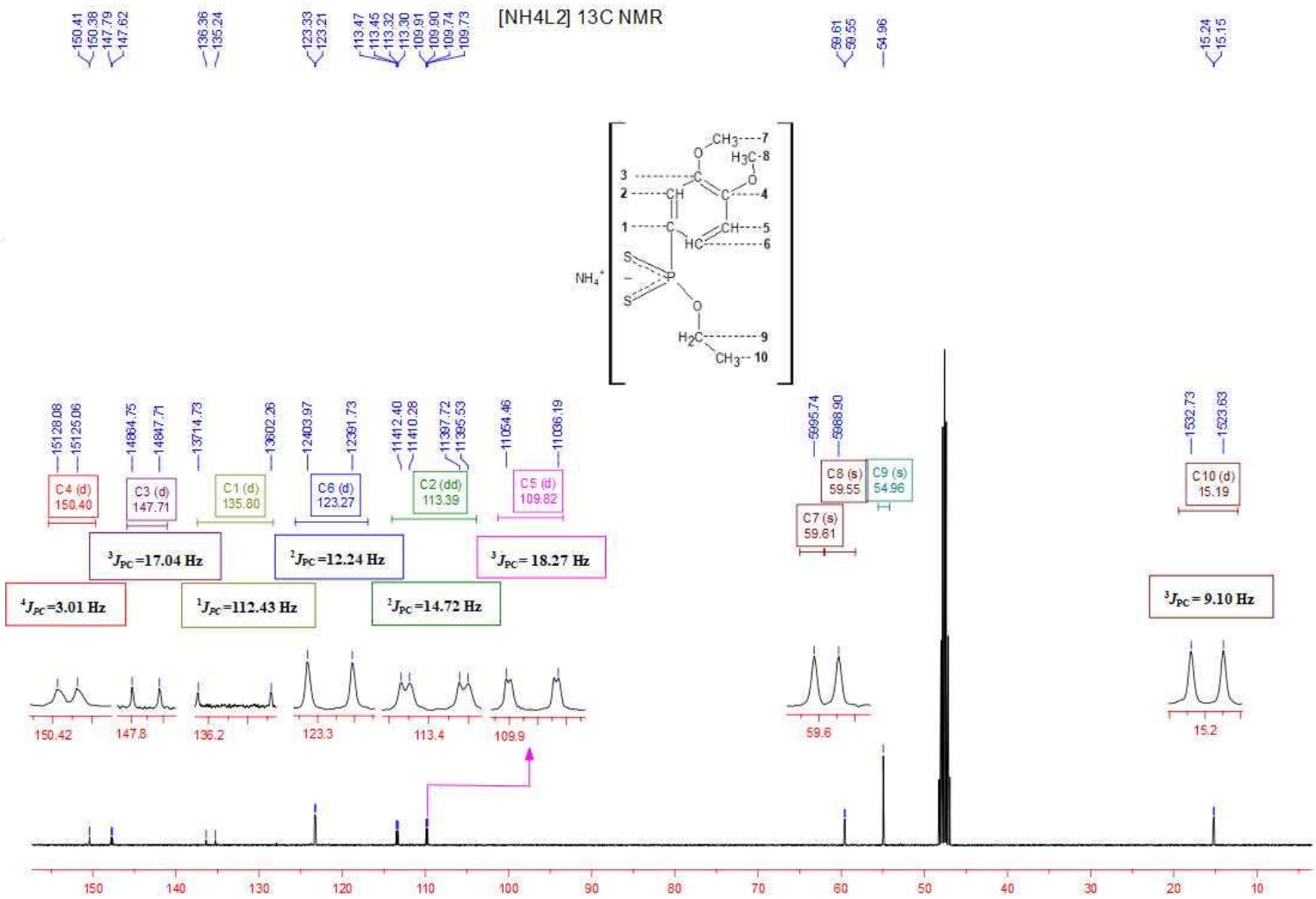


Figure 5.105. $[NH_4][S_2P(R^x)(OR2)]$ ^{13}C-NMR spectrum.

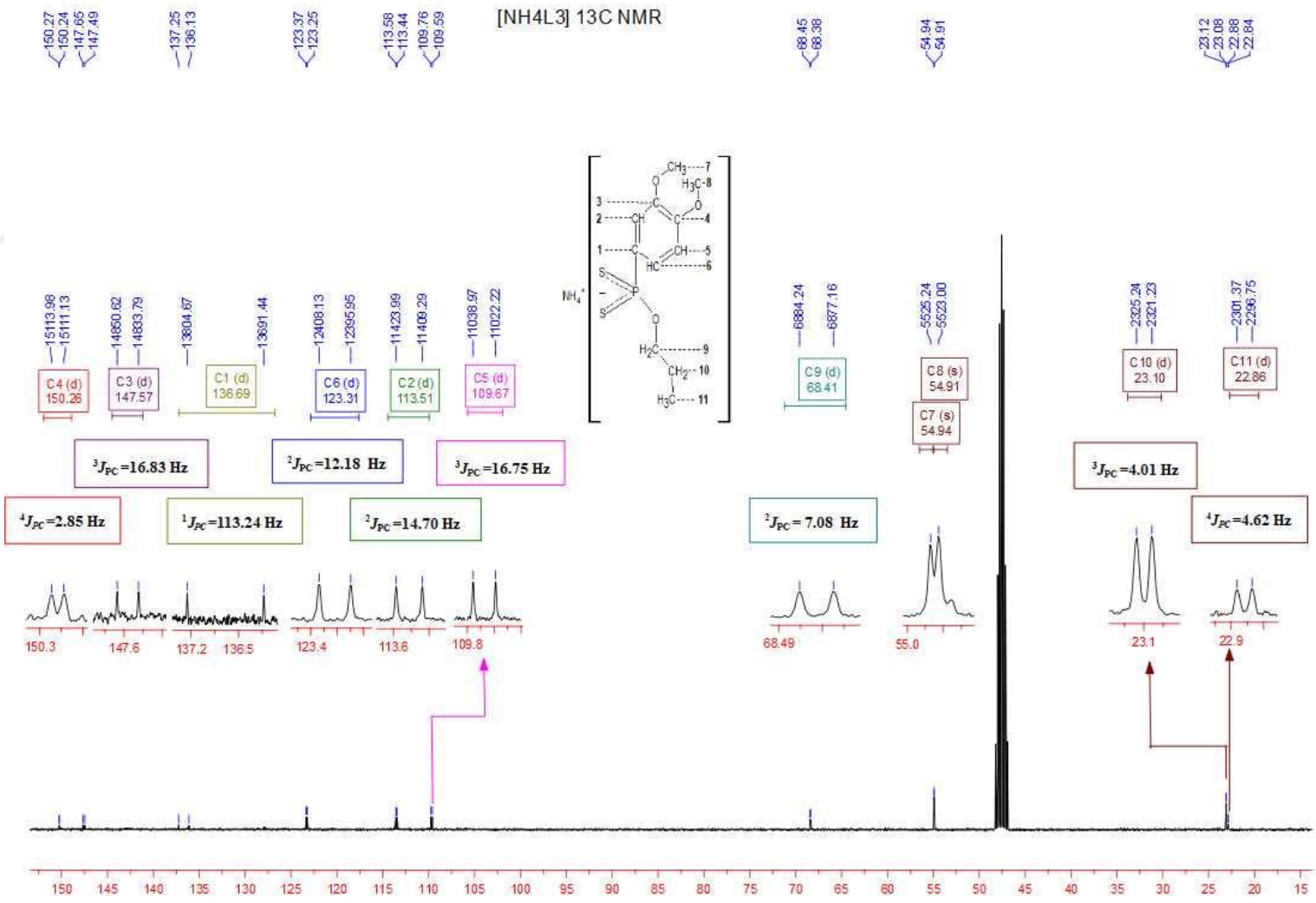


Figure 5.106. $[NH_4][S_2P(R^x)(OR3)]$ ^{13}C-NMR spectrum.

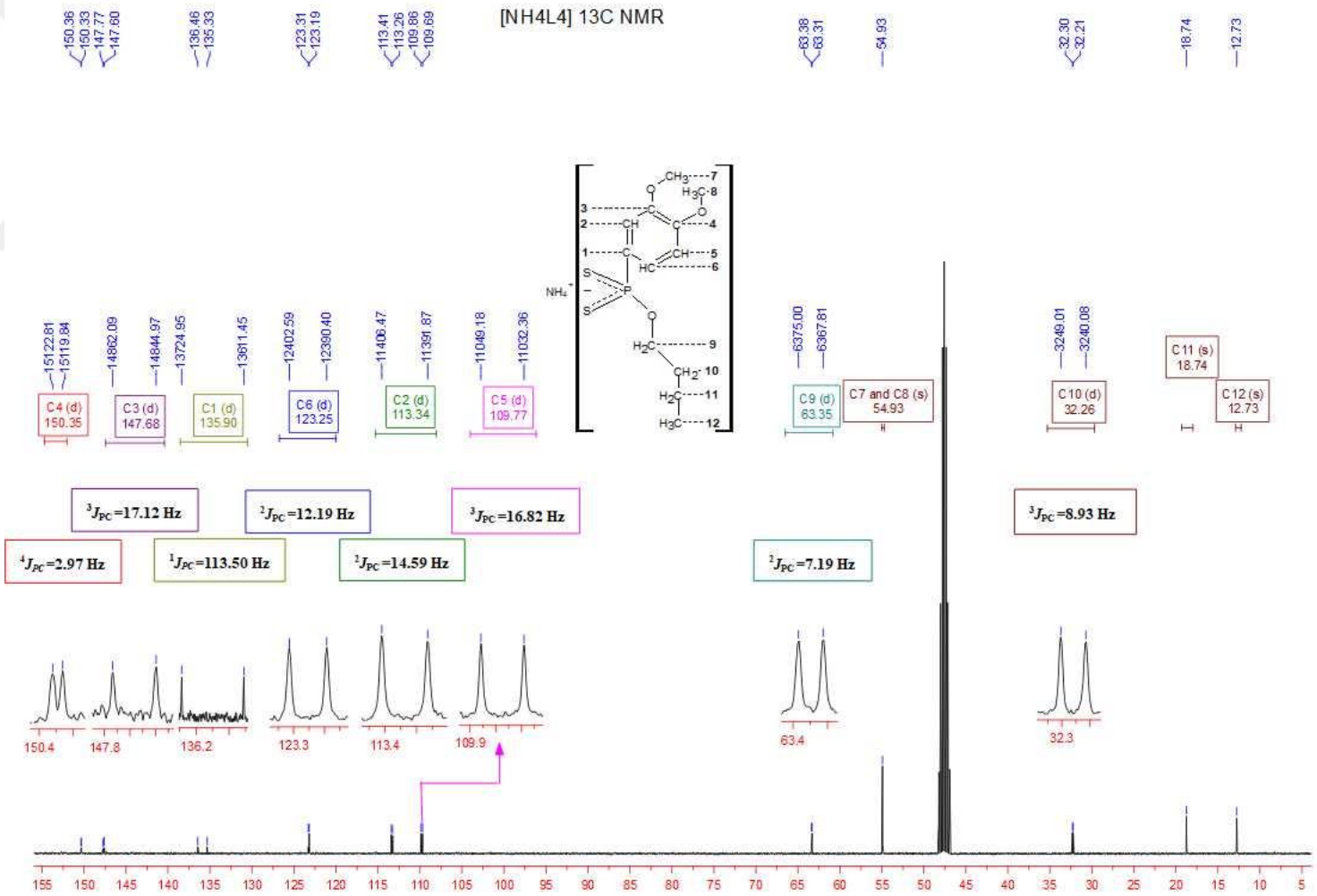


Figure 5.107. $[NH_4][S_2P(R^x)(OR4)]$ ^{13}C-NMR spectrum.

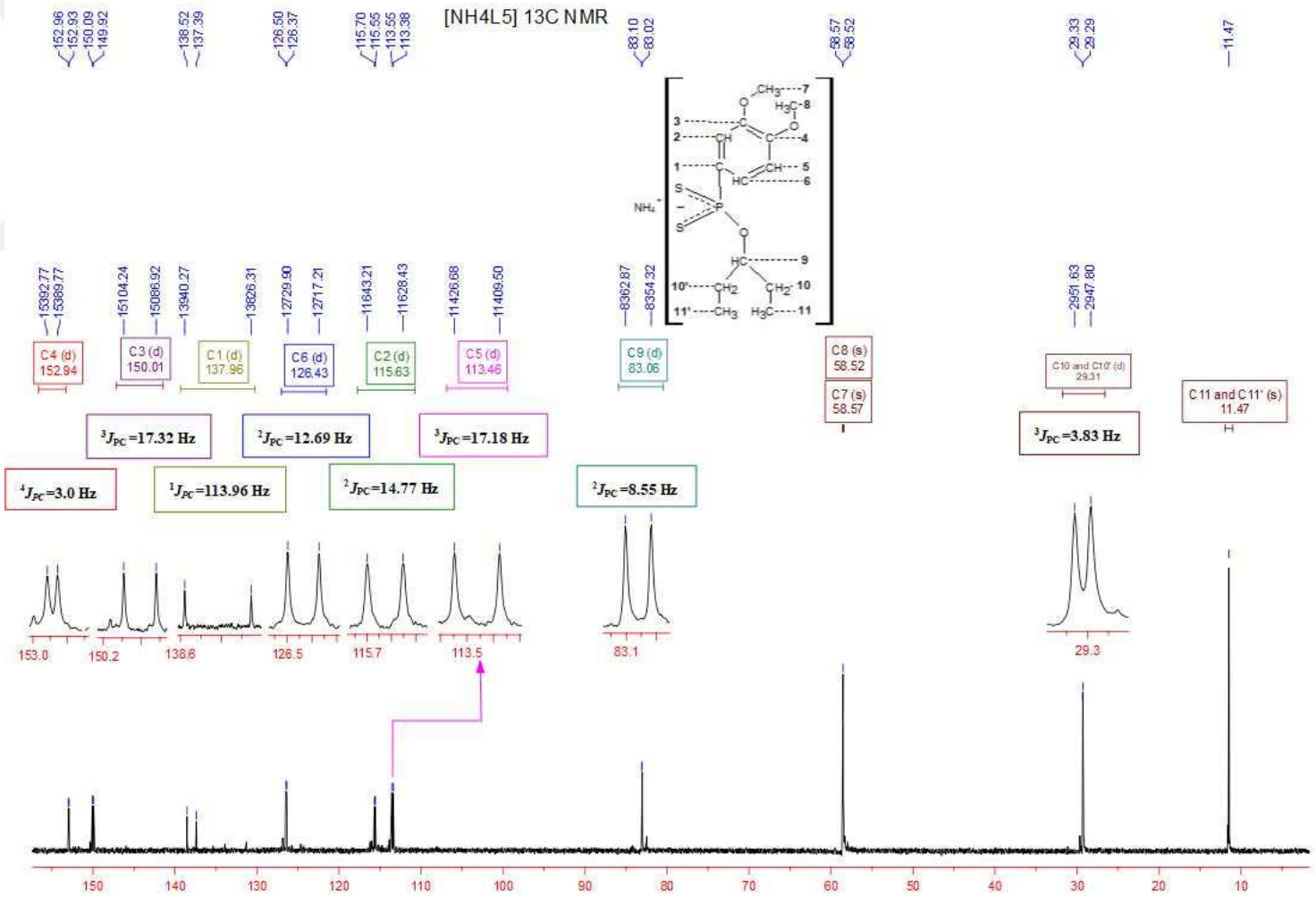


Figure 5.108. $[NH_4][S_2P(R^x)(OR5)]$ ^{13}C-NMR spectrum.

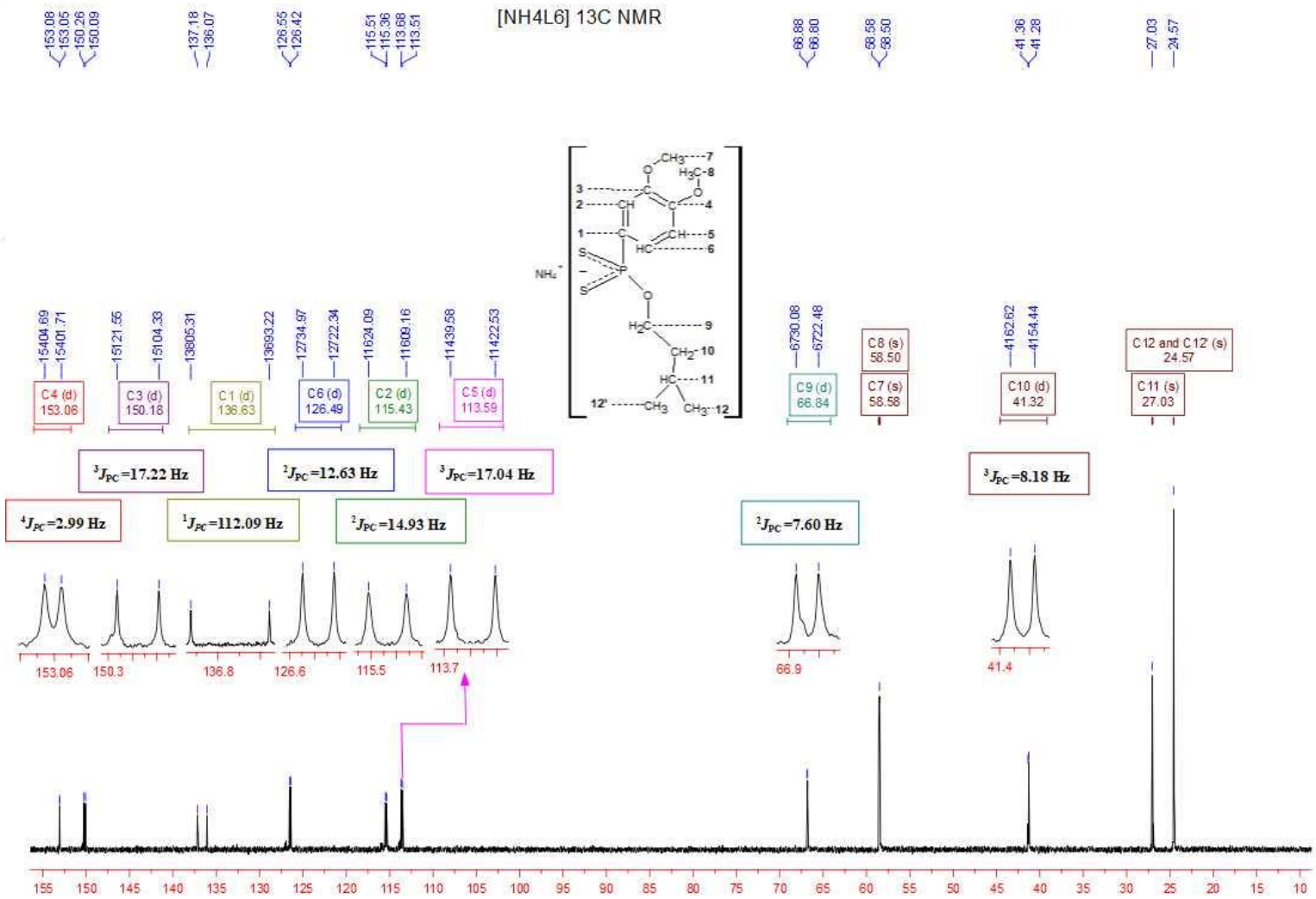


Figure 5.109. $[NH_4][S_2P(R^x)(OR6)]$ ^{13}C-NMR spectrum.

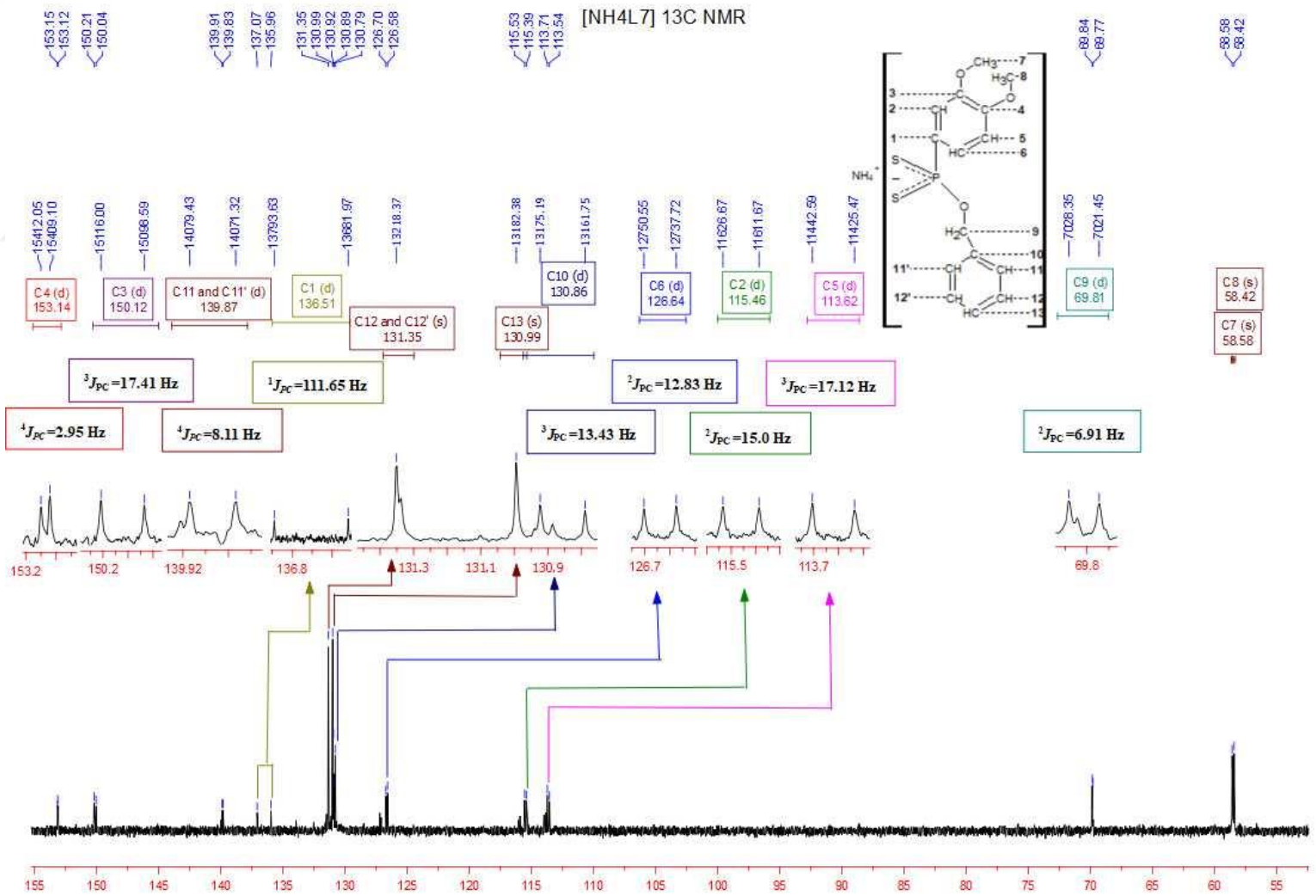


Figure 5.110. $[NH_4][S_2P(R^x)(OR7)]$ ^{13} -NMR spectrum.

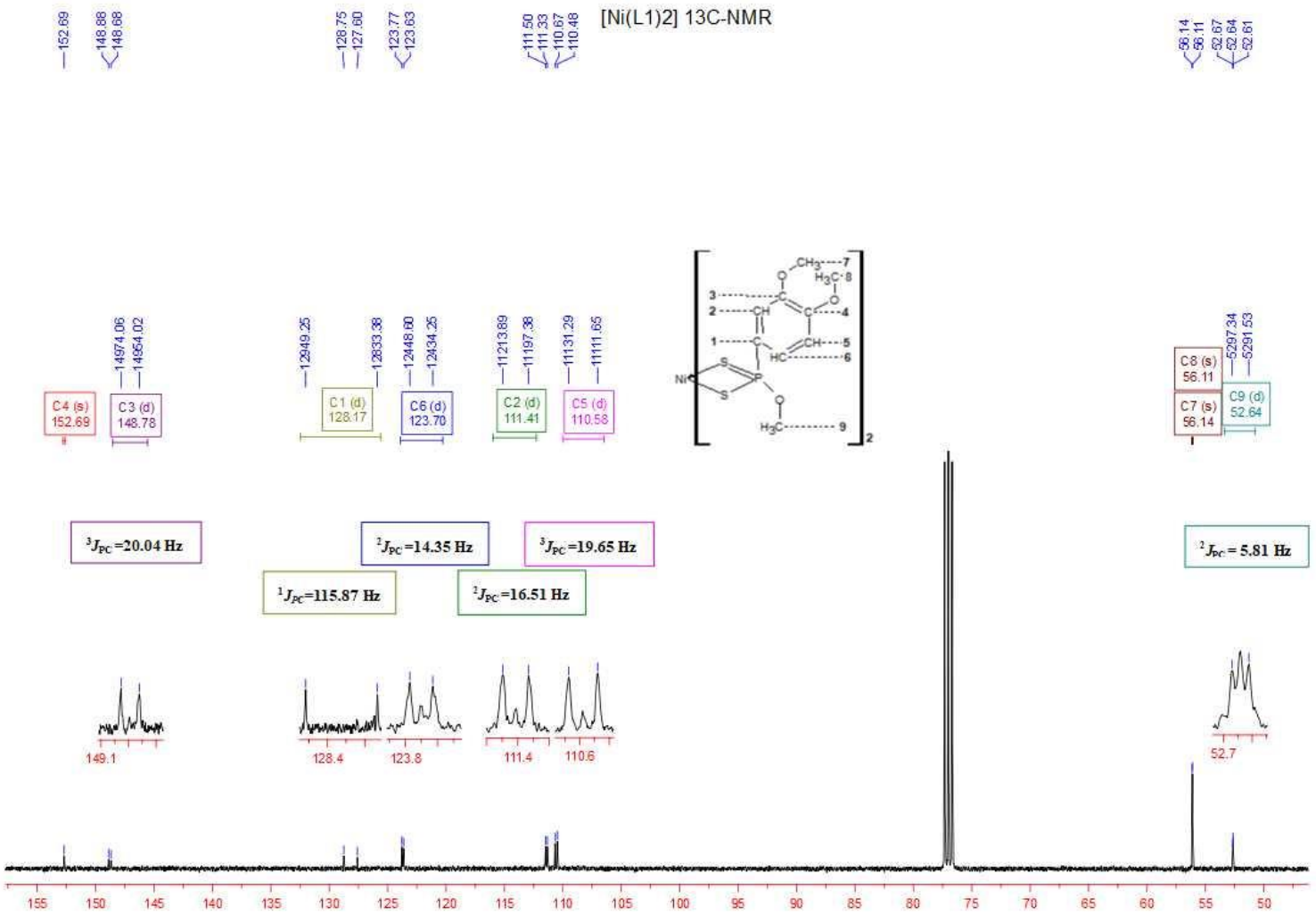


Figure 5.111. [Ni($S_2P(R^x)(OR1))_2$] ^{13}C-NMR spectrum.

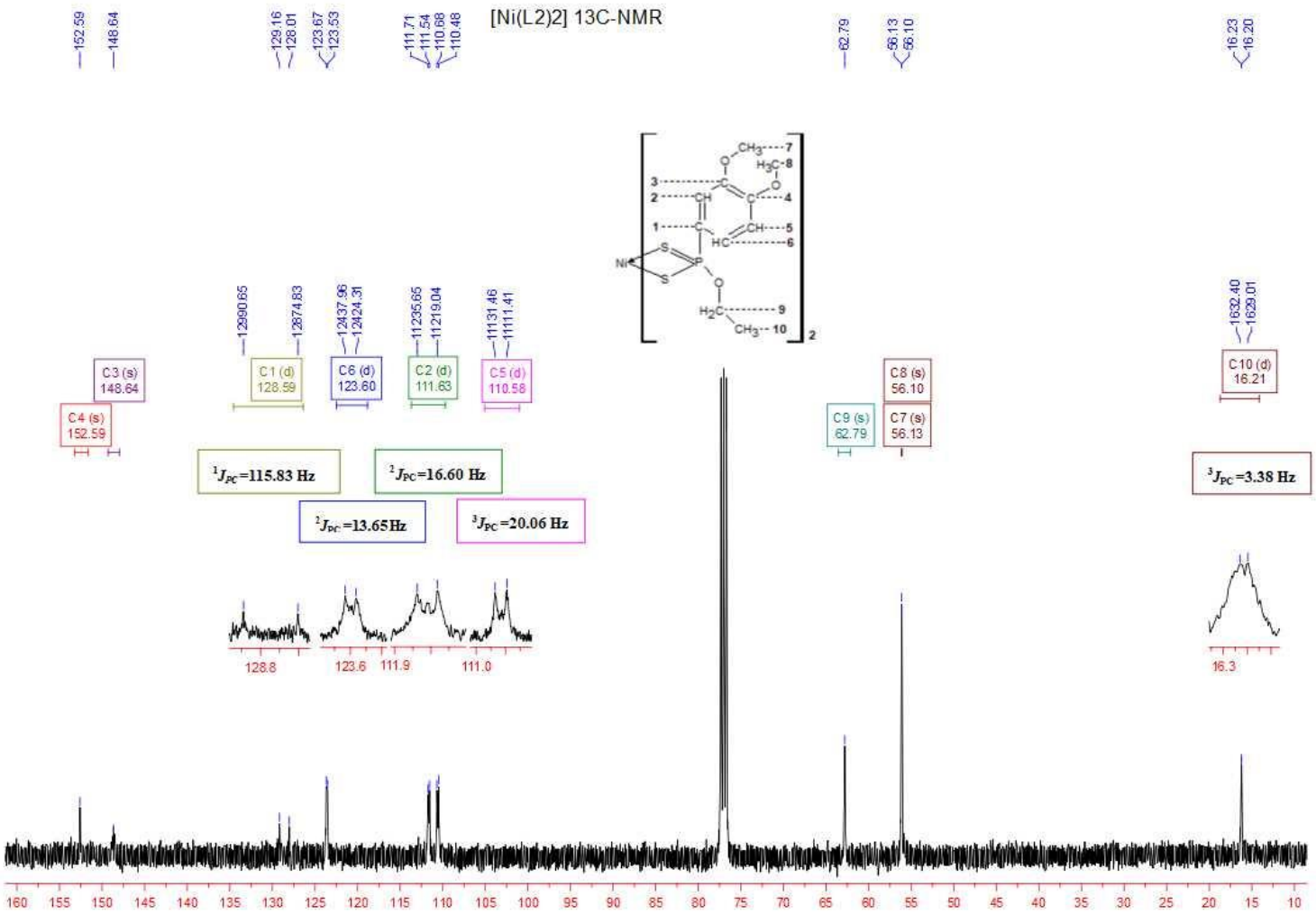


Figure 5.112. $[Ni(S_2P(R^x)(OR2))_2]$ ^{13}C-NMR spectrum.

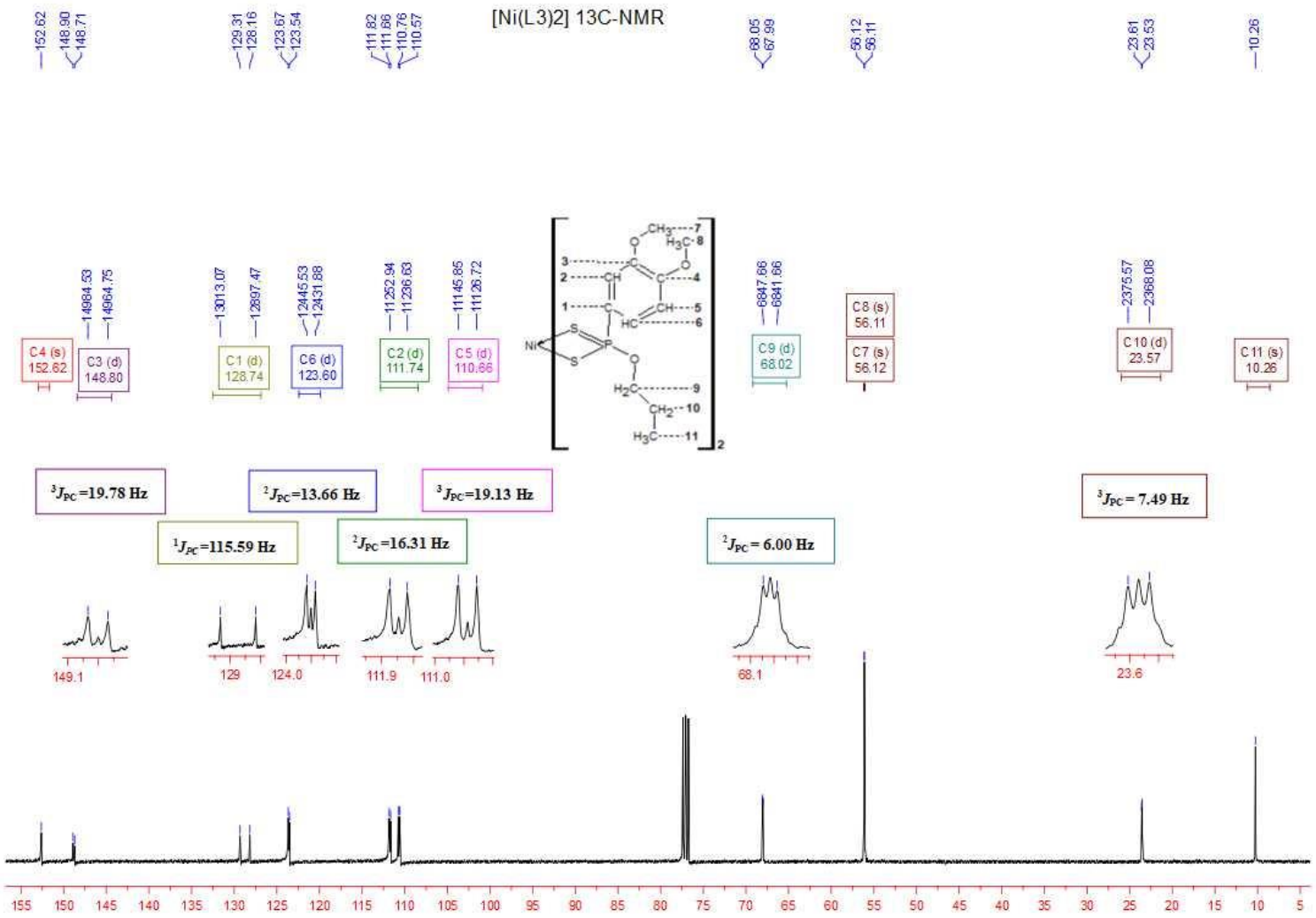


Figure 5.113. [Ni($S_2P(R^x)(OR3))_2$] ^{13}C-NMR spectrum.

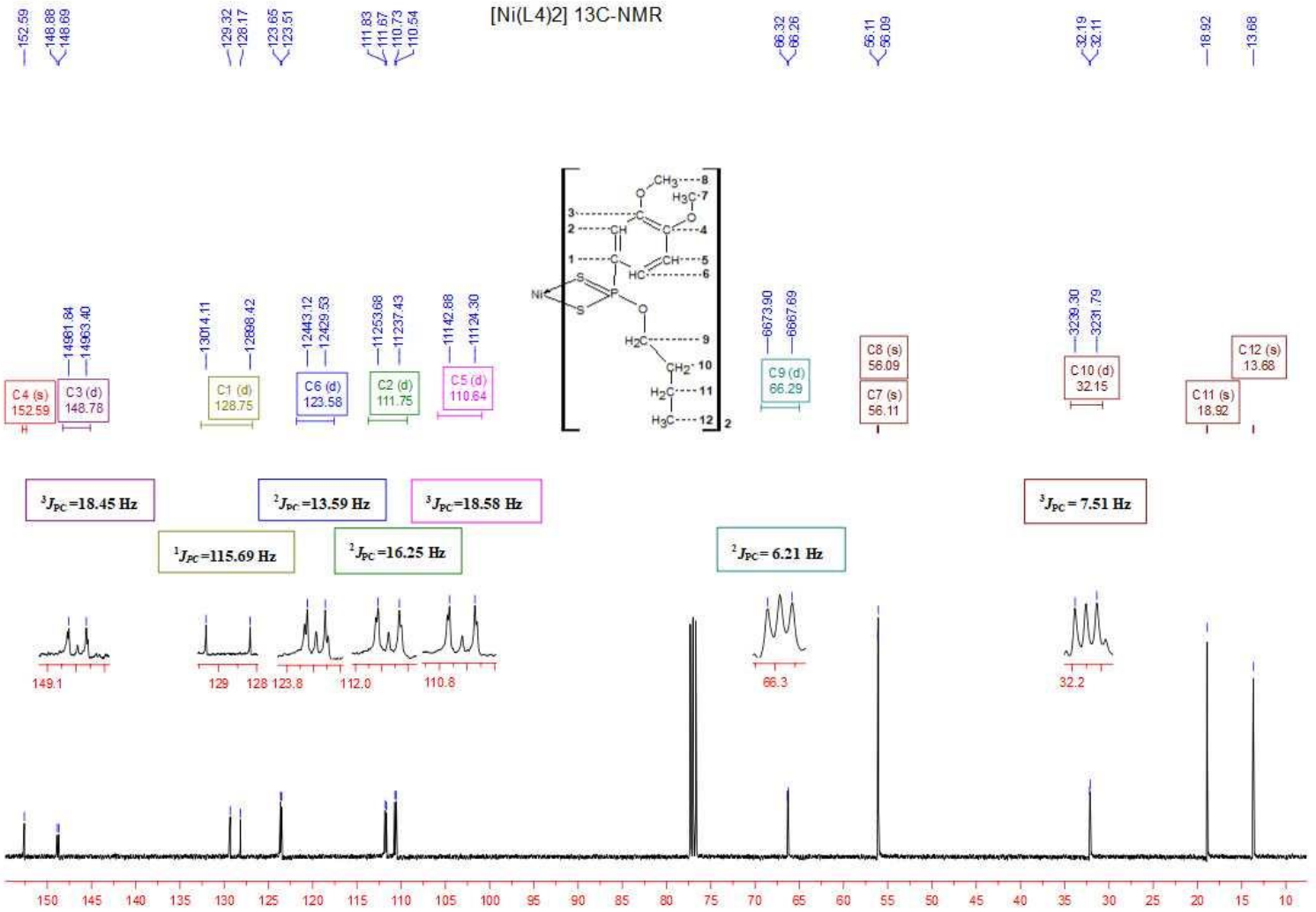


Figure 5.114. [Ni($S_2P(R^x)(OR4))_2$] ^{13}C-NMR spectrum.

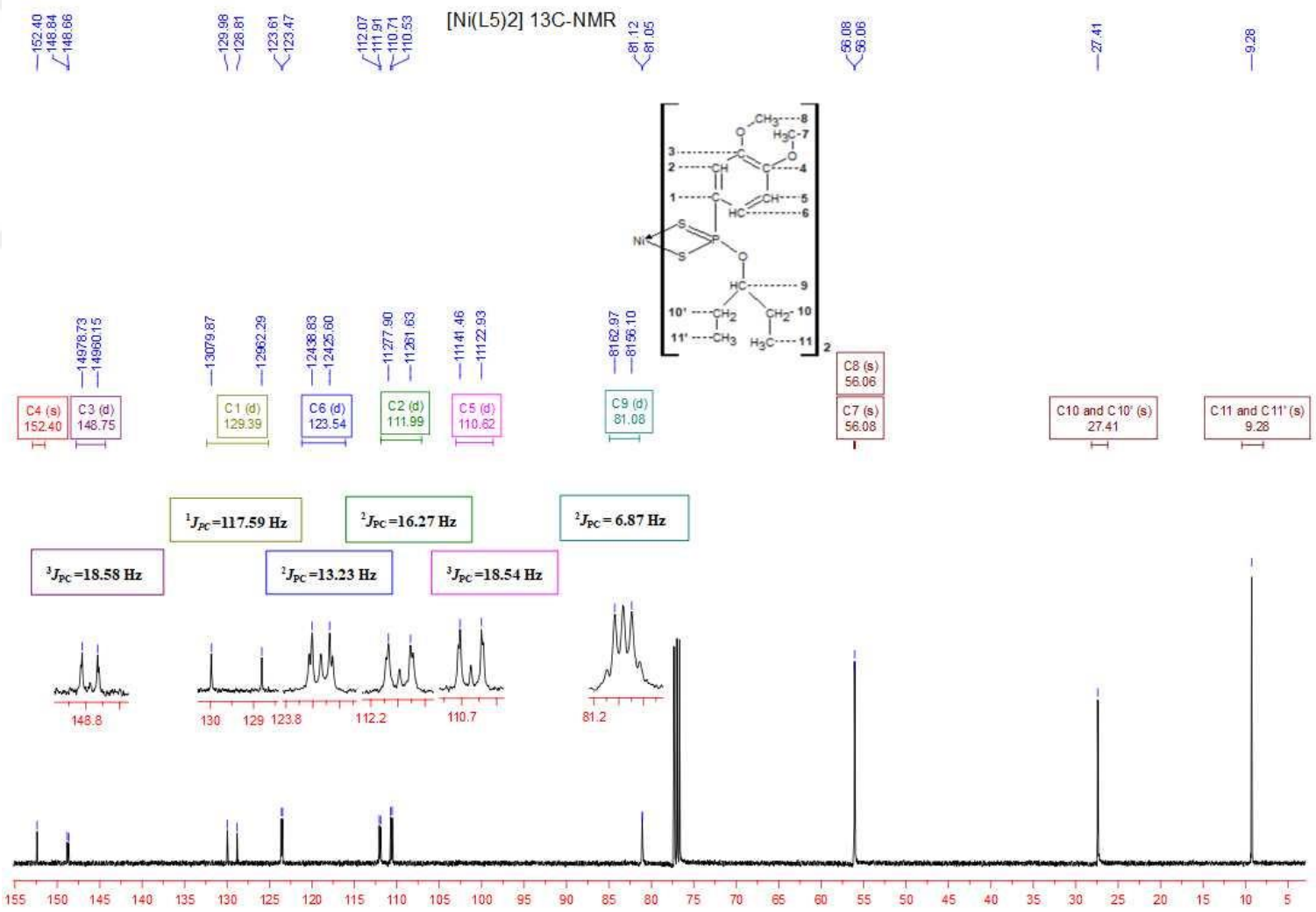


Figure 5.115. $[Ni(S_2P(R^x)(OR5))_2]$ ^{13}C-NMR spectrum.

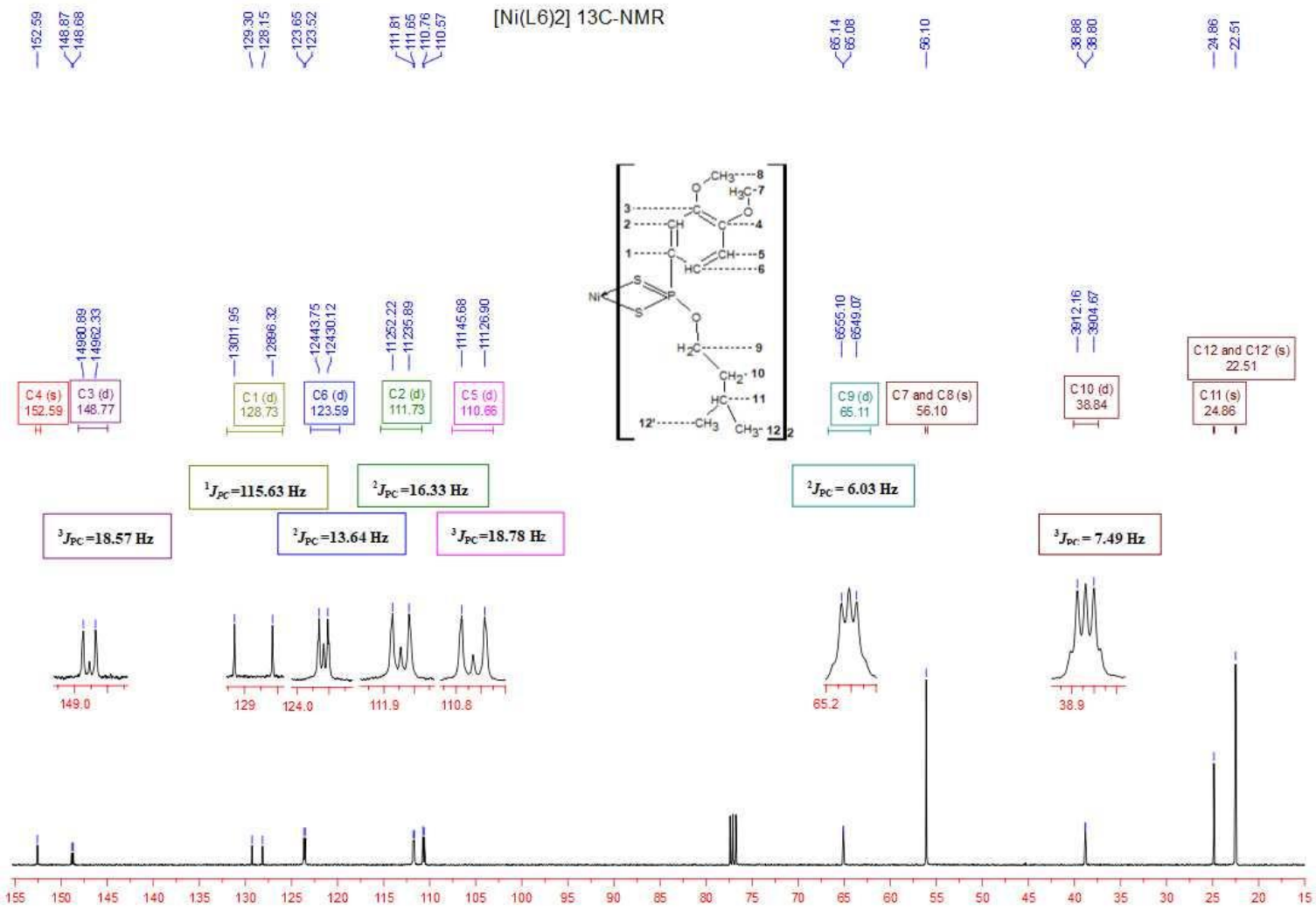


Figure 5.116. [Ni($S_2P(R^x)(OR6))_2$] ^{13}C-NMR spectrum.

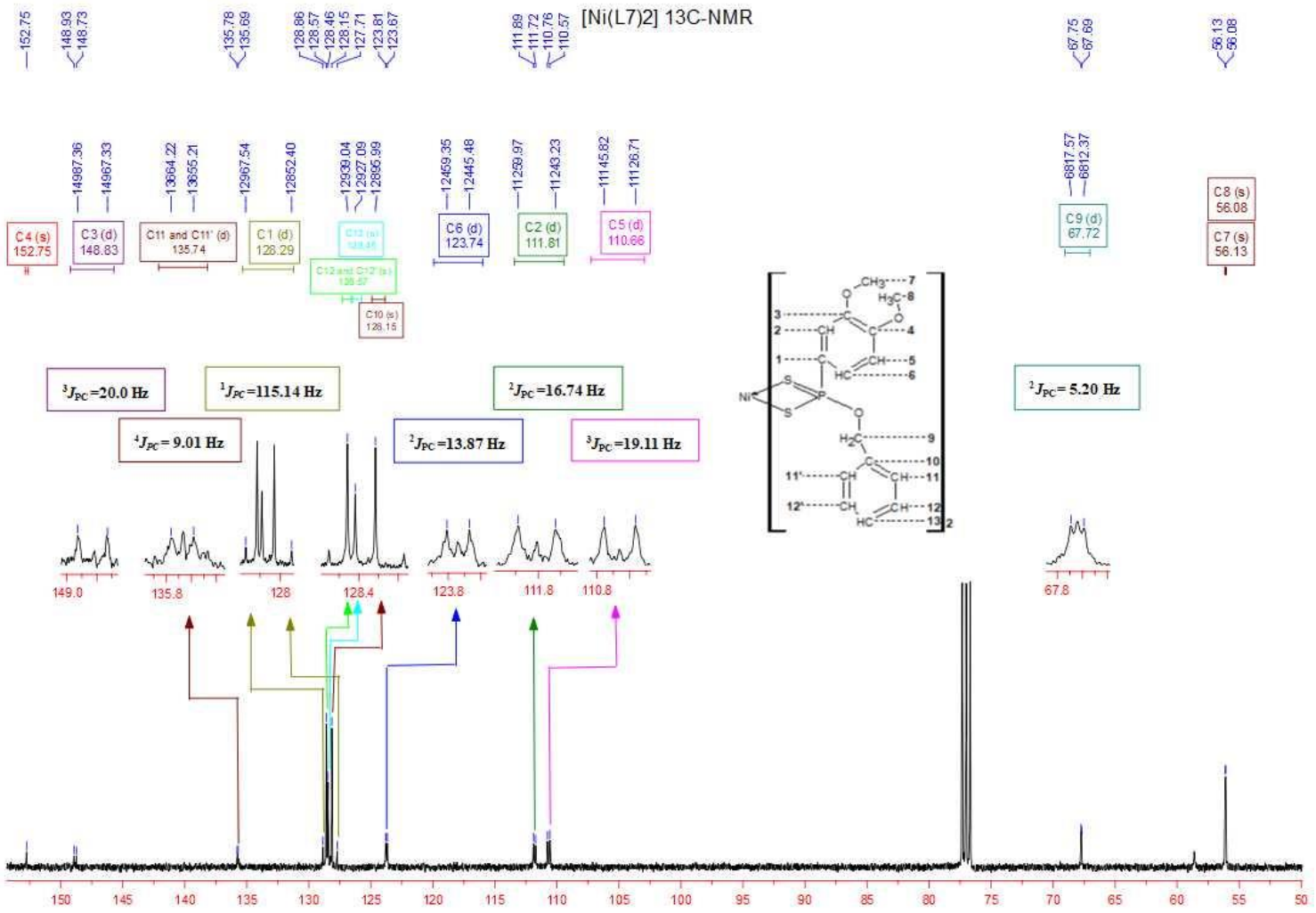


Figure 5.117. $[Ni(S_2P(R^x)(OR7))_2]$ ^{13}C-NMR spectrum.

5.1.7.8. Comments on ^{13}C-NMR Spectra of Part Ib' Compounds

In the ^{13}C-NMR spectra of the ligands, the two bond P-***C*** ($^{2}J_{PC}$) couplings for the carbon atoms in the 3,4-dimethoxyphenyl ring, namely $\boldsymbol{C}_2$ and $\boldsymbol{C}_6$ are in the range 13.8-14.9 Hz and 16.9-17.1 Hz, respectively. For Ni(II) complexes, the same couplings appear in the range 13.8-14.9 Hz and 16.9-17.1 Hz, respectively. These values are comparable to those reported for similar structures [131]. The three bond P-***C*** ($^{3}J_{PC}$) couplings for the $\boldsymbol{C}_3$ and $\boldsymbol{C}_5$ atoms in the ligands are ~17.3 Hz and ~17.0 Hz, respectively. These values are the same with those observed for the complexes. Interestingly, the two-bond P-***C*** coupling values for the $\boldsymbol{C}_2$ and $\boldsymbol{C}_6$ atoms are lower than the three-bond P-***C*** couplings of $\boldsymbol{C}_3$ and $\boldsymbol{C}_5$ atoms; a case reported in the literature for similar structures [132].

The NMR spectra and important NMR data for the ligands and their nickel(II) complexes are presented in Tables 5.10. Spectrum peaks of ^{13}C-NMR are given in Figure 5.118-5.127.

Table 5.10. Part Ib ^{13}C-NMR data of $[NH_4][S_2P(R^x)(ORn)]$ (D_2O) and $[Ni(S_2P(R^x)(ORn))_2]$ ($CDCl_3$) (δ in ppm, J in Hz).

$[NH_4][S_2P(R^x)(OR1)]$	$[NH_4][S_2P(R^x)(OR2)]$	$[NH_4][S_2P(R^x)(OR3)]$	$[NH_4][S_2P(R^x)(OR4)]$	$[NH_4][S_2P(R^x)(OR5)]$		$[Ni(S_2P(R^x)(OR1))_2]$	$[Ni(S_2P(R^x)(OR2))_2]$	$[Ni(S_2P(R^x)(OR3))_2]$	$[Ni(S_2P(R^x)(OR4))_2]$	$[Ni(S_2P(R^x)(OR4))_2]$
136.7, J_{PC}= 111.3	137.6, J_{PC}= 113.0	136.7, J_{PC}= 111.2	134.2, J_{PC}= 145.1	134.7, J_{PC}= 113.7	C_1	128.9, J_{PC}= 115.5	129.2, J_{PC}= 117.0	128.4, J_{PC}= 114.9	129.0, J_{PC}= 116.6	129.2, J_{PC}= 117.0
115.5, $^2J_{PC}$= 14.9	115.7, $^2J_{PC}$= 14.8	115.7, $^2J_{PC}$= 14.9	116.1, $^2J_{PC}$= 13.8	112.7, $^2J_{PC}$= 147.2	C_2	111.9, $^2J_{PC}$= 16.2	119.9, $^2J_{PC}$= 16.5	119.9, $^2J_{PC}$= 17.0	119.9, $^2J_{PC}$= 16.3	119.9, $^2J_{PC}$= 16.2
150.2, $^3J_{PC}$= 17.3	150.0, $^3J_{PC}$= 17.3	150.0,$^3J_{PC}$= 17.3	150.4, $^3J_{PC}$= 17.6	147.2, $^3J_{PC}$= 17.3	C_3	148.8, $^3J_{PC}$= 18.3	148.8, $^3J_{PC}$= 18.8	148.8, $^3J_{PC}$= 19.0	148.8, $^3J_{PC}$= 18.6	148.8, $^3J_{PC}$= 18.6
153.1, $^4J_{PC}$= 3.0	153.0, $^4J_{PC}$= 3.0	152.9, $^4J_{PC}$= 2.9	153.2, $^4J_{PC}$= 3.2	150.1, $^4J_{PC}$= 3.0	C_4	152.7	152.4	152.7	152.5	152.5
113.7, $^3J_{PC}$= 17.1	113.5, $^3J_{PC}$= 17.1	113.2, $^3J_{PC}$= 16.9	114.0, $^3J_{PC}$= 16.9	110.7, $^3J_{PC}$= 17.1	C_5	110.7, $^3J_{PC}$= 18.5	110.6, $^3J_{PC}$= 18.6	110.6, $^3J_{PC}$= 18.9	110.6, $^3J_{PC}$= 18.5	110.6, $^3J_{PC}$= 18.6
126.5, $^2J_{PC}$= 12.6	126.6, $^2J_{PC}$= 12.7	126.5, $^2J_{PC}$= 12.3	126.9, $^2J_{PC}$= 11.2	123.6, $^2J_{PC}$= 12.6	C_6	123.6, $^2J_{PC}$= 13.6	123.5, $^2J_{PC}$= 13.4	123.8, $^2J_{PC}$= 13.9	123.6, $^2J_{PC}$= 13.4	123.6, $^2J_{PC}$= 13.3
58.6	58.6	58.4	58.6	55.7	C_7	56.1	56.1	56.2	56.1	56.1
58.5	58.5	58.3		55.6	C_8	56.1		56.1	56.1	
68.4, $^2J_{PC}$= 7.7	77.0, $^2J_{PC}$= 8.0	69.4, $^2J_{PC}$= 7.0	73.1, $^2J_{PC}$= 6.6	75.5, $^2J_{PC}$= 7.9	C_9	66.6, $^2J_{PC}$= 6.2	75.6, $^2J_{PC}$= 6.4	67.7, $^2J_{PC}$= 4.7	72.3, $^2J_{PC}$= 5.8	30.5, $^2J_{PC}$= 4.7
32.1, $^3J_{PC}$= 8.1	42.1, $^3J_{PC}$= 4.8	137.0, $^3J_{PC}$= 8.9	26.2, $^3J_{PC}$= 5.8	30.0, $^3J_{PC}$= 10.6	C_{10}	29.8.8, $^3J_{PC}$= 7.4	39.8, $^3J_{PC}$= 4.8	132.7, $^3J_{PC}$= 8.8	24.3, $^3J_{PC}$= 3.6	30.3, $^3J_{PC}$= 5.4
30.2	23.9, $^4J_{PC}$= 3.0	130.6	-	20.4, $^4J_{PC}$= 3.0	C_{11}	27.8	22.4	128.1	-	21.8
24.4	20.8	127.5	-	8.9, $^3J_{PC}$= 2.8	C_{12}	22.2	18.6	125.5	-	9.6
16.1	16.1	152.8	-	-	C_{13}	13.9	14.1	151.6	-	-
-	-	36.5	-	-	C_{14}	-	-	34.6	-	-
-	-	33.6	-	-	C_{15}	-	-	31.3	-	-

^{13}C-NMR Spectra of Part Ib [NH_4][$S_2P(R^x)(ORn)$] and [$Ni(S_2P(R^x)(ORn))_2$] Compounds.

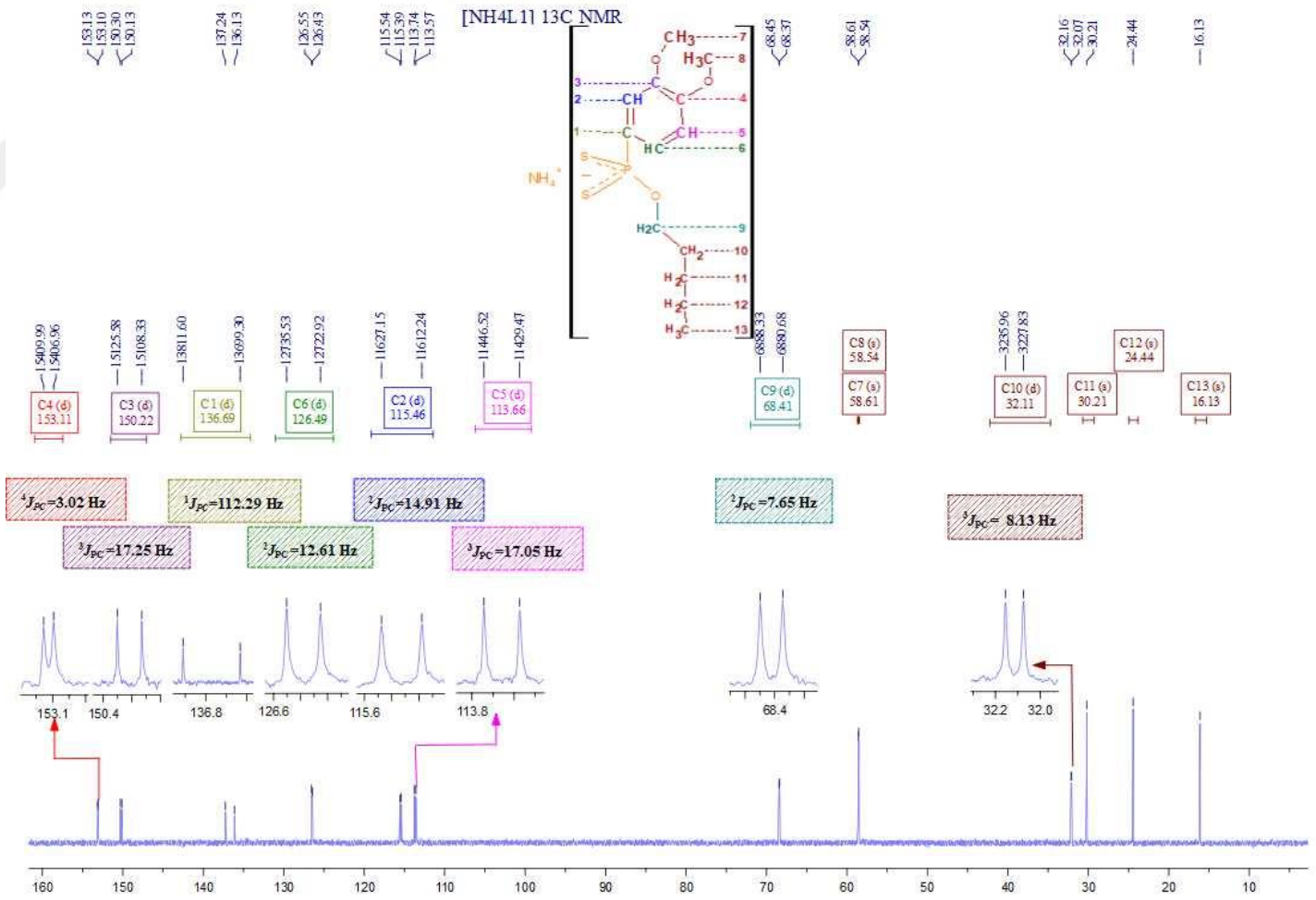


Figure 5.118. [NH_4][$S_2P(R^x)(OR1)$] ^{13}C-NMR spectrum.

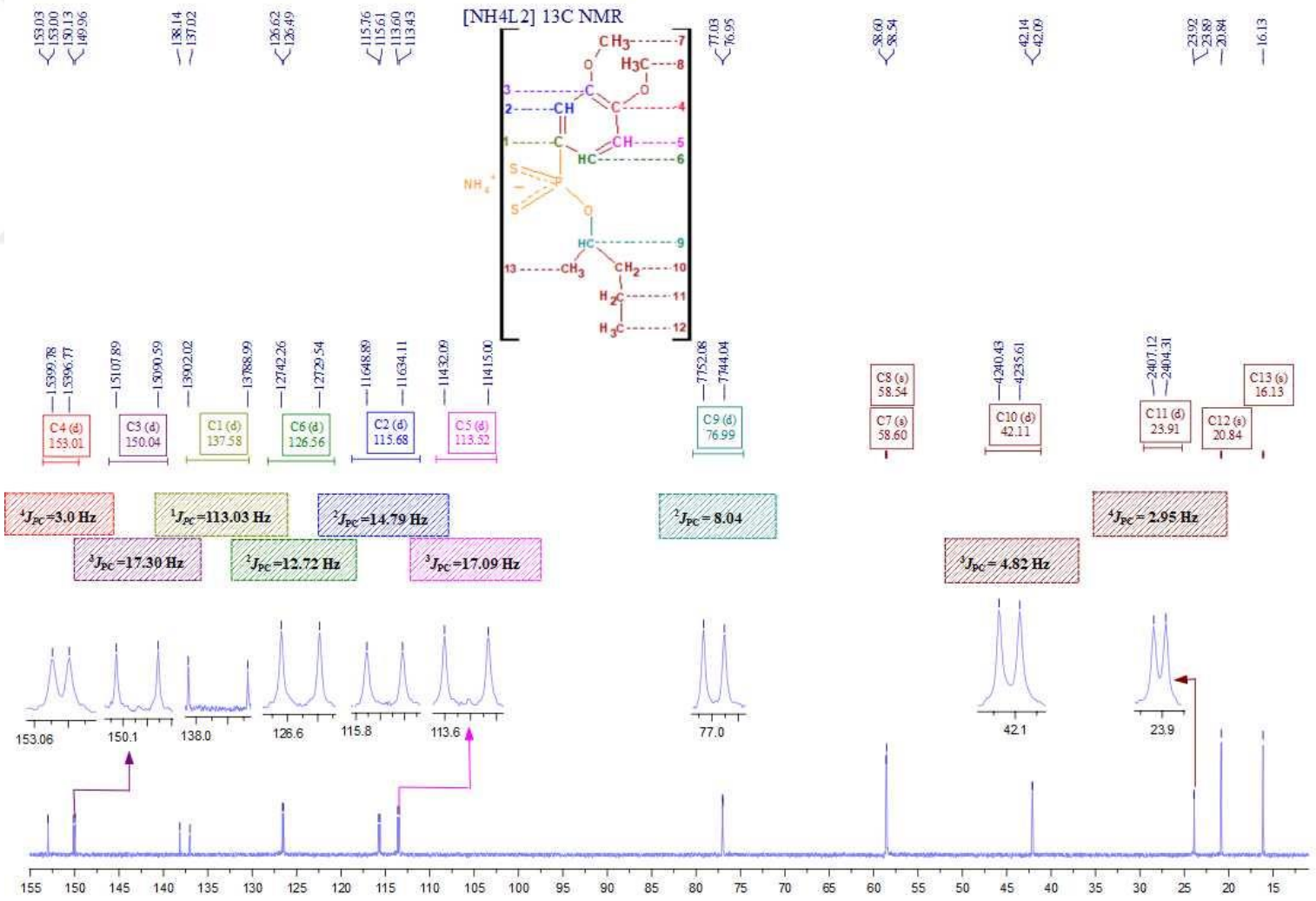


Figure 5.119. $[NH_4][S_2P(R^x)(OR2)]$ ^{13}C-NMR spectrum.

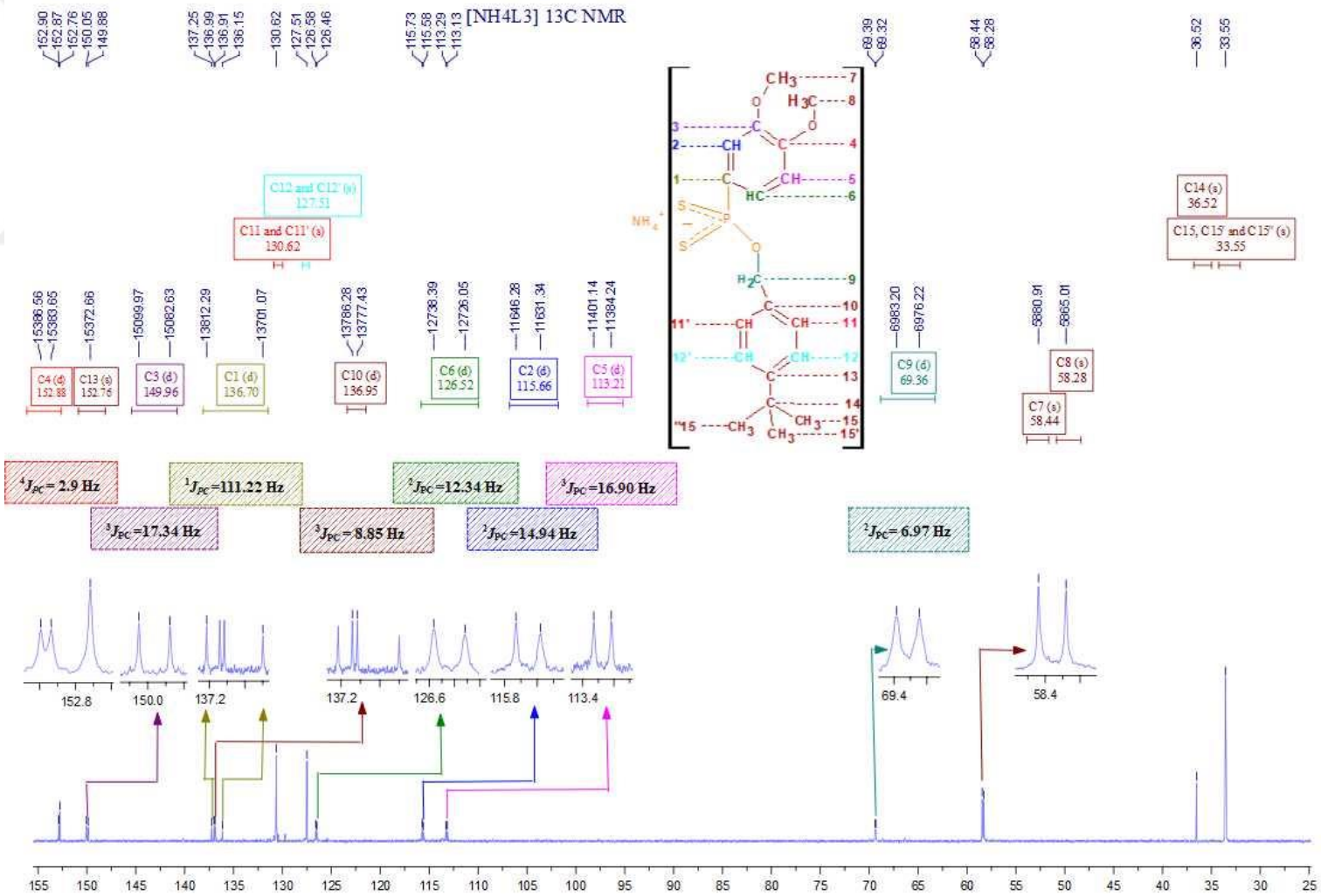


Figure 5.120. $[NH_4][S_2P(R^x)(OR3)]$ ^{13}C-NMR spectrum.

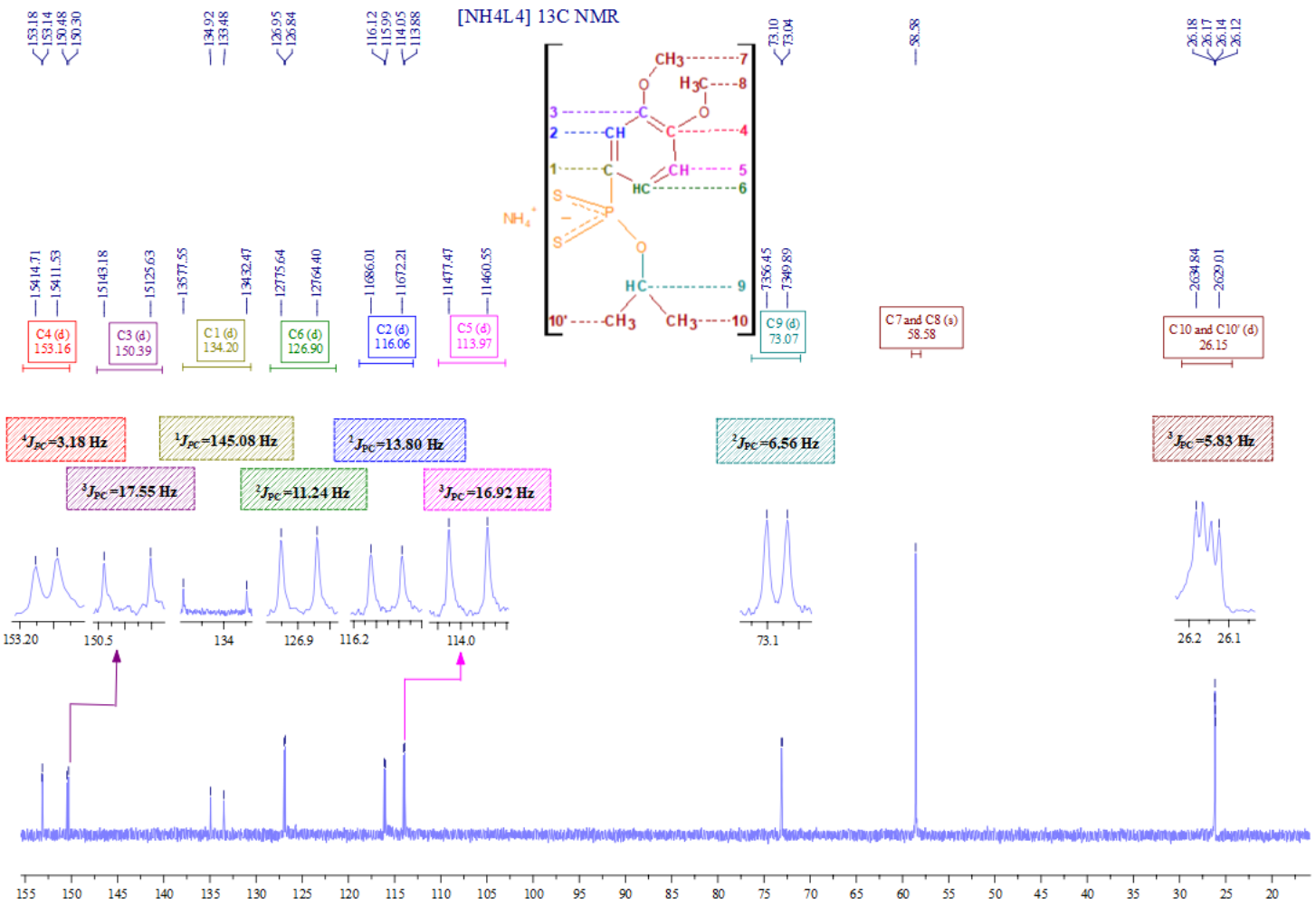


Figure 5.121. $[NH_4][S_2P(R^x)(OR4)]$ ^{13}C-NMR spectrum.

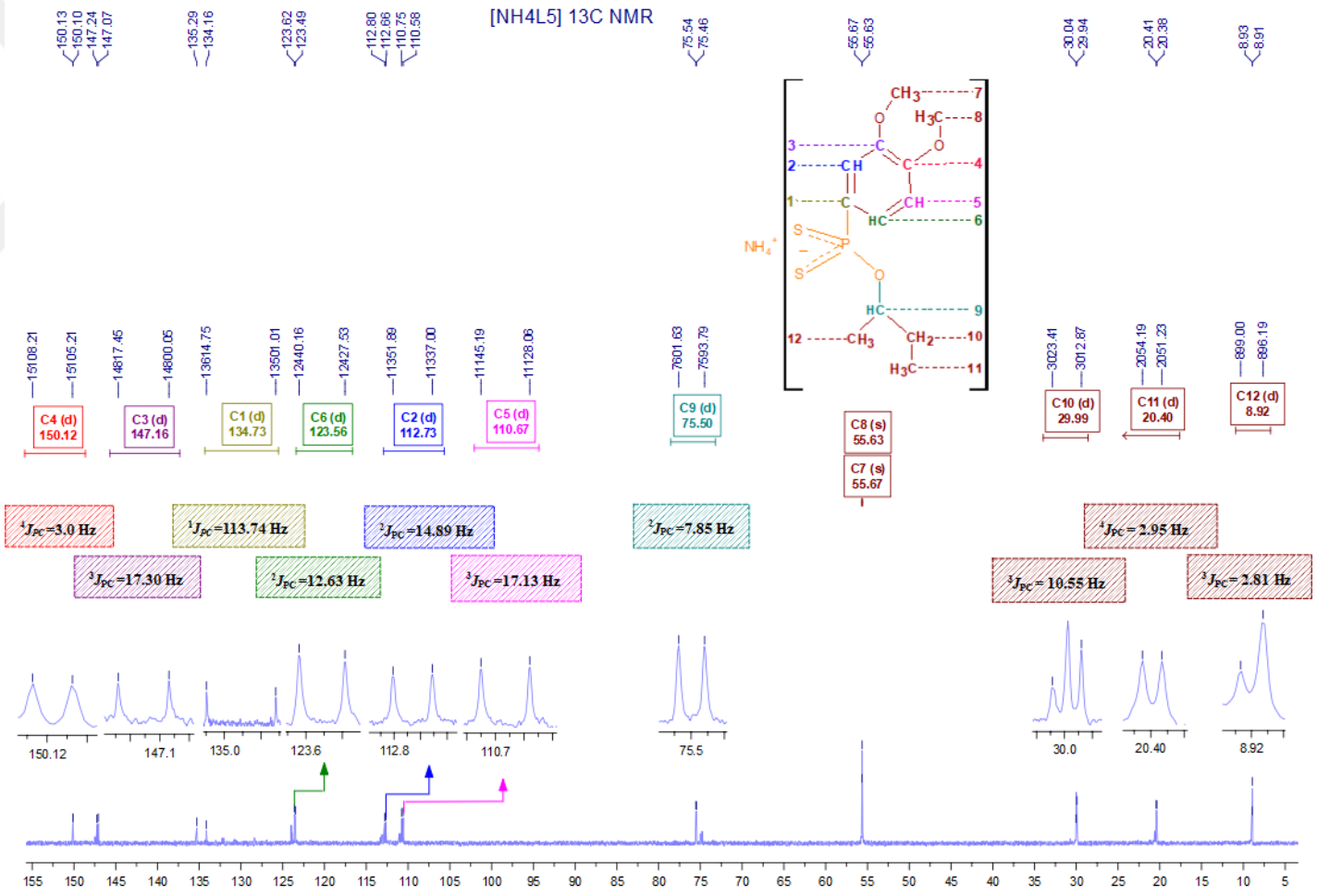


Figure 5.122. $[NH_4][S_2P(R^x)(OR5)]$ ^{13}C-NMR spectrum.

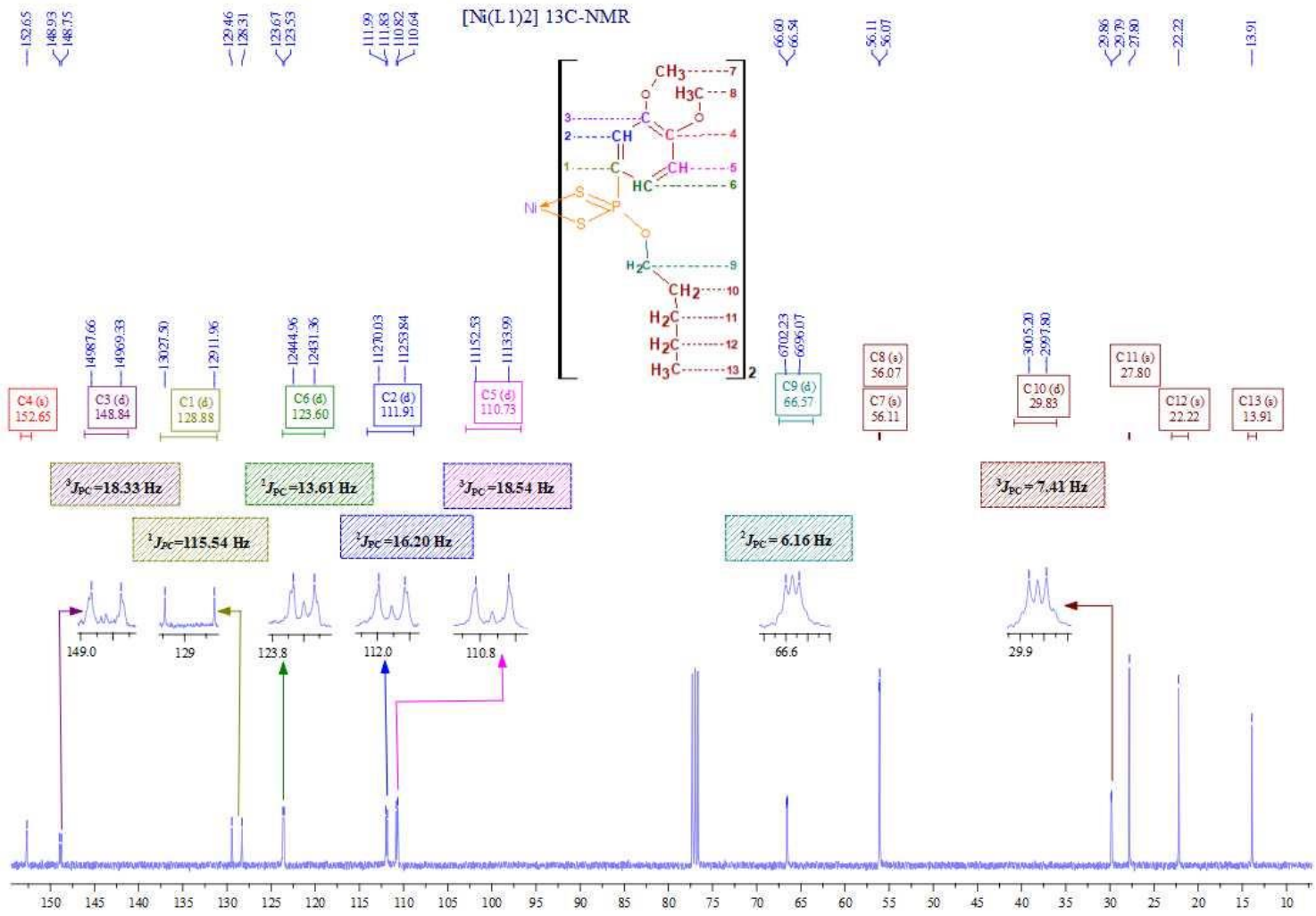


Figure 5.123. [Ni($S_2P(R^x)(OR1))_2$] ^{13}C-NMR spectrum.

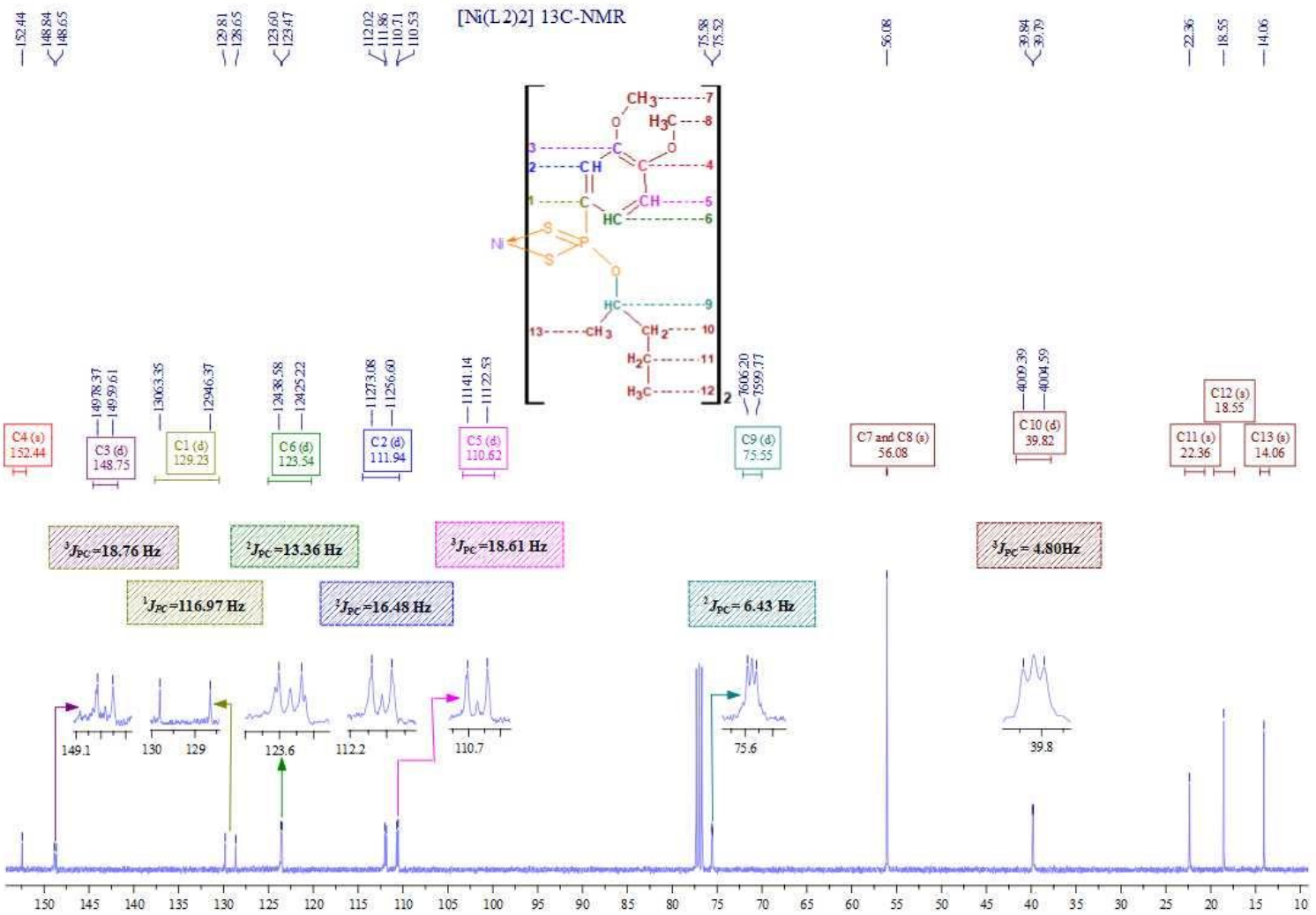


Figure 5.124. $[Ni(S_2P(R^x)(OR2))_2]$ ^{13}C-NMR spectrum.

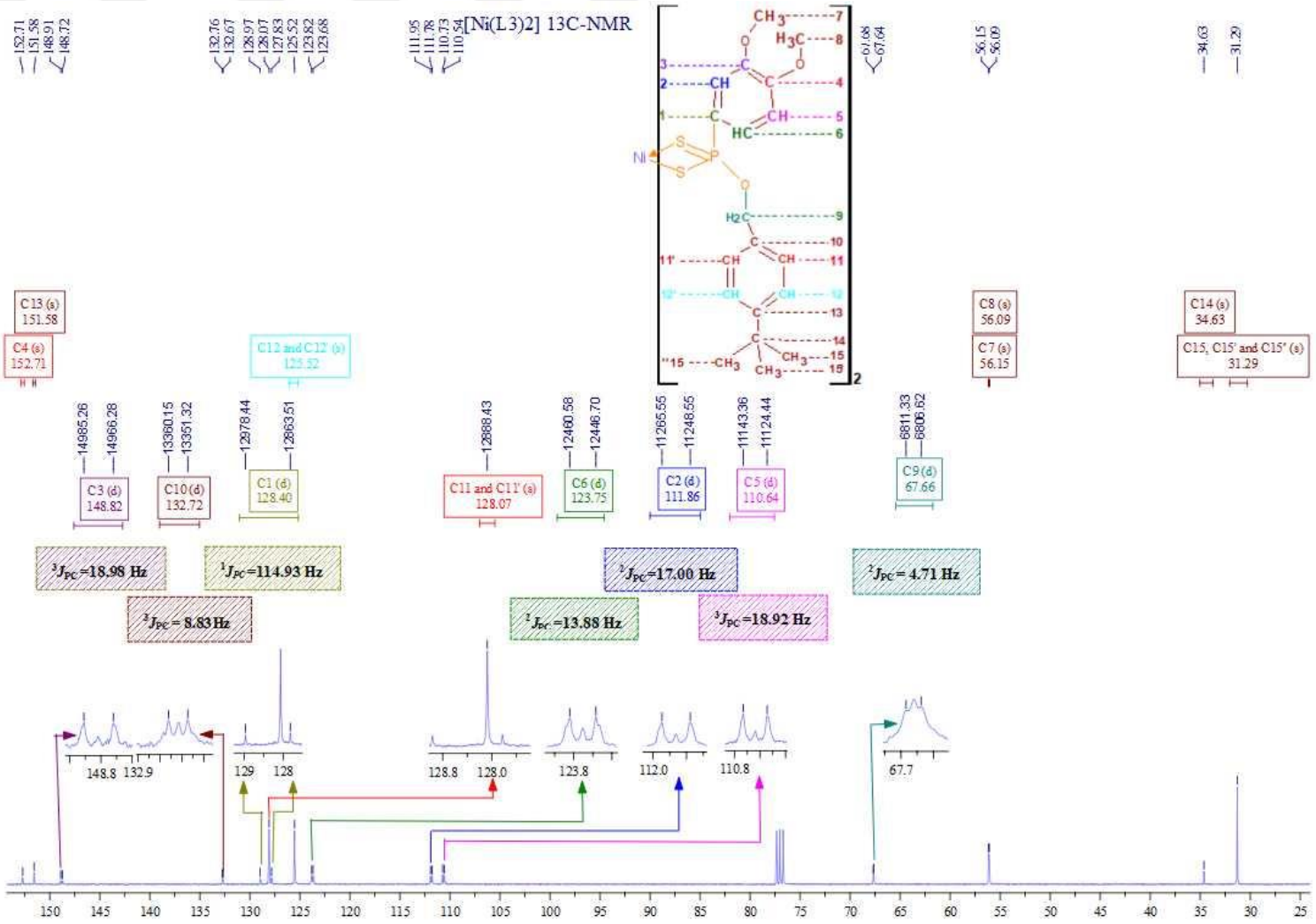


Figure 5.125. $[Ni(S_2P(R^x)(OR3))_2]$ ^{13}C-NMR spectrum.

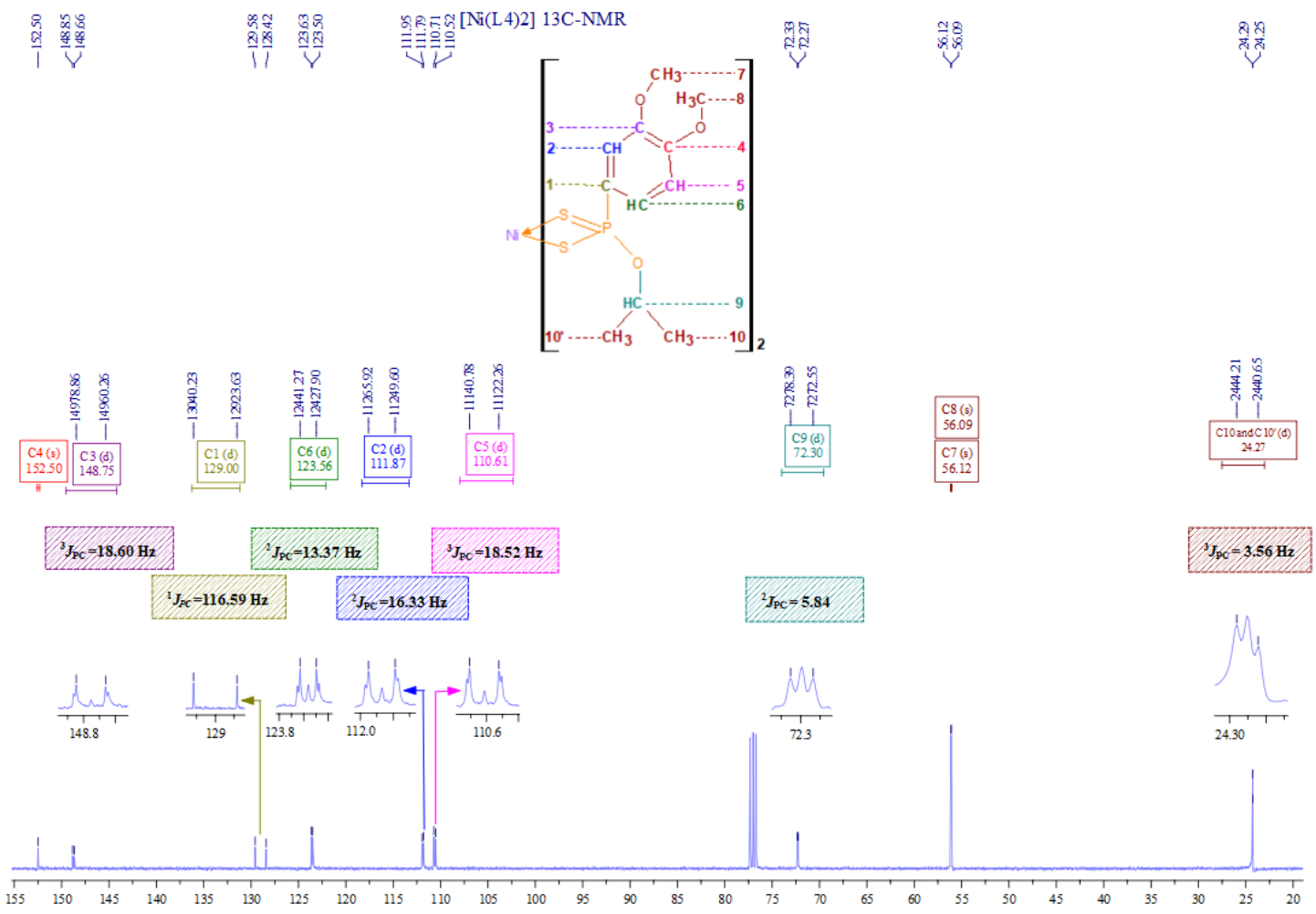


Figure 5.126. $[Ni(S_2P(R^x)(OR4))_2]$ ^{13}C-NMR spectrum.

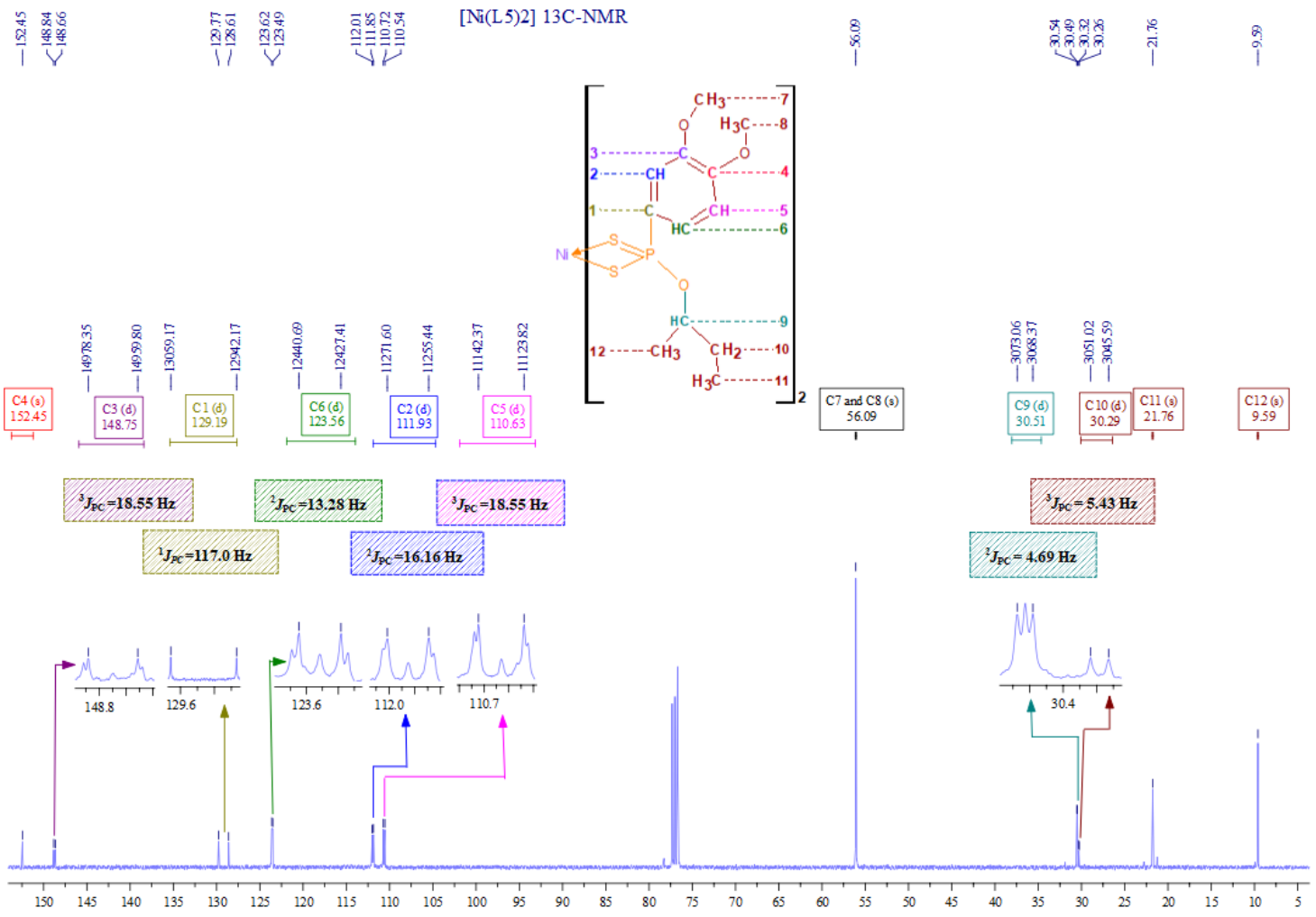


Figure 5.127. [Ni($S_2P(R^x)(OR5)$)$_2$] ^{13}C-NMR spectrum.

5.1.7.9. Comments on ^{13}C-NMR Spectra of the Part II' Compounds

As given in Table 5.11, on the ^{13}C-NMR spectra of the ligands, the signals of the neighboring carbons $\boldsymbol{C}_5$ and $\boldsymbol{C}_6$ are split by the phosphorus in the ranges reported [131] for the two-bond P-***C*** coupling ($^2J_{PC}$= 12.3-13.0 Hz) and the three-bond P-***C*** coupling ($^3J_{PC}$= 14.8-15.0 Hz), respectively. As is the case in many similar structures, the three-bond P-***C*** coupling displayed by the nuclei $\boldsymbol{C}_5$ ($^3J_{PC}$= 14.8-15.0 Hz) is higher than the two-bond couplings of $\boldsymbol{C}_6$ ($^3J_{PC}$= 12.3-13.0 Hz).

Similar trends in the coupling patterns of the 2,4-dimethoxyphenyl ring protons are observed in the ^{13}C-NMR spectra of the complexes.

Table 5.11 ^{13}C-NMR data of the compounds. (D_2O for $[NH_4][S_2P(R^y)(ORn)]$, $CDCl_3$ for $[Ni(S_2P(R^y)(ORn))_2]$; δ in ppm, J in Hz).

	$[NH_4][S_2P(R^y)(OR1)]$	$[NH_4][S_2P(R^y)(OR2)]$	$[NH_4][S_2P(R^y)(OR3)]$	$[NH_4][S_2P(R^y)(OR4)]$	$[Ni(S_2P(R^x)(OR1))_2]$	$[Ni(S_2P(R^x)(OR2))_2]$	$[Ni(S_2P(R^x)(OR3))_2]$	$[Ni(S_2P(R^x)(OR4))_2]$
C_1	124.3, J_{PC}= 114.0	123.3, J_{PC}= 111.0	125.9 overlaps with C11,11'	122.9, J_{PC}= 113.8	116.5, J_{PC}= 118.1	116.1, J_{PC}= 116.8	115.7, J_{PC}= 116.5	115.6, J_{PC}= 116.9
C_2	163.7, $^2J_{PC}$= 3.6	163.5, $^2J_{PC}$= 3.6	162.6, $^2J_{PC}$= 3.3	163.6, $^2J_{PC}$= 3.7	161.8	162.0	162.0	162.0
C_3	101.6, $^3J_{PC}$= 7.9	101.5, $^3J_{PC}$= 7.8	99.5, $^3J_{PC}$= 7.7	101.8, $^3J_{PC}$= 8.0	99.0, $^3J_{PC}$= 7.8	99.0, $^3J_{PC}$= 7.9	99.0, $^3J_{PC}$= 8.0	99.0, $^3J_{PC}$= 8.2
C_4	166.0, $^4J_{PC}$=2.8	166.0, $^4J_{PC}$= 2.9	164.8, $^4J_{PC}$= 2.1	166.2, $^4J_{PC}$= 2.8	164.9	164.9	165.1	165.1
C_5	107.1, $^3J_{PC}$= 15.0	107.2, $^3J_{PC}$= 14.8	107.2, $^3J_{PC}$= 14.8	107.6, $^3J_{PC}$= 14.9	104.3, $^3J_{PC}$= 18.1	104.3, $^3J_{PC}$= 16.9	104.4, $^3J_{PC}$= 16.8	104.4, $^3J_{PC}$= 18.2
C_6	137.6, $^2J_{PC}$= 13.0	137.8, $^2J_{PC}$= 12.7	136.5, $^2J_{PC}$= 12.3	137.6, $^2J_{PC}$= 12.7	134.3, $^2J_{PC}$= 15.3	134.2, $^2J_{PC}$= 14.6	134.3, $^2J_{PC}$= 14.8	134.4, $^2J_{PC}$= 14.5
C_7	58.4	58.4	55.8	54.0	55.6	55.8	55.8	56.0
C_8	58.0	58.2		53.9		55.6	55.6	55.6
C_9	78.2, $^2J_{PC}$= 7.9	68.4, $^2J_{PC}$= 7.9	66.9, $^2J_{PC}$= 6.0	55.7, $^2J_{PC}$= 7.0	76.2	66.3, $^2J_{PC}$= 6.2	67.3, $^2J_{PC}$=5.5	52.5, $^2J_{PC}$= 3.1
C_{10}	32.8, $^3J_{PC}$= 4.6	32.2, $^3J_{PC}$= 8.5	137.0, $^3J_{PC}$= 9.8	-	32.8, $^3J_{PC}$= 4.6	32.2, $^3J_{PC}$= 8.5	137.0, $^3J_{PC}$= 9.8	-
C_{11}	11.7	30.2	125.9 overlaps with C1	-	21.8	27.7	125.3	-
C_{12}	23.0, $^3J_{PC}$= 3.3	24.5	128.9	-	9.5	22.2	127.9	-
C_{13}	-	16.2	151.3	-	-	16.2	151.3	-
C_{14}	-	-	35.3	-	-	-	35.3	-
C_{15}	-	-	31.8	-	-	-	31.8	-

^{13}C-NMR Spectra of Part II [NH_4][$S_2P(R^x)(ORn)$] and [$Ni(S_2P(R^x)(ORn))_2$] Compounds.

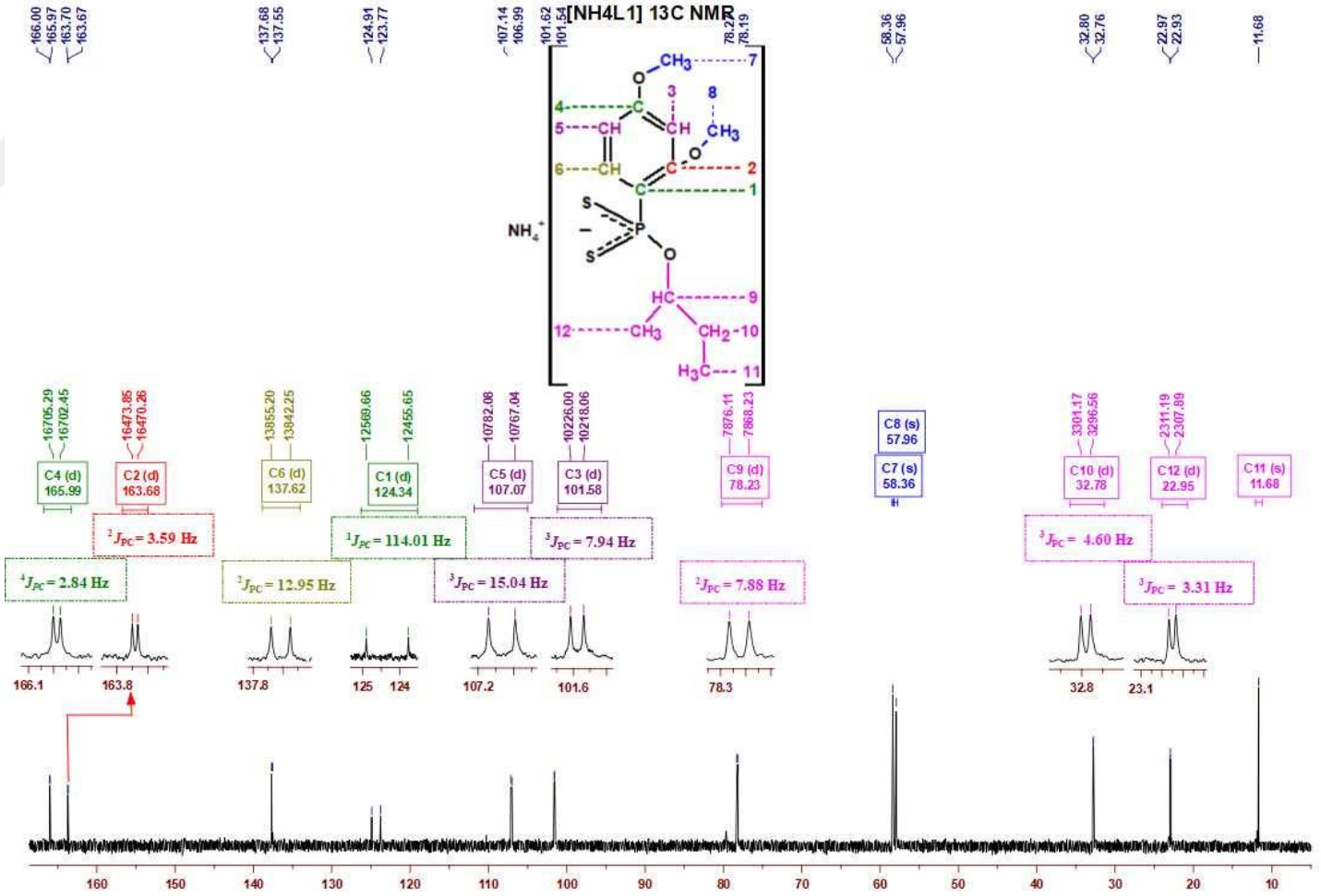


Figure 5.128. [NH_4][$S_2P(R^y)(OR1)$] ^{13}C-NMR spectrum.

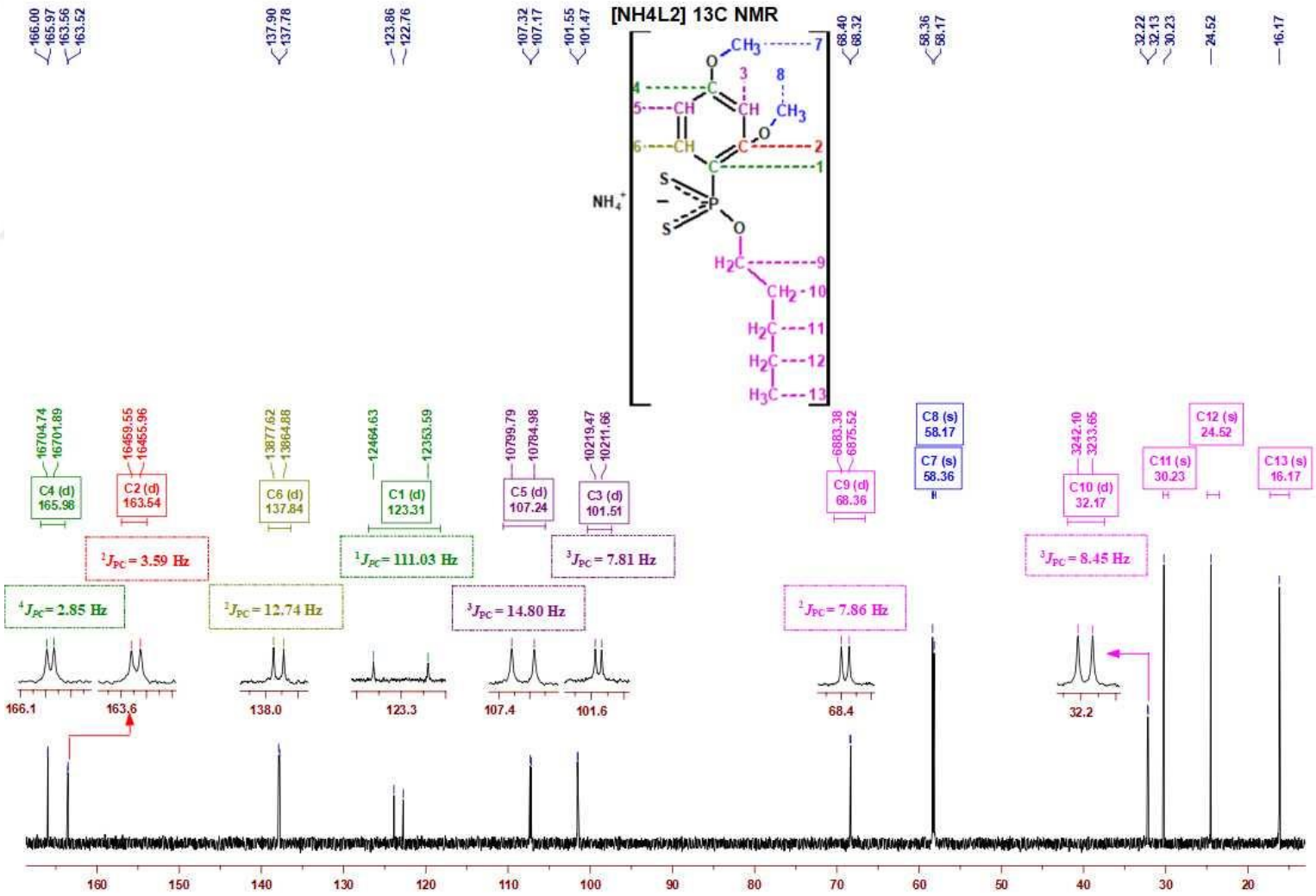


Figure 5.129. $[NH_4][S_2P(R^y)(OR2)]$ ^{13}C-NMR spectrum.

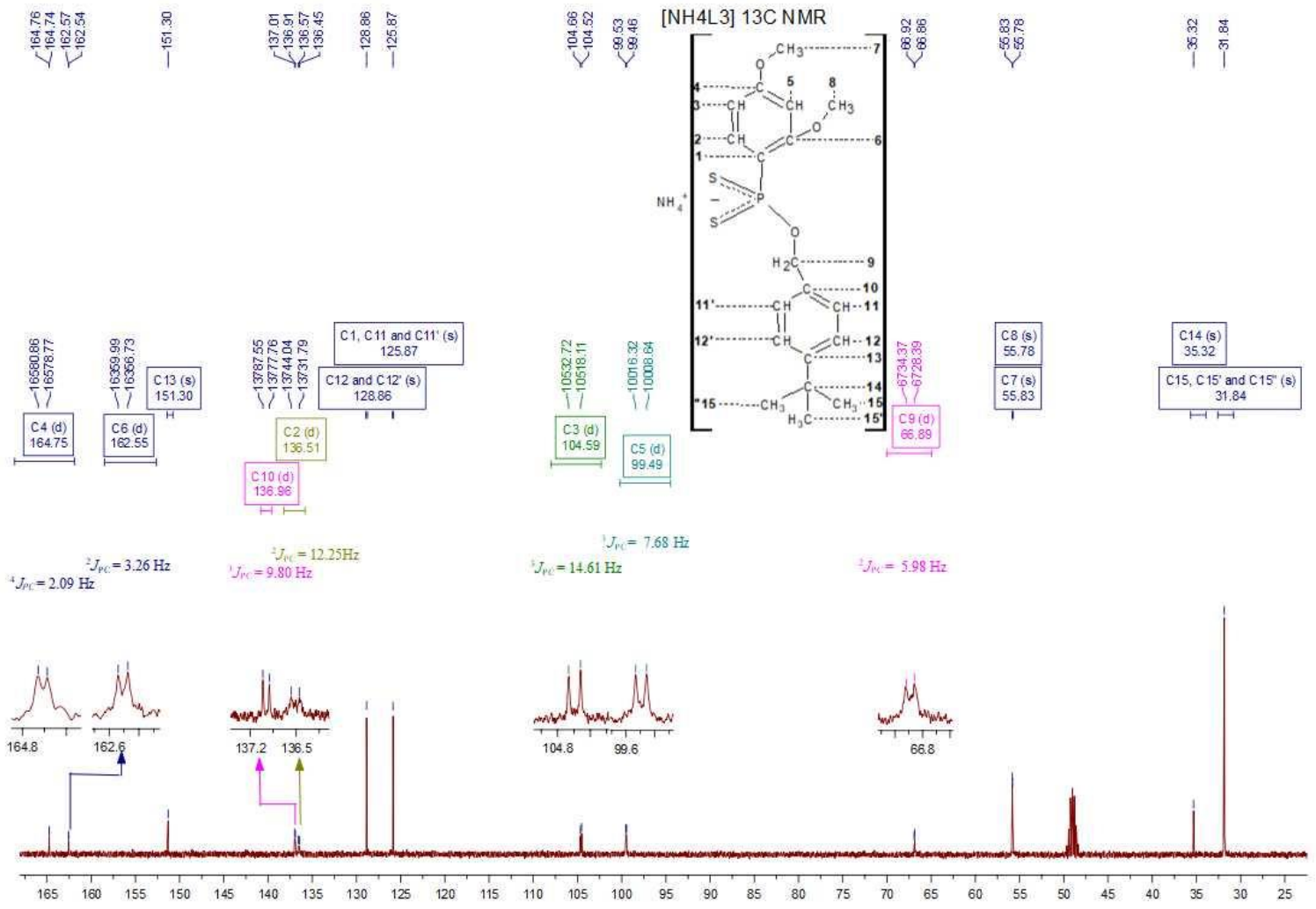


Figure 5.130. $[NH_4][S_2P(R^y)(OR3)]$ ^{13}C-NMR spectrum.

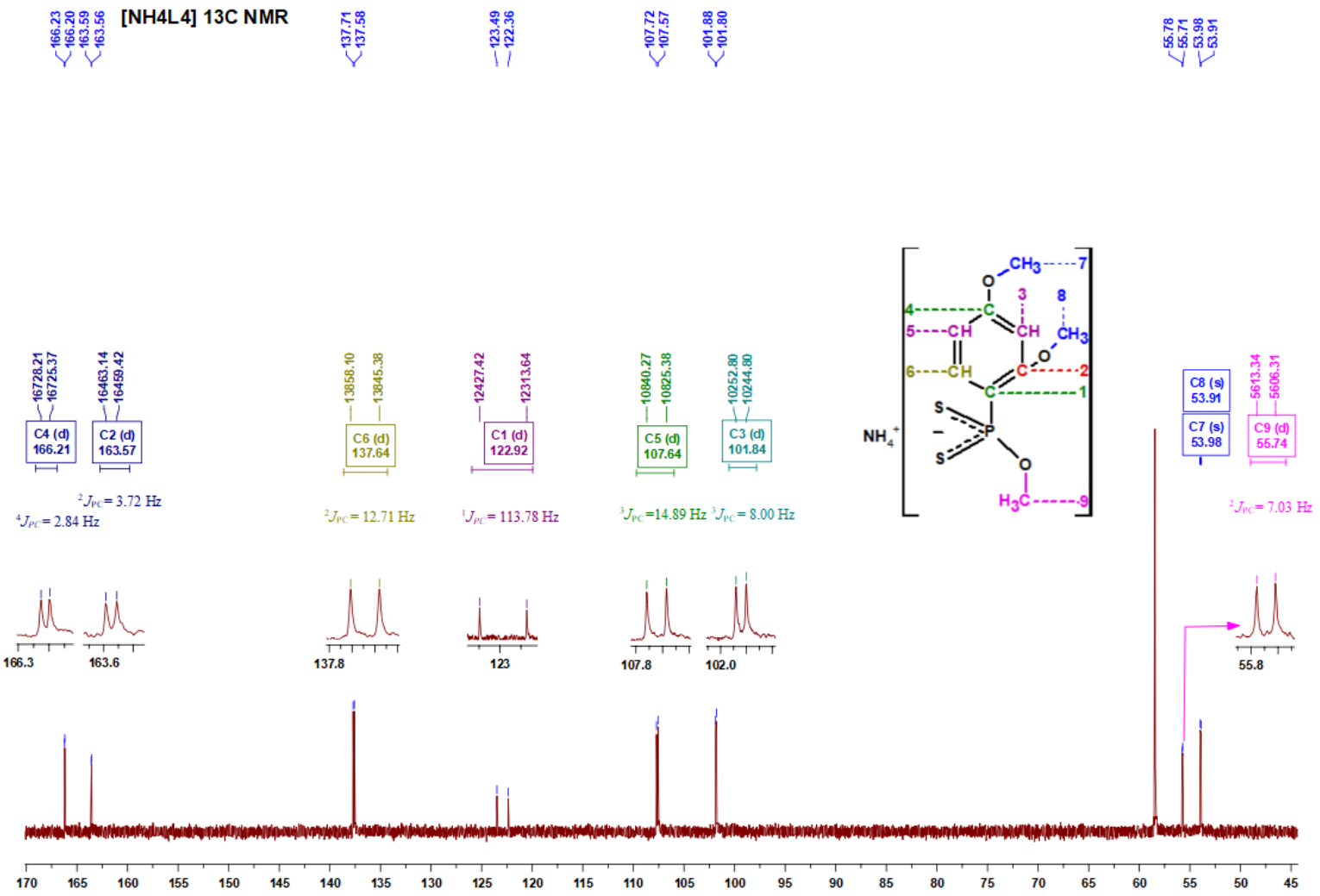


Figure 5.131. $[NH_4][S_2P(R^y)(OR4)]$ ^{13}C-NMR spectrum.

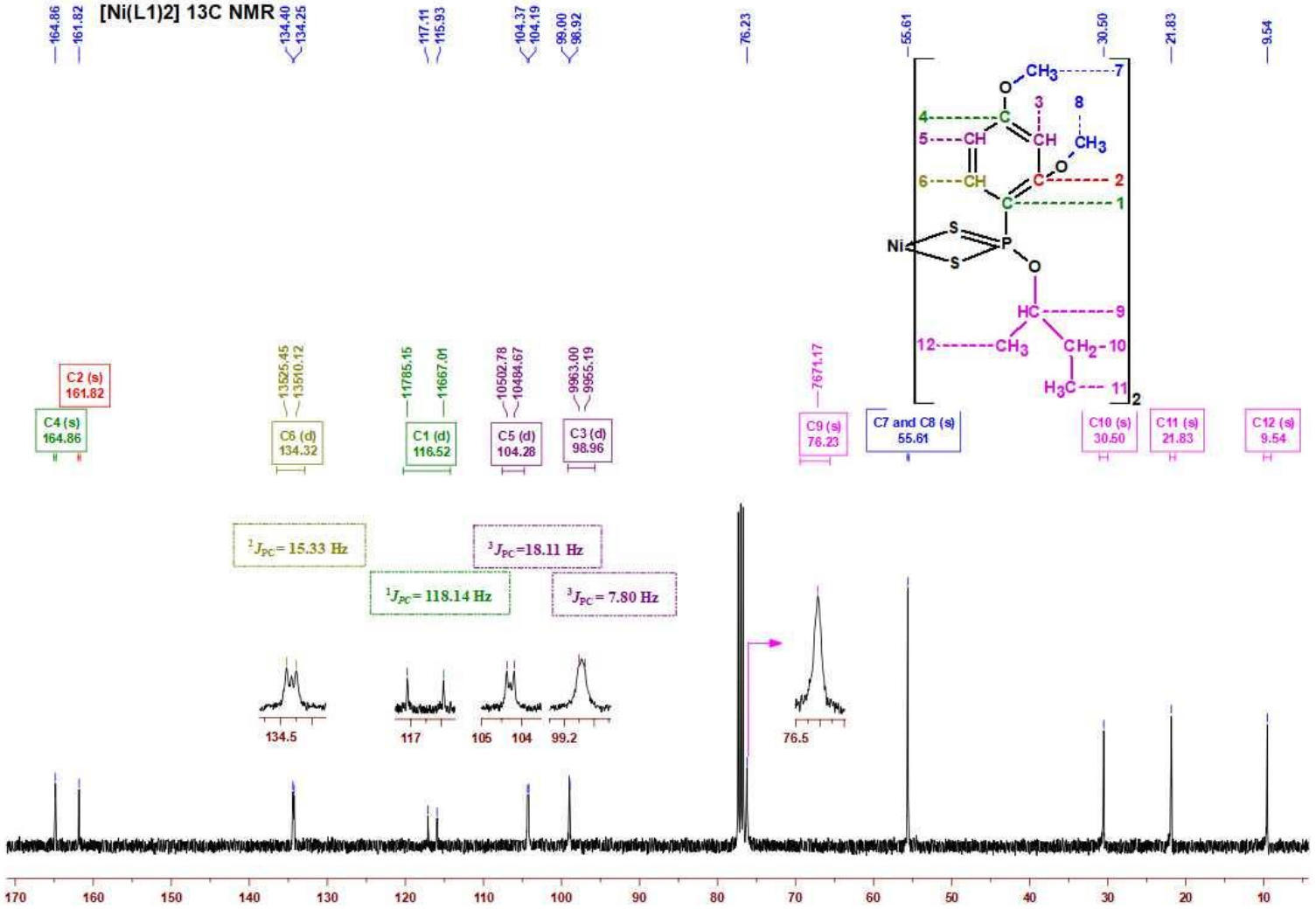


Figure 5.132. [Ni($S_2P(R^y)(OR1))_2$] ^{13}C-NMR spectrum.

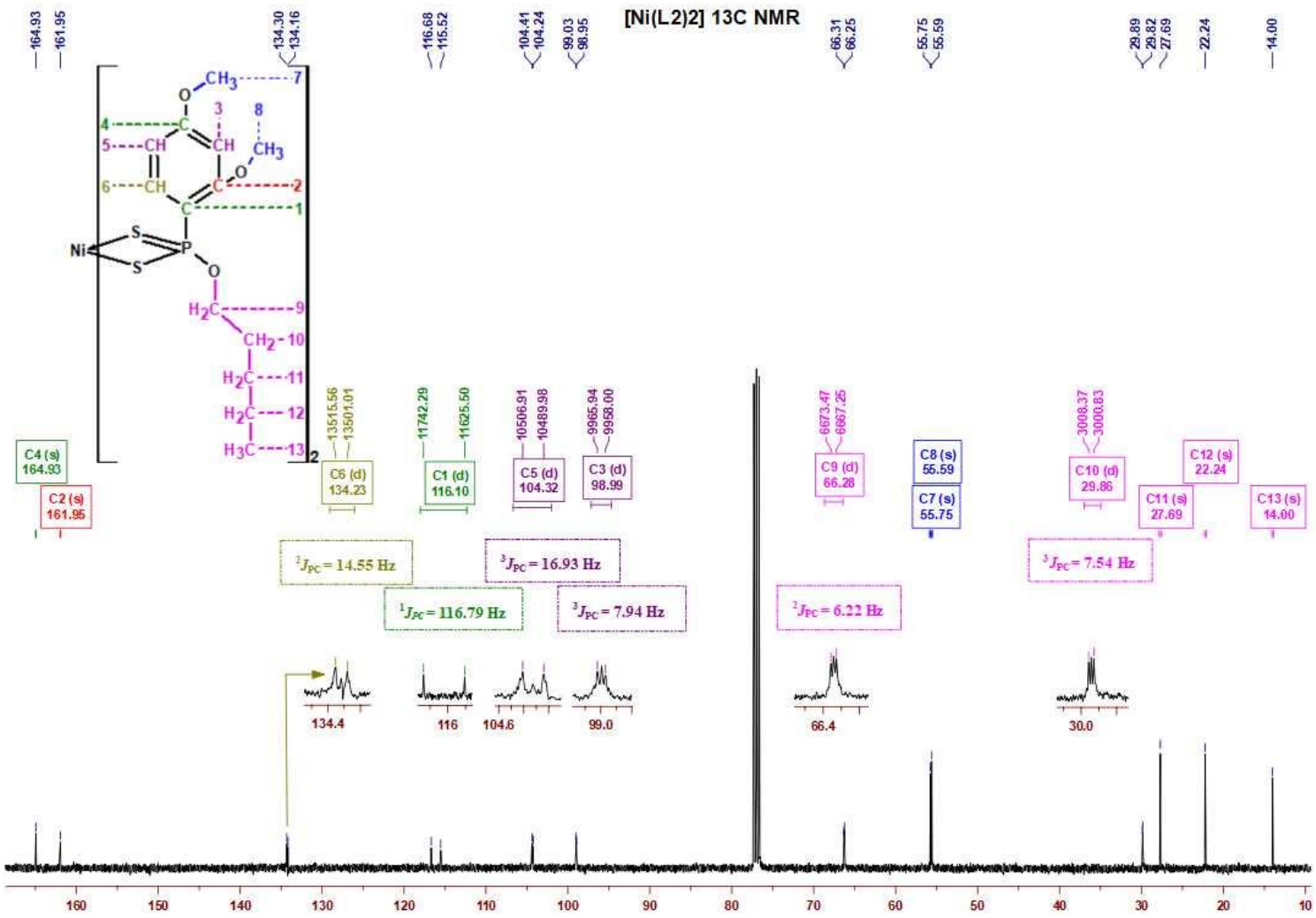


Figure 5.133. [Ni($S_2P(R^y)(OR2))_2$] ^{13}C-NMR spectrum.

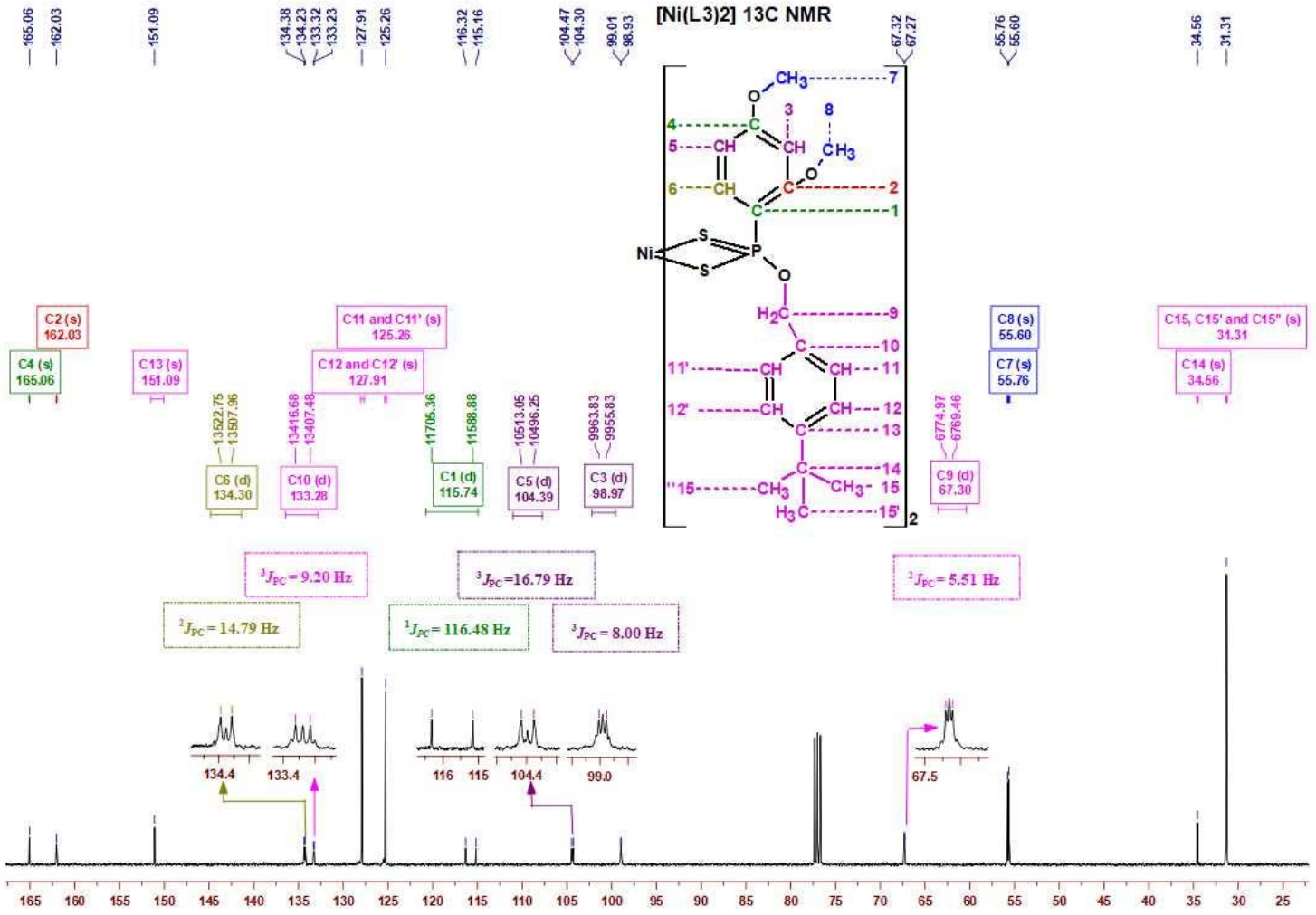


Figure 5.134. [Ni($S_2P(R^y)(OR3)$)$_2$] ^{13}C-NMR spectrum.

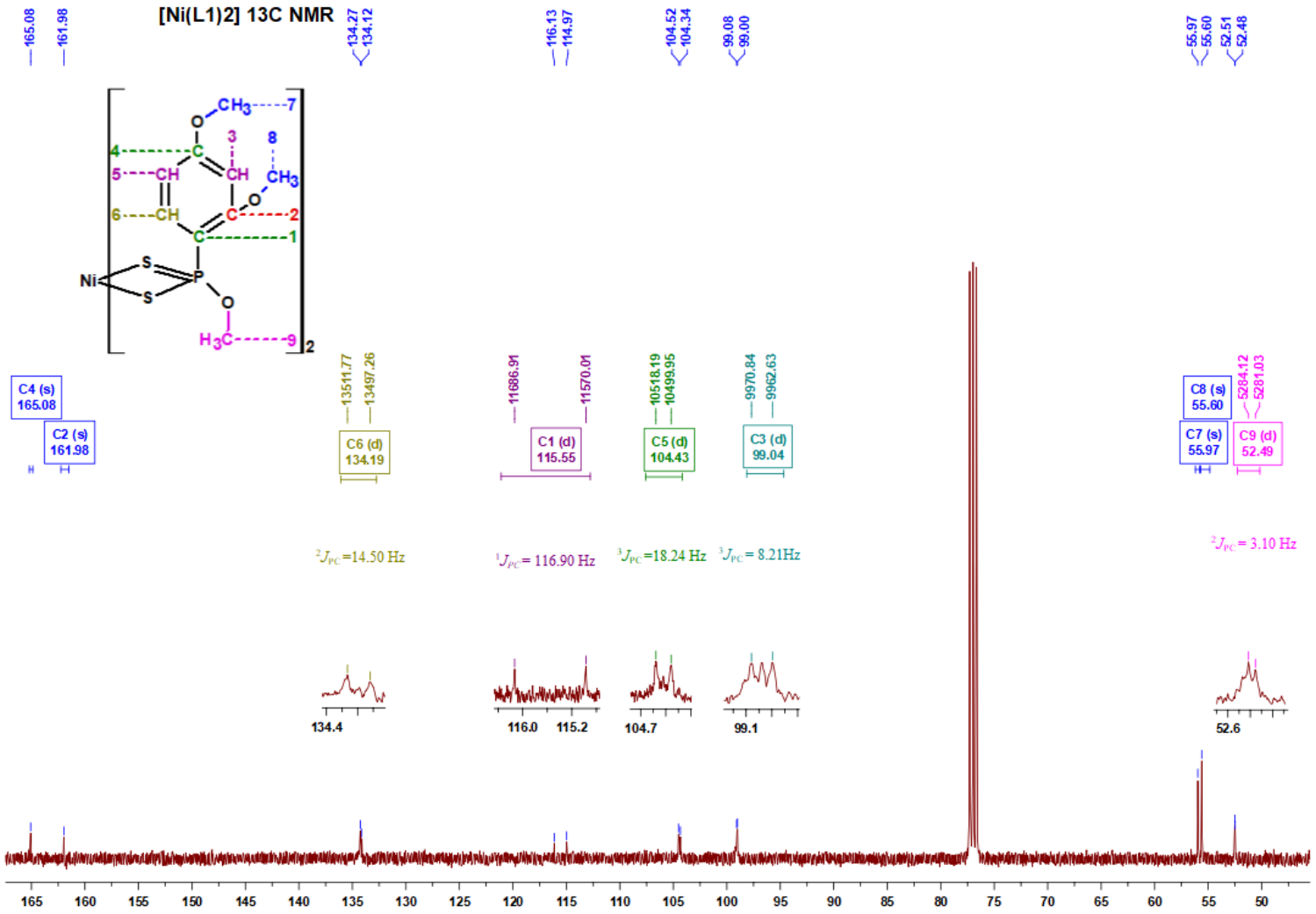


Figure 5.135. $[Ni(S_2P(R^y)(OR4))_2]$ ^{13}C-NMR spectrum.

5.1.7.10. Comments on ^{31}P-NMR Spectra of Part Ia' Compounds

Proton-decoupled ^{31}P-NMR spectra all the compounds comprise single peaks. The chemical ^{31}P chemical shifts of the ligands are located in the range 103.7-109.6 ppm, and those of the complexes in the range 96.3-104.5 ppm, which means that the complex formation causes a shift of δ= ~4-6 ppm to higher fields.

The NMR spectra and important NMR data for the ligands and their nickel(II) complexes are presented in Tables 5.12. Spectrum peaks of ^{31}P-NMR are given in Figure 5.136-5.149.

Table 5.12. ^{31}P-NMR data of the compounds.

Ligands	δ (ppm)		Complexes
$[NH_4][S_2P(R^x)(OR1)]$	109.62	104.45	$[Ni(S_2P(R^x)(OR1))_2]$
$[NH_4][S_2P(R^x)(OR2)]$	106.62	100.97	$[Ni(S_2P(R^x)(OR2))_2]$
$[NH_4][S_2P(R^x)(OR3)]$	105.78	100.81	$[Ni(S_2P(R^x)(OR3))_2]$
$[NH_4][S_2P(R^x)(OR4)]$	105.74	100.72	$[Ni(S_2P(R^x)(OR4))_2]$
$[NH_4][S_2P(R^x)(OR5)]$	103.70	96.30	$[Ni(S_2P(R^x)(OR5))_2]$
$[NH_4][S_2P(R^x)(OR6)]$	105.72	100.55	$[Ni(S_2P(R^x)(OR6))_2]$
$[NH_4][S_2P(R^x)(OR7)]$	107.50	102.65	$[Ni(S_2P(R^x)(OR7))_2]$

^{31}P-NMR Spectra of Part Ia $[NH_4][S_2P(R^x)(ORn)]$ and $[Ni(S_2P(R^x)(ORn))_2]$ Compounds.

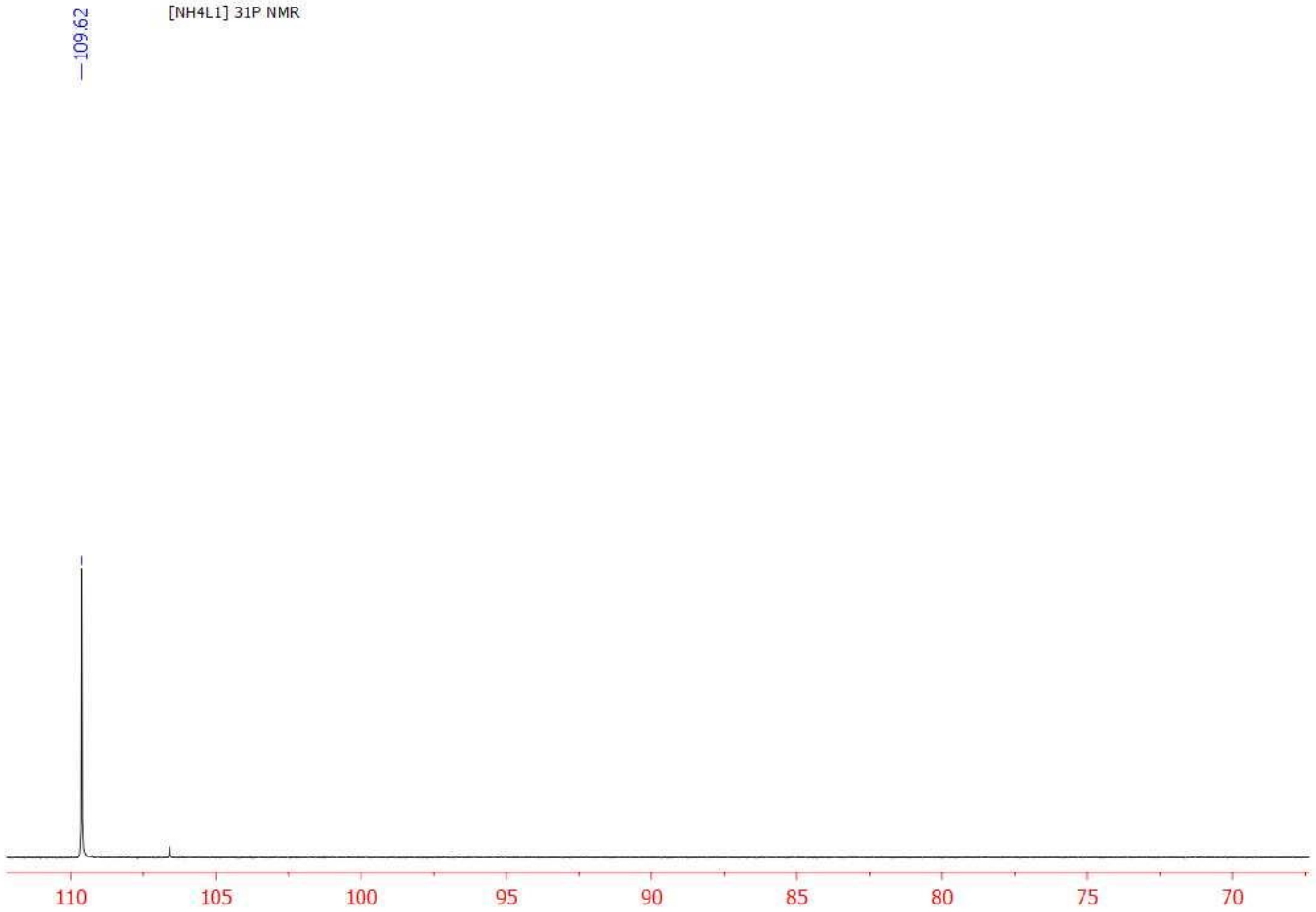


Figure 5.136. $[NH_4][S_2P(R^x)(OR1)]$ ^{31}P-NMR spectrum.

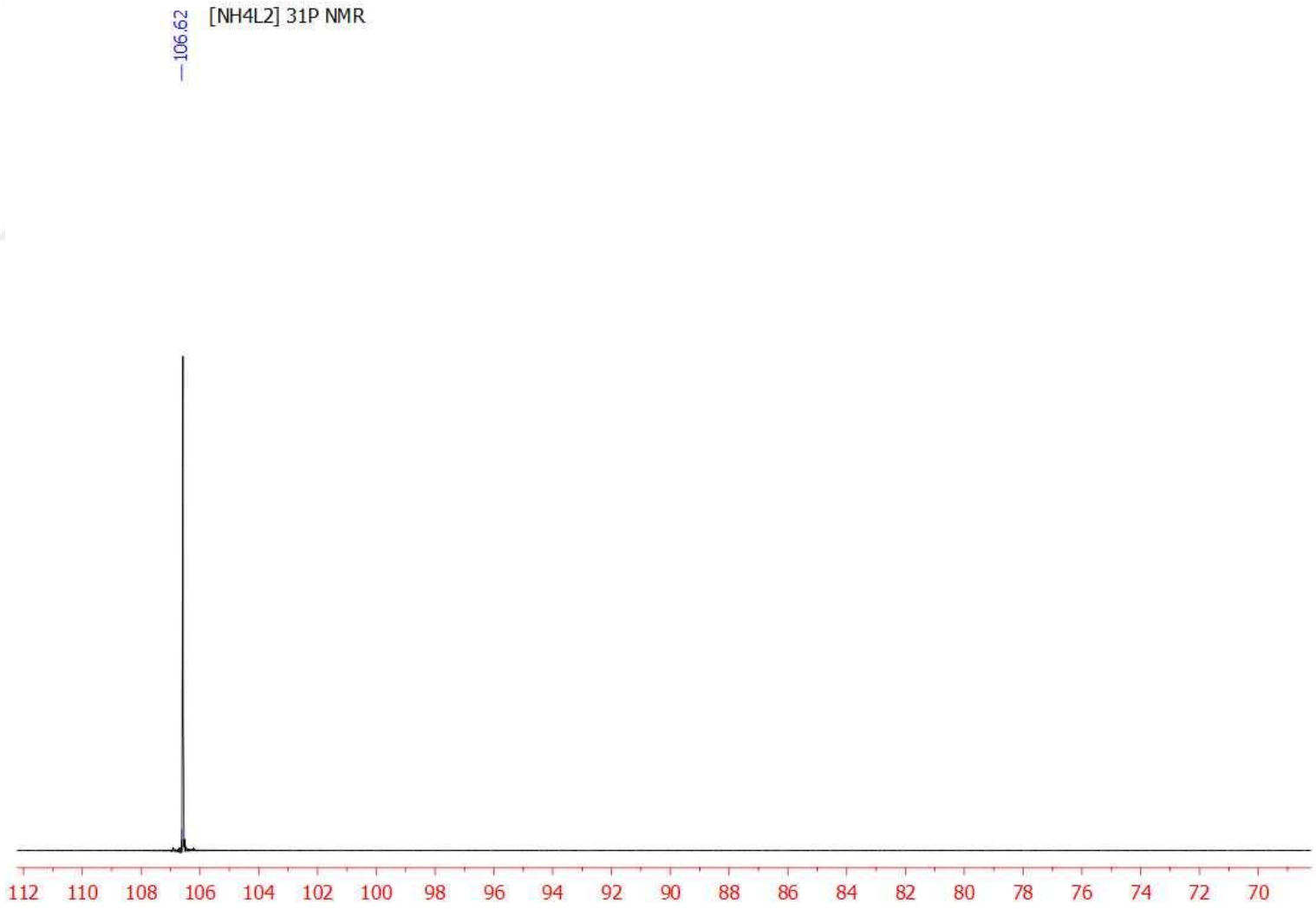


Figure 5.137. $[NH_4][S_2P(R^x)(OR2)]$ ^{31}P-NMR spectrum.

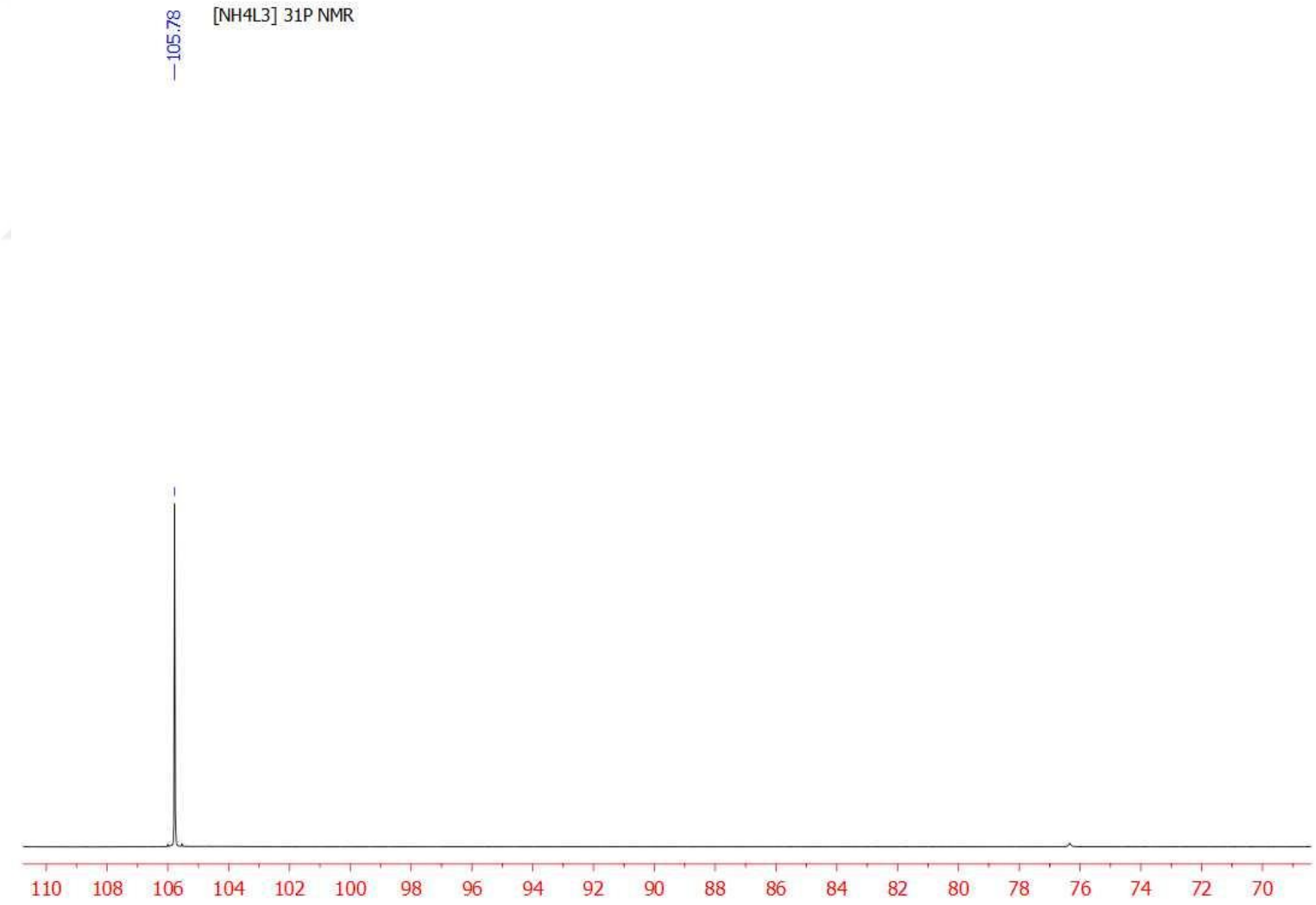


Figure 5.138. $[NH_4][S_2P(R^x)(OR3)]$ ^{31}P-NMR spectrum.

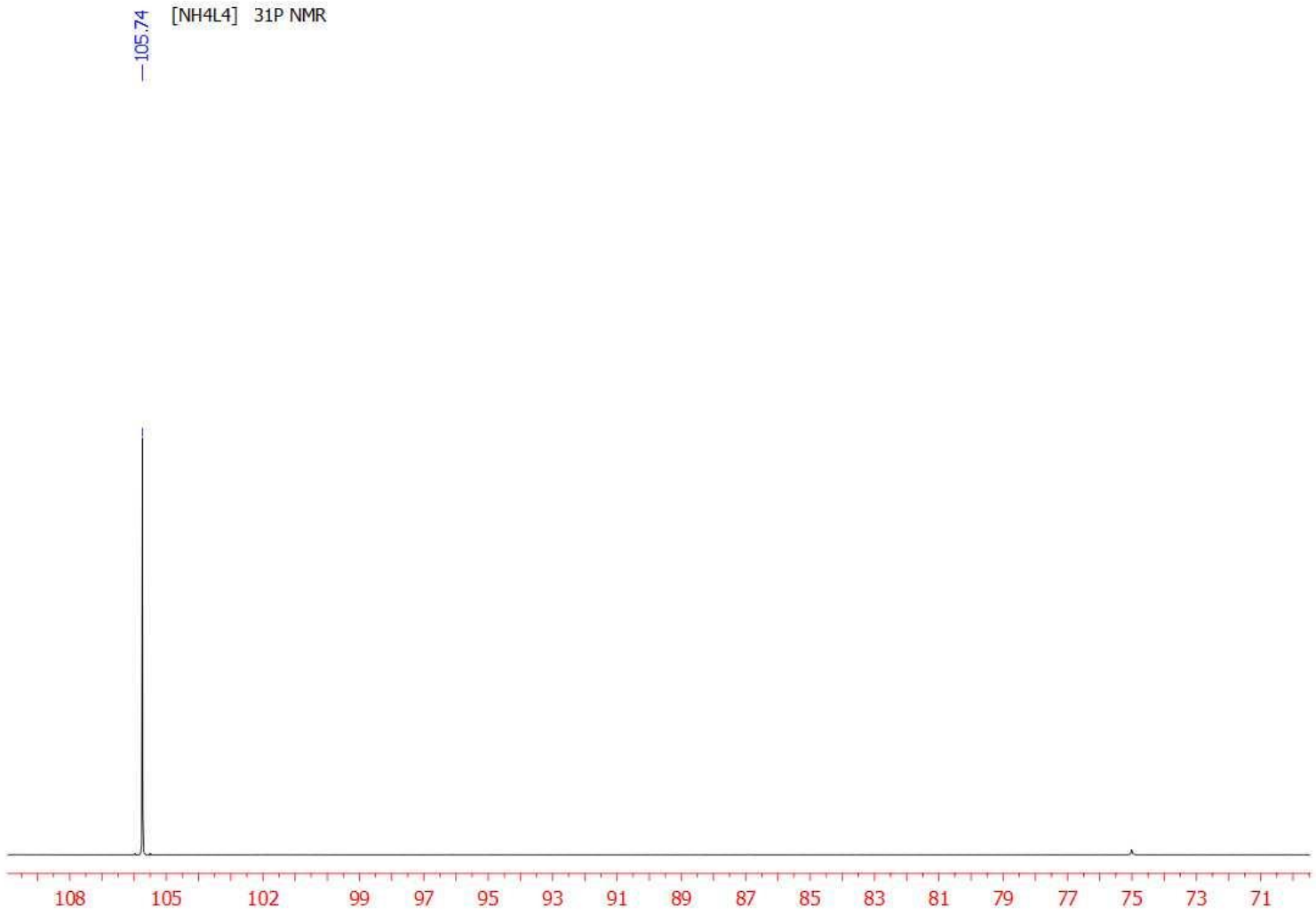


Figure 5.139. $[NH_4][S_2P(R^x)(OR4)]$ ^{31}P-NMR spectrum.

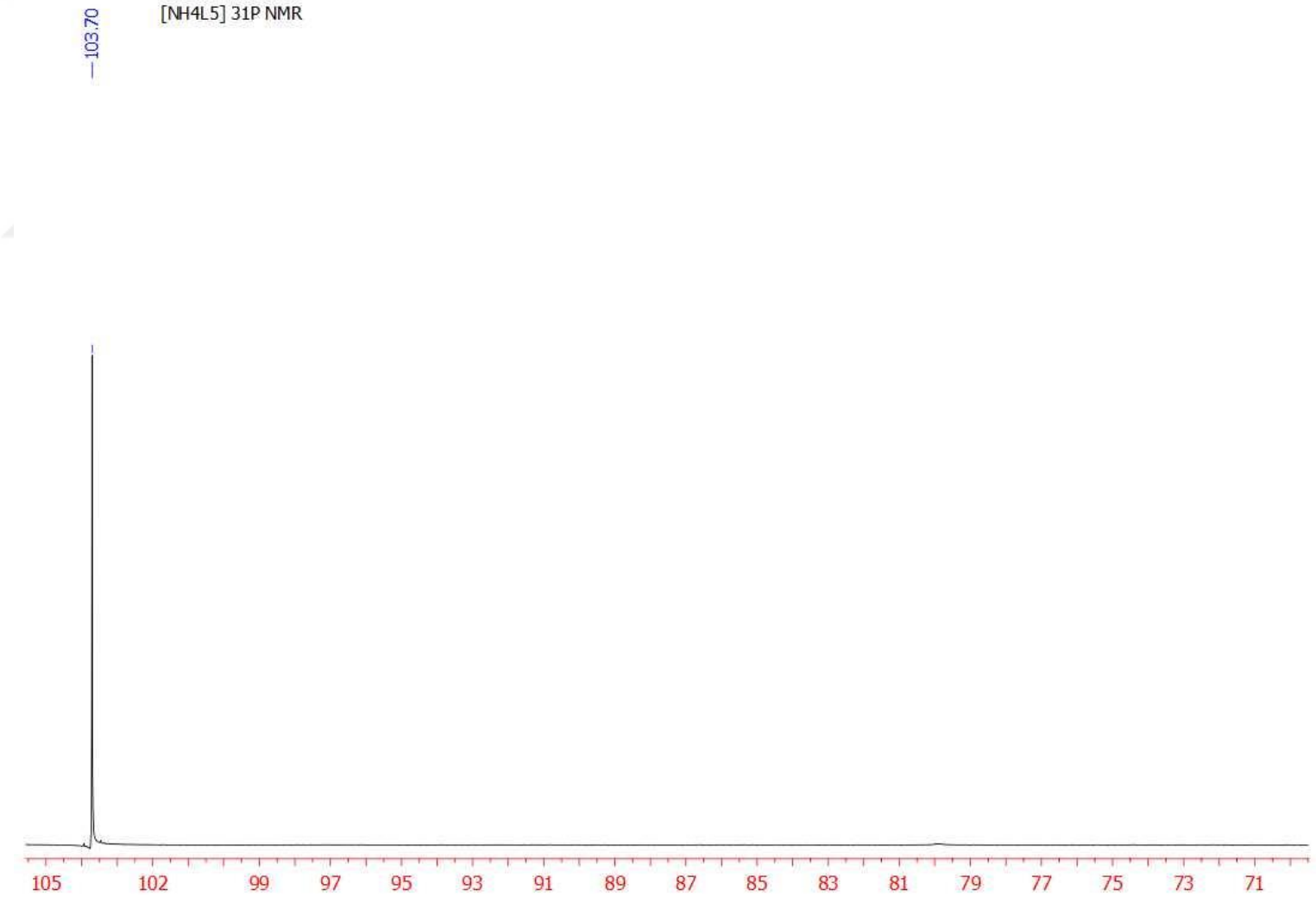


Figure 5.140. $[NH_4][S_2P(R^x)(OR5)]$ ^{31}P-NMR spectrum.

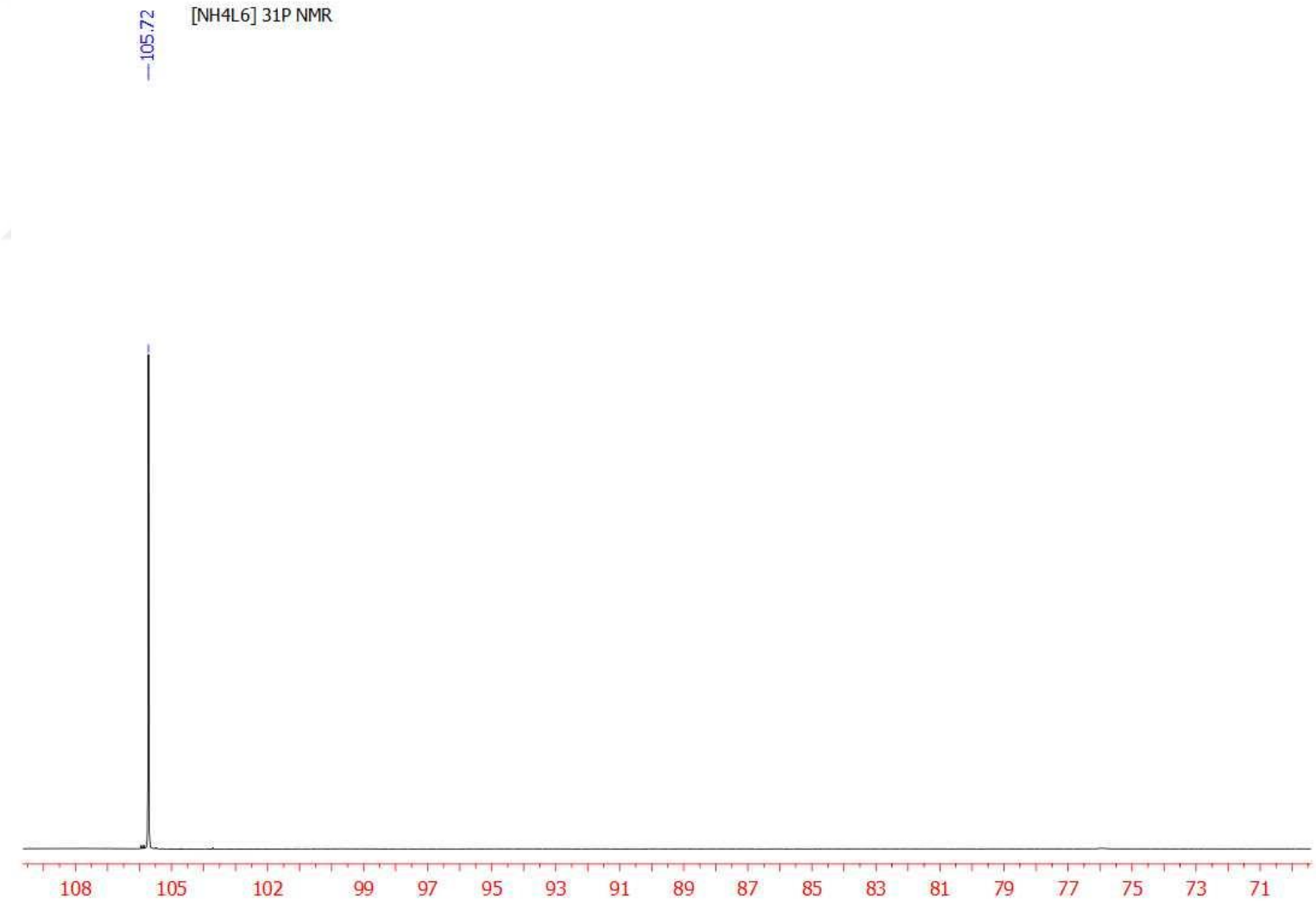


Figure 5.141. $[NH_4][S_2P(R^x)(OR6)]$ ^{31}P-NMR spectrum.



Figure 5.142. $[NH_4][S_2P(R^x)(OR7)]$ ^{31}P-NMR spectrum.



Figure 5.143. $[Ni(S_2P(R^x)(OR1))_2]$ ^{31}P-NMR spectrum.

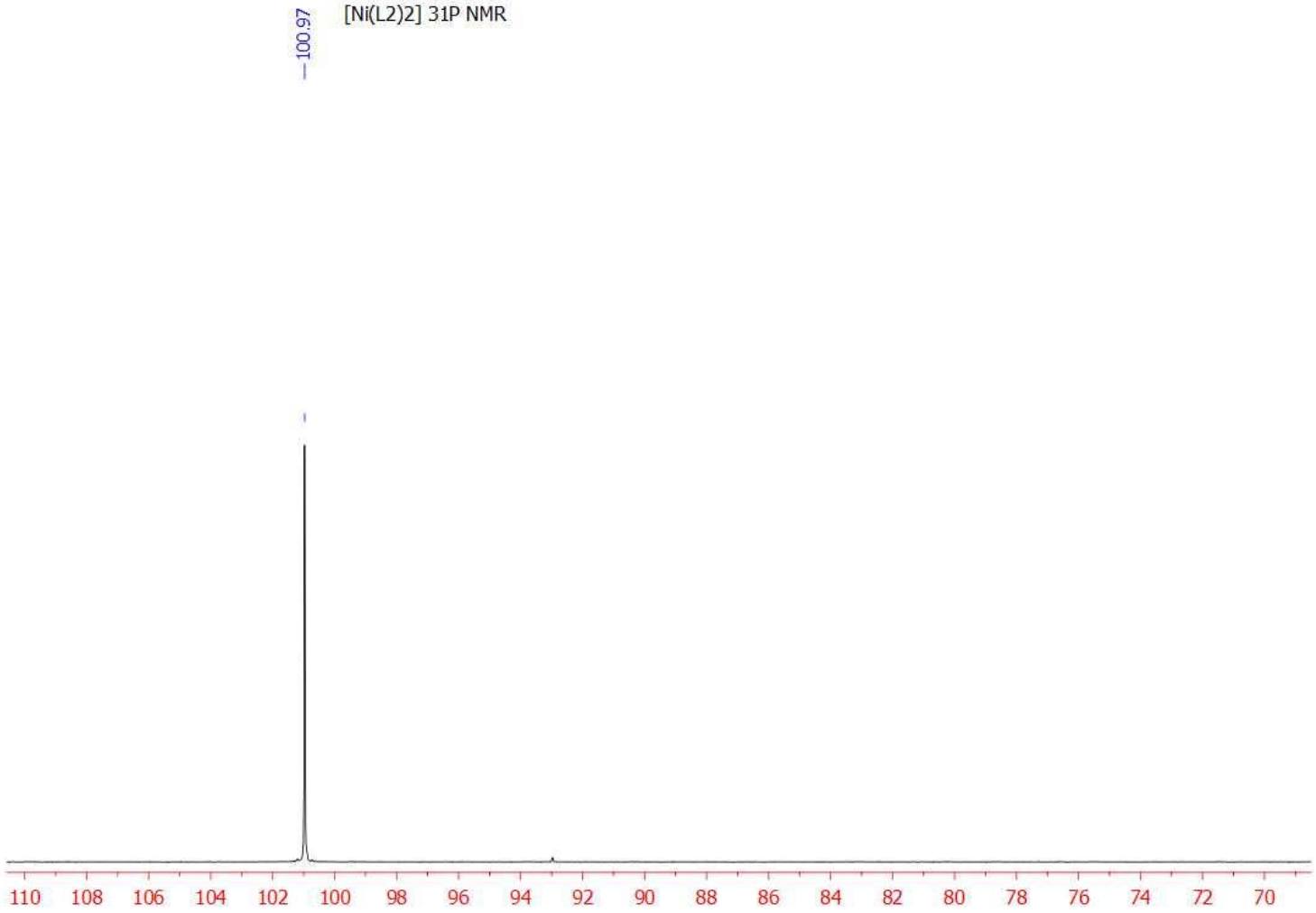


Figure 5.144. $[Ni(S_2P(R^x)(OR2))_2]$ ^{31}P-NMR spectrum.



Figure 5.145. $[Ni(S_2P(R^x)(OR3))_2]$ ^{31}P-NMR spectrum.



Figure 5.146. $[Ni(S_2P(R^x)(OR4))_2]$ ^{31}P-NMR spectrum.

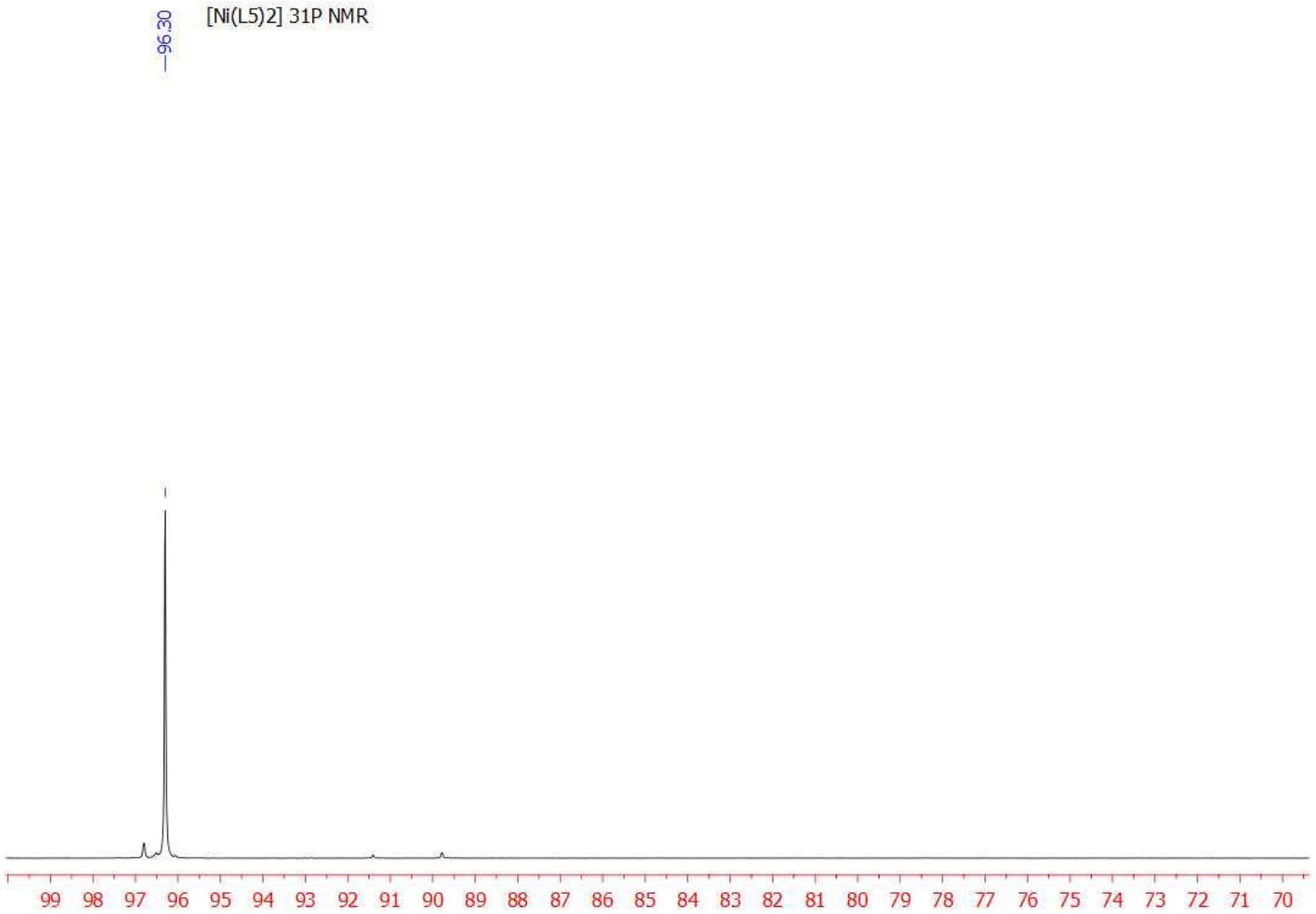


Figure 5.147. [Ni($S_2P(R^x)(OR5)$)$_2$] ^{31}P-NMR spectrum.

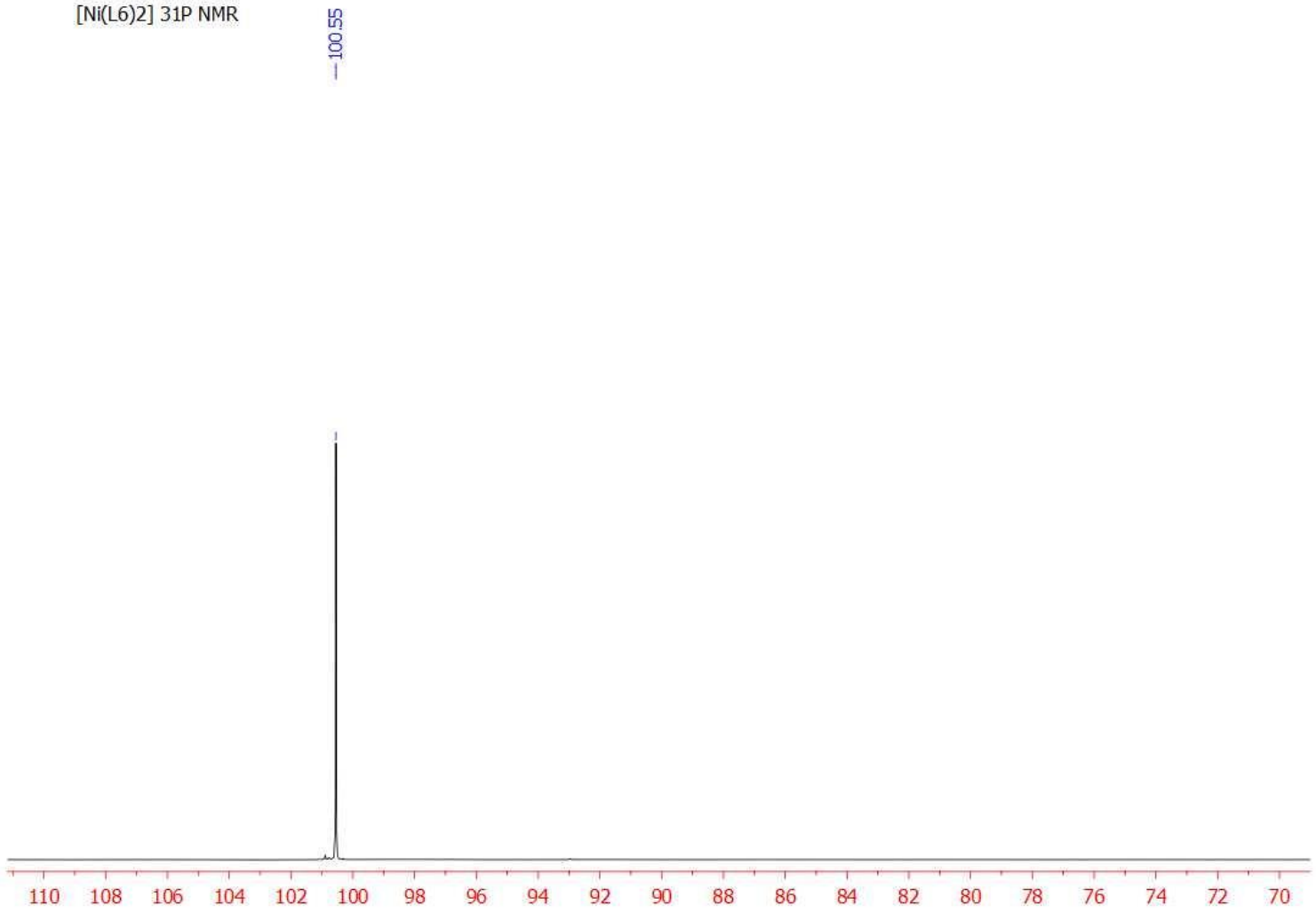


Figure 5.148. [Ni($S_2P(R^x)(OR6))_2$] ^{31}P-NMR spectrum.

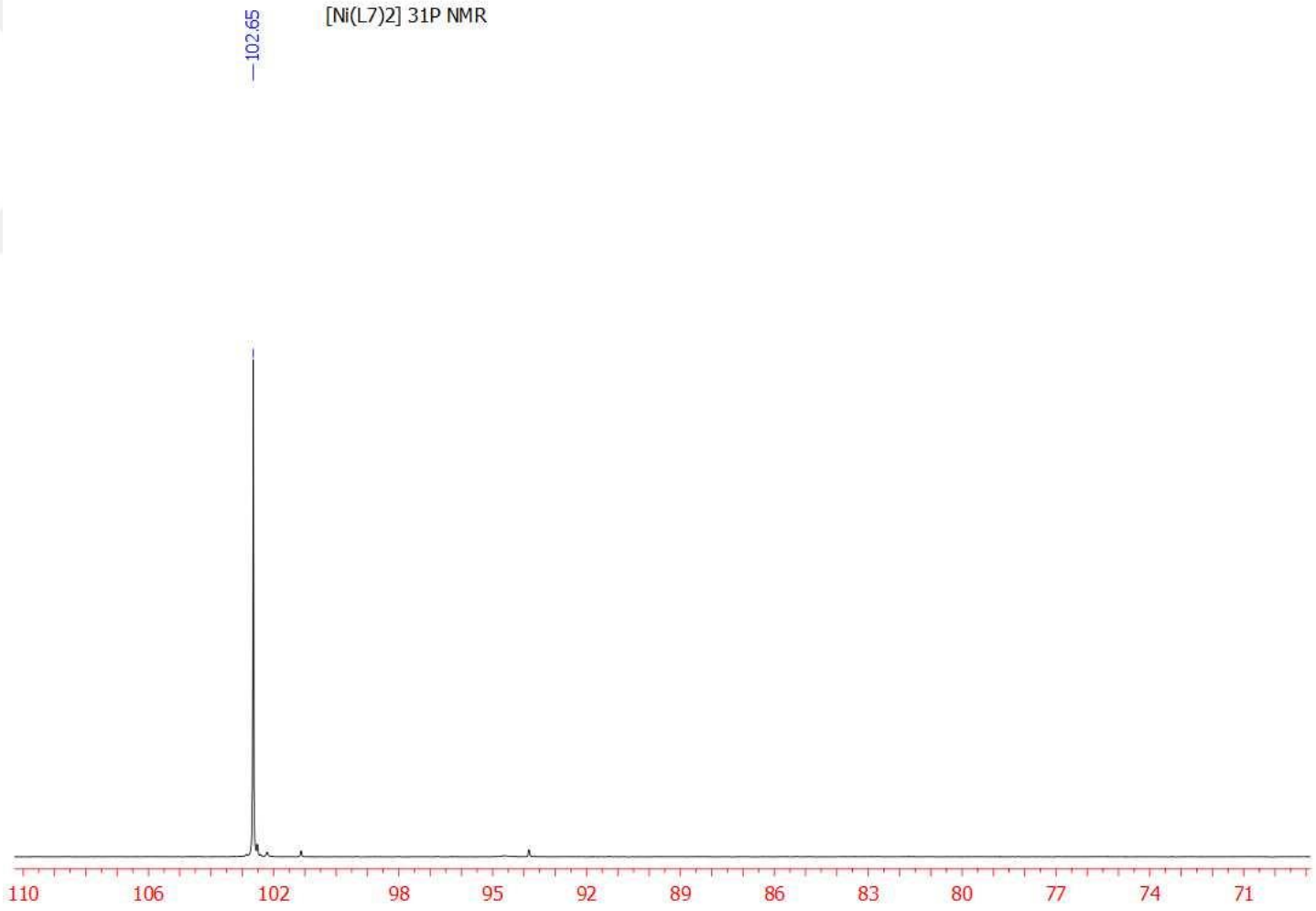


Figure 5.149. $[Ni(S_2P(R^x)(OR7))_2]$ ^{31}P-NMR spectrum.

5.1.7.11. Comments on ^{31}P-NMR Spectra of Part Ib' Compounds

^{31}P-NMR spectra of all the compounds comprise single peaks. The ^{31}P chemical shifts in $[NH_4][S_2P(R^x)(ORn)]$ and $[Ni(S_2P(R^x)(ORn))_2]$ lie in the frequency range 103.7-107.0 ppm and 96.9-102.2 ppm, respectively. These findings mean that the complex formation results in a shift of ~5-7 ppm to higher fields.

The NMR spectra and important NMR data for the ligands and their nickel(II) complexes are presented in Tables 5.13. Spectrum peaks of ^{31}P-NMR are given in Figure 5.150-5.159.

Table 5.13. ^{31}P-NMR data of the compounds.

Ligands	δ (ppm)		Complexes
$[NH_4][S_2P(R^x)(OR1)]$	105.78	100.67	$[Ni(S_2P(R^x)(OR1))_2]$
$[NH_4][S_2P(R^x)(OR2)]$	103.72	96.89	$[Ni(S_2P(R^x)(OR2))_2]$
$[NH_4][S_2P(R^x)(OR3)]$	106.95	100.22	$[Ni(S_2P(R^x)(OR3))_2]$
$[NH_4][S_2P(R^x)(OR4)]$	103.77	97.69	$[Ni(S_2P(R^x)(OR4))_2]$
$[NH_4][S_2P(R^x)(OR5)]$	106.44	97.07	$[Ni(S_2P(R^x)(OR5))_2]$

^{31}P-NMR Spectra of Part Ib [NH_4][$S_2P(R^x)(ORn)$] and [$Ni(S_2P(R^x)(ORn))_2$] Compounds.

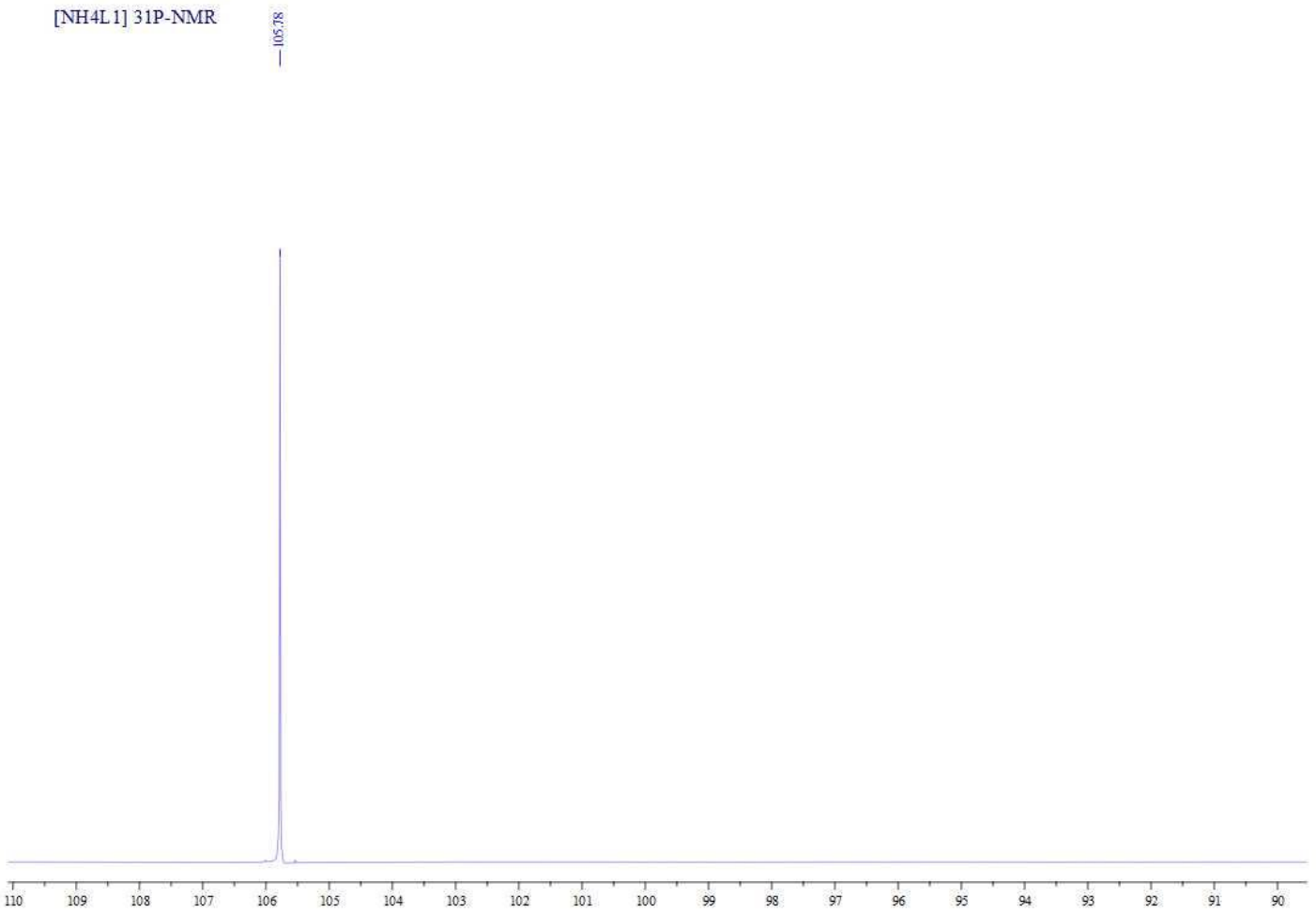


Figure 5.150. [NH_4][$S_2P(R^x)(OR1)$] ^{31}P-NMR spectrum.

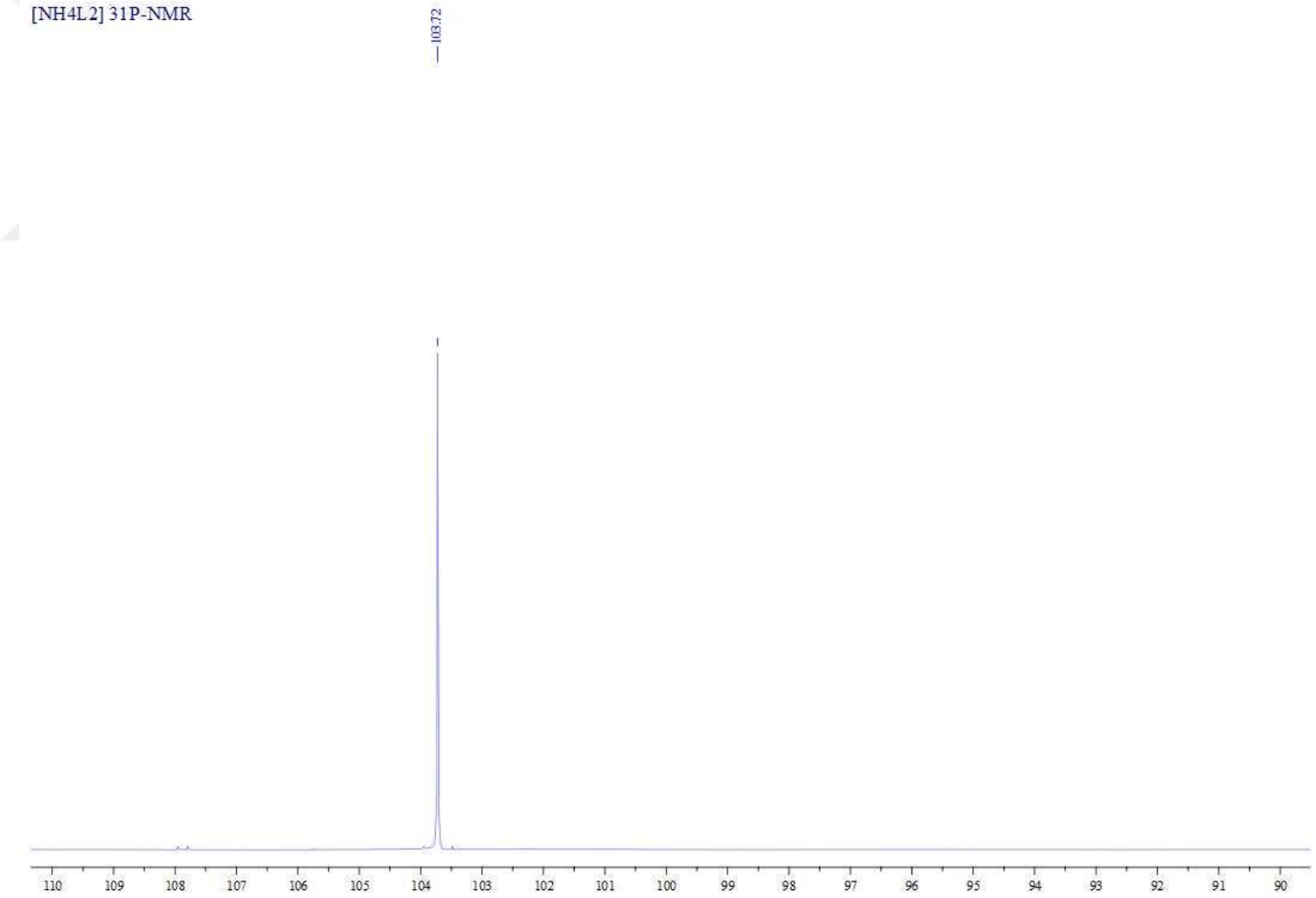


Figure 5.151. $[NH_4][S_2P(R^x)(OR2)]$ ^{31}P-NMR spectrum.

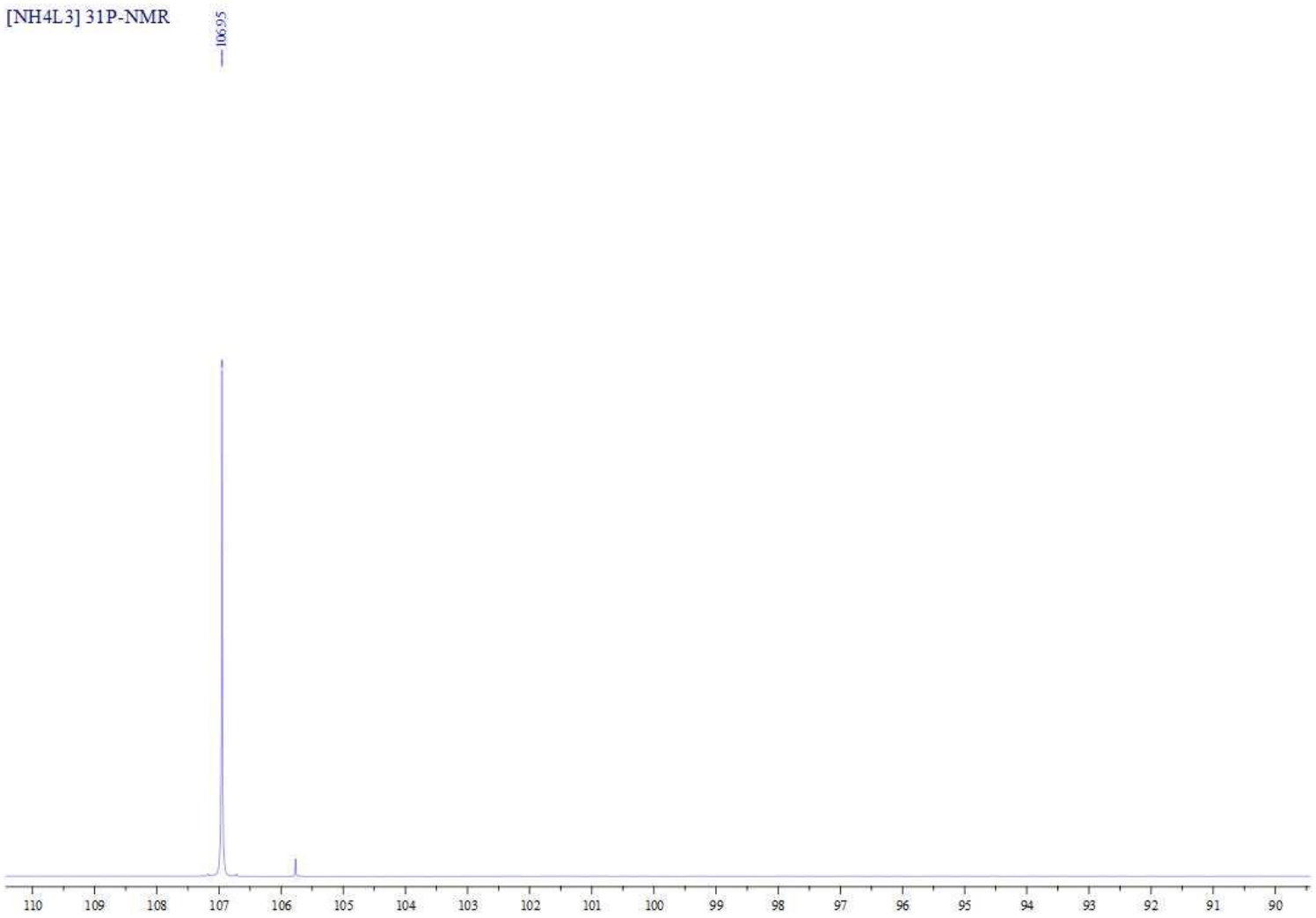


Figure 5.152. $[NH_4][S_2P(R^x)(OR3)]$ ^{31}P-NMR spectrum.

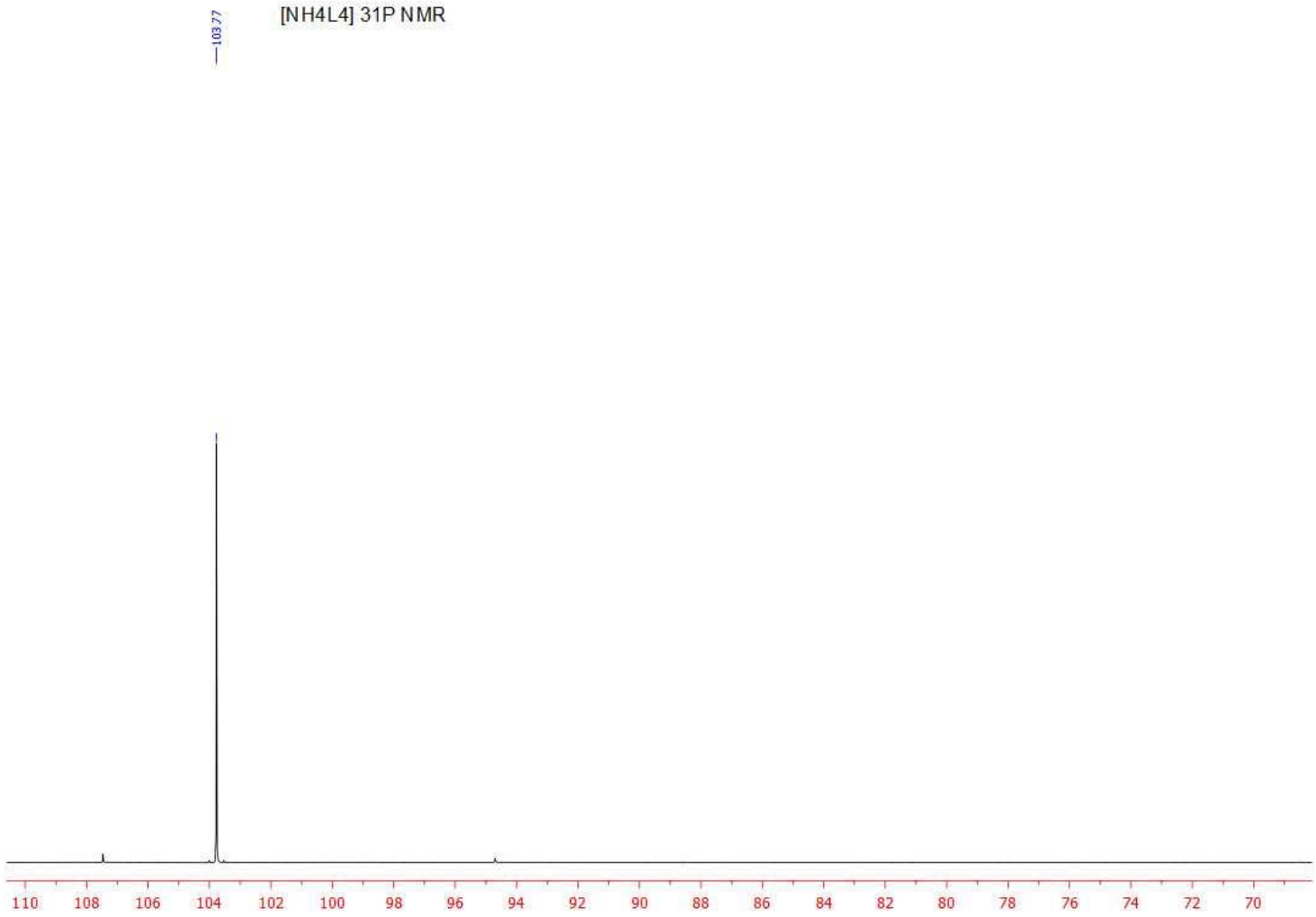


Figure 5.153. $[NH_4][S_2P(R^x)(OR4)]$ ^{31}P-NMR spectrum.



Figure 5.154. $[NH_4][S_2P(R^x)(OR5)]$ ^{31}P-NMR spectrum.

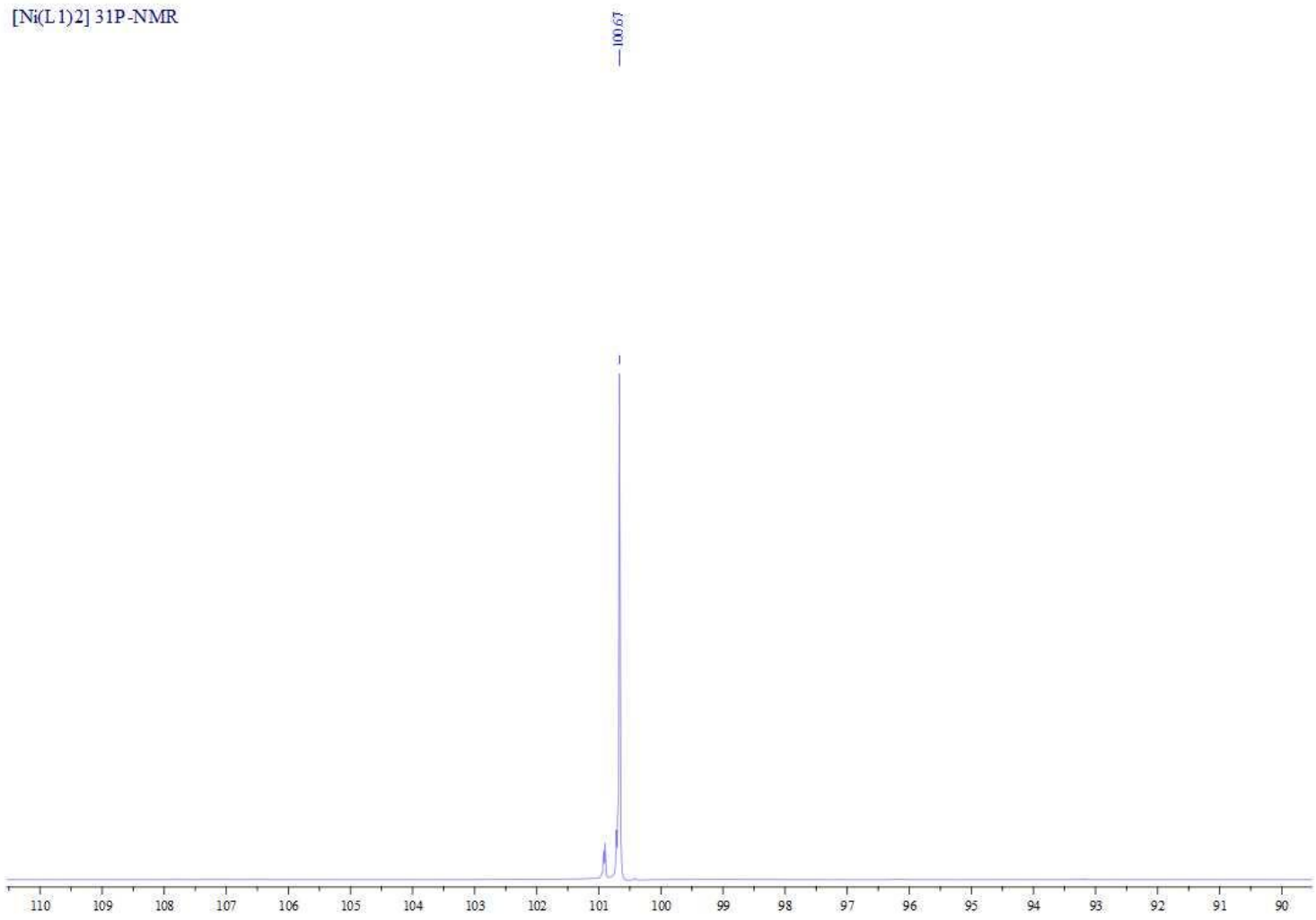


Figure 5.155. $[Ni(S_2P(R^x)(OR1))_2]$ ^{31}P-NMR spectrum.

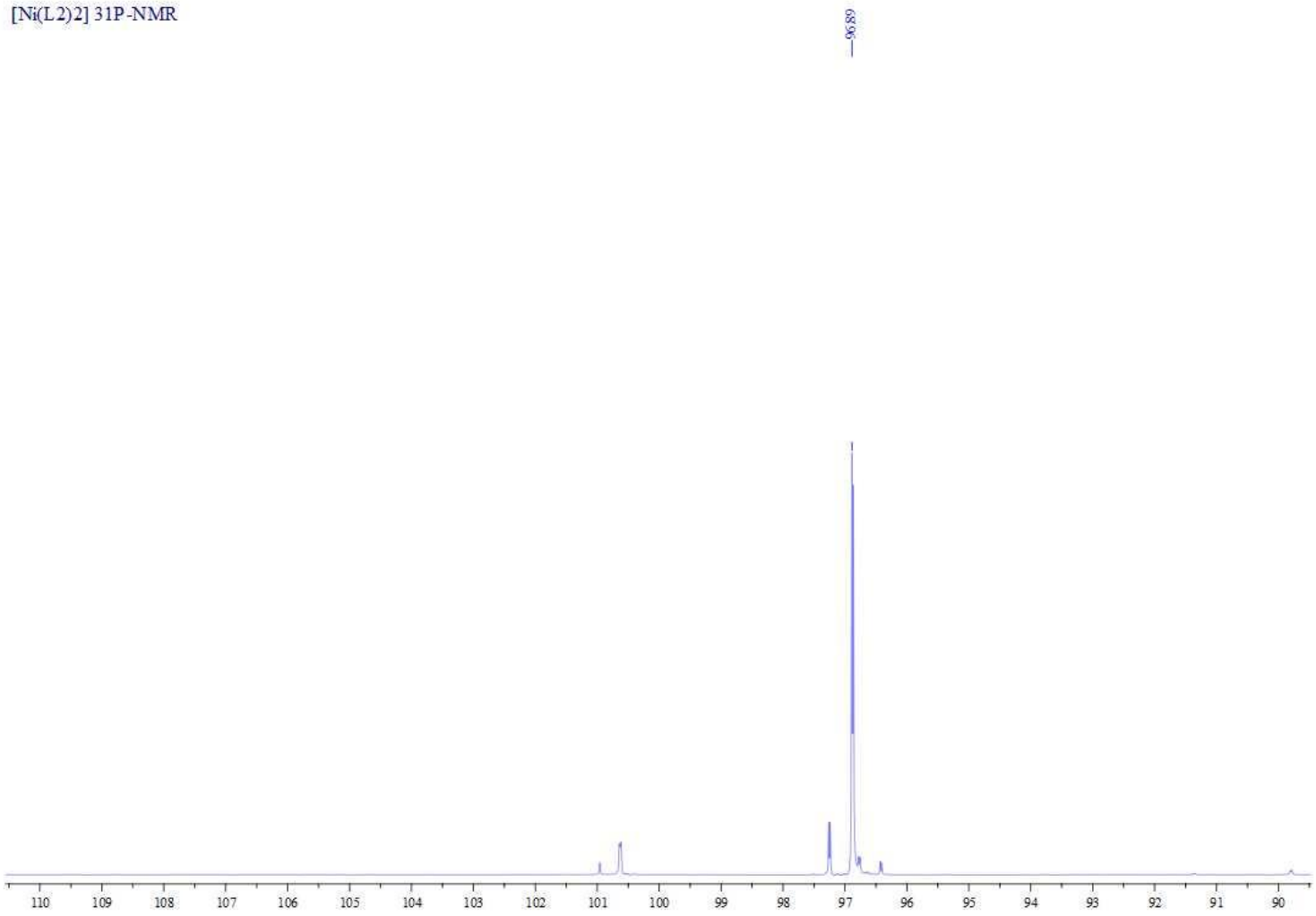


Figure 5.156. $[Ni(S_2P(R^x)(OR2))_2]$ ^{31}P-NMR spectrum.

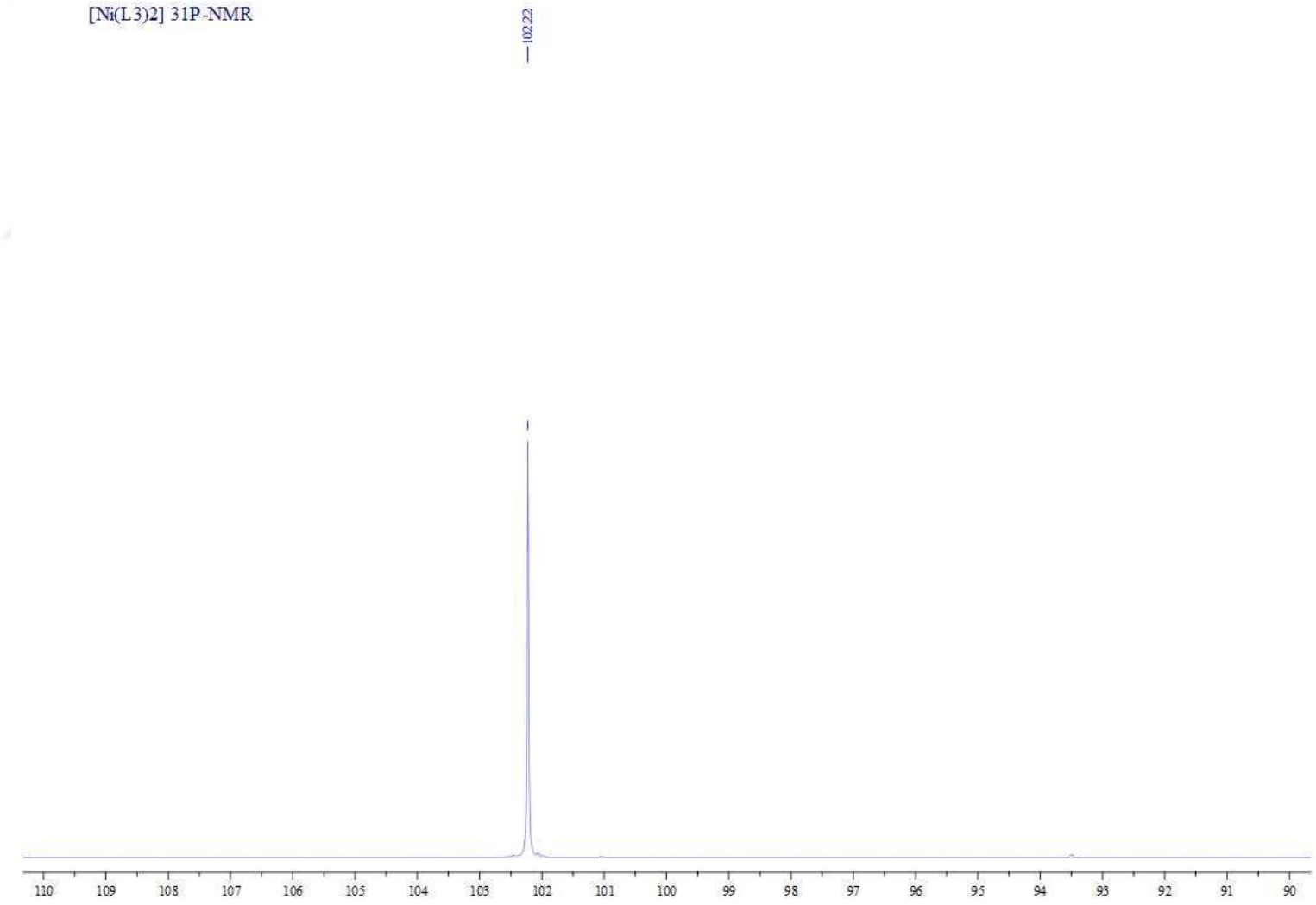


Figure 5.157. $[Ni(S_2P(R^x)(OR3))_2]$ ^{31}P-NMR spectrum.

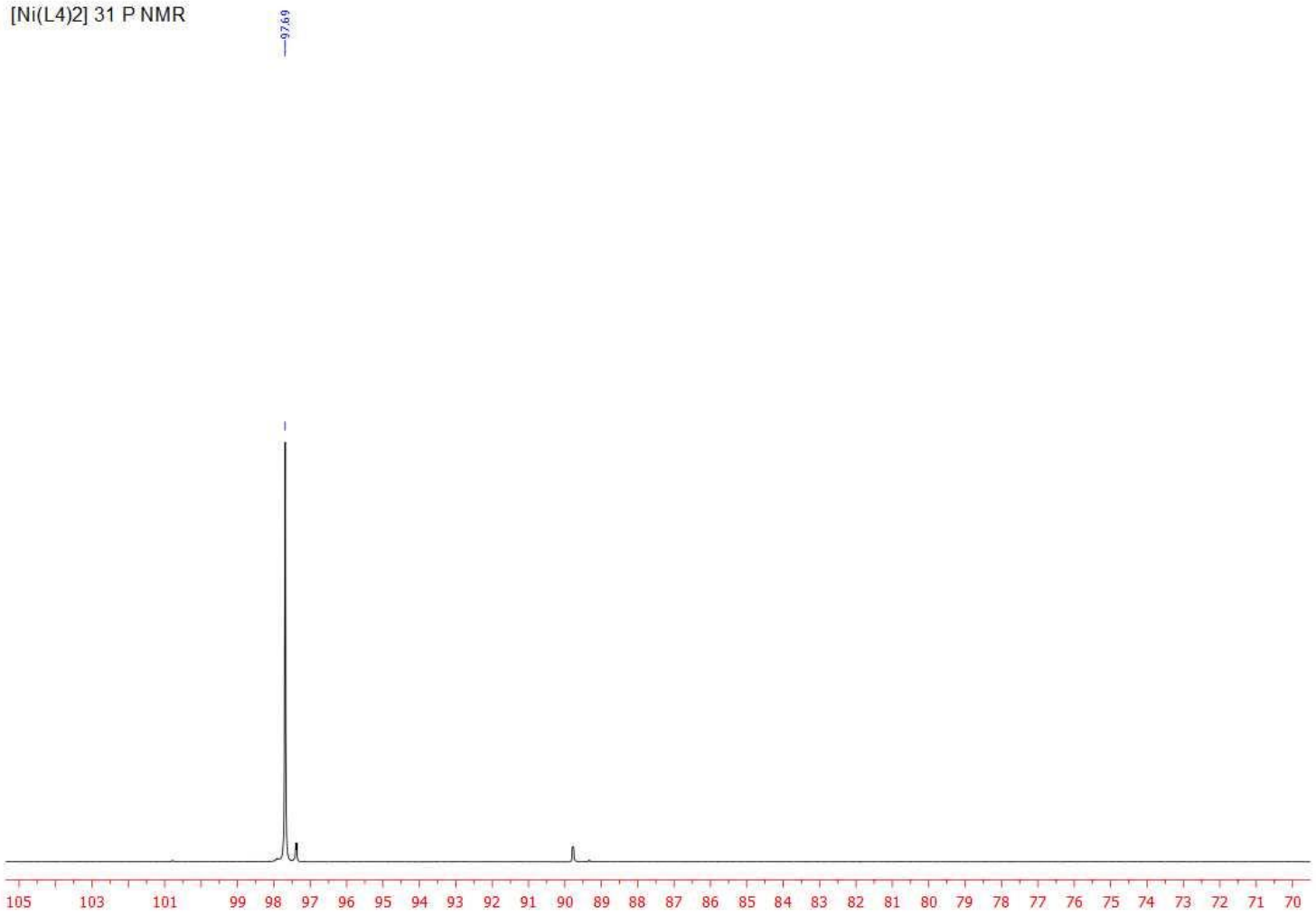


Figure 5.158. $[Ni(S_2P(R^x)(OR4))_2]$ ^{31}P-NMR spectrum.

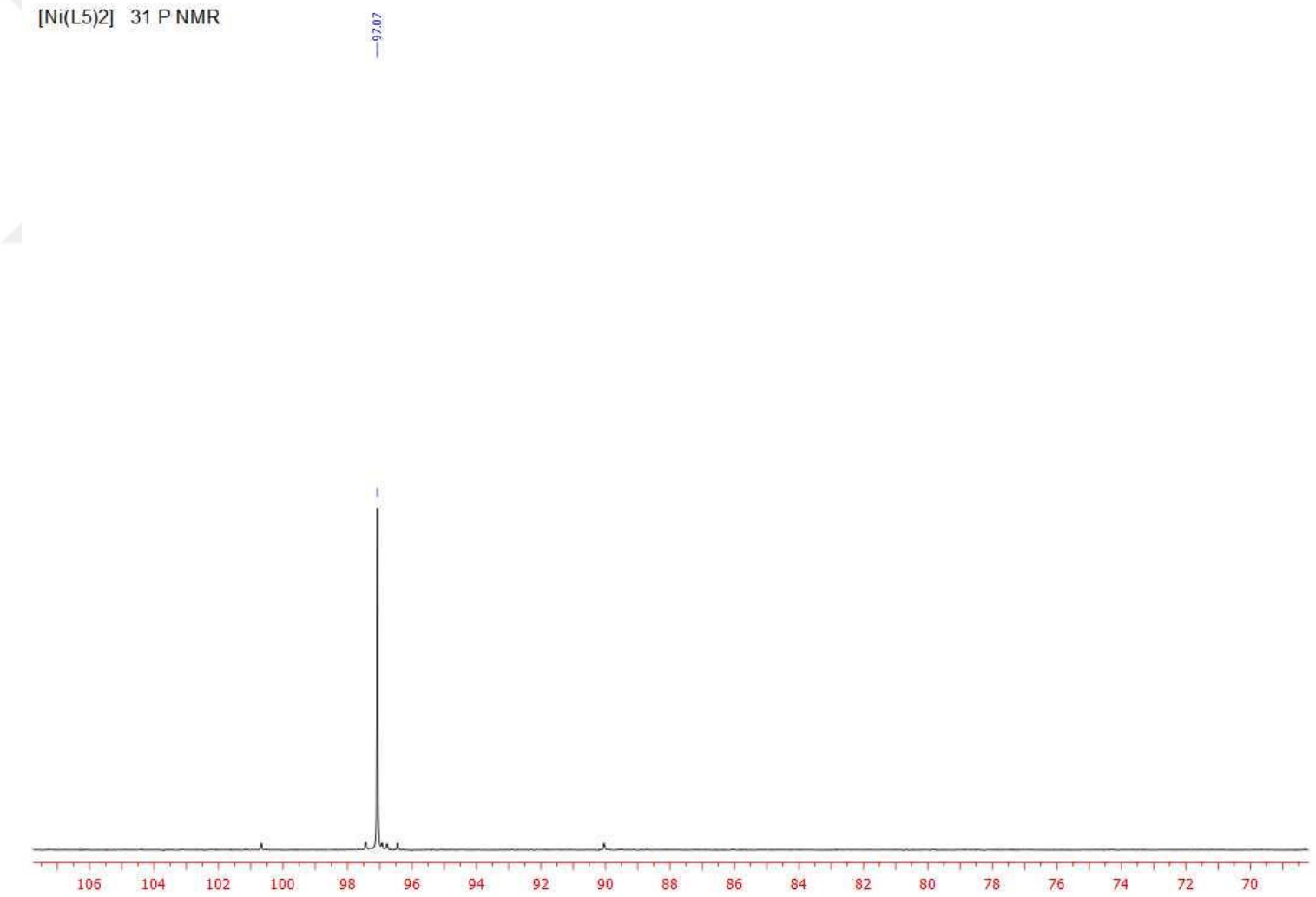


Figure 5.159. $[Ni(S_2P(R^x)(OR5))_2]$ ^{31}P-NMR spectrum.

5.1.7.12. Comments on ^{31}P-NMR Spectra of the Part II' Compounds

^{31}P-NMR spectra of the $[NH_4][S_2P(R^y)(ORn)]$ are of single peaks and ^{31}P chemical shifts of the ligands are observed in the range 99.8-103.4 ppm and those of the complexes in the range 98.5-102.6 ppm.

Table 5.14. ^{31}P-NMR data of the compounds.

Ligands	δ (ppm)		Complexes
$[NH_4][S_2P(R^y)(OR1)]$	99.82	98.46	$[Ni(S_2P(R^y)(OR1))_2]$
$[NH_4][S_2P(R^y)(OR2)]$	102.26	101.36	$[Ni(S_2P(R^y)(OR2))_2]$
$[NH_4][S_2P(R^y)(OR3)]$	103.44	102.61	$[Ni(S_2P(R^y)(OR3))_2]$
$[NH_4][S_2P(R^y)(OR4)]$	105.53	104.99	$[Ni(S_2P(R^y)(OR4))_2]$

^{31}P-NMR Spectra of Part II' $[NH_4][S_2P(R^y)(ORn)]$ and $[Ni(S_2P(R^y)(ORn))_2]$ Compounds.

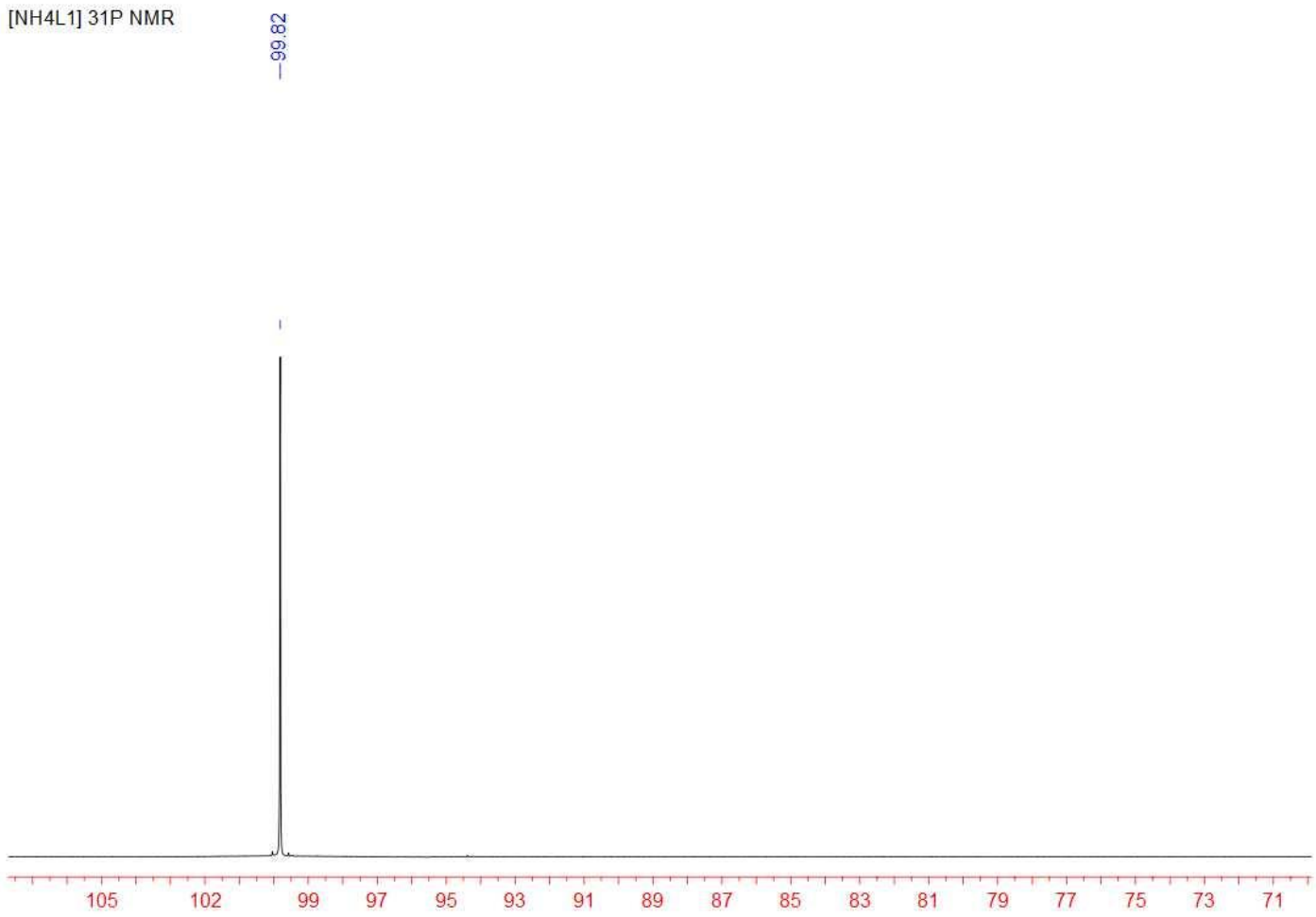


Figure 5.160. $[NH_4][S_2P(R^y)(OR1)]$ ^{31}P-NMR spectrum.

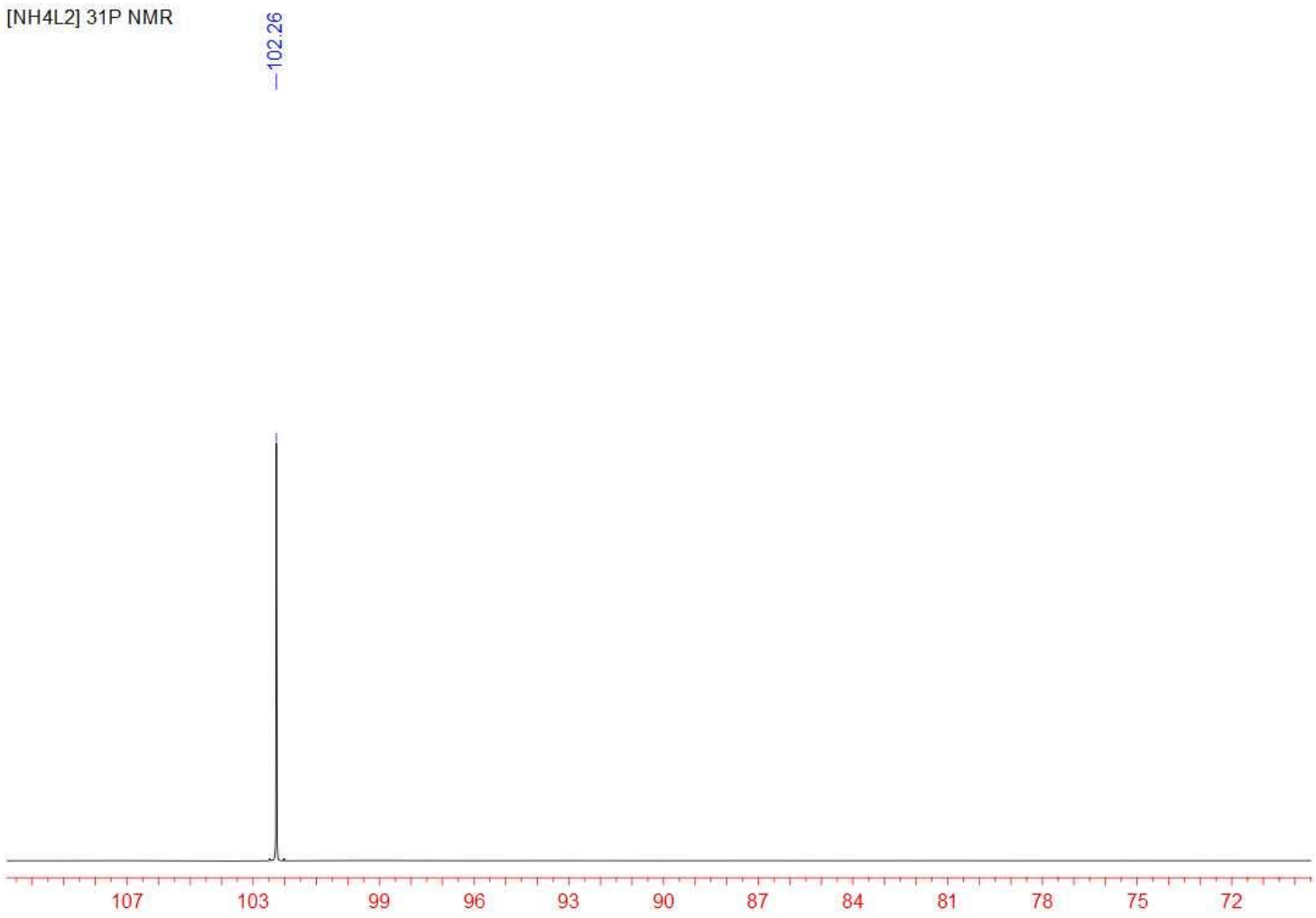


Figure 5.161. $[NH_4][S_2P(R^y)(OR2)]$ ^{31}P-NMR spectrum.

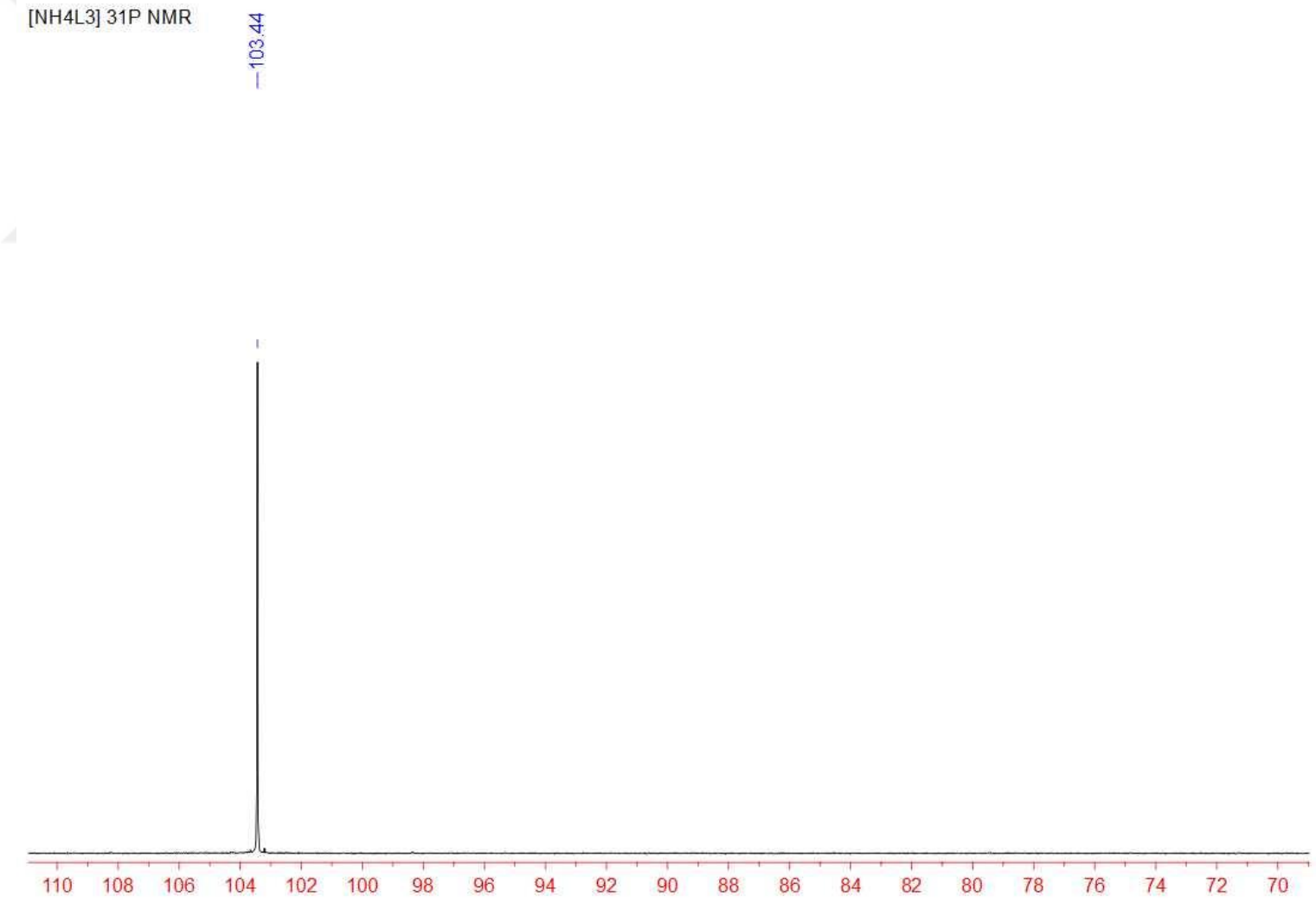


Figure 5.162. $[NH_4][S_2P(R^y)(OR3)]$ ^{31}P-NMR spectrum.

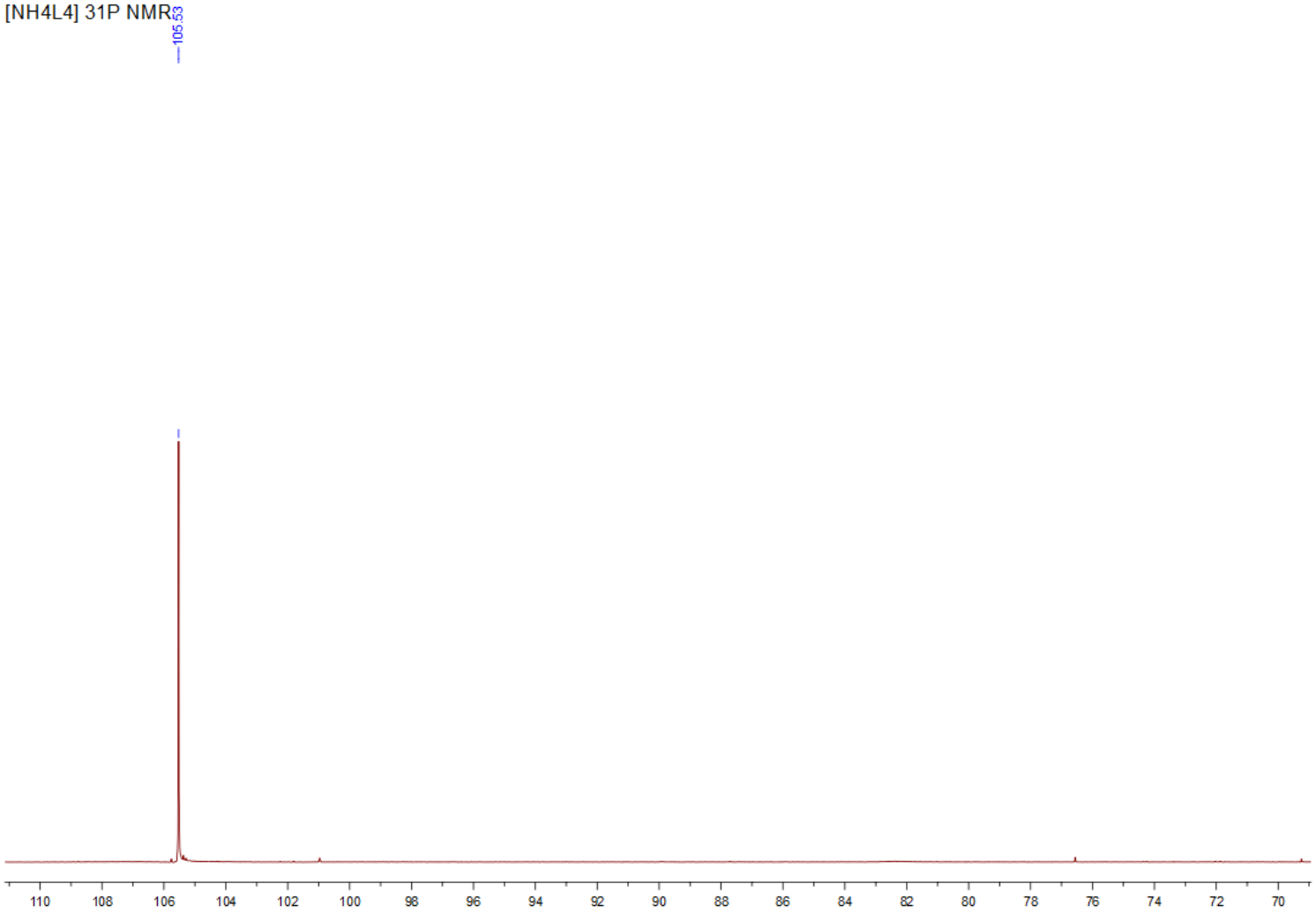


Figure 5.163. $[NH_4][S_2P(R^y)(OR4)]$ ^{31}P-NMR spectrum.

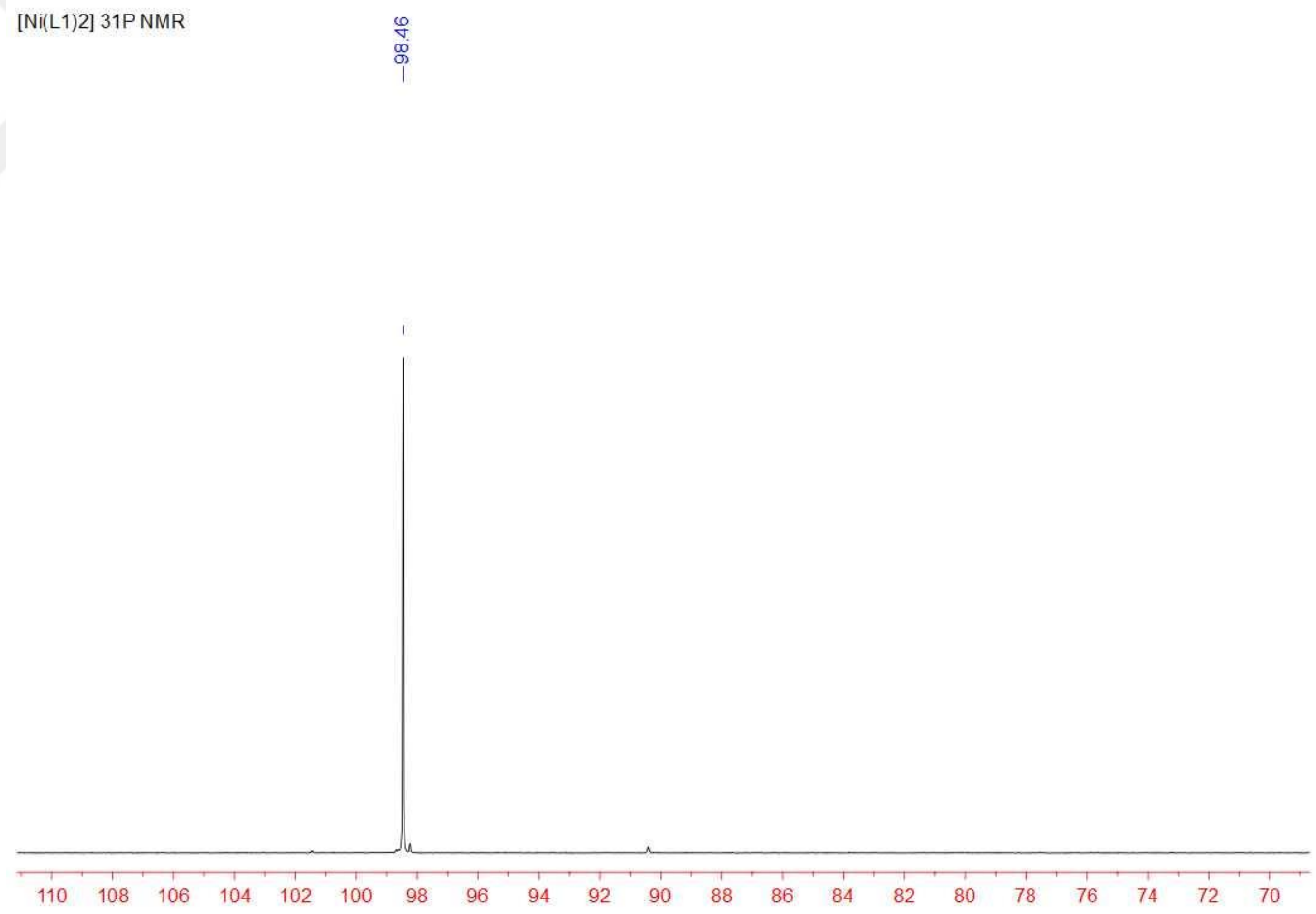


Figure 5.164. $[Ni(S_2P(R^y)(OR1))_2]$ ^{31}P-NMR spectrum.

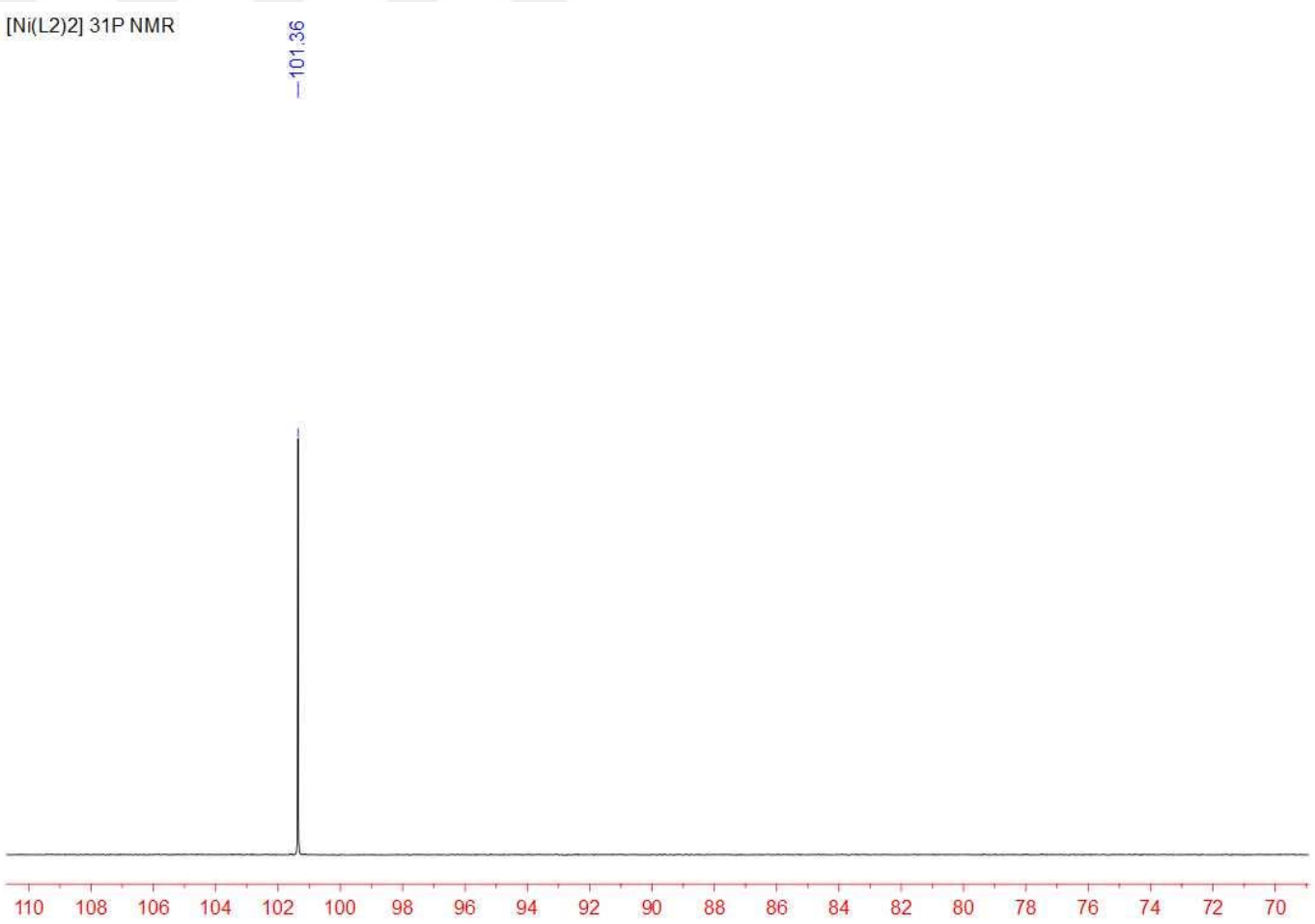


Figure 5.165. $[Ni(S_2P(R^y)(OR2))_2]$ ^{31}P-NMR spectrum.

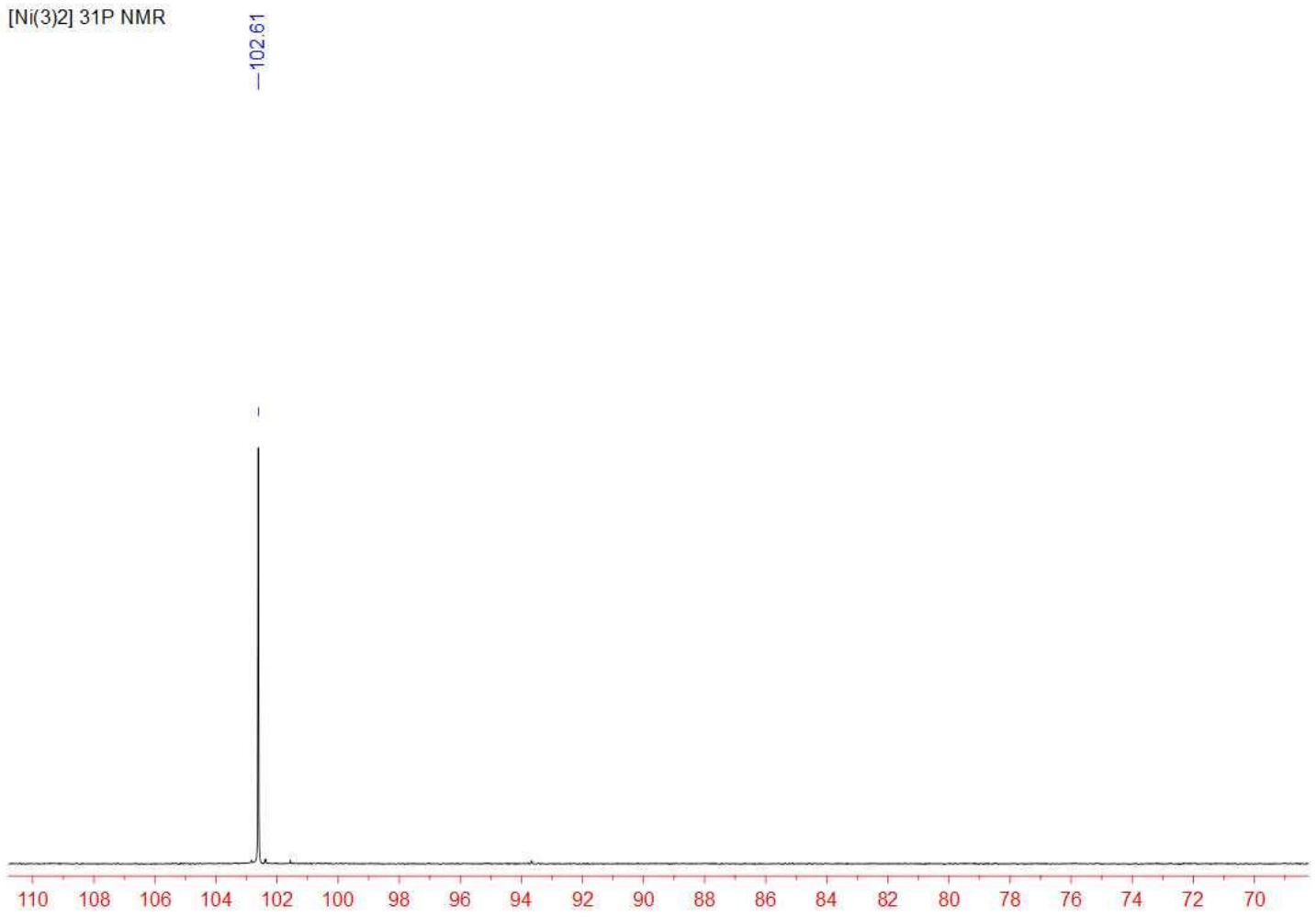


Figure 5.166. $[Ni(S_2P(R^y)(OR3))_2]$ ^{31}P-NMR spectrum.

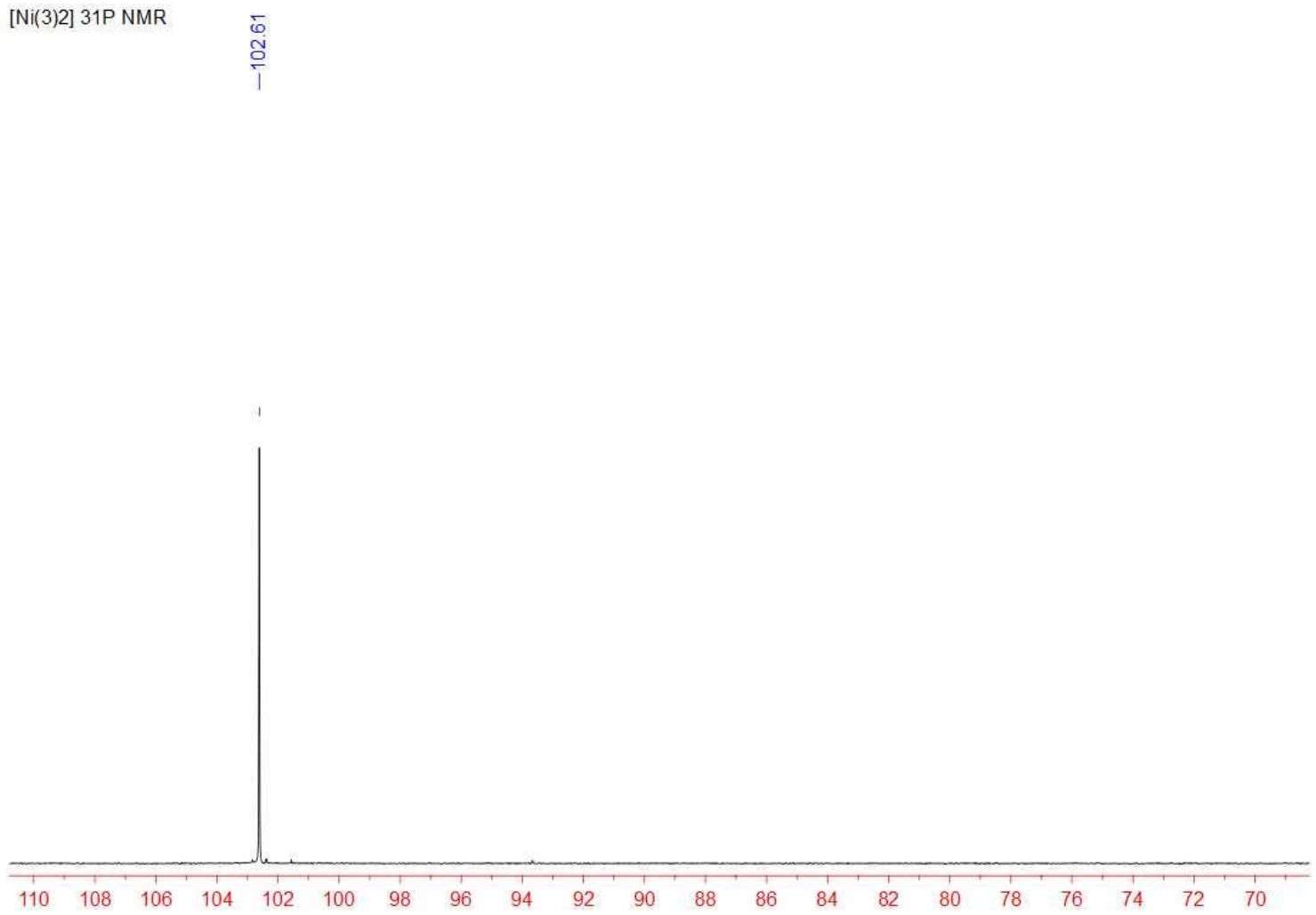


Figure 5.167. $[Ni(S_2P(R^y)(OR4))_2]$ ^{31}P-NMR spectrum**.**

5.2. Crystallographic Descriptions of the Spectra of the Part Ia' Ni(II) Complexes

The crystallographic data and refinement details of the data collection for all complexes are given in Table 5.15. Crystal structures of $[Ni(S_2P(R^x)(ORn))_2]$ (n=1-7) were unambiguously confirmed through single-crystal X-ray diffraction analysis. $[Ni(S_2P(R^x)(OR1))_2]$, $[Ni(S_2P(R^x)(OR2))_2]$, $[Ni(S_2P(R^x)(OR6))_2]$ and $[Ni(S_2P(R^x)(OR7))_2]$ appear to crystallize in the monoclinic system whereas $[Ni(S_2P(R^x)(OR4))_2]$ and $[Ni(S_2P(R^x)(OR5))_2]$ display a triclinic structure with *P*-1. Unlike other complexes, $[Ni(S_2P(R^x)(OR3))_2]$ belongs to orthorhombic *Pbca* space group. Whereas the asymmetric unit of most Ni(II) complexes consists of a single molecule, that of $[Ni(S_2P(R^x)(OR6))_2]$ involves two crystallographically independent compounds.

All the complexes consist of two dithiophosphonate ($[S_2P(R^x)(ORn)]^-$) and one crystallographically distinct Ni(II) ions. The numbering schemes are depicted in Figure 5.168A-5.175A. The Ni(II) ion in each of the complexes has a square planar coordination geometry formed by four sulfur atoms from two dithiophosphonate ligands. In $[Ni(S_2P(R^x)(OR1))_2]$, $[Ni(S_2P(R^x)(OR2))_2]$, $[Ni(S_2P(R^x)(OR3))_2]$, $[Ni(S_2P(R^x)(OR4))_2]$, and $[Ni(S_2P(R^x)(OR5))_2]$, four-coordinate τ_4 parameters for Ni(II) are between 0 - 0.037, and it can be considered as ideal square planar geometry [304]. It is worth noting that the dithiophosphonate moieties in $[Ni(S_2P(R^x)(OR1))_2]$ are in *cis*- configuration with respect to the coordination plane and similar structures with *cis*-arrangement are very rare in the literature [150, 268]. This may be attributed to the relatively less steric hindrance of methyl groups compared to the bulkier alkyl- and aryl- moieties in the other dithiophosphonates.

Table 5.15. Crystal data and refinement parameters for Part Ia' $[Ni(S_2P(R^x)(ORn))_2]$ (n=1-7) complexes.

Compound	$[Ni(S_2P(R^x)(OR1))_2]$	$[Ni(S_2P(R^x)(OR2))_2]$	$[Ni(S_2P(R^x)(OR4))_2]$	$[Ni(S_2P(R^x)(OR4))_2]$	$[Ni(S_2P(R^x)(OR5))_2]$	$[Ni(S_2P(R^x)(OR5))_2]$	$[Ni(S_2P(R^x)(OR5))_2]$
CCDC	2054965	2054966	2104693	2054967	2018565	2097183	2061755
Formula	$C_{18}H_{24}NiO_6P_2S_4$	$C_{20}H_{28}NiO_6P_2S_4$	$C_{22}H_{32}NiO_6P_2S_4$	$C_{24}H_{36}NiO_6P_2S_4$	$C_{26}H_{40}NiO_6P_2S_4$	$C_{26}H_{40}NiO_6P_2S_4$	$C_{30}H_{32}NiO_6P_2S_4$
Formula weight	585.26	613.31	641.36	669.42	697.47	697.47	737.44
Temperature (K)	299	173	298	173	293	298	173
Crystal system	Monoclinic	Monoclinic	Orthorhombic	Triclinic	Triclinic	Monoclinic	Monoclinic
Space group	$P2_1/c$	$P2_1/c$	Pbca	P-1	P-1	$P2_1/c$	$P2_1/n$
a (Å)	16.3817(11)	8.9418(14)	13.6507(8)	7.6989(15)	8.3887(7)	19.9615(13)	13.8324(11)
b (Å)	8.5996(6)	17.118(3)	9.7558(6)	9.3652(18)	14.1029(10)	8.4109(6)	7.9441(6)
c (Å)	18.0039(13)	8.8754(14)	22.1172(13)	11.490(2)	15.0466(11)	22.1262(15)	14.9078(11)
α (°)	90	90	90	106.398(2)	66.894(2)	90	90
β (°)	8.5996(6)	94.757(3)	90	106.975(2)	84.304(3)	116.2830(10)	96.3780(10)
γ (°)	90	90	90	99.988(2)	86.506(3)	90	90
Crystal size (mm^3)	0.23 × 0.13 × 0.12	0.23 × 0.14 × 0.12	0.34 × 0.14 × 0.13	0.46 × 0.18 × 0.01	0.11 × 0.1 × 0.07	0.30 × 0.22 × 0.12	0.14 × 0.08 × 0.06
Volume ($Å^3$)	2525.0(3)	1353.8(4)	2945.4(3)	729.9(2)	1628.7(2)	3330.8(4)	1628.0(2)

Table 5.15. Continues.

Compound	$[Ni(S_2P(R^x)(OR1))_2]$	$[Ni(S_2P(R^x)(OR2))_2]$	$[Ni(S_2P(R^x)(OR4))_2]$	$[Ni(S_2P(R^x)(OR4))_2]$	$[Ni(S_2P(R^x)(OR5))_2]$	$[Ni(S_2P(R^x)(OR5))_2]$	$[Ni(S_2P(R^x)(OR5))_2]$
Z	4	2	4	1	2	4	2
ρcalcd (g. cm^{-3})	1.540	1.505	1.446	1.523	1.422	1.391	1.504
μ (mm^{-1})	1.257	1.176	1.085	1.098	0.987	0.965	0.992
F(000)	1208	636	1336	350	732	1464	764
2θ range for data collection (°)	4.546 to 50.17	4.572 to 50.046	4.74 to 49.992	4.976 to 54.972	5.742 to 49.996	3.71 to 49.994	3.812 to 52.766
Index ranges	-19 ≤ h ≤ 19, -10 ≤ k ≤ 10,-21 ≤ l ≤ 21	-10 ≤ h ≤ 10, -20 ≤ k ≤ 20, -8 ≤ l ≤ 10	-16 ≤ h ≤ 16, -11 ≤ k ≤ 11, -26 ≤ l ≤ 26	-9 ≤ h ≤ 9, -12 ≤ k ≤ 12, -14 ≤ l ≤ 14	-9 ≤ h ≤ 9, -16 ≤ k ≤ 16, -17 ≤ l ≤ 17	-23 ≤ h ≤ 20, -10 ≤ k ≤ 10, -26 ≤ l ≤ 26	17 ≤ h ≤ 17, -9≤ k ≤ 9, -18 ≤ l ≤ 18
Reflections collected	31577	5290	25794	10236	44258	30995	22265
Independent reflections	4489 [R_{int} = 0.0806, R_{sigma} = 0.0551]	2352 [R_{int} = 0.0237, R_{sigma} = 0.0323]	2586 [R_{int} = 0.0316, R_{sigma} = 0.0177]	3316 [R_{int} = 0.0352, R_{sigma} = 0.0365]	5663 [R_{int} = 0.0372, R_{sigma} = 0.0236]	5846 [R_{int} = 0.0405, R_{sigma} = 0.0312]	3322 [R_{int} = 0.0277, R_{sigma} = 0.0172]
Data/restraints/ parameters	4489/0/286	2352/0/154	2586/41/192	3316/0/172	155663/0/361	5846/122/432	3322/0/198
Goodness-of-fit on *F*2 (S)	1.015	1.081	1.081	1.047	1.208	1.064	1.054
Final R indexes [*I*>=2σ (*I*)]	R_1 = 0.0434, wR_2 = 0.0899	R_1 = 0.0290, wR_2 = 0.0723	R_1 = 0.0386, wR_2 = 0.1032	R_1 = 0.0272, wR_2 =0.0736	R_1 = 0.0620, wR_2 = 0.1255	R_1 = 0.0477, wR_2 = 0.1176	R_1 = 0.0233, wR_2 =0.0604
Final R indexes [all data]	R_1 = 0.0825, wR_2 = 0.1051	R_1 = 0.0342, wR_2 = 0.0751	R_1 = 0.0468, wR_2 = 0.1094	R_1 = 0.0304, wR_2 = 0.0758	R_1 = 0.0735, wR_2 = 0.1299	R_1 = 0.0707, wR_2 = 0.1277	R_1 = 0.0279, wR_2 = 0.0634
Largest diff. peak and hole (e.$Å^{-3}$)	0.37/-0.27	0.38/-0.21	0.41/-0.28	0.50/-0.36	0.72/-0.67	0.34/-0.32	0.34/-0.19

The selected bond lengths and bond angles are given in Table 5.23. The Ni–S bond distances in Ni(II) coordination sphere are between 2.2148 (13) - 2.2311 (12) Å / 2.1970 – 2.3501 Å (Exp./Cal.) for $[Ni(S_2P(R^x)(OR1))_2]$, 2.2228 (6) - 2.2267 (6) / 2.3480 – 2.3489 Å (Exp./Cal.) for $[Ni(S_2P(R^x)(OR2))_2]$, 2.2121(8) - 2.2246(8) Å / 2.3483 – 2.3488 Å (Exp./Cal.) for $[Ni(S_2P(R^x)(OR3))_2]$, 2.2288 (6) - 2.2318 (5) Å / 2.3440 - 2.3482 Å (Exp./Cal.) for $[Ni(S_2P(R^x)(OR4))_2]$, 2.2261(15) - 2.2388(14) Å /2.3440 – 2.3482 (Exp./Cal.) for $[Ni(S_2P(R^x)(OR5))_2]$, 2.2217 (11) ~~Å~~ - 2.2294 (9) Å / 2.3482 – 2.3485 Å (Exp./Cal.) for $[Ni(S_2P(R^x)(OR6))_2]$, and 2.2156 (4) - 2.2244 (4) Å / 2.3475 – 2.3476 Å for $[Ni(S_2P(R^x)(OR7))_2]$. The S-Ni-S bond angles exhibit almost the same tendency in all complexes and range from 87.84 (5)° to 180.0°/ 89.325° to 180.0° (Exp./Cal.). As expected, the optimized bond lengths are somewhat longer than the experimental values. These results are not surprising because the optimized results are based on the unpacked isolated molecules while the experimental results are obtained in the solid-state form. The N-S bond distances and S-Ni-S bond angles are compatible with those previously found in dithiophosphonato Ni(II) complexes [150, 250, 251, 254, 265, 268, 296, 305, 306]. The average P-S bond lengths for $[Ni(S_2P(R^x)(ORn))_2]$ are typically about 2.0 Å, which shows that π-electron delocalization prevails in the $-PS_2$ moiety of dithiophosphonates. These values are consistent with the literature reports [252, 264, 265, 307-309]. As indicated in Table 5.16, intermolecular CH···O hydrogen bonding interactions are to be considered 'weak' because the experimental CH···O distance between the CH groups and O atoms in the dithiophosphonato anions ($d_{(O\cdots H)}$ ~ 2.52-2.72 Å) are longer than the corresponding van der Waals distances ($r_{vdw}(O) + r_{vdw}(H) = 2.72$ Å), (Figures. 5.168B-5.186B). On the other hand, the CH···S hydrogen bonding interactions (corresponding van der Waals distances ($r_{vdw}(S) + r_{vdw}(H) = 3.00$ Å) were observed only in $[Ni(S_2P(R^x)(OR1))_2]$, $[Ni(S_2P(R^x)(OR2))_2]$, and $[Ni(S_2P(R^x)(OR7))_2]$ (Figures. 5.168D, 5.169D, and 5.186C). It is noteworthy that, in all the complexes, the short intermolecular π···π interactions with less than 3.8 Å distance in between are not present. But C-H···π interactions for $[Ni(S_2P(R^x)(OR1))_2]$, $[Ni(S_2P(R^x)(OR2))_2]$, $[Ni(S_2P(R^x)(OR3))_2]$, $[Ni(S_2P(R^x)(OR5))_2]$ and $[Ni(S_2P(R^x)(OR7))_2]$ are notable.

Table 5.16. The intermolecular C-H···X (X= O, S, π) interactions (Å and °) for the complexes.

D—H···A	Symmetry	d(D-H)	d(H···A)	d(D-H···A)	D-H···A
$[Ni(S_2P(R^x)(OR1))_2]$					
C12-H12B···S1	x, 5/2-y, -1/2+z	0.96	2.98	3.691	132
C8-H8C···O5	1-x, 2-y,1-z	0.96	2.56	3.454	155
C8-H8A···Cg1	1-x, 1-y,1-z	0.96	2.65	3.479	144
$[Ni(S_2P(R^x)(OR2))_2]$					
C3-H3···S1	1-x, 1-y, 1-z	0.95	2.96	3.692	135
C9-H9B···S2	x, 1/2-y, 1/2+z	0.98	2.95	3.925	172
C7-H9A···O1	x, 1/2-y, -1/2+z	0.99	2.63	3.546	155
C9-H9A···O2	x, 1/2-y, -1/2+z	0.98	2.70	3.117	106
C8-H8A···Cg1	2-x, 1-y, 1-z	0.98	2.72	3.599	150
$[Ni(S_2P(R^x)(OR3))_2]$					
C3-H3···O3	1-x, 1/2+y, 1/2-z	0.93	2.72	3.645	175
C9-H9C···Cg1	1/2-x,-1/2+y, z	0.96	2.97	3.636	128
C10-H10B···Cg1	1-x, -y, -z	0.97	2.72	3.645	159

D—H···A	Symmetry	d(D-H)	d(H···A)	d(D-H···A)	D-H···A
$[Ni(S_2P(R^x)(OR4))_2]$					
C11-H11A···O2	x, y, -1+z	0.99	2.65	3.572	156
$[Ni(S_2P(R^x)(OR5))_2]$					
C12-H12A···O4	2-x, 1-y, -z	0.96	2.71	3.634	162
C12-H12A···O5	2-x, 1-y, -z	0.96	2.52	3.285	136
C9-H9B···O2	1-x, 1-y, 2-z	0.96	2.57	3.525	171
C12-H12B···O3	1-x,1-y,1-z	0.96	2.68	3.618	166
C11-H11C···Cg1	x, y, -1+z	0.96	2.73	3.494	137
$[Ni(S_2P(R^x)(OR6))_2]$					
C18-H18B···O2	1-x,1/2+y,1/2-z	0.96	2.65	3.229	119
C9-H9A···O4	-	0.96	2.66	3.504	147
$[Ni(S_2P(R^x)(OR7))_2]$					
C11-H11···O3	1/2-x, 1/2+y, 1/2-z	0.95	2.67	3.416	136
C14-H14···S1	1-x, 1-y, 1-z	0.95	2.96	3.857	159
C6-H6···S2	3/2-x, -1/2+y, 1/2-z	0.95	2.98	3.894	162
C13-H13···Cg1	1/2+x, 3/2-y, - 1/2+x	0.95	2.70	3.542	147
C15-H15···Cg2	3/2-x, -1/2+y, 1/2-x	0.95	2.95	3.841	157

In $[Ni(S_2P(R^x)(OR1))_2]$, the C8-H8C···O5 ($d_{(C8\cdots O5)}$ = 3.454 Å) contacts link the molecules to form a hydrogen-bonded dimer (Figure 5.168B). HS of $[Ni(S_2P(R^x)(OR1))_2]$ are illustrated in Figure 5.168C, and the O···H/ H···O interactions appear as distinct spikes in the 2D fingerprint plot (Figure 5.170A), which constitute 15.5%. These hydrogen-bonded dimers are expanded into a 1D zigzag hydrogen-bonded chain connected by C12-H2B···S1 ($d_{(C12\cdots S1)}$ = 3.691 Å) contacts running along the *c*-axis (Figure 5.168D). The second most predominant contribution to the total HS by 19.0% is from the S···H/H···S interactions appearing as distinct spikes in the 2D fingerprint plot. Interestingly, as shown in Figure 5.168E, the C8-H8A···π_{phenyl} ($d_{(H\cdots\pi)}$ = 2.65 Å, Figure 5.169A) interaction contributed to stabilization of the 3D supramolecular network to form a honeycomb-like motif viewed down the *a*-axis. The closest C-H···π_{phenyl} interaction is seen in $[Ni(S_2P(R^x)(OR1))_2]$, as illustrated in the shape index-mapped HS (Figure 5.169B).

In $[Ni(S_2P(R^x)(OR2))_2]$, the weak CH···O (C7-H7A···O1, $d_{(C7\cdots O1)}$ = 3.546 Å and C9-H9A···O2, $d_{(C9\cdots O2)}$ = 3.117 Å) and C-H···S (C3-H3···S1, $d_{(C3\cdots S1)}$ = 3.692 Å and C9-H9B···S2, $d_{(C9\cdots S2)}$ = 3.925 Å) hydrogen bonding interactions form a 2D supramolecular layers (Figure 5.171B, 5.171C, 5.171D). The 2D fingerprint regions of $[Ni(S_2P(R^x)(OR2))_2]$ shows that the S···H/H···S and O···H/H···O interactions constitute the significant area of the HS with the ratio of 22.7% and 16.5% (see Figure 5.173A). Moreover, these 2D layers are expanded into a 3D supramolecular network (Figure 5.171E) by the C8-H8A···π_{phenyl} ($d_{(H\cdots\pi)}$ = 2.72 Å, Figure 5.172A) interactions. The C···H/H···C interactions comprise 16.8% of the HS, which represent C–H···π interactions (Figure 5.172).

In $[Ni(S_2P(R^x)(OR3))_2]$, the C3-H3···O3 (d(C3···O3) = 3.645 Å, Figure 5.174C) hydrogen bonding interactions, which comprises the ratio of 12.4% of the HS (Figure 5.176A), sustained by running along the *bc*-plane to form a 2D hydrogen-bonded layers (Figure 5.174B), which are stabilized by the short C–H···π contacts (C10-H10B···π, ($d_{(H\cdots\pi)}$ = 3.645(12) Å). Furthermore, the other C–H···π interactions (C9-H10C···π, ($d_{(H\cdots\pi)}$ = 3.636(4) Å) play a crucial role in the formation of the herringbone-like 3D supramolecular network (Figure 5.174D). The C···H/H···C intermolecular interactions that represent C–H···π interactions (Figure 5.175A) comprise 15.7% of the total HS for

$[Ni(S_2P(R^x)(OR3))_2]$. The HS shape index of $[Ni(S_2P(R^x)(OR3))_2]$ shows concave curvature, where C—H···π interactions occur (Figure 175B).

In $[Ni(S_2P(R^x)(OR4))_2]$, the weak CH···O (C11-H11A···O2, $d_{(C11\cdots O2)}$ = 3.572 Å, Figure 5.177B) hydrogen bonding interactions Figure 5.177C), which comprise 14.1% of the HS (Figure 5.179A), generated a 1D hydrogen-bonded chains along the *c*-axis. These chains are further linked by the short C–H···C contacts (C3-H3···C12, $d_{(H3\cdots C12)}$ = 2.88 Å; C8-H8A···C2, $d_{(H8A\cdots C2)}$ = 2.84 Å; C12-H12B···C5, $d_{(C12B\cdots C5)}$ = 2.82 Å), which are less than corresponding sum of the van der Waals distances ($r_{vdw}(C) + r_{vdw}(H)$ = 2.90 Å), to form a 2D hydrogen-bonded layers (Figure 5.177D). Moreover, the adjacent layers are connected through the weak π···π interactions ($d_{(\pi\cdots\pi)}$ = 4.255 Å) between the phenyl rings (Figure 5.178A) to form a 3D supramolecular network (Figure 5.177E). This π···π interaction is observed by looking at the pattern of adjacent red and blue triangles on the HS shape index map (Figure 5.178B).

In $[Ni(S_2P(R^x)(OR5))_2]$, the intermolecular C–H···O interactions (C12-H12A···O4, $d_{(C12\cdots O4)}$ = 3.634 Å; C12-H12A···O5, $d_{(C12\cdots O5)}$ = 3.285 Å; C9-H9B···O2, $d_{(C9\cdots O2)}$ = 3.525 Å; C12-H12B···O3, $d_{(C12\cdots O3)}$ = 3.618 Å, Figure 5.180B) comprising 11.8% of the HS (Figure 5.180C, Figure 5.182A) form a 2D hydrogen-bonded layers along the *ac*-axis. In addition, the C–H···π interactions (C11-H11C···π, (d(H···π) = 2.73 Å, Figure 5.181A) contribute to the stabilization of the 3D supramolecular network (Figure 180D). The HS shape index of $[Ni(S_2P(R^x)(OR5))_2]$ displays concave curvature, where C—H···π interactions occur (Figure 181B).

In $[Ni(S_2P(R^x)(OR6))_2]$, two molecules in the asymmetric unit interact with each other through the weak intermolecular C—H···O interaction (C9—H9A···O4, $d_{(C9\cdots O4)}$ = 3.504 Å) and moderate π···π interaction ($d_{(\pi\cdots\pi)}$ = 3.838 Å) between the phenyl rings, as shown in Figure 5.183B and Figure 5.184A. The HS shape index displays the evidence of the adjacent red and blue triangles on the shape index surface (Figure 5.184B). The other intermolecular C—H···O interaction (C18—H18B···O2, $d_{(C18\cdots O2)}$ = 3.504 Å) plays a key factor to construct the 3D herringbone-like supramolecular network (Figure 5.183D). As indicated Figure 5.183C, the weak C—H···O interactions make an 8.5% contribution to the total HS, (Figure 5.185A).

In $[Ni(S_2P(R^x)(OR7))_2]$, the 3D supramolecular network is mainly stabilized by the weak

C—H···O interaction (C11—H11···O3, $d_{(C11\cdots O3)}$ = 3.416 Å, Figure 5.186B) and the weak C—H···S interactions (C14—H14···S1, $d_{(C14\cdots S1)}$ = 3.857 Å; C6—H6···S2, $d_{(C6\cdots S2)}$ = 3.894 Å, Figures 5.186C and 5.186D). The C—H···O and C—H···S interactions comprise 14.1% and 12.9% of the total HS, respectively (Figure 5.188A). The C—H···π interactions (C13—H13···π, (d(H···π) = 2.70 Å; C15—H15···π, (d(H···π) = 2.95 Å, Figure 5.187A) also contributed the formation of a 3D network of crystal structure (Figure 5.186E). The C—H···π interactions in $[Ni(S_2P(R^x)(OR7))_2]$ are easily can be seen in the HS shape index exhibiting concave curvature, where C—H···π interactions occur in Figure 5.187B.

To summarize the intermolecular interactions quantitatively, the 2D fingerprint plots exhibit that the most dominant interaction in $[Ni(S_2P(R^x)(ORn))_2]$ (n=1-7) is the H/H interaction contributing to the total HS with the values equal to 41.1%, 42%, 47.5%, 51.5%, 56.7%, 59.4%, and 42.7%, respectively. This is probably due to the abundant aliphatic and aromatic hydrogen atoms in the compounds. The second most contributions to the total HS in $[Ni(S_2P(R^x)(ORn))_2]$ (n=1-6) are from S/H···H/S interactions appearing as distinct spikes, which constitute 22.9%, 22.7%, 21.4%, 17.2%, 14.1, and 18%, respectively. This provides evidence for the important role of the C—H···S interactions in the stabilization of crystal structure. In the presence of benzyl, instead of aliphatic side groups, in $[Ni(S_2P(R^x)(OR7))_2]$, the S/H···H/S interaction rate drops significantly. The fact that the side groups are aromatic makes C—H···π interactions be the second-highest contribution to the HS in $[Ni(S_2P(R^x)(OR7))_2]$. The non-classical C—H···O hydrogen bonds are one of the other weak interactions observed in these complex structures. It can be concluded that, as a general trend, the S/H···H/S interactions are the most important interactions after C—H···S interactions, comprising 15.5%, 16.5%, 12.4%, 14.1%, 11.8%, 8.5%, and 14.1% of the total HS, respectively. It is also worth noting that the C—H···π interactions in $[Ni(S_2P(R^x)(ORn))_2]$ (n=1-7) make a remarkable contribution in the formation of supramolecular network with the ratio of 10.7%, 16.8%, 15.7%, 11.7%, 11.7%, 6.9%, and 25.4%, respectively. The shortest π···π interaction among all Ni(II) complexes was observed in the $[Ni(S_2P(R^x)(OR6))_2]$, as exhibited large flat region on the curvedness mapped on the Hirshfeld surface (Figure 5.185C).

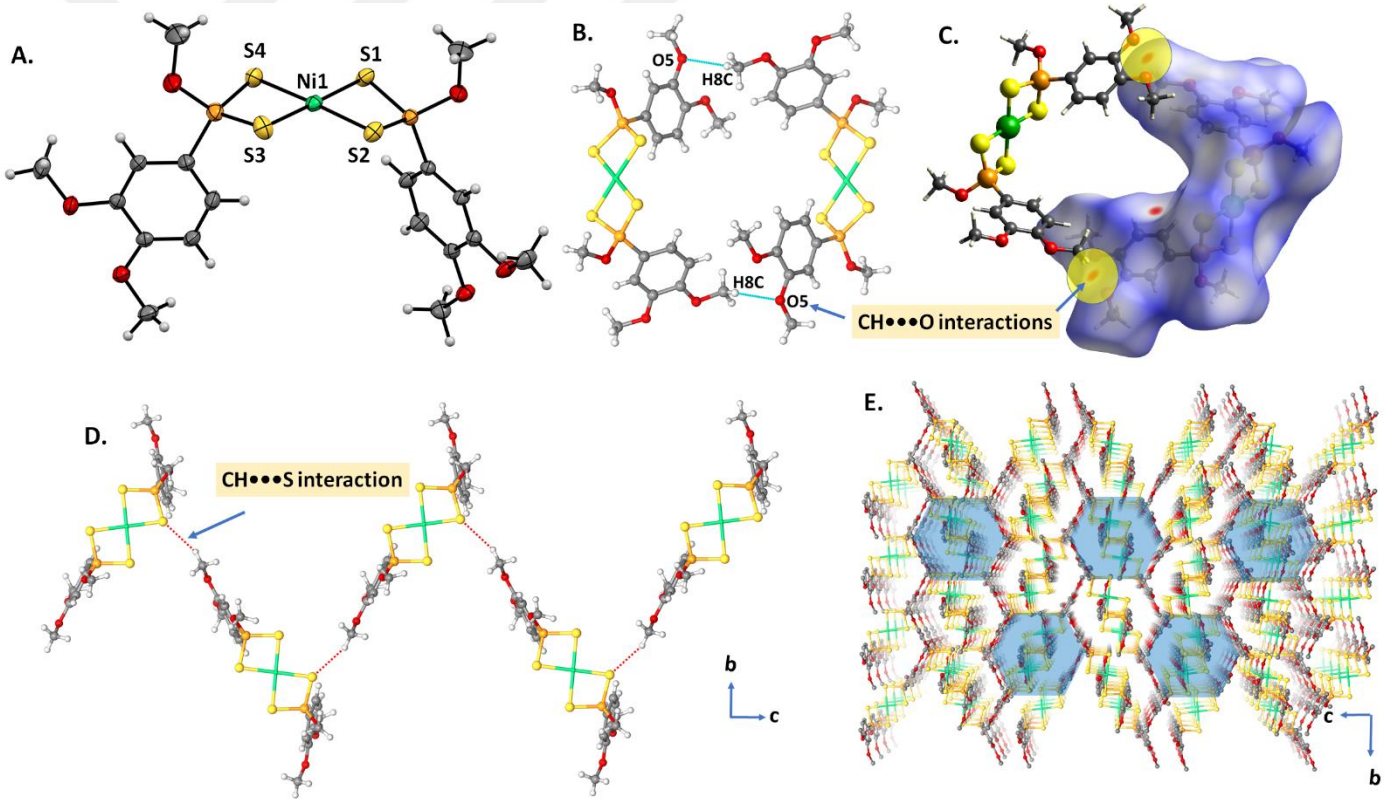


Figure 5.168. A) Crystal structure of $[Ni(S_2P(R^x)(OR1))_2]$ with displacement ellipsoids drawn at the 50% probability level. **B)** and **C)** HS of $[Ni(S_2P(R^x)(OR1))_2]$ mapped with d_{norm}, showing the CH···O hydrogen bonding interactions **D)** View of the one-dimensional CH···S hydrogen-bonded chains running along the crystallographic *c*-axis. **E)** The illustration of the 3D supramolecular network showing the honeycomb-like motif.

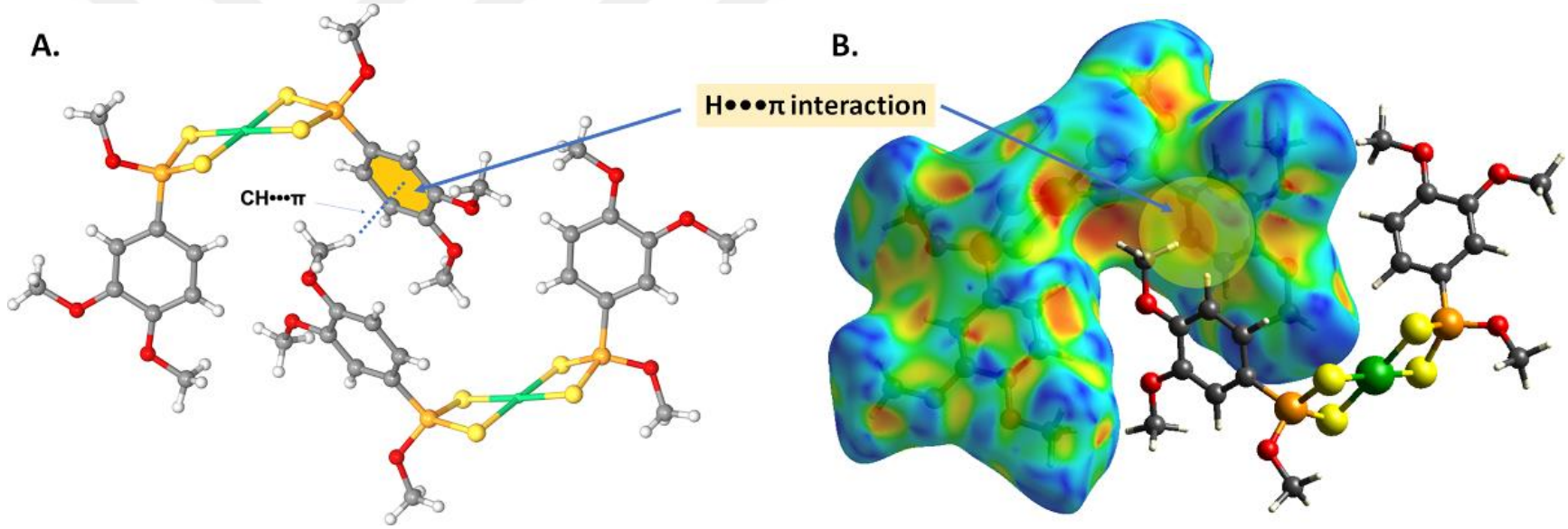


Figure 5.169. A) Representations of the C8-H8A···π_{phenyl} (d(H···π) = 2.65 Å) interactions in [Ni($S_2P(R^x)(OR1))_2$]. B) The HS shape index exhibits concave curvature, where C-H···π interaction occur.

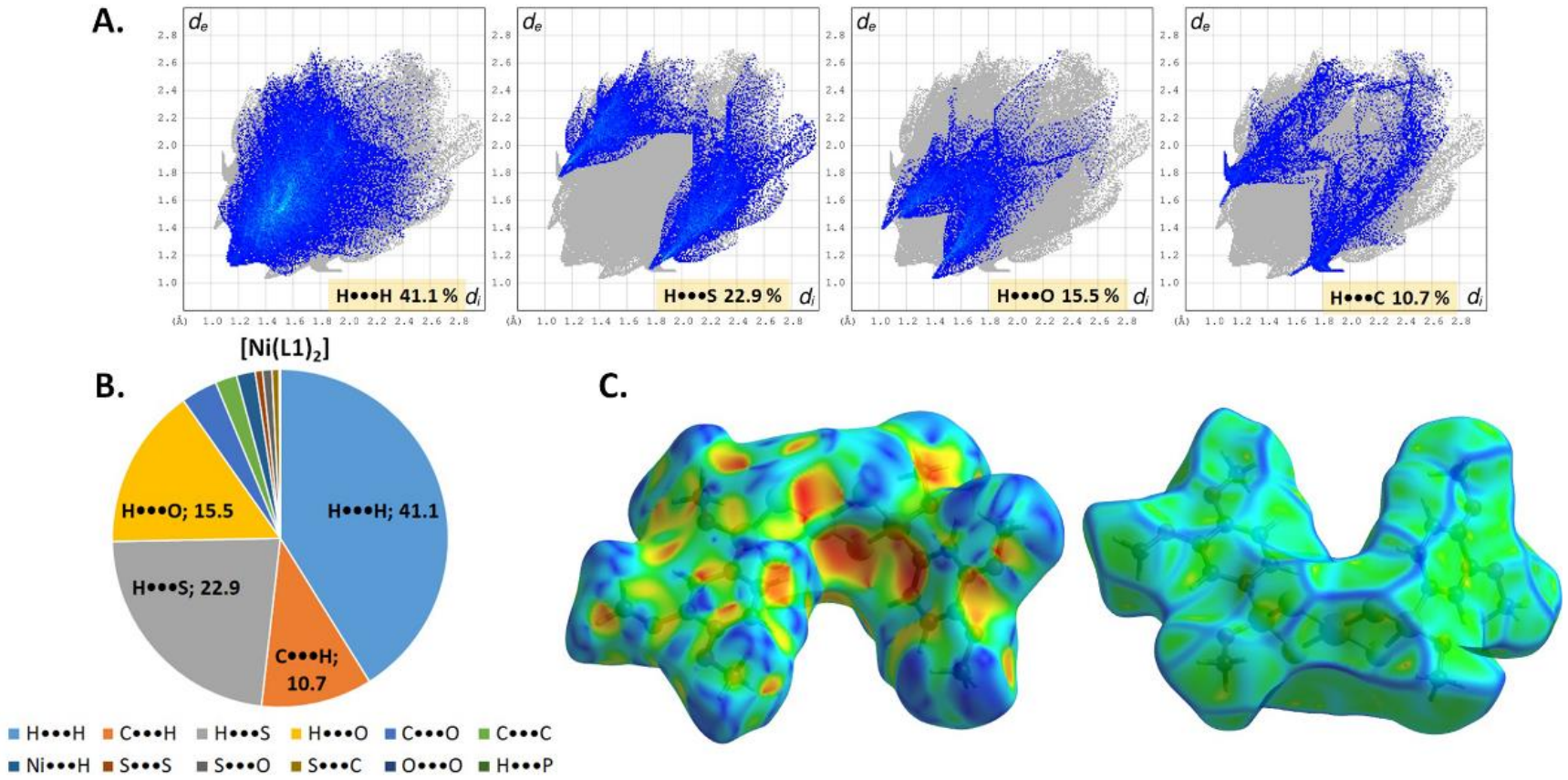


Figure 5.170. The resolved 2D fingerprint plots showing the percentage contributions to the total HS area in [Ni($S_2P(R^x)(OR1)$)$_2$].

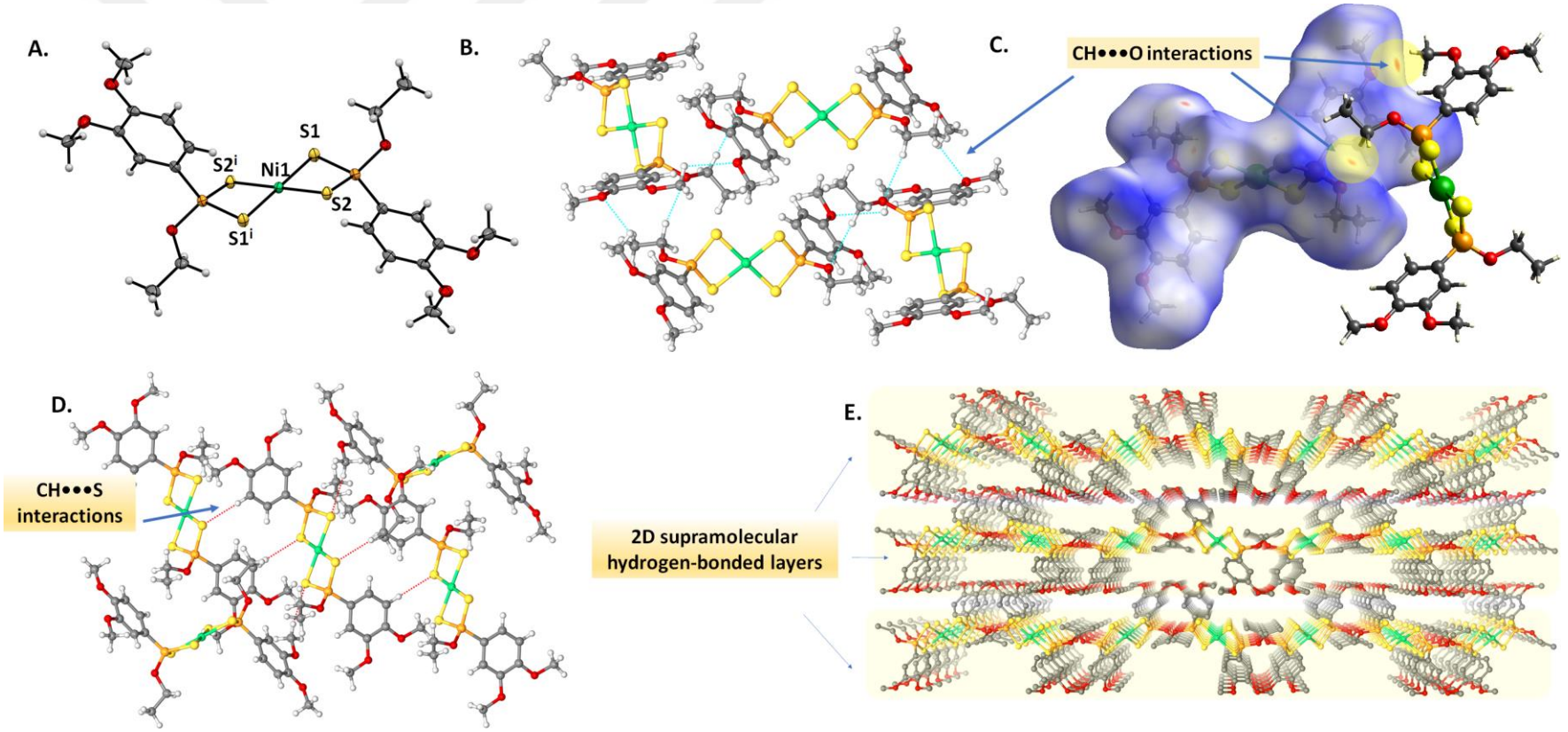


Figure 5.171. A) Crystal structure of $[Ni(S_2P(R^x)(OR2))_2]$ with displacement ellipsoids drawn at the 50% probability level (symmetry code: i: -x+1, -y+1, -z) **B)** and **C)** HS of $[Ni(S_2P(R^x)(OR2))_2]$ mapped with d_{norm}, showing the CH···O hydrogen bonding interactions **D)** View of the CH···S hydrogen bonding interactions in the crystal structure **E)** The illustration of the 3D supramolecular network showing 2D hydrogen-bonded layers.

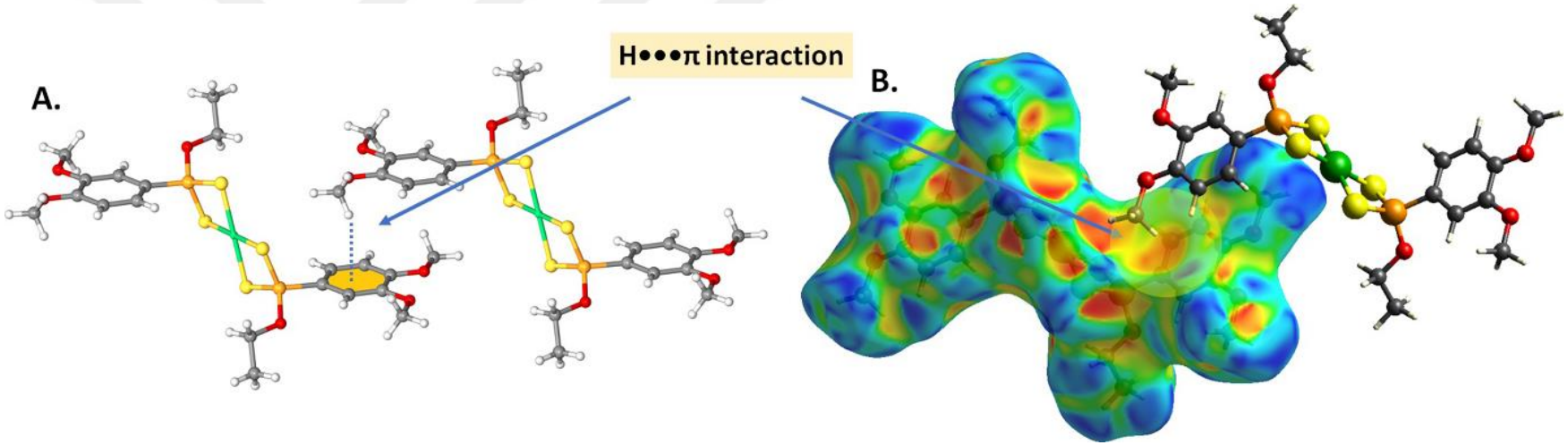


Figure 5.172. A) Representations of the C8-H8A···π_{phenyl} (d(H···π) = 2.72 Å) interactions in [Ni($S_2P(R^x)(OR2)$)$_2$]. B) The HS shape index exhibits concave curvature, where C-H···π interaction occur.

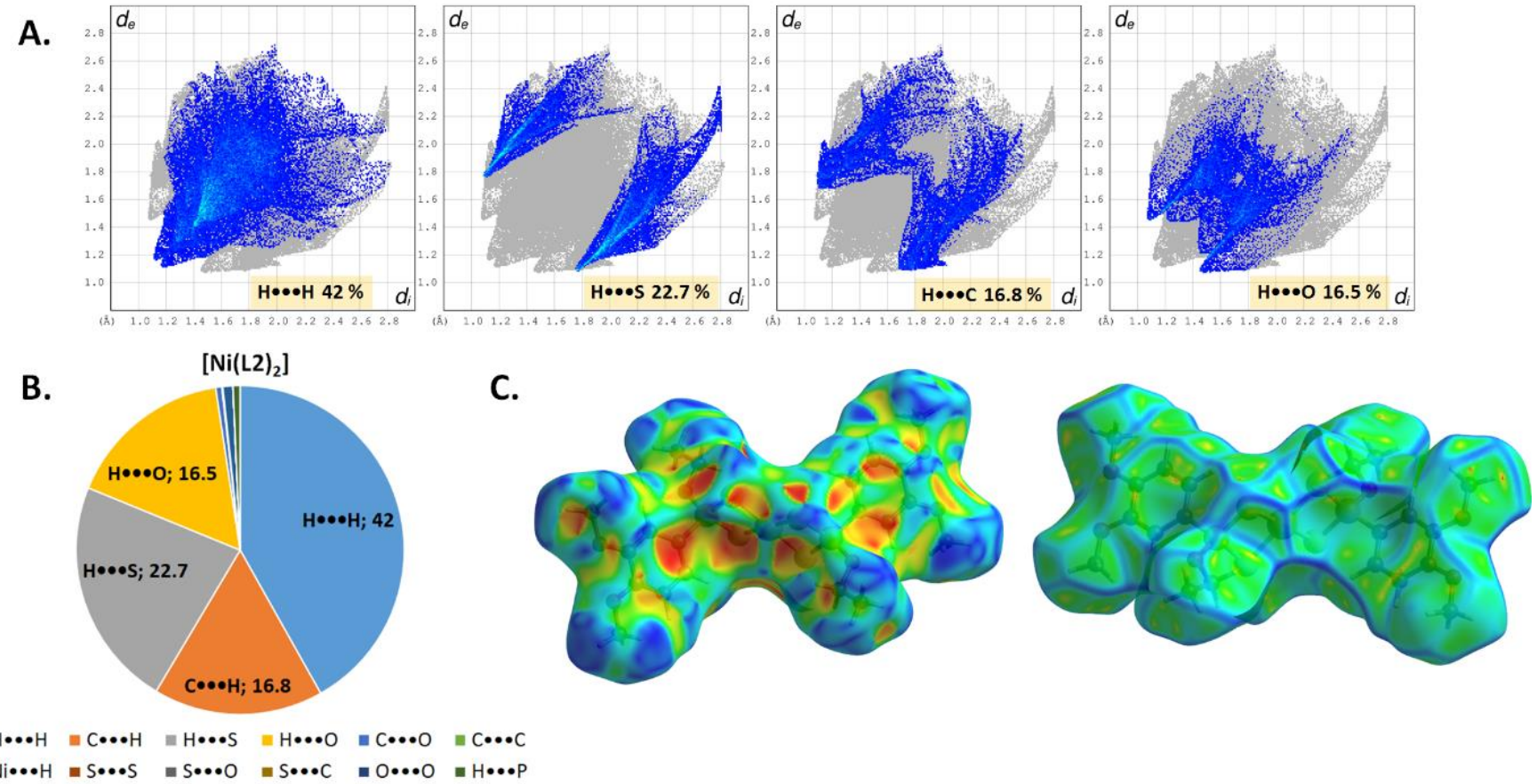


Figure 5.173. The resolved 2D fingerprint plots showing the percentage contributions to the total HS area in $[Ni(S_2P(R^x)(OR2))_2]$.

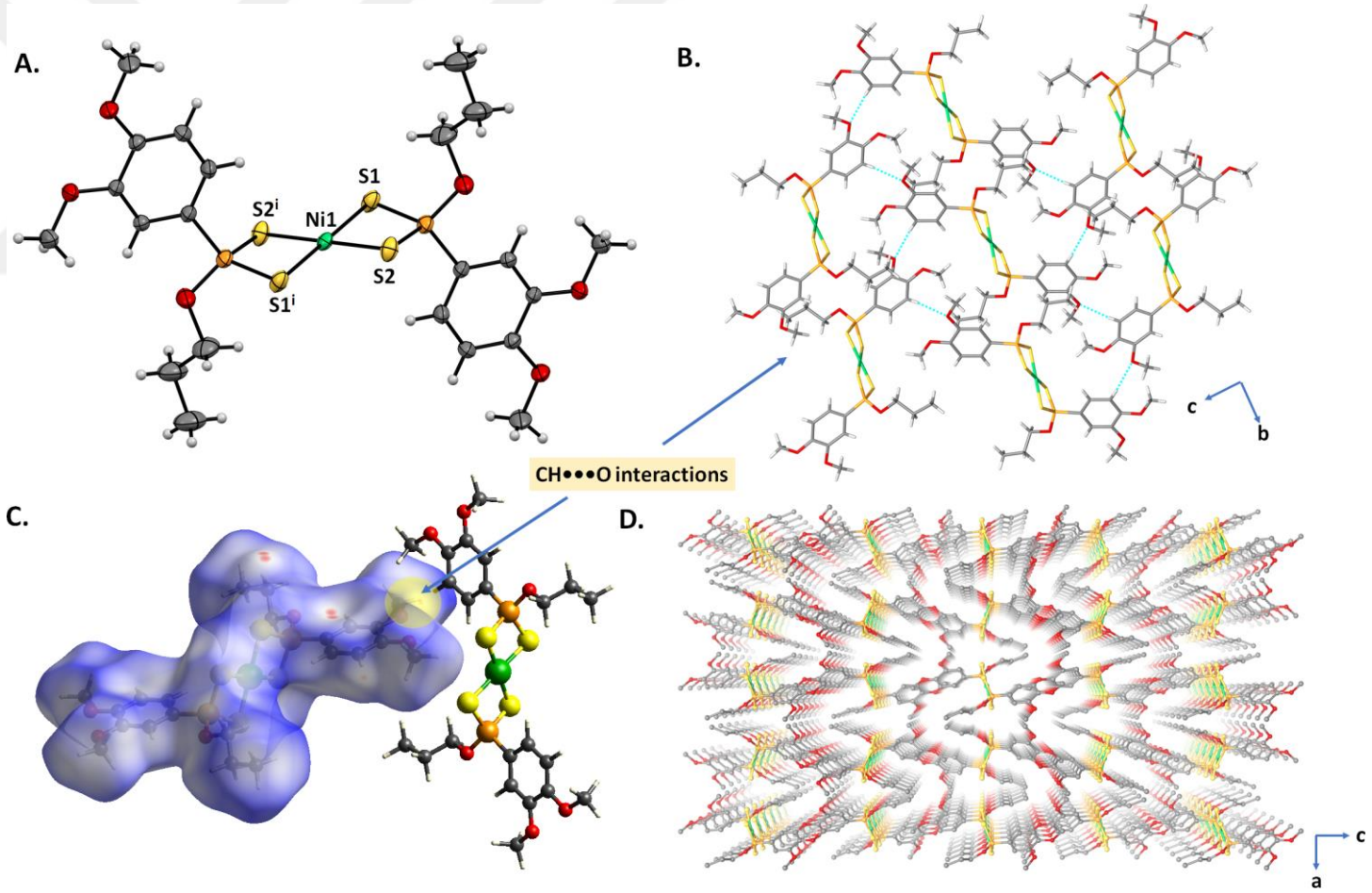


Figure 5.174. A) Crystal structure of $[Ni(S_2P(R^x)(OR3))_2]$ with displacement ellipsoids drawn at the 30% probability level (symmetry code: i: -x+1, -y+1, -z) **B)** and **C)** HS of $[Ni(S_2P(R^x)(OR3))_2]$ mapped with d_{norm}, showing the CH···O hydrogen bonding interactions. **D)** The illustration of the 3D supramolecular network showing the herringbone motif.

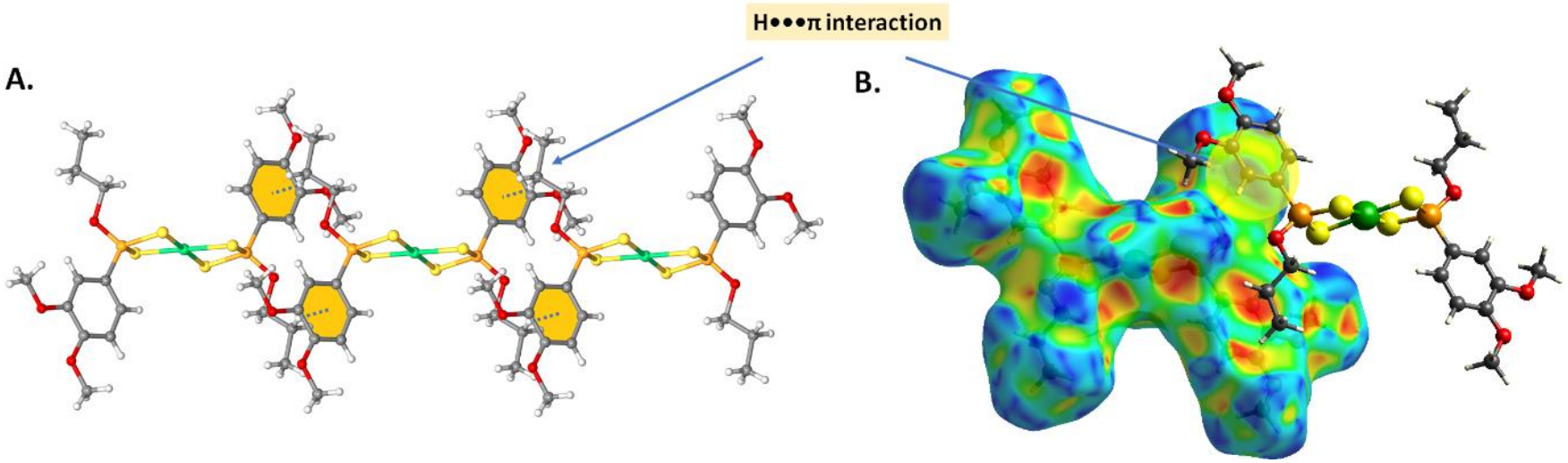


Figure 5.175. A) Representations of the C10-H10B···π_{phenyl} (d(H···π) = 2.72 Å) interactions in [Ni($S_2P(R^x)(OR3))_2$]. B) The HS shape index exhibits concave curvature, where C-H···π interactions occur.

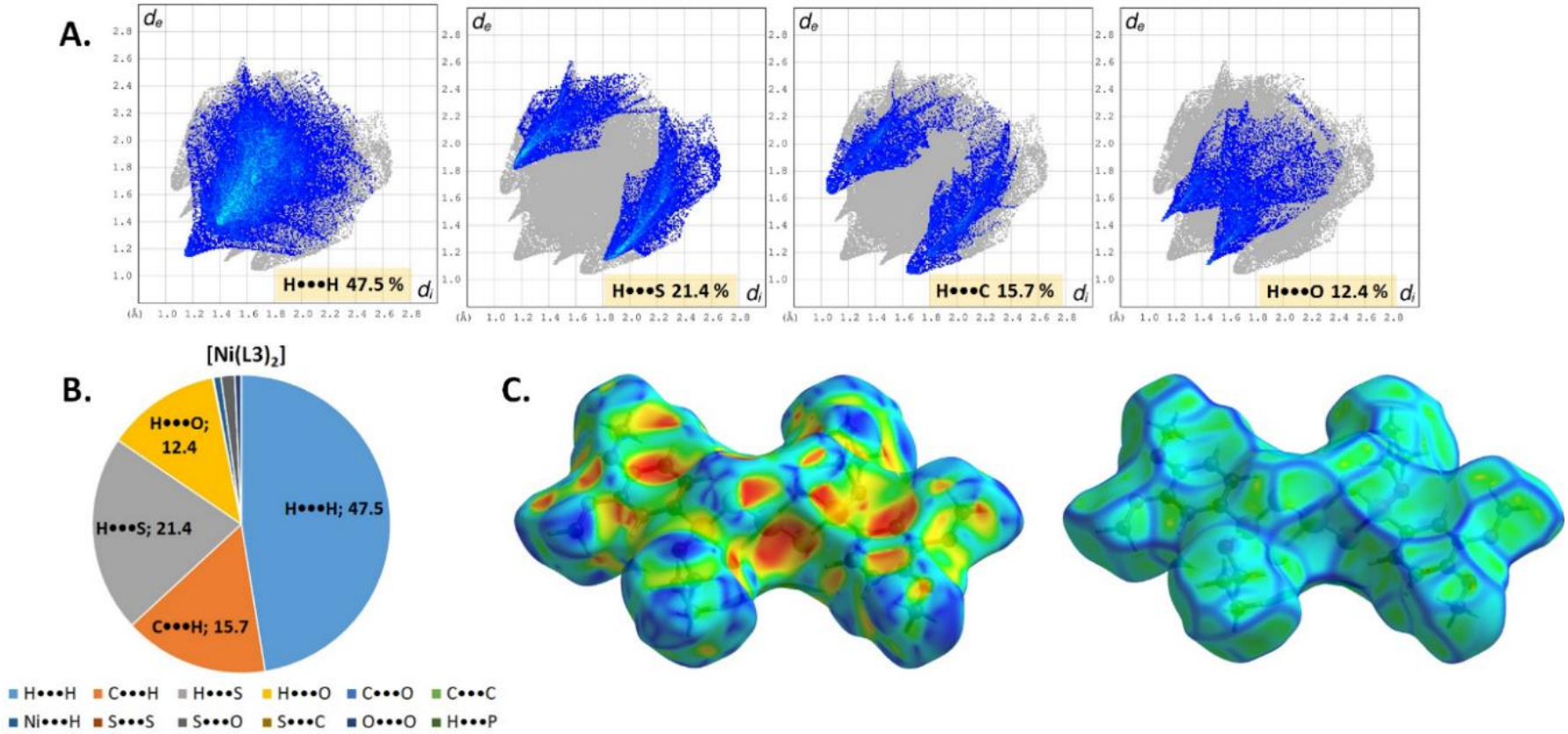


Figure 5.176. The resolved 2D fingerprint plots showing the percentage contributions to the total HS area in [Ni($S_2P(R^x)(OR3)$)$_2$].

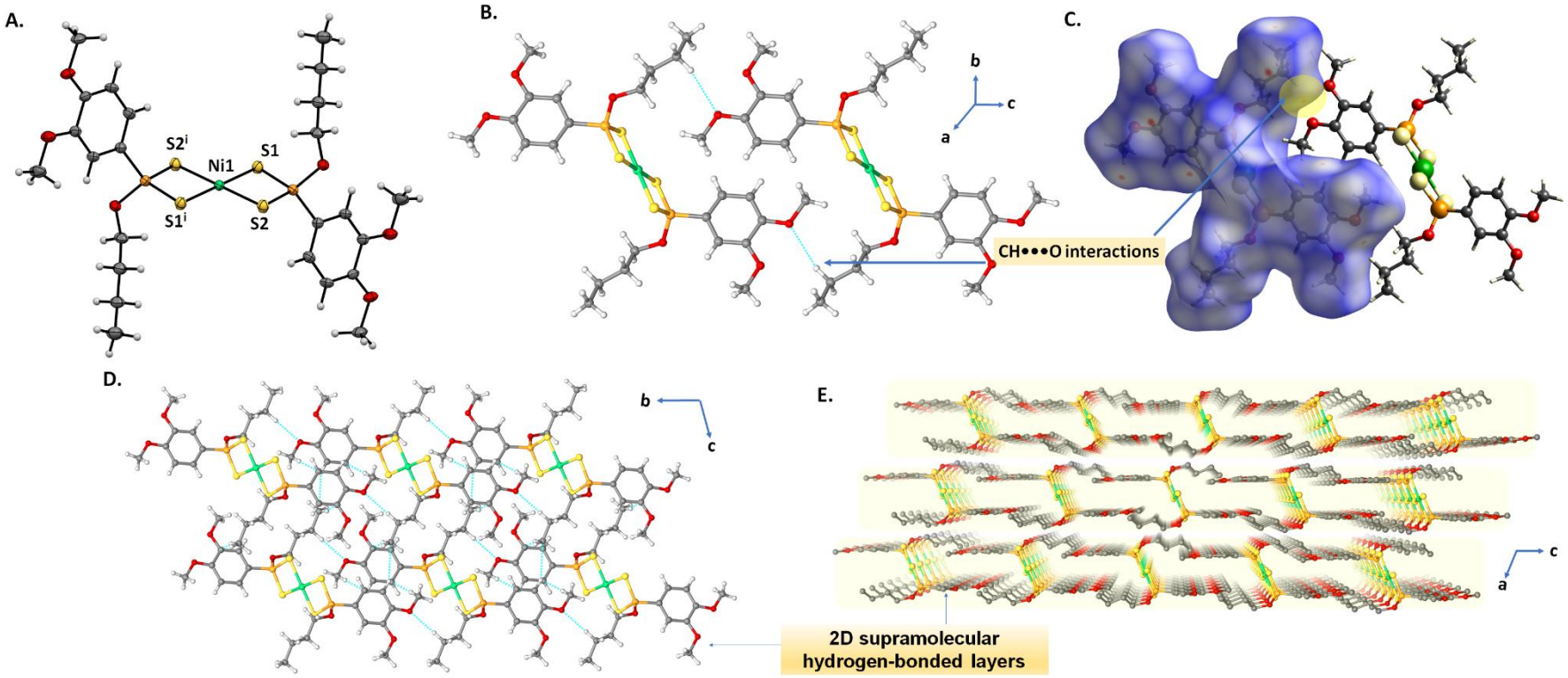


Figure 5.177. A) Crystal structure of $[Ni(S_2P(R^x)(OR4))_2]$ with displacement ellipsoids drawn at the 50% probability level (symmetry code: i: -x+1, -y+2, -z+1) **B)** and **C)** HS of $[Ni(S_2P(R^x)(OR4))_2]$ mapped with d_{norm}, showing the CH···O hydrogen bonding interactions. **D)** The 2D layers connected by the short CH···O and CH···C interactions **E)** Representation of 3D supramolecular network.

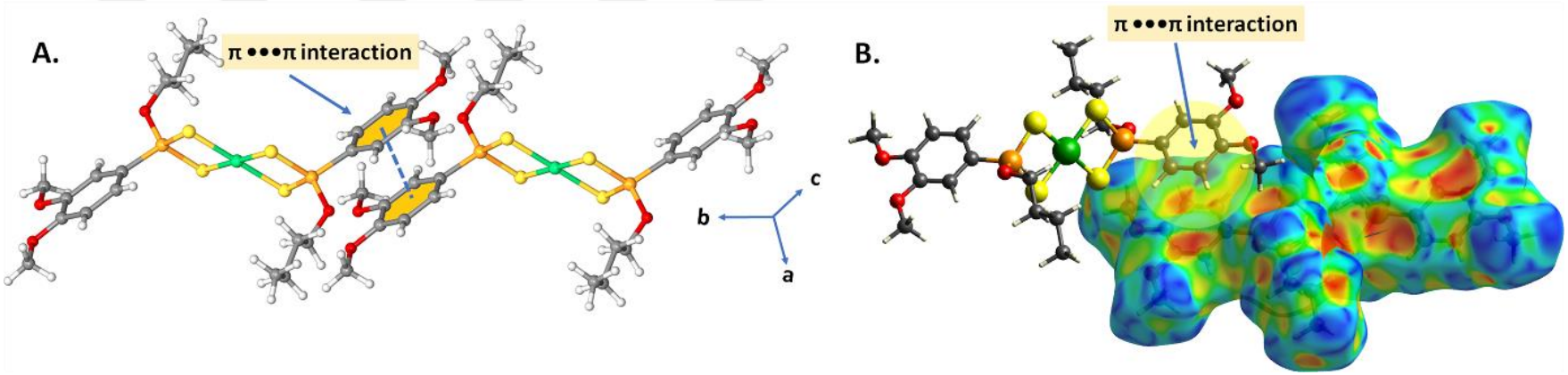


Figure 5.178. A) Representations of the $\pi_{phenyl} \cdots \pi_{phenyl}$ ($d_{(H\cdots\pi)}$ = 4.255 Å) interactions in $[Ni(S_2P(R^x)(OR4))_2]$. B) The HS shape index exhibits the evidence of the adjacent red and blue triangles on the shape index surface.

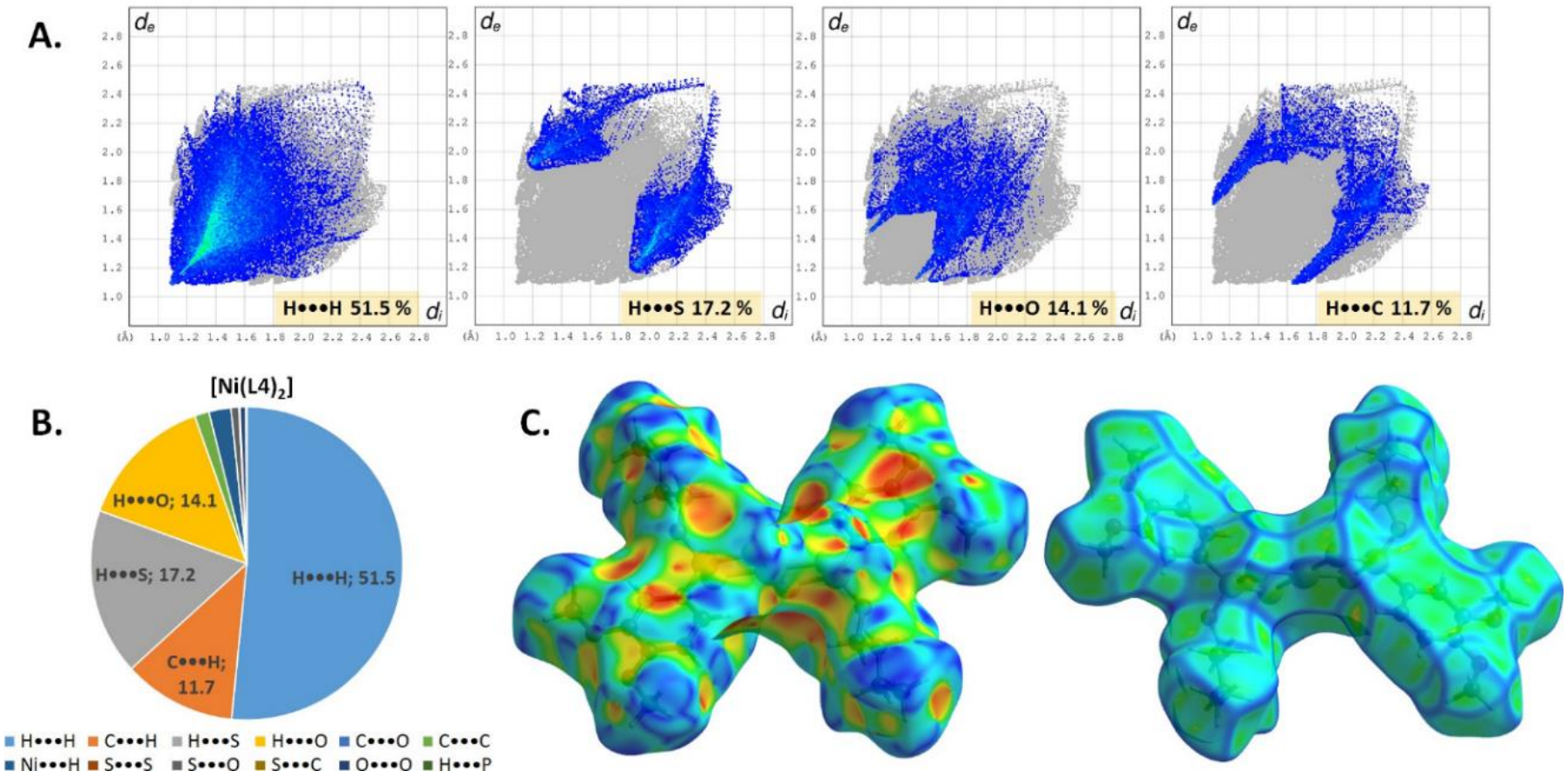


Figure 5.179. The resolved 2D fingerprint plots showing the percentage contributions to the total HS area in $[Ni(S_2P(R^x)(OR4))_2]$.

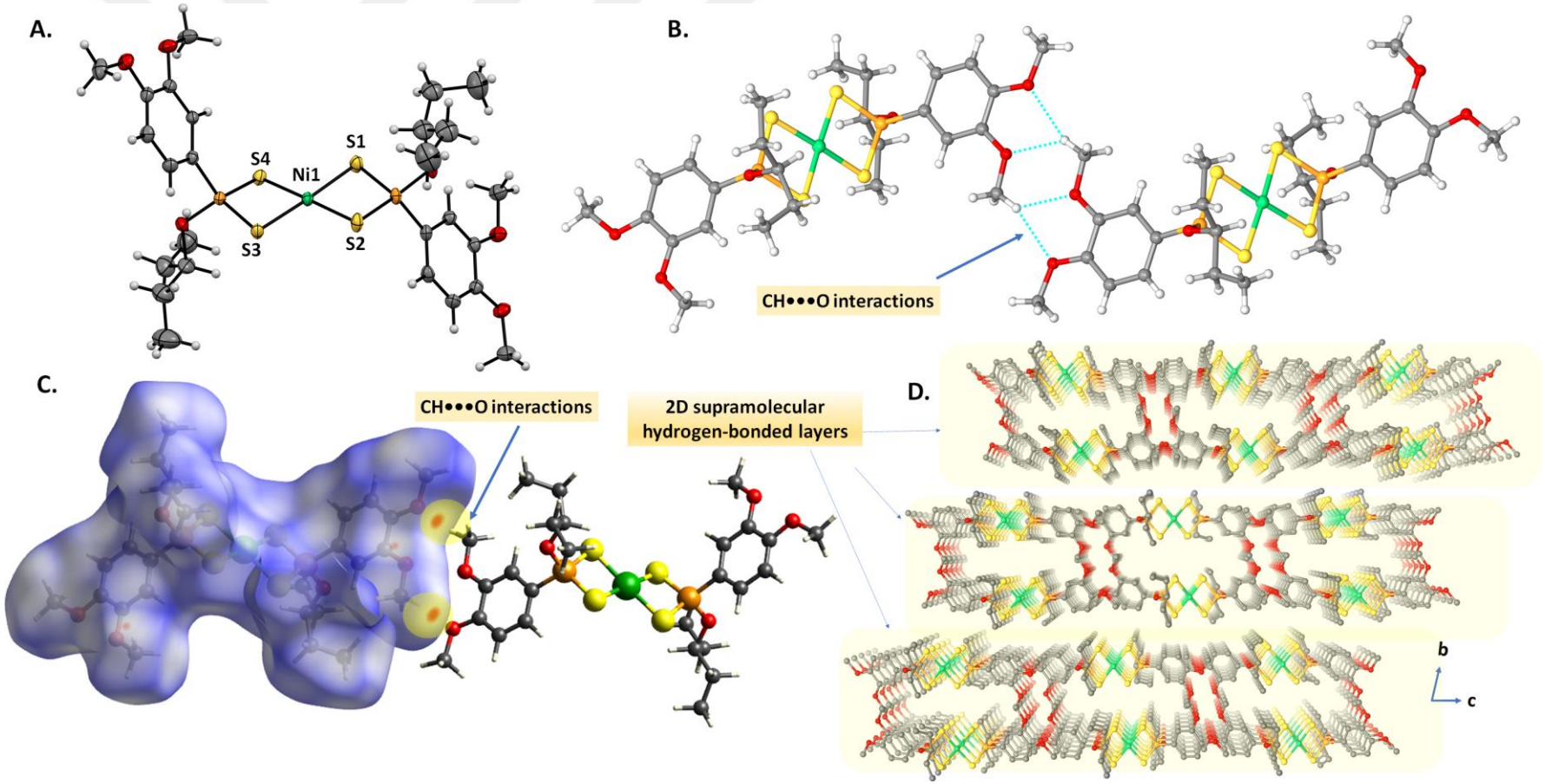


Figure 5.180. A) Crystal structure of [Ni($S_2P(R^x)(OR5)$)$_2$] with displacement ellipsoids drawn at the 30% probability level (symmetry code: i: -x+1, -y+1, -z) **B)** and **C)** HS of [Ni($S_2P(R^x)(OR5)$)$_2$] mapped with d_{norm}, showing the CH···O hydrogen bonding interactions. **D)** Illustration of 3D supramolecular network.

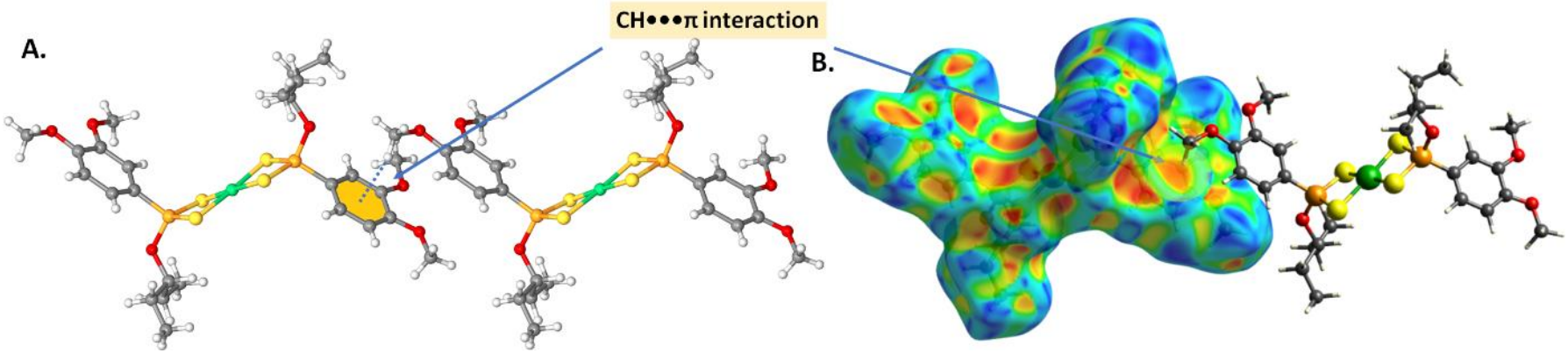


Figure 5.181. A) Representations of the C11-H11C···π_{phenyl} ($d_{(H\cdots\pi)}$ = 2.73 Å) interactions in [Ni($S_2P(R^x)(OR5)$)$_2$]. B) The HS shape index exhibits concave curvature, where C-H···π interactions occur.

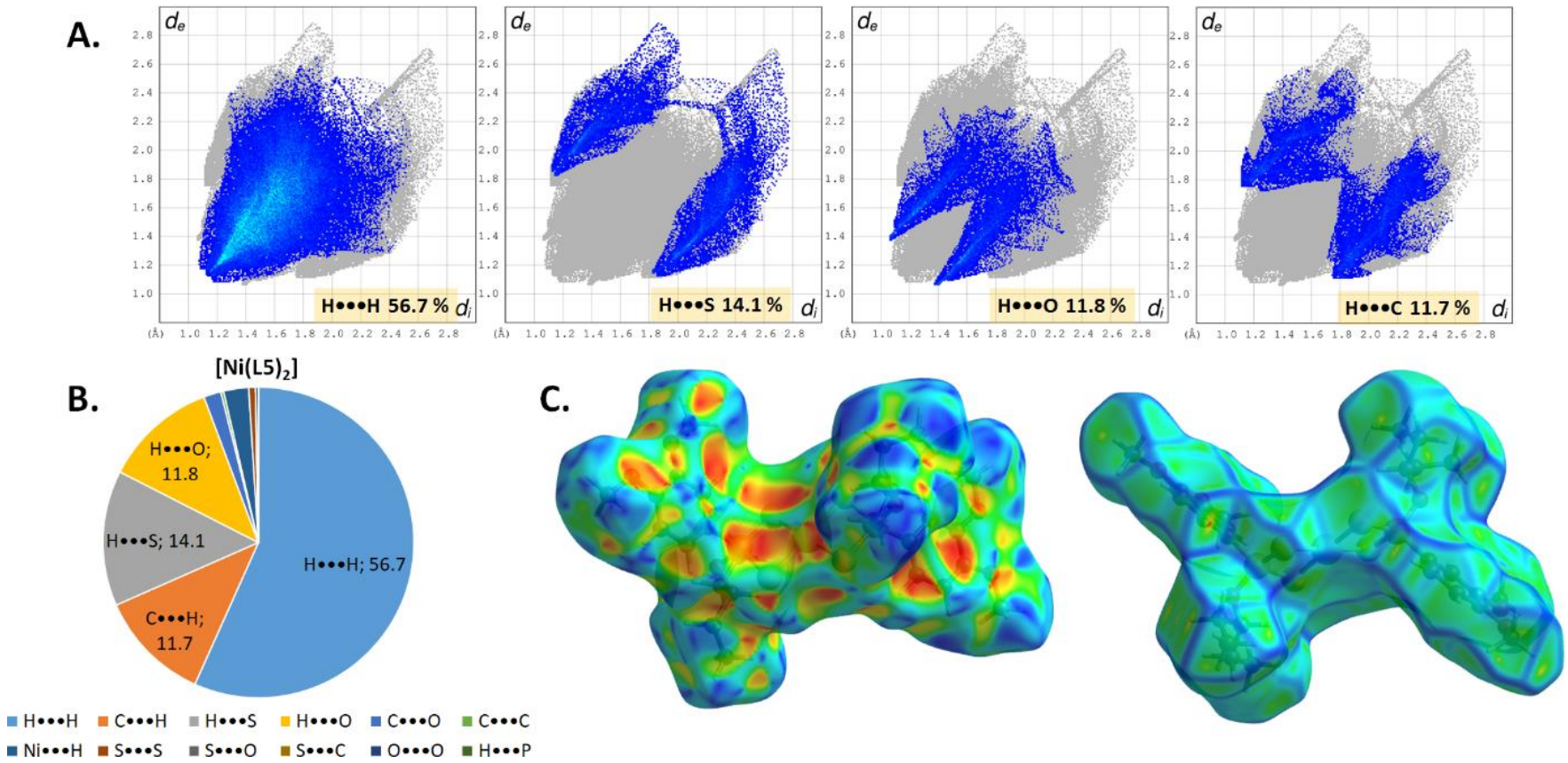


Figure 5.182. The resolved 2D fingerprint plots showing the percentage contributions to the total HS area in $[Ni(S_2P(R^x)(OR5))_2]$.

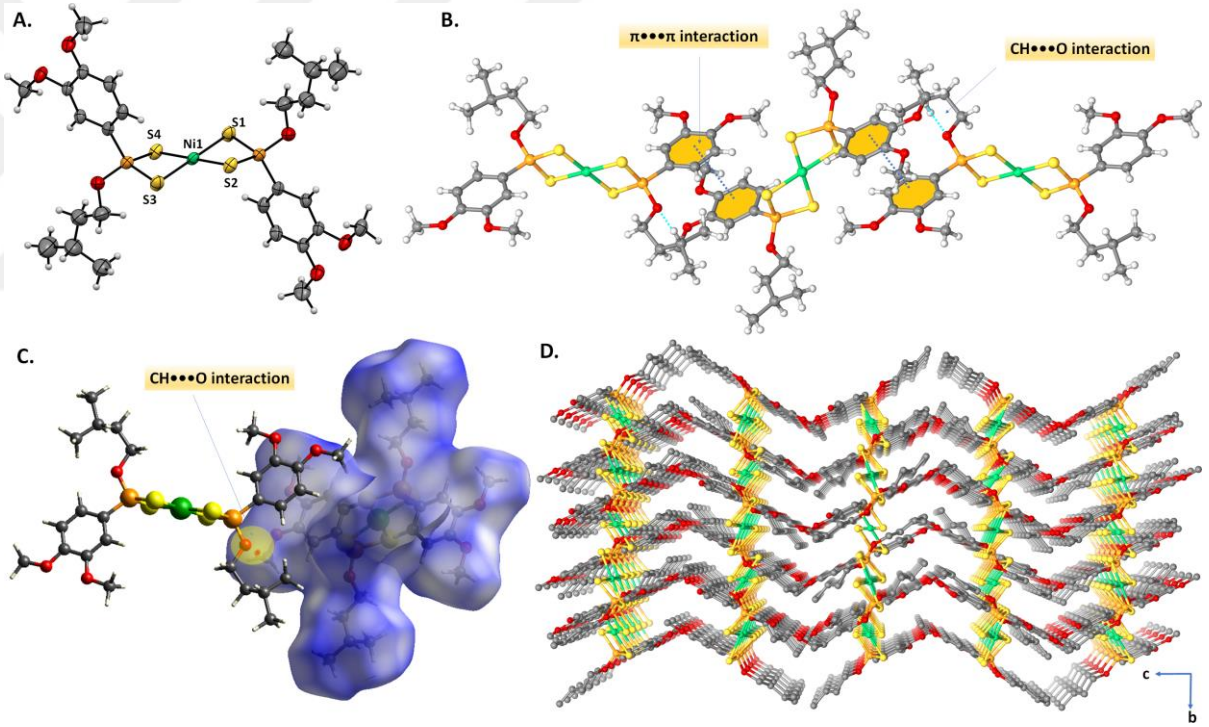


Figure 5.183. A) Crystal structure of [Ni($S_2P(R^x)(OR6)$)$_2$] with displacement ellipsoids drawn at the 30% probability level (symmetry code: i: -x+1, -y+1, -z) **B)** Perspective view of the CH···O hydrogen bonding and the short π ···π interaction **C)** HS of [Ni($S_2P(R^x)(OR6)$)$_2$] mapped with d_{norm}, showing the CH···O hydrogen bonding interactions. **D)** The view of the 3D supramolecular network showing the herringbone motif.

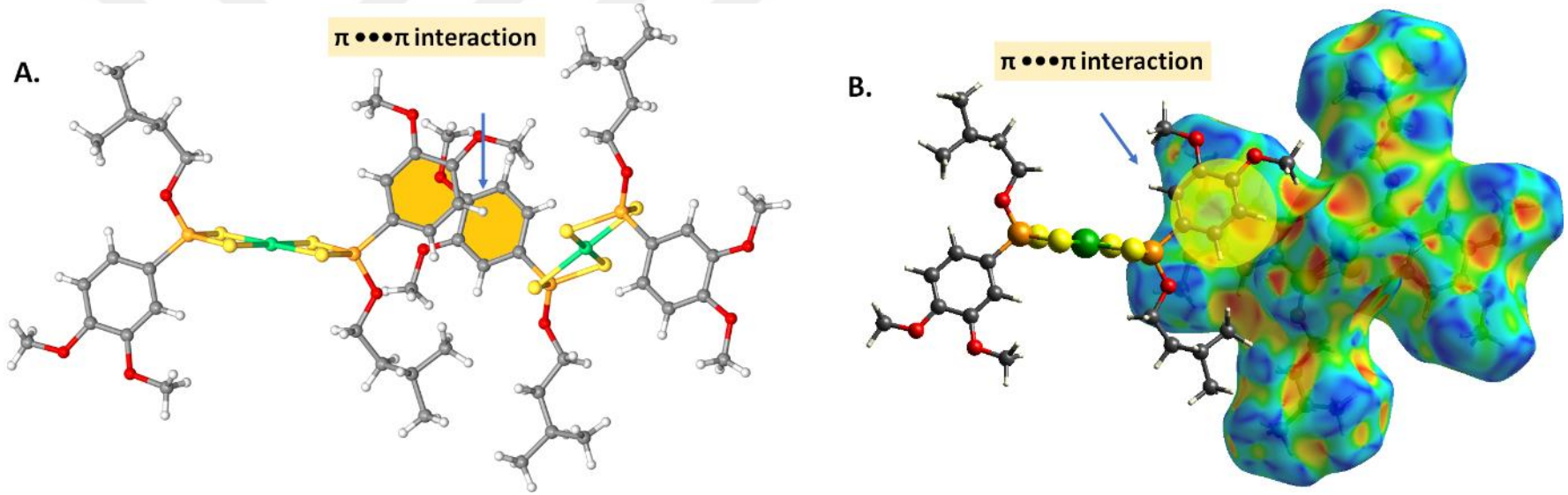


Figure 5.184. A) Representations of the $\pi_{phenyl} \cdots \pi_{phenyl}$ ($d(_{\pi \cdots \pi})$ = 3.838 Å) interactions in $[Ni(S_2P(R^x)(OR6))_2]$. B) The HS shape index exhibits the evidence of the adjacent red and blue triangles on the shape index surface.

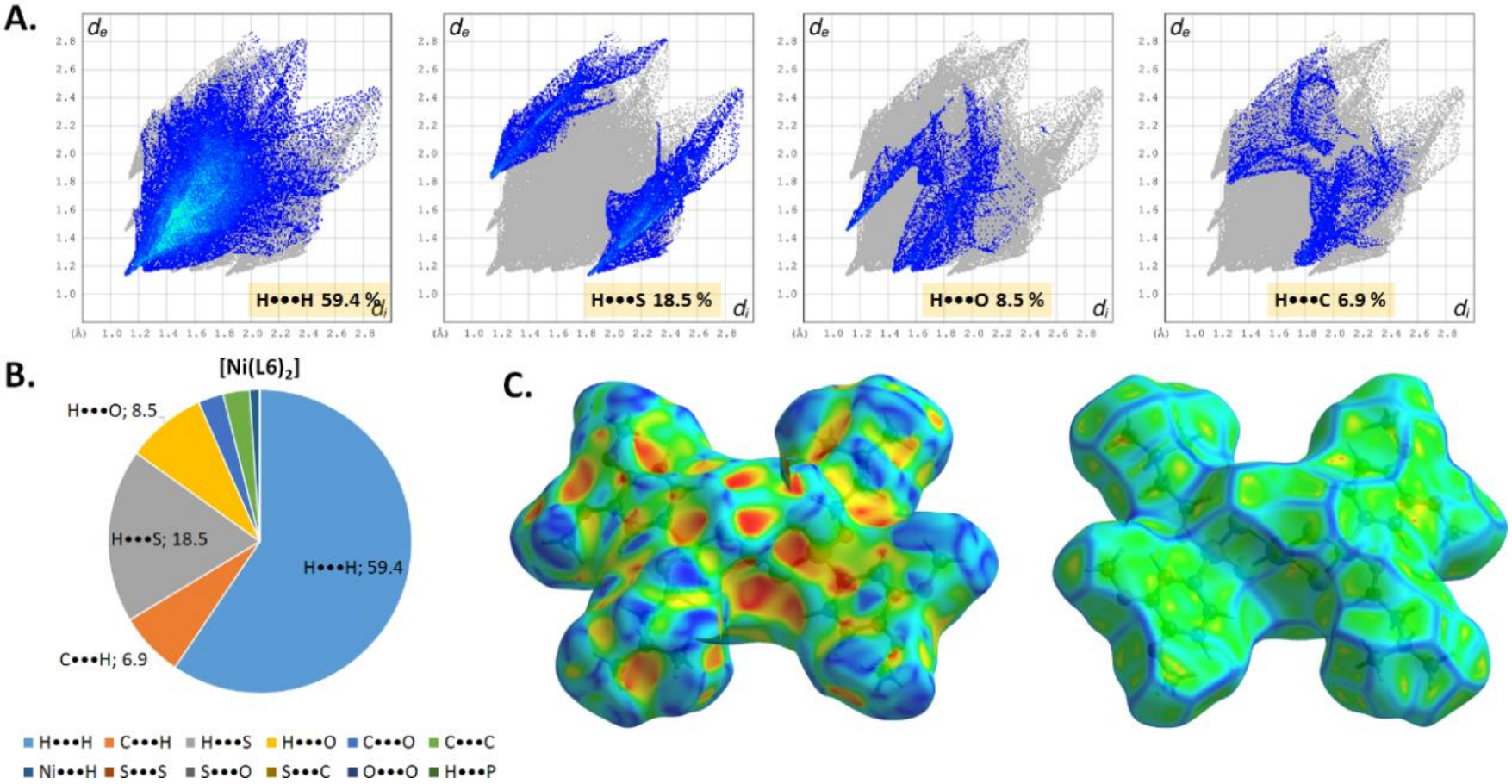


Figure 5.185. The resolved 2D fingerprint plots showing the percentage contributions to the total HS area in [Ni($S_2P(R^x)(OR6)$)$_2$].

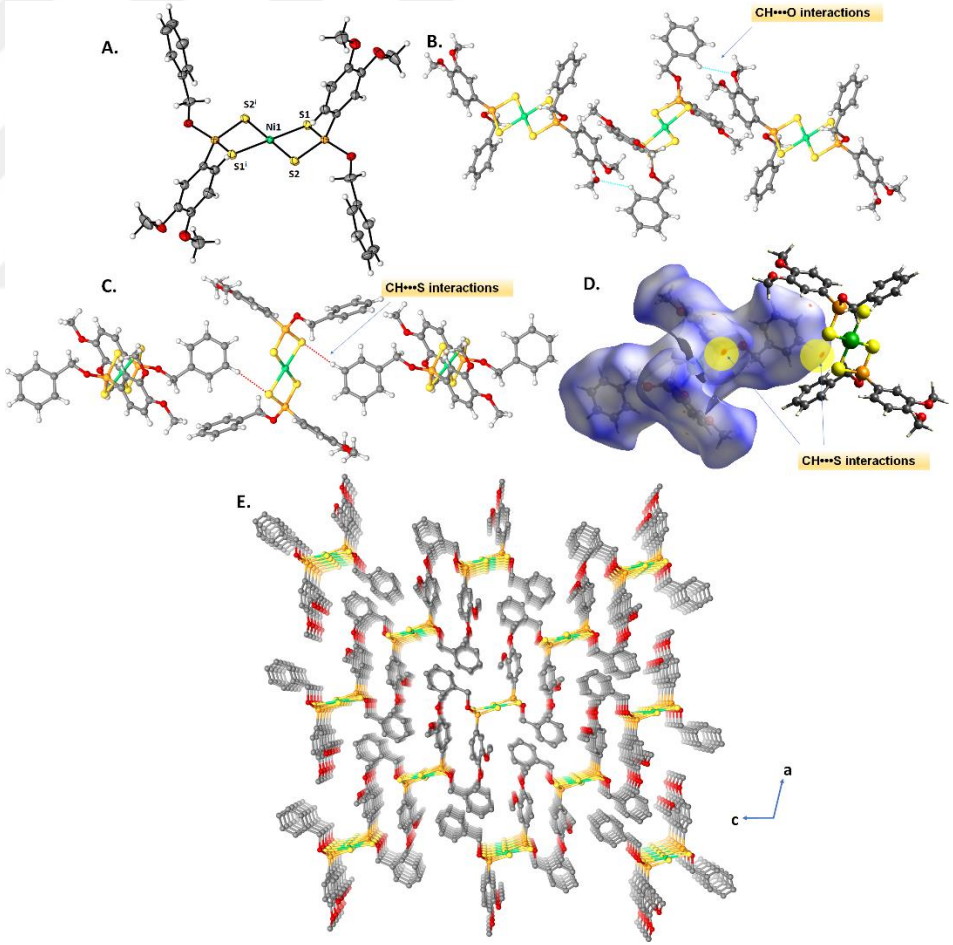


Figure 5.186. A) Crystal structure of $[Ni(S_2P(R^x)(OR7))_2]$ with displacement ellipsoids drawn at the 50% probability level (symmetry code: i: -x+1, -y+2, -z+1) **B)** and **C)** Perspective view of the CH···O and CH···S hydrogen bonding interactions **D)** HS of $[Ni(S_2P(R^x)(OR7))_2]$ mapped with d_{norm}, showing the CH···S hydrogen bonding interactions. **E)** View of the 3D supramolecular network.

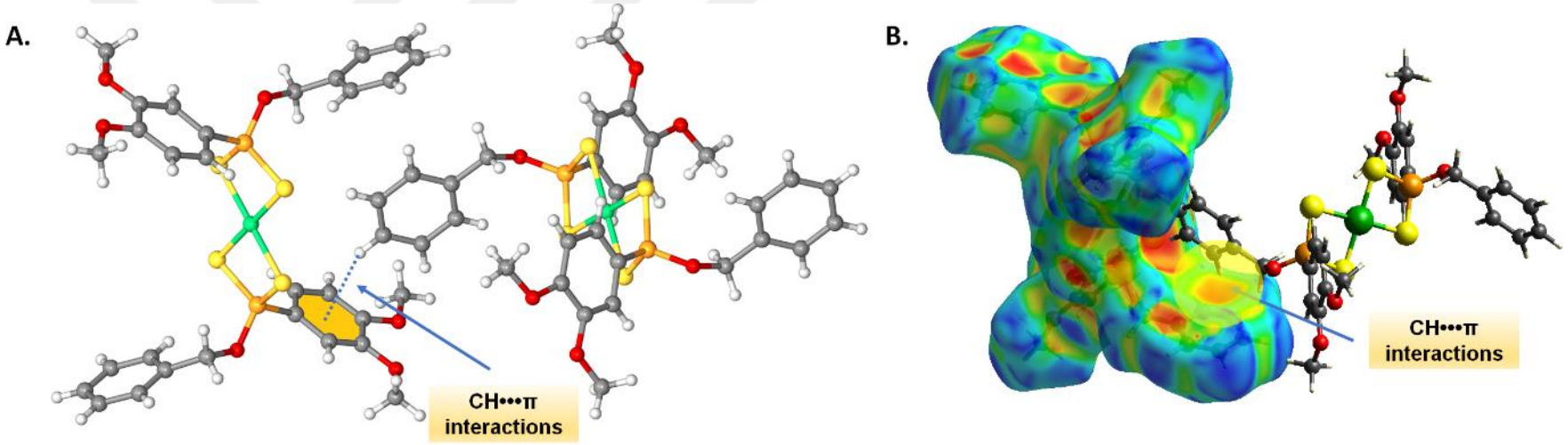


Figure 5.187. A) Representations of the C15-H15···π_{phenyl} ($d_{(H\cdots\pi)}$ = 2.95 Å) interactions in [Ni($S_2P(R^x)(OR7))_2$]. B) The HS shape index exhibits concave curvature, where C-H···π interactions occur.

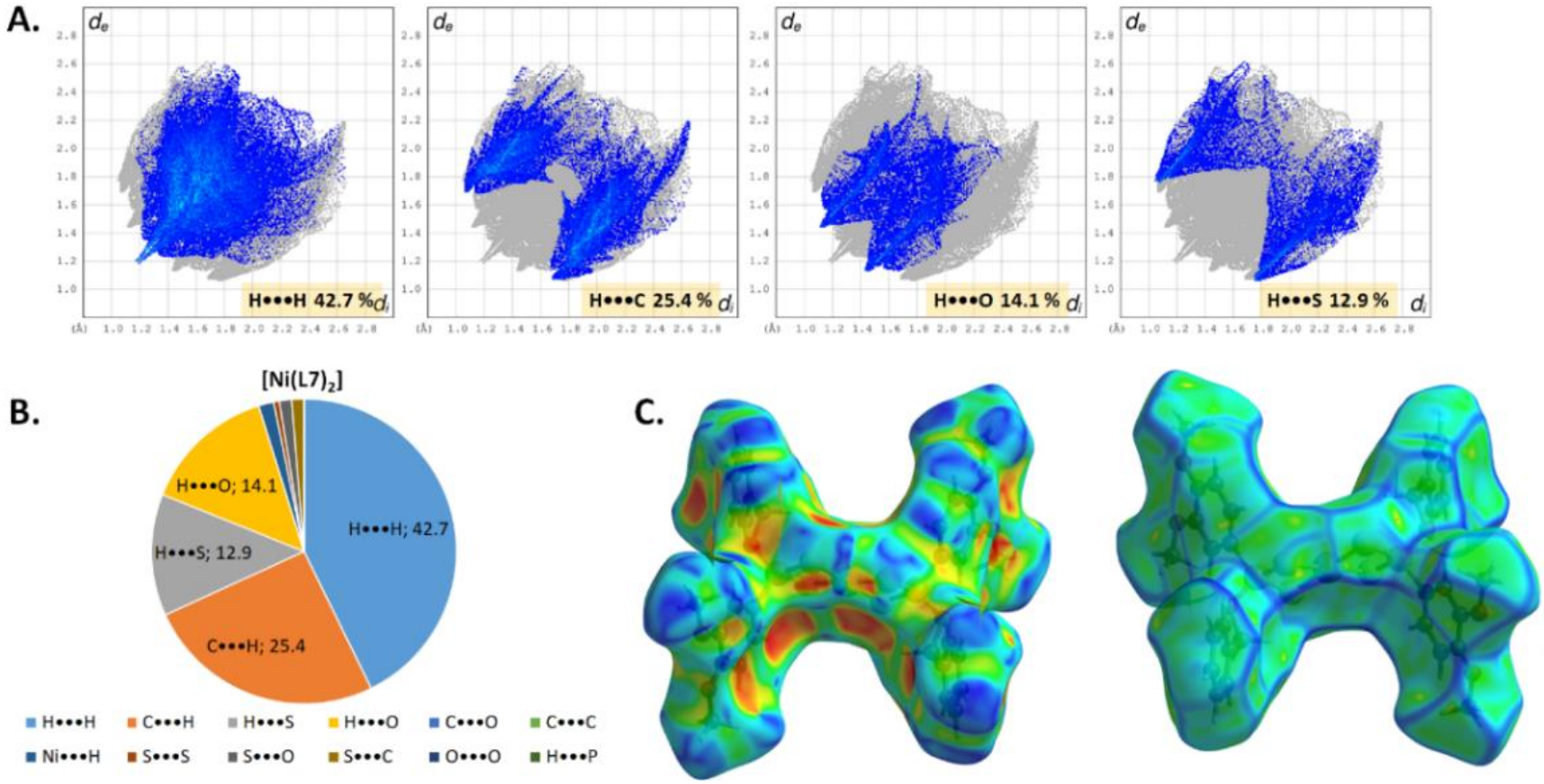


Figure 5.188. The resolved 2D fingerprint plots showing the percentage contributions to the total HS area in [Ni($S_2P(R^x)(OR7)_2$]$_2$].

5.3. Crystallographic Descriptions of the Part Ib' Ni(II) Complexes

Crystallographic data and refinement details for $[Ni(S_2P(R^x)(OR1))_2]$, $[Ni(S_2P(R^x)(OR2))_2]$, $[Ni(S_2P(R^x)(OR4))_2]$ and $[Ni(S_2P(R^x)(OR5))_2]$ are given in Table 5.17. The coordination environment and molecular structure were illustrated in Figures. 5.189A, 5.191A, 5.192A and 5.193A. Selected experimental and calculated bond lengths (Å) and bond angles (°) were given in Table 5.18. Crystallographic investigation revealed that $[Ni(S_2P(R^x)(OR1))_2]$ crystallizes in the orthorhombic $P2_12_12_1$, while the others ($[Ni(S_2P(R^x)(OR2))_2]$, $[Ni(S_2P(R^x)(OR4))_2]$ and $[Ni(S_2P(R^x)(OR5))_2]$) crystallize in triclinic *P*-1 space groups with the asymmetric unit consisting of two dithiophosphonate ligands and one Ni(II) cation.

Table 5.17. Crystal data and refinement details for $[Ni(S_2P(R^x)(ORn))_2]$ (n=1,2,4,5)

Compound	$[Ni(S_2P(R^x)(OR1))_2]$	$[Ni(S_2P(R^x)(OR2))_2]$	$[Ni(S_2P(R^x)(OR4))_2]$	$[Ni(S_2P(R^x)(OR5))_2]$
CCDC	2176951	2218375	2254587	2254588
Formula	$C_{26}H_{40}NiO_6P_2S_4$	$C_{26}H_{40}NiO_6P_2S_4$	$C_{22}H_{32}NiO_6P_2S_4$	$C_{24}H_{36}NiO_6P_2S_4$
Formula weight	697.47	697.47	641.36	669.42
Temperature (K)	298	298	298	298
Crystal system	Orthorhombic	Triclinic	Triclinic	Triclinic
Space group	$P2_12_12_1$	P-1	P-1	P-1
a (Å)	8.1244(7)	8.4631(10)	8.2063(17)	8.1849(10)
b (Å)	18.8194(16)	13.9826(17)	13.710(3)	13.989(5)
c (Å)	21.8529(18)	14.9228(18)	14.659(3)	14.892(6)
α (°)	90	111.446(2)	117.060(4)	65.54(2)
β (°)	90	97.462(2)	92.305(4)	84.24(2)
γ (°)	90	90.443(2)	91.424(4)	85.52(2)
Crystal size (mm^3)	0.21×0.16×0.14	0.31×0.20×0.10	0.24×0.12×0.08	0.34×0.13×0.10
Volume ($Å^3$)	3341.2(5)	1626.8(3)	1465.8(5)	1543(9)

Table 5.17. Continues.

Z	4	2	2	2
ρcalc (g/cm^3)	1.387	1.424	1.453	1.441
μ (mm^{-1})	0.962	0.988	1.090	1.038
F(000)	1464	732	668	700
2θ range for data collection (°)	2.856 to 50.174	2.962 to 49.998	3.126 to 50.244	3.012 to 49.994
Index ranges	-9 ≤ h ≤ 9, -22 ≤ k ≤ 22, -26 ≤ l ≤ 26	-10 ≤ h ≤ 10, -16 ≤ k ≤ 16, -17 ≤ l ≤ 17	-9 ≤ h ≤ 9, -16 ≤ k ≤ 16, -17 ≤ l ≤ 17	-9 ≤ h ≤ 9, -16 ≤ k ≤ 16, -17 ≤ l ≤ 17
Reflections collected	52769	20245	18269	17203
Independent reflections	5933 [R_{int} = 0.0512, R_{sigma} = 0.0307]	5715 [R_{int}= 0.0304, R_{sigma} = 0.0309]	5192 [R_{int}= 0.0421, R_{sigma} = 0.0466]	5448 [R_{int}=0.0461, R_{sigma} = 0.0607]
Data/restraints/ parameters	5933/94/396	5715/282/379	5192/0/324	5445/124/420
Goodness-of-fit on F2 (S)	1.132	1.071	1.083	1.004
Final R indices [*I* > 2σ(*I*)]	R_1 = 0.0419, wR_2 = 0.0996	R_1 = 0.0674, wR_2 = 0.1959	R_1 = 0.0719, wR_2 = 0.2081	R_1 = 0.0449, wR_2 = 0.1023
R indices (all data)	R_1 = 0.0585, wR_2 = 0.1116	R_1 = 0.0870, wR_2 = 0.2075	R_1 = 0.0959, wR_2 = 0.2218	R_1 = 0.0905, wR_2 = 0.1149
Largest diff.peak/ hole (e Å^{-3})	0.29/-0.22	1.19/-0.66	1.21/-1.12	0.29/-0.29

In each of the crystal structures of complexes, the Ni(II) metal center is surrounded by four sulfur atoms from two dithiophosphonate ligands, forming a square planar coordination geometry. As seen in many Ni(II)-DTPOA complexes in the Cambridge Structural Database (CSD Ref. Codes: DUKMIH, HAHDAW, NORFUV, XADKET, ZUNLIG) [250, 252, 254, 296], due to the steric hindrance of bulky alkyl groups, the dithiophosphonate ligands in $[Ni(S_2P(R^x)(OR1))_2]$, $[Ni(S_2P(R^x)(OR2))_2]$, $[Ni(S_2P(R^x)(OR4))_2]$ and $[Ni(S_2P(R^x)(OR5))_2]$ are anti-positioned with respect to the NiS_4 coordination plane. In $[Ni(S_2P(R^x)(OR1))_2]$, the NiS_4P_2 segment exhibits a substantially coplanar, as indicated in the torsion angles for Ni1—S3—P2—S4 and Ni1—S2—P1—S1 are -0.86(9)° and -4.35(9)°, respectively. However, the NiS_4P_2 fragment in $[Ni(S_2P(R^x)(OR2))_2]$, $[Ni(S_2P(R^x)(OR4))_2]$ and $[Ni(S_2P(R^x)(OR5))_2]$ was found to deviate slightly from planarity compared to $[Ni(S_2P(R^x)(OR1))_2]$, as viewed from comparative torsion angles Ni1—S3—P2—S4 and Ni1—S2—P1—S1 are 11.51(8)° and 13.67(8)° to give an example of $[Ni(S_2P(R^x)(OR2))_2]$ (Table 5.18). The 3,4-dimethoxyphenyl aromatic rings in $[Ni(S_2P(R^x)(OR1))_2]$, $[Ni(S_2P(R^x)(OR2))_2]$,

$[Ni(S_2P(R^x)(OR4))_2]$ and $[Ni(S_2P(R^x)(OR5))_2]$ are perfectly parallel to each other, and the dihedral angles are ~4.97°, ~3.01°, ~3.18°, and ~4.64°, respectively. In the NiS_4 coordination sphere, the bond distances between the Ni—S bonds in $[Ni(S_2P(R^x)(OR1))_2]$, $[Ni(S_2P(R^x)(OR2))_2]$, $[Ni(S_2P(R^x)(OR4))_2]$ and $[Ni(S_2P(R^x)(OR5))_2]$ are almost the same, between 2.2200(17) Å - 2.2246(18) Å, 2.2167(15) Å - 2.2363(15) Å, 2.220(2) Å - 2.227(2) Å, and 2.2173(19) Å - 2.2263(19) Å, respectively. This trend in bond lengths is seen in the bond angles as well. The S—Ni—S bond angles are in the ranges between 88.03(6)° to 179.91(9)° for $[Ni(S_2P(R^x)(OR1))_2]$, 88.01(6)° to 176.61(5)° for $[Ni(S_2P(R^x)(OR2))_2]$, 88.59(7)° to 179.94(8)° for $[Ni(S_2P(R^x)(OR4))_2]$, and 88.44(9)° to 178.35(4)°, respectively. The Ni—S bond lengths and the S—Ni—S bond angles are consistent with those previously observed in dithiophosphonato-based Ni(II) complex [305].

In $[Ni(S_2P(R^x)(OR1))_2]$, the weak C—H···S (C7—H7A···S4, d(C7···S4) = 3.845 Å and C2A—H2AB···S1, d(C2A···S1) = 3.892 Å) hydrogen bonding interactions form a 1D chains along the a-axis (Figure 5.189B). The resulting 1D infinite hydrogen-bonded chains are further expanded into a 3D supramolecular network (Figure 5.189D) with herringbone motif by the combination of weak C—H···O interactions (C17—H17C···O3, d(C17···O3) = 3.559 Å, C17—H17B···O3, d(C17···O3) = 3.229Å, C1A—H1AA···O5, d(C1A···O5) = 3.518Å, Table 5.19). The red spots on Hirshfeld surfaces of $[Ni(S_2P(R^x)(OR1))_2]$ mapped with d_{norm} clearly displays the C—H···O hydrogen bonding interactions (Figure 5.189C). The 2D fingerprint regions of $[Ni(S_2P(R^x)(OR1))_2]$ exhibits that the S···H/H···S and O···H/H···O interactions compose the considerable area of the Hirshfeld surfaces with the ratio of 18.0% and 11.6%. Moreover, the weak π···π interactions (d(π···π) = 4.089(4) Å - 4.118(4) Å, Figure 5.189E) between the adjacent complexes support to stabilize the crystal structure of $[Ni(S_2P(R^x)(OR1))_2]$. The C···C contacts attributing to the π···π interactions constitute 3.5% of the total Hirsfeld surfaces in $[Ni(S_2P(R^x)(OR1))_2]$ (Figure 5.189F).

In $[Ni(S_2P(R^x)(OR2))_2]$, the two weak C—H···O hydrogen bonding interactions ((C15—H15A···O2, d(C15···O2) = 3.408 Å and C17—H17B···O5, d(C17···O5) = 3.551 Å) lead a 1D infinite chains (Figure 5.191B). The resulting 1D infinite hydrogen-bonded chains are broadened into a herringbone-like 2D supramolecular network (Figure 5.191D) through the combination of weak C—H···O interactions (C16—H16A···O3, d(C16···O3)

= 3.523 Å, C15—H15B···O4, d(C15···O4) = 3.598 Å, Table 5.19). The red spots on Hirshfeld surfaces of [Ni($S_2P(R^x)(OR2)$)$_2$] clearly displays the C—H···O hydrogen bonding interactions (Figure 5.191C). Also, the C—H···π contacts (C14—H14C···π, d(H14C···π) = 2.78 Å, Figure 5.191E) supported this 2D supramolecular network (Figure 5.191D).

In [Ni($S_2P(R^x)(OR4)$)$_2$], the four weak hydrogen bonding interactions (C14—H14A···O3, (d(C14···O3) = 3.308 Å; C14—H14A···O2, (d(C14···O2) = 3.442 Å; C16—H16C···O4, (d(C16···O4) = 3.334 Å; C16—H16C···O5, d(C16···O5) = 3.352 Å) result in the assembly of a 1D infinite chains (Figure 5.193B). The C—H···O interactions are easily seen as bright red dots on the Hirshfeld surfaces of [Ni($S_2P(R^x)(OR4)$)$_2$] (Figure 5.193C). The 3D supramolecular network (Figure 5.193D) is also stabilized by the C—H···π contacts (C15—H15B···π, d(H15B···π) = 2.69 Å, Figure 5.193E) and the weak C—H···S (C17—H17C···S1, d(C17···S1) = 3.729 Å) interactions.

In [Ni($S_2P(R^x)(OR5)$)$_2$], the 1D infinite chain structure (Figure 5.195B) comes from the four intermolecular C—H···O hydrogen bonding interactions (C14—H14B···O2, d(C14···O2) = 3.389 Å; C14—H14B···O3, d(C14···O3) = 3.333 Å; C16—H16A···O5, d(C16···O5) = 3.286 Å; C16—H16A···O6, d(C16···O6) = 3.527 Å). The resulting 1D chains are expanded into a 2D supramolecular layered netwok by C16—H16B···O3 (d(C16···O3) = 2.632 Å). Hirshfeld surfaces of [Ni($S_2P(R^x)(OR5)$)$_2$] reveal the C—HO interactions as intense red spots (Figure 5.195C). Also, as observed in other complexes, the intermolecular C—H···S (d(C3···S2) = 3.695 Å) and the C—H···π contact (C15—H15C···π, d(H15C···π) = 2.70 Å, Figure 5.195E) contributed to the crystal packing of [Ni($S_2P(R^x)(OR5)$)$_2$] (Figure 5.195D).

According to the 2D fingerprint plots of [Ni($S_2P(R^x)(OR1)$)$_2$], [Ni($S_2P(R^x)(OR2)$)$_2$], [Ni($S_2P(R^x)(OR4)$)$_2$] and [Ni($S_2P(R^x)(OR5)$)$_2$] (Figure 5.190, 5.192, 5.194, 5.196), the most dominant interaction in Ni(II) complexes is the H/H interaction, which constitutes 57.4%, 55.9%, 51.5% and 53.9% of the total Hirshfeld surfaces. This is highly possible because of the abundance of aliphatic hydrogen atoms in the side flexible chains of dithiophosphonate moiety. On the other hand, the C···C contact ratios (~0.3-0.4%) in the 2D fingerprint plots of [Ni($S_2P(R^x)(OR2)$)$_2$], [Ni($S_2P(R^x)(OR4)$)$_2$] and [Ni($S_2P(R^x)(OR5)$)$_2$] explain that there are no important π···π interactions in these

complexes. The CH···π contacts can be viewed by a pair of typical “wings” at the top left and bottom right of the 2D plots (Figure 5.190, 5.192, 5.194, 5.196). The C···H/H···C contacts of $[Ni(S_2P(R^x)(OR1))_2]$, $[Ni(S_2P(R^x)(OR2))_2]$, $[Ni(S_2P(R^x)(OR4))_2]$ and $[Ni(S_2P(R^x)(OR5))_2]$ 5.2%, 11.3%, 12.8% and 12.3% of the total Hirsfeld surface attribute to the CH···π interactions. Figures. 5.191B, 5.192B, 5.195B demonstrate the C···H contact in $[Ni(S_2P(R^x)(OR2))_2]$, $[Ni(S_2P(R^x)(OR4))_2]$ and $[Ni(S_2P(R^x)(OR5))_2]$ and C···H interaction regions are clearly marked on the Hirshfeld surfaces of $[Ni(S_2P(R^x)(OR2))_2]$, $[Ni(S_2P(R^x)(OR4))_2]$, and $[Ni(S_2P(R^x)(OR5))_2]$ when the surfaces are mapped with the shape index. In all crystal structures, all other types of interactions such as C···O and Ni···H are less than 5%.

Table 5.18. Selected experimental and calculated at B3LYP/LANL2DZ level bond lengths (Å), bond angles (°) and torsion angles for $[Ni(S_2P(R^x)(OR1))_2]$, $[Ni(S_2P(R^x)(OR2))_2]$, $[Ni(S_2P(R^x)(OR4))_2]$ and $[Ni(S_2P(R^x)(OR5))_2]$.

	Bond lengths (Å) X-ray				Bond lengths (Å) Calculated			
	$[Ni(S_2P(R^x)(OR1))_2]$	$[Ni(S_2P(R^x)(OR2))_2]$	$[Ni(S_2P(R^x)(OR4))_2]$	$[Ni(S_2P(R^x)(OR5))_2]$	$[Ni(S_2P(R^x)(OR1))_2]$	$[Ni(S_2P(R^x)(OR2))_2]$	$[Ni(S_2P(R^x)(OR4))_2]$	$[Ni(S_2P(R^x)(OR5))_2]$
Ni1—S1	2.2200(17)	2.2233(16)	2.222(2)	2.2173(19)	2.3445	2.3441	2.3454	2.3455
Ni1—S2	2.2217(18)	2.2281(14)	2.224(2)	2.225(2)	2.3409	2.3476	2.3468	2.3462
Ni1—S3	2.2233(17)	2.2363(15)	2.220(2)	2.2263(19)	2.3512	2.3452	2.3485	2.3443
Ni1—S4	2.2246(18)	2.2167(15)	2.227(2)	2.223(2)	2.3450	2.3428	2.3466	2.3457
S1—P1	2.012(2)	1.990(2)	1.999(2)	1.999(2)	2.1978	2.1993	2.1995	2.1963
S2—P1	2.001(2)	1.9999(2)	1.994(3)	1.996(2)	2.1939	2.1972	2.1980	2.1993
S3—P2	2.008(2)	1.9982(2)	1.993(3)	2.003(2)	2.1936	2.1985	2.1995	2.1979
S4—P2	2.005(2)	1.9991(2)	2.001(2)	1.994(2)	2.1977	2.2003	2.1950	2.2003

Table 5.18. Continues.

	Bond angles (°) X-ray				Bond angles (°) Calculated			
	$[Ni(S_2P(R^x)(OR1))_2]$	$[Ni(S_2P(R^x)(OR2))_2]$	$[Ni(S_2P(R^x)(OR4))_2]$	$[Ni(S_2P(R^x)(OR5))_2]$	$[Ni(S_2P(R^x)(OR1))_2]$	$[Ni(S_2P(R^x)(OR2))_2]$	$[Ni(S_2P(R^x)(OR4))_2]$	$[Ni(S_2P(R^x)(OR5))_2]$
S2—Ni1—S1	88.03(6)	88.01(6)	88.59(7)	88.44(9)	89.57	89.50	89.49	89.40
S1—Ni1—S4	91.91(7)	91.06(6)	91.46(7)	90.76(9)	90.32	90.48	90.51	90.60
S3—Ni1—S1	179.91(9)	176.31(6)	179.84(9)	178.35(4)	177.57	178.01	179.85	179.82
S3—Ni1—S2	91.99(7)	93.06(5)	179.84(9)	92.29(9)	90.68	90.73	90.51	90.63
S3—Ni1—S4	88.06(6)	88.06(6)	88.62(8)	88.56(9)	89.52	89.34	89.02	89.21
S4—Ni1—S2	179.30(9)	176.61(5)	179.94(8)	178.03(4)	177.96	178.55	179.75	179.81

Table 5.19. Continues.

	Torsion angles (°) X-ray				Torsion angles (°) Calculated			
	$[Ni(S_2P(R^x)(OR1))_2]$	$[Ni(S_2P(R^x)(OR2))_2]$	$[Ni(S_2P(R^x)(OR4))_2]$	$[Ni(S_2P(R^x)(OR5))_2]$	$[Ni(S_2P(R^x)(OR1))_2]$	$[Ni(S_2P(R^x)(OR2))_2]$	$[Ni(S_2P(R^x)(OR4))_2]$	$[Ni(S_2P(R^x)(OR5))_2]$
Ni1—S1—P1—C1	129.2(2)	108.9(2)	104.5(3)	109.8(1)	128.72	122.38	126.31	125.35
Ni1—S1—P1—O1	-117.6(2)	-137.1(2)	-141.8(2)	-136.8(1)	-116.05	-123.47	117.85	-119.91
Ni1—S2—P1—C1	-129.1(2)	-108.0(2)	-103.9(3)	-109.1(1)	-130.35	-124.30	-124.37	-125.26
Ni1—S2—P1—O1	115.8(2)	136.5(2)	140.5(2)	136.5(1)	114.28	119.94	121.29	119.09
Ni1—S2—P1—S1	-4.35(9)	13.67(8)	16.8(1)	12.70(6)	-4.093	-4.219	-0.49	-1.08
Ni1—S3—P2—S4	-0.86(9)	11.51(8)	15.9(1)	14.47(6)	-1.842	0.657	-1.13	-3.15
Ni1—S3—P2—O6	121.3(2)	135.9(2)	140.5(2)	138.4(1)	116.58	116.60	117.60	118.23
Ni1—S3—P2—C8	-124.4(2)	-109.6(2)	-105.8(3)	-107.2(1)	-127.93	-128.04	-126.37	126.76
Ni1—S4—P2—O6	-120.1(2)	-135.9(2)	-139.9(2)	-138.2(1)	-119.08	-115.73	-120.75	-116.80
Ni1—S4—P2—C8	124.9(2)	110.6(2)	105.5(3)	107.5(1)	125.97	128.28	124.40	127.15

Table 5.19. The intermolecular C—H···X (X= O, S) interactions (Å and °) for the complexes.

D—H···A	Symmetry	d(H···A)	d(D···A)	D—H···A
$[Ni(S_2P(R^x)(OR1))_2]$				
C17—H17C···O3	3/2-x,1-y,-1/2+z	2.617	3.559	166.72
C17—H17B···O3	1-x,-1/2+y,3/2-z	2.593	3.229	123.86
C1A—H1AA···O5	1/2+x,1/2-y,1-z	2.565	3.518	166.73
C7—H7A···S4	1+x,y,z	2.897	3.845	161.85
C2A—H2AB···S1	1+x,y,z	2.964	3.892	160.87
$[Ni(S_2P(R^x)(OR2))_2]$				
C15—H15A···O2	-x, 1-y, -z	2.546	3.408	149.46
C17—H17B···O5	1-x, 1-y, 2-z	2.60	3.551	170.11
C16—H16A···O3	1+x, y, 1+z	2.65	3.523	151.92
C15—H15B···S4	1-x, 1-y, 1-z	2.65	3.598	169.92

D—H···A	Symmetry	d(H···A)	d(D···A)	D—H···A
$[Ni(S_2P(R^x)(OR4))_2]$				
C14—H14A···O2	-x, -y, -z	2.504	3.442	165.11
C14—H14A···O3	-x, -y, -z	2.602	3.308	130.61
C16—H16C···O4	1-x, 2-y, 2-z	2.381	3.334	172.11
C16—H16C···O5	1-x, 2-y, 2-z	2.679	3.352	127.49
C17—H17C···S1	1-x, 2-y, 1-z	2.848	3.729	152.96
$[Ni(S_2P(R^x)(OR5))_2]$				
C14—H14B···O2	1-x, 1-y, 2-z	2.437	3.389	171.36
C14—H14B···O3	1-x, 1-y, 2-z	2.647	3.333	128.73
C16—H16A···O5	2-x, 1-y, -z	2.557	3.286	132.85
C16—H16A···O6	2-x, 1-y, -z	2.596	3.527	163.56
C16—H16B···O3	1-x, 1-y, 1-z	2.632	3.565	164.01
C3—H3···S2	1-x, 2-y, 1-z	2.906	3.695	143.41

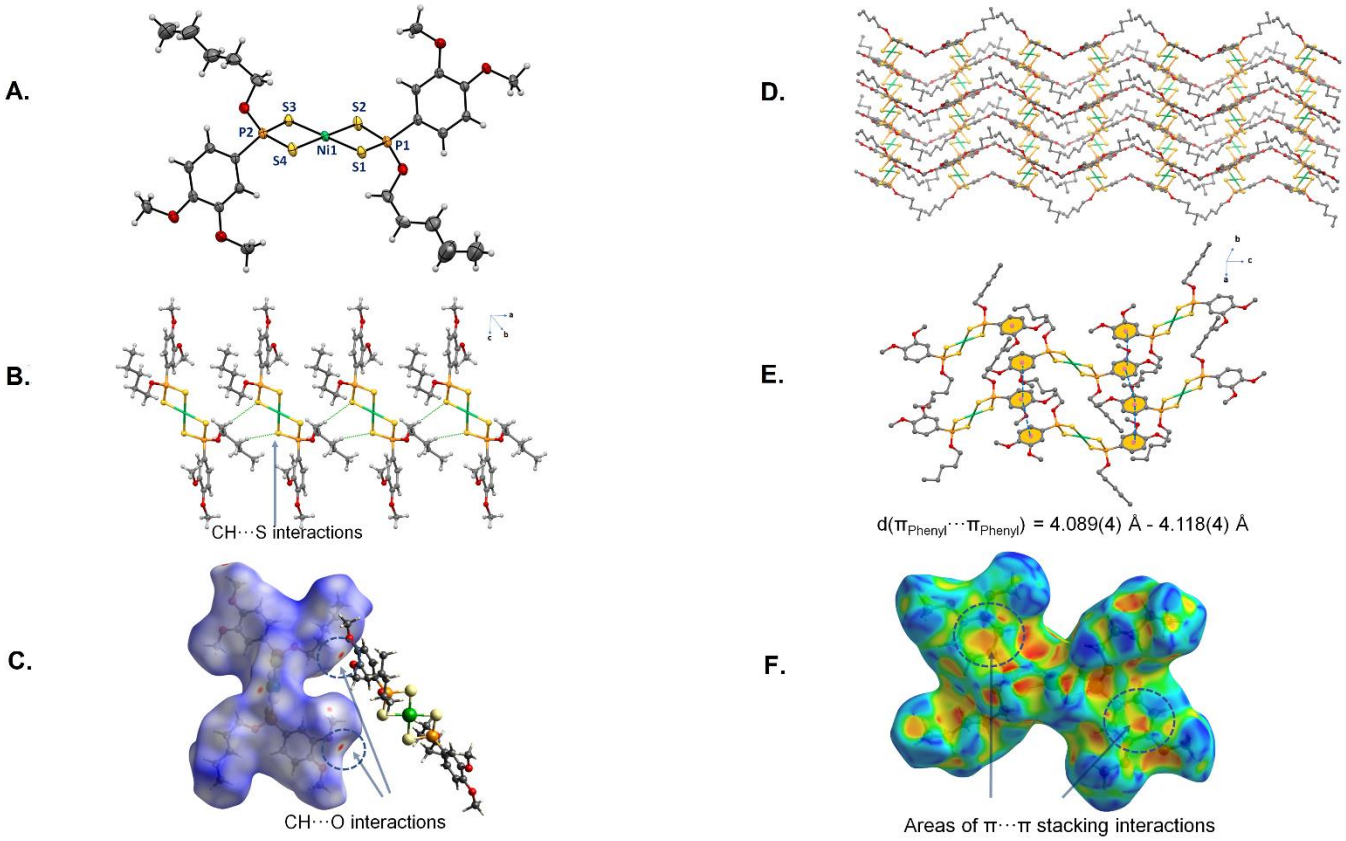


Figure 5.189. A[Ni($S_2P(R^x)(OR1))_2$] crystal structure with displacement ellipsoids drawn at the 25% probability level **B.** The C—H···S hydrogen bonding interactions in the crystal structure view **C.** Hirshfeld surfaces of [Ni($S_2P(R^x)(OR1))_2$] mapped with d_{norm}, showing the C—H···O hydrogen bonding interactions **D.** The illustration of the 3D supramolecular network showing the herringbone motif. **E.** The π···π interactions between the phenyl rings in [Ni($S_2P(R^x)(OR1))_2$] **F.** [Ni($S_2P(R^x)(OR1))_2$]'s Hirshfeld surfaces mapped with shape index depicting the areas of the π···π interactions.

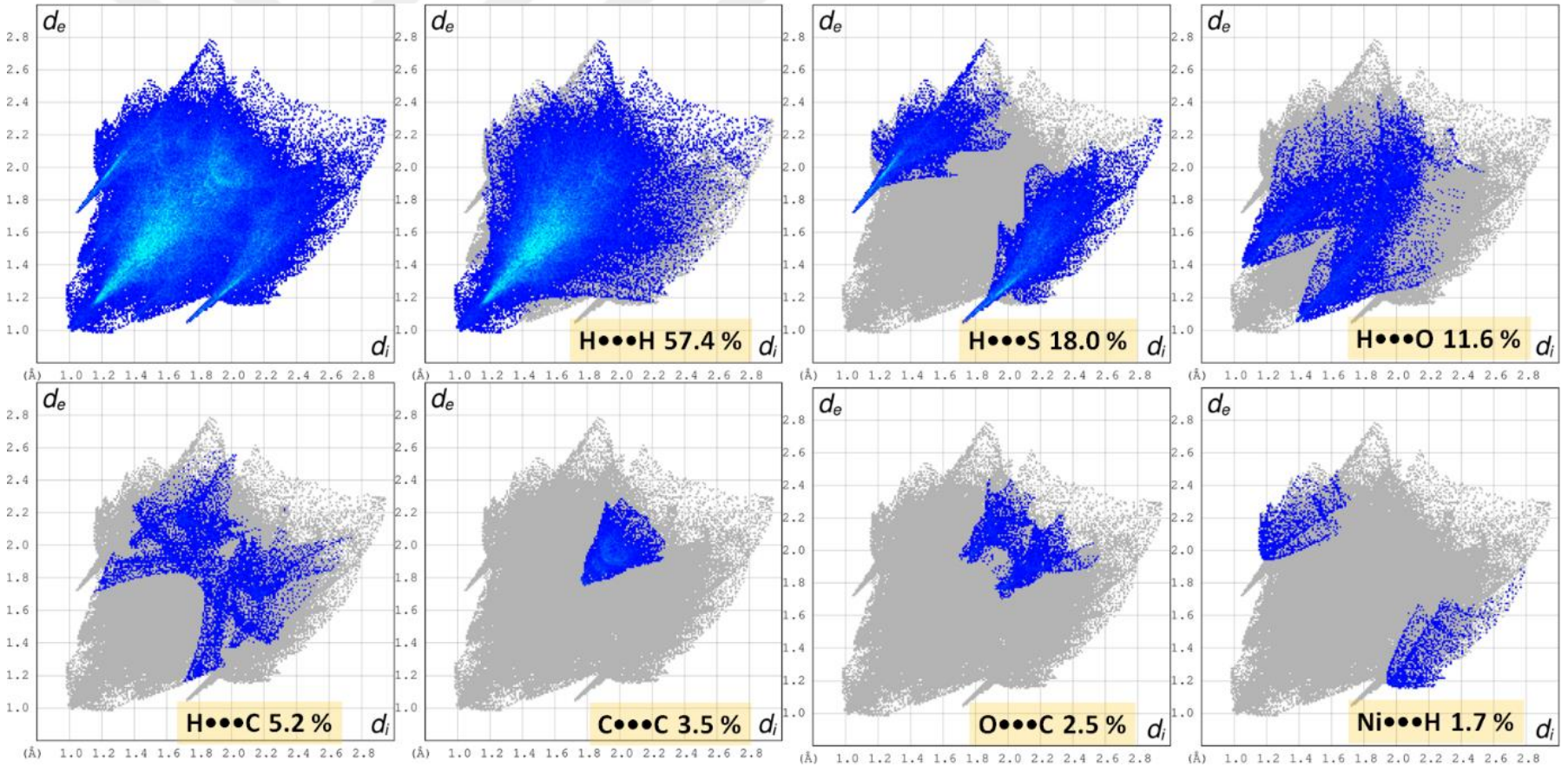


Figure 5.190. The resolved 2D fingerprint plots showing the contributions to the overall Hirshfeld surface area in $[Ni(S_2P(R^x)(OR1))_2]$.

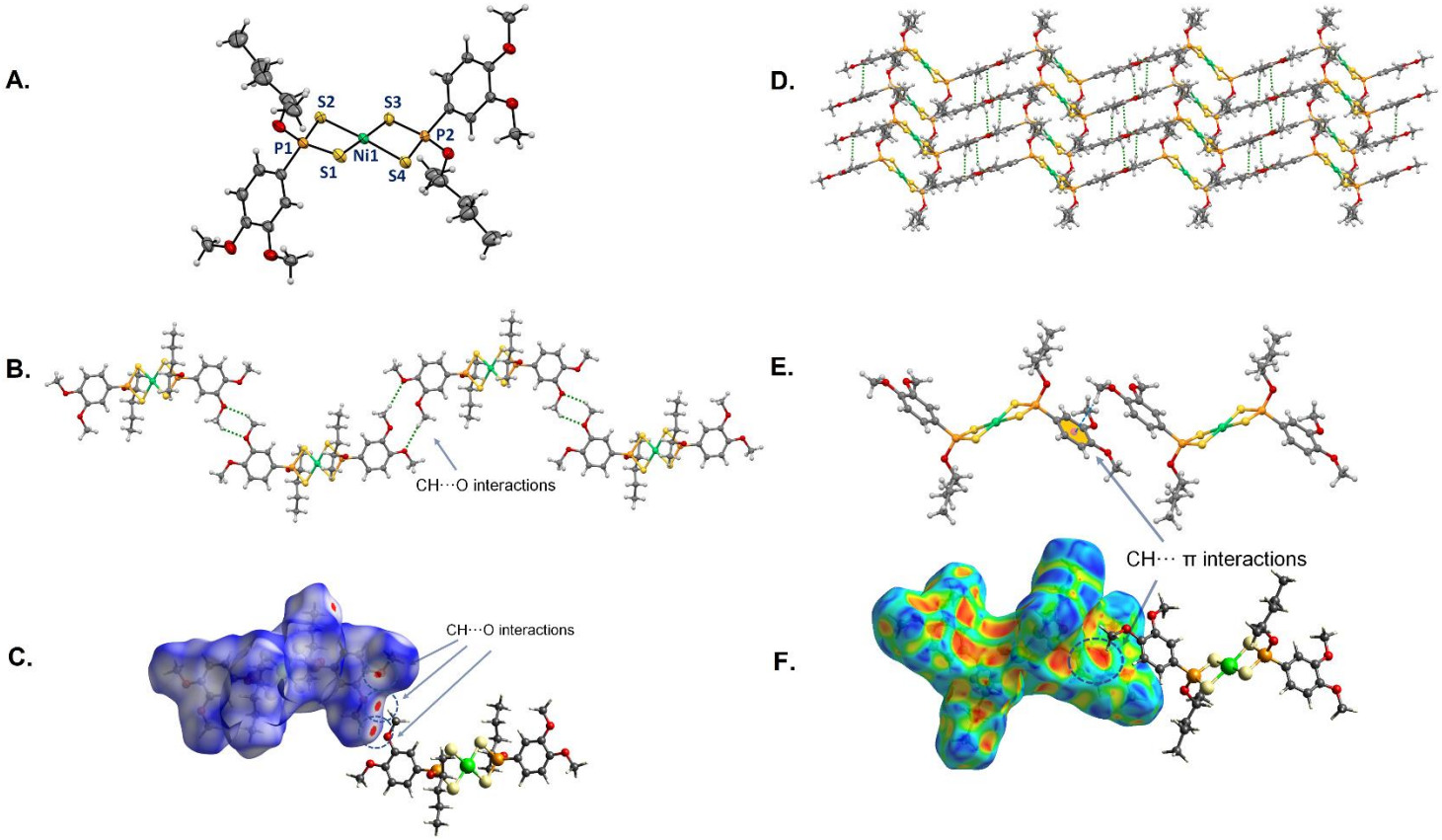


Figure 5.191. A. [Ni($S_2P(R^x)(OR2))_2$] crystal structure with displacement ellipsoids drawn at the 30% probability level **B.** View of the C—H···O hydrogen bonding interactions in the crystal structure **C.** [Ni($S_2P(R^x)(OR2))_2$] Hirshfeld surfaces mapped with d_{norm}, showing the C—H···O hydrogen bonding interactions **D.** The view of the 2D supramolecular network with the herringbone motif. **E.** The CH···π interaction in [Ni($S_2P(R^x)(OR2))_2$] **F.** [Ni($S_2P(R^x)(OR2))_2$] Hirshfeld surfaces mapped with shape index representing the areas of the CH···π interaction.

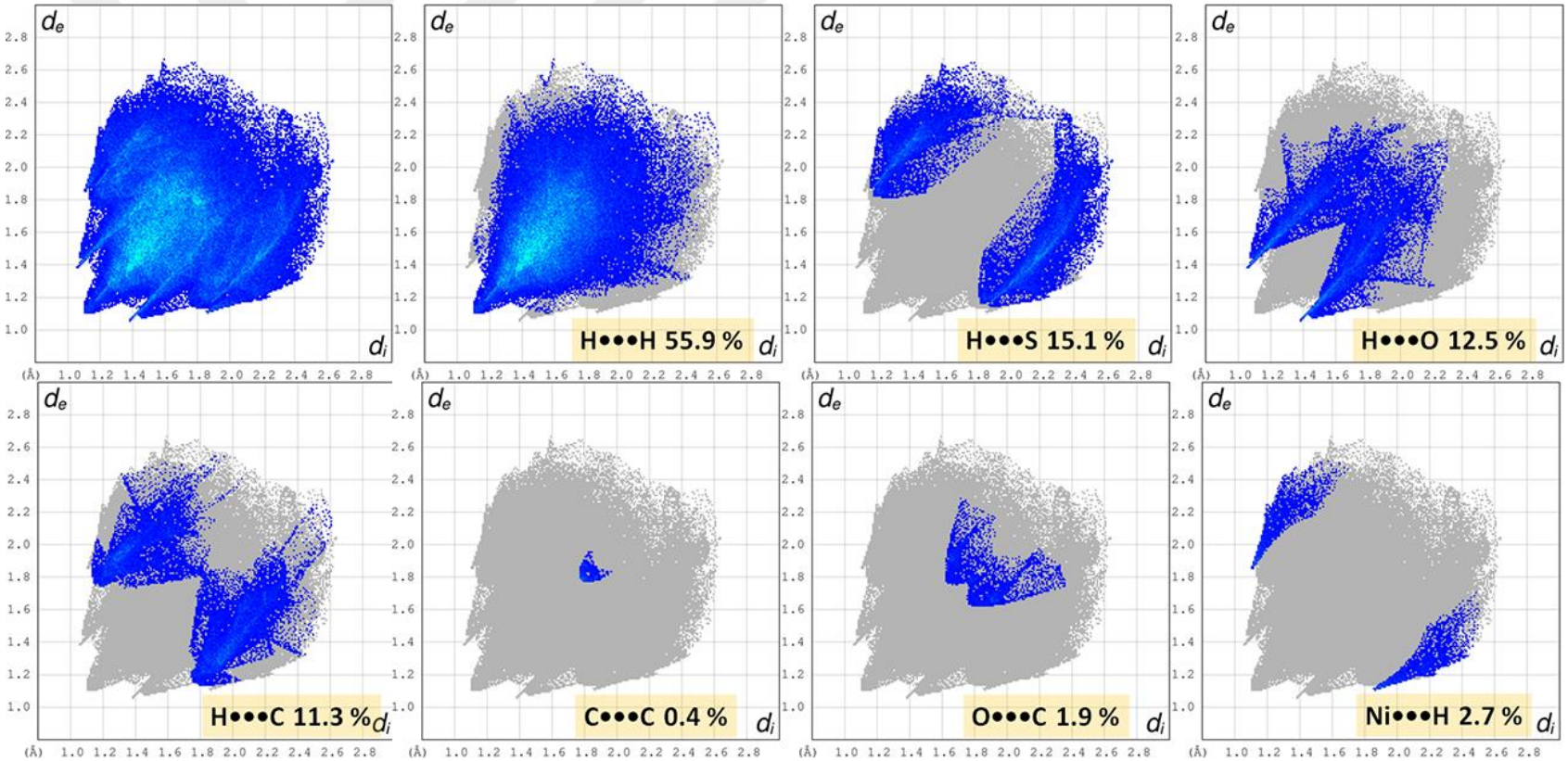


Figure 5.192. The resolved 2D fingerprint plots showing the contributions to the overall Hirshfeld surface area in [Ni($S_2P(R^x)(OR2)$)$_2$].

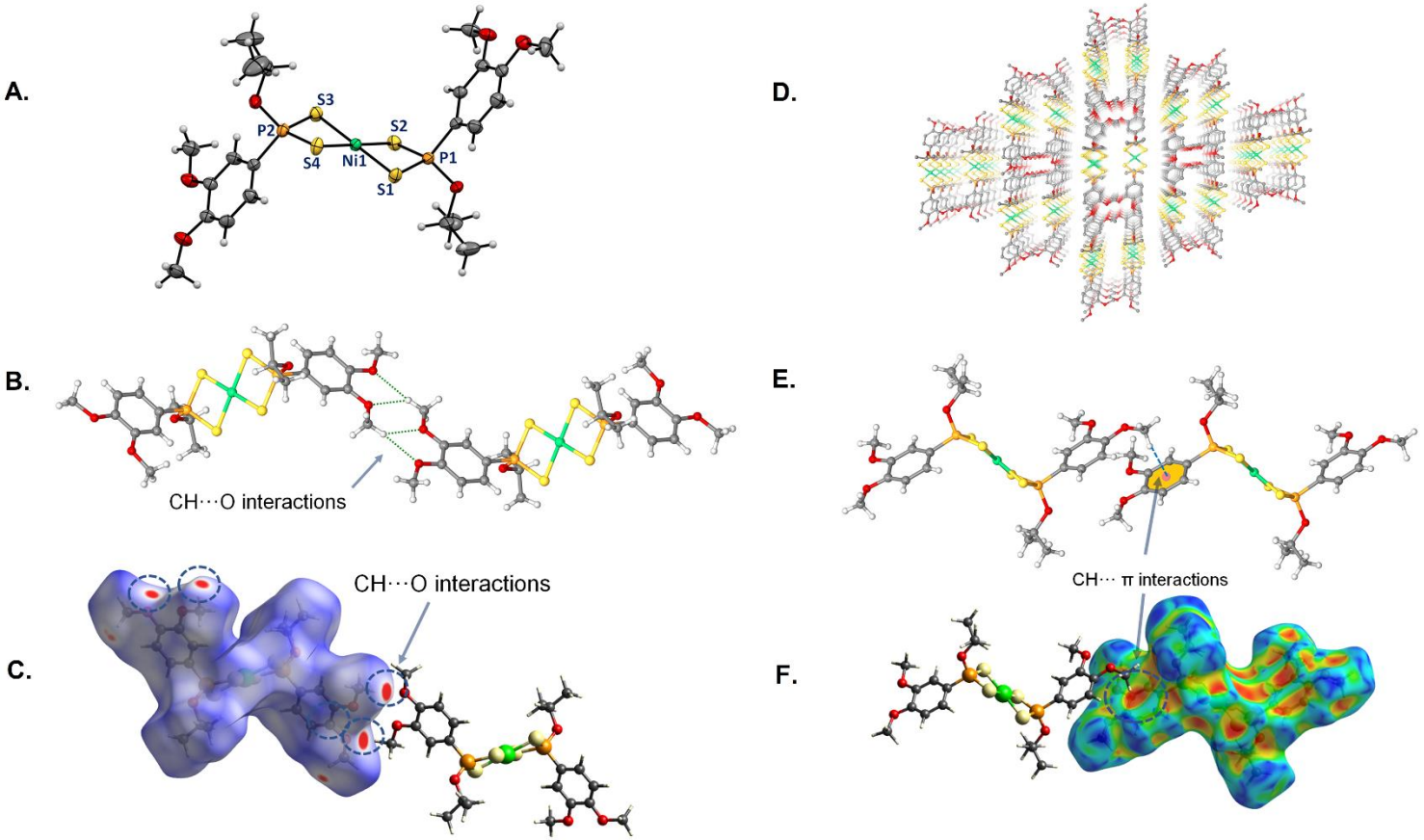


Figure 5.193. A. Crystal structure of [Ni($S_2P(R^x)(OR4))_2$] with displacement ellipsoids drawn at the 30% probability level **B.** View of the C—H···O hydrogen bonding interactions **C.** Hirshfeld surfaces of [Ni($S_2P(R^x)(OR4))_2$] mapped with d_{norm}, showing the C—H···O hydrogen bonding interactions **D.** The view of the 3D supramolecular network of crystal structure of [Ni($S_2P(R^x)(OR4))_2$]. **E.** The CH···π interaction in [Ni($S_2P(R^x)(OR4))_2$] **F.** Hirshfeld surfaces of [Ni($S_2P(R^x)(OR4))_2$] mapped with shape index showing the areas of the CH···π interaction.

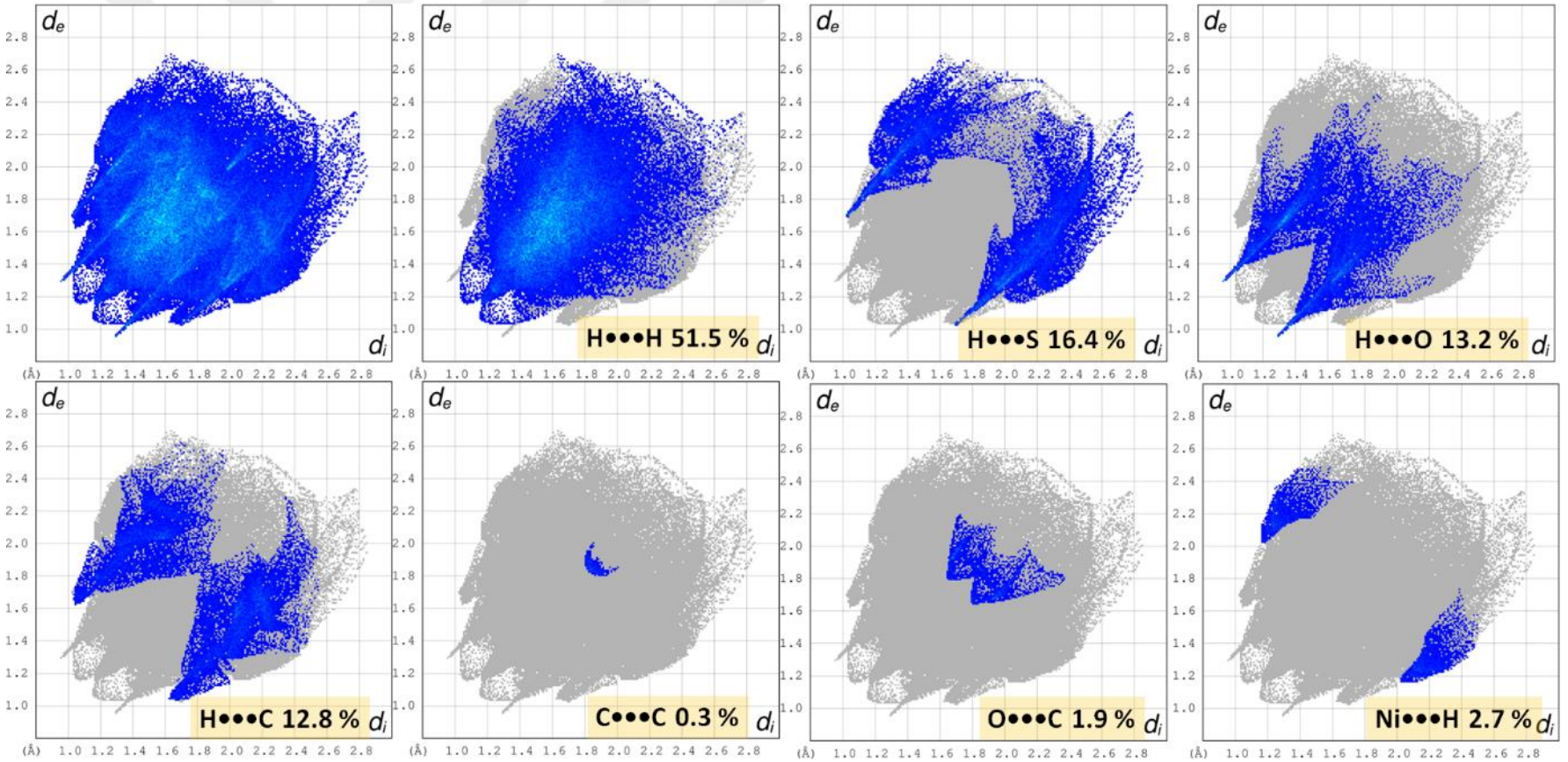


Figure 5.194. The resolved 2D fingerprint plots showing the contributions to the overall Hirshfeld surface area in $[Ni(S_2P(R^x)(OR4))_2]$.

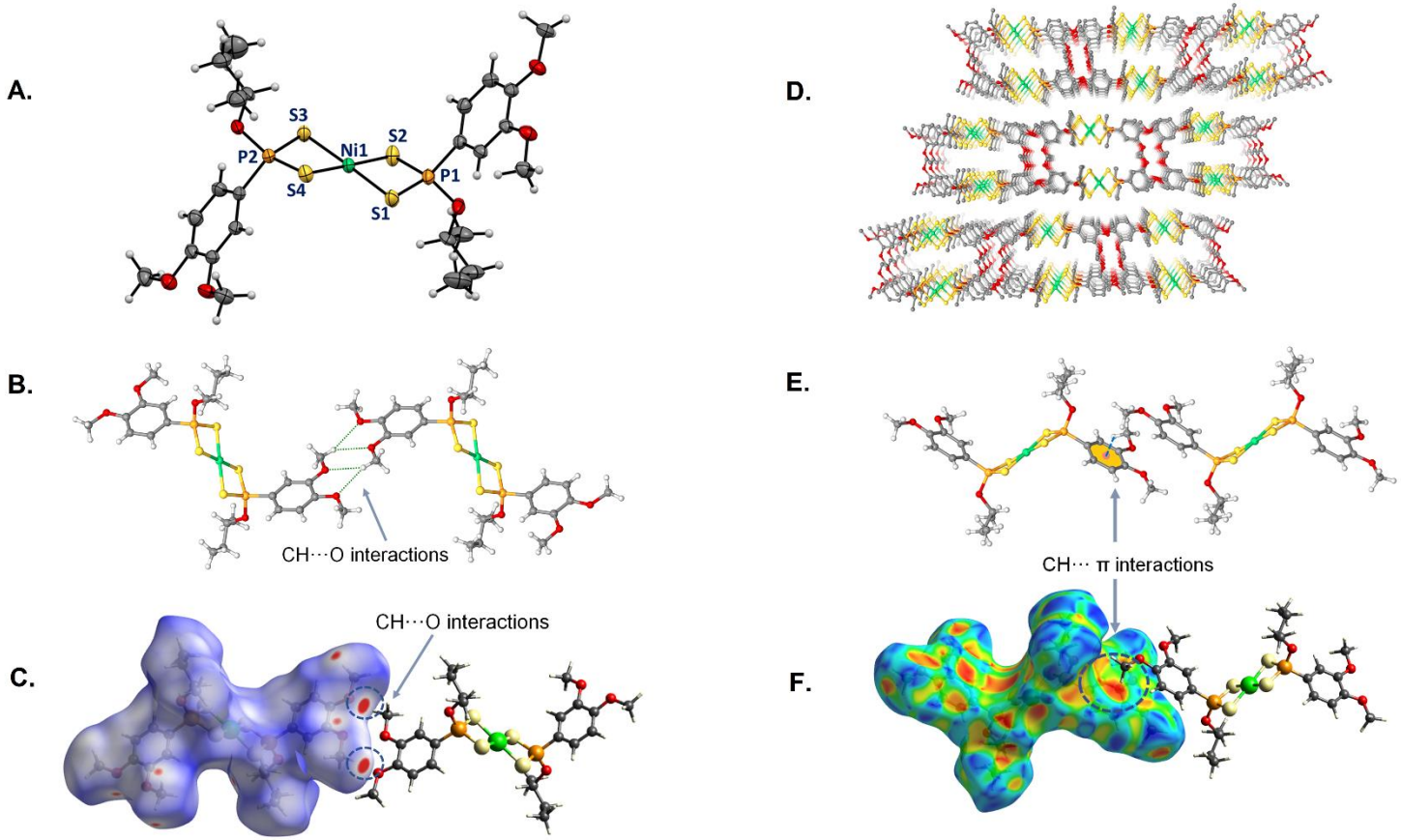


Figure 5.195. A. Crystal structure of [Ni($S_2P(R^x)(OR5)$)$_2$] with displacement ellipsoids drawn at the 30% probability level **B.** View of the C—H···O hydrogen bonding interactions **C.** Hirshfeld surfaces of [Ni($S_2P(R^x)(OR5)$)$_2$] mapped with d_{norm}, showing the C—H···O hydrogen bonding interactions **D.** The view of the 3D supramolecular network of crystal structure of [Ni($S_2P(R^x)(OR5)$)$_2$]. **E.** The CH···π interaction in [Ni($S_2P(R^x)(OR5)$)$_2$] **F.** Hirshfeld surfaces of [Ni($S_2P(R^x)(OR5)$)$_2$] mapped with shape index showing the areas of the CH···π interaction

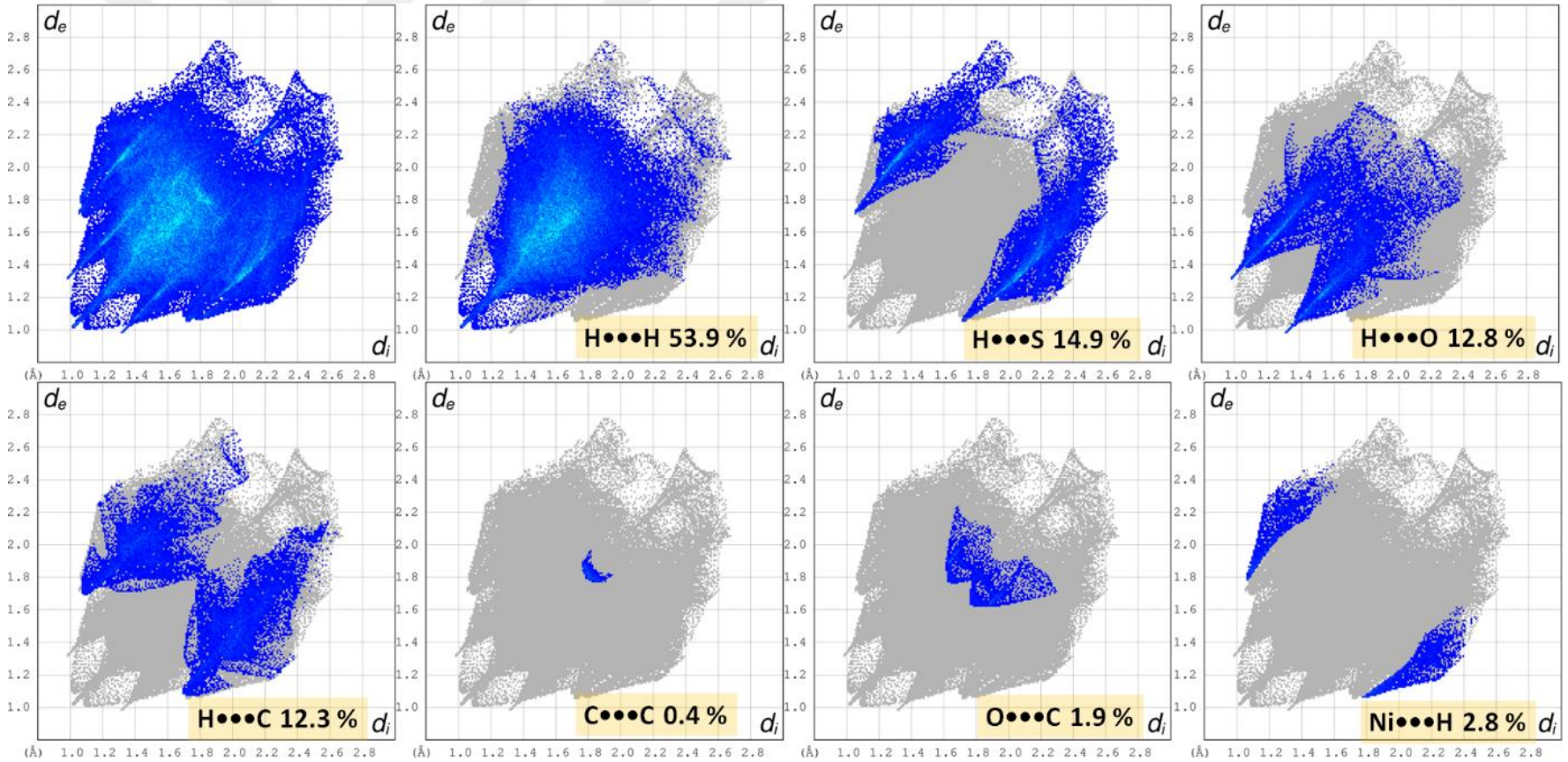


Figure 5.196. The resolved 2D fingerprint plots showing the contributions to the overall Hirshfeld surface area in [Ni($S_2P(R^x)(OR5)$)$_2$].

5.4. Crystallographic Descriptions of the Spectra of the Part II' [Ni(S$_2$P(R^y)(OR2))$_2$] Complex

The crystal structure of [Ni(S$_2$P(R^y)(OR2))$_2$] was unambiguously elucidated through single-crystal X-ray diffraction analysis to better understand its solid-state structure (Figure 5.197A, Table 5.20).

Table 5.20. Crystal data and structure refinement details for [Ni(S$_2$P(R^y)(OR2))$_2$].

Compound	[Ni(S2P(Ry)(OR2))2]
CCDC	2054970
Formula of Refinement Model	$C_{26}H_{40}NiO_6P_2S_4$
Formula weight	697.47
Temperature/K	173
Radiation, Wavelength (Å)	MoKα (λ = 0.71073)
Crystal system	Monoclinic
Space group	*C*2/c
a/Å	7.7485(11)
b/Å	7.9589(12)
c/Å	13.793(2)
α/°	105.315(2)
β/°	99.061(2)
γ/°	91.880(2)
Crystal size/mm3	0.52 × 0.50 × 0.23

Compound	[Ni(S2P(Ry)(OR2))2]
Volume/Å^3	807.7(2)
Z	1
ρcalcg/cm^3	1.434
μ/mm^{-1}	0.995
F(000)	366
2θ range for data collection/°	3.108 to 50
Index ranges	-9 ≤ h ≤ 9, -9 ≤ k ≤ 9, -16 ≤ l ≤ 16
Reflections collected	9941
Independent reflections	2851 [Rint = 0.0260, Rsigma = 0.0222]
Data/restraints/ parameters	2851/0/181
Goodness-of-fit on *F*2 (S)	1.039
Final R indices [*I* > 2σ(*I*)]	R1 = 0.0232, wR2 = 0.0612
R indices (all data)	R1 = 0.0244, wR2 = 0.0619
Largest diff. peak/hole / e Å^{-3}	0.35/-0.26

[Ni(S$_2$P(R^y)(OR2))$_2$] crystallizes in the triclinic crystal system with *P*-1 with the asymmetric unit consisting of one Ni(II) cation and one ligand (L2). The Ni(II) ion is located on a crystallographic inversion center. The dihedral angle between the 2,4-dimethoxyphenyl ring and NiS$_4$ coordination plane in the complex is 61.83° and also the dithiophosphonate moieties are in trans arrangement with respect to the coordination plane. The Ni(II) metal center has a square planar coordination geometry by four sulfur

atoms (S1, $S1^{i}$, S2, $S2^{i}$) from two dithiophosphonate ligands, forming four-membered chelate rings with an S1—Ni1—S2 angle of 87.929(15)°, and these angles agree with those observed in related Ni(II) complexes (CSD. Ref. Code: NORFUV, RIVQUI, RIVRAP) [252, 307]. The Ni—S bond distances (Ni1—S1 = 2.2216(5) Å and Ni1—S2 = 2.2412(5) Å) are in the normal ranges and are well-matched to those found in Ni(II) complexes (CSD Ref. Code: XORKAT, DUKMIH, HAHDAW, LIGFAJ, NIRMAF, NORFUV) [250, 252, 254, 281, 306, 310]. The P1—S1 and P1—S2 bond lengths are 2.0036(6) Å and 2.0093(6) Å, respectively, are intermediate between the P—S (~2.1 Å) and P=S (~1.90 Å) bond distances, which reflect that π-electron delocalization prevails in the $-PS_2$ of dithiophosphonate moiety. Unsurprisingly, the 2D fingerprint plots (Figure 5.198A) exhibit that the most effective contact in solid-state of $[Ni(S_2P(R^y)(OR2))_2]$ is the H/H interaction contributing to the total Hirshfeld surface with the value equal to 54.5% owing to the plentiful hydrogen atoms through aliphatic side groups. The weak C—H•••O (C8-H8C•••O1, (d(C8···O1) = 3.347 Å; C7—H7C•••O3, (d(C7···O3) = 3.325 Å, Table 5.21) hydrogen bonding interactions link the molecules to form 2D hydrogen-bonded layers (Figure 5.197C). The resulting 2D layers are further expanded into a 3D supramolecular network through C11—H11A•••S1 (d(C11···S1) = 3.347 Å) interactions, forming the hydrogen bonding rings with R2,2(18) motif, as shown in Figure 5.197D. HS of $[Ni(S_2P(R^y)(OR2))_2]$ are illustrated in Figure 5.197B and the O•••H/ H•••O and S•••H/ H•••S interactions constitute 13% and 17.3%, respectively, appearing as distinct spikes in the 2D fingerprint plot (Figure 5.198A). The closest C—H•••πphenyl (d(H•••π)) = 2.77 Å, Table 5.21) interaction is illustrated in the shape index-mapped Hirshfeld surfaces (Figure 5.198B) and also help to stabilize the crystal structure of $[Ni(S_2P(R^y)(OR2))_2]$. On the other hand, the curvedness mapped on the HS (Figure 5.198B) does not show a large flat region, which reflects no important π–π stacking interactions less than πphenyl•••πphenyl < 3.8 Å.

Table 5.21. The intermolecular C—H···X (X= O, S, π) interactions (Å and °) for $[Ni(S_2P(R^y)(OR2))_2]$.

D—H···A	Symmetry	d(D—H)	d(H···A)	d(D—H···A)	D—H···A
C8—H8C···O1	2656.01	0.98	2.51	3.347	142.99
C7—H7C···O3	1565.01	0.98	2.59	3.325	131.87
C11—H11A···S1	2667.01	0.99	2.85	3.739	149.23
C8—H8B···Cg2	2756.01	0.98	2.77	3.631	146.47

Represents the ring built up by atoms C1-C2-C3-C4-C5-C6.

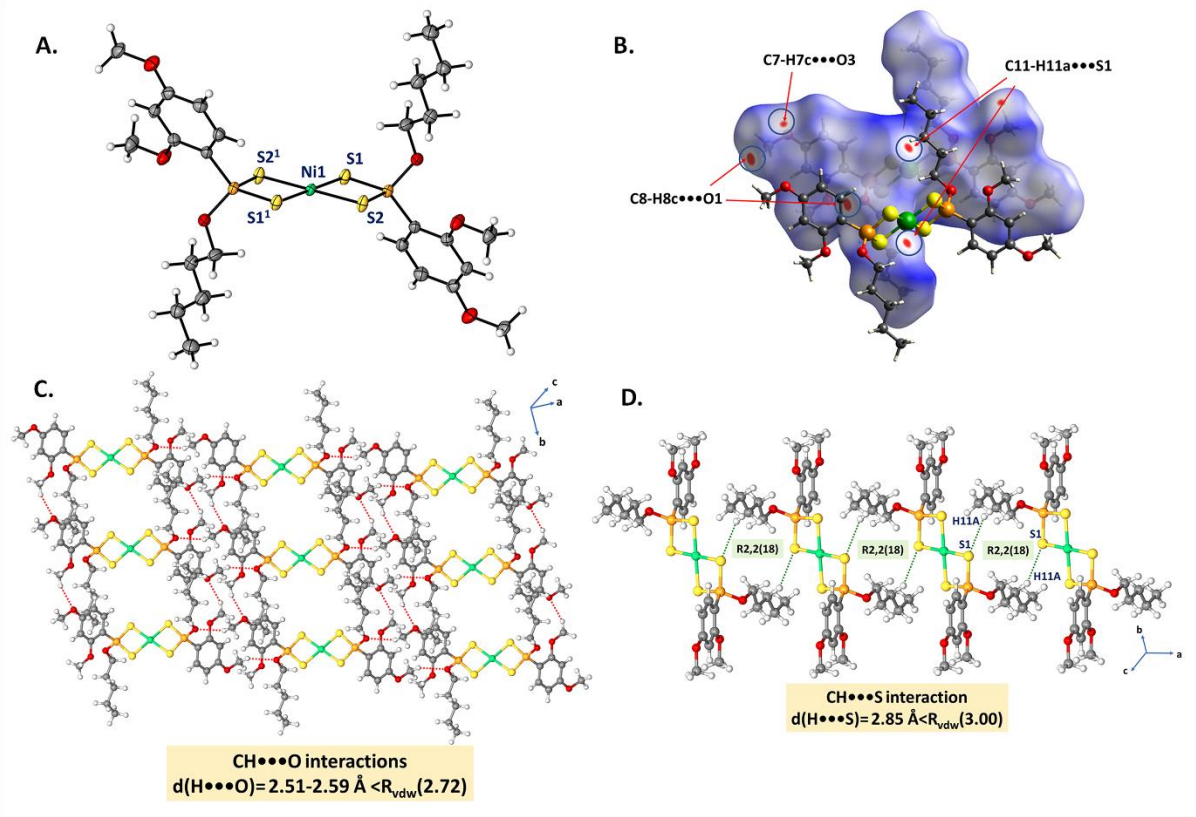


Figure 5.197. A. A view of the structure of [Ni($S_2P(R^y)(OR2))_2$], showing the atom-labeling scheme. Displacement ellipsoids are drawn at the 50% pro bability level. Symmetry code: (a) 2 −x , 1 −y , 2 –z. **B.** HS of [Ni($S_2P(R^y)(OR2))_2$] mapped with d norm , showing the C —H ···O (red dotted lines) and C —H ···S (green dotted lines) hydrogen bonding interactions. **C.** Perspective view of the 2D constructed from

the C —H ···O hydrogen bonds. **D.** The 1D chains constructed from the hydrogen bonding rings with R2,2(18)-graph-set notation.

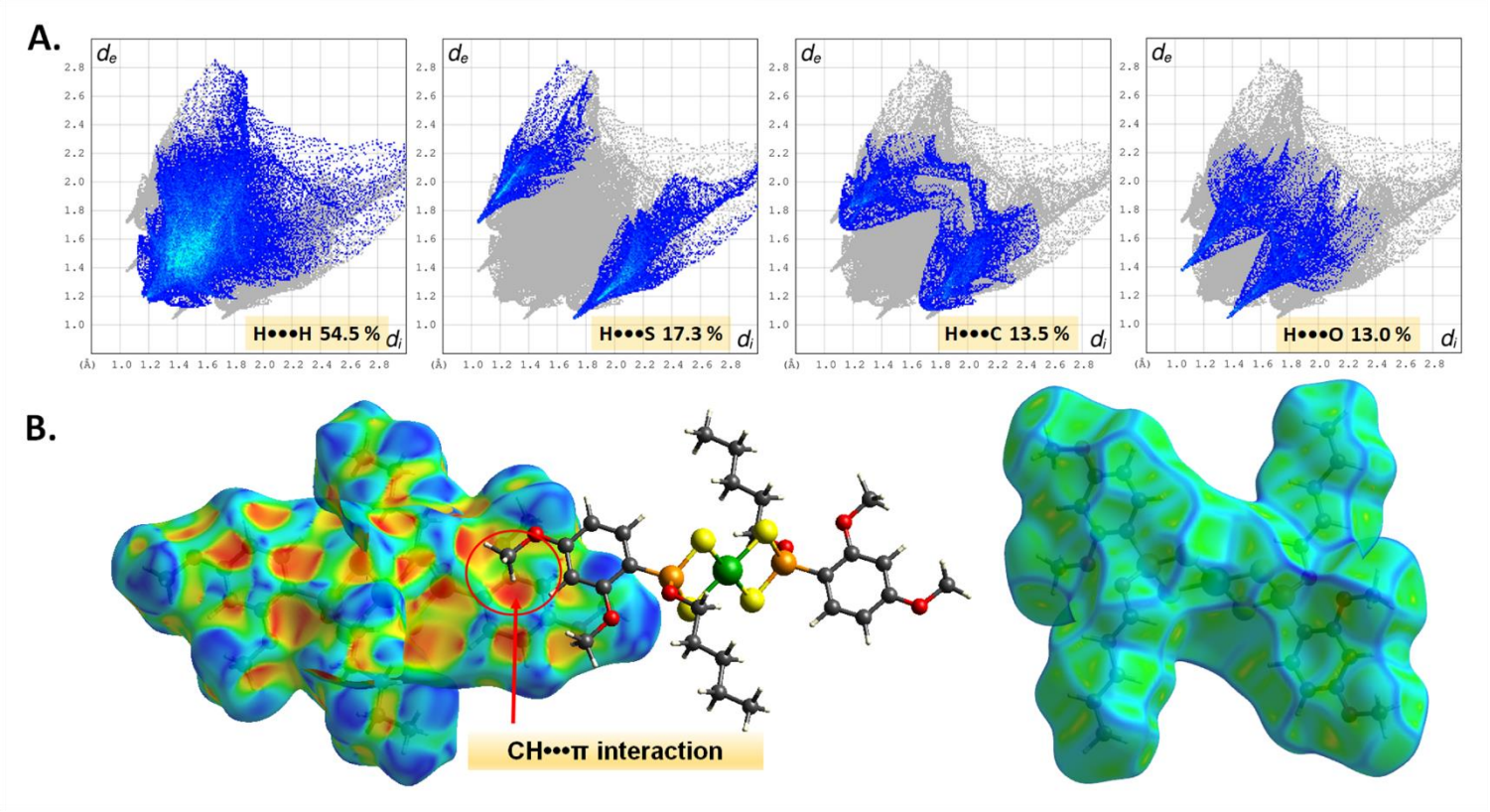


Figure 5.198. A. The resolved 2D fingerprint plots showing the percentage contributions to the total HS area. **B.** HS mapped with shape index (left) and curvedness (right) of [Ni($S_2P(R^y)(OR2)_2$]. The HS shape index exhibits concave curvature, where C —H ···πinteraction occurs.

5.5. Optimized molecular structures of the Part Ia' Ni(II) Complexes

The optimized 3D structural parameters of the complexes investigated were calculated using B3LYP/LANL2DZ/6-31+G(d,p) level in the ground state. The optimized molecular figures of the compounds are depicted in Figure 199A. Experimental and theoretical values of selected bond lengths and angles were listed in Table 5.22.

Table 5.22. Selected experimental and calculated bond lengths (Å) and bond angles (°) for Ni(II) complexes.

Bond lengths (Å)	$[Ni(S_2P(R^x)(OR1))_2]$	$[Ni(S_2P(R^x)(OR2))_2]$	$[Ni(S_2P(R^x)(OR3))_2]$	$[Ni(S_2P(R^x)(OR4))_2]$	$[Ni(S_2P(R^x)(OR5))_2]$	$[Ni(S_2P(R^x)(OR6))_2]$	$[Ni(S_2P(R^x)(OR7))_2]$
Ni1——S1	2.2240 (12)/2.3501*	2.2228(6)/2.3489*	2.2121(8)/2.3488*	2.2288 (6)/2.3455*	2.2272(15)/2.3482*	2.2249(11)/2.3482*	2.2156 (4)/2.3475*
Ni1——S2	2.2311 (12)/2.3483*	2.2267(6)/2.3480*	2.2246(8)/2.3483*	2.2318 (5)/2.3453*	2.2293(15)/2.3445*	2.2217(11)/2.3485*	2.2244 (4)/2.3476*
Ni1——S3	2.2148 (13)/2.3501*	-	-	-	2.2388(14)/2.3440*	-	-
Ni1——S4	2.2287 (12)/2.1970*	-	-	-	2.2261(15)/2.3456*	-	-
Ni2——S3	-	-	-	-	-	2.2235(10)	-
Ni2——S4	-	-	-	-	-	2.2294(9)	-
S1——P1	1.9956 (15)/2.1910*	2.0030(8)/2.1919*	2.0043(12)/2.1925*	2.0149(7)/2.1965*	2.003(2)/2.1960*	1.9975(15)/2.1966*	2.0087 (5)/2.1942*
S2——P1	2.0033 (15)/2.1969*	2.0040(8)/2.1973*	2.0016(12)/2.1954*	2.0035(7)/2.1946*	2.0038(18)/2.1993*	2.0065(15)/2.1914*	1.9966 (6)/2.1941*
S3——P2	2.0019 (17)/2.1901*	-	-	-	2.0092(18)/2.200*	2.0114(13)	-
S4——P2	1.9999 (17)/2.1970*	-	-	-	1.9967(18)/2.1976*	2.0012(14)	-

Table 5.22. Continues.

Bond angles (°)	$[Ni(S_2P(R^x)(OR1))_2]$	$[Ni(S_2P(R^x)(OR2))_2]$	$[Ni(S_2P(R^x)(OR3))_2]$	$[Ni(S_2P(R^x)(OR4))_2]$	$[Ni(S_2P(R^x)(OR5))_2]$	$[Ni(S_2P(R^x)(OR6))_2]$	$[Ni(S_2P(R^x)(OR7))_2]$
S1—Ni1—S1^i	-	180.0/180.0*	180.0/180.0*	180.0/180.0*	-	180.0/180.0*	180.0/180.0*
S2^i—Ni1—S2	-	180.0/180.0*	180.0/180.0*	180.0/180.0*	-	180.0/180.0*	180.0/180.0*
S2—Ni1—S1^i	-	91.83 (2)/90.490*	91.73(3)/90.569*	92.214(16)/90.646*	-	91.81(4)/90.503*	91.306 (14)/90.572*
S2—Ni1—S1	-	-	-	-	-	88.19(4)/89.497*	-
S1—Ni1—S2	88.08 (4)/89.546*	88.17 (2)/89.510*	88.27(3)/89.431*	87.786(16)/89.349*	88.42(5)/89.497*	-	88.693 (14)/89.428*
S1—Ni1—S4	92.19 (5)/90.453*	-	-	-	90.73(6)/90.544*	-	-
S3—Ni1—S1	178.78 (5)/179.770*	-	-	-	177.35(6)/179.605*	-	-
S3—Ni1—S2	91.94 (5)/90.451*	-	-	-	92.59(5)/90.639*	-	-
S3—Ni1—S4	87.84 (5)/ 89.546*	-	-	-	88.36(5)/89.325*	-	-
S4—Ni1—S2	177.64 (5)/178.886*	-	-	-	177.38(6)/179.232*	-	-
S3—Ni2—S3^i	-	-	-	-	-	180.0	-
S4^i—Ni2—S4	-	-	-	-	-	180.0	-
S3—Ni2—S4^i	-	-	-	-	-	92.04(3)	-
S3—Ni2—S4	-	-	-	-	-	87.96(3)	-

*Optimized (theoretical) values at the B3LYP/LANL2DZ/6-31+G(d,p) level in the ground stat

5.6. Frontier orbitals and chemical parameters of the Part Ia' Ni(II) Complexes

Frontier orbitals (HOMOs and LUMOs) are related to electron affinity and ionization potential. These orbitals are very important for chemical reactivity. If the energy values of frontier orbitals are calculated, the chemical parameters such as the ionization potential (IP), the electron affinity, (EA), the chemical hardness, (η), the absolute electronegativity (χ), and the absolute softness (σ) of the molecules can be calculated by using to the Koopmans theorem [292].

The chemical parameters and the energy gaps between HOMOs and LUMOs of the Ni(II) dithiophosphonato complexes were calculated by the DFT in the ground state. The total energies, calculated chemical parameters and the energy gaps $\Delta E_{Gap} = (E_{LUMO} - E_{HOMO})$ were given in Table 5.23. As can be seen in the table, the values of ΔE_{Gap} are 3.3641, 3.3625, 3.3590, 3.3598, 3.3758, 3.3644 and 3.3582 eV for the gas phases of the compounds $[Ni(S_2P(R^x)(ORn))_2]$ (n=1-7), respectively. The configurations of HOMO and LUMO with energy levels are depicted in Figure 5.199B. In all the compounds, HOMOs are mainly localized on the whole molecule except for R_n groups while LUMOs are mainly localized on PS_2 moiety and nickel atoms (Figure 5.199B).

Table 5.23. Calculated total energies, dipole moments and chemical parameters of the complexes.

Parameters	E_{TOTAL}(Hartee)	E_{HOMO} (eV)	E_{LUMO} (eV)	ΔE_{Gap}(eV)	I (eV)	A eV	η (eV)	X (eV)	σ (eV)	μ_p (eV)	ω
$[Ni(S_2P(R^x)(OR1))_2]$	-1374.2867	-5.9223	-2.5581	3.3631	5.9223	2.2581	1.6821	4.2402	0.5945	-4.2402	14.1214
$[Ni(S_2P(R^x)(OR2))_2]$	-1452.9134	-5.8662	-2.5037	3.3625	5.8662	2.5037	1.6813	4.1850	0.5948	-4.1850	14.7228
$[Ni(S_2P(R^x)(OR3))_2]$	-13531.5285	-5.8475	-2.4885	3.3590	5.8475	2.4885	1.6795	4.1680	0.5954	-4.1680	14.5880
$[Ni(S_2P(R^x)(OR4))_2]$	-1610.1400	-5.8543	-2.4945	3.3598	5.8543	2.4945	1.6799	4.1744	0.5953	-4.1744	14.6364
$[Ni(S_2P(R^x)(OR5))_2]$	-1688.7634	-5.8573	-2.4814	3.3758	5.8573	2.4814	1.6879	4.1693	0.5924	-4.1693	14.6709
$[Ni(S_2P(R^x)(OR6))_2]$	-1688.7556	-5.8431	-2.4787	3.3644	5.8431	2.4787	1.6822	4.1609	0.5945	-4.1609	14.5621
$[Ni(S_2P(R^x)(OR7))_2]$	-1836.3230	-5.8719	-2.5138	3.3582	5.8719	2.5138	1.6791	4.1929	0.5956	-4.1929	14.7592

E_{TOTAL} : Total energy.
E_{HOMO} and E_{LUMO} : Energy values of HOMO and LUMO.
ΔE_{Gap}(eV) = (E_{LUMO} - E_{HOMO}) : Gap of energy.

I : Ionization potential.
A : Electron affinity.
η : Absolute hardness. (I - A)/2.

X : Electronegativity. (I + A)/2.
σ : Softness. 1/η.
μ_p : Chemical potential. - (I + A)/2
ω : Electrophilicity. $\mu_p^2/2\eta$.

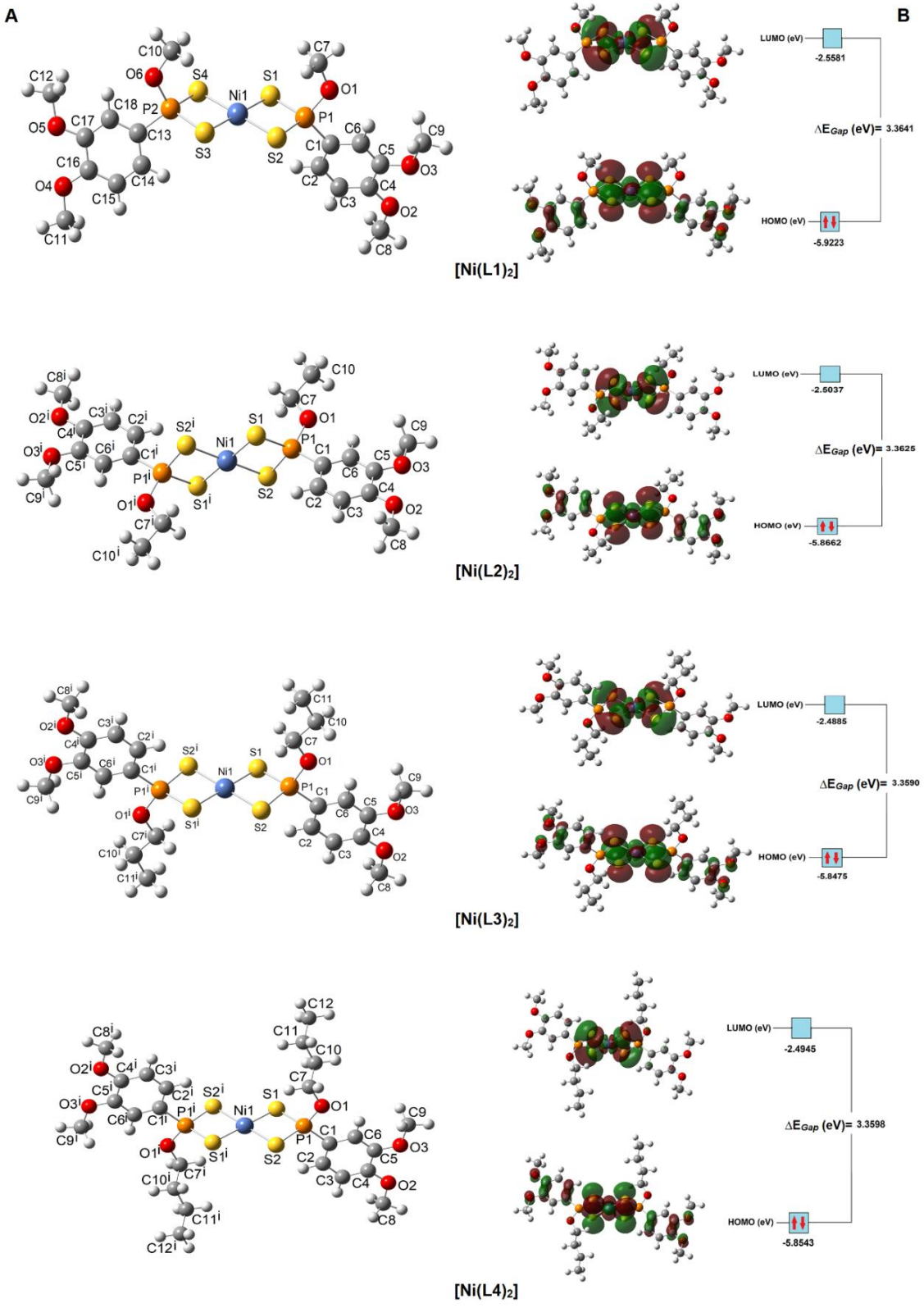


Figure 5.199. The optimized structures (**A**), HOMO and LUMO surfaces electron density and band gap values (eV) (**B**) of the Ni(II) complexes.

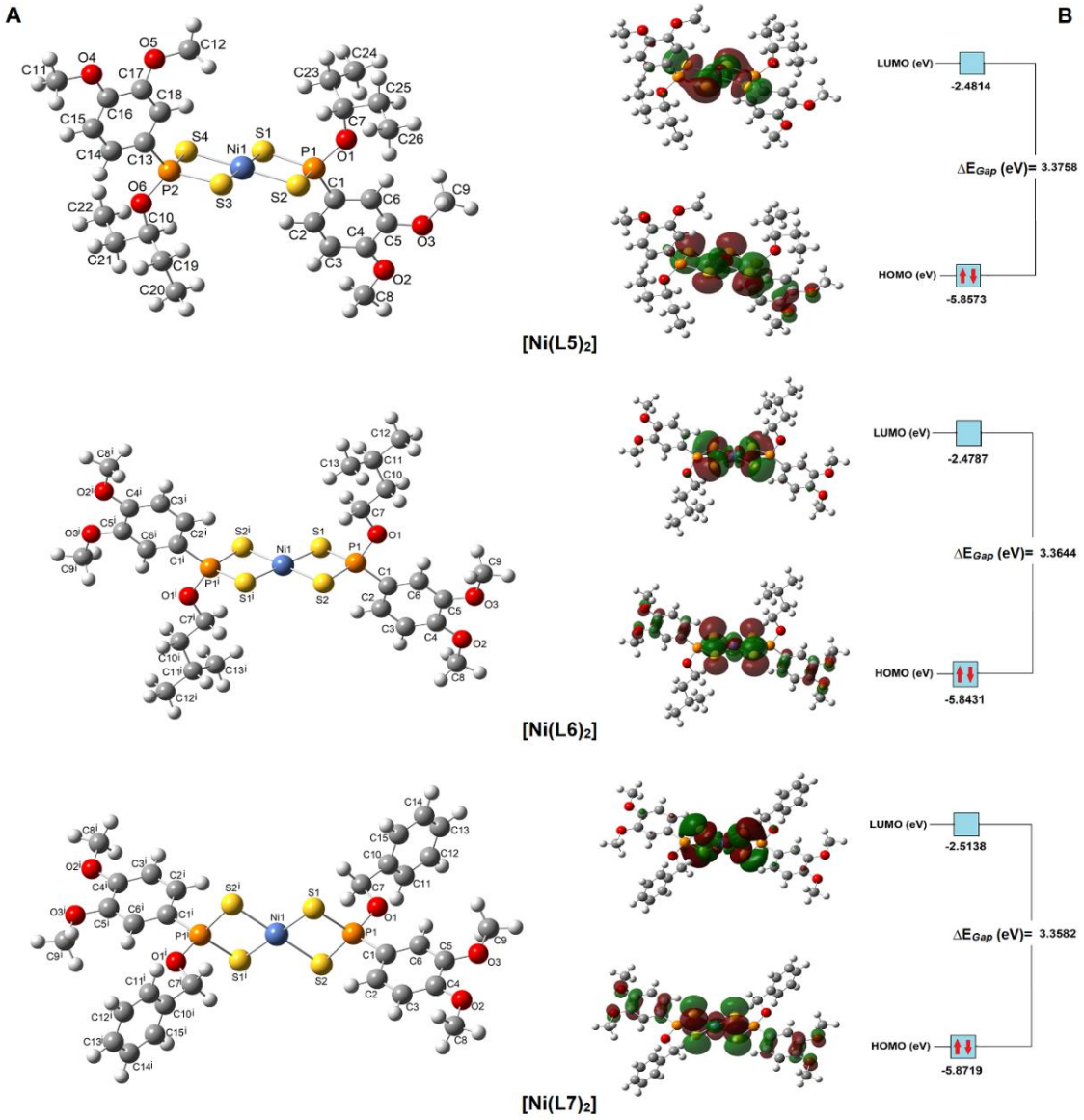


Figure 5.199. Continues.

5.7. Optimized Molecular Structures of the Part Ib' Ni(II) Complexes

The 3D geometrical parameters of the complexes $[Ni(S_2P(R^x)(OR1))_2]$, $[Ni(S_2P(R^x)(OR2))_2]$, $[Ni(S_2P(R^x)(OR4))_2]$ and $[Ni(S_2P(R^x)(OR5))_2]$ were optimized using B3LYP/LANL2DZ. The optimized structures of Ni complexes were given in Figure 5.200A. The findings of selected experimental and theoretical bond lengths and angles were itemized in Table 5.24.

The conformational discrepancies between the optimized structures at the B3LYP/LANL2DZ level and experimental structures (X-ray structure) of $[Ni(S_2P(R^x)(OR1))_2]$, $[Ni(S_2P(R^x)(OR2))_2]$, $[Ni(S_2P(R^x)(OR4))_2]$ and

$[Ni(S_2P(R^x)(OR5))_2]$ can be seen in Figure 5.200B. The comparison of the NiS_4P_2 fragment in the optimized structures and those in the X-ray determined structure shows that the corresponding structrures are fairly approximate. However, optimized structures predict greater rotational freedom for aryl groups compared to freedoms observable in the X-ray structures (Figure 5.200B).

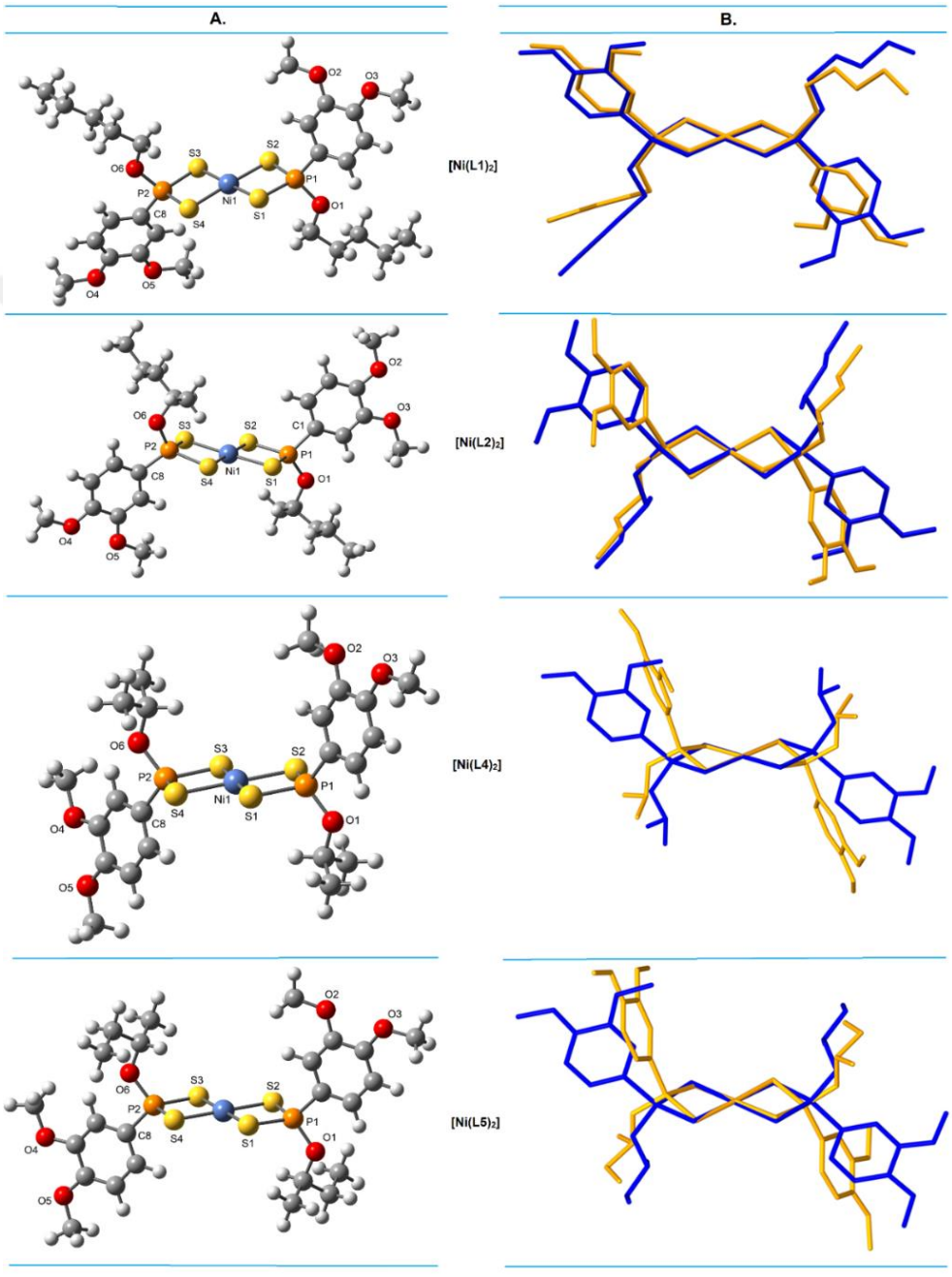


Figure 5.200 A. The optimized structures of the complexes by DFT with B3LYP/LANL2DZ level. **B.** Superimposition of the DFT-optimized (dark blue) and X-ray (yellow) structures of the complexes.

The conformational differences are found in between the experimental and calculated structures of the investigated complexes $[Ni(S_2P(R^x)(OR1))_2]$, $[Ni(S_2P(R^x)(OR2))_2]$, $[Ni(S_2P(R^x)(OR4))_2]$ and $[Ni(S_2P(R^x)(OR5))_2]$ as seen from Table 5.24 and Figure 5.200B. The Ni–S bond lengths in Ni(II) coordination sphere are 2.2200(17)/2.3445, 2.2217(18)/2.3409, 2.2233(17)/2.3512 and 2.2246(18)/2.3450 Å (Exp./Cal.) for $[Ni(S_2P(R^x)(OR1))_2]$, 2.2233(16)/2.3441, 2.2217(18)/2.3476, 2.2233(17)/2.3452 and 2.2246(18)/2.3428 Å (Exp./Cal.) for $[Ni(S_2P(R^x)(OR2))_2]$, 2.222(2)/ 2.3454, 2.224(2)/2.3468, 2.220(2)/2.3485 and 2.227(2)/2.3428 Å (Exp./Cal.) for $[Ni(S_2P(R^x)(OR4))_2]$ and 2.2173(19)/2.3455, 2.225(2)/2.3462, 2.2263(19)/2.3443 and 2.223(2)/ 2.3457 Å (Exp./Cal.) for $[Ni(S_2P(R^x)(OR5))_2]$.

The S─Ni─S bond angles are range from 88.03(6)/89.52 to 179.91(9)°/177.96° (Exp./Cal.) for $[Ni(S_2P(R^x)(OR1))_2]$, 88.01(6)/89.50 to 176.31(6)°/178.55° (Exp./Cal.) for $[Ni(S_2P(R^x)(OR2))_2]$, 88.59(7)/89.02 to 179.84(9)°/179.94° (Exp./Cal.) for $[Ni(S_2P(R^x)(OR4))_2]$ and 88.44(9)/89.21 to 178.35(6)°/179.82° (Exp./Cal.) for $[Ni(S_2P(R^x)(OR5))_2]$.

The fact that the calculated geometric values are a little higher than the experimentally found counterparts is not a surprise, because the experimental data are acquired in the solid-state whereas the optimized DFT data relate to unpacked isolated molecules.

5.8. Chemical Parameters and HOMO and LUMO iso Surfaces of Part Ib' Ni(II) Complexes

The values of total energies, the ΔE_{Gap} and chemical parameters of the $[Ni(S_2P(R^x)(ORn))_2]$, (n= 1,2,4,5) were listed in Table 5.25. With the B3LYP/LANL2DZ level of the DFT, the predicted values of ΔE_{Gap} are 3.4017, 3.3737, 3.3775 and 3.3792 eV. The band gap levels and isosurfaces of HOMOs and LUMOs are pictured in Figure 5.201.

HOMO and LUMO of $[Ni(S_2P(R^x)(OR1))_2]$ are localized essentially on the coordination neighbourhood comprising the Ni and S atoms. LUMO of $[Ni(S_2P(R^x)(OR2))_2]$ and $[Ni(S_2P(R^x)(OR5))_2]$ is mainly localized on the coordination region while HOMOs of $[Ni(S_2P(R^x)(OR2))_2]$, $[Ni(S_2P(R^x)(OR4))_2]$ and $[Ni(S_2P(R^x)(OR5))_2]$ are spread on the regions comprising the central NiS_4 part, oxygens of the aromatic methoxy groups and four carbon atoms from each of 3,4-dimethoxyphenyl ring (Figure 5.201). The low ΔE_{Gap}

value indicates a notable potency for intermolecular charge transfer and bioactivity of the compounds.

Table 5.24 Calculated total energies, dipole moments and chemical parameters of the complexes.

Parameters	$[Ni(S_2P(R^x)(OR1))_2]$	$[Ni(S_2P(R^x)(OR2))_2]$	$[Ni(S_2P(R^x)(OR4))_2]$	$[Ni(S_2P(R^x)(OR5))_2]$
E_{TOTAL}(Hartee)	-1688.7554	-1688.7648	-1531.5381	-1688.7648
E_{HOMO} (eV)	-5.9130	-5.8553	-5.8725	-5.8642
E_{LUMO} (eV)	-2.5113	-2.4817	-2.4950	-2.4849
ΔE_{Gap}(eV)	3.4017	3.3736	3.3775	3.3792
I (eV)	5.9130	5.8553	5.8725	5.8642
A (eV)	2.5113	2.4817	2.4950	2.4849
η (eV)	1.7008	1.6868	1.6887	1.6896
X (eV)	4.2122	4.1685	4.1838	4.1746
σ (eV)	0.5879	0.5928	0.5922	0.5918
μ_p (eV)	-4.2122	-4.1685	-4.1838	-4.1746
ω	15.0887	14.6557	14.7797	14.7226

E_{TOTAL} : Total energy.
E_{HOMO} and E_{LUMO} : Energy values of HOMO and LUMO.
$\Delta E_{Gap}(eV) = (E_{LUMO} - E_{HOMO})$: Gap of energy.
I : Ionization potential.
A : Electron affinity.

η : Absolute hardness. $(I - A)/_2$.
X : Electronegativity. $(I + A)/_2$.
σ : Softness. $1/\eta$.
μp : Chemical potential. $- (I + A)/_2$
ω : Electrophilicity. $\mu p_2/_2\eta$.

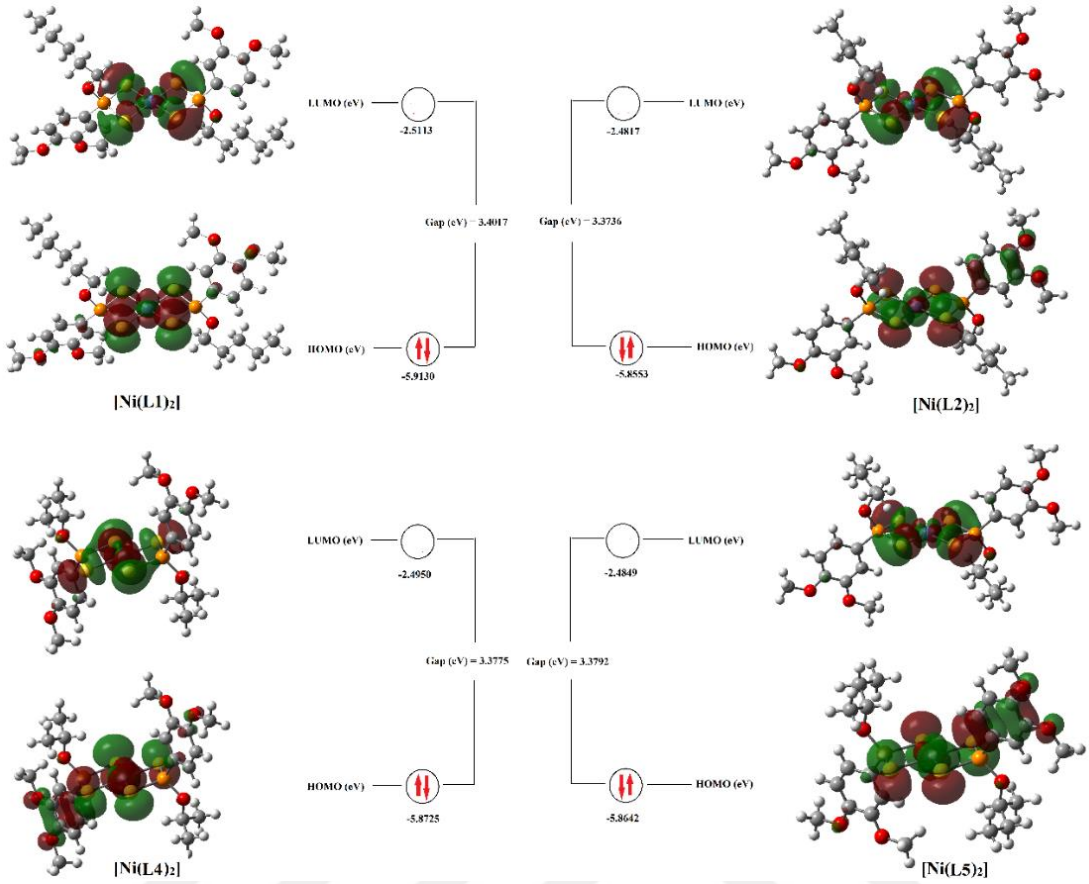


Figure 5.201. The band gap levels and isosurfaces of HOMOs and LUMOs for the complexes $[Ni(S_2P(R^x)(OR1))_2]$, $[Ni(S_2P(R^x)(OR2))_2]$, $[Ni(S_2P(R^x)(OR4))_2]$ and $[Ni(S_2P(R^x)(OR5))_2]$.

5.9. Optimized Molecular Structure of the Part II' $[Ni(S_2P(R^y)(OR2))_2]$ Complex

The optimized 3D structural parameters of the investigated complex $[Ni(S_2P(R^y)(OR2))_2]$ were calculated using B3LYP/LANL2DZ/6-31+G(d,p) level in the ground state. The optimized molecular figure of the complex is given in Figure 5.202. Experimental and theoretical values of selected bond lengths and angles were listed in Table 5.25.

Table 5.25. Selected experimental and calculated [B3LYP/LANL2DZ/6-31+G(d,p) level in the ground state] bond lengths (Å), bond angles (°) and torsion angles for $[Ni(S_2P(R^y)(OR2))_2]$.

Bond lengths (Å)		
	X-ray	Calculated
Ni1—S1	2.222 (2)	2.3506
Ni1—S2	2.241 (2)	2.3490
S1—P1	2.004 (2)	2.1947
S2—P1	2.009 (2)	2.1926
P1—O1	1.582 (2)	1.6231
P1—C1	1.790 (2)	1.8376
O1—C9	1.462 (2)	1.4798
O2—C2	1.359 (2)	1.3843
O2—C7	1.432 (2)	1.4563
O3—C4	1.359 (2)	1.3899
O3—C8	1.435 (2)	1.4576

Bond angles (°)		
	X-ray	Calculated
S1—Ni1—S1^{i}	180.0	180.0
S2^{i}—Ni1—S2	180.0	180.0
S2—Ni1—S1^{i}	92.07 (2)	90.247
S1—Ni1—S2	92.07 (2)	90.247
P1—S1—Ni1	87.93 (2)	85.983
P1—S2—Ni1	87.93 (2)	86.071
S2—P1—S1	101.08 (2)	98.193
O1—P1—S1	113.02 (2)	111.988
O1—P1—S2	113.14 (2)	113.539

Torsion angles (°)		
	X-ray	Calculated
S1—P1—O1—C9	61.6 (1)	60.018
S1—P1—C1—C2	176.1 (1)	-171.223
S1—P1—C1—C6	-7.8 1)	8.758
S2—P1—O1—C9	-52.5 (1)	50.073
S2—P1—C1—C2	-68.4 (1)	-56.791
S2—P1—C1—C6	107.7 (2)	123.190

Torsion angles (°)		
	X-ray	Calculated
P1—O1—C9—C10	122.6 (1)	179.466
P1—C1—C2—O2	-1.3 (2)	0.728
O1—P1—C1—C2	54.8 (1)	-68.518
O1—P1—C1—C6	-129.0 (1)	-111.501
O2—C2—C3—C4	176.1 (2)	179.637
C1—P1—O1—C9	-177.6 (1)	-178.833

As seen from Table 5.25, conformational discrepancies are observed in between the experimental and optimized structures of the investigated complex [Ni($S_2P(R^y)(OR2)$)$_2$]. The Ni—S bond distances in Ni(II) coordination sphere are 2.222(1) / 2.3506 and 2.241(1) / 2.3490 Å (Exp./Cal.) for [Ni($S_2P(R^y)(OR3)$)$_2$]. The S—Ni—S bond angles are range from 92.07(3) / 90.247° to 180.0°/ 180.0° (Exp./Cal.). As expected the optimized bond lengths are a little longer than the experimental values. These results are not surprising because the optimized results are based on the unpacked isolated molecules

while the experimental results are obtained in the solid-state form.

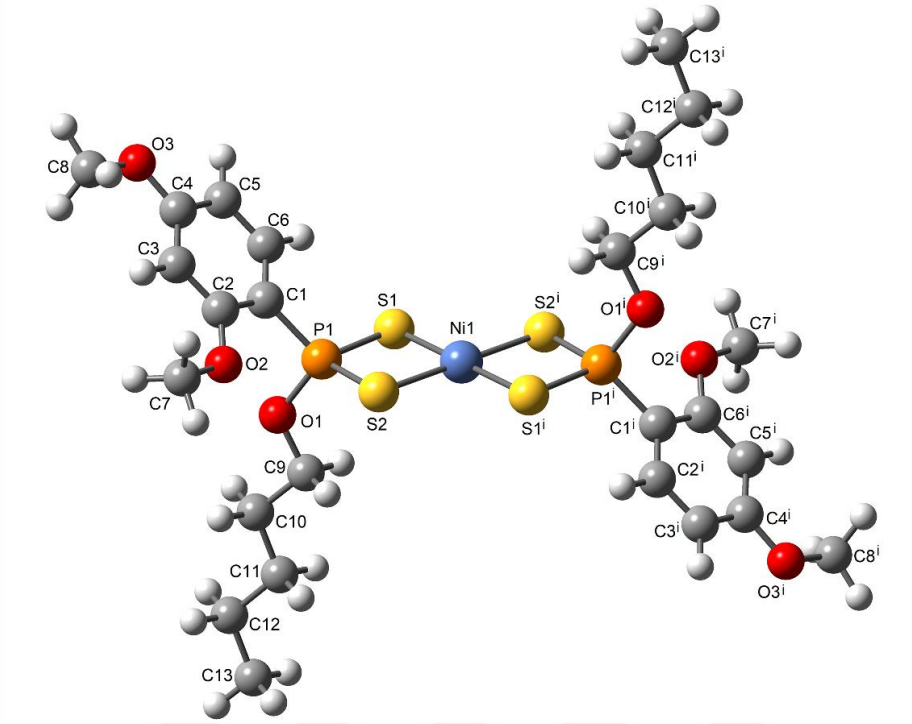


Figure 5.202. The optimized structures of the complex [Ni($S_2P(R^y)(OR2)$)$_2$] by DFT.

5.10. Part II Frontier Orbitals and Chemical Parameters of the Part II' [Ni($S_2P(R^y)(OR2)$)$_2$] Complex

Frontier orbitals (HOMOs and LUMOs) are very important for chemical reactivity and are associated with electron affinity and ionization potential. According to Koopmans theorem [292], chemical parameters such as ionization potential (*IP*), electron affinity (*EA*), chemical hardness (η), absolute electronegativity (χ) and absolute softness (σ) can be calculated if the energy values of the frontier orbitals are determined.

The energy gap, $\Delta E_{Gap} = (E_{LUMO} - E_{HOMO})$, between HOMO and LUMO makes it easy to predict the chemical and electrical properties of molecules. Thus, to determine the chemical parameters of [Ni($S_2P(R^y)(OR2)$)$_2$], the energy gaps between HOMOs and LUMOs were calculated with the B3LYP/LANL2DZ/6-31+G(d,p) level of the DFT in the ground state. The total energies, calculated chemical parameters and energy gaps $\Delta E_{Gap} = (E_{LUMO} - E_{HOMO})$ of [Ni($S_2P(R^y)(OR2)$)$_2$] were given in Table 5.26.

Table 5.26. Calculated total energies, dipole moments and chemical parameters of the compounds $[Ni(S_2P(R^y)(OR2))_2]$.

Parameters	$[Ni(S_2P(R^y)(OR2))_2]$
E_{TOTAL}(Hartee)	-1688.7629
E_{HOMO} (eV)	-5.9226
E_{LUMO} (eV)	0.1442
ΔE_{Gap}(eV)	6.0668
I (eV)	5.9226
A (eV)	-0.1442

Parameters	$[Ni(S_2P(R^y)(OR2))_2]$
η (eV)	3.0334
X (eV)	2.8892
σ (eV)	0.3297
μ_p (eV)	-2.8892
ω	12.6603

E_{TOTAL} : Total energy.
E_{HOMO} and E_{LUMO} : Energy values of HOMO and LUMO.
$\Delta E_{Gap}(eV) = (E_{LUMO} - E_{HOMO})$: Gap of energy.
I : Ionization potential.
A : Electron affinity.

η : Absolute hardness. $(I - A)/_2$.
X : Electronegativity. $(I + A)/_2$.
σ : Softness. $1/\eta$.
μp : Chemical potential. $- (I + A)/_2$
ω : Electrophilicity. $\mu p_2/_2\eta$.

As seen in Table 5.26, the value of ΔE_{Gap} is 6.0668 eV in the gas phase. The energy levels and configurations of HOMO and LUMO are shown in Figure 5.203. HOMO is mainly localized on the $S2^i$ atom of the phosphazene ring, while LUMO is mainly only localized on the phenyl group in $[Ni(S_2P(R^y)(OR2))_2]$ (Figure 5.203). The low energy gap value has a significant effect on the intermolecular charge transfer and bioactivity of the molecule. The low energy gap ΔE_{Gap} value has a significant influence on the intermolecular charge transfer and bioactivity of the molecule.

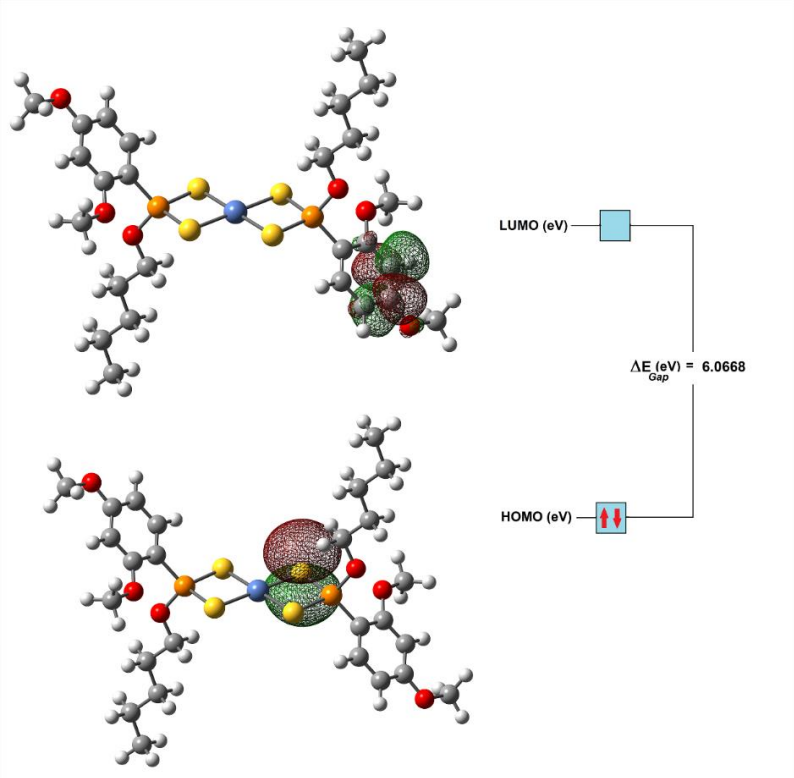


Figure 5.203. HOMO and LUMO electron density isosurfaces and band gap values (eV) of the complex $[Ni(S_2P(R^y)(OR2))_2]$.

5.11. The MEP Surfaces of the Part Ia' Ni(II) Complexes

Electrostatic potential maps (MEPs) are valuable tools to describe the charge-related properties of molecules. They allow us to visualize the size and shape of molecules. The non-covalent interactions predicted by MEPs can allow us to predict the molecule's charge transfer and bioactivity centers. Conventionally, the negative regions are coloured as red while the positive regions are coloured as blue in the MEPs. The negative regions exhibit higher electron density (electrophilic reactivity) whereas the positive regions exhibit low electron density (nucleophilic reactivity) in the MEPs. The MEP surfaces of the complexes were determined and visualized by the Gaussian 09 and Gauss-view visualization programs. MEPs were illustrated in Figure 5.204.

The oxygen atoms O3 (O4 for $[Ni(S_2P(R^x)(OR1))_2]$ and $[Ni(S_2P(R^x)(OR5))_2]$) of 3,4-dimethoxyphenyl groups in the compounds, the MEP diagrams indicated that the maximum electron densities (electrophilic reactivities) are 0.066, 0.067, 0.068, 0.067, 0.067, 0.067 and 0.068 a.u., respectively,(Figure 5.204). The nucleophilic sites are

illustrated in the MEP diagrams Figure 5.204. These regions give preliminary information to predict possible intermolecular interactions.

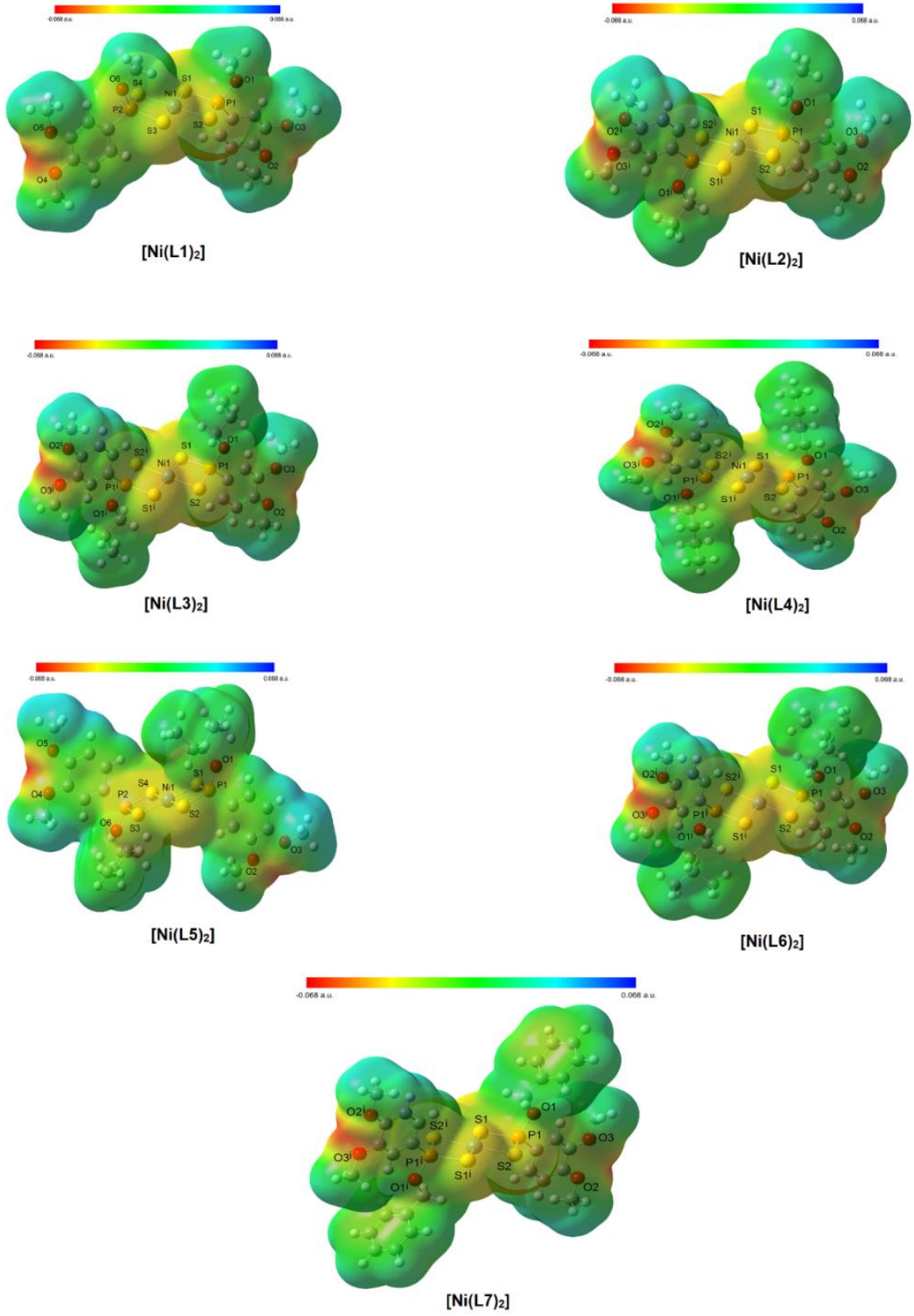


Figure 5.204. Molecular electrostatic potential (MEP) surfaces of the Ni(II) complexes.

5.12. Molecular Electrostatic Potential (MEP) surfaces of Part Ib' Ni(II) Complexes

The intensity of the charges at a particular position due to nuclei and electrons are evaluated using MEP analyses. The MEP analyses provide the value of the electrostatic potential on an electron density surface to get a description of the electrostatic characteristics of the target drug. Thus, the non-covalent interactions can be predicted by MEP analyses. In other words, the MEP graphs can enable us predicted the potential of a molecule for charge transfer and bioactivity. Therefore, the MEP analyses are very useful to get a description of the electrostatic characteristics of the target drug. Coloure 3D shapes of molecules can be drawn by MEP surface analyses. On these pictures, the negative regions are called the nucleophilic sites and represented by a red colour whereas, the positive regions are called electrophilic sites and represented by a blue colour. To predict the nucleophilic and electrophilic reactivity of $[Ni(S_2P(R^x)(OR1))_2]$, $[Ni(S_2P(R^x)(OR2))_2]$, $[Ni(S_2P(R^x)(OR4))_2]$ and $[Ni(S_2P(R^x)(OR5))_2]$, 3D MEP surfaces were designated and viewed by using DFT. The MEP diagram was attributed to Gauss-view visualization program in Figure 5.205.

The maximum electron density (nucleophilic reactivity) values of the region covering O2 and O3 as well as the region covering O4 and O5 were calculated to be 0.067 and 0.068 a.u. for $[Ni(S_2P(R^x)(OR1))_2]$, 0.068 and 0.067 a.u. for $[Ni(S_2P(R^x)(OR2))_2]$, 0.067 to 0.068 a.u. for $[Ni(S_2P(R^x)(OR4))_2]$ and 0.068 to 0.069 a.u. for $[Ni(S_2P(R^x)(OR5))_2]$, respectively. The maximum electron density (nucleophilic reactivity) values of S atoms of the coordination ring (the coordinating region of the Ni atom) covers the range 0.035-0.039 a.u. for $[Ni(S_2P(R^x)(OR1))_2]$, 0.038-0.042 a.u. for $[Ni(S_2P(R^x)(OR2))_2]$, 0.038-0.036 a.u. for $[Ni(S_2P(R^x)(OR4))_2]$ and 0.039-0.037 a.u. for $[Ni(S_2P(R^x)(OR5))_2]$. The regions of electrophilic reactivity are showed in blue in the MEP contour given in Figure 5.205.

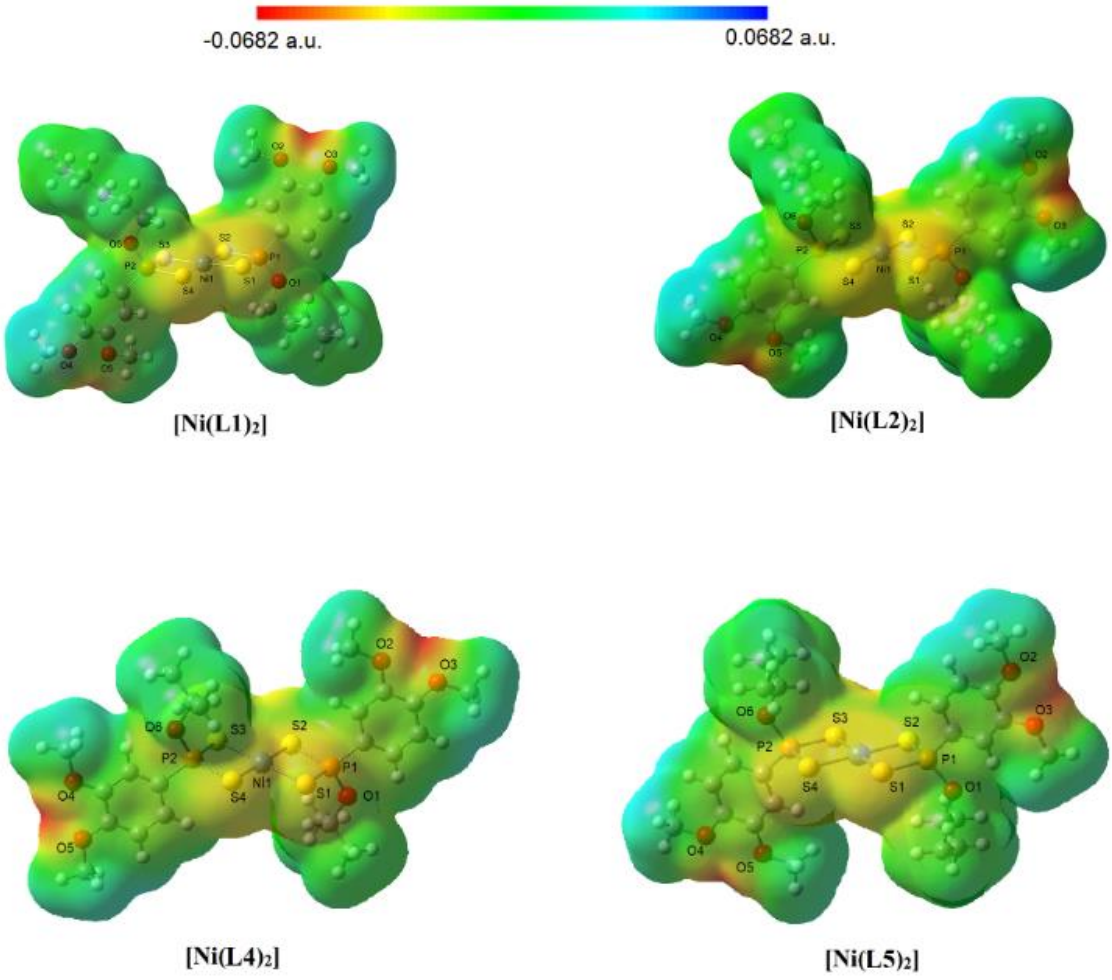


Figure 5.205. $[Ni(S_2P(R^x)(OR1))_2]$, $[Ni(S_2P(R^x)(OR2))_2]$, $[Ni(S_2P(R^x)(OR4))_2]$ and $[Ni(S_2P(R^x)(OR5))_2]$'s MEP surfaces

5.13. Part II The MEP Surfaces of the Part II' $[Ni(S_2P(R^y)(OR2))_2]$ Complex

Electrostatic potential maps (MEPs) are very useful 3D diagrams for visualizing charge distributions of molecules. They are valuable tools for describing the charge-related properties and to visualize the size and shape of molecules. Thus, the non-covalent interactions predicted by MEPs can be a lead to predict the charge transfer and bioactivity centers of the molecule. In MEPs, negative regions colored in red exhibit higher electron density (electrophilic reactivity), while positive regions colored blue exhibit low electron density (nucleophilic reactivity). To determine the electrophilic and nucleophilic reactivity of $[Ni(S_2P(R^y)(OR2))_2]$, MEP surfaces were determined and visualized with

B3LYP/LANL2DZ/6-31+G(d,p) level using Gaussian 09 and Gauss-view visualization programs. The diagram of MEP was illustrated in Figure 5.206. The maximum electron density (electrophilic reactivity) values of O1 ($O1^{i}$), O3 ($O3^{i}$), S1 ($S1^{i}$) and S2 ($S2^{i}$) atoms from the MEP diagram of $[Ni(S_2P(R^y)(OR2))_2]$ were calculated as 0.0519, 0.0355, 0.0425 and 0.0510 a.u. The maximum positive region value is 0.0465 a.u. and the positive region indicating nucleophilic reactivity are shown in the MEP diagrams in Figure 5.206. These regions provide preliminary information to predict intermolecular interactions.

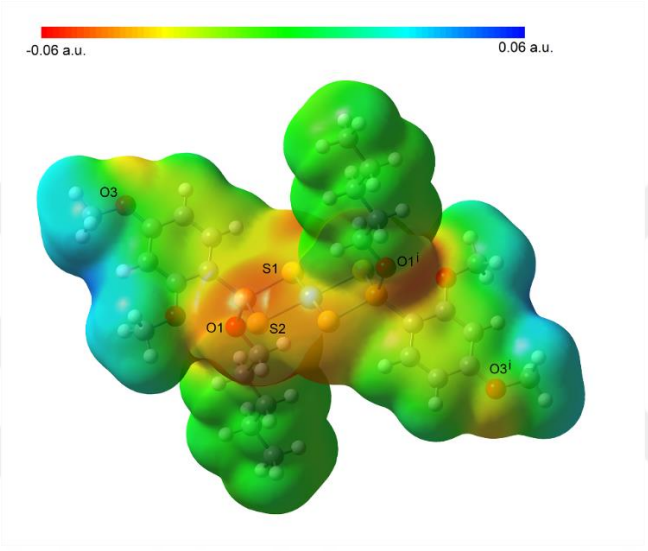


Figure 5.206. Molecular electrostatic potential (MEP) surfaces for the complex $[Ni(S_2P(R^y)(OR2))_2]$.

5.14. Molecular Docking Studies of the Part Ia' Ni(II) Complexes

The MDS can be used to model the interactions between molecules and a target protein at the atomic level. These models serve in drug discovery and development studies and save time, thereby providing low costs. In this study, we first tested the Ni(II) complexes at various concentrations against cancer cell lines including HepG2 and DLD-1. As a second step, we predicted the potential interactions of $[Ni(S_2P(R^x)(ORn))_2]$ (n=1-7) with proteins and compared the results with the corresponding experimental findings. The MDS of the Ni(II) complexes were done with liver cancer protein, PDB ID: 3WZE and colon cancer antigen proteins, ID 2HQ6. Energetically most favorable docked poses were obtained from the rigid molecular docking of each compound with 3WZE and 2HQ6 Figure 5.207A. The 3D illustrations of the non-covalent interactions between $[Ni(S_2P(R^x)(ORn))_2]$ (n=1-7) and the proteins samples 3WZE and 2HQ6 were given in

Figure 5.207B. For the docking interactions of $[Ni(S_2P(R^x)(ORn))_2]$ (n=1-7) with (PDB ID: 3WZE) the relative binding energy values are -6.5, -6.6, -6.5, -5.5, -5.5, -5.6, -5.9 and -8.2 kcal/mol, respectively. The corresponding values for docking studies with (PDB ID: 2HQ6) are -5.8, -5.6, -5,5, -6.7, -7.2, -7.1 and -6.8 kcal/mol.

The complex $[Ni(S_2P(R^x)(OR1))_2]$ binds at the active sites of amino acids, namely ASP1046, ARG1027, PRO1068, ILE1025, ALA881, SER884, ARG1027, LEU889 and ILE888 of the liver cancer protein (PDB ID: 3WZE). The type of interactions are as follows: one the conventional hydrogen bonds, six carbon-involving hydrogen bonds, two (pi-system)-alkyl, one (pi-system)-sigma and one (pi-system)-anion interactions. The conventional hydrogen bond length is 2.994 Å (between an OD2 oxygen on ASP1046 and S2 atom of dithiophosphonate-complex). On the other hand, six particular amino acids ASN103, GLN64, SER73, GLN112, ALA102 and HIS127 of colon cancer antigen proteins (PDB ID: 2HQ6) have been estimated to interact with $[Ni(S_2P(R^x)(OR1))_2]$. The non-covalent interactions are as follows: three conventional hydrogen bonds; two carbon-involving hydrogen bonds; one (pi-system)-donor-metal acceptor bond and one (pi-system)-donor-sulfur bond. The conventional hydrogen bond lengths are 3.157 Å (between NE2 nitrogen on GLN64 and O6 atom of OCH3 group of dithiophosphonate-complex), 3.781 Å (between an O atom on ASN103 and S2 atom of dithiophosphonate-complex) and 3.384 Å (between an O atom on ASN103 and S3 atom of dithiophosphonate-complex).

The complex $[Ni(S_2P(R^x)(OR2))_2]$ appears to be bound to the active sites of the amino acids HIS1026, LEU889, LEU1019, CYS1045, ASP1046, GLU885, ASP1046, ARG1027 in the liver cancer protein (PDB ID: 3WZE) by two conventional hydrogen bonds; two (pi-system)-alkyl interactions; one alkyl-alkyl van der Waals bonds; three carbon-involving hydrogen bonds; one (pi-system)-anion interaction and two (pi-system)-cation interactions. The conventional hydrogen bond lengths are 3.100 Å between HIS1026:O and S1 atom of dithiophosphonato-complex; 3.527 Å between HIS1026:O and S2i atom of dithiophosphonate-complex. The complex binds at the active site of ARG56, ASN103, HIS127, LEU123, ILE62, PHE114, PHE61, LYS126, HIS55 and THR71 of the colon cancer antigen proteins (PDB ID: 2HQ6) by three conventional hydrogen bonds; one unfavorable metal-donor interaction; one T-shaped (pi-system)-(pi-system) interaction; six (pi-system)-alkyl interactions; two inter alkyl interactions, one

(pi-system)-sulfur bond and two carbon-involving hydrogen bond interactions. For the docking of colon cancer antigen proteins (PDB ID: 2HQ6) with $[Ni(S_2P(R^x)(OR2))_2]$, the conventional hydrogen bond lengths are 3.482 Å between ARG56:NH1 and the atom S1 on the dithiophosphonato-complex; 3.686 Å between ARG56:NH1 and the atom S2i on the dithiophosphonate-complex and 3.205 Å between an O atom on ASN103 and the S1 atom of the dithiophosphonato-complex.

The molecular docking results indicate that fourteen amino acids, namely, HIS1026, LEU1049, ILE1053, TYR1082, ARG1027, LEU889, ILE888, TYR1059, ASP1028, ASP1046, GLU815, ARG1027, CYS1024 and ILE888 of the liver cancer protein (PDB ID: 3WZE) are found to interact with $[Ni(S_2P(R^x)(OR3))_2]$ complex. The predicted fourteen non-covalent interactions are of the types: one conventional hydrogen bond, three (pi-system)-alkyl interactions, three alkyl-alkyl van der Waals bonds, four carbon-involving hydrogen bonds and three more interactions between (pi-system)-central cation, (pi-system)-sulfur and (pi-system)-sigma bond. The conventional hydrogen bond length is 3.018 Å between HIS1026:O and the atom S2 of the dithiophosphonate-complex. On the other hand, eight particular amino acids ARG56, HIS127, LEU123, ILE62, PHE114, HIS55, GLY72 and SER73 of colon cancer antigen proteins (PDB ID: 2HQ6) have been estimated to interact with $[Ni(S_2P(R^x)(OR3))_2]$. The eleven non-covalent interactions are as follows: three conventional hydrogen bonds; two (pi-system)-alkyl and two alkyl-alkyl interactions; two carbon-involving hydrogen bonds and three more interactions between (pi system)-sulfur, (pi-system)-sigma bond and one T-shaped (pi-system)-(pi-system) interactions. The conventional hydrogen bond lengths are 3.507 Å (between the NH1 nitrogen atom on ARG56 and one of the S atoms on dithiophosphonato-complex); 3.681 Å (between the NH1 nitrogen atom of ARG56 and another S atom on dithiophosphonato-complex) and 3.303 Å (between an O atom on ASN103 and S atom of dithiophosphonato-complex.

The complex $[Ni(S_2P(R^x)(OR4))_2]$ binds at the active sites of HIS1026, PRO1068, LEU889, TYR1059, LEU1049, ILE1053, TYR1059, ASP1028, ASP1046, ILE888, ARG1027 and CYS1024 of the liver cancer protein (PDB ID: 3WZE). The type of interactions are as follows: one conventional hydrogen bond; two alkyl-alkyl and two (pi-system)-alkyl interactions, three carbon-involving hydrogen bonds and three more interactions between (pi-system)-sigma bond, (pi-system)-cation and (pi-system)-sulfur.

The conventional hydrogen bond length is 3.506 Å (between an O atom on HIS1026 and the S1 atom of dithiophosphonato-complex). The molecular docking results between $[Ni(L4)_2]$ and the colon cancer antigen proteins (PDB ID: 2HQ6) show that the complex binds to active sites on ASN103, HIS127, ILE62, LEU123, HIS127, PHE114, LYS126 and ARG56 of 2HQ6. The non-covalent interactions are as follows: two conventional hydrogen bonds; four (pi-system)-alkyl and two alkyl-alkyl interactions and two more interactions between (pi-system)-sulfur, (pi-system)-cation. The conventional hydrogen bond lengths are 3.163 Å (between an O atom on ASN103 and S1 atom of dithiophosphonate-complex) and 3.551 Å (between NE2 nitrogen on HIS127 and S1 atom of dithiophosphonato-complex).

The docking studies between $[Ni(S_2P(R^x)(OR5))_2]$ and 3WZE indicate that the amino acids HIS1026, ASP1046, ARG1027, LEU889, TYR1082, ILE1053, LEU1049, CYS1024, TYR1059 and GLU815 interact with the complex. The non-covalent interactions between the complex and the liver cancer protein (PDB ID: 3WZE) are as follow: two conventional hydrogen bonds; four (pi-system)-alkyl interactions, two alkyl-alkyl interactions, one (pi-system)-sulfur and one (pi-system)-cation interaction and two carbon involving-hydrogen bond interactions. There are the conventional hydrogen bonds are of the lengths, 3.232 Å (between an O atom on HIS1026 and an S atom on dithiophosphonato-complex) and 3.524 Å (between OD2 oxygen on ASP1046 and S atoms of dithiophosphonato-complex). Docking studies also show that six different amino acids ARG56, ASN103, LYS126, ALA102, LEU123, ALA104 and GLY105 of colon cancer antigen proteins (PDB ID: 2HQ6) interact with the $[Ni(S_2P(R^x)(OR5))_2]$. The non-covalent interactions are: three conventional hydrogen bonds, two (pi-system)-alkyl and three alkyl-alkyl interactions along with one amide-pi stacked interaction and one carbon-involving hydrogen bonds. The conventional hydrogen bond lengths are 3.276 Å (between NH1 nitrogen on ARG56 and S1 atom of dithiophosphonato-complex), 3.441 Å (between an O atom on ASN103 and S2i of dithiophosphonato-complex) and 3.355 Å (between an O atom on ASN103 and S1 atom of dithiophosphonato-complex).

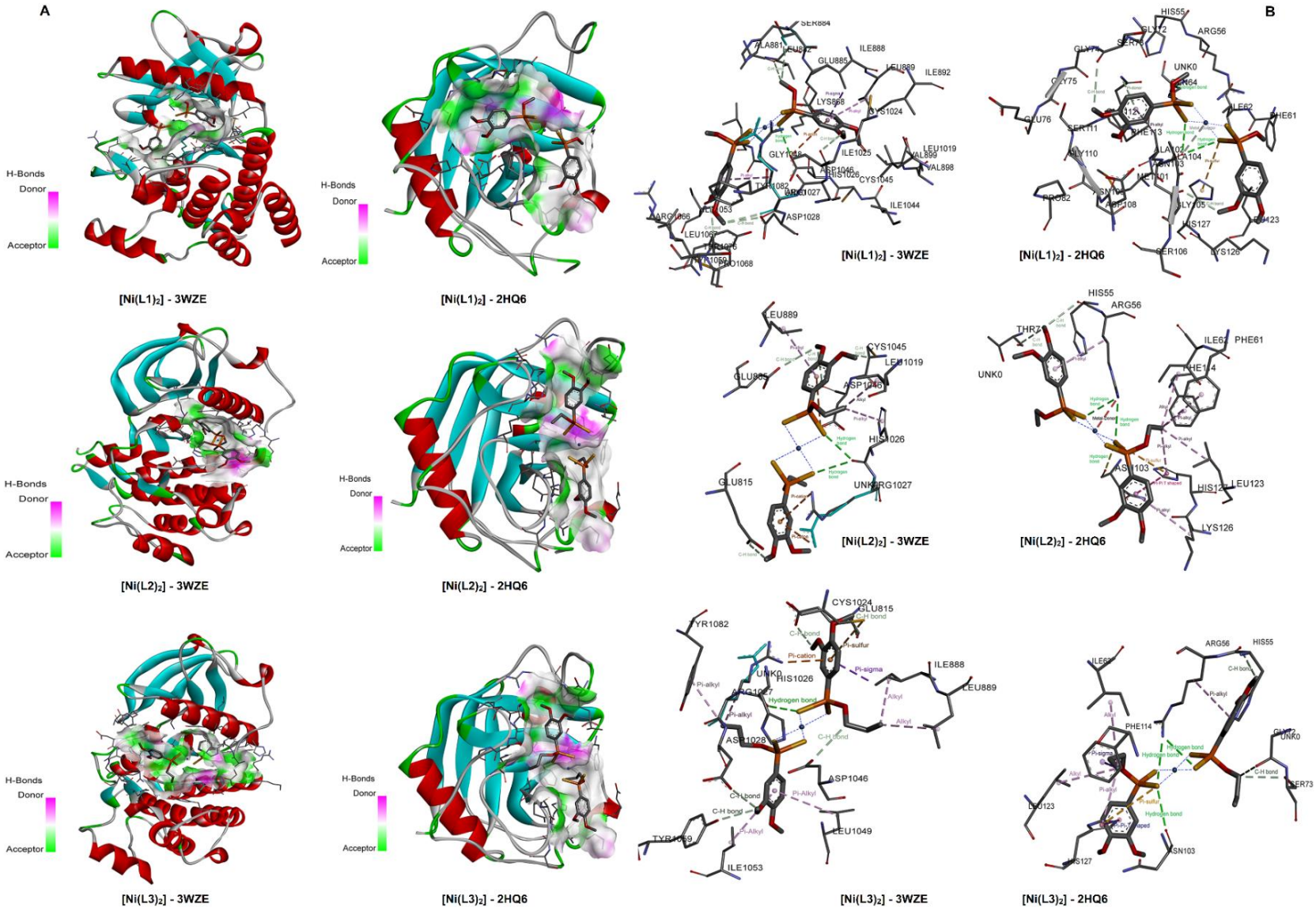
The complex $[Ni(S_2P(R^x)(OR6))_2]$ binds at the active site of HIS1026, ASP1028, TYR1059, GLU815, PRO1068, LEU1067, ILE1053, LEU1049, LEU1019, ILE892, ILE888 and ARG1027 of the liver cancer protein (PDB ID: 3WZE) with one conventional hydrogen bond, one alkyl, eight (pi-system)-alkyl, three carbon involving-hydrogen

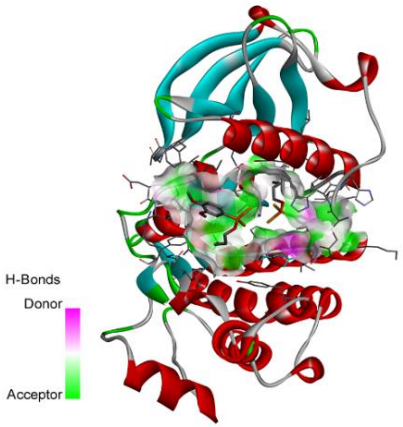
bond, one for (pi-system)-sigma and one (pi-system)-cation interactions. The conventional hydrogen bond length is 3.053 Å (between an O atom on HIS1026 and S1 atom of dithiophosphonato-complex). The molecular docking results between $[Ni(S_2P(R^x)(OR6))_2]$ with the colon cancer antigen proteins (PDB ID: 2HQ6) predicts that the complex $[Ni(S_2P(R^x)(OR6))_2]$ binds at the active site of HIS1026, ASP1028, TYR1059, GLU815, PRO1068, LEU1067, ILE1053, LEU1049, LEU1019, ILE892, ILE888, ARG1027 of 2HQ6. The non-covalent interactions are: one conventional hydrogen bond; eight (pi-system)-alkyl, three carbon involving-hydrogen bond, one (pi-system)-sigma and (pi-system)-cation interactions. The conventional hydrogen bond length is 3.053 Å between HIS1026:O and S1 atom of dithiophosphonato-complex.

The molecular docking results indicate that nine amino acids, namely, HIS1026, ARG1027, LEU889, ILE888, ARG1027, ASP1046, CYS1024, ASP1046 and CYS1045 of the liver cancer protein (PDB ID: 3WZE) are found to interact with $[Ni(S_2P(R^x)(OR7))_2]$ complex. The predicted non-covalent interactions are of the types: two conventional hydrogen bonds; two carbon involving-hydrogen bonds, two (pi-system)-alkyl, one (pi-system)-sigma, one (pi-system)-anion and two (pi-system)-cation interactions. The conventional hydrogen bond lengths are 3.042 Å (between an O atom on HIS1026 and S1 atom of dithiophosphonato-complex) and 3.091 Å (between an O atom on HIS1026 and S2i atom of dithiophosphonato-complex). Finally, docking studies also show that nine different amino acids ARG56, LYS126, ASN103, SER73, LYS126, ALA102, GLN112, ASN103 and GLY72 of colon cancer antigen proteins (PDB ID: 2HQ6) interact with the $[Ni(S_2P(R^x)(OR7))_2]$. The non-covalent interactions are: four conventional hydrogen bonds, two carbon involving-hydrogen bonds, two (pi-system)-alkyl, one (pi-system)-donor hydrogen and one metal acceptor interactions. The conventional hydrogen bond lengths are 3.591 Å between ARG56:NH1 and S1, 3.119 Å between LYS126:NZ and O3i atom of 3,4-dimethoxyphenyl, 3.718 Å between ASN103 and S2i atom of dithiophosphonato-complex and 3.098 Å between GLY72:CA and O3 atom of 3,4-dimethoxyphenyl in the complex.

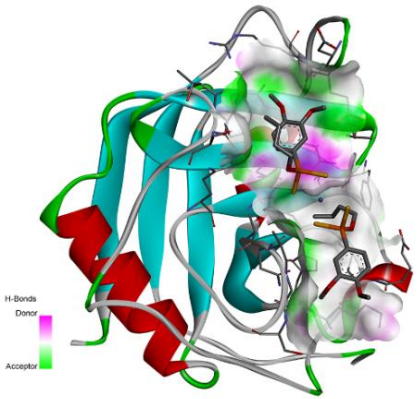
The lowering of the HOMO-LUMO energy gap value has a substantial influence on the intermolecular charge transfer. The low HOMO–LUMO energy gap always refers to lower kinetic stability and higher chemical reactivity. As for the DFT results, the energy gap ΔE_{Gap}(eV) of the complex $[Ni(S_2P(R^x)(OR7))_2]$ is lower than the other Ni complexes

used in this study (Table 5.23**)**. The energy gap, ΔE_{Gap}(eV) of the complex $[Ni(S_2P(R^x)(OR7))_2]$ is especially noteworthy to predict potential non-covalent interactions with colon cancer antigen proteins (PDB ID: 2HQ6). Consequently, according to all of the molecular docking results we can say that the bioactivity of the investigated complexes with 2HQ6 (colon cancer antigen proteins) is higher than that between the investigated Ni complexes and 3WZE (the liver cancer protein).

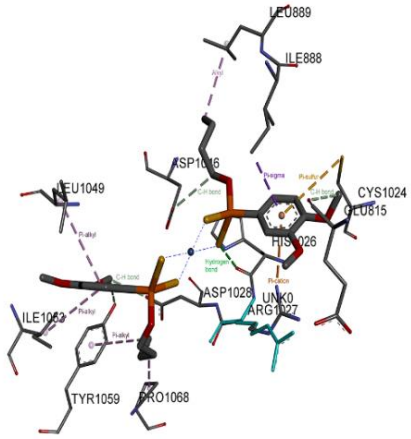

A
B
H-Bonds
Donor
Acceptor
[Ni(L1)2] - 3WZE
[Ni(L1)2] - 2HQ6
[Ni(L1)2] - 3WZE
[Ni(L1)2] - 2HQ6
[Ni(L2)2] - 3WZE
[Ni(L2)2] - 2HQ6
[Ni(L2)2] - 3WZE
[Ni(L2)2] - 2HQ6
[Ni(L3)2] - 3WZE
[Ni(L3)2] - 2HQ6
[Ni(L3)2] - 3WZE
[Ni(L3)2] - 2HQ6



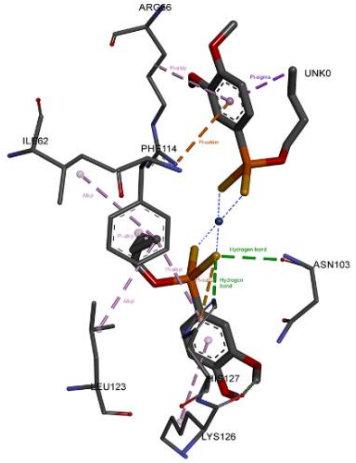
$[Ni(L4)_2]$ - 3WZE



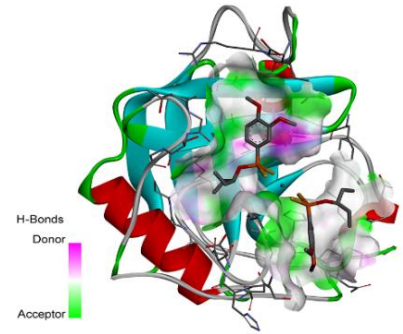
$[Ni(L4)_2]$ - 2HQ6



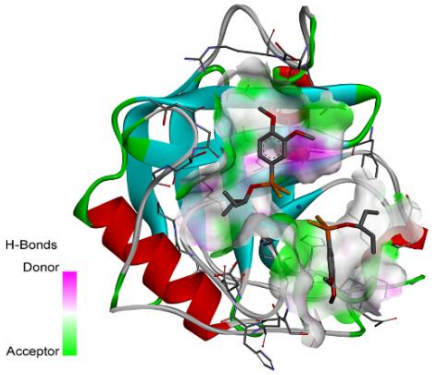
$[Ni(L4)_2]$ - 3WZE



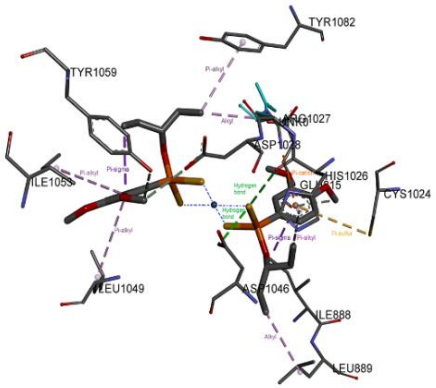
$[Ni(L4)_2]$ - 2HQ6



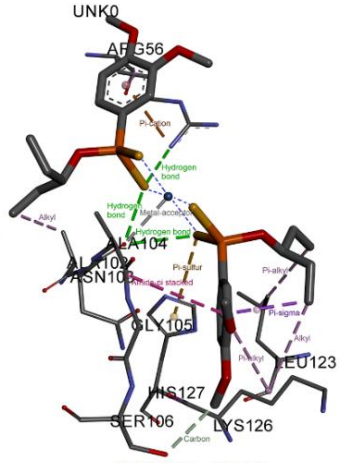
$[Ni(L5)_2]$ - 3WZE



$[Ni(L5)_2]$ - 2HQ6



$[Ni(L5)_2]$ - 3WZE



$[Ni(L5)_2]$ - 2HQ6

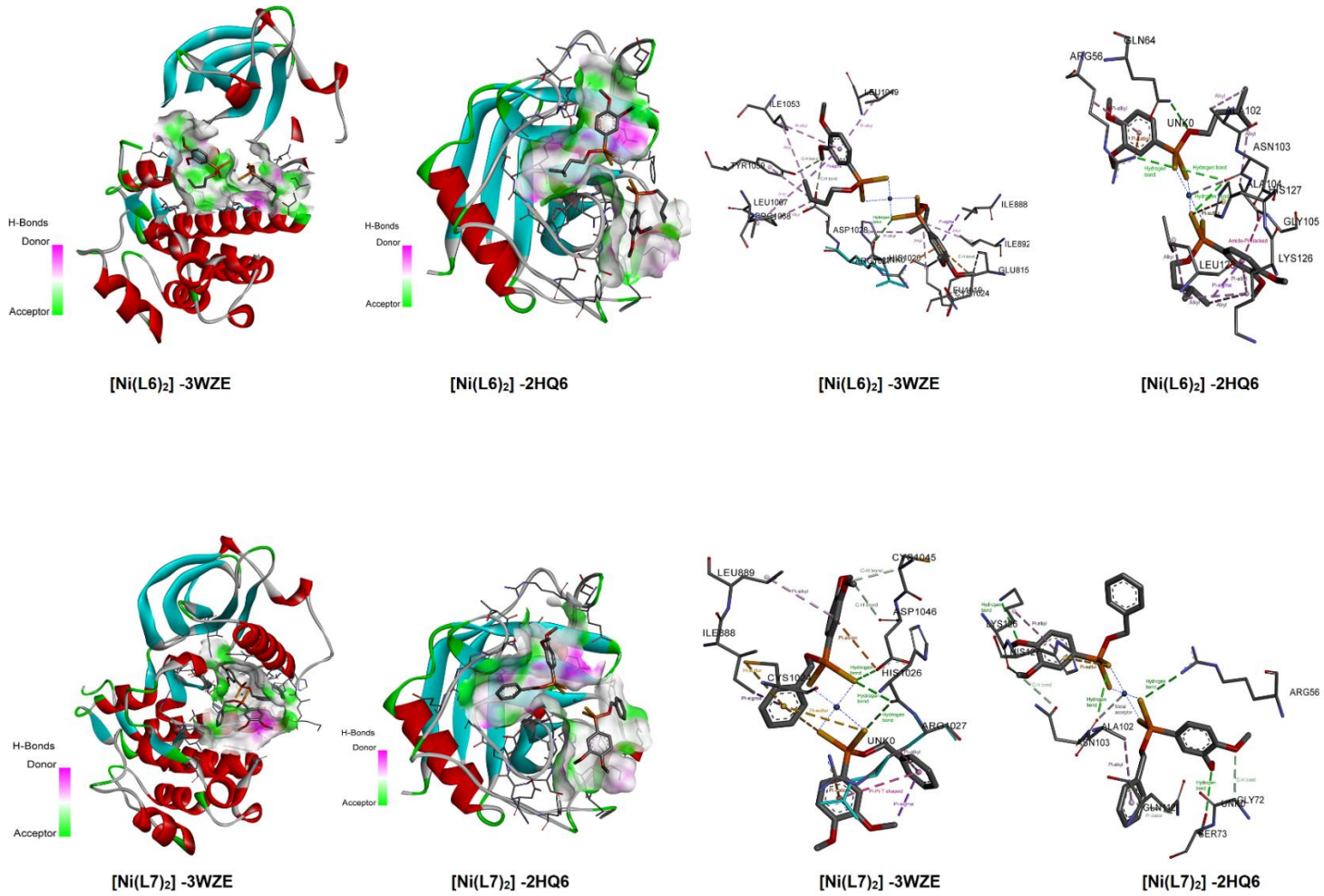


Figure 5.207. Energetically most favorable docked poses obtained from the rigid molecular docking of each complex with 3WZE and 2HQ6 (**A**) and the non-covalent interactions of the Ni(II) complexes (**B**).

5.15. Part Ib. Molecular Docking Studies of $[Ni(S_2P(R^x)(OR1))_2]$, $[Ni(S_2P(R^x)(OR2))_2]$, $[Ni(S_2P(R^x)(OR4))_2]$ and $[Ni(S_2P(R^x)(OR5))_2]$ with Colon Cancer Antigen and Liver Cancer Proteins

Molecular docking (MD) studies contribute to efforts aimed at minimizing high cost and time losses in drug development process by the way of predicting possible interactions between the intended drug molecule and the target protein. The MD studies of $[Ni(S_2P(R^x)(OR1))_2]$, $[Ni(S_2P(R^x)(OR2))_2]$, $[Ni(S_2P(R^x)(OR4))_2]$ and $[Ni(S_2P(R^x)(OR5))_2]$ were performed with colon cancer antigen proteins, ID 2HQ6 and liver cancer protein, PDB ID: 3WZE by AutoDock-Vina software [292] The bonding energies and refining results (RMSD values) for binding sites of the complexes are given in Table 5.27. The docking poses for $[Ni(S_2P(R^x)(OR1))_2]$, $[Ni(S_2P(R^x)(OR2))_2]$, $[Ni(S_2P(R^x)(OR4))_2]$ and $[Ni(S_2P(R^x)(OR5))_2]$ with 2HQ6 and 3WZE were shown in Figure 5.208A. Based on MD studies, the interactions of $[Ni(S_2P(R^x)(OR1))_2]$, $[Ni(S_2P(R^x)(OR2))_2]$, $[Ni(S_2P(R^x)(OR4))_2]$ and $[Ni(S_2P(R^x)(OR5))_2]$ with 2HQ6 and 3WZE were picturized in Figure 5.208 B. The relative affinity energy values for the docking of $[Ni(S_2P(R^x)(OR1))_2]$, $[Ni(S_2P(R^x)(OR2))_2]$, $[Ni(S_2P(R^x)(OR4))_2]$ and $[Ni(S_2P(R^x)(OR5))_2]$ on 2HQ6 are -6.2, -7.1, -6.1, -5.7 kcal/mol, respectively. Corresponding values on 3WZE are 6.2, -7.3, -7.6 and -7.1 kcal/mol, respectively.

Table 5.27. The RMSD values and bonding energies as outcome of MD for $[Ni(S_2P(R^x)(OR1))_2]$, $[Ni(S_2P(R^x)(OR2))_2]$, $[Ni(S_2P(R^x)(OR4))_2]$ and $[Ni(S_2P(R^x)(OR5))_2]$ by using AutoDock-Vina software.

$[Ni(S_2P(R^x)(OR1))_2]$-3WZE

Mode	Affinity (kcal/mol)	Distance from the best mode	
		RMSD l.b.	RMSD u.b.
1	-6.2	0.000	0.000
2	-6.1	2.096	2.831
3	-5.8	0.915	11.349
4	-5.1	1.758	2.207
5	-4.8	1.573	2.112
6	-4.7	2.326	3.239
7	-4.6	4.148	9.283
8	-4.5	4.402	9.116
9	-4.5	4.976	8.604

$[Ni(S_2P(R^x)(OR1))_2]$-2HQ6

Mode	Affinity (kcal/mol)	Distance from the best mode	
		RMSD l.b.	RMSD u.b.
1	-6.2	0.000	0.000
2	-6.0	1.102	11.385
3	-5.6	5.326	8.476
4	-5.5	1.480	2.292
5	-5.4	2.279	11.802
6	-5.3	1.895	11.770
7	-5.1	4.924	11.011
8	-5.0	4.262	9.556
9	-4.9	5.001	9.010

$[Ni(S_2P(R^x)(OR2))_2]$-3WZE

Mode	Affinity (kcal/mol)	Distance from the best mode	
		RMSD l.b.	RMSD u.b.
1	-7.3	0.000	0.000
2	-6.9	0.998	11.713
3	-6.9	2.854	7.059
4	-6.4	2.967	7.433
5	-6.4	3.308	7.824
6	-5.6	2.942	7.048
7	-5.3	16.448	20.740
8	-5.3	17.219	22.705
9	-5.2	16.741	20.642

$[Ni(S_2P(R^x)(OR2))_2]$-2HQ6

Mode	Affinity (kcal/mol)	Distance from the best mode	
		RMSD l.b.	RMSD u.b.
1	-7.1	0.000	0.000
2	-7.0	1.042	11.763
3	-6.9	3.161	9.257
4	-6.7	2.922	7.805
5	-6.7	3.905	8.481
6	-6.6	2.899	7.591
7	-6.6	3.628	8.959
8	-6.4	1.973	2.424
9	-6.3	2.962	9.393

$[Ni(S_2P(R^X)(OR4))_2]$-3WZE

Mode	Affinity (kcal/mol)	Distance from the best mode	
		RMSD l.b.	RMSD u.b.
1	-7.6	0.000	0.000
2	-7.5	2.718	8.756
3	-7.5	0.411	10.471
4	-7.3	2.785	6.840
5	-7.2	2.315	9.167
6	-7.0	2.372	6.034
7	-6.9	3.825	7.798
8	-6.9	1.312	10.531
9	-6.6	1.689	2.359

$[Ni(S_2P(R^X)(OR4))_2]$-2HQ6

Mode	Affinity (kcal/mol)	Distance from the best mode	
		RMSD l.b.	RMSD u.b.
1	-6.1	0.000	0.000
2	-6.0	0.152	10.281
3	-5.5	1.503	10.387
4	-4.7	3.821	8.653
5	-4.6	3.936	8.575
6	-4.5	3.026	10.263
7	-4.4	22.196	25.531
8	-4.3	22.484	25.330
9	-4.3	2.648	3.271

$[Ni(S_2P(R^X)(OR5))_2]$-3WZE

Mode	Affinity (kcal/mol)	Distance from the best mode	
		RMSD l.b.	RMSD u.b.
1	-7.1	0.000	0.000
2	-6.7	3.043	9.320
3	-6.7	3.220	9.321
4	-6.5	3.410	8.947
5	-6.0	3.905	9.169
6	-5.4	16.462	20.704
7	-5.3	16.819	22.264
8	-5.3	17.024	21.236
9	-5.3	17.685	21.940

$[Ni(S_2P(R^X)(OR5))_2]$-2HQ6

Mode	Affinity (kcal/mol)	Distance from the best mode	
		RMSD l.b.	RMSD u.b.
1	-5.7	0.000	0.000
2	-5.7	2.439	11.559
3	-5.7	0.742	11.532
4	-5.5	2.057	2.460
5	-5.5	1.593	2.286
6	-5.4	1.711	11.559
7	-5.2	1.367	11.811
8	-5.2	1.921	2.599
9	-4.9	5.482	8.638

MD studies indicate that eight different amino acids ASN103, ARG56, ALA102, HIS127, LYS126, ILE62, LEU123 and ASP152 of colon cancer antigen proteins (PDB ID: 2HQ6) interact with the $[Ni(S_2P(R^x)(OR1))_2]$ complex. For docking of $[Ni(S_2P(R^x)(OR1))_2]$ on 2HQ6, there are ten different kinds of non-covalent interactions, namely, three conventional hydrogen bonds, three alkyl-alkyl interactions, three (pi-system)-alkyl interactions and one carbon-involving hydrogen bond. The conventional hydrogen bond lengths are 3.532 Å (between S2 atom of $[Ni(S_2P(R^x)(OR1))_2]$ and O oxygen atom on ASN103), 3.351 Å (between S3 atom of $[Ni(S_2P(R^x)(OR1))_2]$ and O oxygen atom on ASN103) and 3.574 Å (between NH1 nitrogen on ARG56 and S2 atom of $[Ni(S_2P(R^x)(OR1))_2]$).

The MD results also indicate that eleven amino acids, namely, ASP1046, HIS1026, LEU889, ILE892, PRO1068, ILE888, ILE1053, CYS1024, ARG1027, TYR1059 and ASP1028 of the liver cancer protein (PDB ID: 3WZE) are found to interact with $[Ni(S_2P(R^x)(OR1))_2]$ complex. The predicted non-covalent interactions are of the following types: three conventional hydrogen bonds, three alkyl-alkyl interactions, two (pi-system)-alkyl interactions, one (pi-system)-sulfur, one (pi-system)-cation and two carbon-involving hydrogen bonds. The conventional hydrogen bond lengths are 3.635 Å (between the S2 atom of $[Ni(S_2P(R^x)(OR2))_2]$ and O oxygen atom on ASP1046); 3.559 Å (between the S3 atom of $[Ni(S_2P(R^x)(OR2))_2]$ and O oxygen atom on ASP1046) and 3.082 Å (between the S2 atom of $[Ni(S_2P(R^x)(OR2))_2]$ and O oxygen on HIS1026).

As to the $[Ni(S_2P(R^x)(OR2))_2]$ complex, it binds at the active sites of eleven amino acids, namely ARG56, GLN64, ASP152, HIS55, ALA104, ALA102, ILE62, LEU123, PHE61, HIS127 and PHE114 of colon cancer antigen proteins (PDB ID: 2HQ6). The type of interactions of the $[Ni(S_2P(R^x)(OR2))_2]$ complex are as follows: three conventional hydrogen bonds, two carbon hydrogen bonds, five alkyl-alkyl interaction, three (pi-system)-alkyl attractions, one (pi-system)-sigma interaction, one (pi-system)-sulfur and one (pi-system)-(pi-system) T-shaped bond interaction. The conventional hydrogen bond lengths are 3.748 Å (between an NH1 nitrogen on A:ARG56 and sulfur S1 atom of $[Ni(S_2P(R^x)(OR2))_2]$), 3.558 Å (between an NE2 nitrogen on A:GLN64 and sulfur S1 atom of $[Ni(S_2P(R^x)(OR2))_2]$), and 3.210 Å (between an NH1 nitrogen on A:ARG56 and sulfur S4 atom of $[Ni(S_2P(R^x)(OR2))_2]$).

The complex $[Ni(S_2P(R^x)(OR3))_2]$ appears to be bound to the active moieties of the amino

acids HIS1026, ASP1046, ASP1028, TYR1059, ARG1027, ILE1053, LEU1049, ILE888 and CYS1024 of the liver cancer protein (PDB ID: 3WZE). The non-covalent interactions are as follows: three conventional hydrogen bonds, two carbon-involving hydrogen bond, one alkyl- alkyl interaction, two (pi-system)-alkyl attractions, two (pi-system)-sigma bonds, one (pi-system)-sulfur and one (pi-system)-cation interaction. The conventional hydrogen bond lengths are 3.169 Å (between an oxygen on A:HIS1026 and sulfur S3 atom of $[Ni(S_2P(R^x)(OR3))_2]$), 3.447 Å (between an OD2 oxygen on A:ASP1046 and sulfur S2 atom of $[Ni(S_2P(R^x)(OR3))_2]$), and 3.694 Å (between an OD' nitrogen on oxygen on A:ASP1046 and sulfur S2 atom of $[Ni(S_2P(R^x)(OR3))_2]$).

Molecular docking studies showed that seven different amino acids on colon cancer antigen proteins, (PDB ID: 2HQ6), namely the ALA104, ALA102, LEU123, ARG56, PHE61, LYS126, HIS127 interact with the $[Ni(S_2P(R^x)(OR4))_2]$ complex. The nine non-covalent interactions involved are: three alkyl-alkyl, four (pi-system)-alkyl, one pi-system-cation and one pi-pi-system-T-shaped bond interactions. Here, there is no conventional hydrogen bond.

The same complex, $[Ni(S_2P(R^x)(OR4))_2]$, appears to be bound to the active moieties of the amino acids LEU889, ILE888, ARG1027, ARG1066, TYR1082, HIS816 and CYS1024 on the liver cancer protein (PDB ID: 3WZE). The non-covalent interactions involved are: six alkyl-alkyl, two (pi-system)-alkyl, two (pi-system)-sigma, one (pi-system)-sulfur and one (pi-system)-cation interactions. There is no conventional hydrogen bond, here.

Twelve different amino acids on colon cancer antigen proteins (PDB ID: 2HQ6), namely, GLN64, ASP152, HIS55, ALA104, ILE62, ARG56, LYS126, HIS127, LEU123, PHE61, PHE6 and HIS127 interact with the $[Ni(S_2P(R^x)(OR5))_2]$ complex. The non-covalent interactions involved are: one conventional hydrogen bond, three alkyl-alkyl, seven (pi-system)-alkyl, one (pi-system)-sulfur and one pi-pi-system-T-shaped interactions along with two carbon-involving hydrogen bonds. The conventional hydrogen bond length is 3.647 Å (between S2 atom of $[Ni(S_2P(R^x)(OR5))_2]$ and N(E2) atom on GLN64).

The eleven amino acids on the liver cancer protein (PDB ID: 3WZE), namely, TYR1059, ASP1028, ASP1046, GLU815, ILE888, CYS1024, ARG1027, HIS1026, TYR1082, ILE1053 and LEU1049 are found to interact with $[Ni(S_2P(R^x)(OR5))_2]$. The predicted non-covalent interactions are as follows: one alkyl-alkyl, four (pi-system)-alkyl, one (pi-

system)-sulfur, one (pi-system)-cation, one (pi-system)-sigma interactions and four carbon-involving hydrogen bonds.

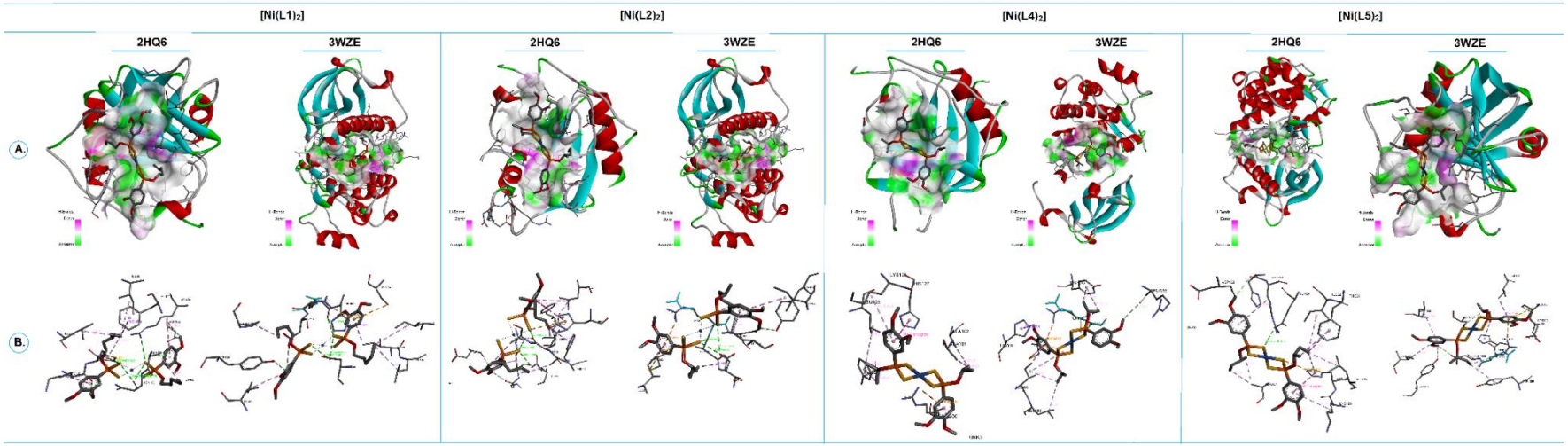


Figure 208 A. The docked poses obtained from the rigid molecular docking $[Ni(S_2P(R^x)(OR1))_2]$, $[Ni(S_2P(R^x)(OR2))_2]$, $[Ni(S_2P(R^x)(OR4))_2]$ and $[Ni(S_2P(R^x)(OR5))_2]$ with 2HQ6 and 3WZE. **B.** non-covalent interactions with 2HQ6 and 3WZE.

5.16. Molecular Docking Studies of the Part II' [Ni($S_2P(R^y)(OR2))_2$] Complex

Molecular docking studies can be used to model interactions between molecules and a target protein at the atomic level. These models serve in drug discovery and development studies and save time, thereby providing low costs. The molecular docking studies of [Ni($S_2P(R^y)(OR2))_2$] were done with liver cancer protein, PDB ID: 3WZE and colon cancer antigen proteins, ID 2HQ6. The bonding energies and RMSD values for each molecular docking study of the investigated compounds are listed comparatively in Table 5.28. Energetically most favorable docked poses obtained from the rigid molecular docking of each compound with 3WZE and 2HQ6 were illustrated in Figure 5.209.

The non-covalent interactions of [Ni($S_2P(R^y)(OR2))_2$] with 3WZE and 2HQ6 using the molecular docking study were revealed and illustrated as 3D in Figure 5.210. The relative binding energy values are -7.3 and -6.0 kcal/mol docked with investigated Ni(II) complex and liver cancer protein (PDB ID: 3WZE) and colon cancer antigen proteins (PDB ID: 2HQ6), respectively.

Table. 5.28. The predicted bonding energies and RMSD values as a consequence of molecular docking for [Ni($S_2P(R^y)(OR2))_2$] by using AutoDock-Vina software.

[Ni($S_2P(R^y)(OR2))_2$]-3WZE

Mode	Affinity (kcal/mol)	Distance from the best mode	
		RMSD l.b.	RMSD u.b.
1	-7.3	0.000	0.000
2	-7.1	1.330	11.481
3	-7.1	1.239	2.137
4	-6.9	2.425	9.777
5	-6.9	2.853	7.008
6	-6.7	2.798	7.222
7	-6.7	3.220	7.605
8	-6.4	2.987	9.285
9	-6.4	3.198	9.127

[Ni($S_2P(R^y)(OR2))_2$]-2HQ6

Mode	Affinity (kcal/mol)	Distance from the best mode	
		RMSD l.b.	RMSD u.b.
1	-6.0	0.000	0.000
2	-5.8	1.608	11.182
3	-5.8	0.554	11.266
4	-5.8	1.863	2.562
5	-5.2	2.206	10.963
6	-5.0	3.223	4.214
7	-5.0	5.454	11.593
8	-4.8	3.806	11.220
9	-4.7	4.427	11.131

The molecular docking results indicate that nine amino acids, namely, ASP1046, HIS1026, ILE1053, TYR1082, ARG1027, CYS1024, ILE888, LEU889, and GLU815 of the liver cancer protein (PDB ID: 3WZE) are found to interact with $[Ni(S_2P(R^y)(OR2))_2]$ complex. The predicted non-covalent interactions are of types: three conventional hydrogen bonds, one carbon-involving hydrogen bond, two (pi-system)-alkyl interaction, one (pi-system)-sigma bond, one (pi-system)-cation, one (pi-system)-sulfur and one alkyl interactions. The conventional hydrogen bond lengths are 3.137 (between the O oxygen atom on HIS1026 and S2i atom of dithiophosphonato-complex); 3.477 Å (between the OD2 oxygen on ASP1046 and S2i atom of dithiophosphonato-complex) and 3.614 Å (between the OD2 oxygen on ASP1046 and S1 atom of dithiophosphonato-complex).

Docking studies also show that ten different amino acids ARG56, GLN64, LYS126, PHE61, LEU123, HIS127, SER106, ASP152 LYS126 and ASN103 of colon cancer antigen proteins (PDB ID: 2HQ6) interact with the $[Ni(S_2P(R^y)(OR2))_2]$ complex. The non-covalent interactions are: two conventional hydrogen bonds, three carbon-involving hydrogen bonds, one (pi-system)-cation bond, three (pi-system)-alkyl, two (pi-system)-sulfur, one metal acceptor and alkyl interactions. The conventional hydrogen bond lengths are 3.079 Å (between NH1 nitrogen on ARG56 and S1 atom of dithiophosphonato-complex), 3.148 Å (between NE2 nitrogen on GLN64 and O1 atom of the *n*-pentyl group in dithiophosphonato-complex).

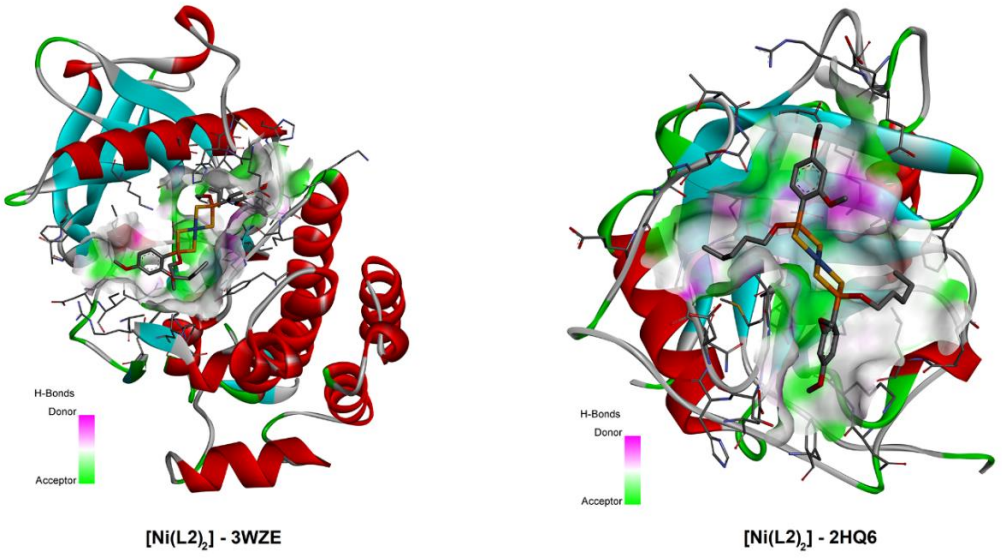


Figure 5.209. Energetically most favorable docked poses were obtained from the rigid molecular docking of $[Ni(S_2P(R^y)(OR2))_2]$ with 3WZE and 2HQ6.

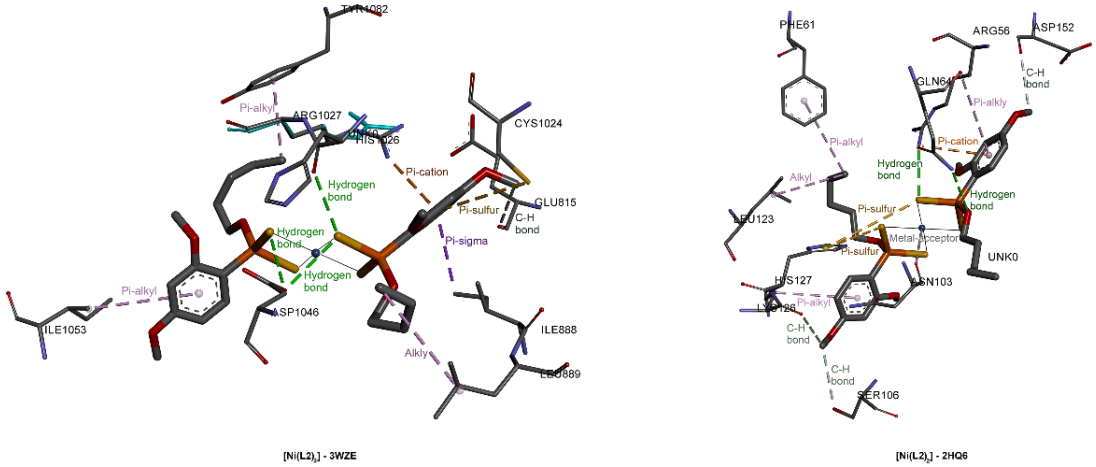


Figure 5.210. The non-covalent interactions of $[Ni(S_2P(R^y)(OR2))_2]$ with 3WZE and 2HQ6.

5.17. *In vitro* Cytotoxic Activity Studies of the Part Ia' Compounds

The cytotoxic activities of compounds were tested at 5 µM, 10 µM, 20 µM, 50 µM, 100 µM and 200 µM concentrations in two human cancer cell lines, including HepG2 and DLD-1 for 48 h. The results are given in Table 5.29.

Table 5.29. IC_{50} results for compounds against cancer cell lines.

Compounds	IC_{50} (μM)	
	DLD-1	HepG2
$[NH_4][S_2P(R^x)(OR1)]$	143.00	> 200
$[NH_4][S_2P(R^x)(OR2)]$	82.73	> 200
$[NH_4][S_2P(R^x)(OR3)]$	> 200	178.40
$[NH_4][S_2P(R^x)(OR4)]$	86.20	> 200
$[NH_4][S_2P(R^x)(OR5)]$	74.87	> 200
$[NH_4][S_2P(R^x)(OR6)]$	41.96	53.49
$[NH_4][S_2P(R^x)(OR7)]$	41.96	53.49
Cisplatin	41.96	53.49

Compounds	IC_{50} (μM)	
	DLD-1	HepG2
$[Ni(S_2P(R^x)(OR1))_2]$	> 200	164.10
$[Ni(S_2P(R^x)(OR2))_2]$	> 200	> 200
$[Ni(S_2P(R^x)(OR3))_2]$	93.38	144.70
$[Ni(S_2P(R^x)(OR4))_2]$	> 200	> 200
$[Ni(S_2P(R^x)(OR5))_2]$	> 200	> 200
$[Ni(S_2P(R^x)(OR6))_2]$	41.96	53.49
$[Ni(S_2P(R^x)(OR7))_2]$	41.96	53.49
Cisplatin	41.96	53.49

As can be seen in the results in Table 5.29, while the designed organic molecules were not effective in the HepG2 cell line, it was observed that two of the nickel complexes of these molecules were effective on cell growth. These two complexes having the codes of $[Ni(S_2P(R^x)(OR4))_2]$ and $[Ni(S_2P(R^x)(OR7))_2]$ had cytotoxic activity on HepG2 cell line with IC_{50} values of 181.1 μM, 173.2 μM, respectively. These $[Ni(S_2P(R^x)(OR4))_2]$ and $[Ni(S_2P(R^x)(OR7))_2]$ complexes, which contain *n*-butyl and benzyl groups in their structures, respectively, demonstrated more toxic effects on liver cells than on colon cancer cells. However, other compounds ($[Ni(S_2P(R^x)(ORn))_2]$ (n=1-7), $[Ni(S_2P(R^x)(OR1))_2]$-$[Ni(S_2P(R^x)(OR3))_2]$, $[Ni(S_2P(R^x)(OR5))_2]$, $[Ni(S_2P(R^x)(OR6))_2]$) except of these mentioned complexes ($[Ni(S_2P(R^x)(OR4))_2]$ and $[Ni(S_2P(R^x)(OR7))_2]$) did not have a significant effect on the growth of liver cancer cells and the calculated IC_{50} values were found to be greater than 200 μM.

Comparison of the data obtained within the set of synthesized compounds $[NH_4][S_2P(R^x)(ORn)]$ and $[Ni(S_2P(R^x)(ORn))_2]$ (n=1-7) show that aliphatic side chains

revealed a drastic change in the activities of these compounds. According to the structure-activity relationship (SAR) studies, a compound $[NH_4][S_2P(R^x)(OR5)]$containing 3-pentyl substituent on the phenyl ring demonstrated more antiproliferative activity compared to that of other synthesized new compounds $[NH_4][S_2P(R^x)(OR1)]$-$[NH_4][S_2P(R^x)(OR4)]$, $[NH_4][S_2P(R^x)(OR6)]$, $[NH_4][S_2P(R^x)(OR7)]$ and $[Ni(S_2P(R^x)(OR1))_2]$-$[Ni(S_2P(R^x)(OR7))_2]$ with IC_{50} value of 68.2 μM in DLD-1 cell line. Other compounds active towards the DLD-1 cell line were: $[NH_4][S_2P(R^x)(OR2)]$, $[NH_4][S_2P(R^x)(OR3)]$ and $[NH_4][S_2P(R^x)(OR6)]$ with IC_{50} values of 131.3 μM, 151.2 μM, 118.0 μM, respectively. However, under the same experimental conditions, it was observed that none of the nickel complexes were effective on colon cancer, and the related cancer cells grew as in the negative control. In a nutshell, all tested molecules and their nickel complexes exhibited lower cytotoxic activity in both liver and colon cancer cell lines than that of conventional chemotherapeutic drug *cis*-platin.

The compounds $[NH_4][S_2P(R^x)(OR5)]$, $[Ni(S_2P(R^x)(OR5))_2]$ including 3-pentyl substituent, and $[NH_4][S_2P(R^x)(OR6)]$ including 3-methyl-1-butyl substituent, demonstrated similar IC_{50} values against the HepG2 cell line, whereas ligand $[NH_4][S_2P(R^x)(OR5)]$ exhibited approximately two-time and five-time higher activity than $[NH_4][S_2P(R^x)(OR6)]$ and $[Ni(S_2P(R^x)(OR5))_2]$ against the DLD-1 cell line, respectively. A nickel complex $[Ni(S_2P(R^x)(OR6))_2]$, having a 3-methyl-1-butyl substituent, showed nearly the same toxic effects on both cell lines.

The dose-dependent effects of new compounds on cell viability ratio are given in Figures 5.211 and 5.212.

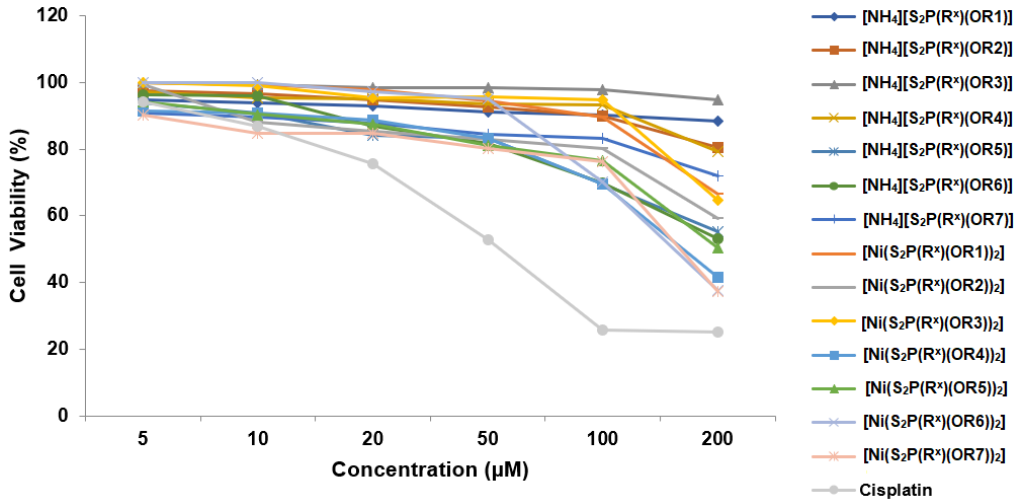


Figure 5.211. Dose-dependent antiproliferative effect of compounds and *cis*-platin on HepG2 cells for 48 h.

As can be seen in Figures 5.211 and 5.212, the viability ratio of cells changed depending on concentrations tested of the compounds and *cis*-platin for two cell lines. For the majority of compounds tested in this study, the highest cell viability was seen at concentrations of 5 µM, 10 µM, 20 µM, 50 µM, and 100 µM. Cell viability ratios were calculated as 88.36%, 80.37%, 94.75%, 79.12%, 55.26%, 53.00%, 71.96%, 66.63%, 59.14%, 64.64%, 41.51%, 50.30%, 37.64%, 37.23% in HepG2 cells at 200 µM concentration of compounds $[NH_4][S_2P(R^x)(ORn)]$ and $[Ni(S_2P(R^x)(ORn))_2]$ (n=1-7), respectively. At 200 µM concentration of compounds $[NH_4][S_2P(R^x)(ORn)]$ and $[Ni(S_2P(R^x)(ORn))_2]$ (n=1-7), the viability ratios were calculated as 62.10%, 52.49%, 57.26%, 64.54%, 48.57%, 52.17%, 64.58%, 95.82%, 98.56%, 96.61%, 69.36%, 53.20%, 48.92%, 55.64% for DLD-1 cells, respectively.

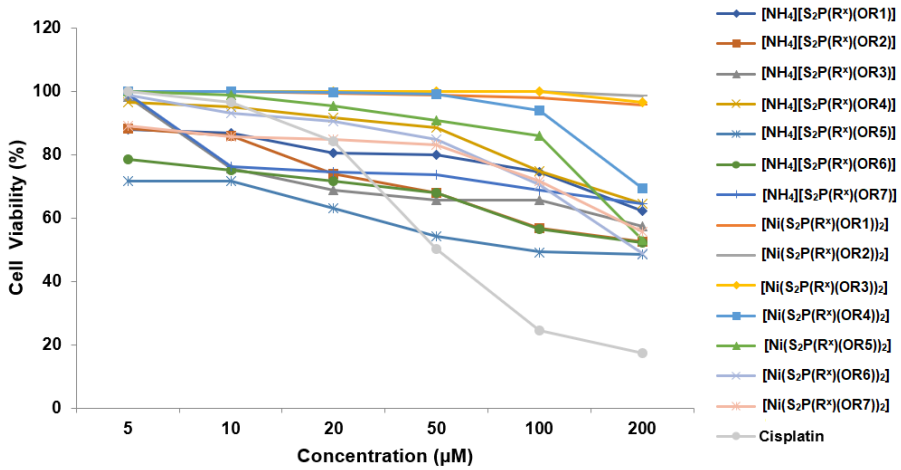


Figure 5.212. Dose-dependent antiproliferative effect of compounds and *cis*-platin on DLD-1 cells for 48 h.

It is seen in Figure 5.212 that the activity of ligands in colon cancer cells is higher than their nickel complexes. For example, while the cell viability ratio was obtained as 56.77% in 100 µM of $[NH_4][S_2P(R^x)(OR2)]$, this ratio was calculated as 100% when the complex of this compound was used.

5.18. *In vitro* Cytotoxic Activity Studies of the Part Ib' Compounds

The cytotoxic activities of the ligands and their nickel complexes were screened at various concentrations in human liver and colon human cancer cell lines for 48 h. The observed results are presented in Table 5.30.

Table 5.30. IC_{50} results for $[NH_4][S_2P(R^x)(ORn)]$ and $[Ni(S_2P(R^x)(ORn))_2]$ against cancer cell lines.

Ligands	IC_{50} (µM)	
	DLD-1	HepG2
$[NH_4][S_2P(R^x)(OR1)]$	143.00	> 200
$[NH_4][S_2P(R^x)(OR2)]$	82.73	> 200
$[NH_4][S_2P(R^x)(OR3)]$	> 200	178.40
$[NH_4][S_2P(R^x)(OR4)]$	86.20	> 200
$[NH_4][S_2P(R^x)(OR5)]$	74.87	> 200
cis-platin	41.96	53.49

Complexes	IC_{50} (µM)	
	DLD-1	HepG2
$[Ni(S_2P(R^x)(OR1))_2]$	> 200	164.10
$[Ni(S_2P(R^x)(OR2))_2]$	> 200	> 200
$[Ni(S_2P(R^x)(OR3))_2]$	93.38	144.70
$[Ni(S_2P(R^x)(OR4))_2]$	> 200	> 200
$[Ni(S_2P(R^x)(OR5))_2]$	> 200	> 200
cis-platin	41.96	53.49

Five new ligands, $[NH_4][S_2P(R^x)(ORn)]$ and their nickel complexes, $[Ni(S_2P(R^x)(ORn))_2]$, were screened in HepG2 cell line *in vitro*. Four ligands ($[NH_4][S_2P(R^x)(OR1)]$, $[NH_4][S_2P(R^x)(OR2)]$, $[NH_4][S_2P(R^x)(OR4)]$, $[NH_4][S_2P(R^x)(OR5)]$) were found to be inactive in the liver cancer cell line at the studied time and concentration range with IC_{50} values higher than 200 µM. The ligand $[NH_4][S_2P(R^x)(OR3)]$ proved to have a notable cytotoxic effect with an IC_{50} value of 178.4 µM in HepG2. The complexes $[Ni(S_2P(R^x)(OR1))_2]$ and $[Ni(S_2P(R^x)(OR3))_2]$ showed measurable cytotoxic effects on the same cell line with IC_{50} values of 164.10 and

144.70 μM, respectively. The other three complexes appear to be inactive. The activity of the two metal complexes were negligible compare to the positive control drug (cisplatin) tested.

In vitro studies showed that four of the ligands ($[NH_4][S_2P(R^x)(OR1)]$, $[NH_4][S_2P(R^x)(OR2)]$, $[NH_4][S_2P(R^x)(OR4)]$, $[NH_4][S_2P(R^x)(OR5)]$) and one of the complexes $[Ni(S_2P(R^x)(OR3))_2]$ were effective against colon cancer cell line with IC_{50} values 143.00, 82.73, 86.20, 74.87 and 93.38 μM, respectively. Ligands ($[NH_4][S_2P(R^x)(OR1)]$, $[NH_4][S_2P(R^x)(OR2)]$, $[NH_4][S_2P(R^x)(OR4)]$, $[NH_4][S_2P(R^x)(OR5)]$) that were inactive in the HepG2 cell line tests were effective in inhibiting the growth of cells in the DLD-1 cell line. A 48 h test shows that among the compounds tested, the ligand $[NH_4][S_2P(R^x)(OR5)]$ has the highest cytotoxic activity on colon cancer cell line with a IC_{50} value of 74.87 μM. While the complexes ($[Ni(S_2P(R^x)(OR1))_2]$, $[Ni(S_2P(R^x)(OR2))_2]$, $[Ni(S_2P(R^x)(OR4))_2]$ and $[Ni(S_2P(R^x)(OR5))_2]$) were found to be inactive, the complex $[Ni(S_2P(R^x)(OR3))_2]$ had cytotoxic activity against DLD-1. The complex $[Ni(S_2P(R^x)(OR3))_2]$ showed cytotoxic effect in both cancer cell lines. The variation of the cytotoxic effect of the ligands and the complexes at various concentrations is given in Figure 5.213.

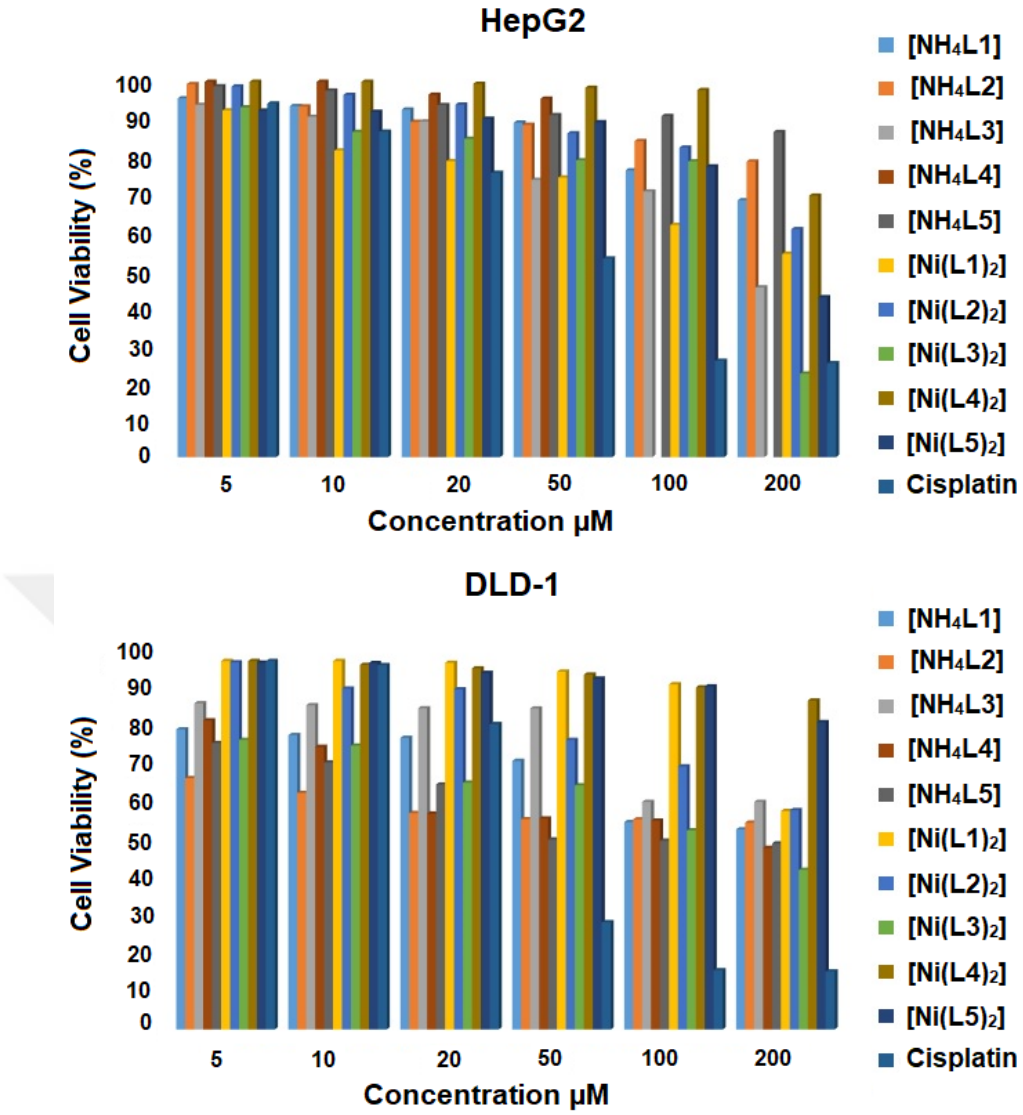


Figure 5.213. Anticancer effect of compounds on cancer cells.

As seen in Figure 5.213, the viability ratios of HepG2 cells at 5 µM concentrations of the ligands, $[NH_4][S_2P(R^x)(ORn)]$ (n=1-5), complexes $[Ni(S_2P(R^x)(ORn))_2]$ (n=1-5) and cisplatin were 95.60%, 99.37%, 93.85%, 100%, 98.83%, 92.37%, 98.76, 93.19%, 100%, 92.31% and 94.21%, respectively. When the concentration of the same compounds and cisplatin were rised to 100 µM, the viability ratios of the cells changed to 76.39%, 84.20%, 70.77%, 95.59%, 90.89%, 61.86%, 82.47%, 78.80%, 97.79%, 77.43% and 25.65%, respectively. Consequently, the compounds tested appear to be not particularly effective against colon cancer cells at the concentration range, 5-50 µM.

5.19. *In vitro* cytotoxic activity studies of the Part II' Compounds

The antiproliferative activity of ligands and their nickel complexes were tested at different concentrations against liver and colon human cancer cell lines for 48 h. The results are given in Table 5.31.

The tested $[NH_4][S_2P(R^y)(ORn)]$ and $[Ni(S_2P(R^y)(ORn))_2]$ (n=1-3, except for n= 4) exhibited IC_{50} values in the ranges of values 65.67 and >200 μM in the human colon adenocarcinoma cell line (DLD-1). According to this made structure-activity relationship (SAR) study, substituents on the molecule structures certainly have a significant effect on DLD-1. For example, one of the Ni complexes $[Ni(S_2P(R^y)(OR3))_2]$ containing 4-*tert*-but-benzyl group showed a very effective result with 65.67 μM compared to the other compounds in DLD-1, and this value is very close to the IC_{50} value obtained from the positive control drug cisplatin. On the other hand, the complex $[Ni(S_2P(R^y)(OR3))_2]$ exhibited nearly two times higher cytotoxic activity than other synthesized compounds in the DLD-1 cell line. At the same time, the ligand $[Ni(S_2P(R^y)(OR3))_2]$ of this metal complex $[NH_4][S_2P(R^y)(OR3)]$ demonstrated higher antiproliferative activity on the DLD-1 cell line compared to the other two ligands $[NH_4][S_2P(R^y)(OR1)]$ and $[NH_4][S_2P(R^y)(OR2)]$ with IC_{50} value of 127.50 μM. This clearly shows that the substituents on the structure affect the activity of the molecule. Complex $[NH_4][S_2P(R^y)(OR1)]$ with IC_{50} value of 131.40 μM, had moderate toxic effect on the inhibition of colon cancer cell growth as *in vitro.* However, compounds $[NH_4][S_2P(R^y)(OR1)]$, $[NH_4][S_2P(R^y)(OR2)]$ and $[Ni(S_2P(R^y)(OR2))_2]$ were found to be inactive towards DLD-1 for the tested concentrations and incubation time.

We also evaluated *in vitro* antiproliferative activity of compounds towards the HepG2 cell line. Interestingly, all tested compounds were found to be inactive in this cell line. Even, the most effective complex $[Ni(S_2P(R^y)(OR3))_2]$ in the DLD-1 cell line was found to have an IC_{50} value higher than 200 μM in HepG2. The variation of the antiproliferative effect of the compounds on cells for 48 hours depending on the concentrations is given in Figures 5.214 and 5.215.

As seen in Figure 5.214, the compounds $[NH_4][S_2P(R^y)(OR3)]$, $[Ni(S_2P(R^y)(OR1))_2]$-$[Ni(S_2P(R^y)(OR3))_2]$ tested inhibited the proliferation of dividing colon and liver cancer cells in a dose-dependent manner. However, compounds $[NH_4][S_2P(R^y)(OR1)]$ and $[NH_4][S_2P(R^y)(OR2)]$ did not show any effect on cell viability ratio even at a

concentration as high such as 200 µM. The viability ratios of DLD-1 cells were obtained in 93.48%, 94.25%, 92.49%, 71.27%, 94.78%, 66.99% and 81.54% at 20 µM concentration of $[NH_4][S_2P(R^y)(ORn)]$, $[Ni(S_2P(R^y)(ORn))_2]$ and (n=1-3) and cisplatin, respectively. When the concentrations of tested compounds were increased to 200 µM, the viability ratio of DLD-1 cells changed as follows: 91.89%, 86.76%, 21.78%, 53.25%, 56.47%, 15.13%, 19.68% for $[NH_4][S_2P(R^y)(ORn)]$, $[Ni(S_2P(R^y)(ORn))_2]$ (n=1-3) and cisplatin, respectively. The results show that the ligand $[NH_4][S_2P(R^y)(OR3)]$ and its metal complex have a significant toxic effect on DLD-1 at 200 µM concentration and greatly inhibit cell growth.

The synthesized ligands and complexes generally do not effect on liver cancer cells growth. The viability ratios of HepG2 cells were obtained in 83.40%, 92.19%, 94.55%, 59.93%, 51.65%, 19.62%, 23.52% at 200 µM concentration of $[NH_4][S_2P(R^y)(ORn)]$, $[Ni(S_2P(R^y)(ORn))_2]$ (n=1-3) and cisplatin, respectively. When 100 µM of complex $[Ni(S_2P(R^y)(OR3))_2]$ was used, the cell viability ratio was measured as 87.13%. This ratio was dramatically reduced to 19.62% with 200 µM of the same complex. However, there was no significant change in liver cancer cell inhibition with the concentration change of the other compounds (Figure 5.215).

Table 5.31. IC_{50} results for the compounds against cancer cell lines.

Ligands	IC_{50} (µM)	
	DLD-1	HepG2
$[NH_4][S_2P(R^y)(OR1)]$	> 200	> 200
$[NH_4][S_2P(R^y)(OR2)]$	> 200	> 200
$[NH_4][S_2P(R^y)(OR3)]$	127.50	> 200
cis-platin	48.83	31.91

Complexes	IC_{50} (µM)	
	DLD-1	HepG2
$[Ni(S_2P(R^y)(OR1))_2]$	131.40	> 200
$[Ni(S_2P(R^y)(OR2))_2]$	> 200	> 200
$[Ni(S_2P(R^y)(OR3))_2]$	> 65.67	> 200
cis-platin	48.83	31.91

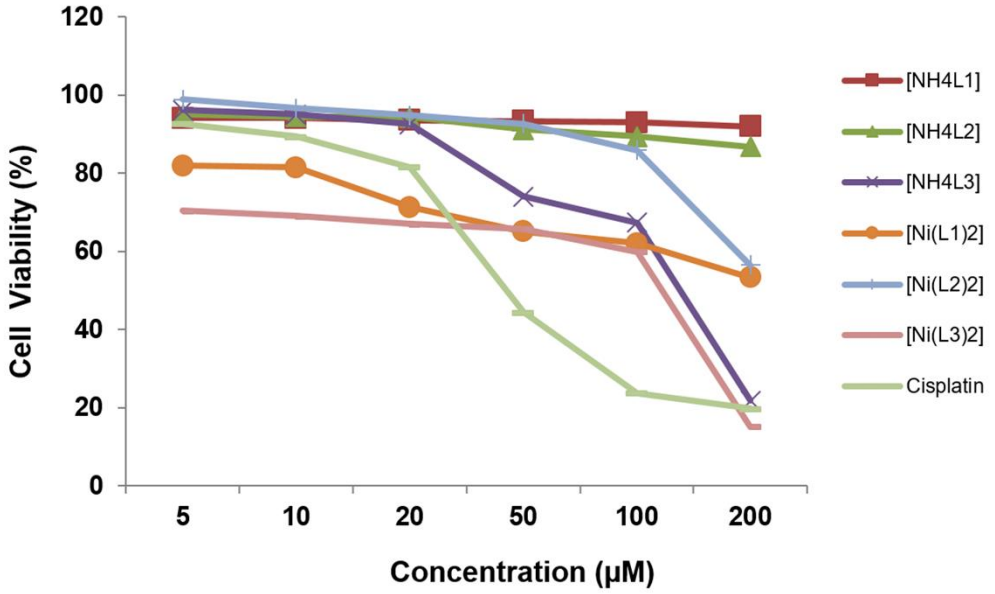


Figure 5.214. Antiproliferative effect of compounds on DLD-1 cells.

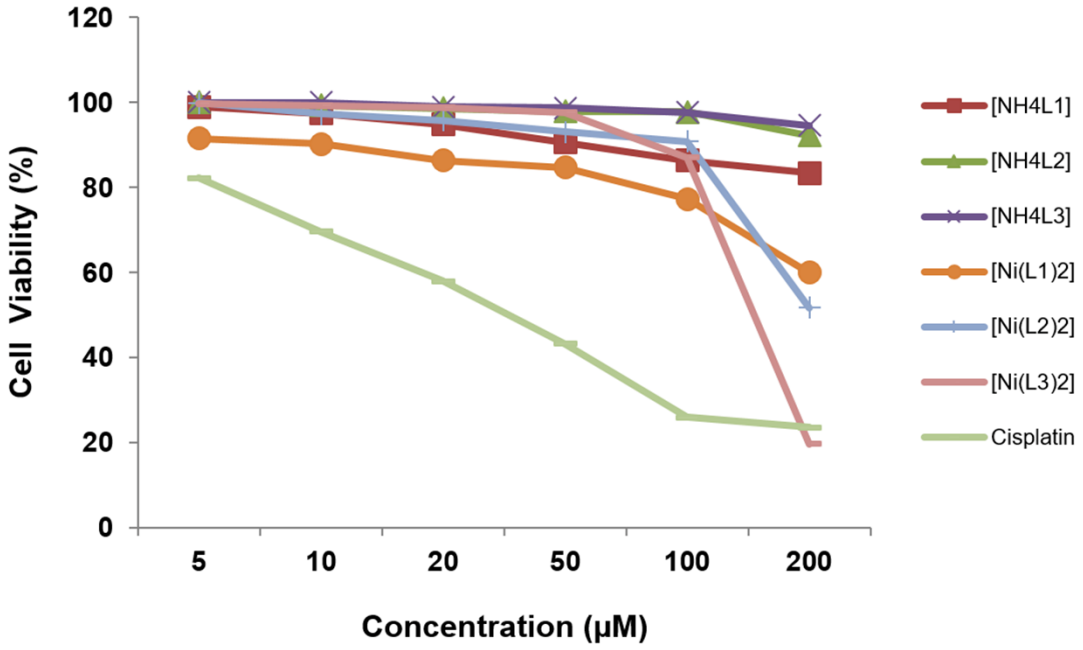


Figure 5.215. Antiproliferative effect of compounds on HepG2 cells.

6. CONCLUSIONS

In an effort to create alternatives to the well-known 1,3,2,4-dithiadiphosphetane-2,4-disulfides such as Lawesson reagent and Belleau reagents, we investigated on the new reagent, SAV-A1 and SAV-A2 ($[R^{x,y}\text{-}P(S)S]_2$, R^x= 3,4-dimethoxyphenyl, SAV-A1; R^y= 2,4-dimethoxyphenyl, SAV-A2), with an emphasis on a less laborious procedure. These compounds were used in the synthesis of structurally diverse organo-dithiophosphonates ligands ($[NH_4][S_2P(R^{x,y})(ORn)]$) and the anions of these salts were used in the preparation of new dithiophosphonato Ni(II) complexes ($[Ni(S_2P(R^{x,y})(ORn)]$). New ligands and complexes were analyzed by mass, FT-IR, NMR, (1D ^{1}H-, ^{13}C-, ^{31}P-NMR and 2D HSQC for $[Ni(S_2P(R^x)(OR6)]$ and $[Ni(S_2P(R^y)(OR2)]$) spectroscopies together with elemental analysis. The ^{13}C-NMR spectra of the aromatic parts of the compounds display interesting features. The ambiguity regarding the assignments of ^{1}H- and ^{13}C-NMR peaks of $[Ni(S_2P(R^x)(OR6)]$ complex and $[Ni(S_2P(R^y)(OR2)]$ complex were dealt with by using HSQC spectra (Figure 5.67 and Figure 5.94, respectively). In addition, the structures of the complexes were done by the X-ray diffraction method ($[Ni(S_2P(R^x)(ORn)]$, n=1-7 for Part Ia; $[Ni(S_2P(R^x)(ORn)]$, n=1,2,4,5 for Part Ib and $[Ni(S_2P(R^y)(OR2)]$ for II). Theoretical calculations (density functional theory, molecular docking) of the complexes whose structure is characterized by X-rays and anticancer studies of the compounds were carried out as an application.

For Part Ia studies; the theoretically calculated structural parameters of the $[Ni(S_2P(R^x)(ORn)]$ (Rn, R1=methyl-, R2=Ethyl-, R3=n-propyl-, R4=n-butyl-, R5=3-pentyl-, R6=3-methyl-1-butyl-, R7=benzyl-) complexes were compared with the molecular structures obtained from X-ray analysis by using DFT. Total molecular energies, HOMO-LUMO band energy gaps, the chemical parameters, the HOMO and LUMO diagrams and MEP analysis of the complexes were reported by the quantum mechanical calculations. Energetically the most favorable poses during docking were also obtained from the rigid molecular docking of each Ni complex with liver cancer protein, PDB ID: 3WZE and colon cancer antigen proteins, ID 2HQ6. The binding sites, types of interaction and bond distances are predicted by MDS of the compounds. According to the theoretical results, the HOMO–LUMO band energy gap ΔE_{Gap}(eV) of the complex $[Ni(S_2P(R^x)(OR7)]$ is lower than those of the others.

Molecular docking results show that the bioactivities of the investigated complexes with 2HQ6 (colon cancer antigen proteins) are higher than that between the complexes and 3WZE (the liver cancer protein).

The compounds concerned were also tested against two different cell lines for evaluating the anti-cancer potentials. It was found that some of the compounds prepared have a toxic effect on the screened cell lines. In particular, the ligand $[NH_4][S_2P(R^x)(OR5)]$ was found to be more cytotoxic effect with an IC_{50} value of 68.2 μM in DLD-1. The theoretical calculation results appear to agree well with the experimental findings. $[Ni(S_2P(R^x)(OR7)]$ was found to be the most effective complex, among metals against HepG2 cells.

For Part Ib studies; the DFT calculations of the four of the square-planar Ni(II) complexes, $[Ni(S_2P(R^x)(OR1)]$, $[Ni(S_2P(R^x)(OR2)]$, $[Ni(S_2P(R^x)(OR4)]$ and $[Ni(S_2P(R^x)(OR5)]$ were carried out to compare the geometrical features of the molecules in solid and gas state. The total molecular energies, HOMO-LUMO energy values, HOMO and LUMO surface diagrams, HOMO-LUMO band gaps, dipole moments and other chemical parameters were computed. MEP analyses of them were also done by quantum mechanical calculations. Energetically, the most favorable docked poses of the molecules on colon cancer antigen proteins, ID 2HQ6, and liver cancer protein, PDB ID: 3WZE were also obtained from the rigid MD of the complexes. The binding sites, binding types and docking bond distances are predicted by MD studies.

The compounds were screened in human cancer cell lines, and it was found that nine of the ten compounds have negligible toxic effects. Only the compound $[NH_4][S_2P(R^x)(OR5)]$ was found to be notably effective with an IC_{50} value of 74.87 μM in DLD-1.

For Part II studies; the DFT calculations of $[Ni(S_2P(R^y)(OR2)]$ were presented. Calculated structural parameters of the Ni complexes were compared with the molecular structures obtained from X-ray analysis by using DFT. Total molecular energies, the energy values of HOMO-LUMO band gaps, the chemical parameters, the HOMO and LUMO diagrams and MEP analysis of the complexes were reported by the quantum mechanical calculations. Energetically most favorable docked poses were also obtained from the rigid molecular docking of investigated Ni complex with liver cancer protein,

PDB ID: 3WZE and colon cancer antigen proteins, ID 2HQ6. The binding sites, binding types and bond distances are predicted by molecular docking studies of the compounds.

The compounds were screened in human cell lines, and it was found that some compounds have toxic effects. In particular, a complex [Ni($S_2P(R^y)$(OR3)] was found to be more effective than the others with an IC_{50} value of 65.67 μM in DLD-1.

To sum up;

- New 2,4-*bis*($R^{x,y}$)-1,3,2,4-dithiadiphosphetane-2,4-disulfides were synthesized as starting materials (SAV-A1 and SAV-A2).
- Different types dithiophosphonic acids ([$R^{x,y}$)(RnO)P(S)SH]), ligands ([NH_4][$S_2P(R^{x,y})$(ORn)]) and complexes ([Ni($S_2P(R^{x,y})$(ORn)]) were synthesized from these starting materials.
- The characteristic ν_{N-H} stretching bands of the ligands on the IR spectra disappear in complexes proving the substitution of the ammonium group by metal cations.
- Molecular ion peaks belonging to ligands and complexes have been observed noticeably in the Mass spectra.
- ^{1}H- and ^{13}C-NMR spectra of the compounds confirm the suggested structures.
- The single peak seen in the ^{31}P-NMR spectra of the ligands indicates a single phosphorus atom in the structure of the ligands, whereas the single peak seen in the ^{31}P-NMR spectra of the complexes indicates that the two phosphorus atoms in the structure are symmetric.
- Complementary structural information was provided by the HSQC spectrum of the complexes. The structures of the starting materials are deduced from the structures of derivatives thereof. That is, the suggested structure for the 3,4-dimethoxyphenyl- group in the main framework of SAV-A1 and the 2,4-dimethoxyphenyl- group in the main framework of SAV-A2 are indirectly confirmed by 2D NMR analysis (HSQC) of the complexes [Ni($S_2P(R^x)$(OR6)] and [Ni($S_2P(R^y)$(OR2)].
- Single crystal X-ray studies show that the bond lengths between the "P-S" atoms in the structure are almost equal, indicating that the S-P-S electrons are delocalized.

- Single crystal X-ray studies also show that the structures of the complexes are square planes. However, this structure is slightly distorted from the ideal geometry.

- Density Functional Theory (DFT) calculations of the complexes ([Ni($S_2P(R^x)$(ORn)], n= 1-7 for Part Ia; [Ni($S_2P(R^x)$(ORn)], n= 1,2,4,5 for Part Ib and [Ni($S_2P(R^y)$(OR2)] for Part II) were done. Theoretical calculations of complexes whose structure is elucidated by X-ray analysis have also found that the structure is a square plane.

- The molecular docking studies of the Ni(II) complexes with colon cancer antigen proteins, ID 2HQ6 and liver cancer protein, PDB ID: 3WZE were done to foresee the interactions of the complexes.

- The ligands and their nickel complexes were tested on human liver and colon cancer cell lines using (MTT) assay method. Some of the ligands ([NH_4][$S_2P(R^x)$(*O*-3-pentyl)] for Part Ia; [NH_4][$S_2P(R^x)$(*O*-2-pentyl)], [NH_4][$S_2P(R^x)$(*O*-2-butyl)] for Part Ib) demonstrated more antiproliferative effects than others in colon cancer cell line with IC50. On the other hand, among the complexes tested of the Part II study, just [Ni($S_2P(R^y)$(O-*4-tert*-but-benzyl)] complex showed an activity closer to that of cisplatin against the colon cancer cell line.

Two manuscripts in prestigious journals within the scope of Science Citiation Index have emerged from this thesis (Figure 6.1 and 6.2). In addition to the thesis, it has been presented in national [311, 312] and international [313, 314] congresses. In addition, one publication is in the process of being sent.

In the future, we would say that this study could constitute an infrastructure for the synthesis of different types organo-dithiophosphorus compounds with new starting materials in terms of scientific point of view. For example, the study investigated the reaction of starting materials with alcohols. Reactions with Grignard reagents or amines have not been studied. Furthermore, only Ni(II) complexes have been synthesized in this study. Complexes of other metals remain to be synthesized. Lewis-based coordination compounds with six coordination have also been expected to be synthesized by researchers. The potential application of the compounds to be synthesized from these samples in medicine, industry and nuclear chemistry are still to be investigated. We hope that even the compounds synthesized within the scope of this thesis can be an alternative

to chemical compounds used in the disposal of nuclear waste and provide an infrastructure for chemotherapeutic drugs in anticancer cancer treatment.

Received: 5 April 2022 | Revised: 9 June 2022 | Accepted: 6 July 2022
DOI: 10.1002/aoc.6821

RESEARCH ARTICLE

Applied Organometallic Chemistry WILEY

Ni(II) complexes with 1,3,2,4-dithiadiphosphetane 2,4-disulfide-based ligands: Structural insights, theoretical studies, and anticancer activities

Elif Bulat[1,2] | Ertuğrul Gazi Sağlam[1,2] | Celal Tuğrul Zeyrek[3] | Senem Akkoç[4,5] | Yunus Zorlu[6] | Hakan Dal[7]

[1]Department of Chemistry, Yozgat Bozok University, Yozgat, Turkey
[2]Department of Chemistry, Marmara University, İstanbul, Turkey
[3]Department of Medical Services and Techniques, Çankırı Karatekin University, Çankırı, Turkey
[4]Department of Basic Pharmaceutical Science, Süleyman Demirel University, Isparta, Turkey
[5]Faculty of Engineering and Natural Sciences, Bahçeşehir University, Istanbul, 34353, Turkey
[6]Department of Chemistry, Gebze Technical University, Gebze, Turkey
[7]Department of Medical Services and Techniques, Anadolu University, Eskişehir, Turkey

Correspondence
Ertuğrul Gazi Sağlam, Department of Chemistry, Yozgat Bozok University, Yozgat 66900, Turkey; Department of Chemistry, Marmara University, Göztepe, İstanbul 34722, Turkey.
Email: ertugrulgazi.saglam@yobu.edu.tr; egazi@marmara.edu.tr; saglameg@gmail.com

Funding information
Yozgat Bozok Üniversitesi, Grant/Award Number: BAP 6602c-FEN/20-359; Marmara Üniversitesi, Grant/Award Number: BAPKO; Project No: FDK- FDK-2021-10339; Türkiye Bilimsel ve Teknolojik Araştırma Kurumu, ULAKBIM: High Performance and Grid Computing Center (TRUBA; Suleyman Demirel University Research Fund, Grant/Award Number: TSG-2021-8458; Marmara University; Yozgat Bozok University

The first synthesis of 2,4-*bis*(3,4-dimethoxyphenyl)-1,3-dithia-2,4-diphosphetane 2,4-disulfide (SAV-A1 reagent) was achieved. Seven oxo-alkyl esters (HLn) were synthesized thereof. Ni(II) complexes ([Ni(Ln)$_2$]) of these ligands were prepared in ethanol. The structures were identified by spectral studies. Ni(II) complexes were unambiguously determined by X-ray crystallography. In addition, the ligands and their Ni(II) complexes were tested on two different human cancer cell lines, including liver and colon. Moreover, density functional theory (DFT) calculations of the Ni(II) complexes were performed, and the molecular docking studies of these compounds with liver cancer protein, PDB ID: 3WZE and colon cancer antigen proteins, ID 2HQ6 were presented to investigate and predict potential interactions.

KEYWORDS
2,4-diorganyl-1,3,2,4-dithiadiphosphetan-2,4-disulfide, anticancer, density functional theory, dithiophosphonato complexes, perthiophosphonic acid anhydrides

1 | INTRODUCTION

Over the past few decades, the compounds bearing a P_2S_2 moiety are dubbed 2,4-diorganyl-1,3,2,4-dithiadiphosphetane-2,4-disulfide (DTPS, $(RP(S)S)_2$) have attracted much attention, because they serve as the starting material of a series of new organodithiophosphorus compounds.[1–7] The prototype of the DTPSs is the so-called Lawesson reagent.[8] Other analogs, for example, Belleau reagent,[9] Yokoyama reagent,[10] and Davy reagent[11] have been reported afterward (Figure 1).

Lawesson's and Davy's reagents are commercially available,[12] whereas other DTPSs are synthesized as needed. There are three routes for the syntheses of these reagents: the reaction of thiophosphine dichlorides with H_2S[13]; the treatment of the diphosphines with elemental

 © 2022 John Wiley & Sons Ltd.

Figure 6.1. The article published 1 within the scope of the thesis.

Journal of Molecular Structure 1272 (2023) 134197

Contents lists available at ScienceDirect

Journal of Molecular Structure

journal homepage: www.elsevier.com/locate/molstr

2,4-*Bis*(2,4-dimethoxyphenyl)-1,3-dithia-2,4-diphosphetane 2,4-disulfide and its derivatives: Syntheses, structural characterizations, anticancer activities, and theoretical studies on some dithiophosphonato Ni(II) complex

Ertuğrul Gazi Sağlam[a,*], Elif Bulat[a], Celal Tuğrul Zeyrek[b], Senem Akkoç[c,d], Yunus Zorlu[e], Hamza Yılmaz[f]

[a] Department of Chemistry, Marmara University, Göztepe, İstanbul 34722, Türkiye
[b] Department of Medical Services and Techniques, Çankırı Karatekin University, Çankırı 18100, Türkiye
[c] Department of Basic Pharmaceutical Science, Süleyman Demirel University, Isparta 32260, Türkiye
[d] Faculty of Engineering and Natural Sciences, Bahçeşehir University, 34353, İstanbul, Türkiye
[e] Department of Chemistry, Gebze Technical University, Kocaeli 41400, Türkiye
[f] Department of Chemistry, Ankara University, Tandoğan, Ankara 06100, Türkiye

ARTICLE INFO

Article history:
Received 5 June 2022
Revised 6 September 2022
Accepted 21 September 2022
Available online 22 September 2022

Keywords:
Perthiophosphonic acid anhydrides
2,4-diorganyl-1,3,2,4-dithiadiphosphetan-2,4-disulfide
Phosphonodithioates
Dithiophosphonates
Organodithiophosphorus compounds
Single crystal X-ray analysis
Density functional theory
Molecular docking
Antiproliferative activity
Anticancer

ABSTRACT

New 2,4-*bis*(2,4-dimethoxyphenyl)-1,3-dithia-2,4-diphosphetane 2,4-disulfide, (SAV-A2), was synthesized from the reaction P_4S_{10} and 1,3-dimethoxybenzene. SAV-A2 was reacted with alcohols to form dithiophosphonic acid monoesters (HLn, $HS_2P((2,4\text{-}CH_3O)_2C_6H_3)(ORn)$; *n*=1–3, R1=2-butyl-; R2=*n*-pentyl-; R3=*4-tert*-but-benzyl-). The acids were converted to the ammonium salts ($[NH_4Ln]$) to serve as the source of the ligands (Ln), to obtain Ni(II) complexes, ($[Ni(Ln)_2]$). $[Ni(L2)_2]$ crystal structure was elucidated by single-crystal X-ray diffraction analysis. In addition, Density Functional Theory (DFT) calculations of $[Ni(L2)_2]$ was performed. The molecular docking studies of the complex with liver cancer protein, PDB ID: 3WZE and colon cancer antigen proteins, ID 2HQ6 were done compare with experimental and theoretical results. All compounds were tested on liver- and colon cancer cell lines. Among the complexes tested, $[Ni(L3)_2]$ showed an activity closer to that of cisplatin against the colon cancer cell line. The other compounds were found to be have less active.

© 2022 Elsevier B.V. All rights reserved.

1. Introduction

Phosphor-1,1-dithiolates including dithiophosphate (DTP), dithiophosphinate (DTPA) and dithiophosphonate (DTPOA) ligands and their derivatives have many commercial applications such as floatation reagents in the recovery of industrial metal cations [1], as additives in lubricants [2], as pesticides in agriculture [3] and as precursors for chemical warfare [4]. They are also deemed to be a potential candidates to be used in the synthesis of antibiotics [5] and anticancoregenes against some tumors [6].

Organo-dithiophoshorus compounds have been the subject of a few studies on the field of cancer therapeutics. There are hardly any studies on the antiproliferative activities of dithiophosphinic- [7] and dithiophosphonic acids [8–10]. Anti-cancer studies with dithiophosphoric acids, on the other hand, are slightly more common [11]. Pt-dithiophosphoric acid complexes, for example, were found to be active against cancer, by Lowe et al. [12]. Cytotoxic activities of some vanadium dithiophosphates have been demonstrated by Kumar et al. in the cancers of the lung, prostate and blood [13]. So, the preliminary motives are ready to make investigations on the cancerogenic activity of dithiophosphinate and dithiophosphonate compounds.

Due to the soft-base character of dithiophosphorus-compounds, phosphor-1,1-dithiolate ligands form stable complexes with cations of soft-acid nature. There are several papers available giving the details of the synthesis, structures and chemistry, especially the metal complexes of dithiophosphorus-compounds. The

* Corresponding author.
E-mail address: egazi@marmara.edu.tr (E.G. Sağlam).

https://doi.org/10.1016/j.molstruc.2022.134197
0022-2860/© 2022 Elsevier B.V. All rights reserved.

Figure 6.2. The article published 2 within the scope of the thesis.

POSTER PRESENTATIONS

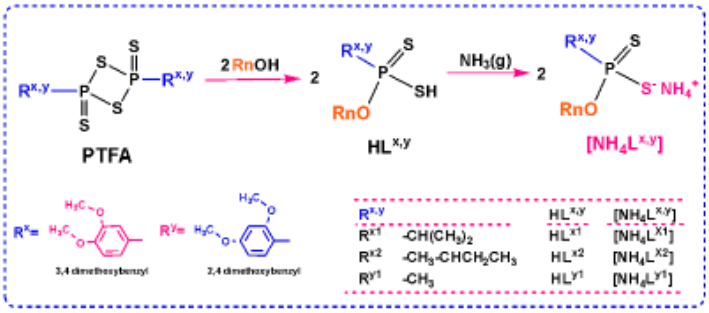
Synthesis and characterization of New Dithiophosphonate Ligands

Elif Bulat[1*,2], Ertuğrul Gazi Sağlam[1,2], Hakan Dal[3]

[1]Department of Chemistry, Marmara University, 34722, Göztepe, İstanbul, Türkiye
[2]Department of Chemistry, Yozgat Bozok University, 66900, Yozgat, Türkiye
[3]Department of Medical Services and Techniques, Anadolu University, Eskişehir, Türkiye
Email: bulatelif55@gmail.com

Perthiophosphonic acid anhydrides (PTPA) are used as a starting agent in the synthesis of dithiophosphonic acids (DTPOA)[1].

In this survey, we synthesized new DTPOAs starting from PTPAs formerly synthesized by us [2]. That is, new DTPOAs ($HS_2P((2,4\text{-}CH_3O)_2\text{-}C_6H_3)(ORn)$, $HL^{x,y}$; R^{x1}=n-propyl-, R^{x2}=2-butyl-, R^{y}=methyl- were synthesized by reaction of 2,4-bis(3,4-dimethoxyphenyl)-1,3-dithia-2,4-diphosphetane 2,4-disulfide, (SAV-A1) and 2,4-bis(2,4-dimethoxyphenyl)-1,3-dithia-2,4-diphosphetane 2,4-disulfide, (SAV-A2) with aliphatic alcohols. All DTPOAs were transformed to relating to ammonium salts, $[NH_4L^{x,y}]$ (Scheme 1).



Scheme 1. Synthesis reaction of DTFOAs

The characterization of $[NH_4L^{x,y}]$ ligands was performed by elemental analysis as well as mass spectroscopy, FT-IR and ^{1}H-, ^{13}C- and ^{31}P-NMR spectroscopies.

This study was supported by Project Coordination Application and Research Center of Yozgat Bozok (BAP 6602c-FEN/20-359) and Marmara University [FDK-2021–10339].

References:

[1] Bulat, E.; Saglam, E.G.; Yılmaz, H.; The Syntheses and Characterization of New Dithiophosphonates derived from Novel 2,4-Bis(methoxytolyl)-1,3-dithia-2,4-diphosphetane 2,4-disulfides and Their Ni(II) Complexes. J. Turkish Chem. Soc. A: Chem., 2020, 7, 3, 789-800

[2] Saglam, E.G.; Bulat, E.; Zeyrek, C.T.; Akkoç, S.; Zorlu,Y.; Yılmaz, H.; 2,4- Bis (2,4-dimethoxyphenyl)-1,3-dithia-2,4-diphosphetane 2,4-disulfide and its derivatives: Syntheses, structural characterizations, anticancer activities, and theoretical studies on some dithiophosphonato Ni(II) complex. J. Mol. Struc., 2023, 1272, 134197

Figure 6.3. The international congress 1 within the scope of the thesis.

POSTER PRESENTATIONS

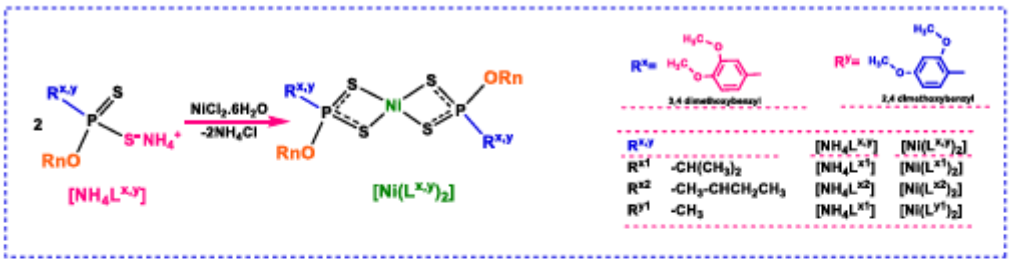
New Dithiophosphonato Ni(II) Complexes: Synthesis, characterization, theoretical and *in vitro* cytotoxicity studies

Elif Bulat[1*,2], Ertuğrul Gazi Sağlam[1,2], Senem Akkoç[3,4], Celal Tuğrul Zeyrek[5], Yunus Zorlu[6], Hakan Dal[7]

[1]*Department of Chemistry, Marmara University, 34722, Göztepe, İstanbul, Türkiye*
[2]*Department of Chemistry, Yozgat Bozok University, 66900, Yozgat, Türkiye*
[3]*Department of Basic Pharmaceutical Science, Süleyman Demirel University, 32260, Isparta, Türkiye*
[4]*Faculty of Engineering and Natural Sciences, Bahçesehir University, 34353, İstanbul, Türkiye*
[5]*Department of Medical Services and Techniques, Çankırı Karatekin University, 18100, Çankırı, Türkiye*
[6]*Department of Chemistry, Gebze Technical University, 41400 Kocaeli, Türkiye*
[7]*Department of Medical Services and Techniques, Anadolu University, Eskişehir, Türkiye*
Email: bulatelif55@gmail.com

Dithiophosphonic acids (DTFOA), one of the members of the Organo-dithiophosphorus Compounds, have been preferred more in studies because they are easier to synthesize and have higher yields than other organo-dithiophosphorus compounds [1,2].

In this study; new Ni(II) complexes, $[Ni(L^{x,y})_2]$ were obtained by the reaction of $NiCl_2.6H_2O$ and corresponding dithiophosphonate salts, $[NH_4L^{x,y}]$. These complexes were elucidated by spectroscopic methods. They were also studied by single crystal X-ray diffraction analysis, theoretical and molecular docking studies as well as *in vitro* anticancer activities.



Scheme 1. The synthesis reaction of $[Ni(L^{x,y})_2]$ complexes

References

[1] Van Zyl, W.E.; Woollins, J.D.; The coordination chemistry of dithiophosphonates: An emerging and versatile ligand class. Coord. Chem. Rev. 2013, 257, 718–731

[2] Bulat, E.; Saglam, E.G.; Zeyrek, C.T.; Akkoç, S.; Zorlu,Y.; Dal,H; Ni(II) complexes with 1,3,2,4-dithiadiphosphetane 2,4-disulfide-based ligands: Structural insights, theoretical studies and anticancer activities. Appl. Organometal. Chem. 2022, 36, e6821

This study was supported by Project Coordination Application and Research Center of Yozgat Bozok (BAP 6602c-FEN/20-359), Marmara University [FDK-2021–10339], Suleyman Demirel University (TSG-2021–8458) and The Scientific and Technological Research Council of Turkey, ULAKBIM - TRUBA resources.

Figure 6.4. The international congress 2 within the scope of the thesis.

33. Ulusal Online Kimya Kongresi
7-9 Ekim 2021 Kimyanın Gücü

İnteraktif E-Posterler

PS-004

Veratrol İçerikli Yeni Ditiyofosfonat ve Nikel Komplekslerinin Sentezi ve Yapısal Karakterizasyonu

Ertuğrul Gazi Sağlam[1], Elif Bulat[1], Hakan Dal[2]

[1]Marmara Üniversitesi
[2]Anadolu Üniversitesi

Organo-ditiyofosfor bileşikleri; ditiyofosfat, ditiyofosfinat ve ditiyofosfonatlar olarak sınıflandırılır (Haiduc,2001). Bu bileşikler, ziraatte zararlı haşere ve bitkilerin yok edilmesinde kullanılan maddelerin içeriğine ilave edilmektedir (Kabra,2009). Ditiyofosfonatlar yapılarındaki kükürt atomlarının Lewis bazı özelliğinden dolayı peryodik sistemdeki hemen hemen bütün metallerle değişik koordinasyonlarda (dörtlü veya altılı yapıda) ve farklı yapılarda (tek metal merkezli/monomerik; iki metal merkezli/dimerik) kompleksler verirler (Haiduc,2003). Bu çalışmada, orjinal ditiyofosfonat ligandları sentezlendi ([S2P(R')(ORn)]-; R'=(o-CH3O)2C6H3-, veratril; R1=n-propil-; R2=2-propil-; R3=2-butil-; R4=n-pentil-; R5=2-pentil-; R6=3-metil-1-butil-; R7=4-tert-butilbenzil-). Bu ligandların NiCl2.6H2O ile yeni tek metal merkezli Ni(II) kompleksleri ([Ni(S2P(R')(ORn))2]) elde edildi (Şekil 1). Bileşiklerin yapıları elementel analiz, kütle spektroskopisi, titreşim spektroskopisi (IR) ve NMR spektroskopisi (^{1}H-, ^{13}C- ve ^{31}P-) yöntemleriyle aydınlatıldı.

KAYNAKLAR:

[1.] Haiduc I., J. Org. Chem., 623, 29-42, 2001.

[2.] Kabra V., Mitharwal S., Singh S., Phosphorus, Sulfur Silicon Relat. Elem., 184, 2431-2442, 2009.

[3.] Haiduc I., in Comprehensive Coord. Chem. II, eds. McCleverty J. A., Meyer T. J., Pergamon, Oxford, 2003.

Teşekkür: Bu çalışma Yozgat Bozok Üniversitesi, Proje Koordinasyon Uygulama ve Araştırma Merkezi, BAP 6602c-FEN/20-359 kodlu projesiyle desteklenmektedir.

Anahtar Kelimeler: 1,1 Ditiyolatlar, Fosfinoditioatlar, Organo-ditiyofosfor Kompleksleri, Ditiyofosfonik Asit, Ditiyofosfonato kompleksleri

Şekil 1. Ditiyofosfonato Ni(II) komplekslerinin sentez reaksiyonu.

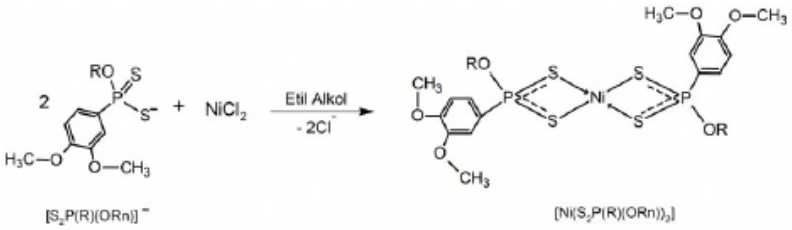


Figure 6.5. National congress 1 within the scope of the thesis.

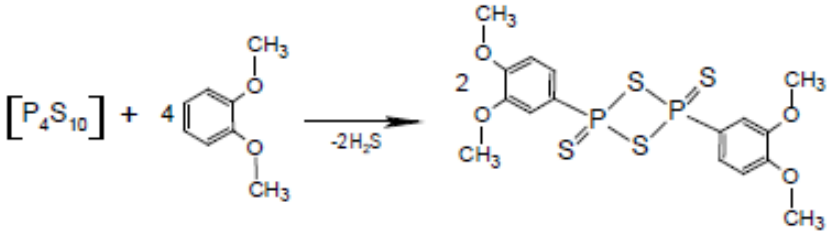
P-011

YENİ 2,4-*bis*(1,2-DİMETOKSİFENİL)-1,3-DİTHİA-2,4-DİFOSFETAN 2,4-DİSÜLFÜR TÜREVLERİNİN SENTEZİ VE KARAKTERİZASYONU

Ertuğrul Gazi Sağlam [1,2], ***Elif Bulat*** [1,2], ***Hakan Dal*** [3]

[1] *Yozgat Bozok Universitesi, Fen Edebiyat Fakültesi, Kimya Bölümü, YOZGAT*
[2] *Marmara Universitesi, Fen Edebiyat Fakültesi, Kimya Bölümü, İSTANBUL*
[3] *Anadolu Üniversitesi, Açık Öğretim Fakültesi, Tıbbi Hizmetler ve Teknikler Bölümü, ESKİŞEHİR*
saglameg@gmail.com

1,3,2,4-ditiadifosfetan-2,4-disülfürler (pertiyofosfonik asit anhidritler) organoditiyofosfor bileşiklerinin sentezinde kullanılan başlangıç maddesidir [1,2]. Organo-ditiyofosfor bileşiklerinin birçok endüstriyel alanda uygulaması vardır. Bunlara, makina parçalarındaki yağlayıcılarda antioksidant katkı maddesi olarak ilave edilmesi bir örnektir [3]. Bu çalışmada, yeni organo-ditiyofosfor bileşiklerinin sentezinde altenatif olarak öngörülen orijinal bir pertiyofosfonik asit anhidriti Berzelius reaktifinin 1,2-dimetoksibenzenle reaksiyonundan sentezlenmiştir (Şekil 1). 2,4-*bis*(1,2-dimetoksifenil)-1,3-dithia-2,4-difosfetan 2,4-disülfür'ün çeşitli aromatik ve alifatik alkollerle nükleofilik reaksiyonundan, yeni ditiyofosfonik asitleri elde edildi ([HLn, n=1, metil-; n=2, etil-; n=3, n-butil-; n=4, 3-pentil-; n=5, benzil-). Bu asitler daha sonra amonyum ditiyofosfonat tuzlarına dönüştürüldü (NH_4Ln). Amonyum ditiyofosfonatların Ni(II) tuzuyla reaksiyonundan, yeni dört koordinasyonlu Ni(II) ditiyofosfonat kompleksleri sentezlendi ($[Ni(Ln)_2]$). Bileşiklerin yapıları, elementel analizi, kütle spektroskopisi, FTIR, ^1H-, ^{13}C-, ^{31}P- NMR spektroskopisiyle karakterize edildi.



Şekil 1. Yeni 2,4-*bis*(1,2-dimetoksifenil)-1,3-dithia-2,4-difosfetan 2,4-disülfür sentez reaksiyonu.

Anahtar Kelimeler: Pertiyofosfonik asit anhidritler, 1,3,2,4-ditiadifosfetan-2,4-disülfidler, Ditiyofosfonik Asit, Ditiyofosfonato kompleksleri, Organo-ditiyofosfor Kompleksleri

Teşekkür: Bu çalışma Yozgat Bozok Üniversitesi, Proje Koordinasyon Uygulama ve Araştırma Merkezi, BAP 6602c-FEN/20-359 kodlu projesiyle desteklenmektedir.

KAYNAKLAR:

[1.] Van Zyl W.E., Fackler JP., *Phosphorus, Sulfur Silicon Relat. Elem.*, 167, 117-132, 2000.
[2.] Fay P., Lankelma H.P., *J. Am. Chem. Soc.*, 74, 4933-4935, 1952.
[3.] Colclough Soyad T., Soyad A., *Ind. Eng. Chem. Res.*, 26, 1888-1895, 1987.

Figure 6.6. National congress 2 within the scope of the thesis.

7. REFERENCES

[1] G.M. Kosolapoff, J. Wiley, Organophosphorus compounds. By Gennady M. Kosolapoff. John Wiley and Sons, Inc., New York, 1950. 376 pp, Journal of the American Pharmaceutical Association (Scientific ed.), 39 (1950) 704.

[2] L. Malatesta, R. Pizzotti, CA 2012."The reaction betwen phosphorus pentasulfide and Grignard compounds", Gazz. Chim. Italy, 76 (1947) 167-181.

[3] V. Kabra, S. Mitharwal, S. Singh, Synthesis and Insecticidal Activity of Novel Dithiophosphonates, Phosphorus, Sulfur, and Silicon and the Related Elements, 184 (2009) 2431-2442.

[4] G.M. Kishore, D.M. Shah, Amino Acid Biosynthesis Inhibitors As Herbicides, Annual Review of Biochemistry, 57 (1988) 627-663.

[5] A. Amir, A.H. Sayer, A. Ezra, B. Fischer, Methylenediphosphonotetrathioate: Synthesis, Characterization, and Chemical Properties, Inorganic Chemistry, 52 (2013) 3133-3140.

[6] T. Dang, I.S. Nizamov, R.Z. Salikhov, L.R. Sabirzyanova, V.V. Vorobev, T.I. Burganova, M.M. Shaidoullina, E.S. Batyeva, R.A. Cherkasov, T.I. Abdullin, Synthesis and characterization of pyridoxine, nicotine and nicotinamide salts of dithiophosphoric acids as antibacterial agents against resistant wound infection, Bioorganic & Medicinal Chemistry, 27 (2019) 100-109.

[7] I.S. Nizamov, T.G. Belov, I.D. Nizamov, Y.N. Nikitin, G.R. Akhmedova, O.V. Shilnikova, I.D. Timushev, R.Z. Salikhov, M.P. Shulaeva, O.K. Pozdeev, E.S. Batyeva, R.A. Cherkasov, Pyridoxonium salts of chiral and cyclic dithiophosphoric and bisdithiophosphonic acids and their antimicrobial activities, Phosphorus, Sulfur, and Silicon and the Related Elements, 196 (2021) 431-438.

[8] E.G. Sağlam, S. Akkoç, Y. Zorlu, E. Bulat, A. Akgün, New phenanthroline nickel(II) organodithio-phosphorus complexes: Syntheses, structural characterizations and in vitro cytotoxic activity studies, Polyhedron, 199 (2021) 115097.

[9] H.P.S. Chauhan, A. Bakshi, S. Bhatiya, Synthetic, spectral as well as in vitro antimicrobial studies on some bismuth(III) bis(N,N-dialkyldithiocarbamato) alkylenedithiophosphates, Applied Organometallic Chemistry, 24 (2010) 317-325.

[10] A. Rotar, A. Silvestru, C. Silvestru, J.E. Drake, M.B. Hursthouse, M.E. Light, L. Bunaciu, P. Bunaciu, Structure and in vitro antibacterial activity of

BuSnCl3−n[(OPPh2)(SPPh2)N]n (n = 1, 2), Applied Organometallic Chemistry, 19 (2005) 555-562.
[11] S. Bhatiya, H.P.S. Chauhan, N. Carpenter, Preparation, spectroscopic, thermal and powder X-ray diffraction characterization, and antimicrobial activities of mixed bis(O,O′-diisopropyldithiophosphato-S,S′)antimony(III) derivatives with some oxygen and sulfur donor ligands, Applied Organometallic Chemistry, 32 (2018) e4026.
[12] I.Y. Fleitlikh, N.A. Grigorieva, O.A. Logutenko, Extraction of Non-Ferrous Metals and Iron with Systems based on Bis(2,4,4-Trimethylpentyl)Dithiophosphinic Acid (CYANEX 301), A Review, Solvent Extraction and Ion Exchange, 36 (2018) 1-21.
[13] M. Jafari, S. Chehreh Chelgani, S.Z. Shafaie, H. Abdollahi, E. Hadavandi, Study effects of conventional flotation reagents on bioleaching of zinc sulfide, Journal of Industrial and Engineering Chemistry, 78 (2019) 364-371.
[14] N. Tercero, D.R. Nagaraj, R. Farinato, A Critical Overview of Dithiophosphinate and Dithiophosphate Interactions with Base Metal Sulfides and Precious Metals, Mining, Metallurgy & Exploration, 36 (2019) 99-110.
[15] İ. Çelik, A. Çeker, R. Belge, Nükleer Enerji: Türkiye ve Dünya Ölçeğinde Bir Değerlendirme, Yeni Fikir Dergisi, 7 (2015) 55-68.
[16] J. Chen, M. Wei, X. Liu, J. Wang, Back-end of nuclear fuel cycle in China, Progress in Nuclear Energy, 54 (2012) 46-48.
[17] Z. Wang, N. Pu, Y. Tian, C. Xu, F. Wang, Y. Liu, L. Zhang, J. Chen, S. Ding, Highly Selective Separation of Actinides from Lanthanides by Dithiophosphinic Acids: An in-Depth Investigation on Extraction, Complexation, and DFT Calculations, Inorganic Chemistry, 58 (2019) 5457-5467.
[18] E. Bellande, V. Comazzi, J. Laine, M. Lecayon, R. Pasqualini, A. Duatti, D. Hoffschir, Synthesis and biodistribution of nitrido technetium-99m radiopharmaceuticals with dithiophosphinate ligands: a class of brain imaging agents, Nuclear Medicine and Biology, 22 (1995) 315-320.
[19] B.F. Monzyk, P.J. Usinowicz, D.R. Heiss, V.V. Gadkari, J.T. Stropki, Formulations and methods to reduce hexavalent chrome contamination, in, 2017.
[20] J. Chen, X. He, J. Wang, Nuclear fuel cycle-oriented actinides separation in China, Radiochimica Acta, 102 (2014) 41-51.
[21] A.T. Kassem, Y.T. Selim, N. El-Said, Hollow Fiber Supported Liquid Membrane

for Separation and Recovery of ¹⁵²⁺¹⁵⁴Eu and ⁹⁰Sr from Aqueous Acidic Wastes, American Journal of Analytical Chemistry, 06 (2015) 631-643.
[22] V.N.H. Nguyen, T.H. Nguyen, M.S. Lee, Review on the Comparison of the Chemical Reactivity of Cyanex 272, Cyanex 301 and Cyanex 302 for Their Application to Metal Separation from Acid Media, Metals, 10 (2020) 1105.
[23] X. Yang, L. Xu, A. Zhang, C. Xiao, Organophosphorus Extractants: A Critical Choice for Actinides/Lanthanides Separation in Nuclear Fuel Cycle, Chemistry – A European Journal, 29 (2023) e202300456.
[24] M. Oh, K. Lee, R.I. Foster, I.-S. Kim, C.-H. Lee, Applicability Study of Co and Eu Extraction Using Solvent from Ca Rich HCl Solution, Archives of Metallurgy and Materials, vol. 68 (2023) 123-126.
[25] S.M. Ghoreishi, K. Ansari, H.S. Ghaziaskar, Supercritical extraction of toxic heavy metals from aqueous waste via Cyanex 301 as chelating agent, The Journal of Supercritical Fluids, 72 (2012) 288-297.
[26] I.S. Nizamov, A.A. Yakovlev, I.D. Nizamov, D.A. Terenzhev, K.A. Ivshin, O.N. Kataeva, M.P. Shulaeva, O.K. Pozdeev, E.S. Batyeva, R.A. Cherkasov, Chiral S-stannyl dithiophosphates and dithiophosphonates on the basis of monoterpenols, Applied Organometallic Chemistry, 32 (2018) e4320.
[27] A. Saadat, A. Banaee, P. McArdle, K. Zare, K. Gholivand, A.A. Ebrahimi Valmoozi, Ni(II) complexes of dithiophosphonic acids, Journal of Chemical Sciences, 126 (2014) 1125-1133.
[28] C. Aydemir, S. Solak, G. Acar Doganlı, T. Sensoy, D. Arar, N. Bozbeyoglu, N. Mercan Dogan, P. Lönnecke, E. Hey-Hawkins, M. Sekerci, M. Karakus, Synthesis, Characterization, and Antibacterial Activity of Dithiophosphonates and Amidodithiophosphonates, Phosphorus, Sulfur, and Silicon and the Related Elements, 190 (2015) 300-309.
[29] B.K. Keppler, C. Silvestru, I. Haiduc, Antitumour Organometallics. III. In Vivo Activity of Diphenylantimony(III) and Diorganotin(IV) Dithiophosphorus Derivatives Against P388 Leukemia, Metal-based drugs, 1 (1994) 73-77.
[30] B.C. Froehler, C.A. Buhr, Hydrogen phosphonodithioate compositions, in, 1993.
[31] B.C. Froehler, C.A. Buhr, Nucleoside hydrogen phosphonodithioate diesters and

activated phosphonodithioate analogues, in, 2004.
[32] W. Feng, X.-Y. Teo, W. Novera, P.M. Ramanujulu, D. Liang, D. Huang, P.K. Moore, L.-W. Deng, B.W. Dymock, Discovery of New H2S Releasing Phosphordithioates and 2,3-Dihydro-2-phenyl-2-sulfanylenebenzo[d][1,3,2]oxazaphospholes with Improved Antiproliferative Activity, Journal of Medicinal Chemistry, 58 (2015) 6456-6480.
[33] X.-b. Yang, Methods and compositions of improved modified siRNA, in, 2015.
[34] A. Lowe, M. Whittaker, P. Dieterich, M. Polywka, E. Cossimino, Dithiophosphato-Platinum-Complexes for The Treatment of Cancer, in, 2005.
[35] S. Kumar, A. Syed, S. Andotra, R. Kaur, Vikas, S.K. Pandey, Investigation of synthesized new vanadium(III) complexes of ditolyldithiophosphate ligands by spectroscopic, cyclic voltammetric, DFT, antimicrobial and cytotoxic studies, Journal of Molecular Structure, 1154 (2018) 165-178.
[36] T. Ozturk, E. Ertas, O. Mert, A Berzelius Reagent, Phosphorus Decasulfide (P4S10), in Organic Syntheses, Chemical Reviews, 110 (2010) 3419-3478.
[37] Demselben, Ueber die Verbindungen des Phosphors mit Schwefel, Justus Liebigs Annalen der Chemie, 46 (1843) 251-281.
[38] A.H. Cowley, The structures and reactions of the phosphorus sulfides, Journal of Chemical Education, 41 (1964) 530.
[39] C.J. Romieux, L.J. Christmann, Rubber accelerator and method of using the same, in, 1927.
[40] D. Sharma, A. Radha, P. Kumar, S. Kumar, A.K. Jassal, S. Lata, Vikas, S.K. Pandey, N-donor stabilized complexes of nickel(II) diphenyldithiophosphates: single-crystal X-ray, HSA and computational analysis, Transition Metal Chemistry, 45 (2020) 531-544.
[41] S.M. Darling, L. Chien-Wei, Lubricating oil additive, in, 1956.
[42] H.Z. Lecher, R.A. Greenwood, K.C. Whitehouse, T.H. Chao, The Phosphonation of Aromatic Compounds with Phosphorus Pentasulfide, Journal of the American Chemical Society, 78 (1956) 5018-5022.
[43] P.J. Wheatley, 50. An X-ray diffraction determination of the crystal and molecular structure of “methyl metadithiophosphonate,”[CH3·PS2]2, Journal of the Chemical Society (Resumed), (1962) 300-302.
[44] P.E. Newallis, J.P. Chupp, L.C.D. Groenweghe, Thionophosphine Sulfides. I. Preparation and Use in the Friedel-Crafts Reaction1, The Journal of Organic Chemistry,

27 (1962) 3829-3831.
[45] G. Salbeck, Synthese Neuer Phosphor Enthaltender Heterocyclen (Umsetzung Bifunktioneller Verbindüngen Mit Dithiophosphonsäureanhydriden), Phosphorus and Sulfur and the Related Elements, 9 (1980) 175-181.
[46] R. Appel, F. Knoch, H. Kunze, The First Organodithioxophosphorane, Angewandte Chemie International Edition in English, 22 (1983) 1004-1005.
[47] H. Keck, W. Kuchen, Massenspektrometrische Untersuchungen An Organophosphorverbindüngen I Zum Massenspektrometrischen Fragmentierungsverhalten von Dithio- und Thiophosphonsäureanhydriden, Phosphorus and Sulfur and the Related Elements, 4 (1978) 173-178.
[48] H. Bock, M. Kremer, B. Solouki, M. Binnewies, Gasphasen-Reaktionen, 85[1] Darstellung und Photoelektronen-Spektrum von Ethyldithioxo-λ5-phosphoran H5C2-P(=S)2, Chemische Berichte, 125 (1992) 315-320.
[49] K. Krüger, G. Grossmann, U. Fleischer, R. Franke, W. Kutzelnigg, Ab initio IGLO calculations of 31P NMR shielding tensors of thiophosphoryl compounds. I—dithiadiphosphetanes and dithioxophosphoranes, Magnetic Resonance in Chemistry, 32 (1994) 596-604.
[50] H. Beckmann, G. Großmann, G. Ohms, J. Sieler, New perthiophosphonic acid anhydrides and the direct indication of the dimer-monomer equilibrium. NMR and X-Ray Studies, Heteroatom Chemistry, 5 (1994) 73-83.
[51] G. Ohms, A. Treichler, G. Grossmann, Die Struktur Von Alkyl- Und Arylperthiophosphonsäureanhydriden In Losung, Phosphorus, Sulfur, and Silicon and the Related Elements, 45 (1989) 95-101.
[52] G. Ohms, G. Großmann, B. Buchta, A. Treichler, NMR-spektroskopische Untersuchung von 2,4-Dilsopropyl-2,4-dithioxo-1,3,2λ5-,4λ5-dithiadiphosphetan, Zeitschrift für Chemie, 29 (1989) 138-139.
[53] C. Lensch, W. Clegg, G.M. Sheldrick, Preparation and crystal structures of two phosphorus–sulphur rings: (PhP)3S3 and (PhP)2S4, Journal of the Chemical Society, Dalton Transactions, (1984) 723-725.
[54] C. Lensch, G.M. Sheldrick, Preparation and crystal structures of two phosphorus–sulphur rings: (RPS)4 and (RPS2)2(R = C6H2Me3-2,4,6), Journal of the Chemical Society, Dalton Transactions, (1984) 2855-2857.

[55] A.M.Z. Slawin, D.J. Williams, P.T. Wood, J.D. Woollins, The preparation and X-ray structure of naphthalenedithiadiphosphetanedisulphide, Journal of the Chemical Society, Chemical Communications, (1987) 1741-1741.

[56] J.T. Shore, W.T. Pennington, M.C. Noble, A.W. Cordes, Crystal Structure of t-bütyl Perthiophosphonic Anhydride, (t-C4H9PS2)2, and its Selenium Analog (t-C4H9PSe2)2, Phosphorus and Sulfur and the Related Elements, 39 (1988) 153-157.

[57] G. Ohms, G. Grossmann, H. Beckmann, Dithiadiphosphetanes. NMR Studies in Solution and Solid State, Phosphorus, Sulfur, and Silicon and the Related Elements, 65 (1992) 127-130.

[58] J.J. Daly, A Least-squares Rejinement of the Xtructure of "Methyl Metadithiophosphonate" [CH3PS2]2, Journal of the Chemical Society (Resumed), (1964) 4065.

[59] W.E. Van Zyl, J.P. Fackler, A General and Convenient Route to Dithiophosphonate Salt Derivatives, Phosphorus, Sulfur, and Silicon and the Related Elements, 167 (2000) 117-132.

[60] M. Baudler, H.-W. Valpertz, Notizen: Beiträge zur Chemie des Phosphors XXXV. Reaktion von Organyl-dichlor-phosphinen mit Disulfan, Zeitschrift für Naturforschung B, 22 (1967) 222-223.

[61] P. Kilian, A.M.Z. Slawin, J.D. Woollins, Novel small organo-P–S/Se heterocycles, Chemical Communications, (2001) 2288-2289.

[62] M.R.S.J. Foreman, A.M.Z. Slawin, J.D. Woollins, 2,4-Diferrocenyl-1,3-dithiadiphosphetane 2,4-disulfide; structure and reactions with catechols and [PtCl2(PR3)2](R = Et or Bun), Journal of the Chemical Society, Dalton Transactions, (1996) 3653-3657.

[63] M. R. StJ. Foreman, J. Novosad, A. M. Z. Slawin, J. Derek Woollins, New organophosphorus–sulfur heterocycles, Journal of the Chemical Society, Dalton Transactions, (1997) 1347-1350.

[64] P.T. Wood, J.D. Woollins, New Phosphorus-Selenium Heterdcycles, Phosphorus, Sulfur, and Silicon and the Related Elements, 41 (1989) 51-56.

[65] R. Kempe, J. Sieler, Crystal structure of 2,4-bis(p-methoxyphenyl)-2,4-dithioxo-1,3,2-λ5,4λ5-dithiadiphosphetane, C14H14P2S4, Zeitschrift für Kristallographie, 202 (1992) 159-160.

[66] G. Grossmann, G. Ohms, K. Krüger, G. Jeschke, P.G. Jones, A. Fischer, Solid-State NMR Studies and Crystal Structure of the Lawesson-Reagent, Phosphorus, Sulfur, and Silicon and the Related Elements, 107 (1995) 57-68.

[67] V. Kaiser, F. Menzel, Crystal structure of 2,4-bis(methylthio)-1,3-dithiaphosphetane-2,4-disulfide, (CH3S)2(P2S2)S2, Zeitschrift für Kristallographie - Crystalline Materials, 206 (1993) 279-280.

[68] F. Menzel, V. Kaiser, W. Brockner, M. Ystenes, Investigation of the conformation of 2,4-bis(methylthio)-2,4-dithioxo-1,3,2,4-dithiadiphosphetane, (CH3S)2P2S4, by crystal structure determination, vibrational analysis and quantum mechanical calculations, Polyhedron, 13 (1994) 579-589.

[69] V. Kaiser, F. Menzel, W. Brockner, M. Ystenes, Crystal structure of 2,4-bis(ethylthio)-2,4-dithioxo- 1,3,2,4-dithiadiphosphetane, (C2H5S)2(P2S2)S2, Zeitschrift für Kristallographie - Crystalline Materials, 207 (1993) 306-307.

[70] M.S.J. Foreman, A.M.Z. Slawin, J.D. Woollins, The preparation of a solubilized form of Lawessons reagent and its thionation reactions, Heteroatom Chemistry, 10 (1999) 651-657.

[71] I.S. Nizamov, D.A. Terenzhev, G.G. Shumatbaev, I.D. Nizamov, D.R. Islamov, O.V. Kataeva, R.A. Cherkasov, 2,4-Diorganyl 1,3,2,4-dithiadiphosphetane-2,4-disulfides, their structure and S-silyl dithiophosphonic derivatives, Phosphorus, Sulfur, and Silicon and the Related Elements, 191 (2016) 1576-1577.

[72] E. Fluck, G. Gonzalez, K. Peters, H.-G. Von Schnering, N, N-Dimethylamido-trithiophosphorsäure-anhydrid, Zeitschrift für anorganische und allgemeine Chemie, 473 (1981) 51-58.

[73] I.y.S. Nizamov, O.V. Bolshakova, L.A. Al'metkina, I.n.D. Nizamov, G.G. Sergeenko, L.V. Frolova, D.B. Krivolapov, E.S. Batyeva, I.A. Litvinov, Synthesis and thermal stability of S-trimethylsilyl esters of tetracoordinated phosphorus amidothioacids, Heteroatom Chemistry, 17 (2006) 670-675.

[74] A. Dimitrov, I. Hartwich, P. Neubauer, M. Meisel, 2,4-N,N′-Bis(dialkylamido)-2,4-dithioxo-1,3,2λ5,4λ5-dithiadiphosphetanes, European Journal of Inorganic Chemistry, 2004 (2004) 3842-3845.

[75] M. Meisel, H. Bock, B. Solouki, M. Kremer, Generation and Ionization Pattern of the Iso(valence)electronic Compounds CIP(=O)2 and CIP(=)S)2, Angewandte Chemie

International Edition in English, 28 (1989) 1373-1376.
[76] S. Scheibye, R. Shabana, S.O. Lawesson, C. Rømming, Studies on organophosphorus compounds—XL: Reactions of ketones with 2,4-bis(4-methoxyphenyl)-1,3,2,4-dithiadiphosphetane 2,4-disulfide, Tetrahedron, 38 (1982) 993-1001.
[77] N.M. Yousif, Ylide Chemistry, Part II. Addition Reactions of Triphenyl-Phosphine(Carbonyl)Methylenes with 1,3-Dithia-2,4-Diphosphetane-2,4-Disulfides, Phosphorus, Sulfur, and Silicon and the Related Elements, 46 (1989) 169-174.
[78] Y. Masaaki, T. Kozo, A. Kaori, I. Naoki, Isolation and Characterization of a Stable Dithioxophosphorane, Chemistry Letters, 13 (1984) 317-318.
[79] Z. Kaleta, T. Soós, R. Dembinski, 2,4-Bis[4-[(5,5,6,6,7,7,8,8,9,9,10,10,10-tridecafluorodecyl)oxy]phenyl]-1,3,2,4-dithiadiphosphetane 2,4-Disulfide (Fluorous Lawesson's Reagent), in: Encyclopedia of Reagents for Organic Synthesis (EROS), 2009.
[80] T.B. Rauchfuss, G.A. Zank, Mechanistic studies on the thiation of carbonyls by Lawesson's reagent: The role of a 3-coordinate phosphorus(V) species, Tetrahedron Letters, 27 (1986) 3445-3448.
[81] L. Maier, Organische Phosphorverbindungen VII. Zur Kenntnis der Reaktion von Phenylphosphin mit Schwefel, Helvetica Chimica Acta, 46 (1963) 1812-1818.
[82] J. Navech, J.P. Majoral, R. Kraemer, Synthesis of the first stable metadithiophosphonate, Tetrahedron Letters, 24 (1983) 5885-5886.
[83] T.A. van der Knaap, F. Bickelhaupt, Intermediates in the reaction of a triarylphosphaethene with sulfur, Journal of Organometallic Chemistry, 277 (1984) 351-357.
[84] J. Navech, M. Revel, R. Kraemer, Etude De L'action Du Soufre Sur La tris(tertiobütyl)phenylphosphine, Phosphorus and Sulfur and the Related Elements, 21 (1984) 105-110.
[85] T. Kozo, Y. Masaaki, H. Ken, Sulfurization Reaction of 1,3-Diphosphaallene. X-Ray Structure of cis-2,4-Bis(2,4,6-tri-t-butylphenyl)-1,2,4-thiadiphosphetane 2,4-Disulfide, Chemistry Letters, 19 (1990) 643-646.
[86] T. Sasamori, N. Takeda, N. Tokitoh, Synthesis and reactions of new diphosphenes bearing extremely bulky substituents, Journal of Physical Organic Chemistry, 16 (2003) 450-462.

[87] T. Sasamori, M. Sakagami, N. Tokitoh, Step-wise sulfurization of stable 1,2-bis(ferrocenyl)diphosphene, Journal of Sulfur Chemistry, 34 (2013) 677-683.
[88] T. Sasamori, Y. Suzuki, M. Sakagami, H. Miyake, N. Tokitoh, Structure of Stable Telluradiphosphirane Bearing Bulky Ferrocenyl Ligands, Chemistry Letters, 43 (2014) 1464-1466.
[89] A. Mardyukov, D. Niedek, P.R. Schreiner, Unravelling Lawesson's reagent: the structure of monomeric (4-methoxyphenyl)phosphine disulfide, Chemical Communications, 54 (2018) 2715-2718.
[90] Y. Masaaki, A. De-Lie, T. Kozo, Y. Masafumi, Preparations and Sulfurization Reactions of (2,4-Di-t-butyl-6-methoxyphenyl)phosphine and 1-(2,4-Di-t-butyl-6-methoxyphenyl)-2-(2,4,6-tri-t-butylphenyl)diphosphene, Chemistry Letters, 22 (1993) 2069-2072.
[91] M. Yoshifuji, D.-L. An, K. Toyota, M. Yasunami, 2,4-Di-t-butyl-6-methoxyphenyldithioxophosphorane as a probe for the mechanistic studies of Lawesson's reagent, Tetrahedron Letters, 35 (1994) 4379-4382.
[92] H. Köhler, A. Michaelis, Ueber Phenylphosphin und Phosphobenzol (Diphosphenyl), Berichte der deutschen chemischen Gesellschaft, 10 (1877) 807-814.
[93] M. Yoshifuji, I. Shima, N. Inamoto, K. Hirotsu, T. Higuchi, Synthesis and structure of bis(2,4,6-tri-tert-butylphenyl)diphosphene: isolation of a true phosphobenzene, Journal of the American Chemical Society, 103 (1981) 4587-4589.
[94] R.C. Fischer, P.P. Power, π-Bonding and the Lone Pair Effect in Multiple Bonds Involving Heavier Main Group Elements: Developments in the New Millennium, Chemical Reviews, 110 (2010) 3877-3923.
[95] M. Yoshifuji, K. Shibayama, N. Inamoto, K. Hirotsu, T. Higuchi, Reaction of the diphosphene ArP□PAr (Ar = 2,4,6-But3C6H2) with sulphur: isolation and X-ray structure of the diphosphene monosulphide, Journal of the Chemical Society, Chemical Communications, (1983) 862-863.
[96] S. Takahiro, M. Eiko, T. Norihiro, Chalcogenation Reactions of Overcrowded Doubly Bonded Systems between Heavier Group 15 Elements, Bulletin of the Chemical Society of Japan, 80 (2007) 2425-2435.
[97] T. Sasamori, M. Sakagami, M. Niwa, H. Sakai, Y. Furukawa, N. Tokitoh, Synthesis of a stable 1,2-bis(ferrocenyl)diphosphene, Chemical Communications, 48 (2012) 8562-

8564.
[98] P.E. Newallis, J.P. Chupp, Esters of phosphonodithioic acid, in, 1963.
[99] A.M. Kinnear, E.A. Perren, 661. Formation of organo-phosphorus compounds by the reaction of alkyl chlorides with phosphorus trichloride in the presence of aluminium chloride, Journal of the Chemical Society (Resumed), (1952) 3437-3445.
[100] R. Coelln, G.H.C. Schrader, Process for the preparation of alkyl or aryl dithiophosphonic acid anhydrides, in, 1959.
[101] H. Beckmann, G. Ohms, G. Großmann, K. Krüger, K. Klostermann, V. Kaiser, Synthesis, crystal structure, and NMR spectroscopy of a 1,3,2λ5,4λ5-oxathiadiphosphetane, Heteroatom Chemistry, 7 (1996) 111-118.
[102] Chlorocyclohexyltrithiophosphonic thioanhydride, in, 1974.
[103] W. Kuchen, H. Buchwald, Zur Kenntnis der Organophosphorverbindungen, I. Das Tetraphenyl-cyclo-tetraphosphin, Chemische Berichte, 91 (1958) 2296-2304.
[104] M. Yoshifuji, M. Hirano, K. Toyota, Stable dithioxophosphorane, diselenoxophosphorane, and selenoxophosphine bearing 2,4-Di-t-butyl- 6-(dimethylamino)phenyl group as a new sterically protecting auxiliary, Tetrahedron Letters, 34 (1993) 1043-1046.
[105] M. Ludwig, Process for preparing organic dimeric dithiophosphonic anhydrides, in, 1967.
[106] B. Ziemer, H.-U. Steinberger, A monoclinic polymorph of bis(tert-butylperthiophosphonic) dianhydride, Acta Crystallographica Section C, 56 (2000) e95.
[107] G. Ohms, G. Grossmann, N.A. Mukmeneva, E.N. Cheresova, NMR-spektroskopische Untersuchung von 2,4-Bis(3,5-di-tert.-butyl-4-hydroxyphenyl)-2,4-dithioxo-1,3,2λ5,4λ5-dithiadiphosphetan und ausgewählten Alkoholyseprodukten, Journal für Praktische Chemie, 331 (1989) 361-364.
[108] T.H. Chao, H.Z. Lecher, R.A. Greenwood, Preparation of arylphosphonic acids, in, 1958.
[109] H.Z. Lecher, R.A. Greenwood, Preparation of phosphonothioic dichlorides, tetrachlorophosphoranes, and phosphonic dichlorides, in, 1959.
[110] J.D. Bartleson, Furnace oils containing organic phosphorus compounds, in, 1954.
[111] P. Fay, H.P. Lankelma, The Reaction of Cyclohexene with Phosphorus Pentasulfide, Journal of the American Chemical Society, 74 (1952) 4933-4935.

[112] B.S. Pedersen, S. Scheibye, K. Clausen, S.-O. Lawesson, Studies on organophosphorus compounds XXII The dimer of p-methoxyphenylthionophosphine sulfide as thiation reagent. a new route to O-substituted thioesters and dithioesters, Bulletin des Sociétés Chimiques Belges, 87 (1978) 293-297.

[113] I. Thomsen, K. Clausen, S. Scheibye, S.O. Lawesson, Thiation With 2,4-bis(4-methoxyphenyl)-1,3,2,4-Dithiadiphosphetane 2,4-Disülfide: N-Methylthiopyrrolidone [2-pyrrolidinethione, 1-methyl-], Organic Syntheses, 62 (1984) 158.

[114] G. Lajoie, F. Lépine, L. Maziak, B. Belleau, Facile regioselective formation of thiopeptide linkages from oligopeptides with new thionation reagents, Tetrahedron Letters, 24 (1983) 3815-3818.

[115] M. Yokoyama, Y. Hasegawa, H. Hatanaka, Y. Kawazoe, T. Imamoto, Improved O/S Exchange Reagents, Synthesis, 1984 (1984) 827-829.

[116] C.B. Scott, A. Menefee, D.O. Alford, Synthesis of Unsymmetrical Trialkyl Phosphorotetrathioates, The Journal of Organic Chemistry, 22 (1957) 789-791.

[117] P. Wipf, C. Jenny, H. Heimgartner, 2,4-Bis(4-methylpheylthio)-1,3,2λ5,4λ5-dithiadiphosphetan-2,4-dithion: Ein neues Reagens zur Schwefelung von N,N-disubstituierten Amiden, Helvetica Chimica Acta, 70 (1987) 1001-1011.

[118] H. Davy, A direct conversion of carboxylic acids into dithioesters, Journal of the Chemical Society, Chemical Communications, (1982) 457-458.

[119] N.M. Yousif, U. Pedersen, B. Yde, S.O. Lawesson, Studies on organophosphorus compounds XLVIII Synthesis of Dithioesters from P,S-Containing Reagents and Carboxylic Acids and Their Derivatives, Tetrahedron, 40 (1984) 2663-2669.

[120] J. Mai, Über Schwefelphosphorverbindungen, Berichte der deutschen chemischen Gesellschaft, 44 (1911) 1229-1233.

[121] I.H. Derby, O.D. Cunningham, Froth-flotation process and product for effecting same, in, 1930.

[122] G. Grossmann, H. Beckmann, O. Rademacher, K. Krüger, G. Ohms, Crystal structure, nuclear magnetic resonance spectroscopy and individual gauge for localised orbitals (IGLO) calculations of C6H4P2S6, a new tetrathiadiphosphorinane, and comparison with related P–S compounds, Journal of the Chemical Society, Dalton Transactions, (1995) 2797-2803.

[123] C.M. Loane, J.W. Gaynor, Lubricant, in, 1943.

[124] R.L. May, Reaction products of aliphatic alcohols and terpene-phosphorus sulfide, in, 1944.
[125] H.S. Angel, E.W. Fuller, H.G. Berger, Mineral oil, in, 1945.
[126] H.M. Hajime, H. Yoshioka, C. Austin, Thienyl (2) dithiophosphonic anhydride, in.
[127] H.M. Hajime, H. Yoshioka, 2-thienyl thionophosphine sulfide, in, 1971.
[128] Z. Kaleta, B.T. Makowski, T. Soós, R. Dembinski, Thionation Using Fluorous Lawesson's Reagent, Organic Letters, 8 (2006) 1625-1628.
[129] Z. Kaleta, G. Tárkányi, Á. Gömöry, F. Kálmán, T. Nagy, T. Soós, Synthesis and Application of a Fluorous Lawesson's Reagent: Convenient Chromatography-Free Product Purification, Organic Letters, 8 (2006) 1093-1095.
[130] I.y.S. Nizamov, L.A. Al'Metkina, V.A. Kuznetzov, E.S. Batyeva, 2,4-N,N'-bis(dialkylamido)-2,4-Dithioxo-1,3,2λ 5,4λ5-Dithiadiphosphetanes, Phosphorus, Sulfur, and Silicon and the Related Elements, 92 (1994) 139-147.
[131] E.G. Sağlam, E. Bulat, H. Yılmaz, The Syntheses and Characterization of New Dithiophosphonates derived from Novel 2,4-Bis(methoxytolyl)-1,3-dithia-2,4-diphosphetane 2,4-disulfides and Their Ni(II) Complexes, Journal of The Turkish Chemical Society, 7 (2020) 789-800.
[132] E. Bulat, E.G. Sağlam, C.T. Zeyrek, S. Akkoç, Y. Zorlu, H. Dal, Ni(II) complexes with 1,3,2,4-dithiadiphosphetane 2,4-disulfide-based ligands: Structural insights, theoretical studies, and anticancer activities, Applied Organometallic Chemistry, 36 (2022) e6821.
[133] E.G. Sağlam, E. Bulat, C.T. Zeyrek, S. Akkoç, Y. Zorlu, H. Yılmaz, 2,4-Bis(2,4-dimethoxyphenyl)-1,3-dithia-2,4-diphosphetane 2,4-disulfide and its derivatives: Syntheses, structural characterizations, anticancer activities, and theoretical studies on some dithiophosphonato Ni(II) complex, Journal of Molecular Structure, 1272 (2023) 134197.
[134] D. Picthall, B.A. Surgenor, P. Kilian, Convenient and Scalable Synthesis of Aryldichlorophosphines and Primary Arylphosphines via Perthiophosphonic Anhydrides, Synthesis, 55 (2023) 919-926.
[135] M. Meisel, C. Donath, Formation and Structural Aspects of Four-, Five-, and Six-Membered Phosphorus Nitrogen Ring Compounds, Phosphorus, Sulfur, and Silicon and the Related Elements, 64 (1992) 63-69.

[136] W. Klingen, R. Ott, H. Hahn, Uber die Darstellung und Eigenschaften von Hexathio- und Hexaselenohypodiphosphaten, Zeitschrift für anorganische und allgemeine Chemie, 396 (1973) 271-278.
[137] P. Toffoli, P. Khodadad, N. Rodier, Structure cristalline de l'hexathiodimetaphosphate d'argent, Ag2P2S6, Acta Crystallographica Section B, 34 (1978) 3561-3564.
[138] C. Wibbelmann, W. Brockner, B. Eisenmann, H. Schäfer, Kristallstruktur und Schwingungsspektren des Thalliumhexathiometadiphosphates Tl2P2S6 / Crystal Structure and Vibrational Spectra of Tl2P2S6, Zeitschrift für Naturforschung B, 38 (1983) 1575-1580.
[139] W. Klingen, G. Eulenberger, H. Hahn, Uber die Kristallstrukturen von Fe2P2Se6 und Fe2P2S6, Zeitschrift für anorganische und allgemeine Chemie, 401 (1973) 97-112.
[140] C. Gieck, F. Rocker, V. Ksenofontov, P. Gütlich, W. Tremel, “Supramolecular” Solid-State Chemistry: Interpenetrating Diamond-Type Frameworks of U4+ Ions Linked by S,S′-Bidentate P2S62− Molecular Rods in UP4S12, Angewandte Chemie International Edition, 40 (2001) 908-911.
[141] C. Neuhausen, S.T. Hatscher, M. Panthöfer, W. Urland, W. Tremel, Comprehensive Uranium Thiophosphate Chemistry: Framework Compounds Based on Pseudotetrahedrally Coordinated Central Metal Atoms, Zeitschrift für anorganische und allgemeine Chemie, 639 (2013) 2836-2845.
[142] M. Gjikaj, C. Ehrhardt, W. Brockner, Rb2P2S6 – A New Alkali Thiophosphate: Crystal Structure and Vibrational Spectra of Rubidium Hexathiodiphosphate(V), Zeitschrift für Naturforschung B, 61 (2006) 1049-1053.
[143] A. Kuhn, R. Eger, J. Nuss, B.V. Lotsch, Synthesis and Structural Characterization of the Alkali Thiophosphates Na2P2S6, Na4P2S6, K4P2S6, and Rb4P2S6, Zeitschrift für anorganische und allgemeine Chemie, 640 (2014) 689-692.
[144] G.B. Jin, S. Skanthakumar, R.G. Haire, L. Soderholm, J.A. Ibers, Neptunium Thiophosphate Chemistry: Intermediate Behavior between Uranium and Plutonium, Inorganic Chemistry, 50 (2011) 9688-9695.
[145] A. Kuhn, L.M. Schoop, R. Eger, B.V. Lotsch, Synthesis and Characterization of Copper Hexathiometadiphosphate Cu2P2S6, Zeitschrift für anorganische und allgemeine Chemie, 642 (2016) 356-360.

[146] E.G. Sağlam, S. Erden, Ö. Tutsak, D.E. Bayraktepe, Z.Y. Durmuş, H. Dal, A. Ebinç, Syntheses, characterization of and studies on the electrochemical behaviour of ferrocenyl dithiophosphonates and 4-methoxyphenyl dithiophosphonates, Phosphorus, Sulfur, and Silicon and the Related Elements, 192 (2017) 322-329.

[147] M.-E. Eleftheriou, J. Novosad, D.J. Williams, J.D. Woollins, Reactions of 1,3-epithionaphtho[1,8-cd][1,2λ5,6λ5]thiadiphosphinine-1,3-dithione; the preparation and X-ray structure of NpP(S)(SMe)SP(S)(OMe), the first C3P2S ring, Journal of the Chemical Society, Chemical Communications, (1991) 116-117.

[148] R. Shabana, L.S. Boulos, Y.M. Shaker, The reaction of Lawesson's reagent with trihydroxy compounds, Heteroatom Chemistry, 10 (1999) 25-30.

[149] C.M. Thomas, A. Neels, H. Stœckli-Evans, G. Süss-Fink, Synthesis and structure of [(C5H5)Fe(C5H4PS2OCH2C6H4N3)]−, a new phosphonodithioate derivative, and its coordination chemistry with rhodium(I) and nickel(II), Journal of Organometallic Chemistry, 633 (2001) 85-90.

[150] I.P. Gray, H.L. Milton, A.M.Z. Slawin, J.D. Woollins, Synthesis and structure of [Fc(RO)PS2]− complexes, Dalton Transactions, (2003) 3450-3457.

[151] M. Karakus, P. Lönnecke, D. Yakhvarov, E. Hey-Hawkins, Heterobimetallic Nickel(II) Complexes of Ferrocenyldithiophosphonates. Molecular Structures of [{FcP(OR)S2}2Ni] [Fc = Fe(η5-C5H4)(η5-C5H5), R = Et, Pri, Bus, Bui], Zeitschrift für anorganische und allgemeine Chemie, 630 (2004) 1444-1450.

[152] P.I. Gryaznov, O.E. Naumova, D.R. Alimova, D.B. Krivolapov, I.A. Litvinov, V.A. Al'fonsov, Reaction of Lawesson Reagent with 1,2-(N-Benzyliden)iminoalcohols, Russian Journal of General Chemistry, 75 (2005) 1744-1749.

[153] A.A. El-Kateb, N.M. Abd El-Rahman, Synthesis of New Heterocyclic Compounds Using Lawesson Reagent, Phosphorus, Sulfur, and Silicon and the Related Elements, 181 (2006) 249-254.

[154] I. Haiduc, G. Mezei, R. Micu-Semeniuc, F.T. Edelmann, A. Fischer, Differing Coordination Modes of (O-Alkyl)-p-Ethoxyphenyldithiophosphonato Ligands in Copper(I), Silver(I) and Gold(I) Triphenylphosphine Complexes, Zeitschrift für anorganische und allgemeine Chemie, 632 (2006) 295-300.

[155] M.d.C. Hernández-Galindo, V. Jancik, M.M. Moya-Cabrera, R.A. Toscano, R. Cea-Olivares, 2D hydrogen bond networks in the crystals of

[(NH4·H2O)2][(RO)(Fc)P(S)2]2 (R=3-(BzO)-Bz, 4-(n-Bu)-Bz, Bz=benzyl), Journal of Organometallic Chemistry, 692 (2007) 5295-5302.

[156] M. Karakus, P. Lönnecke, M. Hildebrand, E. Hey-Hawkins, Chiral Heterobimetallic Gold(I) Ferrocenyldithiophosphonato Complexes, Zeitschrift für anorganische und allgemeine Chemie, 637 (2011) 983-987.

[157] L.S. Boulos, H.A. Abdel-Malek, N.F. El-Sayed, M.E. Moharam, Scope and Limitation of the Reactions of 3-Imino Derivatives of Pentane-2,4-Diones with Organophosphorus Reagents, Phosphorus, Sulfur, and Silicon and the Related Elements, 187 (2012) 697-710.

[158] R.A. Cherkasov, I.S. Nizamov, Y.M. Martianov, L.A. Almetkina, Y.N. Nikitin, R.R. Shamilov, Thiophosphorylation of Pharmacophoric Phenols, Diols, and Triols, Phosphorus, Sulfur, and Silicon and the Related Elements, 188 (2013) 24-26.

[159] I.S. Nizamov, G.T. Gabdullina, L.A. Al'metkina, R.R. Shamilov, R.A. Cherkasov, Thiophosphorylation of thymol with phosphorus sulfides, Russian Journal of Organic Chemistry, 49 (2013) 145-146.

[160] G.K. Çılgı, M. Karakuş, M. Ak, Ferrocenyl dithiophosphonate functionalized inorganic–organic hybrid conductive polymer with green color in neutral state, Synthetic Metals, 180 (2013) 25-31.

[161] I.S. Nizamov, E.S. Batyeva, G.G. Shumatbaev, I.D. Nizamov, R.A. Cherkasov, Dithiophosphorylation of paracetamol, Russian Journal of Organic Chemistry, 50 (2014) 1755-1756.

[162] M.d.C. Hernández-Galindo, M. Moya-Cabrera, V. Jancik, R.A. Toscano, R. Cea-Olivares, Synthesis and structural characterization of organotellurium(IV) complexes bearing ferrocenyldithiophosphonate ligands. The first examples of tellurium dithiophosphonates, Journal of Organometallic Chemistry, 772-773 (2014) 280-286.

[163] T. Soganci, M. Ak, S. Ocal, M. Karakus, Ferrocenyldithiophosphonate Containing Conducting Polymers and Theirs Electrochromic Application, Journal of Inorganic and Organometallic Polymers and Materials, 25 (2015) 1011-1018.

[164] I.S. Nizamov, E.N. Nikitin, E.S. Batyeva, I.D. Nizamov, M.P. Shulaeva, O.K. Pozdeev, R.A. Cherkasov, Dithiophosphonation of 4-(1H-pyrrol-1-yl)phenol and 4-(1H-imidazol-1-yl)phenol, Russian Journal of Organic Chemistry, 51 (2015) 1272-1276.

[165] I.S. Nizamov, D.A. Terenzhev, I.D. Nizamov, G.G. Shumatbaev, E.S. Batyeva,

R.A. Cherkasov, Dithiophosphorylation of trimethylsilyl ethers of carvacrol and thymol, Russian Journal of General Chemistry, 86 (2016) 564-569.
[166] E.G. Sağlam, E. Bulat, A. Yildirim, Synthesis and Characterization of New Ferrocenyl and 3-methoxytolyl Dithiophosphonates, Hittite Journal of Science and Engineering, 9 (2022) 183-191.
[167] E.G. Sağlam, E. Bulat, C.T. Zeyrek, H. Dal, T. Hökelek, Syntheses of and structural studies on some square planar dithiophosphonato Ni(II) complexes, octahedral pyridine derivatives thereof and X-ray crystallography, DFT and molecular docking studies of the latter, Journal of Molecular Structure, 1178 (2019) 112-125.
[168] W.E. van Zyl, J.M. López-de-Luzuriaga, A.A. Mohamed, R.J. Staples, J.P. Fackler, Dinuclear Gold(I) Dithiophosphonate Complexes: Synthesis, Luminescent Properties, and X-ray Crystal Structures of [AuS2PR(OR‘)]2 (R = Ph, R‘ = C5H9; R = 4-C6H4OMe, R‘ = (1S,5R,2S)-(−)-Menthyl; R = Fc, R‘ = (CH2)2O(CH2)2OMe), Inorganic Chemistry, 41 (2002) 4579-4589.
[169] A.V. Sofronov, L.A. Al’metkina, E.N. Nikitin, I.S. Nizamov, R.A. Cherkasov, Optically active aryldithiophosphonic acids and their salts based on L-(−)-menthol and D-(+)-menthol, Russian Journal of Organic Chemistry, 46 (2010) 300-301.
[170] I.S. Nizamov, G.T. Gabdullina, L.A. Al’metkina, R.R. Shamilov, E.S. Batyeva, R.A. Cherkasov, (1S)-endo-(−)-borneol in the synthesis of optically active phosphorus dithioacids, Russian Journal of General Chemistry, 82 (2012) 1751-1752.
[171] I.S. Nizamov, L.A. Al’metkina, G.T. Gabdullina, R.R. Shamilov, A.V. Sofronov, L.E. Nikitina, S.A. Lisovskaya, N.I. Glushko, R.A. Cherkasov, Chiral phosphorus dithio acids derived from (1S,2S,3S,5R)-(+)-isopinocampheol. Synthesis and fungicidal activity, Russian Chemical Bulletin, 61 (2012) 2370-2371.
[172] I.S. Nizamov, Y.N. Nikitin, I.D. Nizamov, T.G. Belov, A.D. Voloshina, E.S. Batyeva, R.A. Cherkasov, α-d-Glucofuranose and α-d-allofuranose diacetonides and silyl ether of α-d-glucofuranose diacetonide in dithiophosphorylation reactions, Heteroatom Chemistry, 27 (2016) 345-352.
[173] I.S. Nizamov, G.G. Shumatbaev, I.D. Nizamov, R.Z. Salikhov, Y.N. Nikitin, M.P. Shulaeva, O.K. Pozdeev, E.S. Batyeva, R.A. Cherkasov, Cinchona Alkaloids in the Synthesis of Chiral Salts of Phosphorus Dithioacids on the Basis of 1,2:3,4-Di-O-isopropylidene-α-D-galactopyranose, ChemistrySelect, 4 (2019) 1681-1684.

[174] R.A. Cherkasov, I.S. Nizamov, G.T. Gabdullina, L.A. Almetkina, R.R. Shamilov, A.V. Sofronov, Dithiophosphoric and Dithiophosphonic Acids and Their Derivatives on the Basis of Thymol: Synthesis and Antimicrobial Activity, Phosphorus, Sulfur, and Silicon and the Related Elements, 188 (2013) 33-35.
[175] Production of alkyl or aryl dithiophosphonic-acid anhydrides, Chemisches Zentralblatt, 132(27), 9597-9597 (1961) 9597.
[176] N.A. Andreev, O.N. Grishina, Organylphosphonic acid anhydrides and their thio analogs, Zhurnal Obshchei Khimii 52 (1982) 1785-1792.
[177] N.A. Andreev, O.N. Grishina, Sulfonation of cyclopolyphosphines by dithiophosphonic acid anhydrides, Zhurnal Obshchei Khimii, 54 (1984) 1533-1536.
[178] E. Cherezova, O. Cherkasova, N.A. Mukmeneva, Sterically hindered phosphorus dithio acids, Zhurnal Obshchei Khimii, 57 (1987) 2696-2708.
[179] S. Soyleyici, M. Karakus, M. Ak, Transparent-Blue Colored Dual Type Electrochromic Device: Switchable Glass Application of Conducting Organic-Inorganic Hybrid Carbazole Polymer, Journal of The Electrochemical Society, 163 (2016) H679.
[180] A. Bayer, Dithiophosphonic acid esters, in, 1962.
[181] I.P. Gray, A.M.Z. Slawin, J.D. Woollins, Synthesis and Structure of [Fc(EtO)PS2]-Complexes, Zeitschrift für anorganische und allgemeine Chemie, 630 (2004) 1851-1857.
[182] W. Shi, M. Shafaei-Fallah, C.E. Anson, A. Rothenberger, Metal thiophosphonates and related compounds: an emerging area of supramolecular coordination chemistry, Dalton Transactions, (2006) 3257-3262.
[183] M.R.S.J. Foreman, A.M.Z. Slawin, J.D. Woollins, Preparation and X-ray structure of a new organo-P–O–S heterocycle, Journal of the Chemical Society, Chemical Communications, (1995) 2217-2218.
[184] P. Kilián, Jirítouzín, J. Marek, J. Derek Woollins, J. Novosad, Reaction of Naphthalenedithiadiphosphetanedisulphide with Ethylene Glycol, Main Group Chemistry, 1 (1996) 425-429.
[185] M. Karakus, H. Yilmaz, E. Bulak, Synthesis and Characterization of Zn(II) and Cd(II) Complexes with Bisdithiophosphonates, Russian Journal of Coordination Chemistry, 31 (2005) 316-321.
[186] L.A. Al'metkina, I.S. Nizamov, A.V. Sofronov, D.A. Terenzhev, R.A. Cherkasov, (+)-Dimethyl tartrate in the synthesis of optically active bis-arylphosphonodithioic acids,

Russian Journal of Organic Chemistry, 46 (2010) 1581-1582.
[187] M.N. Pillay, B. Omondi, R.J. Staples, W.E. van Zyl, A hexanuclear gold(i) metallatriangle derived from a chiral dithiophosphate: synthesis, structure, luminescence and oxidative bromination reactivity, CrystEngComm, 15 (2013) 4417-4421.
[188] M.N. Pillay, H. van der Walt, R.J. Staples, W.E. van Zyl, C/O/P/S cycles derived from oxidative intramolecular disulfide (–S–S–) coupling of ferrocenyl dithiophosphonates, Journal of Organometallic Chemistry, 794 (2015) 33-39.
[189] I.S. Nizamov, Y.N. Nikitin, T.G. Belov, I.D. Nizamov, A.D. Voloshina, R.A. Cherkasov, 1,2:5,6-Di-O-Cyclohexylidene-d-Mannitol and Its Bis(Trimethylsilyl) Ether in the Dithiophosphorylation Reactions, Heteroatom Chemistry, 27 (2016) 108-113.
[190] G.A. Kutyrev, O.S. Korolev, N.R. Safiullina, E.G. Yarkova, O.E. Lebedeva, R.A. Cherkasov, A.N. Pudovik, Synthesis and properties of bis(dithiophosphonic acids), Zhurnal Obshchei Khimii, 56 (1986) 1227-1233.
[191] W. Przychodzeń, New Products of Reaction of Lawesson's Reagent Wih Diols, Phosphorus, Sulfur, and Silicon and the Related Elements, 179 (2004) 1621-1633.
[192] M. Karakus, H. Yilmaz, Synthesis and characterization of Ni(II), Zn(II), and Cd(II) complexes with dithiophosphonate derivatives, Russian Journal of Coordination Chemistry, 32 (2006) 437-443.
[193] I.y.S. Nizamov, G.T. Gabdullina, I.D. Nizamov, Y.N. Nikitin, L.A. Al'metkina, R.A. Cherkasov, Bisaryldithiophosphonic Acids: Synthesis and Their Reactions with Organyl Chlorosilanes, Germanes, Stannanes, and Plumbanes, Phosphorus, Sulfur, and Silicon and the Related Elements, 185 (2010) 732-742.
[194] R.F. Semeniuc, R.R. Baum, J.J. Veach, K.A. Wheeler, P.J. Pellechia, Metal complexes of ditopic dithiophosphonate ligands built on a naphthalenediimide core, Inorganica Chimica Acta, 400 (2013) 228-238.
[195] G.E. Ayom, S.J. Zamisa, T. Singh, W.E. van Zyl, Polymorphism in pentaerythritol-derived ferrocenyl dithiophosphonates with intramolecular S-S coupling: a structural and computational study, Phosphorus, Sulfur, and Silicon and the Related Elements, (2023) 1-10.
[196] I.S. Nizamov, L.A. Al’metkina, E.N. Nikitin, G.R. Sabirzyanova, A.R. Burilov, M.A. Pudovik, Thiophosphorylation of calix[4]resorcinarenes with 2,4-diaryl-1,3-dithia-2λ5,4λ5-diphosphetane 2,4-disulfides, Russian Journal of Organic Chemistry, 47 (2011)

1504-1507.
[197] I.S. Nizamov, Y.N. Nikitin, L.A. Almetkina, G.R. Sabirzyanova, A.R. Burilov, M.A. Pudovik, Reactions of 2,4-diaryl 1,3,2,4-dithiadiphosphetane- 2,4-disulfides with resorcinol and 1,3-bis(2-hydroxyethoxy) benzene, Journal of Sulfur Chemistry, 32 (2011) 413-417.
[198] I.S. Nizamov, L.A. Al'metkina, G.R. Sabirzyanova, E.N. Nikitin, A.R. Burilov, M.A. Pudovik, Reaction of 2,4-Diaryl-1,3-dithia-2,4-diphosphetane-2,4-disulfides with resorcinol, Russian Journal of General Chemistry, 82 (2012) 342-343.
[199] I.S. Nizamov, G.T. Gabdullina, L.A. Al'metkina, I.D. Nizamov, R.A. Cherkasov, O,O′-ethylenedioxydiethylene bis[S-(triphenylplumbyl)(3,5-di-tert-butyl-4-hydroxyphenyl)phosphonodithioate], Russian Journal of General Chemistry, 78 (2008) 1466-1468.
[200] G. Hua, D.B. Cordes, A.M.Z. Slawin, J.D. Woollins, Application of four-membered ring chalcogenation reagents to the synthesis of new phosphorus-chalcogen heterocycles, ARKIVOC, 2017 (2016) 9-20.
[201] R. Shabana, F.H. Osman, S.S. Atrees, Organophosphorus compounds XIII. The reaction of 2,4-bis(4-methoxyphenyl)-1,3,2,4-dithiadiphosphetane-2,4-disulfide (LR) with dihydric alcohols. A new route to 1,3,2-dioxaphosphorinane, Tetrahedron, 49 (1993) 1271-1282.
[202] R. Shabana, F.H. Osman, S.S. Atrees, Organophosphorus compounds XV. The reaction of 2,4-bis(4-methoxyphenyl)-1,3,2,4-dithiadiphosphetane-2,4-disulfide (Lawesson's Reagent) with aromatic dihydroxy compounds. Simple new route to 1,3,2-dioxaphospholane-2-sulfide, Tetrahedron, 50 (1994) 6975-6988.
[203] G. Hua, D.B. Cordes, A.M.Z. Slawin, J.D. Woollins, Application of One-Pot Three-Component Condensation Reaction for the Synthesis of New Organophosphorus–Sulfur Macrocycles, Synlett, 29 (2018) 1496-1501.
[204] F.M. Raymo, J.F. Stoddart, Interlocked Macromolecules, Chemical Reviews, 99 (1999) 1643.
[205] Y.Z. Shu, Recent Natural Products Based Drug Development: A Pharmaceutical Industry Perspective, journal of Natural Products, 61 (1998) 1053.
[206] E.M. Driggers, S.P. Hale, J. Lee, N.K. Terrett, The exploration of macrocycles for drug discovery — an underexploited structural class, Nature Reviews Drug Discovery, 7

(2008) 608-624.
[207] E. Marsault, M.L. Peterson, Macrocycles Are Great Cycles: Applications, Opportunities, and Challenges of Synthetic Macrocycles in Drug Discovery, Journal of Medicinal Chemistry 54 (2011) 1961.
[208] F. Giordanetto, J. Kihlberg, Macrocyclic Drugs and Clinical Candidates: What Can Medicinal Chemists Learn from Their Properties?, Journal of Medicinal Chemistry, 57 (2014) 278.
[209] A.K. Yudin, Macrocycles: lessons from the distant past, recent developments, and future directions, Chemical Science, 6 (2015) 30.
[210] S. Down, M.B. Dewal, D. Sobransingh, M. Paderes, A.C. Wibowo, M.D. Smaith, J.A. Krause, P.J. Pellechia, L.S. Shimizu, Self-Assembled Phenylethynylene Bis-urea Macrocycles Facilitate the Selective Photodimerization of Coumarin, Journal of the American Chemical Society, 133 (2011) 7025.
[211] J. Montenegro, M.R. Ghadiri, J.R. Granja, Ion Channel Models Based on Self-Assembling Cyclic Peptide Nanotubes, Accounts of Chemical Research, 46 (2013) 2955.
[212] K.E. Griffiths, J.F. Stoddart, Template-directed synthesis of donor/acceptor [2]catenanes and [2]rotaxanes, Pure and Applied Chemistry, 80 (2008) 485.
[213] N.H. Evans, P.D. Beer, Progress in the synthesis and exploitation of catenanes since the Millennium, Chemical Society Reviews, 43 (2014) 4658.
[214] M. Xue, Y. Yang, X. Chi, X. Yan, F. Huang, Development of Pseudorotaxanes and Rotaxanes: From Synthesis to Stimuli-Responsive Motions to Applications, Chemical Reviews, 115 (2015) 7398.
[215] J. Atwood, Comprehensive Supramolecular Chemistry, Pergamon, Oxford, 1996.
[216] G. Hua, J. Du, A.M.Z. Slawin, J.D. Woollins, One-Pot Approach to Organo-Phosphorus–Chalcogen Macrocycles Incorporating Double OP(S)SCn or OP(Se)SeCn Scaffolds: A Synthetic and Structural Study, Chemistry – A European Journal, 22 (2016) 7782-7791.
[217] G. Hua, J. Du, D.B. Cordes, A.M.Z. Slawin, J.D. Woollins, One-Pot Three-Component Condensation Synthesis and Structural Features of Organophosphorus–Sulfur Macrocycles, The Journal of Organic Chemistry, 81 (2016) 4210-4225.
[218] G. Hua, K. Davidson, D. Cordes, J. Du, A. Slawin, J. Woollins, Phosphorus-Sulfur Heterocycles Incorporating an O-P(S)-O or O-P(S)-S-S-P(S)-O Scaffold: One-Pot

Synthesis and Crystal Structure Study, Molecules, 22 (2017) 1687.
[219] I.P. Gray, A.M.Z. Slawin, J. Derek Woollins, Synthesis and characterisation of disulfides and esters derived from their sodium organodithiophosphonate salts, New Journal of Chemistry, 28 (2004) 1383-1389.
[220] J.B. Stanley, Olefin-thionophosphine sulfide reaction products, their derivatives and use thereof as oil and fuel additives, in, 1977.
[221] R. Shabana, M.R. Mahran, T.S. Hafez, Studies on Organophosphorus Compounds Part VIII.1 The Action of 1,3,2,4-Dithiadiphosphetane-2,4-Disülfides on Benzilmonoanils. Novel Synthesis of 4,5-Diphenyl δ4-1,3,2-Thiazaphospholine-2-Sülfide Derivatives, Phosphorus and Sulfur and the Related Elements, 31 (1987) 1-6.
[222] N.M. Yousif, Addition Reactions of Pyridinium-and Related N-Ylides With 1,3,2,4-Dithiadiphosphetane-2,4-Disulfides, Phosphorus, Sulfur, and Silicon and the Related Elements, 44 (1989) 249-254.
[223] A.A. Fahmy, T.S. Hafez, A.F. El-farargy, M.M. Hamad, Studies on Organophosphorus Compounds Reactions of 1,3,2,4-Dithiadiphosphetane-2,4-Disulfides and Alkyl Phosphites with Coumarin Derivatives, Phosphorus, Sulfur, and Silicon and the Related Elements, 57 (1991) 211-215.
[224] A.A. Fahmy, New Organophosphorus Compounds From 2-Hydroxy-4-Amino Benzoic Acid, Phosphorus, Sulfur, and Silicon and the Related Elements, 63 (1991) 81-86.
[225] A.A. Fahmy, Simple New Routes To Phosphorins from 2- Mercapto-1,3,4-Oxa- and Thiadiazole and 3- Mercapto-1,2,4-Triazole, Phosphorus, Sulfur, and Silicon and the Related Elements, 68 (1992) 139-145.
[226] N.M. Yousif, Reaction of Amidoximes with 1,3-Dithia-2,4-Diphosphetane-2,4-Disulfides, Phosphorus, Sulfur, and Silicon and the Related Elements, 73 (1992) 93-98.
[227] R. Shabana, S.S. Atrees, Studies on Organophosphorus Compounds, Part XVI.1 The Reaction of 1,3,2,4- Dithiadiphosphetane-2,4-Disulfide with Benzil Dianils. A Novel Synthesis of 2h-1,3,6,2-Thiadiazaphosphorine-2-Sulfide Derivatives, Phosphorus, Sulfur, and Silicon and the Related Elements, 102 (1995) 9-13.
[228] M. R. StJ. Foreman, A. M. Z. Slawin, J. Derek Woollins, Phosphorus–sulfur–nitrogen heterocycles from diferrocenyl dithiadiphosphetane disulfide, Chemical Communications, (1997) 1269-1270.

[229] M.R.S.J. Foreman, A.M.Z. Slawin, J.D. Woollins, Heterocycles from Diferrocenyl Dithiadiphosphetane Disulfide, Phosphorus, Sulfur, and Silicon and the Related Elements, 124 (1997) 469-472.
[230] M. R. St. John Foreman, A. M. Z. Slawin, J. Derek Woollins, The reaction of dithiadiphosphetane disulfides with dienes, alkenes and thioaldehydes, Journal of the Chemical Society, Dalton Transactions, (1999) 1175-1184.
[231] M.H.N. Arsanious, S.S. Maigali, L.S. Boulos, Scope and Limitation of the Reaction of Benzocycloalkanone Oximes with Lawesson's Reagents, Phosphorus, Sulfur, and Silicon and the Related Elements, 185 (2009) 57-64.
[232] M. El-Hussieny, M.A. Abd-El-Maksoud, S.S. Maigali, F.M. Soliman, A.M. Soliman, Chemistry of Phosphorus Ylides Part 42: Reaction of Dipyridyl Ethanedione with Phosphorus Reagents. Cytotoxic Activity of Phosphanylidene-Cyclobutane, Oxaphosphetane, and Pyridazinone, Phosphorus, Sulfur, and Silicon and the Related Elements, 190 (2015) 1845-1856.
[233] D.-L. AN, Y.-J. ZHANG, Z.-H. PENG, Synthesis and x-ray crystal structure of a novel cyclic phosphonic acid anhydride, Acta Chimica Sinica, 62 (2004) 1166.
[234] A. Ecker, I. Boie, U. Schmidt, Cycloadditionen mit Dithiophosphonsäure-anhydriden; Bildung von Dien-dithiophosphinsäuren, Angewandte Chemie, 83 (1971) 178-178.
[235] A. Ecker, I. Boie, U. Schmidt, Über 3,6-Dihydro-2H-1,2-thiaphosphorin-2-sulfide, Monatshefte für Chemie / Chemical Monthly, 104 (1973) 503-514.
[236] M.R.S. Foreman, A.M.Z. Slawin, J. Derek Woollins, Novel 1,2-thiaphosphetanes from diferrocenyldithiadiphosphetane disulfide, Chemical Communications, (1997) 855-856.
[237] W.E. van Zyl, J.D. Woollins, The coordination chemistry of dithiophosphonates: An emerging and versatile ligand class, Coordination Chemistry Reviews, 257 (2013) 718-731.
[238] I. Haiduc, D.B. Sowerby, S.-F. Lu, Stereochemical aspects of phosphor-1,1-dithiolato metal complexes (dithiophosphates, dithiophosphinates): Coordination patterns, molecular structures and supramolecular associations—I, Polyhedron, 14 (1995) 3389-3472.
[239] I. Haiduc, D.B. Sowerby, Stereochemical aspects of phosphor-1,1-dithiolato metal

complexes: Coordination patterns, molecular structures and supramolecular associations in dithiophosphinates and related compounds, Polyhedron, 15 (1996) 2469-2521.
[240] R.G. Pearson, Hard and Soft Acids and Bases, Journal of the American Chemical Society, 85 (1963) 3533-3539.
[241] H.-L. Liu, H.-Y. Mao, C. Xu, H.-Y. Zhang, H.-W. Hou, Q.-a. Wu, Y. Zhu, B.-X. Ye, L.-J. Yuan, Four novel sulfur-rich complexes: syntheses, crystal structures of three nickel(II) and one cobalt(II) complex with derivatives of Lawesson's Reagent, Polyhedron, 23 (2004) 1799-1804.
[242] G.A. Zank, T.B. Rauchfuss, Thiophosphoryl complexes of bis(cyclopentadienyl)titanium. 1. Synthesis, interconversions, and structures, Organometallics, 3 (1984) 1191-1199.
[243] I.y.S. Nizamov, V.A. Kuznetzov, E.S. Batyeva, Reactions of dithioxo-1,3,2λ5,4λ5-dithiadiphosphetanes with triorganolead derivatives, Heteroatom Chemistry, 8 (1997) 323-327.
[244] R. Jones, D.J. Williams, P.T. Wood, J.D. Woollins, Oxidative addition reaction between lawesson's reagent and Pt(C2H4)(PPh3)2: The preparation and X-ray structure of [Pt{(S2P(S)(C6H4OMe)}(PPh3)2], Polyhedron, 6 (1987) 539-542.
[245] P.T. Wood, J.D. Woollins, The preparation of M(PR3)2 (S2(S)PC6H4OMe) (M=Ni, Pd, Pt) from Lawessons reagent, Transition Metal Chemistry, 12 (1987) 403-405.
[246] I.y.S. Nizamov, G.n.G. Sergeenko, E.S. Batyeva, N.M. Azancheev, V.A. Al'fonsov, Reactions of 1,3,2,4-Dithiadiphosphetane-2,4-disulfides with Alkyl Borates, Main Group Chemistry, 3 (2000) 129-135.
[247] A. Rothenberger, M. Shafaei-Fallah, W. Shi, A recipe for new organometallic polymers and oligomers? Synthesis and structure of an oligo- and a polymeric arrangement of P–S anions, Chemical Communications, (2007) 1499-1501.
[248] X.-Y. Wang, H.-T. Shi, Q. Ma, Q.-F. Zhang, Syntheses and Structures of Silver(I) and Palladium(II) Complexes with Ferrocenyl-phosphonodithiolate Ligands, Zeitschrift für Naturforschung B, 65 (2010) 32-36.
[249] M.C. Aragoni, M. Arca, F. Demartin, F.A. Devillanova, A. Garau, F. Isaia, F. Lelj, V. Lippolis, G. Verani, New [M(R,R'timdt)2] Metal-Dithiolenes and Related Compounds (M = Ni, Pd, Pt; R,R'timdt = Monoanion of Disubstituted Imidazolidine-2,4,5-trithiones): An Experimental and Theoretical Investigation, Journal of the American

Chemical Society, 121 (1999) 7098-7107.
[250] I.P. Gray, A.M. Slawin, J.D. Woollins, Synthesis and structure of [An(RO)PS2]-complexes, Dalton transactions (Cambridge, England : 2003), (2004) 2477-2486.
[251] Y. Özcan, S. İde, M. Karaku, H. Yilmaz, Crystal and Molecular Structures of trans-Nickel(II)-bis[(O-propyln)-(p-methoxyphenyl)dithiophosphonate], Analytical Sciences, 18 (2002) 1285-1286.
[252] M. Arca, A. Cornia, F.A. Devillanova, A.C. Fabretti, F. Isaia, V. Lippolis, G. Verani, New perspectives in phosphonodithioate coordination chemistry. Synthesis and X-ray crystal structure of trans-bis-[O-ethyl-(4-methoxyphenyl)phosphonodithioato] nickel(II), Inorganica Chimica Acta, 262 (1997) 81-84.
[253] H. Hartung, Nickel(II) phenyl-O-ethyldithiophosphonate, Zeitschrift für Chemie, 7 (1967) 241.
[254] E.G. Sağlam, A. Ebinç, C.T. Zeyrek, H. Ünver, T. Hökelek, Structural studies on some dithiophosphonato complexes of Ni(II), Cd(II), Hg(II) and theoretical studies on a dithiophosphonato Ni(II) complex using density functional theory, Journal of Molecular Structure, 1099 (2015) 490-501.
[255] J.P. Fackler, L.D. Thompson, Sulfur chelates 36. Structural characterization of the Trans isomers of the O-ethylphenyldithiophosphonates of Pd(II) and Pt(II), M[S2P(OC2H5)C6H5]2. Cis-Trans isomerization of the planar Pd(II) complex, Inorganica Chimica Acta, 48 (1981) 45-52.
[256] M.C. Aragoni, M. Arca, F. Demartin, Francesco A. Devillanova, C. Graiff, F. Isaia, V. Lippolis, A. Tiripicchio, G. Verani, Ring-Opening of Lawesson's Reagent: New Syntheses of Phosphono- and Amidophosphono-Dithioato Complexes − Structural and CP-MAS 31P-NMR Characterization of [p-CH3OPh(X)PS2]2M (X = MeO, iPrNH; M = NiII, PdII, and PtII), European Journal of Inorganic Chemistry, 2000 (2000) 2239-2244.
[257] E.G. Sağlam, C.T. Zeyrek, H. Dal, H. Ünver, A. Ebinç, New {bis-pyridine-bis-[3-methyl-1-butoxy-(p-methoxyphenyl)phosphonodithioato]}nickel(II) complex: Synthesis, characterization, single crystal structure and theoretical studies, Journal of Molecular Structure, 1201 (2020) 127185.
[258] E.G. Sağlam, S. Akkoç, C.T. Zeyrek, H. Dal, Ö. Tutsak, New heterobimetallic nickel(II) ferrocenyldithiophosphonato complexes: Syntheses, characterization, antiproliferative activity and X-ray, DFT, molecular docking studies on trans-bis-[O-3-

methyl-1-butyl-(ferrocenyl)dithiophosphonato]nickel(II), Inorganica Chimica Acta, 514 (2021) 119991.
[259] S. Sewpersad, New Dithiophosphonate Complexes Of Nickel, Cadmium, Mercury ve Lead, in, Kwazulu Unıversity, South Africa, 2013.
[260] G. Sánchez, J.n. García, D.J. Meseguer, J.L. Serrano, J. Pérez, E.e. Molins, G. López, Organometallic nickel(II) complexes with dithiophosphate, dithiophosphonate and monothiophosphonate ligands, Inorganica Chimica Acta, 357 (2004) 677-683.
[261] M. Karakus, H. Yilmaz, E. Bulak, P. Lönnecke, Crystallographic report: Bis{μ-[O-cyclopentyl(4-methoxyphenyl) dithiophosphonato]1κ:S,2κ:S-[O-cyclopentyl(4-methoxyphenyl)dithiophosphonato]1κ2S,S′} dizinc(II), Applied Organometallic Chemistry, 19 (2005) 396-397.
[262] A.R. Gataulina, D.A. Safin, T.R. Gimadiev, M.V. Pinus, Complexes of podand-containing bis(dithiophosphonate) ligands with cobalt(II), nickel(II) and cadmium(II): recognition of CH2Cl2, Transition Metal Chemistry, 33 (2008) 921-924.
[263] Sağlam E, Bulat E, Acar N, D. İ., New Homodinuclear Alkyl- and Aryl-Dithiophosphonato Cd(II) and Hg(II) complexes: Syntheses and Characterizations, Journal of the Turkish Chemical Society Section A: Chemistry, 7 (2020) 49-64.
[264] M.C. Aragoni, M. Arca, N.R. Champness, M. De Pasquale, F.A. Devillanova, F. Isaia, V. Lippolis, N.S. Oxtoby, C. Wilson, Synthesis and structural characterisation of coordination polymers designed using discrete phosphonodithioato NiII complexes and dipyridyl donor ligands, CrystEngComm, 7 (2005) 363-369.
[265] M.C. Aragoni, M. Arca, F.A. Devillanova, M.B. Hursthouse, S.L. Huth, F. Isaia, V. Lippolis, A. Mancini, S. Soddu, G. Verani, Investigation into the reactivity of the coordinatively unsaturated phosphonodithioato [Ni(MeOpdt)2] towards 2,4,6-tris(2-pyridyl)-1,3,5-triazine: goals and achievements, Dalton transactions (Cambridge, England : 2003), (2007) 2127-2134.
[266] M.C. Aragoni, M. Arca, M. Crespo, F.A. Devillanova, M.B. Hursthouse, S.L. Huth, F. Isaia, V. Lippolis, G. Verani, Investigation on the reactivity of dithiophosphonato/dithiophosphato NiII complexes towards 2,4,6-tris-2-pyridyl-1,3,5-triazine: developments and new perspectives, Dalton Transactions, (2009) 2510-2520.
[267] Y. Ozcan, S. Ide, M. Karakus, H. Yilmaz, trans-Bis[O-2,4-di-tert-butylphenyl (4-methoxyphenyl)dithiophosphonato-kappa(2)S,S']nickel(II), Acta crystallographica.

Section C, Crystal structure communications, 58 (2002) m388-389.
[268] V.G. Albano, M.C. Aragoni, M. Arca, C. Castellari, F. Demartin, F.A. Devillanova, F. Isaia, V. Lippolis, L. Loddo, G. Verani, An unprecedented example of a cis-phosphonodithioato nickel(ii) complex built by an extensive hydrogen bonding supramolecular network, Chemical Communications, (2002) 1170-1171.
[269] APEX2, Version 2014.11-0, Bruker (2014), Bruker AXS Inc., Madison, WI (2014).
[270] v.A. SAINT, Bruker (2013), Bruker AXS Inc., Madison, WI,, (2014).
[271] v. SADABS, Bruker (2014), Bruker AXS Inc., Madison, WI, (2014).
[272] G. Sheldrick, SHELXT - Integrated space-group and crystal-structure determination, Acta Crystallographica Section A, 71 (2015) 3-8.
[273] G. Sheldrick, Crystal structure refinement with SHELXL, Acta Crystallographica Section C, 71 (2015) 3-8.
[274] O.V. Dolomanov, L.J. Bourhis, R.J. Gildea, J.A.K. Howard, H. Puschmann, OLEX2: a complete structure solution, refinement and analysis program, Journal of Applied Crystallography, 42 (2009) 339-341.
[275] A. Spek, Structure validation in chemical crystallography, Acta Crystallographica Section D, 65 (2009) 148-155.
[276] C.F. Macrae, P.R. Edgington, P. McCabe, E. Pidcock, G.P. Shields, R. Taylor, M. Towler, J. van de Streek, Mercury: visualization and analysis of crystal structures, Journal of Applied Crystallography, 39 (2006) 453-457.
[277] M.A. Spackman, D. Jayatilaka, Hirshfeld surface analysis, CrystEngComm, 11 (2009) 19-32.
[278] M.A. Spackman, J.J. McKinnon, Fingerprinting intermolecular interactions in molecular crystals, CrystEngComm, 4 (2002) 378-392.
[279] M.J. Turner, J.J. McKinnon, S.K. Wolff, D.J. Grimwood, P.R. Spackman, D. Jayatilaka, M.A. Spackman, CrystalExplorer17, University of Western Australia, 2017.
[280] J.J. McKinnon, M.A. Spackman, A.S. Mitchell, Novel tools for visualizing and exploring intermolecular interactions in molecular crystals, Acta Crystallographica Section B, 60 (2004) 627-668.
[281] J.J. McKinnon, D. Jayatilaka, M.A. Spackman, Towards quantitative analysis of intermolecular interactions with Hirshfeld surfaces, Chemical Communications, (2007) 3814-3816.

[282] Frisch MJ. Trucks GW. Schlegel HB. Scuseria GE. Robb MA. Cheeseman JR. Scalmani G. Barone V. Mennucci B. Petersson GA. Nakatsuji H. Caricato M. Li X. Hratchian HP. Izmaylov AF. Bloino J. Zheng G. Sonnenberg JL. Hada M. Ehara M. Toyota K. Fukuda R. Hasegawa J. Ishida M. Nakajima T. Honda Y. Kitao O. Nakai H. Vreven T. Montgomery JA. Jr JEP. Ogliaro F. Bearpark M. Heyd JJ. Brothers E. Kudin KN. Staroverov VN. Kobayashi R. Normand J. Raghavachari K. Rendell A. Burant JC. Iyengar SS. Tomasi J. Cossi M. Rega N. Millam JM. Klene M. Knox JE. Cross JB. Bakken V. Adamo C. Jaramillo J. Gomperts R. Stratmann RE. Yazyev O. Austin AJ. Cammi R. Pomelli C. Ochterski JW. Martin RL. Morokuma K. Zakrzewski VG. Voth GA. Salvador P. Dannenberg JJ. Dapprich S. Daniels AD. Farkas Ö. Foresman JB. Ortiz JV. Cioslowski J. Fox DJ (2009) Gaussian 09. Revision A.02. Gaussian. Inc.. Wallingford CT.

[283] Dennington R. Keith T. Millam J (2009) GaussView. Version 5. Semichem. Inc.. Shawnee Mission. KS.

[284] T.H.D. Jr., P.J. Hay, in Modern Theoretical Chemistry, in: P. Ed. H. F. Schaefer III (Ed.), Ed. H. F. Schaefer III, Plenum, New York, 1977, pp. 1-28.

[285] A.D. Becke, Density-functional thermochemistry. IV. A new dynamical correlation functional and implications for exact-exchange mixing, The Journal of Chemical Physics, 104 (1996) 1040-1046.

[286] J.-P. Blaudeau, M.P. McGrath, L.A. Curtiss, L. Radom, Extension of Gaussian-2 (G2) theory to molecules containing third-row atoms K and Ca, The Journal of Chemical Physics, 107 (1997) 5016-5021.

[287] O. Trott, A.J. Olson, AutoDock Vina: Improving the speed and accuracy of docking with a new scoring function, efficient optimization, and multithreading, Journal of Computational Chemistry, 31 (2010) 455-461.

[288] Discovery Studio Visualizer Software. V16.1.015350 (2015). Dassault Systemes Biovia Corp. http://www.accelrys.com.

[289] M.F. Sanner, Python: a programming language for software integration and development, J. Mol. Graph. Model, 17 (1999) 57-61.

[290] B. Kramer, M. Rarey, T. Lengauer, Evaluation of the FLEXX incremental construction algorithm for protein–ligand docking, Proteins: Structure, Function, and Bioinformatics, 37 (1999) 228-241.

[291] A.B. Gurung, M.A. Ali, A. Bhattacharjee, M. AbulFarah, F. Al-Hemaid, F.M. Abou-Tarboush, K.M. Al-Anazi, F.S. Al-Anazi, J. Lee, Molecular docking of the anticancer bioactive compound proceraside with macromolecules involved in the cell cycle and DNA replication, Genetics and molecular research : GMR, 15 (2016).
[292] T. Koopmans, Über die Zuordnung von Wellenfunktionen und Eigenwerten zu den Einzelnen Elektronen Eines Atoms, Physica, 1 (1934) 104-113.
[293] S. Akkoç, Derivatives of 1-(2-(Piperidin-1-yl)ethyl)-1H-benzo[d]imidazole: Synthesis, Characterization, Determining of Electronic Properties and Cytotoxicity Studies, ChemistrySelect, 4 (2019) 4938-4943.
[294] S. Akkoç, Antiproliferative activities of 2-hydroxyethyl substituted benzimidazolium salts and their palladium complexes against human cancerous cell lines, Synthetic Communications, 49 (2019) 2903-2914.
[295] I. Haiduc, Supramolecular aspects of tin and lead chemistry, Applied Organometallic Chemistry, 21 (2007) 476-482.
[296] T.L. Yusuf, C.U. Ibeji, W.E. van Zyl, Nickel(II) complexes from phosphor-dichalcogenide (P/Se2 and P/S2) type ligands: Synthesis, structure and theoretical calculations, Journal of Molecular Structure, 1218 (2020) 128517.
[297] T.J. Ajayi, M. Shapi, Solvent-free mechanochemical synthesis, hirshfeld surface analysis, crystal structure, spectroscopic characterization and NBO analysis of Bis(ammonium) Bis((4-methoxyphenyl) phosphonodithioato)-nickel (II) dihydrate with DFT studies, Journal of Molecular Structure, 1202 (2020) 127254.
[298] M. Karakus, H. Yilmaz, Y. Ozcan, S. Ide, Crystallographic report: Bis{μ-[O-cyclopentyl(4-methoxyphenyl)dithiophosphonato]1κ:S,2κ:S-[O-cyclopentyl(4-methoxyphenyl)dithiophosphonato]-1κ2S,S′}dicadmium(II), Applied Organometallic Chemistry, 18 (2004) 141-142.
[299] L. Ernst, 13C n.m.r. spectroscopy of diethyl alkyl- and benzyl-phosphonates. A study of phosphorus–carbon spin–spin coupling constants over one to seven bonds, Organic Magnetic Resonance, 9 (1977) 35-43.
[300] G.A. Gray, S.E. Cremer, Carbon-13 nuclear magnetic resonance of organophosphorus compounds. III. Phosphorus heterocycles, The Journal of Organic Chemistry, 37 (1972) 3458-3469.
[301] J.M.A. Al-Rawi, M.A. Sheat, N. Ayed, Carbon-13 NMR of some

organophosphorus compounds. 2—chemical shifts and P□C coupling constants of diaryl-, dialkoxy- and diaryloxy-phosphine amines with general formula Y2PNRR', Organic Magnetic Resonance, 22 (1984) 336-339.
[302] G. Kallinowski, W. Vogt, 13C nuclear magnetic resonance study of some phosphinolipids: Assignments and conformational studies, Magnetic Resonance in Chemistry, 27 (1989) 647-652.
[303] G.A. Gray, Carbon-13 nuclear magnetic resonance of organophosphorus compounds. I. Diethyl phosphonates, Journal of the American Chemical Society, 93 (1971) 2132-2140.
[304] L. Yang, D.R. Powell, R.P. Houser, Structural variation in copper(i) complexes with pyridylmethylamide ligands: structural analysis with a new four-coordinate geometry index, τ4, Dalton Transactions, (2007) 955-964.
[305] G.E. Ayom, M.D. Khan, T. Ingsel, W. Lin, R.K. Gupta, S.J. Zamisa, W.E. van Zyl, N. Revaprasadu, Flexible Molecular Precursors for Selective Decomposition to Nickel Sulfide or Nickel Phosphide for Water Splitting and Supercapacitance, Chemistry – A European Journal, 26 (2020) 2693-2704.
[306] T.J. Ajayi, M. Ollengo, L. le Roux, M.N. Pillay, R.J. Staples, S.M. Biros, K. Wenderich, B. Mei, W.E. van Zyl, Heterodimetallic Ferrocenyl Dithiophosphonate Complexes of Nickel(II), Zinc(II) and Cadmium(II) as Sensitizers for TiO2-Based Dye-Sensitized Solar Cells, ChemistrySelect, 4 (2019) 7416-7424.
[307] M.C. Aragoni, M. Arca, F. Demartin, F.A. Devillanova, C. Graiff, F. Isaia, V. Lippolis, A. Tiripicchio, G. Verani, Reactivity of phosphonodithioato NiII complexes: solution equilibria, solid state studies and theoretical calculations on the adduct formation with some pyridine derivatives, Journal of the Chemical Society, Dalton Transactions, (2001) 2671-2677.
[308] M.C. Aragoni, M. Arca, M. Crespo, F.A. Devillanova, M.B. Hursthouse, S.L. Huth, F. Isaia, V. Lippolis, G. Verani, Predictable and unpredictable reactions between 4,4′-dipyridyldisulfide and phosphonodithioato/dithiophosphato NiII complexes: novel coordination polymers and the unique example of 4,4′-dipyridyltrisulfide, CrystEngComm, 9 (2007) 873-878.
[309] M.C. Aragoni, M. Arca, S.J. Coles, M. Crespo Alonso, S.L. Coles, R.P. Davies, M.B. Hursthouse, F. Isaia, R. Lai, V. Lippolis, Coordination polymers and polygons using

di-pyridyl-thiadiazole spacers and substituted phosphorodithioato NiII complexes: potential and limitations for inorganic crystal engineering, CrystEngComm, 18 (2016) 5620-5629.
[310] W. Shi, R. Kelting, M. Shafaei-Fallah, A. Rothenberger, Transformations of P-chalcogenide precursors with a hydrated metal salt, Journal of Organometallic Chemistry, 692 (2007) 2678-2682.
[311] S.E. G, B. E, Veratrol İçerikli Yeni Ditiyofosfonat ve Nikel Komplekslerinin Sentezi ve Yapısal Karakterizasyonu, 33. Ulusal Kimya Kongresi, (2021).
[312] S.E. G, B. E, H. Dal, Yeni 2,4-bis(1,2-Dimetoksifenil)-1,3-Dithia-2,4-Difosfetan 2,4-Disülfür Türevlerinin Sentezi ve Karakterizasyonu, Ulusal Anorganik Kimya Kongresi, (2021).
[313] B. E, S.E. G, H. Dal, Synthesis and characterization of New Dithiophosphonate Ligands, Frühjahrssymposium 2023, (2023).
[314] B. E, S.E. G, S. Akkoç, C.T. Zeyrek, Y. Zorlu, H. Dal, New Dithiophosphonato Ni(II) Complexes: Synthesis, characterization, theoretical and in vitro cytotoxicity studies, Frühjahrssymposium 2023, (2023).

8. CURRICULUM VITAE

Summary

Elif BULAT research interests are:

- Inorganic Chemistry,
- Inorganic Cyclic Compounds,
- Coordination Chemistry,
- Organometallic Chemistry,
- New Ligands,
- Organic Spectroscopy,

Education

PhD in Inorganic Chemistry

August 2023 - Marmara University, Istanbul, Türkiye

Master in Chemistry

July 2018 - Yozgat Bozok University, Yozgat, Türkiye

Bachelor in Chemistry

July 2016 – Yozgat Bozok University, Yozgat, Türkiye

Publications

(1) Ertuğrul Gazi Sağlam*, **Elif Bulat**, Celal Tuğrul Zeyrek, Hakan Dal, and Tuncer Hökelek, "Syntheses of and structural studies on some square planar dithiophosphonato Ni(II) complexes, octahedral pyridine derivatives thereof and X-ray crystallography, DFT and molecular docking studies of the latter", J. Mol. Struct., 1178, 112-125, 2019. https://doi.org/10.1016/j.molstruc.2018.09.084

(2) Ertuğrul Gazi Sağlam*, Senem Akkoç, Yunus Zorlu, **Elif Bulat**, Aziz Akgün, "New phenanthroline nickel(II) organodithio-phosphorus complexes: Syntheses, structural characterizations and *in vitro* cytotoxic activity studies", Polyhedron, 199, 11509791, 1-13, 2021. https://doi.org/10.1016/j.poly.2021.115097

(3) **Elif Bulat**, Ertuğrul Gazi Sağlam*, Celal Tuğrul Zeyrek, Senem Akkoç, Yunus Zorlu, Hakan Dal, "Ni(II) complexes with 1,3,2,4-dithiadiphosphetane 2,4-disulfide-based ligands: Structural insights, theoretical studies, and anticancer activities", Appl

Organomet Chem., e6821, 1-23, 2022. https://doi.org/10.1002/aoc.6821

(4) Ertuğrul Gazi Sağlam*, **Elif Bulat**, Celal Tuğrul Zeyrek, Senem Akkoç, Yunus Zorlu, Hamza Yılmaz, "2,4-Bis(2,4-dimethoxyphenyl)-1,3-dithia-2,4-diphosphetane 2,4-disulfide and its derivatives: Syntheses, structural characterizations, anticancer activities, and theoretical studies on some dithiophosphonato Ni(II) complex", J. Mol. Struct., 1272, 134197, 2023. https://doi.org/10.1016/j.molstruc.2022.134197

(5) Ertuğrul Gazi Sağlam*, **Elif Bulat**, Nurcan Acar and İbrahim Demirel, "New Homodinuclear Alkyl- and Aryl- Dithiophosphonato Cd(II) and Hg(II) complexes: Syntheses and Characterizations." J. Turkish Chem. Soc., Section A: Chemistry (JOTCSA), 7(1), 49-64, 2020. https://doi.org/10.18596/jotcsa.565642

(6) Ertuğrul Gazi Sağlam*, **Elif Bulat**, Hamza Yılmaz, "The Syntheses and Characterization of New Dithiophosphonates derived from Novel 2,4-Bis(methoxytolyl)-1,3-dithia-2,4-diphosphetane 2,4- disulfides and Their Ni(II) Complexes", J. Turkish Chem. Soc., Section A: Chemistry (JOTCSA), 7(3), 789-800, 2020. https://doi.org/10.18596/jotcsa.773478

(7) Ertuğrul Gazi Sağlam*, **Elif Bulat**, Ayşe Yıldırım, "Synthesis and Characterization of New Ferrocenyl and 3-methoxytolyl Dithiophosphonates", HJSE, 9 (3) 183-191, 2022. https://doi.org/10.17350/HJSE19030000270

(8) Ertuğrul Gazi Sağlam*, **Elif Bulat**, Mustafa Saçmacı, Servet Yıldız, "Çift Metal Merkezli Fosfor 1,1-Ditiyolat Cd(II) Komplekslerinin Sentez ve Yapılarının Aydınlatılması", Düzce Üniversitesi Bilim ve Teknoloji Dergisi, 11 (2), 759-774, **2023**. https://doi.org/10.29130/dubited.1104231

(9) **Elif Bulat** *, Ertuğrul Gazi Sağlam, Senem Akkoç, Celal Tuğrul Zeyrek, Yunus Zorlu, Hakan Dal, "Studies on new dithiophosphonic acid derivatives: Synthesis, characterization, DFT and molecular docking calculations and in vitro cytotoxicity assessment", **in publication**

Conferences

(1) **Bulat Elif,** Ertuğrul Gazi Sağlam**,** Hakan Dal, "Syntheses of and Structural Studies on Some Four Coordinated Dithiophosphonato Ni(II) Complexes" International Chemistry Biology Conference'18 (Özet Bildiri/Sözlü Sunum) 11-14.07.2018, Sharm El-Sheikh, EGYPT.

(2) **Bulat Elif,** Ertuğrul Gazi Sağlam**,** Hakan Dal, Tuncer Hökelek, "Syntheses of and

Structural Characterization on Octahedral Pyridino Dithiophosphonato Complexes and X ray Study on a Ni(II) Pyridino complex." International Chemistry Biology Conference'18 (Özet Bildiri/Poster), 11-14.07.2018, Sharm El-Sheikh, EGYPT.

(3) Ertuğrul Gazi Sağlam, Senem Akkoç, Yunus Zorlu, **Elif Bulat,** Aziz Akgün, "New phenanthroline nickel(II) organodithio-phosphorus complexes: Syntheses, structural characterizations and in vitro cytotoxic activity studies." 3rd International Eurasian Conference on Biological and Chemical Sciences (EurasianBioChem 2020) (Özet Bildiri/Poster), 19-20.03.2020, Ankara, TÜRKİYE

(4) Ertuğrul Gazi Sağlam, **Elif Bulat**, Hakan Dal, "Yeni 2,4-*bis*(1,2-Dimetoksifenil)-1,3-Dithia-2,4-Difosfetan 2,4-Disülfür Türevlerinin Sentezi ve Karakterizasyonu", (Özet Bildiri/Poster), VIII. Ulusal Anorganik Kimya Kongresi, 02-05 Eylül 2021, Tekirdağ Namık Kemal Üniversitesi, Tekirdağ.

(5) Ertuğrul Gazi Sağlam, **Elif Bulat,** "Yeni 2-Metoksifeniltiyofosforik Halkalı Di(Tiyoanhidriti)'nin Türevlerinin Sentezi ve Yapılarının Aydınlatılması", (Özet Bildiri/Poster), VIII. Ulusal Anorganik Kimya Kongresi, 02-05 Eylül 2021, Tekirdağ Namık Kemal Üniversitesi, Tekirdağ.

(6) Ertuğrul Gazi Sağlam**, Elif Bulat**, Hakan Dal, "Yeni 2,4-*bis*(3-metoksitolil)-1,3-dithia-2,4-difosfetan 2,4-disülfidinden Yeni Ditiyofosfonat ve Ni(II) Komplekslerinin Sentez ve Karakterizasyonu", (Özet Bildiri/Poster), 33. Ulusal Kimya Kongresi, 07-09 Ekim 2021, Tekirdağ Namık Kemal Üniversitesi, Tekirdağ.

(7) Ertuğrul Gazi Sağlam, **Elif Bulat,** "Veratrol İçerikli Yeni Ditiyofosfonat ve Nikel Komplekslerinin Sentezi ve Yapısal Karakterizasyonu", (Özet Bildiri/Poster), 33. Ulusal Kimya Kongresi, 07-09 Ekim 2021, Tekirdağ Namık Kemal Üniversitesi, Tekirdağ.

(8) **Elif Bulat,** Ertuğrul Gazi Sağlam, Hakan Dal, "Synthesis and characterization of New Dithiophosphonate Ligands." Frühjahrssymposium 2023, (Özet Bildiri/Poster), 21-24.03.2023, Giessen, GERMANY

(9) **Elif Bulat,** Ertuğrul Gazi Sağlam, Senem Akkoç, Celal Tuğrul Zeyrek, Yunus Zorlu, Hakan Dal, "New Dithiophosphonato Ni(II) Complexes: Synthesis, characterization, theoretical and in vitro cytotoxicity studies." Frühjahrssymposium 2023, (Özet Bildiri/Poster), 21-24.03.2023, Giessen, GERMANY

Research Projects

(1) Yozgat Bozok Üniv., BAP, **6602c FEF/17-120** "Kükürt-Fosfor Grubu Komplekslerinin Sentezi ve Yapısal Karakterizasyonu" **2017-2018.**

(2) Yozgat Bozok Üniv., BAP, **6602c-FEN/20-359** "2,4-diorganil-1,3,2,4-ditiyadifosfetan-2,4-disülfüründen Yeni Ditiyofosfonik Asit, Türev ve Komplekslerinin Sentezi ve Yapısal Karakterizasyonu." **2020-2022**

(3) Marmara Üniv, BAP, **FDK-2021-10339**"2,4-diorganil-1,3,2,4-ditiyadifosfetan-2,4- disülfüründen Yeni Ditiyofosfonik asit Türev ve Komplekslerinin Sentezi ve Yapısal Karakterizasyonu." **2021-2023**

(4) Ankara Üniversitesi, BAP, **FBA-2023-2736** "Organo-ditiyofosfor Türevlerinin Sentezi ve Yapılarının Aydınlatılması." **2023-2025.**

Dissertations

Doctorate

Synthesis and Structural Characterization of New Dithiophosphonic Acid, Derivatives and Complexes from 2,4-diorganyl-1,3,2,4-dithiadiphosphetane-2,4-disulfide, Marmara University, Institute for Graduate Studies in Pure and Applied Sciences, 2021 (Advisor: Prof. Dr. E.G. SAĞLAM).

Master

Dört ve altı koordinasyonlu nikel ditiyofosfonat komplekslerinin sentezi ve yapısal karakterizasyonu, Yozgat Bozok University, Institute for Graduate Studies in Pure and Applied Sciences, 2018 (Advisor: Prof. Dr. E.G. SAĞLAM).